

**COMPARISON OF FINITE DIFFERENCE AND FINITE ELEMENT HYDRODYNAMIC
MODELS APPLIED TO THE LAGUNA MADRE ESTUARY, TEXAS**

A Thesis

by

KARL EDWARD MCARTHUR

Submitted to the Office of Graduate Studies of
Texas A&M University
in partial fulfillment of the requirements for the degree of

MASTER OF SCIENCE

December 1996

Major Subject: Civil Engineering

**COMPARISON OF FINITE DIFFERENCE AND FINITE ELEMENT HYDRODYNAMIC
MODELS APPLIED TO THE LAGUNA MADRE ESTUARY, TEXAS**

A Thesis

by

KARL EDWARD MCARTHUR

Submitted to the Office of Graduate Studies of
Texas A&M University
in partial fulfillment of the requirements for the degree of

MASTER OF SCIENCE

December 1996

Major Subject: Civil Engineering

**COMPARISON OF FINITE DIFFERENCE AND FINITE ELEMENT HYDRODYNAMIC
MODELS APPLIED TO THE LAGUNA MADRE ESTUARY, TEXAS**

A Thesis

by

KARL EDWARD MCARTHUR

Submitted to Texas A&M University
in partial fulfillment of the requirements
for the degree of

MASTER OF SCIENCE

Approved as to style and content by:

Ralph A Wurbs
(Chair of Committee)

Wayne R. Jordan
(Member)

Juan B. Valdés
(Member)

Ingacio Rodríguez-Iturbe
(Head of Department)

December 1996

Major Subject: Civil Engineering

ABSTRACT

Comparison of Finite Difference and Finite Element Hydrodynamic Models Applied to the Laguna Madre Estuary, Texas. (December 1996)

Karl Edward McArthur, B.S., The University of Texas at Austin

Chair of Advisory Committee: Dr. Ralph A. Wurbs

The U.S. Geological Survey Surface Water Flow and Transport Model in Two-Dimensions (SWIFT2D) model was applied to the northern half of the Laguna Madre Estuary. SWIFT2D is a two-dimensional hydrodynamic and transport model for well-mixed estuaries, coastal embayments, harbors, lakes, rivers, and inland waterways. The model numerically solves finite difference forms of the vertically integrated equations of mass and momentum conservation in conjunction with transport equations for heat, salt, and constituent fluxes. The finite difference scheme in SWIFT2D is based on a spatial discretization of the water body as a grid of equal sized, square cells. The model includes the effects of wetting and drying, wind, inflows and return flows, flow barriers, and hydraulic structures.

The results of the SWIFT2D model were compared to results from an application of the TxBLEND model by Texas Water Development Board to the same part of the estuary. TxBLEND is a two-dimensional hydrodynamic model based on the finite element method. The model employs triangular elements with linear basis functions and solves the generalized wave continuity formulation of the shallow water equations. TxBLEND is an expanded version of the BLEND model to additional features that include the coupling of the density and momentum equations, the inclusion of evaporation and direct precipitation, and the addition tributary inflows. The TxBLEND model simulations discussed in this study were performed by personnel at the TWDB.

The two models were calibrated to a June 1991 data set from a TWDB intensive inflow survey of the Laguna Madre. Velocity and water quality data were available for the three days of the survey. Tide data for a much longer period were available from TCOON network stations. Results of the two models were compared at seven tide stations, eight velocity stations, and eleven flow cross sections. Simulated water surface elevations, velocities, and circulation patterns were comparable between models. The models were also compared on the basis of the ease of application and the computational efficiencies of the two models. The results indicate that, in the case of the Laguna Madre Estuary, TxBLEND is the more efficient of the two models.

ACKNOWLEDGEMENTS

I would like to express my sincerest appreciation to Dr. Ralph Wurbs, whose patience, understanding, and guidance were essential to the completion of this thesis. I would also like to thank the other members of my committee, Dr. Juan Valdés and Dr. Wayne Jordan. The funds for this study were provided by the Texas Water Development Board in cooperation with the U.S. Geological Survey. I would like to express my sincerest appreciation to Dr. Ruben Solis and Dr. Junji Matsumoto of the Water Development Board, whose guidance and input were invaluable to the completion of this thesis.

I would also like to thank the U.S. Geological Survey and Texas District USGS personnel who made this project possible. In particular, I would like to thank Mr. Marshall Jennings, who has been a mentor to me during my four years as an undergraduate and graduate co-op student with the USGS. His help and guidance have been greatly appreciated. I would also like to thank Mr. Ray Schaffranek and Mr. Bob Baltzer for their assistance in the early stages of this project.

I would like to thank my parents, Mr. and Mrs. Roland McArthur, for their love, support, and encouragement. I especially appreciate the patience of my wife to be, Flora, who has worked at a full time engineering job, planned our wedding without my help, and put up with my long hours of work on this project. Without her support, understanding, and encouragement, this thesis would never have been completed.

TABLE OF CONTENTS

		Page
	ABSTRACT	iii
	ACKNOWLEDGEMENTS	iv
	TABLE OF CONTENTS	v
	LIST OF FIGURES	vii
	LIST OF TABLES	x
I	INTRODUCTION.....	1
	Background.....	1
	Estuary Modeling.....	3
	Research Objectives	4
II	LITERATURE REVIEW	5
	The Laguna Madre Estuary	5
	General Hydrodynamic Modeling.....	6
	Previous Studies in the Laguna Madre	9
	TxBLEND and SWIFT2D.....	10
III	DESCRIPTION OF MODELS	12
	SWIFT2D	12
	TxBLEND	22
IV	PROCEDURE.....	30
	Data	30
	Bathymetry Generation	34
	Grid Cell Size Selection	37
	Simulation	42
	Calibration.....	43
	Verification.....	45
V	RESULTS OF SWIFT2D SIMULATIONS.....	46
	Results	46
	Sensitivity Analysis.....	58
VI	COMPARISON WITH TxBLEND RESULTS.....	76
	TxBLEND Model Application	76
	Comparison of Models	77
	Comparison of Results	81

TABLE OF CONTENTS -- continued

	Page
VII SUMMARY AND CONCLUSIONS	104
Summary	104
Conclusions	105
Recommendations for Future Study	107
REFERENCES	108
APPENDIX A	112
APPENDIX B	143
APPENDIX C	152
VITA	175

LIST OF FIGURES

FIGURE	Page
1 Location Map of the Laguna Madre Estuary	2
2 Location of Variables on the Model Grid	18
3 Simple SWIFT2D Computational Grid with Arbitrary Openings	20
4 Example of a Regular, Square Finite Difference Grid	25
5 Example of a Linear, Triangular Finite Element Mesh	25
6 Upper Laguna Madre Study Area Simulated with SWIFT2D and TxBLEND	31
7 Distribution of Wind Directions Observed at the Corpus Christi NAS Wind Station	33
8 Distribution of Wind Speeds Observed at the Corpus Christi NAS Wind Station	34
9 Upper Laguna Madre 400 Meter Grid (148x213 cells)	39
10 Upper Laguna Madre 200 Meter Grid (296x426 cells)	40
11 Typical SWIFT2D Grid Section Which Shows the Stair-step Effect in the Representation of Channels with a Regular, Square Grid	41
12 Locations of Tide Stations at Which Simulated and Observed Water Levels Were Compared	47
13 Locations of Velocity Stations at Which Simulated and Observed Velocities Were Compared	48
14 Locations of Cross Sections at which Simulated Flows Were Compared	49
15 Calibrated Water Levels at the Corpus Christi Naval Air Station Tide Station	51
16 Calibrated Water Levels at the Packery Channel Tide Station	51
17 Calibrated Water Levels at the Pita Island Tide Station	51
18 Calibrated Water Levels at the South Bird Island Tide Station	52
19 Calibrated Water Levels at the Yarbrough Pass Tide Station	52
20 Calibrated Water Levels at the Riviera Beach Tide Station	52
21 Calibrated Water Levels at the El Toro Island Tide Station	53
22 Calibrated Velocity at the Humble Channel Station	55
23 Calibrated Velocity at the GIWW at JFK Causeway Station	55
24 Calibrated Velocity at the GIWW Marker 199 Station	55
25 Calibrated Velocity at the North of Baffin Bay Station	56
26 Calibrated Velocity at the Mouth of Baffin Bay Station	56
27 Calibrated Velocity at the South of Baffin Bay - Middle Station	56
28 Calibrated Velocity at the South of Baffin Bay - West Station	57
29 Calibrated Velocity at the North Land Cut Station	57
30 Differences in Water Levels Due to the Time Step, Pita Island	63

LIST OF FIGURES - continued

FIGURE	Page
31 Differences in Water Levels Due to the Time Step, Riviera Beach	63
32 Differences in Velocity Due to the Time Step, GIWW at JFK Causeway.....	63
33 Differences in Velocity Due to the Time Step, South of Baffin Bay-Middle	64
34 Differences in Flow Due to the Time Step, GIWW at JFK Causeway.....	64
35 Differences in Flow Due to the Time Step, Baffin Bay.....	64
36 Differences in Water Levels Due to the Wind Stress, Pita Island	67
37 Differences in Water Levels Due to the Wind Stress, Riviera Beach	67
38 Differences in Velocity Due to the Wind Stress, GIWW at JFK Causeway.....	67
39 Differences in Velocity Due to the Wind Stress, South of Baffin Bay-Middle.....	68
40 Differences in Flow Due to the Wind Stress, GIWW at JFK Causeway	68
41 Differences in Flow Due to the Wind Stress, Baffin Bay.....	68
42 Differences in Water Levels Due to Manning's n, Pita Island.....	71
43 Differences in Water Levels Due to Manning's n, Riviera Beach.....	71
44 Differences in Velocity Due to Manning's n, GIWW at JFK Causeway	71
45 Differences in Velocity Due to Manning's n, South of Baffin Bay-Middle	72
46 Differences in Flow Due to Manning's n, GIWW at JFK Causeway.....	72
47 Differences in Flow Due to Manning's n, Baffin Bay.....	72
48 Differences in Velocity Due to Viscosity, GIWW at JFK Causeway	73
49 Differences in Flow Due to Viscosity, GIWW at JFK Causeway	73
50 Differences in Flow Due to the Advection Option, LM at North Land Cut.....	74
51 TxBLEND Finite Element Mesh for the Upper Laguna Madre Estuary, Corpus Christi Bay, and Copano Bay System	79
52 Close-up of the TxBLEND Mesh in the Vicinity of the JFK Causeway	80
53 Comparison of Water Levels at the Corpus Christi Naval Air Station Tide Station	82
54 Comparison of Water Levels at the Packery Channel Tide Station.....	82
55 Comparison of Water Levels at the Pita Island Tide Station	82
56 Comparison of Water Levels at the South Bird Island Tide Station.....	83
57 Comparison of Water Levels at the Yarborough Pass Tide Station.....	83
58 Comparison of Water Levels at the Riviera Beach Tide Station	83
59 Comparison of Water Levels at the El Toro Island Tide Station.....	84
60 Comparison of Velocity at the Humble Channel Station	86

LIST OF FIGURES - continued

FIGURE	Page
61 Comparison of Velocity at the GIWW at JFK Causeway Station.....	86
62 Comparison of Velocity at the GIWW Marker 199 Station	86
63 Comparison of Velocity at the North of Baffin Bay Station.....	87
64 Comparison of Velocity at the Mouth of Baffin Bay Station.....	87
65 Comparison of Velocity at the South of Baffin Bay - Middle Station.....	87
66 Comparison of Velocity at the South of Baffin Bay - West Station.....	88
67 Comparison of Velocity at the North Land Cut Station.....	88
68 Comparison of Flow at the GIWW at Corpus Christi Cross Section.....	89
69 Comparison of Flow at the Corpus Christi NAS Cross Section	89
70 Comparison of Flow at the Packery Channel Cross Section	89
71 Comparison of Flow at the Humble Channel Cross Section	90
72 Comparison of Flow at the GIWW at JFK Causeway Cross Section.....	90
73 Comparison of Flow at the Laguna Madre at Pita Island Cross Section.....	90
74 Comparison of Flow at the Laguna Madre at South Bird Island Cross Section.....	91
75 Comparison of Flow at the Laguna Madre at Green Hill Cross Section.....	91
76 Comparison of Flow at the Mouth of Baffin Bay Cross Section.....	91
77 Comparison of Flow at the Laguna Madre at Yarborough Pass Cross Section.....	92
78 Comparison of Flow at the Laguna Madre at North Land Cut Cross Section.....	92
79 TxBLEND Simulated Velocity Vectors, June 10, 09:00.....	95
80 SWIFT2D Simulated Velocity Vectors, June 10, 09:00.....	96
81 SWIFT2D Simulated Velocity Vectors near the John F. Kennedy Causeway, June 10, 09:00	97
82 TxBLEND Simulated Velocity Vectors, June 10, 18:00.....	98
83 SWIFT2D Simulated Velocity Vectors, June 10, 18:00.....	99
84 SWIFT2D Simulated Velocity Vectors near the John F. Kennedy Causeway, June 10, 18:00	100
85 TxBLEND Simulated Velocity Vectors, June 11, 00:00.....	101
86 SWIFT2D Simulated Velocity Vectors, June 11, 00:00.....	102
87 SWIFT2D Simulated Velocity Vectors near the John F. Kennedy Causeway, June 11, 00:00	103

LIST OF TABLES

TABLE	Page
1 Description of the Integration Correction Schemes Available in SWIFT2D	19
2 Data Observation Stations Used in the Study of the Upper Laguna Madre Estuary.....	32
3 Nautical Charts Used in the Development of the Bathymetry Data for the Laguna Madre Estuary	35
4 Root Mean Squared Errors between Simulated and Observed Water Levels.....	53
5 Root Mean Squared Errors between Simulated and Observed Velocities.....	54
6 SWIFT2D Model Parameters Varied for the Sensitivity Analysis	59
7 Courant Numbers Associated with the Time Steps Used in SWIFT2D for the Sensitivity Analysis.....	61
8 Root Mean Squared Errors between Simulated and Observed Water Levels for Simulations with Different Time Steps	61
9 Root Mean Squared Errors between Simulated and Observed Velocities for Simulations with Different Time Steps	62
10 Root Mean Squared Errors between Simulated and Observed Water Levels for Simulations with Different Wind Stress Coefficients	65
11 Root Mean Squared Errors between Simulated and Observed Velocities for Simulations with Different Wind Stress Coefficients	66
12 Root Mean Squared Errors between Simulated and Observed Water Levels for Simulations with Different Manning's Roughness Coefficients	69
13 Root Mean Squared Errors between Simulated and Observed Velocities for Simulations with Different Manning's Roughness Coefficients	70
14 Summary of the Wetting and Drying of Grid Cells during the 15 Day Sensitivity Analysis Simulations.....	75
15 Geometric Characteristics of the SWIFT2D Finite Difference Grid and the TxBLEND Finite Element Mesh	77
16 Root Mean Squared Errors between SWIFT2D and TxBLEND Simulated Water Levels and Observed Water Levels.....	84
17 Root Mean Squared Errors between SWIFT2D and TxBLEND Simulated Velocities and Observed Velocities.....	85
18 Root Mean Squared Errors between SWIFT2D and TxBLEND Simulated Flows.....	93

I INTRODUCTION

BACKGROUND

The need for freshwater inflows to maintain the ecological stability of bays and estuaries has provided the impetus for a wide range of studies along the Texas Coast. Texas Senate Bill 137 passed in 1975 mandated comprehensive studies of freshwater inflows to Texas bays and estuaries (Texas Department of Water Resources 1983). These studies led to a series of reports on the influence of fresh water inflows on the seven major bay and estuary systems along the Texas coast. Similar legislation passed in 1985 mandated an update of the earlier studies. In an effort to help predict the impact of various schedules of freshwater inflows, the Texas Water Development Board began a series of investigations and hydrodynamic modeling studies of Texas bays and estuaries (Longley 1994).

The Laguna Madre estuary is one of only three oceanic, hypersaline, lagoonal areas in the world. The system is composed primarily of shallow tidal flats that extend from Corpus Christi to Brownsville. The estuary is divided into two parts by a wide land bridge south of Baffin Bay. The Gulf Intracoastal Waterway (GIWW) is the only connection between the upper and lower portions of the estuary. The Laguna Madre estuary supports a significant portion of the commercial fishing industry in Texas (Laguna Madre, 1983) and is central to the economy of a large section of the Texas coast. Construction of the GIWW in the late forties significantly changed the patterns of flow in the Estuary. The GIWW created a continuous conduit for flow that extended the entire length of the estuary. The dredging required to maintain the channel has resulted in a chain of spoil islands that are intermittently spaced along the length of the estuary parallel to the GIWW. The spoil islands have also had an influence on circulation patterns in the estuary. The Location of the Laguna Madre is shown in Fig. 1.

The unique nature of the Laguna Madre Estuary presents a number of problems that make the system difficult to model. The presence of large tidal flats requires a hydrodynamic model that is able to simulate the flooding and drying of model computational cells. The unusual characteristics of the estuary system prompted the Texas Water Development Board (TWDB) to evaluate alternatives to the TxBLEND two-dimensional, finite element model which they have applied to several systems along the Texas Gulf Coast.

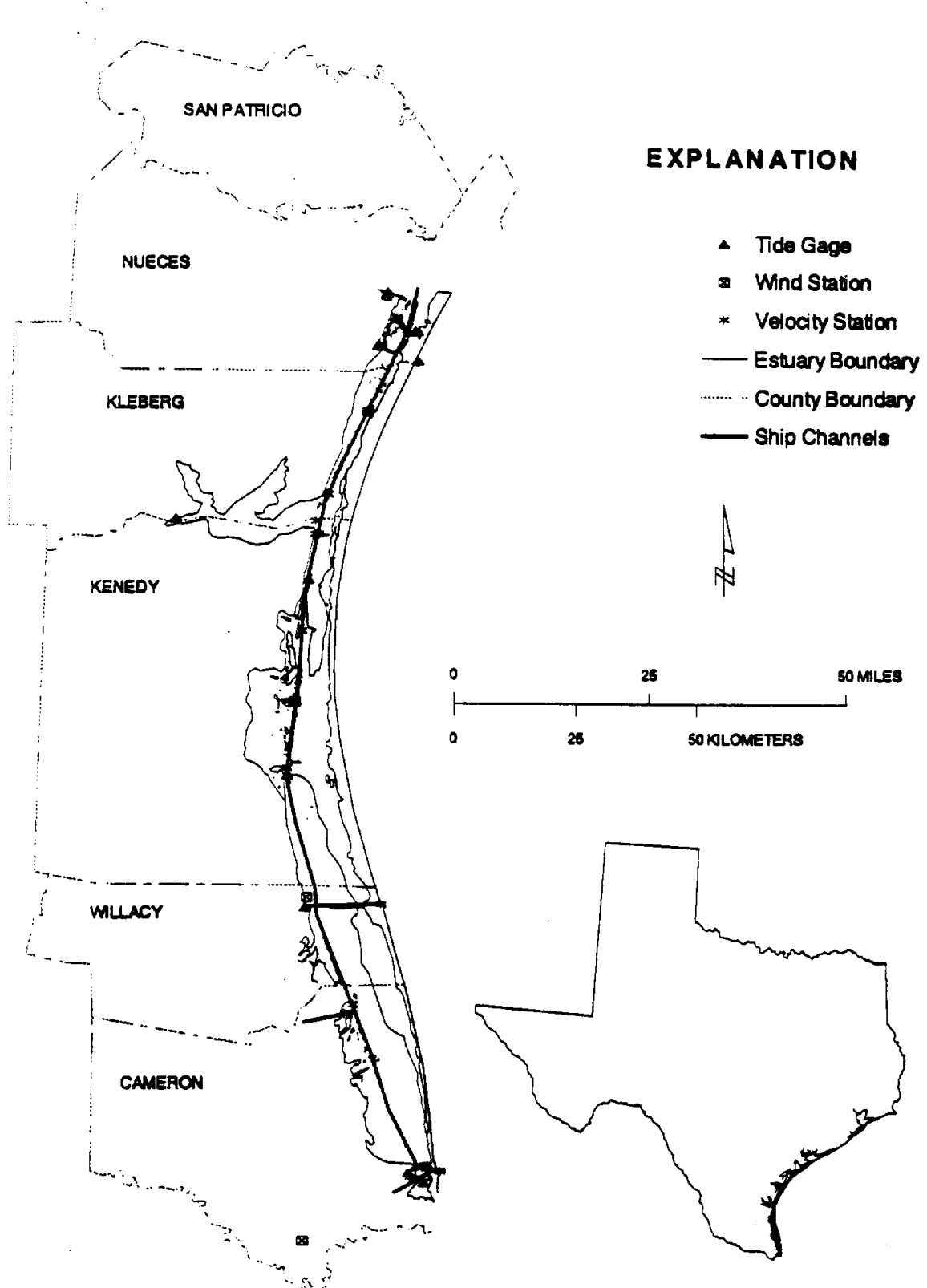


FIG. 1. Location Map of the Laguna Madre Estuary

The U. S. Geological Survey (USGS), under contract with the TWDB, has tested the applicability of the USGS Surface-Water, Integrated, Flow and Transport hydrodynamic model (SWIFT2D) to the Laguna Madre System. The SWIFT2D model is a two-dimensional, vertically integrated, finite difference model with the capability to simulate both flow and constituent transport. The results of the SWIFT2D modeling effort are compared to the available results from the modeling efforts of the TWDB.

The TxBLEND model has not yet been applied to the lower portion of the Laguna Madre south of the land cut. This study will focus on the ability of the models to simulate the upper portion of the Laguna Madre north of the land cut. The SWIFT2D model, calibrated for hydrodynamics, allows for a comparison of the ability of the two models to handle a number of important forcing functions. The effects of wind on the behavior of the model are especially interesting in the case of the Laguna Madre Estuary. The model will also allow an evaluation of the effects of wetting and drying on the extensive tidal flats in the estuary.

One of the major goals of the study is to consider the ability of the simple, regular, square grid finite difference representation of the estuary required for SWIFT2D to match the more geometrically accurate linear triangular finite element representation required for the TxBLEND model. The requirement in SWIFT2D for regular grid cell sizes is somewhat of a liability in the case of the Laguna Madre. The large area and the unusual flow characteristics of the estuary requires a fairly small cell size. The Gulf Intercoastal Water Way (GIWW), which for most of its length has a width of approximately 38 meters (125 feet) and a project depth of 3.7 meters (12 feet), transmits a large part of the flow in the estuary. In order to accurately represent the true bathymetry of the channel, a cell size on the order of the width of the GIWW would be required. Such a grid size would require approximately 3.15 million cells in order to represent upper portion of the Laguna Madre Estuary. The triangular finite element representation used by TxBLEND allows for variation of cell sizes. The cells can be very small in the vicinity of the GIWW or other important features, while cells in the wide, shallow flats can be significantly larger. However, elements which are too large can cause numerical instabilities in the TxBLEND model as discussed by Solis (1991). The limitations on cell size and computer power necessitated separation of the Laguna Madre into two parts for the SWIFT2D modeling.

ESTUARY MODELING

The primary concerns in estuary modeling are the simulation of flow patterns and salinity distributions. Both of these factors are of vital concern to the health and productivity of bay and

estuary systems. The effects of fresh water inflows to bays and estuaries has been studied extensively in the state of Texas. State law mandates that the necessary fresh water inflows to such systems be insured. Hydrodynamic simulation models are often used to determine the relationship between fresh water inflows, circulation patterns, and salinity. Results from hydrodynamic simulations are used in conjunction with planning level optimization models to operate systems of reservoirs upstream of the estuaries to insure the health of the estuary.

There exists a wide range of estuary hydrodynamic models in the literature. Both finite difference and finite element models have been used extensively, and the models have increased in complexity as computer resources have improved. Finite difference solution schemes were more successful in early hydrodynamic models, however, the introduction of the wave continuity equation formulation has led to the creation of many robust finite element schemes (Westerink, 1991). Both finite difference and finite element techniques have been used in a wide variety of two and three-dimensional hydrodynamic models. The advent of more powerful computer resources has spurred the growth in the number of three-dimensional models.

RESEARCH OBJECTIVES

The primary goal of the study is to evaluate the SWIFT2D model as an alternative to the TxBLEND model used by the Texas Water Development Board. Consideration will be given to the ease of application of the model as well as the quality and usefulness of the model results. The specific objectives of the study are:

1. Calibrate and verify the SWIFT2D model for the upper and lower Laguna Madre Estuary with data from the Texas Water Development Board, Texas Coastal Ocean Observation Network, National Oceanic and Atmospheric Administration, and any other available data sources;
2. Compare the quality of the model result and the efficiency of the model application with that of the TWDB's TxBLEND finite element model. Results are compared through evaluations of root mean squared errors between simulated and observed values and through visual inspection of plots of simulated and observed values.

The results of the study will be discussed in the thesis and also will be delivered to the TWDB.

II LITERATURE REVIEW

THE LAGUNA MADRE ESTUARY

The Laguna Madre Estuary system presents special problems in any effort to apply a hydrodynamic model. The estuary is one of only three oceanic, lagoonal, hypersaline areas in the world. Most of the Laguna Madre is composed of shallow flats, which extend the length of the estuary from Corpus Christi to Port Isabel. The upper and lower Laguna Madre is separated by a wide sand flat below Port Mansfield, Texas. The total surface area of the estuary at mean water level is approximately 1658 square kilometers (640 square miles), while the area at mean low water the surface area is approximately 1137 square kilometers (439 square miles). As the difference in surface area between mean water level and mean low water indicates, there are large areas of shallow tidal flats that tend to flood dry periodically. The Gulf Intracoastal Waterway (GIWW), which runs the entire length of the estuary at an average project depth of approximately 12 feet, is the only connection between the two halves of the Laguna Madre. The Laguna Madre has only five connections with the ocean and adjacent waters. At the north end, the estuary opens onto Corpus Christi Bay at the Humble Channel, Gulf Intracoastal Waterway, and Packery Channel. The southern half of the estuary opens onto the Gulf of Mexico at the Port Mansfield and Port Isabel ship channels. A limited amount of freshwater inflow to the estuary enters primarily from Baffin Bay in the upper Laguna and the Arroyo Colorado in the lower Laguna. Circulation in the estuary is primarily wind driven, and the tidal range is generally on the order of half a foot or less (Texas Department of Water Resources 1983). In a report mandated by Senate Bill 137 passed in 1975, the Texas Department of Water resources (1983) discusses in detail the characteristics of the Laguna Madre Estuary. The discussion ranges from the hydrology, circulation, and salinity to the nutrient processes and productivity of the estuary. The report on freshwater inflows to Texas bays and Estuaries edited by Longley (1994) was the result of similar legislation passed in 1985.

Kjerfve (1987) presents a summary of the characteristics of the Laguna Madre that is drawn from a number of sources. The Laguna Madre is the southernmost of the estuaries along the Texas coast. The regional climate of the coastal zone of south Texas is listed as tropical semiarid and is anomalous enough to be considered a "problem climate." The average precipitation rate in the region approximately equals the rate of evaporation. Additionally, there is little freshwater inflow into the northern Laguna Madre. Inflows from Baffin Bay average approximately one cubic meter per second and may cease altogether during periods of little precipitation (Kjerfve 1987). Direct precipitation accounts for an average of 65% of the freshwater inflow to the Laguna Madre (Texas Department of

Water Resources 1983). Kjerfve also discusses the hypersaline nature of the estuary. Before completion of the GIWW, the northern half of the estuary was thought to be in good condition when the salinity fell within the range of 40 to 60 parts per thousand (ppt). The salinity was observed to approach 100 ppt during periods of unusually low rainfall. Construction of the GIWW improved the exchange of water between Corpus Christi Bay and the upper Laguna Madre, however the estuary remains hypersaline. The salinity is highest at locations beyond the reach of tidal and low-frequency exchanges. The mean salinity at the northern end of the estuary was 31.5 ppt. The salinity increased southward at a rate of approximately 0.18 ppt/km (Kjerfve 1987).

A recent article by Cartwright (1996) discusses the economic and ecological impact of the Gulf Intracoastal Waterway on the Laguna Madre Estuary. The article focuses primarily on the impact of maintenance dredging of the GIWW on the health and stability of the estuary. Studies have concluded that the maintenance dredging is destroying the sea grass beds in the estuary. Sea grass forms the base on which life in the Laguna Madre is dependent. The reduction in sea grass has led to serious reductions in the productivity of the estuary. Cartwright (1996) states that while the connection of the upper and lower Laguna Madre as a result of the GIWW land cut increased circulation and productivity in the estuary, significant detrimental effects also were created. Barge traffic along the GIWW causes substantial erosion of sea grass habitat in the flats adjacent to the channel. The spoil islands created as a result of the maintenance dredging have had a significant effect on circulation patterns in the estuary. The islands range in size from 20,000 square meters to over 200,000 square meters. Cartwright (1996) also discussed the possibility of a 420 km extension of the GIWW into Mexico. The extension of the channel would dramatically increase the traffic through the Laguna Madre portion of the GIWW.

Numerous additional works discuss items such as estuary productivity, ecology, and other characteristics. While informative, these works have little bearing on the simulation of hydrodynamics in the estuary and are not included in this report.

GENERAL HYDRODYNAMIC MODELING

A wide variety of hydrodynamic models are discussed in the literature. Both two and three-dimensional models have been used extensively in applications to bay and estuary systems. Efficient finite difference and finite element codes are available from a number of sources. The development of these models has generally kept pace with the rapid pace of improvements in computer systems. Hydrodynamic modeling seems to have a higher priority in Europe, Asia, and Canada (Westerink and Gray 1991). Although U.S. contributions in the area of hydrodynamic modeling are a small fraction

of the world total, the present discussion will be limited primarily to contributions made by U.S. model developers.

Model Developments

Finite difference based spatial discretizations were the most successful schemes in the early development of hydrodynamic models due to the use of staggered spatial grids (Westerink and Gray 1991). Early finite element schemes were burdened by severe spurious modes that required the heavy-handed addition of nonphysical dissipation. The introduction of the wave continuity equation by Lynch and Gray (1979) led to more robust finite element schemes. Numerical schemes based on coordinate transformations also were under development in the late 1970's. These schemes led to finite difference codes with increased grid flexibility and boundary fitting characteristics. As a result, the features of finite difference and finite element based solutions to the shallow water equations have become much more similar (Westerink and Gray 1991).

Significant progress has been made in the development of robust hydrodynamic models, however, a wide range of shortcomings remain to be addressed. Several issues related to depth averaged flow computations need to be addressed. These include time stepping limitations, long term stability, conservation of integral invariants, resolution of sharp fronts, supercritical flows, wetting and drying of land boundaries, convective term treatment, and lateral momentum transport (Westerink and Gray 1991). The size of depth integrated flow problems and the abilities of hydrodynamic models have increased along with available computer capacities.

Two-dimensional Finite difference Models

Most of the finite difference models in current use apply spatially staggered discretization. The SIMSYS2D, which is the previous version of SWIFT2D is based on the staggered grid Alternating Direction Implicit (ADI) solution. An alternative Turkel-Zwas scheme that attempts to overcome the severity of the Courant time step limitation is discussed by Navon and deVilliers (1987). The method discretizes the Coriolis term on a coarser mesh with a fourth order approximation. Casulli and Cheng (1990) studied the stability and accuracy of Eulerian-Lagrangian methods which appear to take advantage of larger time steps.

Efforts to improve the ability of finite difference models to accurately represent irregular geometry have led to the use of coordinate transformation schemes and irregular grid sizes. Extensions of these efforts to problems of flooding in tidal flats have led to models with meshes that deform to fit the shape of the changing physical domain. The traditional approach has been to apply fixed spatial grids and specify small threshold depths over the area subject to inundation and drying. Austria and Aldama (1990) solve the one dimensional shallow water equations using a coordinate

transformation which maps a deforming physical domain with moving boundaries into a fixed computational domain.

Two-dimensional Finite element Models

Finite element schemes have become more common than finite difference schemes for the solution of the shallow water equations, however, some of the same ideas are being examined in both. Time discretization schemes similar to those used in finite difference models have been used in finite element schemes to take advantage of the ability of the method to perform long term simulations. Frequency domain based schemes have also been used for tidal circulation or other periodic events. The frequency domain scheme has the advantage of efficiency for long term simulations, no stability constraints on the time step, and the ability to study nonlinear tidal constituent interactions in a controlled manner (Westerink and Gray 1991).

Flooding and drying effects also have been addressed in finite element models. Akanbi and Katopodes (1988) solved the primitive shallow water equations through the implementation of a scheme which employs moving and deforming finite element mesh. The deforming mesh exactly follows the land water interface. Siden and Louch (1988) use the wave continuity form of the shallow water equations with moving boundaries. The method also exactly follows the interface and uses a time stepping scheme with elastic mapping of interior nodes.

The TABS system developed by the U.S. Army Corps of Engineers Waterways Experiment Station hydraulic group has been used in a number of applications. The TABS system is comprised of the Geometry File Generation program (GFGEN), RMA2, RMA4, and SED2D. The GFGEN software provides an extensive system for the development of the finite element meshes required by the system. Jones and Richards (1992) discuss an early version of the GFGEN software, which in an earlier form was called FastTABS. RMA2 is a one/two-dimensional, vertically-averaged, fully-implicit finite element model. The model can use both one and two-dimensional elements. The two-dimensional elements may be either triangular or trapezoidal and the side can be curved to fit boundary conditions. RMA4 is a one/two-dimensional depth averaged constituent transport finite element model, and SED2D is a two-dimensional, vertically averaged, sediment transport finite element model.

Three-dimensional Models

Most fully three-dimensional models have used the finite difference approach. Three-dimensional models are distinguished by the inclusion of property variation in the vertical. The vertical length scale is typically much smaller than the horizontal scale, therefore, algorithms must be developed which are not restricted in the time step by the small vertical scale (Westerink and Gray 1991). The σ -coordinate system is commonly used to simplify the calculations in the vertical.

Problems of poor accuracy have been observed with the σ - coordinate system used over areas with steep topography.

The Chesapeake Bay is one of the largest estuaries in the world and has been the subject of a number of investigations. Sheng et al. (1990) discuss aspects of curvilinear grids and vertical σ - coordinate transformations in the application of the CH3D model to the Chesapeake Bay. The CH3D model is a three-dimensional hydrodynamic model which makes use of a boundary fitted coordinate system and a turbulence closure model.

Grenier et al. (1993) discuss an application of the Advanced Three-dimensional Circulation Model for Shelves, Coasts, and Estuaries (ADCIRC) in both two-dimensional and three-dimensional forms to the Bight of Abaco. The ADCIRC model employs the generalized wave continuity equation to solve for the surface elevations and then uses a terrain-following σ - coordinate system in the vertical. A complete discussion of the model is presented by Luetlich et al. (1992).

PREVIOUS STUDIES IN THE LAGUNA MADRE

A limited number of hydrodynamic modeling studies of the Laguna Madre have been made since the 1983 study of the estuary by the Texas Department of Water Resources. Most of the models to date have focused on small parts of the estuary, especially in the vicinity of the JFK Causeway at the northern end of the estuary. The causeway has a significant effect on circulation in the estuary and has received considerable attention. Efforts are currently underway to execute models for the entire Laguna Madre Estuary systems. A comprehensive model of the entire estuary would provide valuable information for planning purposes.

The first effort to model the system was initiated as a result of the mandate from Texas Senate Bill 137. The set of models used in the study are described by Masch (1971). Separate models were used for the hydrodynamics and the conservative transport of salinity. Both models operated on a rectangular grid of square cells. The hydrodynamic model was a vertically integrated, explicit scheme, finite difference model. The transport model employed an alternating direction implicit (ADI) solution of the convective-dispersion equation. The computational grid for the Laguna Madre was created, however, a satisfactory calibration was never obtained.

Additional modeling studies of the Laguna Madre have recently been performed by the Conrad Blucher Institute for Surveying and Science. The Blucher Institute has used a two-dimensional, explicit finite difference hydrodynamic model (M2D) for two studies in the area. The M2D model uses a spatially-centered, finite difference scheme. The model operates on a rectilinear, irregularly-spaced finite difference grid. Militello and Kraus (1994) describe an application of the

M2D model to predict current and sediment movement in the Lower Laguna Madre as a result of U.S. Army Corps of Engineer dredging projects along the GIWW. Brown et al. (1995) describe an application of the M2D model to evaluate the effects of changes to the John F. Kennedy Causeway on circulation in the upper Laguna Madre. The M2D model grid for the JFK Causeway application consisted of approximately 13,000 cells with grid cell dimensions ranging from 40 to 592 meters. The second application of the M2D model was similar to TWDB efforts to model changes to the John F. Kennedy Causeway with the TxBLEND model. Neither Blucher Institute study attempted to apply the M2D model to the entire Laguna Madre Estuary.

TxBLEND AND SWIFT2D

The TWDB has undertaken hydrodynamic modeling studies in all seven of the major bay and estuary systems along the Texas Coast (Sabine-Neches, Trinity-San Jacinto, Lavaca-Colorado, Guadalupe, Mission-Aransas, Nueces, and Laguna Madre Estuaries) The TxBLEND model has been used in all of the TWDB modeling efforts to date. TxBLEND is an expanded version of the BLEND model developed by Dr. William G. Gray of Notre Dame University. The original BLEND model is a depth-averaged, two-dimensional finite element model and employs linear triangular elements (Lynch and Gray 1979). The BLEND model was modified with the addition of input routines for tides, river inflows, winds, evaporation, and concentration (Longley 1994). The TWDB has developed finite element grids for use with the TxBLEND model for each of the seven major Texas estuaries.

Limited applications of the model have been performed for the northern most end of the Laguna Madre in the area near the John F. Kennedy Causeway. These modeling efforts which are discussed in reports by Duke (1990), Solis (1991), and Matsumoto (1991), raised questions about the ability of the current version of the TxBLEND model to accurately reproduce the hydrodynamics of the Laguna Madre.

In an attempt to reduce numerical instabilities and conservation of mass problems, the TWDB is currently refining the TxBLEND model and experimenting with a variation of the model called the Finite element Texas Method (FETEX). The FETEX model attempts to combine the flexibility of discretization of finite element methods with the more simple mathematics of finite difference methods. Early applications of the model were not as successful as expected (Matsumoto 1992).

The SWIFT2D hydrodynamic model was selected by the USGS and TWDB for evaluation as an alternative to the TxBLEND model. SWIFT2D is a two-dimensional, depth averaged hydrodynamic/transport model for simulation of vertically well-mixed estuaries, coastal seas, harbors, lakes, rivers, and inland waterways. The SWIFT2D model numerically solves finite difference forms

of the vertically integrated equations of mass and momentum conservation in conjunction with transport equations for heat, salt, and constituent fluxes (Regan and Schaffranek 1993). The theoretical basis of the model is discussed in a report by the Rand Corporation (Leendertse 1987).

The SWIFT2D model has been used in a number of applications around the United States. Schaffranek (1986) discusses an application of the model for a simulation of the upper Potomac Estuary in Maryland. The study was performed as part of an intensive interdisciplinary investigation of the tidal Potomac River and Estuary. The model was successfully used to investigate the hydrodynamics and certain aspects of transport. Lee et al. (1994) discusses the simulation of the effects of highway embankments on the circulation of the Port Royal Sound Estuary. The Port Royal Sound application is similar to the John F. Kennedy Causeway modeling studies performed by the TWDB and the Blucher Institute. A data collection program and application of the SWIFT2D model to the Pamlico River Estuary, North Carolina, are discussed in Bales (1990) and Giese and Bales (1992). The SWIFT2D model has proven to be an effective tool in each of these applications.

III DESCRIPTION OF MODELS

Estuary hydrodynamic models solve the shallow water forms of the equations of conservation of mass transport and momentum conservation. Finite difference and finite element representations of the equations are the most commonly used solution schemes. Two-dimensional models are based on the assumptions of well-mixed conditions in the vertical dimension, small depths in comparison to the horizontal dimensions, and hydrostatic pressure. The Laguna Madre Estuary is primarily shallow with depths of a meter or less over much of the estuary. While the estuary has significant salinity gradients from north to south, the properties in the vertical are generally consistent. Two-dimensional models, therefore, are appropriate to represent the hydrodynamics. Both SWIFT2D and TxBLEND consider vertically averaged velocities and constituent concentrations. The two models provide an excellent contrast between the abilities and applicability of fixed-grid finite difference and a linear, triangular-mesh finite element solution schemes.

SWIFT2D

Capabilities

The basic purpose of the Surface-Water, Integrated Flow and Transport Two-Dimensional Model is the two-dimensional simulation of hydrodynamic, transport, and water quality in well-mixed water bodies. The model was created to model time-dependent, variable-density, fluid flows in bodies of water whose depths, though varying, are small compared with their horizontal dimensions (Leendertse 1987). The original version of the SWIFT2D model was developed in the late 1960's and early 1970's for an application in Jamaica Bay on the New York coast. Work on the SIMSYS2D modeling system which evolved from the original Jamaica Bay application was sponsored by the USGS and the Netherlands Rijkswaterstaat. The original documentation was published in a set of reports written by the RAND corporation for the USGS (Leendertse 1987). The program has been modified and updated several times since completion of the original code. The version of SWIFT2D used in this study was last updated in June, 1995. The SWIFT2D documentation is at present unpublished, however, information about the model and documentation may be obtained from the USGS. The point of contact for SWIFT2D is U.S. Geological Survey, Hydrologic Analysis Software Support Team, R. Steven Regan, 437 National Center, Reston, VA 22092, (electronic mail: h2osoft@usgs.gov). The model has been used by USGS personnel in a number of applications throughout the United States.

SWIFT2D is a robust model based on the alternating direction, implicit (ADI) solution of the two-dimensional equations of conservation, momentum, and mass transport. The model can be applied to a wide range of well mixed, shallow, surface water problems. Possible applications include estuaries, coastal embayments, harbors, lakes, rivers and inland waterways. The program can be used to investigate tidal influences, residual circulation, wind effects, and the fate of discharged substances in water bodies. It can be used to analyze flow through bridge openings, over highway embankments, around causeways and through culverts, at highway crossings of riverine flood plains, and estuarine wetlands. Circulation in lake and enclosed embayments under the influence of wind, storm surges in coastal areas, bays, and estuaries, and harbor oscillations also can be investigated with the program (Regan and Schaffranek 1993).

The finite difference grid for the model can be defined to simulate non-rectangular geographical areas and areas bounded by any combination of closed (land) and open (water) boundaries. Both time-varying data (water levels, velocities, or transport rates) and Fourier functions (phase and amplitude) can be specified as driving conditions at open boundaries. The ability to simulate sources of discharge such as rivers and outfalls allows the model to account for fresh water inflows which are an issue of concern for the health and stability of estuaries. SWIFT2D can be structured to simulate islands, dams and movable barriers or sluices. The ability of the model to simulate wetting and dewatering of tidal flats is especially important in estuaries such as the Laguna Madre which are comprised of vast expanses of fertile tidal flats which support extensive growths of sea grass.

SWIFT2D also has fairly extensive water quality simulation capabilities. The convection-diffusion form of the mass-balance transport equation is incorporated in the model. The equation includes terms which account for the generation, decay, and interaction of constituents. SWIFT2D water-quality computations can handle up to seven constituents simultaneously. The modular structure of the model source code makes the inclusion of more detailed constituent interaction algorithms fairly simple. SWIFT2D includes an equation of state for salt balance to account for pressure-gradient effects in the momentum equation. The presence of the pressure gradient term in the momentum equation provides a direct coupling of hydrodynamic and transport computations. The present version of the model also simulates temperature, however, the simulated temperature is not currently included in the computation of salinity density gradients. Future modifications may couple the temperature and salinity calculations.

The SWIFT2D source code is highly modular and coded entirely in standard, transportable FORTRAN 77, which makes the program compatible with a variety of mainframe, workstation, and microcomputer systems. The principal parts of the SWIFT2D modeling system are the main SWIFT2D program and an input data processor (SWIFTIDP). A number of associated programs are

available which aid in the application of the model. The Time Dependent Data System (TDDS) and the netCDF software system can be used to provide extensive data storage, manipulation, and display functions for time series data. The TDDS is a system of data-management programs developed by the USGS for handling sequences of time-dependent data. The TDDS has several routines written especially for the output of data in the proper format for use with SWIFT2D. Unidata's network Common Data Form (netCDF) is similar in function to the TDDS and provides an efficient set of software for scientific data storage, retrieval, and manipulation (Jenter and Signell 1992). Two programs called RDMAP and RDHIST provide for graphic output of results from SWIFT2D. RDMAP has the capability to create vector and contour plots for each computational grid cell in a model. RDHIST provides time-series plots of water levels, velocities, flows, and constituent transport. A separate program called GRIDEDIT provides an interactive, graphical capability to create, edit, verify, and view two-dimensional arrays of input data or output results.

Theory

The SWIFT2D model is based on the full set of dynamic, vertically-averaged, two-dimensional, flow and transport equations. The equations are derived from the full, Eulerian, three-dimensional representation of flow (conservation and momentum) by ignoring vertical accelerations and by replacing the horizontal velocity components with their respective vertically averaged components. The model is applicable for computation of time-dependent, variable-density flow in vertically well-mixed bodies with depths that are small in comparison with their horizontal dimensions

The partial-differential equations used in the model to express the conservation of mass, momentum, and constituents in the x and y directions (Leendertse 1987) are

Conservation of Mass

$$\frac{\partial \zeta}{\partial t} + \frac{\partial(HU)}{\partial x} + \frac{\partial(HV)}{\partial y} = 0 \dots\dots\dots(1)$$

Conservation of Momentum

$$\frac{\partial U}{\partial t} + U \frac{\partial U}{\partial x} + V \frac{\partial U}{\partial y} - fV + g \frac{\partial \zeta}{\partial x} + \frac{g}{2} \frac{H}{\rho} \frac{\partial \rho}{\partial x} + RU - \frac{\xi}{H} W^2 \sin \phi - k \left(\frac{\partial^2 U}{\partial x^2} + \frac{\partial^2 U}{\partial y^2} \right) = 0 \dots\dots\dots(2)$$

$$\frac{\partial V}{\partial t} + U \frac{\partial V}{\partial x} + V \frac{\partial V}{\partial y} + fU + g \frac{\partial \zeta}{\partial y} + \frac{g}{2} \frac{H}{r} \frac{\partial r}{\partial y} + RV - \frac{x}{H} W^2 \cos j - k \left(\frac{\partial^2 V}{\partial x^2} + \frac{\partial^2 V}{\partial y^2} \right) = 0 \dots\dots\dots(3)$$

$$\frac{\partial(H\dot{P})}{\partial t} + \frac{\partial(HUP)}{\partial x} + \frac{\partial(HVP)}{\partial y} - \frac{\partial(HD_x \partial P / \partial x)}{\partial x} - \frac{\partial(HD_y \partial P / \partial y)}{\partial y} - HS = 0 \dots\dots\dots(4)$$

where:

D_x, D_y = diffusion coefficients of dissolved substances,

f = Coriolis parameter,

g = acceleration due to gravity,

h = distance from the bottom to a horizontal reference plane,

H = temporal depth ($h + \zeta$),

k = horizontal exchange coefficient,

S = vector of sources of fluid with dissolved substances,

U = vertically averaged velocity component in x direction,

V = vertically averaged velocity component in y direction,

R = expression for the bottom friction,

W = wind speed,

ζ = water-surface elevation relative to horizontal reference plane,

ξ = wind stress coefficient, and

ϕ = angle between wind direction and the positive y direction.

In these equations, t represents time and x and y are the coordinate axes in the horizontal plane. The first equation (1) represents the conservation of mass, (2) and (3) express momentum conservation in the x and y coordinate directions, respectively, and (4) expresses the mass balance of dissolved constituents.

The variables U and V in the conservation and momentum equations represent the vertically averaged velocity in the x and y coordinate directions and are defined as

$$U = \frac{1}{H} \int_{-h}^{\zeta} u dz \dots\dots\dots(5)$$

$$V = \frac{1}{H} \int_{-h}^{\zeta} v dz \dots\dots\dots(6)$$

where dz is the increment in the vertical by which the u and v point velocities are integrated over the temporal depth H . The constituent concentration is expressed in a similar fashion as:

$$P = \frac{1}{H} \int_{-h}^{\zeta} p_i dz \dots\dots\dots(7)$$

where p_i is the concentration of the i -th constituent.

The Coriolis term represents the acceleration induced by the rotation of the earth. The Coriolis term can be significant in wide water bodies. The Coriolis effect is a function of the angle of latitude of the water body and is expressed as

$$f = 2\omega \sin \varphi \dots\dots\dots(8)$$

where ω is the angular velocity of the earth and φ is the geographical latitude of the water body. The Coriolis effect causes a clockwise acceleration in the northern hemisphere and a counter-clockwise acceleration in the southern hemisphere.

SWIFT2D has two options for the treatment of the bottom stress term represented by R in (1) and (2). The first option is the conventional quadratic-stress representation common in steady-state hydraulics expressed as

$$R = \frac{g}{C^2 H} (U^2 + V^2)^{1/2} \dots\dots\dots(9)$$

The Chézy coefficient, C , is computed dynamically in the model as

$$C = \frac{\lambda}{n} H^{1/5} \dots\dots\dots(10)$$

where n is the Manning roughness coefficient and λ is a factor equal to 1 for SI units and 1.486 when U.S. Customary units are used. A spatially variable Chézy coefficient field, which changes during a simulation due to changes in water levels, is computed from a constant field of specified Manning's n values. Horizontal density gradients due to salinity in a water body force the Chézy values to be dependent on the direction of flow in addition to the depth. SWIFT2D treats the Chézy value as a linear function of the salinity gradient as

$$C = \frac{\lambda}{n} H^{1/5} \left[1 + \alpha_1 \frac{(U(\partial s/\partial x) + V(\partial s/\partial y))}{(U^2 + V^2)^{1/2}} \right] \dots\dots\dots(11)$$

where s is salinity in ppt and α_1 is the salinity correction coefficient. The density equation increases the effects of bottom friction during the flood tide cycle and decreases bottom stress during the ebb tide cycle. The increase and decrease of bottom stress influences mean water levels in certain regions of the model and has an effect on the generation of overtides.

The second expression for R is a turbulence-closure form. In this form the bottom stress is not computed directly from the velocity components. The subgrid-scale energy intensity level, e , is computed by a transport equation and then the bottom stress coefficient is evaluated according to

$$R = \frac{a_3}{H} \sqrt{e} \dots\dots\dots(12)$$

where a_2 is a turbulence closure parameter. Energy is computed as a constituent and transported by (4) with both generation and decay components, and the local bottom stress coefficient is updated according to (12).

Wind has a strong effect on wide, shallow estuaries such as the Laguna Madre. The wind stress coefficient, ξ , is a measure of the drag exerted on the water surface by wind. The dimensionless coefficient is expressed as

$$\xi = C_w \frac{\rho_a}{\rho} \dots\dots\dots(13)$$

where C_w is the water-surface drag coefficient, ρ_a is the air density, and ρ_w is the water density. Experiments have shown that the value of the water surface drag coefficient depends on the height, steepness, and celerity of wind generated surface waves. Representative values for the wind stress coefficient range from 1.5×10^{-3} for light winds to 2.6×10^{-3} for strong winds.

Theoretically, the horizontal momentum diffusion is small when the water in the system is well mixed and a small viscosity coefficient is required for the computation. When the estuary is not well mixed, however, a much larger effective momentum exchange is present. The viscosity term is introduced to account for several physical phenomena. The value of the viscosity coefficient is dependent on the grid size used in the model. Grids with high resolution adequately describe the velocity field in time and space. Part of these motions cannot be represented with a much larger grid size and momentum transfers are incorporated in the viscosity term (Leendertse 1987). Horizontal momentum diffusion can optionally be treated as a function of the vorticity gradient normal to the direction of flow. Horizontal momentum diffusion is generally small in well mixed water bodies, however, when the water body is not well mixed, a much larger effective momentum exchange is present (Leendertse 1987). The horizontal momentum exchange coefficient, k in (2) and (3), is computed as

$$k = k_0 + k' |\partial_y \omega| (\Delta s)^2 \dots\dots\dots(14)$$

where k_0 is a spatially variable coefficient, k' is a constant coefficient over the computational field, Δs is the grid cell size, and ω is the vorticity $[(\partial U / \partial y) - (\partial V / \partial x)]$.

The pressure terms in (2) and (3) represent forcing due to salinity-dependent density gradients. These terms become important in water bodies in which a significant horizontal density gradient exists. An equation of state is solved for every point in the computational grid at every time step to define the relationship between salinity and water density. The distribution of salinity is determined by (4). The equation of state is expressed in a form of the Turmlirz equation in which pressure and volume are related by empirical constants as

$$\rho = S' / \left[(1779.5 + 11.25T - 0.0745T^2) - (3.8 + 0.01T)s + S' \right] \dots\dots\dots(15)$$

where $S' = 0.5890 + 38T - 0.375T^2 + 3s$, in which T is temperature in degrees Celsius and s is salinity in g/kg. Spatial variations in temperature are not computed in the model, therefore, a constant temperature is used for the entire water body.

Hydrodynamic Computation Features

The governing partial differential equations for the conservation of mass and momentum are solved by an alternating-direction, implicit (ADI) method on a space staggered grid (Leendertse 1987). The ADI method is unconditionally stable and does not create artificial (numerical) viscosity. Although the implicit nature of the ADI method relieves the numerical stability constraint on the time step, the time step in practice is often limited by accuracy requirements. Serious errors have been found for large time steps. Stelling et al. (1986) determined that the inaccuracy is a fundamental property of the numerical integration scheme. The so-called ADI effect is discussed further in the section of this report which deals with the Laguna Madre application sensitivity analysis. The space-staggered grid representation (Fig. 2) defines the water depth (h) with respect to a horizontal datum at the center of each grid cell, water surface elevations (ζ) referenced to the horizontal datum at the four corners of the cell, and velocity components (u, v) along the sides of the cell.

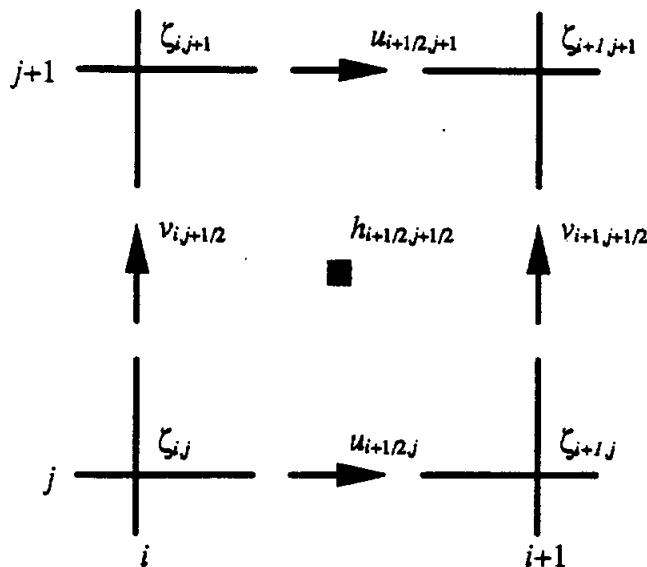


FIG 2. Location of Variables on the Model Grid

The model grid is initially established by delineation of the study area as a rectangle that minimizes the permanent dry area. The rectangle may be rotated from north to minimize the land area. The computational scheme essentially uses four grids, one each for depth, water surface elevation, velocity in the x direction, and velocity in the y direction. The computations proceed in increments of one half of the specified time step. Water levels and concentrations are computed each half time step, while the velocity components are computed at alternate half time steps. Therefore the computed U and V velocities are never coincident in time.

The numerical integration for velocity in the advection term of the momentum equations (2 and 3) and water level in the continuity equation (1) are performed with two different operations. Each operation has options for the time level at which the approximation of certain terms are made and also of the spatial representation of certain terms (Leendertse 1987). The time level indicates whether the variable is at the prior, present, or subsequent time step. In one operation the new velocity and water level components are computed at time step $t+.5$ in the x direction. In the second operation, the components at time step $t+1$ are computed from information available at time step $t+.5$ and t in the y direction. Table 1 summarizes the various corrections performed on computed values for the seven integration options.

TABLE 1. Description of the Integration Correction Schemes Available in SWIFT2D

Integration Option	Velocity in the Advection term		Water level in the continuity equation	
	Every Other Time Step	Every Other Time Step	Every Other Time Step	Every Other Time Step
0	Previous	Previous	Previous	Previous
1	Predicted	Predicted	Previous	Previous
2	Average	Average	Previous	Previous
3	Previous	Predicted	Previous	Previous
4	Predicted	Predicted	Predicted	Predicted
5	Average	Average	Predicted	Predicted
6	Previous	Predicted	Previous	Predicted

When velocities are significant, option 0 becomes unstable due to negative viscosity introduced by the advection terms. Option 5 approaches second-order accuracy after a few iterations as the advection terms become centered in time. Option 5 is considered the most accurate (Leenderts 1987) and was used in the simulations for this study. The model provides three options for the approximation of the

advection terms in the momentum equation. The Arakawa option conserves vorticity and squared vorticity, but is more time consuming. The Leendertse option is a standard central difference approximation and is less time consuming. The third option completely eliminates the advection component.

The model performs calculations on a subset of the full rectangular grid called the computational grid. The purpose of the computational grid is to reduce the number of grid cells involved in the calculations. The computational grid can be defined to exclude large areas of dry land which could include both cells on the shore above the maximum water level and islands. The computational grid need not be rectangular provided the internal angles between line segments are 90° , 135° , 225° , or 270° ; there are at least two grid spaces between a reversal of direction; and computational grid polygons are separated by at least one grid space. The default computational grid which encompasses the entire rectangular grid is shown in Fig. 3.

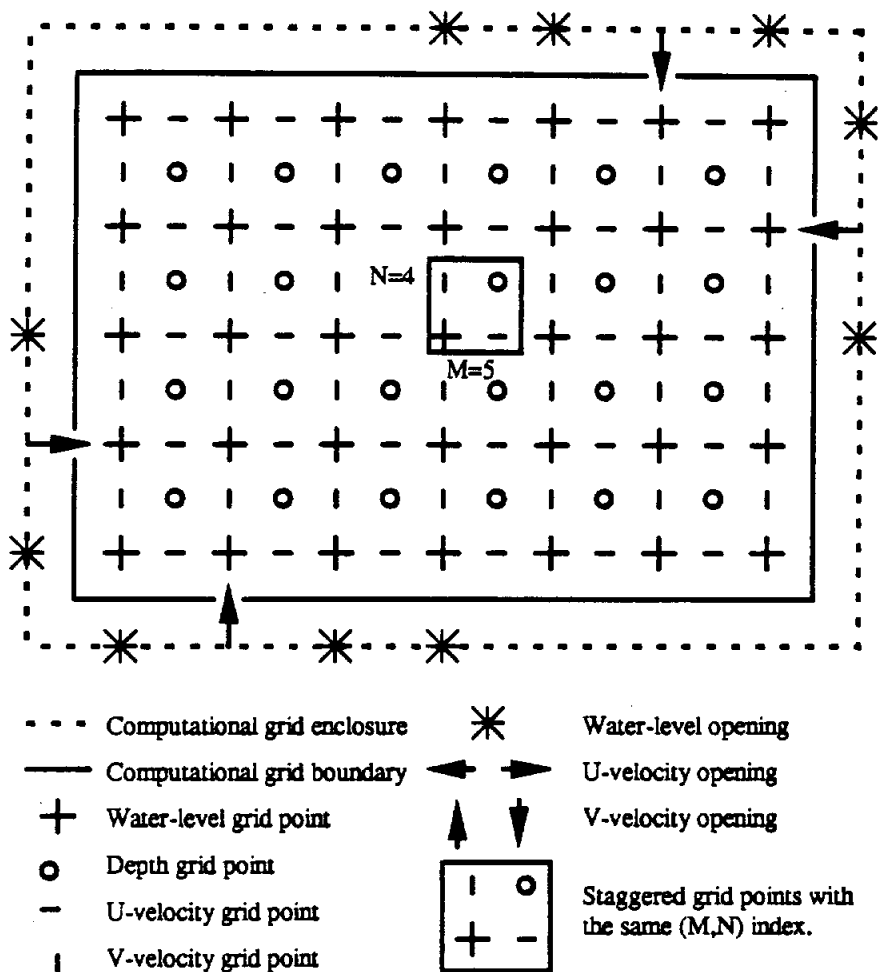


FIG. 3. Simple SWIFT2D Computational Grid with Arbitrary Openings

SWIFT2D supports boundary conditions for tides, velocities, and mass transport. These boundary condition grid cells must be located on the outermost cells of the computational grid.

The forcing functions that drive SWIFT2D include water levels, velocities, and transport rates at open boundaries, along with wind, discharges, and salinity. Open boundary data can be input in the form of time-varying data or Fourier components of amplitude and phase. Time-varying water level, velocity, or transport data at open boundaries are specified for each end of the opening. Values along the opening are interpolated between the two endpoints. Time-varying wind data can be input as a single value for the entire grid or as a coarse grid with wind data interpolated from two or more wind stations. Data for discharge sources which represent stream inflows, return flows, or withdrawals can be input at the edges of the computational grid.

The flooding and drying of shallow areas is simulated through the inclusion or exclusion of water-surface-elevation points from the computation as local water levels rise and fall. The simulation of these areas present a number of computational problems which have been accounted for in the model. The major problem is the discrete nature of the changes. When an area is taken out of the computation the sudden changes generates a small wave. The wave can cause flooding or drying of adjacent areas, which in turn generates more waves. This chain reaction can cause stability problems in large simulations with large tidal flats. Two measures are implemented in the model to deal with the stability problem. First, the assessment of shallow areas that are flooding or drying are made at periodic intervals larger than the computational time step. The disturbances have time to dissipate between the assessments. The second measure sets the Chézy coefficient of shallow-depth points to a small value specified when the depth falls below a small, designated value. The depth and Chézy coefficient are specified in the input file.

SWIFT2D also supports options for the simulation of sluices or barriers to flow, dam or permanently dry points, and particle movement. The barrier option allows for the simulation of structures such as weirs, gates, sills or bridges. The particles in the particle movement routines are assumed to represent some quantity of substance that moves with the water but does not influence the water movement. The particles movement routines could be used to simulate the movement of an oil spill in the estuary. Neither of these options were invoked in the SWIFT2D model of the upper Laguna Madre, however, the barrier options should be used for more detailed analyses such as flow patterns near the JFK Causeway.

TxBLEND

The TxBLEND, like SWIFT2D, is a two-dimensional, vertically integrated, hydrodynamic model capable of simulating flow, salinity, and constituent transport. TxBLEND, however, is based on a finite element solution of the shallow water, Saint-Venant equations. The TxBLEND model is the result of successive evaluations of and improvements to the Fast Linear Element Explicit in Time (FLEET) triangular finite element models for tidal circulation developed by Dr. William G. Gray at the University of Notre Dame (Matsumoto 1993). The original FLEET model, described in the user's manual by Gray (1987), provides several options for the solution of the shallow water equations of continuity and conservation of mass. The FLEET solution scheme is based on an explicit finite element solution of the governing equations. BLEND was the next step in the evolution of the model. The BLEND model contains the complete FLEET model with the addition of two important features; an implicit solution scheme capability and salinity modeling capability. The BLEND model was further modified by the TWDB to create the current TxBLEND hydrodynamic model. Several additions which were deemed important to the modeling of estuaries along the Texas Gulf Coast were added to the model. These features include the introduction of the density term, direct precipitation, evaporation, and source or sink terms incorporated into the governing equations.

The FLEET Model

The original fleet model was as much a research and learning tools as a model to be used for the simulation of real world scenarios. The model was developed in the mid-1980's by the Department of Civil Engineering at the University of Notre Dame under a grant from the National Science Foundation. The purpose of the code was to provide a simple tool for the investigation of the physical and numerical aspects of the modeling of two-dimensional areal circulation in surface water bodies due to tidal and atmospheric forcing (Gray 1987). Output from the model includes the time-varying, vertically-averaged stage and horizontal velocity components of the flow in the modeled water body.

FLEET was a generalization of an older model (WAVETL) which first introduced the wave equation formulation of the continuity and momentum equations to finite element modeling of shallow water bodies. The distinguishing feature of the wave equation model is that the primitive equations (1) and (2) are operated upon before the finite element discretization is applied, such that second derivative of depth with respect to space appear in the continuity equation. The driving force in the development of the wave equation model was the presence of spurious short wavelength spatial oscillations which were a common source of numerical difficulty in earlier finite element models. The

wave equations have been shown to both damp and propagate this short wavelength noise, while maintaining high accuracy for the predominant waves. More complete descriptions of the theoretical basis for application of the wave formulations of the governing equations can be found in Lynch and Gray (1979).

The FLEET model package is actually a set of models which use various forms of the governing shallow water equations. The model allows the user to select between several different forms and time weightings of the equations. FLEET is dependent on the same shallow water assumptions as SWIFT2D, however the model does not account for density variations in the flow. The options for the governing equations in the model are as follows:

Conservation of Mass

Option 1

$$\begin{aligned} & \frac{\partial^2 H}{\partial t^2} + \frac{\partial H}{\partial t} - \frac{\partial}{\partial x} \left[\frac{\partial(HUU)}{\partial x} + \frac{\partial(HUV)}{\partial y} + gH \frac{\partial(H-h)}{\partial x} - fHV - A_x \right] \\ & - \frac{\partial}{\partial y} \left[\frac{\partial(HUV)}{\partial x} + \frac{\partial(HVV)}{\partial y} + gH \frac{\partial(H-h)}{\partial y} + fHU - A_y \right] \dots\dots\dots(16) \\ & - HU \frac{\partial \tau}{\partial x} - HV \frac{\partial \tau}{\partial y} = 0 \end{aligned}$$

Option 2

$$\frac{\partial H}{\partial t} + \frac{\partial(HU)}{\partial x} + \frac{\partial(HV)}{\partial y} = 0 \dots\dots\dots(17)$$

Conservation of Momentum

Option 1

$$\begin{aligned} & \frac{\partial^2(HU)}{\partial t^2} + \tau \frac{\partial(HU)}{\partial t} + HU \frac{\partial \tau}{\partial t} + \frac{\partial}{\partial t} \left[\frac{\partial(HUU)}{\partial x} + \frac{\partial(HUV)}{\partial y} - fHV - A_x \right] \dots\dots\dots(18a) \\ & - \frac{\partial}{\partial x} \left[gH \frac{\partial(HU)}{\partial x} + gH \frac{\partial(HV)}{\partial y} \right] + g \frac{\partial h}{\partial x} \left[\frac{\partial(HU)}{\partial x} + \frac{\partial(HV)}{\partial y} \right] = 0 \end{aligned}$$

$$\begin{aligned} & \frac{\partial^2(HV)}{\partial t^2} + \tau \frac{\partial(HV)}{\partial t} + HV \frac{\partial \tau}{\partial t} + \frac{\partial}{\partial t} \left[\frac{\partial(HUV)}{\partial x} + \frac{\partial(HVV)}{\partial y} + fHU - A_y \right] \dots\dots\dots(18b) \\ & - \frac{\partial}{\partial y} \left[gH \frac{\partial(HU)}{\partial x} + gH \frac{\partial(HV)}{\partial y} \right] + g \frac{\partial h}{\partial y} \left[\frac{\partial(HU)}{\partial x} + \frac{\partial(HV)}{\partial y} \right] = 0 \end{aligned}$$

Option 2

$$\frac{\partial U}{\partial t} + U \frac{\partial U}{\partial x} + V \frac{\partial U}{\partial y} + g \frac{\partial(H-h)}{\partial x} - fV + \tau U - \frac{A_x}{H} = 0 \dots\dots\dots(19a)$$

$$\frac{\partial V}{\partial t} + U \frac{\partial V}{\partial x} + V \frac{\partial V}{\partial y} + g \frac{\partial(H-h)}{\partial y} + fU + \tau V - \frac{A_y}{H} = 0 \dots\dots\dots(19b)$$

Option 3

$$\frac{\partial(HU)}{\partial t} + \frac{\partial(HUU)}{\partial x} + \frac{\partial(HUV)}{\partial y} + gH \frac{\partial(H-h)}{\partial x} - fHV + \tau HU - A_x = 0 \dots\dots(20a)$$

$$\frac{\partial(HV)}{\partial t} + \frac{\partial(HUV)}{\partial x} + \frac{\partial(HVV)}{\partial y} + gH \frac{\partial(H-h)}{\partial y} + fHU + \tau HV - A_y = 0 \dots\dots(20b)$$

Option 4

$$\begin{aligned} & \frac{\partial^2 U}{\partial t^2} + \frac{\partial U}{\partial t} - g \frac{\partial}{\partial x} \left[\frac{\partial(HU)}{\partial x} + \frac{\partial(HV)}{\partial y} \right] - f \frac{\partial V}{\partial t} + U \frac{\partial \tau}{\partial t} - \frac{\partial}{\partial t} \left(\frac{A_x}{H} \right) \\ & + \frac{\partial}{\partial t} \left[U \frac{\partial U}{\partial x} + V \frac{\partial U}{\partial y} \right] = 0 \end{aligned} \dots\dots\dots(21a)$$

$$\begin{aligned} & \frac{\partial^2 V}{\partial t^2} + \frac{\partial V}{\partial t} - g \frac{\partial}{\partial y} \left[\frac{\partial(HU)}{\partial x} + \frac{\partial(HV)}{\partial y} \right] + f \frac{\partial U}{\partial t} + V \frac{\partial \tau}{\partial t} - \frac{\partial}{\partial t} \left(\frac{A_y}{H} \right) \\ & + \frac{\partial}{\partial t} \left[U \frac{\partial V}{\partial x} + V \frac{\partial V}{\partial y} \right] = 0 \end{aligned} \dots\dots\dots(21b)$$

where:

t = time,

U = vertically averaged velocity in the x direction,

V = vertically averaged velocity in the y direction,

H = total depth of water,

h = depth below a horizontal reference datum,

g = gravity,

f = Coriolis parameter,

τ = bottom friction,

A_x = atmospheric forcing in the x direction,

A_y = atmospheric forcing in the y direction.

Equations (17), (19a), and (19b), which comprise option 2 for both the mass and conservation equations, are the primitive forms similar to the governing equations in SWIFT2D. The primary

difference is the lack of density and momentum diffusion terms in the FLEET equations. Equations (16), (18), and (21) are wave equation formulations of the shallow water equations.

The FLEET model uses the finite element technique for the solution of the shallow water equations. The study region must be divided into small, discrete triangular elements as shown in Fig. 5. Each element must have three nodes at which the water surface elevation and velocity solutions are computed. Uniform sizes and orientations of the elements are not required.

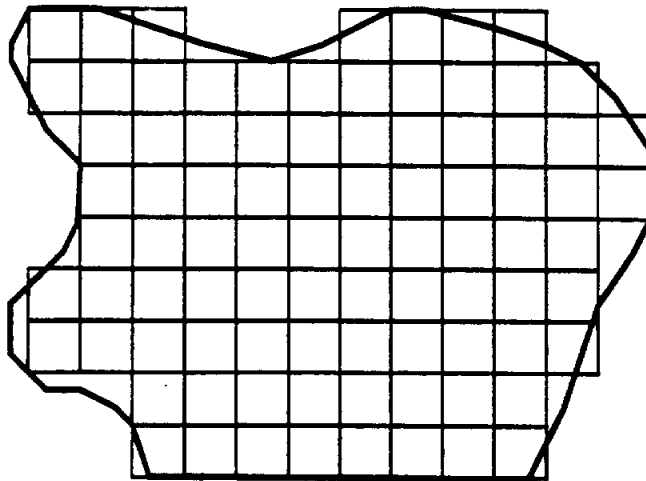


FIG. 4. Example of a Regular, Square Finite Difference Grid

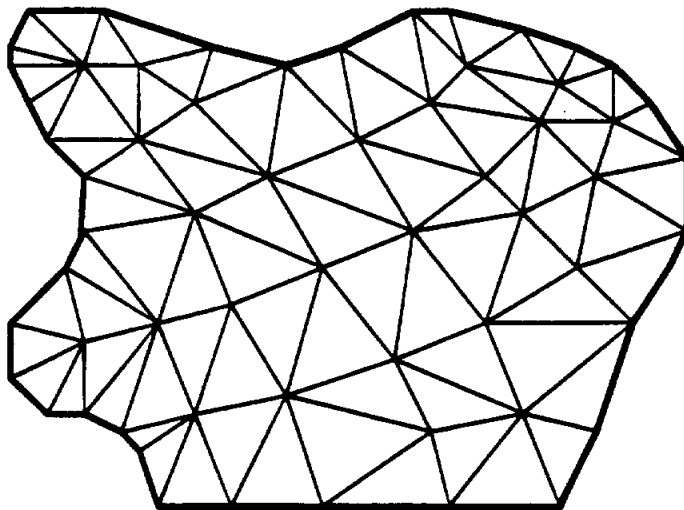


FIG. 5. Example of a Linear, Triangular Finite Element Mesh

The finite element mesh offers several advantages over traditional finite difference grids such as the one shown in Fig. 4. Triangular elements provide a much better fit along the boundaries of the water bodies. In addition, the ability to use varied cell sizes allows the user to more accurately represent important features with small triangles, while larger triangles can be used in less important areas. This feature provides greater computational efficiency in areas where large triangles are appropriate. The triangular elements used to describe the mesh should resemble equilateral triangles as closely as possible. Severely distorted elements may adversely affect the numerical computations of the model.

The FLEET model requires essentially the same input data as SWIFT2D. The latitude must be given for computation of the Coriolis acceleration. The bathymetry and geometry of the basin must be defined and a set of roughness coefficients must be supplied. The roughness coefficient may be in the form of Manning's n , Chézy C , or a time invariant roughness. Boundary, initial, and driving conditions must be supplied. The primary differences between the required inputs for SWIFT2D and the FLEET model result from the description of the finite element mesh. The FLEET model requires an incidence list which defines the nodes contained in each triangular element. The incidence list establishes the connections between elements which are required for the definition of the equation solution matrixes.

The FLEET model applies an explicit method to the solution of the finite element representations of mass and momentum conservation. All terms in the wave equation, except the time derivatives, are evaluated from the information at a each time step. The explicit nature of the solution scheme severely limits the time step that can be used in a simulation. The time step is subject to two upper limits:

1. The time step should never exceed five percent of the period of motion (tidal period).
2. The Courant-Friedrich-Lewy stability condition on the wave celerity which is evaluated based on the dimensionless Courant number C

$$C = \frac{\Delta t}{\Delta S} (gh)^{1/2} \dots\dots\dots(22)$$

where Δt is the time step, ΔS is the maximum distance between nodes in an element, and h is the depth, must not exceed a certain value.

The maximum allowable value of the Courant number depends on the geometry of the finite element mesh and the nature of the features represented. The upper limit on the time step for the conditions in the FLEET model is

$$\Delta \tau < \frac{0.6\Delta S}{\sqrt{gh}} \dots\dots\dots(23)$$

The time step must theoretically be less than the value of this parameter at any point on the grid.

The BLEND Model

The FLEET model was primarily a research tool and a first step toward more sophisticated finite element models for the simulation of two-dimensional hydrodynamics. The BLEND expanded on the original FLEET model with the addition of two important features. The BLEND model incorporated an implicit scheme for the solution of the wave equations of continuity and momentum, and included salinity modeling routines.

The strict limits on the time step in the FLEET model were overcome by the addition of implicit scheme capability in BLEND. BLEND included three new parameters to control the behavior of the implicit scheme. The first parameter determines which form of the implicit scheme to use in the model. A value of 0.0 for the parameter executes the basic explicit scheme. For values between 0.0 and 0.5 the Courant number stability constraint still governs the time step. The Crank-Nicolson scheme is used with a value of 0.5, and a value between 0.5 and 1.0 invokes the explicit scheme. The other two terms pertain to an experimental implicit scheme which uses the Taylor series expansion. The TWDB does not currently use the Taylor series option (Matsumoto 1993). The theoretical details of the implicit scheme are discussed by Gray and Kinnmark (1984). The second major improvement over FLEET was the inclusion of a salinity model. The subroutine which performs the salinity modeling has both a conservative and non-conservative option, and can easily be modified in order to simulate constituents other than salinity. The forms of the convective-diffusion equations incorporated in the model were

Conservative Form

$$\begin{aligned} & \frac{\partial(HC)}{\partial t} + \frac{\partial(HUC)}{\partial x} + \frac{\partial(HVC)}{\partial y} \\ & = \frac{\partial}{\partial x} \left(HD_{xx} \frac{\partial C}{\partial x} \right) + \frac{\partial}{\partial xy} \left(HD_{xy} \frac{\partial C}{\partial y} \right) + \frac{\partial}{\partial y} \left(HD_{yx} \frac{\partial C}{\partial x} \right) + \frac{\partial}{\partial y} \left(HD_{yy} \frac{\partial C}{\partial y} \right) \end{aligned} \quad \dots\dots\dots(24)$$

Non-Conservative Form

$$\begin{aligned} & \frac{\partial(C)}{\partial t} + \frac{\partial(UC)}{\partial x} + \frac{\partial(VC)}{\partial y} \\ & = \frac{\partial}{\partial x} \left(D_{xx} \frac{\partial C}{\partial x} \right) + \frac{\partial}{\partial xy} \left(D_{xy} \frac{\partial C}{\partial y} \right) + \frac{\partial}{\partial y} \left(D_{yx} \frac{\partial C}{\partial x} \right) + \frac{\partial}{\partial y} \left(D_{yy} \frac{\partial C}{\partial y} \right) \end{aligned} \quad \dots\dots\dots(25)$$

where C is the concentration, and D_{xx} , D_{xy} , D_{yx} , D_{yy} are the dispersion coefficients (Matsumoto 1993).

The presence of the salinity model required the addition of an input section for dispersion coefficients and initial concentrations. The salinity model in BLEND was an important addition, however, it was not joined to the governing equations through a density term in the momentum equation.

The TxBLEND Model

The TWDB adopted the BLEND and earlier FLEET as the basic model for use in the simulation of the bays and estuaries along the Texas Gulf Coast. The code was significantly modified by personnel at the TWDB to include several additional options important to the simulation of Texas bays and estuaries. Considerable density gradients exist in Texas estuaries. These density gradients can have a significant effect on the circulation patterns in the estuary. The BLEND salinity model was coupled with the governing equations of flow through the addition of a density term in the momentum equation. A second important features added to the model was a pair of terms to account for evaporation and direct precipitation. Evaporation is especially important in shallow estuaries, such as the Laguna Madre, where evaporation can significantly increase the salinity in the estuary. The evaporation and direct precipitation terms enter directly into the continuity equation in the form

$$\frac{\partial H}{\partial t} + \frac{\partial(HU)}{\partial x} + \frac{\partial(HV)}{\partial y} = r - e \dots\dots\dots(26)$$

where r the direct precipitation and e is evaporation. This is a simple modification of equation (17) in the FLEET model and equation (1) in the SWIFT2D model. The precipitation and evaporation terms are similarly added to the wave continuity as $\tau(r-e)$ which replaces the zero on the right-hand side of equation (18). The third feature was the addition of a source term in the convective-diffusion equation. The source term is directly related to evaporation in the case of salinity. The ability to include inflows or discharges from streams, return flows, and other sources also was added to the model. A final addition to the model was the "bigG" parameter, which helps the model maintain flow continuity.

A primary concern with the TxBLEND model has been a persistent question about the accuracy of the mass balance or flow continuity. The continuity problem was encountered in the work by Duke (1990) described in Chapter II and the further discussed in reports by Matsumoto (1991) and Solis (1991). The continuity question is an important one and has been extensively evaluated by the TWDB. The size of mesh cells has a significant impact on the ability of the model to maintain continuity. Cells that are too large can cause inaccuracies. The TxBLEND users guide (Matsumoto 1993) describes four test cases which check the maintenance of continuity in the model.

The bigG parameter was added to aid in the mass balance problems of the model. The parameter adds G times the primitive continuity equation to the wave continuity equation to produce a generalized wave continuity equation. G is a numerical parameter, not necessarily related to the

bottom friction. The larger the value for G , the more the continuity relationship is enforced, however, the numerical difficulty will correspondingly increase. The model has been observed to create flow when very small value for G are used (Matusumoto 1993). The values for G used in the TxBLEND model are generated by a semi-logarithmic equation. The value for G at the smallest and largest depths are input and the semi-logarithmic equation is used to estimate G for the depths in between. Kinmark (1984) explains the nature of the G parameter in the formulation of the generalized wave equations.

The TxBLEND model used for estuaries along the Texas coast incorporates the original FLEET model and the subsequent improvements described above. TxBLEND uses the wave continuity equation (16), which corresponds to option 1 for the continuity equation in the FLEET model and the primitive form of the momentum equations (20a and 20b), which corresponds to option 3 for the momentum equation in the FLEET model. Early continuity problems have largely been overcome with the introduction of the bigG parameter and careful definition of the finite element mesh.

IV PROCEDURE

The generation and manipulation of data sets, creation of bathymetry data, and calibration and verification of a hydrodynamic model require an extensive amount of time and computer resources. Calibration and verification data sets must be measured in the field. Ideally, two separate data sets would be collected to allow for extensive calibration and verification of the simulation model. The sheer size of the Laguna Madre Estuary makes such data collections extremely expensive and difficult. The TWDB performs only three days of intensive data collections on a single estuary or bay in a year. The best available data set for the Laguna Madre Estuary contained only three days worth of velocity data which was considered insufficient to serve as both a calibration and verification data set. The TWDB plans a new data collection effort on the Laguna Madre in 1997. The model could be verified with this new data set. A second option would be to obtain the old data set used in the early applications of the TxBLEND model by Duke (1990). The bathymetry data available at the time of this study consisted of digitized data from National Ocean Service (NOS) nautical charts and a set of bathymetry data from hydrographic survey completed for the U.S. Army Corps of Engineers in 1995. The TxBLEND model results included in this study were based on bathymetry data from the nautical charts, therefore, the nautical chart data also was used in the SWIFT2D model to insure comparable results.

DATA

The primary data set available for calibration of the model was a set of data from a TWDB intensive inflow study performed for the entire Laguna Madre Estuary in June, 1991. The TWDB performs a three day intensive survey of the inflows, currents, and watery quality for one estuary or bay system each year. Measurements are taken at approximately hourly intervals, 24 hours per day. The 1991 survey of the Laguna Madre covered the days of June 10 through June 13. The data set included measurements of velocities and water quality at 22 points throughout the estuary (10 in the upper Laguna Madre), and additional water quality data from 6 datasondes (3 in the upper portion). The water quality data are comprised of temperature, pH, dissolved oxygen, conductivity, and salinity. Rating surveys for the study were conducted in November, 1990 and April, May, 1991. The ratings serve to relate measured velocities to discharges at the inflow and outflow points. Table 2 contains a list of all data sites in the upper Laguna Madre which were used for this study. The locations of the data sites are shown in Fig. 6.

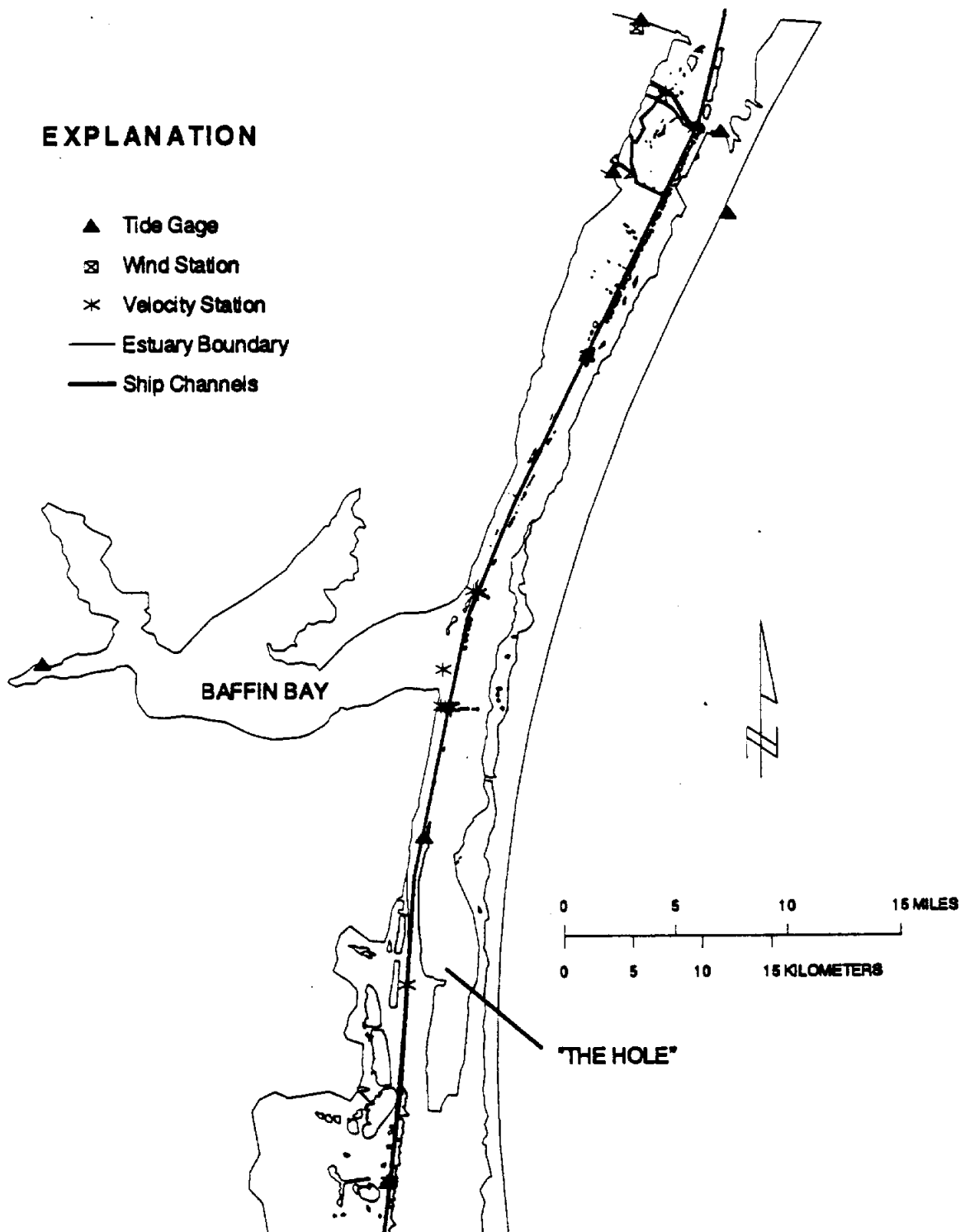


FIG. 6. Upper Laguna Madre Study Area Simulated with SWIFT2D and TxBLEND

TABLE 2. Data Observation Stations Used in the Study of the Upper Laguna Madre Estuary

Station Name	Type of Data	Latitude (Degrees)	Longitude (Degrees)
Corpus Christi NAS	water level / wind	27.7050	97.2800
Packery Channel	water level	27.6333	97.2217
Pita Island	water level	27.6050	97.3000
South Bird Island	water level / wind	27.4850	97.3183
Riviera Beach	water level	27.2767	97.7083
Yarborough Pass	water level	27.1667	97.4333
El Toro Island	water level / wind	26.9417	97.4567
Humble Channel	velocity / water quality	27.6575	97.2611
GIWW JFK Causeway	velocity / water quality	27.6344	97.2397
GIWW, Marker 199	velocity / water quality	27.3267	97.3958
North of Baffin Bay	velocity / water quality	27.3283	97.3989
Mouth of Baffin Bay	velocity / water quality	27.2761	97.4200
South of Baffin Bay (East)	velocity / water quality	27.2514	97.4139
South of Baffin Bay (Mid)	velocity / water quality	27.2517	97.4158
South of Baffin Bay (West)	velocity / water quality	27.2517	97.4183
South of Baffin Bay (FrWest)	velocity / water quality	27.2519	97.4214
North Landcut	velocity / water quality	27.0694	97.4444
JFK Causeway	data sonde	27.6344	97.2394
Riviera Beach	data sonde	27.2825	97.6394
Baffin Bay	data sonde	27.2778	97.4208

Tide data were available for 12 stations in the Texas Coastal Ocean Observation Network (TCOON). Seven of the tide stations were located inside or at the tidal boundaries of the upper Laguna Madre. The TCOON network is an extensive network of tide and wind gages located along the Texas coast. The network of water-level gages was established in cooperation with the Texas General Land Office, Texas Water Development Board, Lamar University-Beaumont, and the National Oceanic and Atmospheric Administration and is operated by the Conrad Blucher Institute for Surveying and Science (CBI) (Jeffress 1995). Tide and wind data for the month of June 1991 were obtained from personnel at the Conrad Blucher Institute network.

One of the initial problems in the application and evaluation of a hydrodynamic model is the accuracy of tidal datums. As of this study, The tide stations in the TCOON network were not tied

together to a consistent datum. Each gage has a set of benchmarks which are used to check the elevation of the tide gage, however, these benchmarks are not tied between gages. In order to allow comparisons between the water levels at the tide stations a consistent reference level was required. The mean water level was assumed constant between the various stations in the upper Laguna Madre and used as the reference level for calculations in the model. The mean water level at each station were calculated as the mean water level over the period of record.

Wind is a primary driving force in the Laguna Madre Estuary. Wind data were available from TCOON for the South Bird Island and El Toro sites. Additional wind data at the Corpus Christi Naval Air Station (NAS) were obtained from the National Weather Service (NWS). The South Bird Island wind sensor was installed in March 1991 and the El Toro Island sensor was installed in November 1990. The data obtained for the Corpus Christi NAS station covered the period from 1970 to 1995. Data from the two TCOON stations had significant gaps during the month of June 1991. The NAS data were more complete than the data from the TCOON stations and provided a better picture of the prevailing wind patterns in the Laguna Madre area. An analysis of the NAS data showed that the prevailing winds during the spring and summer period, which corresponds to the time of the SWIFT2D simulations, blow from the south and south-east. The results of the analysis of the NAS wind data are shown in Figs. 7 and 8.

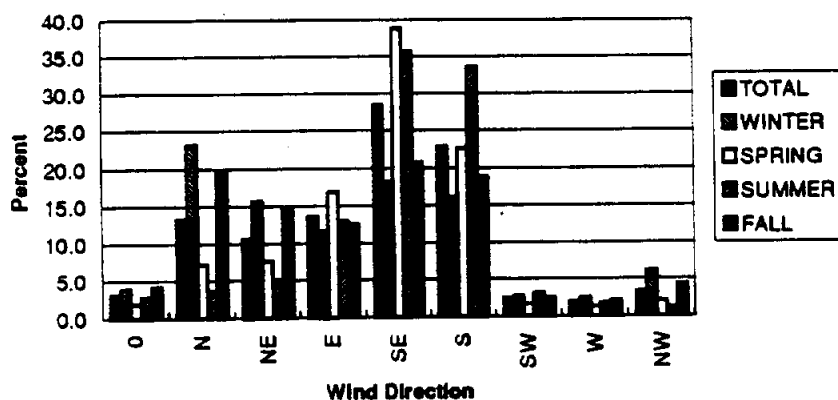


FIG. 7. Distribution of Wind Directions Observed at the Corpus Christi NAS Wind Station

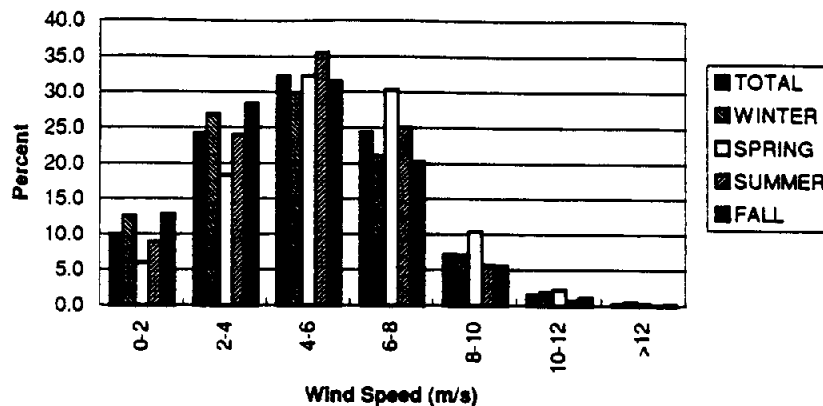


FIG. 8. Distribution of Wind Speeds Observed at the Corpus Christi NAS Wind Station

The wind speed is typically in the 2 to 8 meter per second range. The characteristics of the wind data during June 1991 were similar to the historical distributions. The wind was from the south and south-east 74 percent of the month, while wind speeds were between 6 and 10 meters per second for 70 percent of the month. The strong south and south easterly winds had a strong influence on the SWIFT2D simulation of the Laguna Madre.

BATHYMETRY GENERATION

One of the most important phases of any hydrodynamic modeling study is the development of an accurate representation of the bathymetry of the body of water under study. Regardless of the type of mesh scheme used in computations by the model, the depths at the mesh cells must be accurate. The square-grid representation is easier to generate than the more complicated networks of triangles or quadrilaterals used in finite element models, however the square grid is just as dependent on accurate depth information. The ARC/INFO Geographic Information System (GIS) was chosen to develop the model grid used for the SWIFT2D runs. The triangulated irregular network (TIN) and GRID data structures in the GIS were used for the surface modeling. A similar application of a GIS system to a SWIFT2D project is discussed by Bales and Douglas (1991).

The initial step in the application of the SWIFT2D model to the Laguna Madre Estuary was the development of a set of bathymetry data that would accurately reflect the characteristics of the system. An initial search for bathymetry data already in digital format was largely unsuccessful. The most readily available source of hydrographic survey data is a set of CD-ROM's which contain bathymetric sounding information for U.S. Coastal Waters collected by the National Ocean Survey

(NOS) and distributed by the National Geophysical Data Center (NGDC) which is part of the National Oceanic and Atmospheric Administration (NOAA). A set of data for the Laguna Madre area obtained from the NOS CD-ROM's contained information for Baffin Bay, Corpus Christi Bay, and the coastal waters on the Gulf side of Padre Island. There were no data points present for the main body of the Laguna Madre. In 1994, the Corps of Engineers contracted with John Chance and Associates Consulting Engineers to perform a hydrographic survey to update the data in the Laguna Madre Estuary. The survey was motivated by concerns about the impacts of dredging and sediment transport problems related to the GIWW. The survey was finished in the summer of 1995, however the data were not available for the present study until April, 1996. Due to time constraints on project funding and the desire to make the results compatible with the TWDB TxBLEND model, bathymetry data were digitized from a set of nautical charts.

NOAA nautical charts provided the most current source of bathymetry data available. The four nautical charts shown in Table 3 cover the entire Laguna Madre study area. Table 3 also includes the dates the nautical charts were published. The underlying hydrographic data are older than the maps themselves. Nautical Charts 11308 and 11306 which cover the upper Laguna Madre Estuary from Corpus Christi to the land cut are the pertinent charts for the simulations performed for the current study. The lower Laguna Madre was also simulated, but not included in this discussion. At the date of this report the TWDB has not simulated the lower Laguna Madre, therefore a comparison could not be made with the TxBLEND model for the lower half of the estuary.

TABLE 3. Nautical Charts Used in the Development of Bathymetry Data for the Laguna Madre Estuary

NOAA Chart Number	Date of Publication	Title of NOAA Nautical Chart
11314	April, 1994	Texas Intracoastal Waterway, Carlos Bay to Redfish Bay including Copano Bay
11308	October, 1994	Texas, Intracoastal Waterway, Redfish Bay to Middle Ground, including Baffin Bay
11306	August, 1992	Texas, Intracoastal Waterway, Laguna Madre, Middle Ground to Chubby Island
11303	March, 1994	Texas, Intracoastal Waterway, Laguna Madre, Chubby Island to Stover Point, including the Arroyo Colorado
11302	July, 1994	Texas, Intracoastal Waterway, Laguna Madre, Stover Point to Port Brownsville, including Brazos Santiago Pass

The depth information from these charts was digitized into GIS coverages. The digitized nautical charts provided a fairly extensive set of data, but did not provide as much detail as is typically found in the complete digital databases for other estuary systems along the Texas and U.S. coast. The depth data were especially sparse along the shallow eastern side of the estuary near Padre Island. In addition, the maps did not provide current depths for the GIWW and other channels located throughout the estuary. The GIWW is responsible for much of the circulation in the estuary, therefore a reasonably accurate representation is essential to the application of a hydrodynamic model to the estuary. Despite the shortcomings mentioned, the nautical charts provided the most complete data set available at the time of the study. The nautical charts were used as the basis for the earlier studies by Duke (1990), Matsumoto (1991), Militello (1994), and Brown (1995), and for the SWIFT2D and TxBLEND simulations in this study.

The bathymetry data from a hydrographic survey of the Laguna Madre completed in 1995 was obtained from personnel at the U.S. Army Corps of Engineers Waterways Experiment Station in April, 1996. The new data (approximately 30,000 data points) provides much more complete depth information for the Laguna Madre. The TxBLEND model does not yet incorporate the new bathymetry data, therefore, the model comparisons for this report are based on bathymetry data generated from the Nautical charts. The new data will be processed and incorporated in the GIS database and used for future simulations of the estuary.

The procedures for creation of the model grid are similar for both the nautical chart data set and the 1995 hydrographic survey data set. The GIS was used to create and store coverages (data layers) for depths, land boundaries, navigation channels, and measurement station locations. U.S. Geological Survey 1:100000 scale digital line graphs (DLG) were used to define the land boundary. The land boundary was spot checked at several locations to insure agreement with the boundaries shown on the nautical charts. The use of preexisting DLGs instead of hand digitized boundaries from the Nautical Charts saved substantial time in the creation of the GIS data set. The 1:100,000 scale DLGs are readily available on CD-ROM and over the Internet.

The coverages were used to create a Triangulated Irregular Network (TIN) representation of the bathymetry of the Laguna Madre. The TIN data structure provides a powerful tool for representation of a surface with a network of triangles for which the elevation is known or interpolated at each node. A TIN is a set of adjacent, non-overlapping triangles computed from irregularly spaced points with x, y coordinates and z values. The triangulation method for creation of TIN's in ARC/INFO satisfies the Delaunay criterion. Delaunay triangulation is a proximal method that satisfies the requirement that a circle drawn through the three nodes of a triangle will contain no other point. Delaunay triangulation insures that

1. triangles are as equi-angular as possible, which reduces potential numerical precision problems,
2. any point on the surface is as close as possible to a node,
3. the triangulation is independent of the order in which the points are processed.

Two interpolation schemes may be used to create the TIN data structure: linear interpolation and breakline, bivariate quintic. Both methods honor the z values present in the input data set. In linear interpolation, the surface value to be interpolated is calculated based solely on the z values for the nodes of the triangle which contains the point. Quintic interpolation employs an algorithm which uses a bivariate fifth-degree polynomial in x and y . Quintic interpolation creates a smoother surface than linear interpolation (Environmental System Research Institute, Inc. 1991b).

GRID is a raster- or cell-based geoprocessing toolbox that is ideal for projects which require the representation of continuous surfaces as regularly spaced, discrete units. GRID is based on a hierarchical tile-block structure. The grid is first divided into uniform square units called tiles. Each tile is subdivided into blocks which in turn are comprised of individual square cells. This hierarchical structure allows GRID to quickly access data from anywhere in the grid, regardless of the size of the area (Environmental System Research Institute, Inc. 1991a). The square cell representation provides direct compatibility with the regular, square grid used in SWIFT2D.

In the case of the nautical chart data set, the coverages needed to create the TIN were the digitized depths, the land boundary outline, and a set of points in shallow areas input by hand. The TIN was then converted to a lattice, which is equivalent to the raster data structure used in GRID. The input point distance tolerances in TIN creation algorithms were too large to allow an accurate representation of the channels in the TIN, therefore, separate grids were created for the island and channel coverages. The resulting set of three grids was merged to create the final grid which incorporated all of the available input data. The lattice and grid data structures allowed for easy manipulation of the cell size and area of the resultant merged grid. The generated grids were exported to ASCII text files and then checked and edited with separate software packages. The GRIDEDIT software package which comes bundled with SWIFT2D and the Surfer for Windows software package were used to perform the final edits of the grids. The current version of the ARC/INFO Grid routines does not allow for manipulation of single grid cells.

GRID CELL SIZE SELECTION

The primary difficulty in the application of SWIFT2D to the Laguna Madre Estuary was the restriction of the model grid to uniform, square grid cells. The areal extent of the estuary makes the

use of a large grid size desirable, however, much of the flow in the estuary is conducted by the GIWW which has an average width of 100 to 150 feet. In order to provide adequate resolution for the channels a fairly small grid size was required. The use of small grid cells to represent the channels limits the entire grid to a small cell size. As a result, computation times are greatly increased. The 200 meter grid size used in this study was a compromise between the need to adequately represent the channels in the Laguna Madre without increasing computational times to intolerable levels. The depths of cells representing channels were adjusted to maintain the proper flow conveyance and cross sectional area of the channels. A cell size of 200 meters still substantially distorts the cross sections of the channel, however, it was sufficiently small to allow the channels to remain distinguishable from the natural portions of the estuary.

Initial runs of the model were performed with a 400 meter grid cells. These runs showed that a cell size of 400 meters does not allow for accurate representation of important features in the estuary. The 400 meter cells exaggerated the effect of island on circulation patterns in the estuary. Many of the spoil islands present in the Laguna Madre are much narrower than 400 meters. These spoil islands accounted for an unacceptable fraction of estuary cross sections when included in the model grid. The spoil islands are a major issue of concern in the estuary and, therefore, should be modeled as accurately as possible in the model. The second major concern with the 400 meter cell size was the representation of the GIWW and other navigation channels. In order to maintain reasonable approximations of channel cross sectional areas, the cell depths had to be reduced to an extent that they were no longer distinguishable from adjacent grid cells. This problem is, unfortunately, still evident with the 200 meter grid in the area south of Baffin Bay. Figs. 9 and 10 show shaded representations of the 400 and 200 meter grids respectively. Darker areas represent deeper grid cells. The GIWW can be easily seen as a dark line running the length of the estuary from north to south. Spoil islands show up as light colored areas primarily adjacent to the GIWW. These light colored cells which represent islands and the shoreline and the dark cells which represent the GIWW are significantly larger on the 400 meter grid.



FIG. 9. Upper Laguna Madre 400 Meter Grid (148x213 cells)



FIG 10. Upper Laguna Madre 200 Meter Grid (296x426 cells)

A second problem caused by the resolution of the grid was the stair-stepping effect seen in the cells representing the channel. This effect is illustrated in Fig. 11.

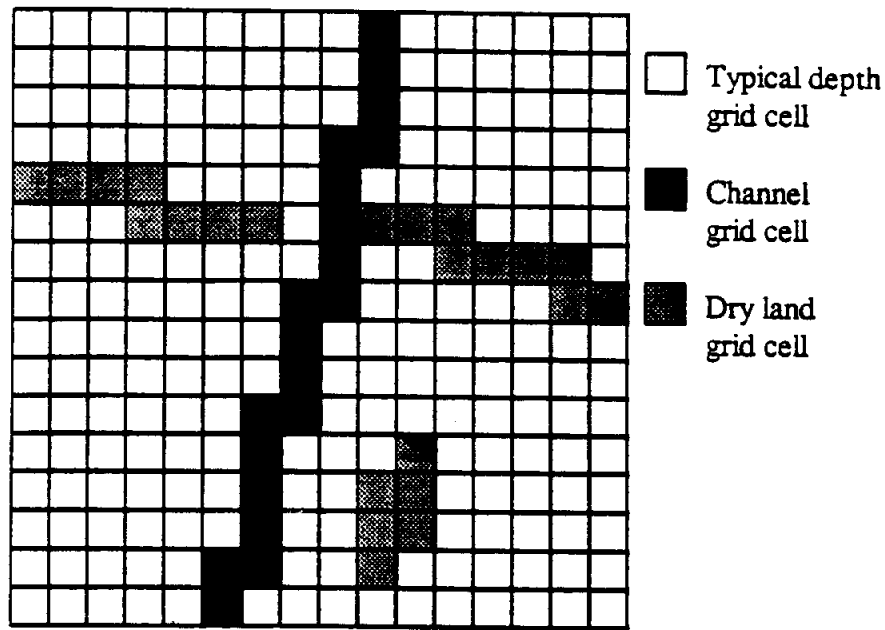


FIG. 11. Typical SWIFT2D Grid Section Which Shows the Stair-step Effect in the Representation of Channels with a Regular, Square Grid

The stair-stepping effect distorts the flow pattern to some degree, however this effect is probably much less serious than the effect of the distortions of channel cross sections. SWIFT2D simulations with the square grid produced reasonable flows at all of the flow cross sections (matching those used in the TxBLEND model) evaluated in the study.

The reduction in grid cell size from 400 meters to 200 meters dramatically increased the number of computations required for the simulation. The computational grid for the original 400 meter cell size would have contained approximately 3,700 active computational cells while the 200 meter computational grid contained approximately 15,000 active computational cells. The increase in complexity and the resulting increase in run times, although significant, were deemed necessary to properly represent the actual conditions in the estuary. The dramatic increase in the number of cells required to simulate small features with reasonable accuracy illustrates the major disadvantage of a model grid with a constant cell size.

SIMULATION

The upper portion of the Laguna Madre Estuary from Corpus Christi to the land cut south of Baffin Bay was chosen for simulations and comparison with the TxBLEND model. The original goal of the modeling study had been to simulate the entire estuary from Corpus Christi to Brownsville. Ideally the model would also include the Corpus Christi Bay system so that the driving tides in the Gulf of Mexico would completely define the input for the model. Simulation of only a section of the estuary required driving tides internal to the system. A complete model of the entire system would require less input data than the partial models and would therefore be more desirable for long range planning efforts. The choice to split the estuary into separate sections for the modeling effort was necessitated by the need for manageable simulation times and data sets. A model grid or mesh comprised of the entire system would also aid in the data needs for simulation of salinity. Salinity for the entire system would also be defined completely by the ambient salinity in the Gulf of Mexico which would be essentially constant compared to the salinity at points internal to the system. Salinity simulations of separate portions of the system would require long-term measurement of salinity at internal points in the estuary.

Simulation efforts for this study centered on the accurate reproduction of flows and water levels in the estuary. The northern half of the estuary selected required two sets of driving tide conditions. The Corpus Christi NAS tide gage at the north end of the model grid and the El Toro tide gage at the southern end provided the data required for the model. A section across the southern end of Corpus Christi Bay adjacent to the Naval Air station formed the northern boundary of the model grid. The Corpus Christi NAS tide data were input as a constant elevation across this section. SWIFT2D requires a water surface elevation at either end of the tidal boundary section. The option for the same elevation at both ends of the cross section was selected for both the NAS boundary and the Land Cut boundary. This assumption should be fairly accurate for the narrow GIWW channel which forms the tidal input at the lower section, however the assumption is not as good for the much wider section across from the Naval Air Station.

The Laguna Madre Estuary receives the smallest amount of fresh water inflows of any estuary in Texas. There are no significant perennial streams and no gaged streams which flow into the upper Laguna Madre. Since the present simulation was performed during the dry summer months, no fresh water inflows were included in the model. A more detailed model would require estimates of fresh water inflows to the system and would also account for power plant withdrawals near Pita Island (need more details - see TWDB reports) at the upper end of the northern estuary.

The data from the Corpus Christi NAS site was the only wind data used for the SWIFT2D simulation runs. The model supports the use of more than one wind station through the use of a wind input grid, however, the single wind input was judged to be sufficient for several reasons. The wind data sets for the South Bird Island and El Toro sites contained missing data and were not considered as reliable as the NAS data for the June, 1991, calibration period. In addition, the hydrodynamic study performed by Brown (1995) determined that the winds at the NAS and at South Bird Island were similar, and only used the NAS data.

CALIBRATION

The calibration of the SWIFT2D model of the Laguna Madre proceeded in two phases. The first phase of the calibration required significant hand editing of the model grid in order to adjust channel cross-sectional areas to match those in used in the TxBLEND model, and to insure that flow was maintained through all narrow passes between land boundaries and islands. The second phase of calibration involved the adjustment of model parameters to provide the best possible fit to measured data. The model was considered calibrated when changes in parameter values no longer provided substantial improvements in the root mean squared errors between simulated and observed values. Visual inspection of plots of simulated and observed values also aided in the calibration of the model. The SWIFT2D model proved to be very robust to changes in most of the model parameters. Adjustment of the model grid and wind stress coefficient produced the largest effect on the model calibration.

Grid Adjustments

The first phase of the calibration required adjustments to some of the depth points in the computational grid. The grid cell resolution improvement of the 200 meter grids over the 400 meter grid was not sufficient to completely eliminate the need for additional processing of the grid output by ARC/INFO. The GRIDEDIT program was used to perform the final edits of the grid. Corrections also were made to bring the grid into closer agreement with the finite element mesh for TxBLEND.

The areas in the most need of editing were narrow passes, areas near islands, and areas along the boundary of the estuary. Early model runs failed to reproduce measured velocities at the Humble Channel and GIWW at JFK causeway. Conditions at these two points control a majority of the flow into and out of the upper Laguna Madre and are, therefore, vital to the simulation of the estuary. The cells which represented navigation channels and adjacent areas in the vicinity of the JFK Causeway were modified to more closely match actual measured cross sections at the two points. Data from the

TxBLEND finite element mesh also were used to guide the adjustment of the bathymetry grid. Model runs with the modified grid produced more reasonable flows and velocities at the Humble Channel and GIWW at JFK Causeway control points.

Parameter Adjustments

SWIFT2D contains several parameters which can be adjusted to calibrate the model to measured data. Important calibration parameters for simulation of circulation and water levels include:

1. wind stress coefficient,
2. Manning's n (constant or spatially varied),
3. vorticity-related viscosity factor (k in the ninth term in momentum equations (2) and (3)),
4. shallow depth parameters for wetting and drying of cells.

Other parameters such as the time step, advection option, and integration method also have an influence on the results of the simulation. The initial values for the Laguna Madre model parameters were modified from example input files for the SWIFT2D application on the upper Potomac Estuary discussed by Schaffraneck (1986).

The wind stress and Manning's n were found to have the greatest effect on the calibration. Early model runs were performed with a constant n throughout the computational grid. The GIWW was expected to provide the majority of the circulation in the estuary, however, the flows and velocity vectors from these early runs did not show a dramatic effect due to the GIWW. In order to more accurately represent the difference in bottom stress between shall areas with dense growths of sea grass and deeper bays or channels, The n value distribution was changed from a constant value to a set of spatially varying values. The spatial variation of the n value was based on the distribution of roughness coefficients used in the TxBLEND model. The GIWW was assigned an n value of 0.025 while secondary channels were assigned an n value of 0.031. Other cells near the channel or in the deeper portions of the grid were assigned values of 0.035. The remainder of the grid was assigned a value of 0.040. The areas assigned a value of 0.040 were primarily shallow tidal flats, which generally support extensive growths of sea grass. SWIFT2D assigns a separate, high roughness coefficient to cells that drop below a specified depth. The intention is to use a small Chezy value for these shallow depths so that when the water becomes shallow the friction increases considerably, and thus the currents decrease.

Variation of the wind stress coefficient produced the most dramatic effect on the simulated results.

Wind stress values ranging from 0.0001 to 0.0026 were tested in an attempt to match the simulated and observed water levels at the internal tide stations. The water levels at the Packery Channel, Pita Island, and South Bird Island tide stations are driven primarily by the tide in Corpus Christi Bay which in turn is driven by the tide in the Gulf of Mexico. The tides are progressively more damped as the tide signal passes south through the narrow passes in the JFK Causeway and the GIWW. The tide signal is almost completely damped when it reaches the South Bird Island gage. The Riviera Beach and Yarrowborough Pass tide gages receive essentially no diurnal tide signal. As a result, wind is the primary driving force in the portion of the estuary south of Bird Island.

The remaining calibration parameters had only limited effects on the SWIFT2D simulation results. These parameters are discussed further in the section which describes the model sensitivity analysis.

VERIFICATION

The small data set available for the Laguna Madre limited the possibilities for verification of the model. The three days of velocity data present in the data set were not considered adequate for separation into separate calibration and verification data sets. Calibration runs of the model considered the dates from June 1, to June 14, 1991. After calibration, the simulations were extended to include the remainder of the month of June. The agreement between modeled and observed water levels for the second half of June was equivalent to the results of the first half of the month. Due to the limited data available, the verification process was considered complete with the runs for the month of June.

Several options could be explored for verification of the model in future studies. Acoustic velocity meters were installed at the Humble Channel and GIWW openings in the JFK Causeway in 1994. The meters were installed as part of the ECOON network of data collection platforms (Brown, 1995). The acoustic velocity meter data were not publicly available at the time of this study. The second option would involve verification of the model with a second set of intensive inflow survey data. The TWDB currently plans to perform an intensive inflow survey for the Laguna Madre in 1997. A third option would require a long-term simulation over several months to a year. Such a simulation would provide adequate data for a check of the mass balance of inflows and outflows in the Laguna Madre.

V RESULTS OF SWIFT2D SIMULATIONS

RESULTS

The calibrated SWIFT2D model of the upper Laguna Madre produced results in good agreement with observed values. The quality of results was evaluated based on the calculated root mean squared errors (RMSE) between simulated and observed values and by visual inspection of plots of the simulated and observed time series. The RMSE was calculated as the average of the squared difference between each simulated and observed data point. Visual inspection of the time series provided a means to check for consistently low or high simulated values and for similarities in the phase and amplitude of the simulated and observed time series. The calibrated model provided a small RMSE and reproduced the phase and amplitude of the measured time series as faithfully as possible. Additional parameter adjustments may have provided a slightly better fit to observed data, however, the length of time required for SWIFT2D simulations limited the number of runs that could be afforded. Run times for a fifteen day simulation with the calibrated model averaged around 2.3 hours.

Simulated and observed time series were compared at locations throughout the upper Laguna Madre Estuary. The simulated water levels at the five internal tide stations and velocities at eight locations throughout the estuary were compared to the observed values at these locations. Fig. 12 shows the seven tide stations (five internal and two driving tides), while Fig. 13 shows the velocity stations. Simulated flows were output at eleven cross sections, the locations of which are shown in Fig. 14. Model parameters were adjusted as discussed in the section on calibration until the simulated time series matched the observed time series as closely as possible. The calibrated model employed a spatially varied Manning's n which ranged from 0.025 for channels to 0.040 for shallow tidal flats; a wind stress coefficient of 0.0015; minimal viscosity, and a 360 second (6 minute) time step. The results for water levels and velocities are discussed in the following sections. Comparisons of results from simulations with varied parameters are discussed in the section that describes the sensitivity analysis.

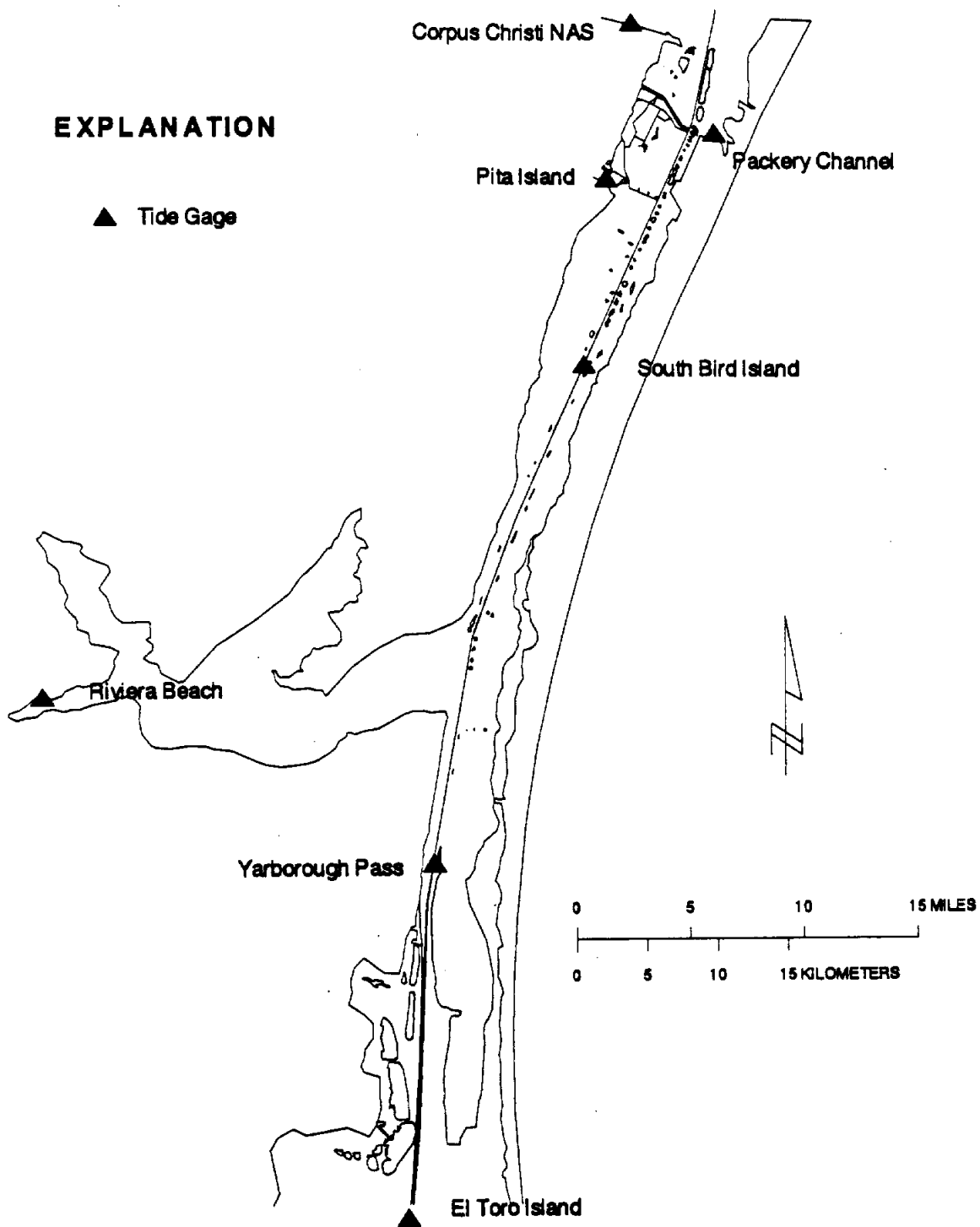


FIG. 12. Locations of Tide Stations at Which Simulated and Observed Water Levels Were Compared

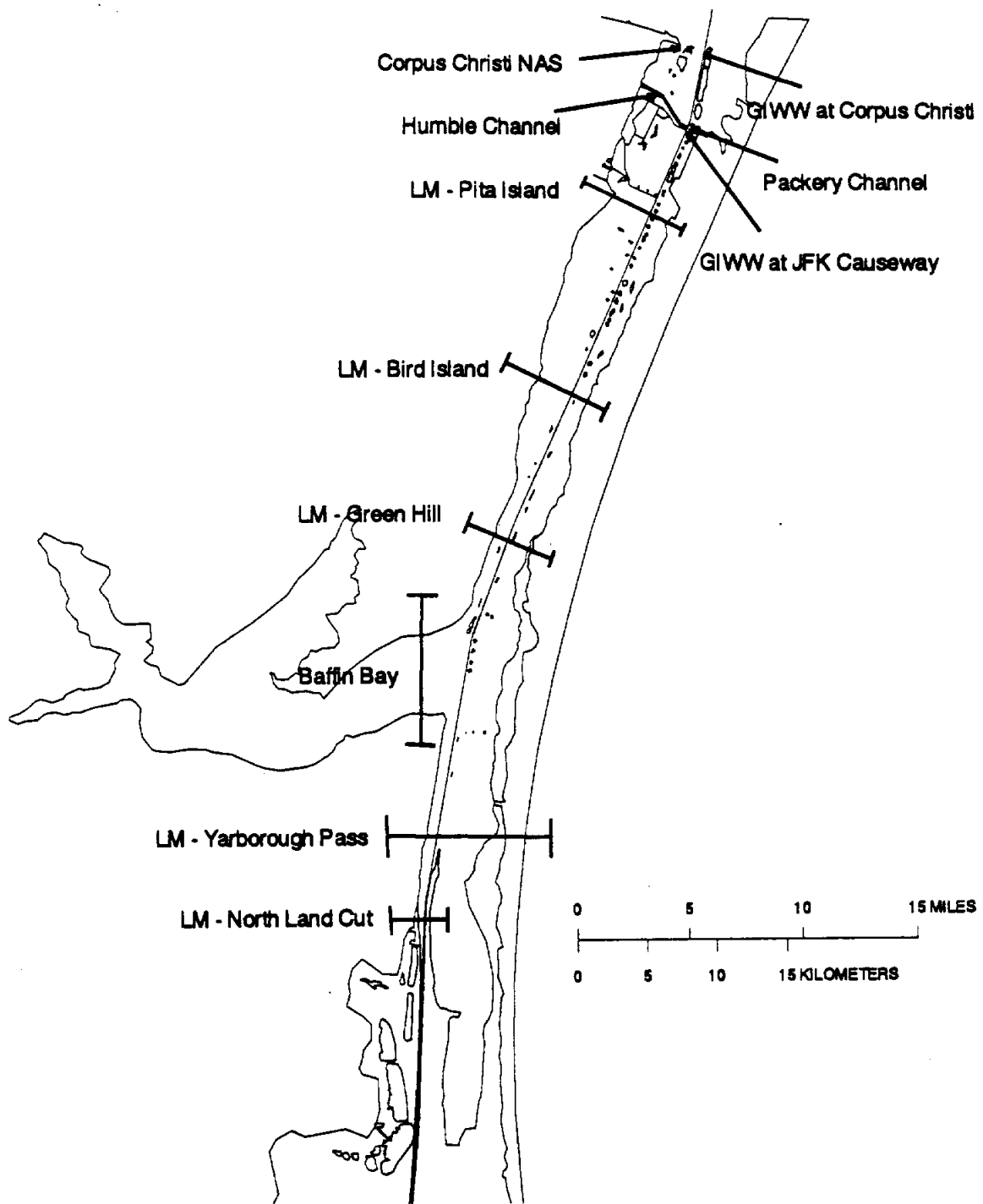


FIG. 14. Locations of Cross Sections at Which Simulated Flows Were Compared

Water Levels

The simulations showed a dramatic contrast between the factors which drive the variations in water levels at northern stations closest to the JFK Causeway and the tide stations toward the south and in Baffin Bay. The simulated water levels at the northern tide station (Packery Channel, Pita Island, and South Bird Island) appear to be primarily influenced by the driving tidal signal at the Corpus Christi Naval Air Station. This influence can be seen to dissipate as the signal passes south through the estuary. The tidal cycle is significantly damped by the time it reaches the South Bird Island tide station. The water levels at the Yarborough Pass and Riviera Beach tide stations, which are the most distant from the JFK Causeway, seem to be primarily influenced by wind. The tide stations near the Causeway are affected to a much smaller degree by the wind.

The water level variations at the Yarborough pass and Riviera Beach tide stations exhibit significantly more noise than the northern tide stations. The time series of water levels at the stations near the JFK Causeway exhibit the smooth, daily oscillations expected at points influenced by a strong diurnal tidal cycle. The water level fluctuations at the Yarborough Pass station and especially at the Riviera Beach station seem to be strongly influenced by wind. The Riviera Beach station is located in the western most arm of Baffin Bay. As a result the station is as far removed from the influence of Gulf of Mexico tides as possible in the Laguna Madre system. The strong summer winds which blow primarily from the south and southeast appear to cause substantial flow into Baffin Bay and a corresponding wind driven set-up of water levels on the northwestern portions of the Bay. The strong convective winds caused by the summer heat probably provide the primary driving force for the daily oscillation of water levels at stations where the amplitude of the tidal signal is damped.

The simulated and observed water levels at the seven tide stations are shown in Figs. 15 through 21. The water levels at the Corpus Christi NAS and El Toro tide stations are the driving tides. The simulated water levels for these two tide stations are immediately adjacent to the tidal boundaries and, therefore, are almost identical to the observed tides. The tidal damping is faithfully reproduced by the SWIFT2D simulations. The larger amplitude in the simulated tidal cycle at Packery Channel is probably due to the definition of the model grid. The water levels shown in Figs. 15 through 21 are referenced to mean water level at each station.

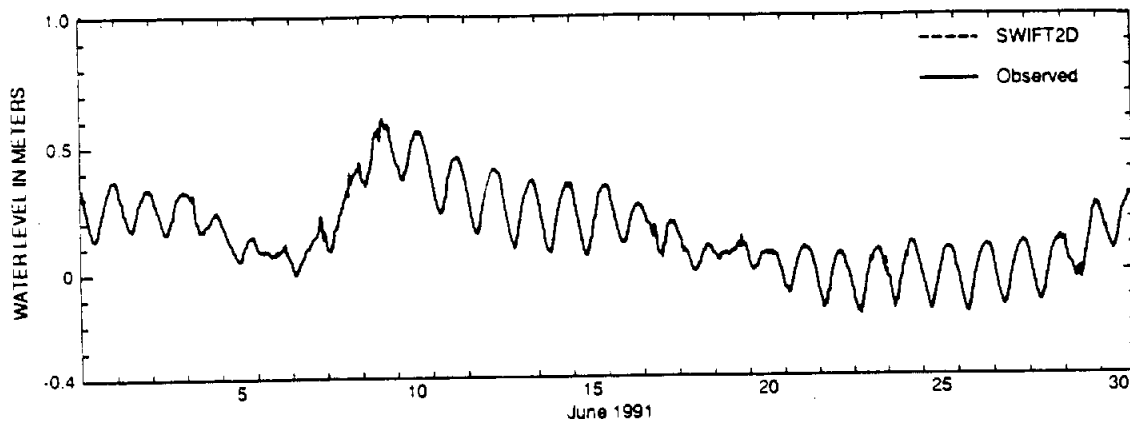


FIG. 15. Callbrated Water Levels at the Corpus Christi Naval Air Station Tide Station

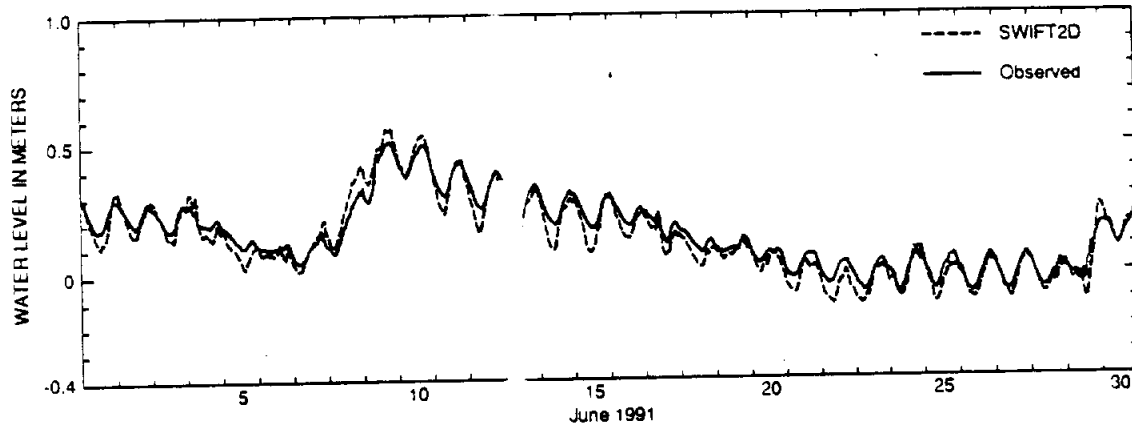


FIG. 16. Callbrated Water Levels at the Hackery Channel Tide Station

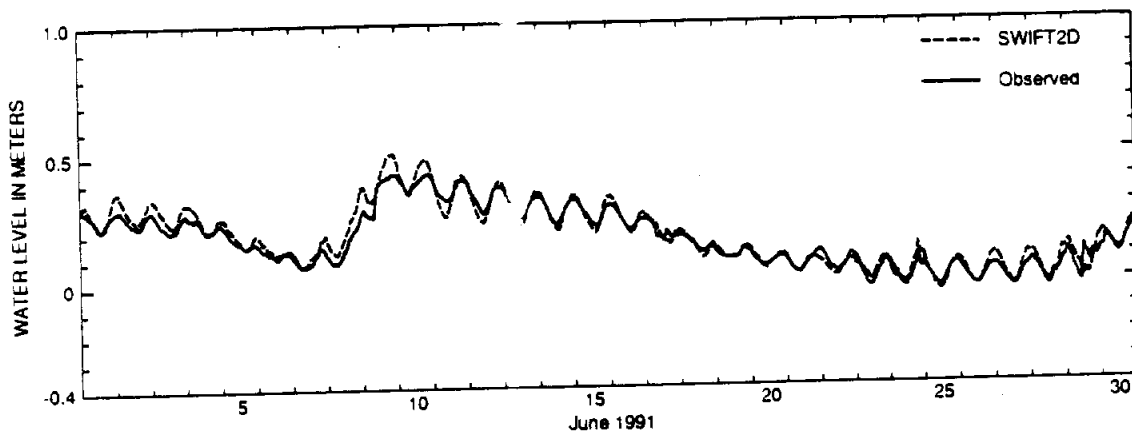


FIG. 17. Callbrated Water Levels at the Pita Island Tide Station

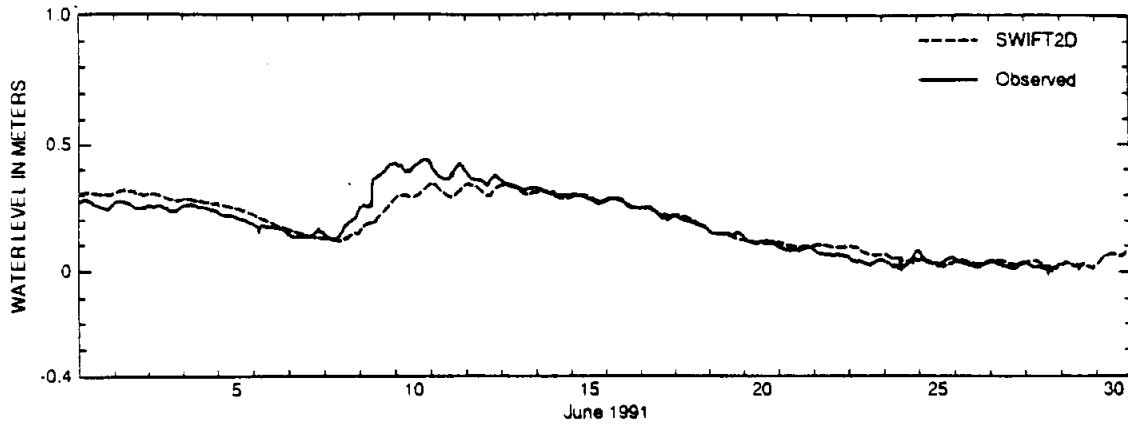


FIG. 18. Calibrated Water Levels at the South Bird Island Tide Station

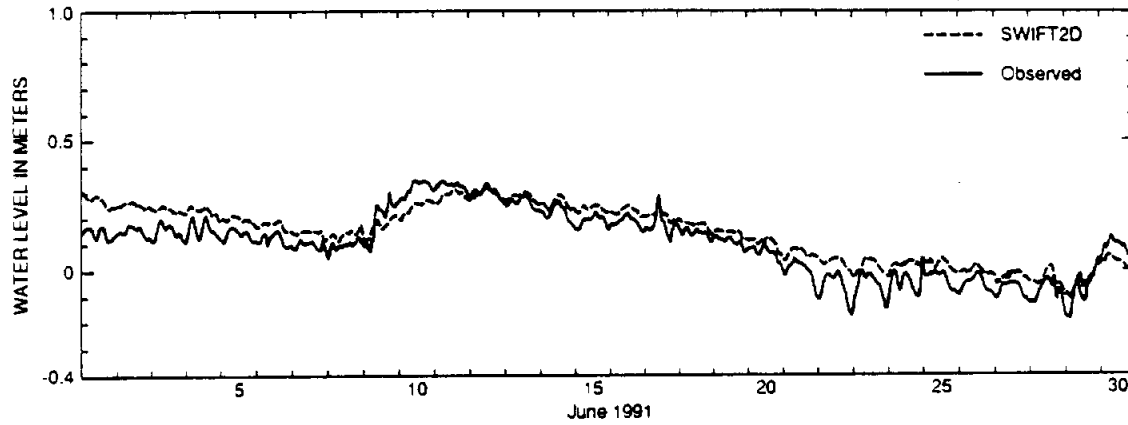


FIG. 19. Calibrated Water Levels at the Yarborough Pass Tide Station

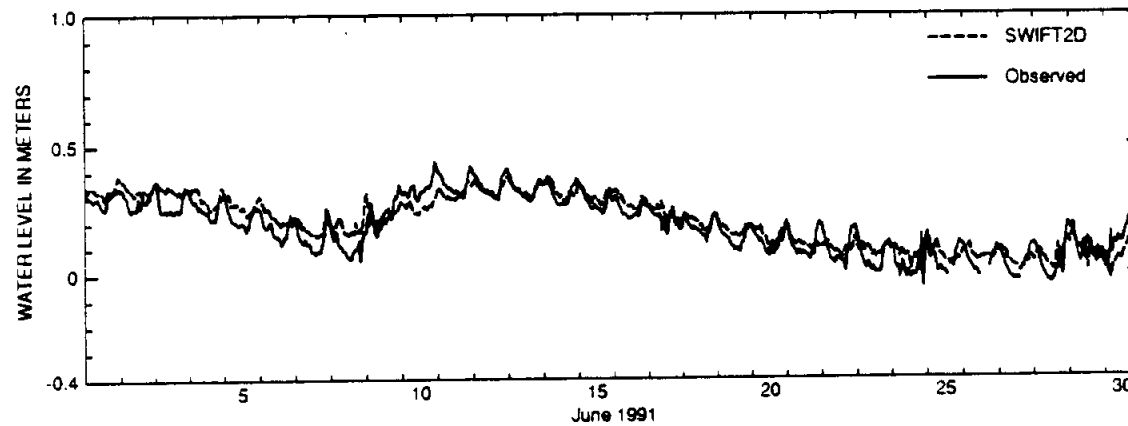


FIG. 20. Calibrated Water Levels at the Riviera Beach Tide Station

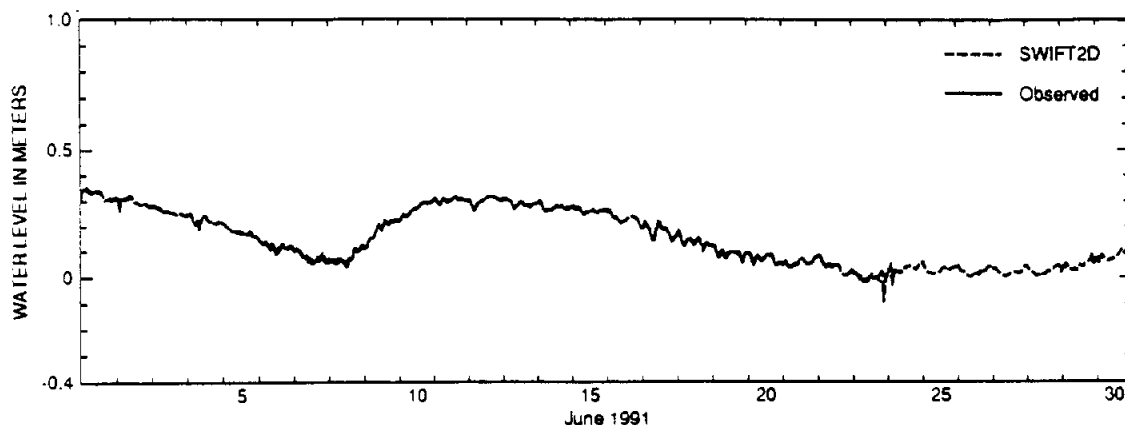


FIG. 21. Calibrated Water Levels at the El Toro Island Tide Station

The RMSE's between simulated and observed water levels are shown in Table 4. The Corpus Christi NAS and El Toro Island tide stations provided the driving tides in the simulations, therefore, the errors between simulated and observed tides at these locations should be very small.

TABLE 4. Root Mean Squared Errors between Simulated and Observed Water Levels

Water Level Station	RMSE (meters)
Corpus Christi NAS	0.001
Packery Channel	0.043
Pita Island	0.036
South Bird Island	0.059
Yarborough Pass	0.067
Riviera Beach	0.124
El Toro Island	0.006
Average	0.048

The largest error was observed at the Riviera Beach tide station. This station is the most distant from the influence of the tidal signal at the northern end of the estuary. The amplitude of the simulated water levels is not as large as that of the observed water levels. The RMSE generally increases with distance from the JFK Causeway. This would seem to indicate that the model handles the effects of tidal signals better than the effects of wind. Additional variation of the wind stress coefficient and the use of spatially distributed wind input (multiple wind sites) might improve the results.

Velocity

The simulated velocities also matched the observed time series reasonably well, although the results were not as good as those for water levels. Table 5 shows the RMSE's between the simulated and observed velocities.

TABLE 5. Root Mean Squared Errors between Simulated and Observed Velocities

Velocity Station	RMSE (meters per second)
Humble Channel	0.13
GIWW at the JFK Causeway	0.16
GIWW at Marker 199	0.19
North of Baffin Bay	0.10
Mouth of Baffin Bay	0.08
South of Baffin Bay-Middle	0.11
South of Baffin Bay-West	0.08
North Land Cut	0.12
Average	0.12

The largest errors occurred at the Humble Channel, GIWW at the JFK Causeway, and GIWW at Marker 199 stations. These stations are located in the major channels in the estuary. The large errors are probably a result of the representation of the channel geometry in the model. The channels are represented by a single, 200 meter wide grid cell within the model, however, the actual channel widths range from approximately 40 meters for the majority of the GIWW to approximately 120 meters near the JFK Causeway. The RMSE of 0.19 meters per second is approximately half of the amplitude of the velocity at the GIWW at Marker 199 Station.

Comparisons of observed and simulated velocity time series at the eight measurement points indicated in Fig. 14 are shown in Figs. 22 through 29. Positive velocities in the plots indicate flow toward the north. Localized velocities are much more dependent on the realistic representation of the actual geometry of the water body. The primary factor which influenced the quality of the simulated velocities was the approximation required for the generation of the model grid. The openings at the Humble Channel and the GIWW at the JFK Causeway provide the conduits for a majority of the circulation in the estuary. The simulated velocities in these two channels agree fairly well with the observed velocities, especially in regard to the period of the velocity variations.

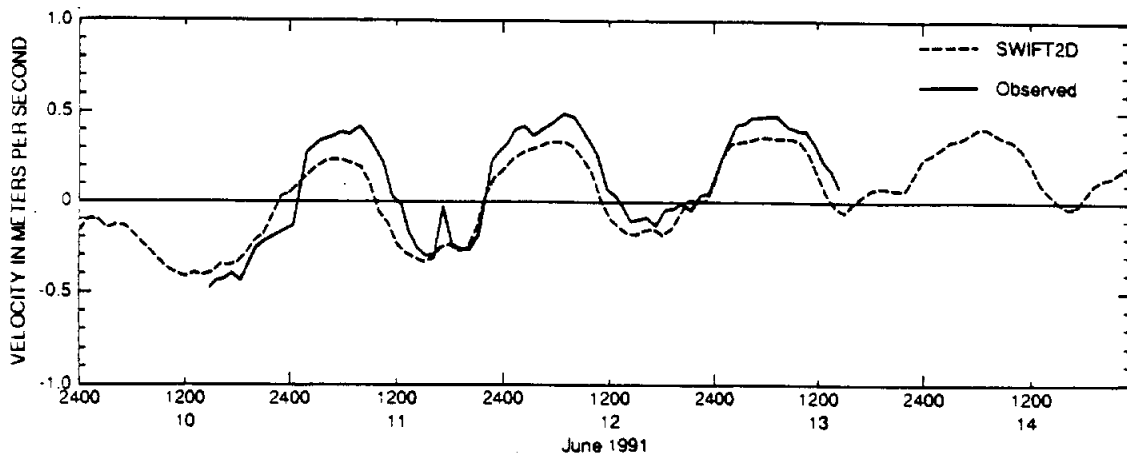


FIG. 22. Calibrated Velocity at the Humble Channel Station

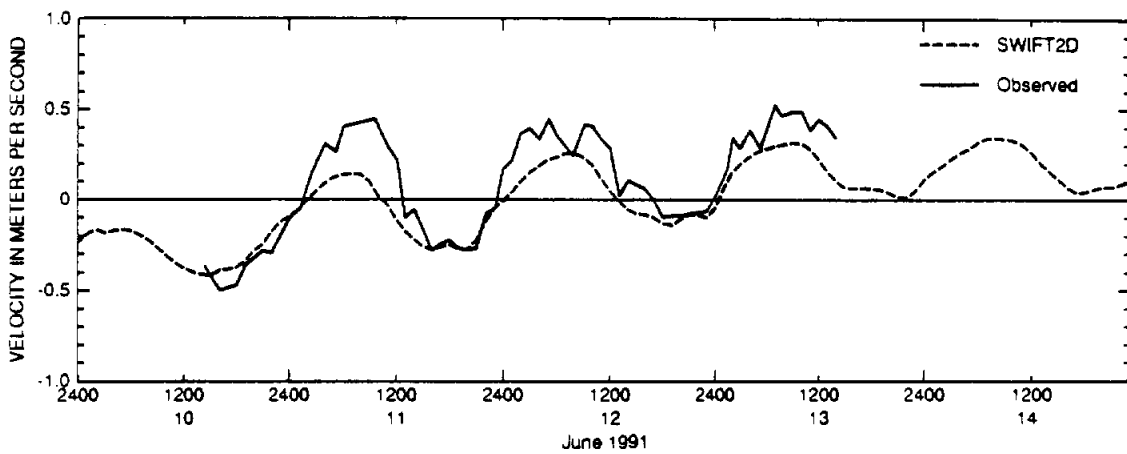


FIG. 23. Calibrated Velocity at the GIWW at JFK Causeway Station

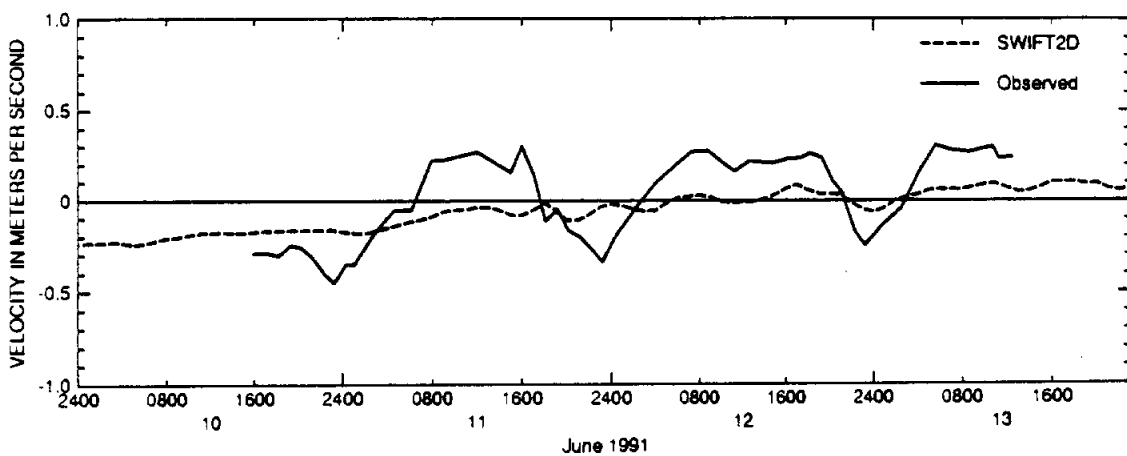


FIG. 24. Calibrated Velocity at the GIWW Marker 199 Station

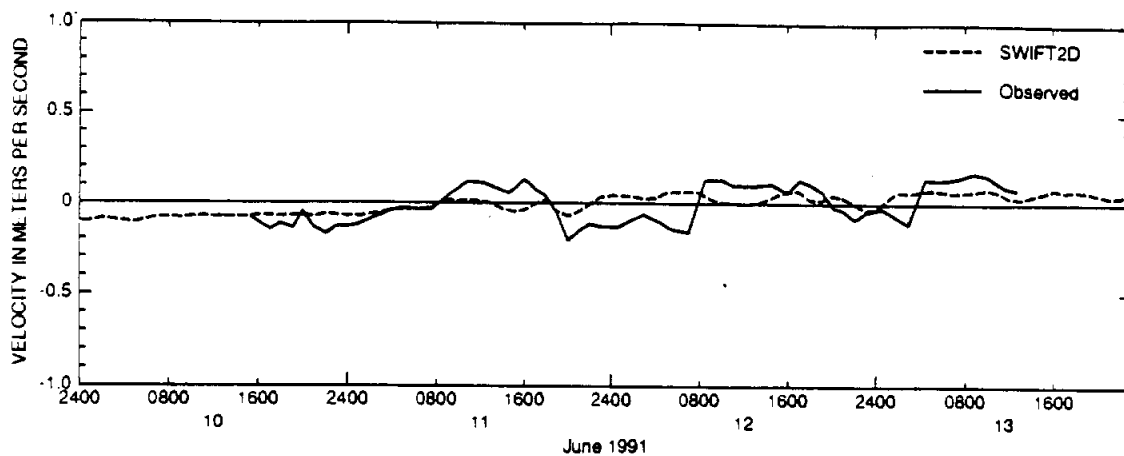


FIG. 25. Calibrated Velocity at the North of Baffin Bay Station

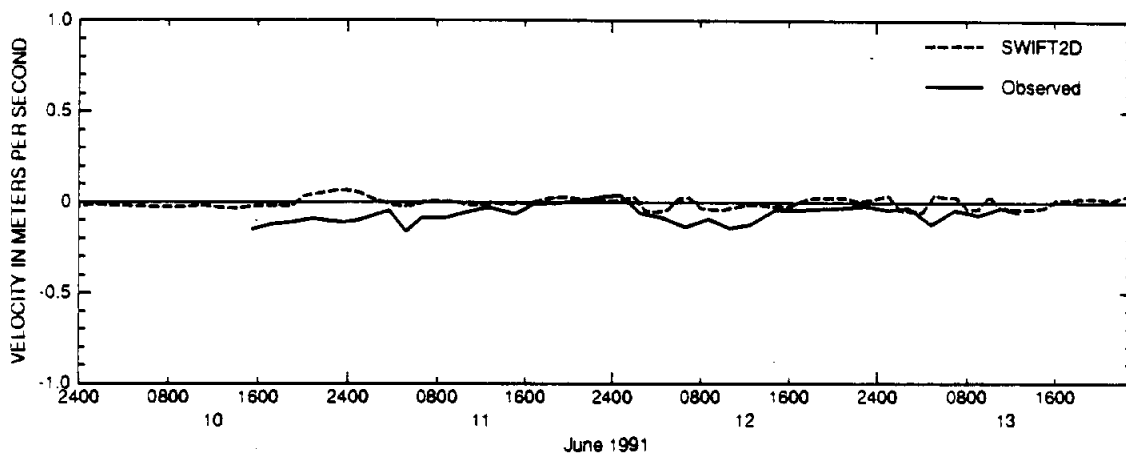


FIG. 26. Calibrated Velocity at the Mouth of Baffin Bay Station

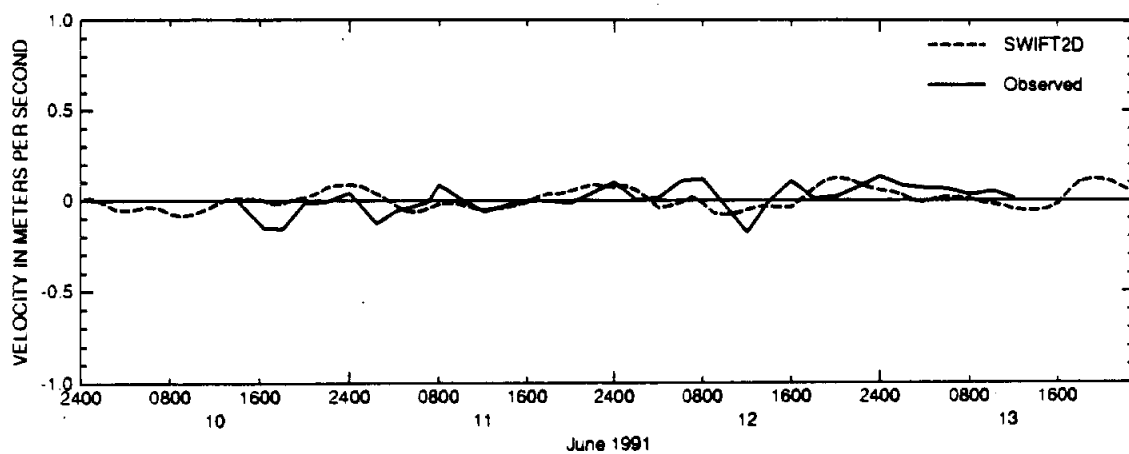


FIG. 27. Calibrated Velocity at the South of Baffin Bay-Middle Station

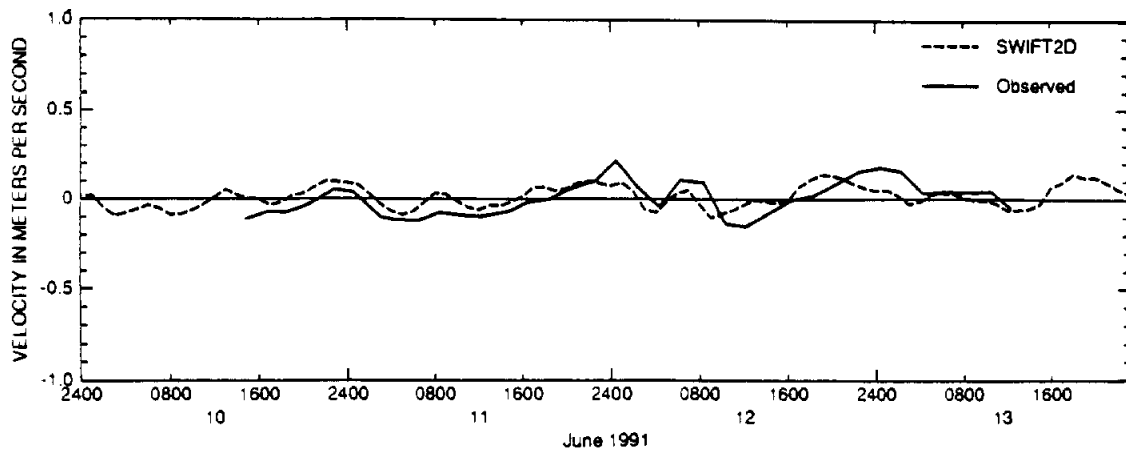


FIG. 28. Calibrated Velocity at the South of Baffin Bay-West Station

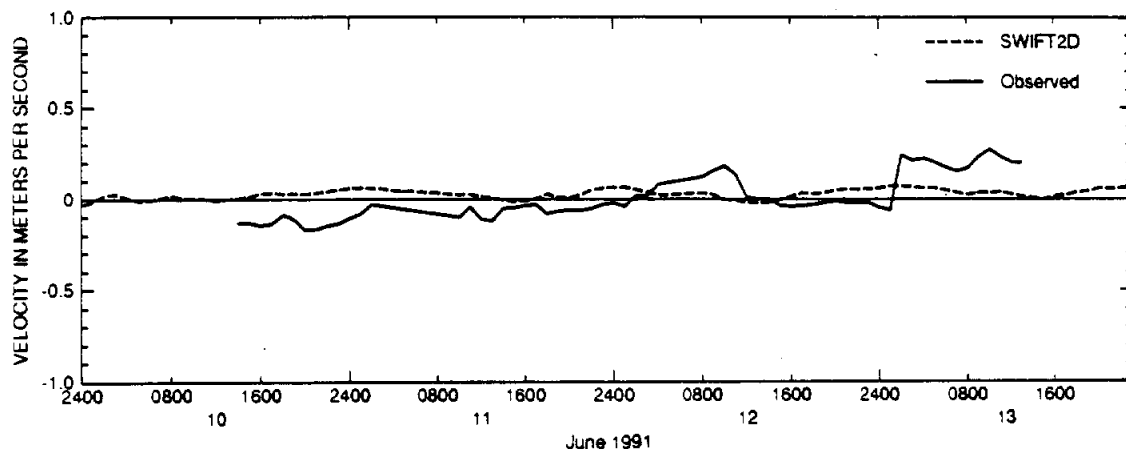


FIG. 29. Calibrated Velocity at the North Land Cut Station

The simulated velocities are generally smaller than expected, primarily due to the finite difference grid representation of the channels. The actual widths of the channels are approximately 95 and 125 meters for the GIWW at JFK Causeway and the Humble Channel, respectively. These widths are smaller than the width of a single grid cell, however, the SWIFT2D requires passes between no flow barriers to be at least two cells wide. The corresponding reduction in the amount of restriction on the flow tended to decrease the simulated velocities. The depth of the grid cells was reduced to compensate for the increased width of the passes. The resulting wider and shallower channels tended to reduce the simulated velocities. A similar problem probably caused the disparity between simulated and observed velocities at the GIWW at Marker 199 station. The SWIFT2D representation of the

GIWW is both wider and more shallow than the actual channel. The result is a substantial reduction in velocity. The observed velocities at the southern end of the estuary, in contrast, are small and appear to be largely dependent on wind.

The SWIFT2D simulated velocities match as closely as can be expected when the grid resolution and wind driven nature of the circulation are considered. The use of additional wind data from a station located in the southern part of the upper Laguna Madre might improve the representation of velocities, however, the actual observed velocities are so small that the potential gain in accuracy may be offset by the increased data requirements.

Flow

Simulated flows were output for the eleven cross sections shown in Fig. 14. These cross sections represent the primary connections with the driving tides at the Corpus Christi NAS and El Toro Island stations, major conduits of flow, and representative sections across the width of the estuary. Actual flows were not measured during the time period simulated by the SWIFT2D and TxBLEND models, therefore a discussion of flow is reserved for the section on the sensitivity analysis and Chapter V which compares the results from the two models. Comparisons between simulated flows are made in these sections.

SENSITIVITY ANALYSIS

SWIFT2D provides a number of calibration parameters which can be adjusted to yield the best possible fit to measured data. A simple sensitivity analysis was performed to evaluate the effects of variations in the different parameters on model results. The set of five parameters shown in Table 6 were adjusted to illustrate the effect of each parameter on the model.

TABLE 6. SWIFT2D Model Parameters Varied for the Sensitivity Analysis.

Parameter	Low Value	Calibrated Value	High Value	Other
Time Step (seconds)	180	360	720	
Wind Stress	0.0001	0.0015	0.0026	
Viscosity (m ² /s)	0	1	10	
Advection Option	Arakawa	Leendertse	No Advection	
Manning's <i>n</i>	25% reduction (Distributed)	0.025-0.040 (Distributed)	25% increase (Distributed)	0.030 (Constant)

The wind stress coefficient and the Manning's *n* value were observed to have the largest effect on model results. Selection of the time step also has a significant effect on the model results. The other parameters had much smaller effects on the calibration.

Time Step

The length of the time step can contribute significantly to inaccuracies in the computations of the model. Despite the unconditional stability of the ADI method, serious errors can arise when large time steps are used. Substantial errors have been observed in the simulation of both water levels and velocities at large time steps. Stelling et al. (1986) describe this so-called ADI effect as a fundamental property of numerical integration by a splitting method, despite the splitting technique applied and despite the irregularity of the model boundaries.

The Courant number, which serves as an upper limit on the time step for explicit models, is defined by

$$Cf = \tau \left\{ gH \left[\frac{1}{\left(\frac{1}{2}\Delta x\right)^2} + \frac{1}{\left(\frac{1}{2}\Delta y\right)^2} \right] \right\}^{1/2} \dots\dots\dots(27)$$

where *Cf* is the Courant number, *g* is the acceleration of gravity, *H* is the cell depth, and Δx and Δy are the dimension of the cell in the *x* and *y* directions respectively. In the case of SWIFT2D Δx equals Δy and (26) reduces to

$$Cf = \frac{2\tau(2gH)^{1/2}}{\Delta s} \dots\dots\dots(28)$$

where Δs is the length of a side of the square grid cells. If Δx equals Δy then the Courant limitation implies a restriction on the time step of the form

$$\tau < \frac{\Delta s}{[2(2gH)^{1/2}]} \dots\dots\dots(29)$$

Significant numerical errors may occur at time steps much larger than this limiting value. Analytical estimates of the ADI effect are difficult to make, since quantitatively the effect depends on the shape of the geometry or bathymetry combined with the spatial grid size.

An essential feature of an ADI method for the approximation of shallow water equations is that for one time step the finite difference equations are solved alternatively implicit in the x direction and implicit in the y direction in two consecutive computational steps. Due to this, a tidal signal cannot be transferred more than once through an angle of 90° in one complete ADI time step. Hence, in one time step a signal cannot travel more than once through two bends in e.g., a zigzagging channel, halfway around an island or tidal flat, or around a peninsula shaped projection of the coastline. For accurate representation of hydraulics, however, this may be required (Stelling et al. 1986). The larger the Courant number, the larger the analytical area of influence of a grid feature on surrounding grid cells. Since the tidal signal can not pass more than once through an angle of 90° in a time step, the actual area of influence will be smaller than the analytical area of influence implied by a large Courant number.

The SWIFT2D grid for the upper Laguna Madre incorporates all of the features described by Stelling et al. (1986), which lead the ADI effect. The GIWW is a zigzagging narrow channel which runs the length of the estuary and provides much of the circulation. The spoil islands created by the maintenance dredging of the GIWW are also prevalent in the estuary. In addition, there exist large areas of tidal flats and several peninsulas in the model grid. The effects of these features is readily apparent in plots which compare water levels and velocities simulated at large time steps to observed values. The SWIFT2D calibrated model of the upper Laguna Madre was run with time steps of 180, 360, and 720 seconds. Table 7 lists the time steps with the associated Courant numbers. The courant numbers were calculated with both the average and maximum depths, and the average depth of the GIWW in the model grid.

TABLE 7. Courant Numbers Associated with the Time Steps Used in SWIFT2D for the Sensitivity Analysis

Time Step in Seconds (Minutes)	Courant Numbers		
	Average Grid Cell Depth	Maximum Grid Cell Depth	Average Depth of Cells in the GIWW
180 (3)	8.1	17.8	13.6
360 (6)	16.2	35.7	27.2
720 (12)	32.3	71.3	54.3

As expected, the three minute time step yielded the most accurate simulation of water levels and velocities.

RMSE's and Plots of water levels at the Pita Island tide station and RMSE's and velocities at the GIWW at the JFK Causeway velocity station show a clear deterioration in the simulated time series as the time step increases. Tables 8 and 9 show the RMSE's between observed and simulated water levels and velocities.

TABLE 8. Root Mean Squared Errors between Simulated and Observed Water Levels for Simulations with Different Time Steps

Water Level Station	RMSE (meters)		
	360 seconds (Calibrated)	180 seconds	720 seconds
Corpus Christi NAS	0.001	0.001	0.001
Packery Channel	0.043	0.042	0.045
Pita Island	0.036	0.036	0.038
South Bird Island	0.059	0.058	0.062
Yarborough Pass	0.067	0.066	0.069
Riviera Beach	0.124	0.124	0.126
El Toro Island	0.006	0.006	0.005
Average	0.048	0.048	0.049

TABLE 9. Root Mean Squared Errors between Simulated and Observed Velocities for Simulations with Different Time Steps

Water Level Station	RMSE (meters per second)		
	360 seconds (Calibrated)	180 seconds	720 seconds
Humble Channel	0.13	0.13	0.12
GIWW at the JFK Causeway	0.16	0.16	0.19
GIWW at Marker 199	0.19	0.17	0.21
North of Baffin Bay	0.10	0.10	0.10
Mouth of Baffin Bay	0.08	0.08	0.09
South of Baffin Bay-Middle	0.11	0.11	0.11
South of Baffin Bay-West	0.08	0.07	0.07
North Land Cut	0.12	0.12	0.13
Average	0.12	0.12	0.13

An evaluation of the RMSE's showed that the errors increased with increasing length of the time step at almost every station. The largest increases in the RMSE occurred at stations located in the GIWW. The largest increase in the error between simulated and observed velocities occurred at the GIWW at Marker 199 station which is the southern most velocity station in the GIWW still affected by the tidal signal.

The ADI effect is much more evident in plots of the simulated and observed times series. Figs. 30 through 35 show the effect of the time step on the simulation of water levels, velocities, and flows. There are no measured data available during the time of the simulations at the cross sections used in the model comparisons. Results with the 720 second time step show a clear lag in phase for both water levels and flows. This lag is a direct result of the ADI effect described by Stelling et al. (1986). The results at the two stations are dependent on flows through stair-stepped reaches of channels. The large time step does not allow accurate propagation of flow through multiple bends in the channel. The 180 second time step produced the most accurate results, however, the 360 second time step was selected for the simulation runs discussed in this report. The 360 second time step offered much shorter simulation times with minimal losses in accuracy. Run times for a 15 day simulation with a three minute time step were on the order of 4.25 hours while run times for the 6 and 12 minute time steps were 2.3 and 1.3 hours, respectively.

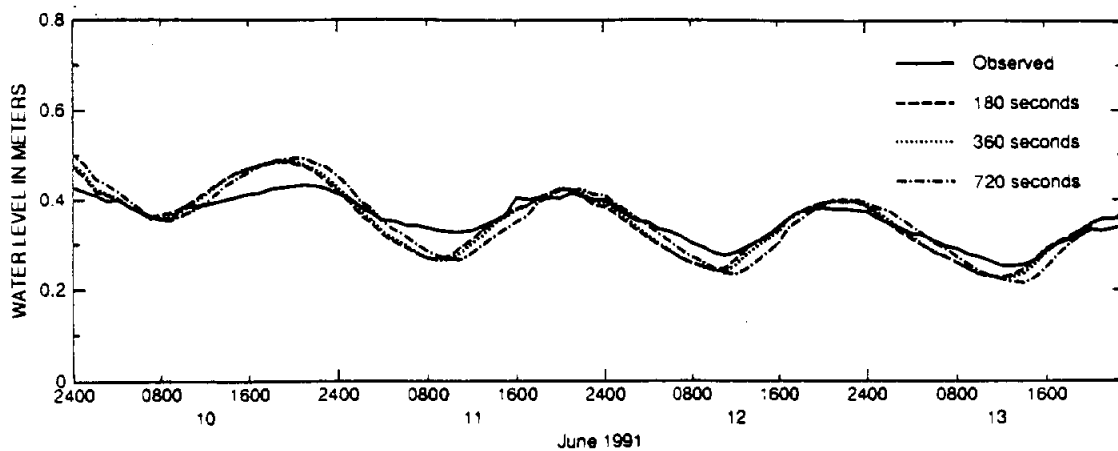


FIG. 30. Differences in Water Levels Due to the Time Step, Pita Island

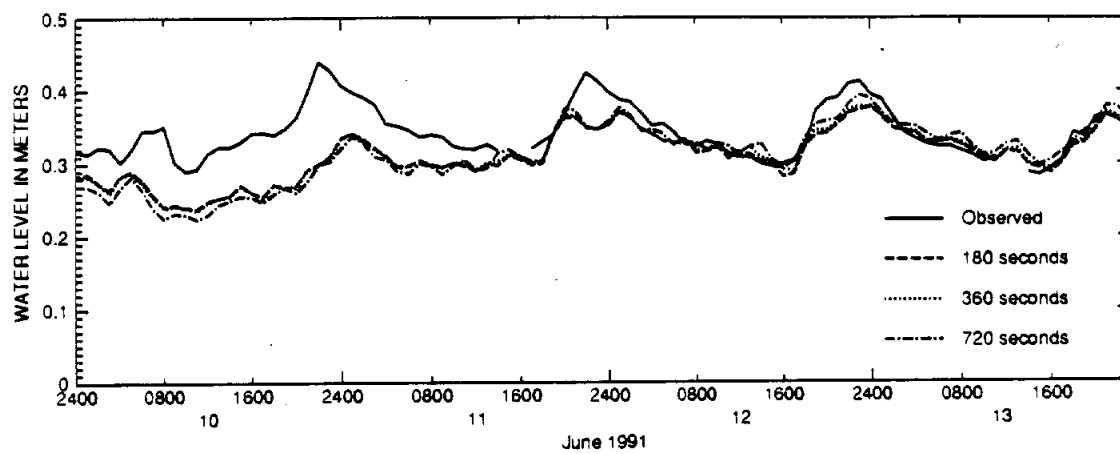


FIG. 31. Differences in Water Levels Due to the Time Step, Riviera Beach

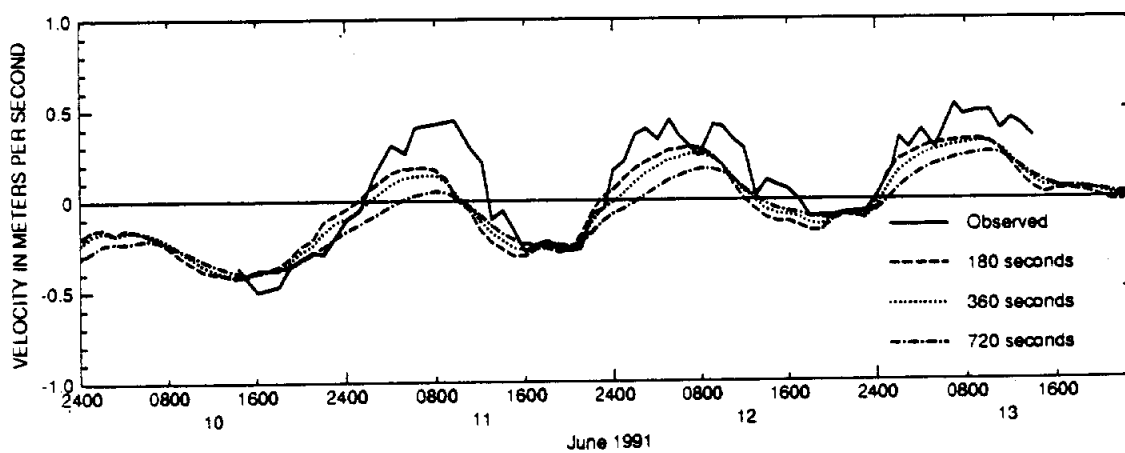


FIG. 32. Differences in Velocity Due to the Time Step, GIWW at JFK Causeway

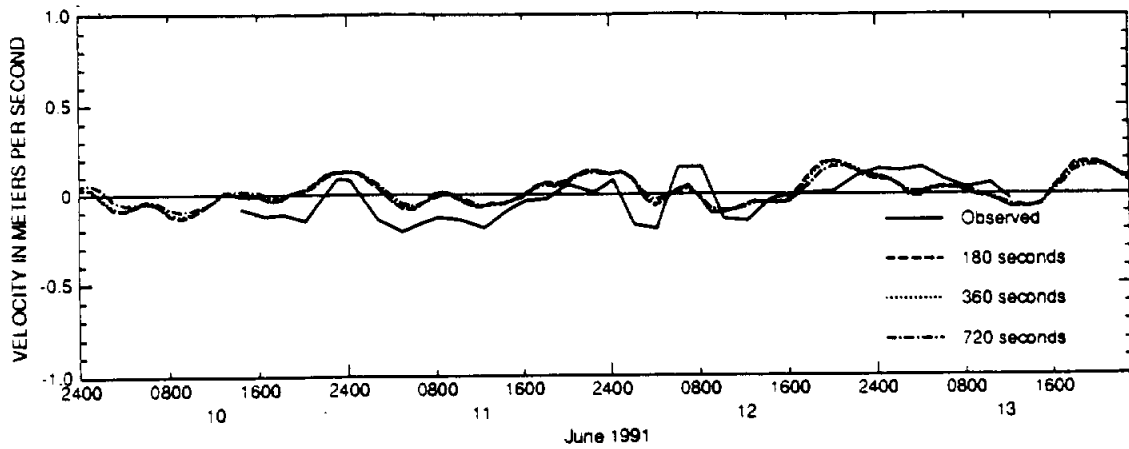


FIG. 33. Differences in Velocity Due to the Time Step, South of Baffin Bay-Middle

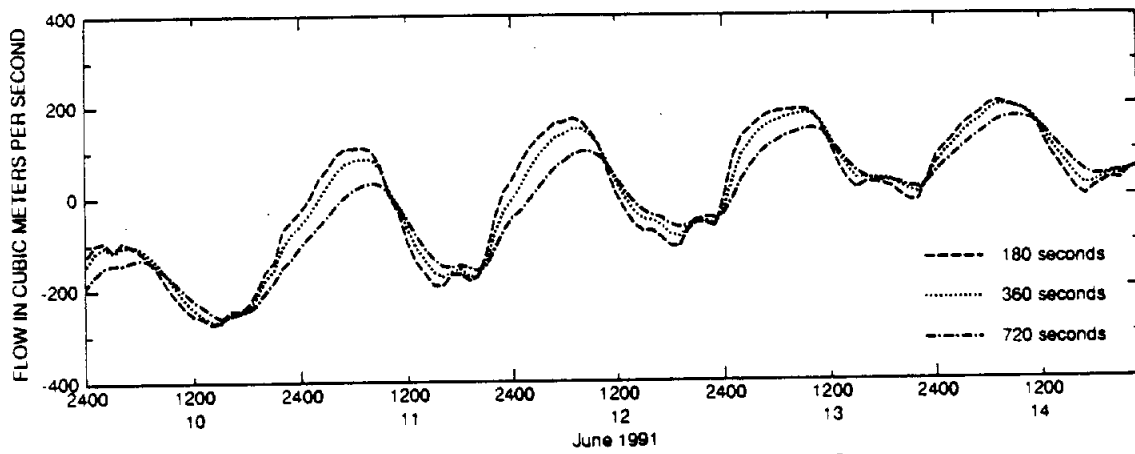


FIG. 34. Differences in Flow Due to the Time Step, GIWW at JFK Causeway

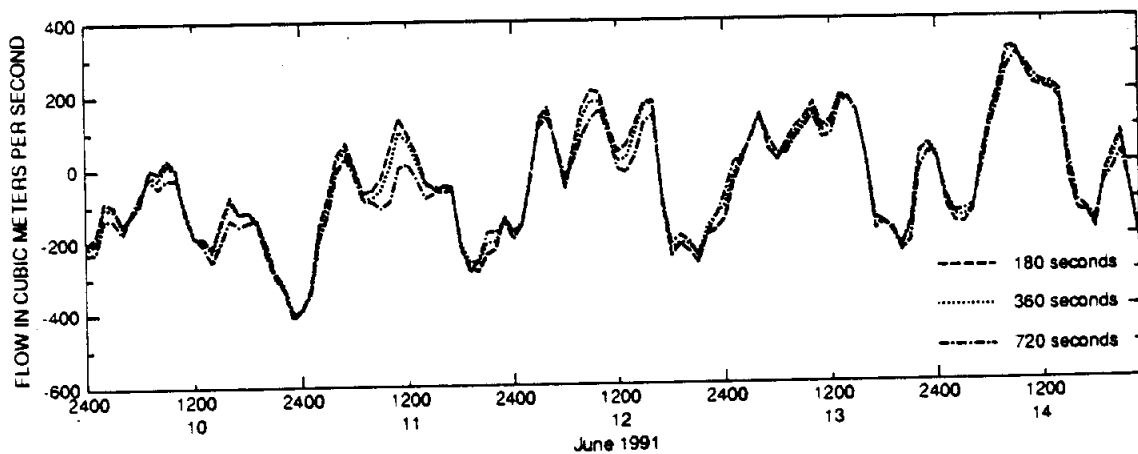


FIG. 35. Differences in Flow Due to the Time Step, Baffin Bay

Wind Stress

The value of the wind stress coefficient had the greatest influence on model results of any of the parameters evaluated. Figs. 36 through 41 show the effects of the wind stress coefficient on water levels at the Pita Island and Riviera Beach tide stations, velocities for the GIWW at the JFK Causeway and South of Baffin Bay-Middle current stations, and the GIWW at the JFK Causeway and Baffin Bay flow cross sections, respectively. Wind stress coefficients of 0.0001, 0.0015 and 0.0026 were used for the sensitivity analysis. The calibrated model used the wind stress of 0.0015. The wind exerts a noticeably greater influence over station in the southern end of the upper Laguna Madre. The RMSE's between simulated and observed water levels and velocities are shown in Tables 10 and 11, respectively.

TABLE 10. Root Mean Squared Errors between Simulated and Observed Water Levels for Simulations with Different Wind Stress Coefficients

Water Level Station	RMSE (meters)		
	0.0015 (Calibrated)	0.0001	0.0026
Corpus Christi NAS	0.001	0.001	0.002
Packery Channel	0.043	0.036	0.063
Pita Island	0.036	0.032	0.044
South Bird Island	0.059	0.055	0.063
Yarborough Pass	0.067	0.091	0.054
Riviera Beach	0.124	0.124	0.135
El Toro Island	0.006	0.006	0.007
Average	0.048	0.049	0.053

Wind appears to cause very little change in the water levels at the Pita Island station, which is strongly associated with the tidal signal from the Gulf of Mexico via Corpus Christi Bay. Larger wind stress coefficients actually increased the error at the three northern most internal stations. The error with a wind stress coefficient of 0.015 was improved by 2.4 centimeters at Yarborough Pass. The second increase of wind stress to 0.0026 only reduced the error at the Yarborough Pass station. The daily variations in water level at the Riviera Beach station appear to be almost entirely due to the effects of wind. The model results for the Riviera Beach station with negligible wind stress, shown as a dashed line on Fig. 37, produced a water level time series with smooth, long period oscillations.

These long period oscillations seem to correspond to the length of the lunar tidal cycle. A simulation run which spans several months to a year would be required to more conclusively evaluate this observation. The calibrated model with a wind stress coefficient of 0.0015 produced the smallest RMSE of the three options evaluated.

Velocities and flows were similarly affected by changes in the wind stress coefficient. The prevailing southerly and south easterly winds generally caused an increase in flow and velocity toward the north. Simulated velocities were improved by the larger wind stress coefficients. A value of 0.0015 produced an average improvement of 0.02 meters per second, while a value of 0.0026 yielded an average improvement of 0.03 meters per second. The improvement in velocities with the 0.0026 wind stress coefficient was outweighed by the decrease in accuracy of the water levels. The greatest effect of wind can be observed in Fig. 41, which shows the flow at the Baffin Bay cross section. The wind stress coefficient caused dramatic fluctuations in the flow which were not present in the results with a negligible wind stress.

TABLE 11. Root Mean Squared Errors between Simulated and Observed Velocities for Simulations with Different Wind Stress Coefficients

Water Level Station	RMSE (meters per second)		
	0.0015 (Calibrated)	0.0001	0.0026
Humble Channel	0.13	0.18	0.11
GIWW at the JFK Causeway	0.16	0.20	0.14
GIWW at Marker 199	0.19	0.22	0.18
North of Baffin Bay	0.10	0.09	0.10
Mouth of Baffin Bay	0.08	0.09	0.09
South of Baffin Bay-Middle	0.11	0.12	0.12
South of Baffin Bay-West	0.08	0.10	0.07
North Land Cut	0.12	0.15	0.11
Average	0.12	0.14	0.11

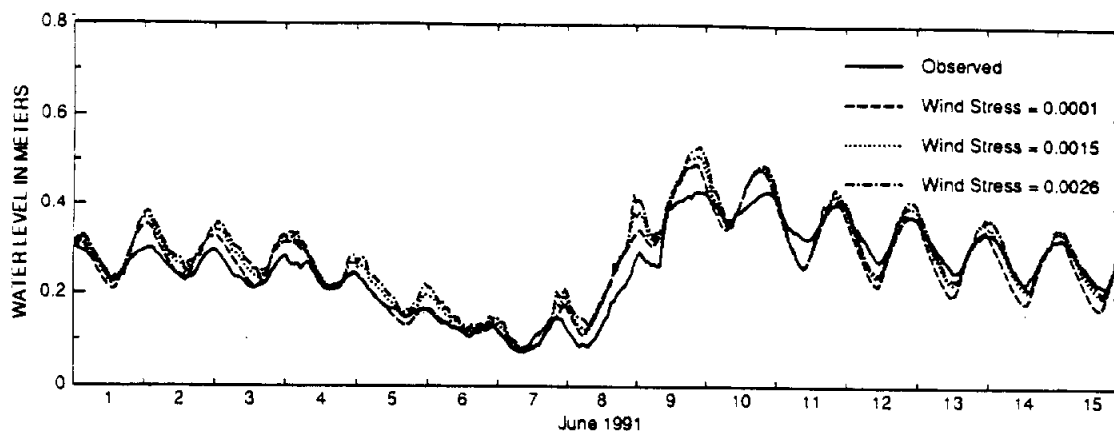


FIG. 36. Differences in Water Levels Due to the Wind Stress, Pita Island

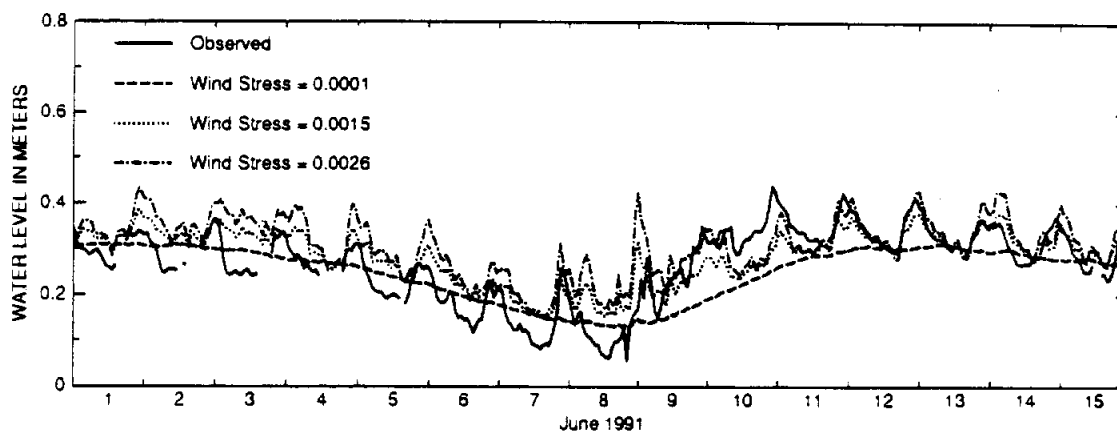


FIG. 37. Differences in Water Levels Due to the Wind Stress, Riviera Beach

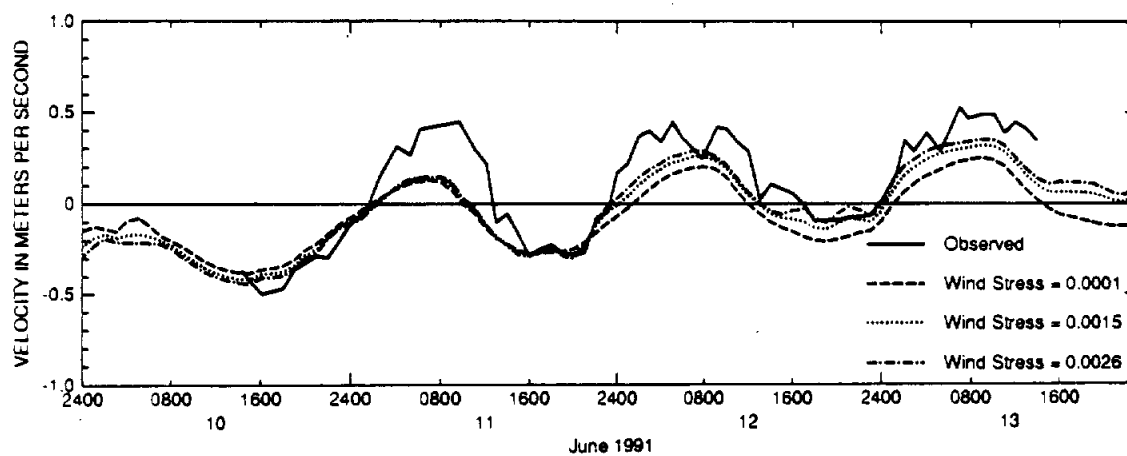


FIG. 38. Differences in Velocity Due to the Wind Stress, GIWW at JFK Causeway

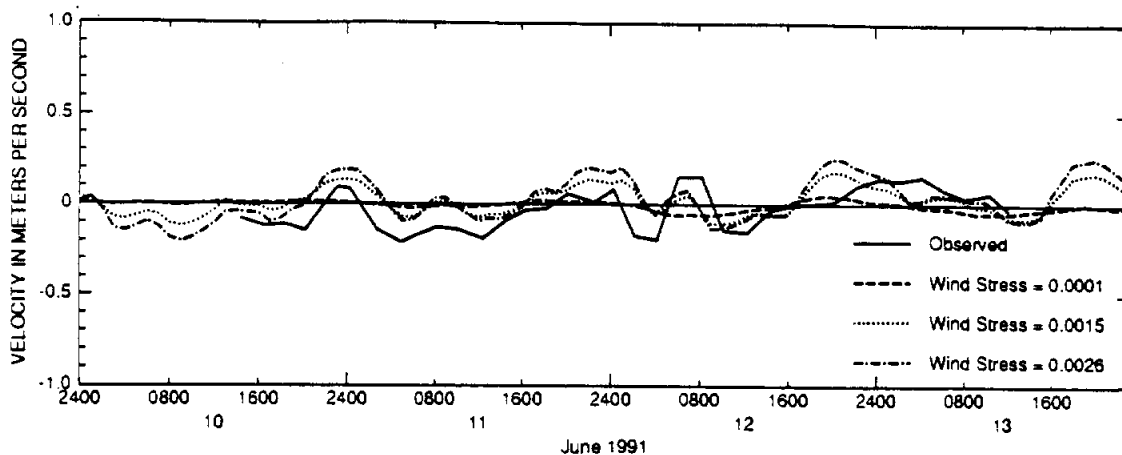


FIG. 39. Differences in Velocity Due to the Wind Stress, South of Baffin Bay-Middle

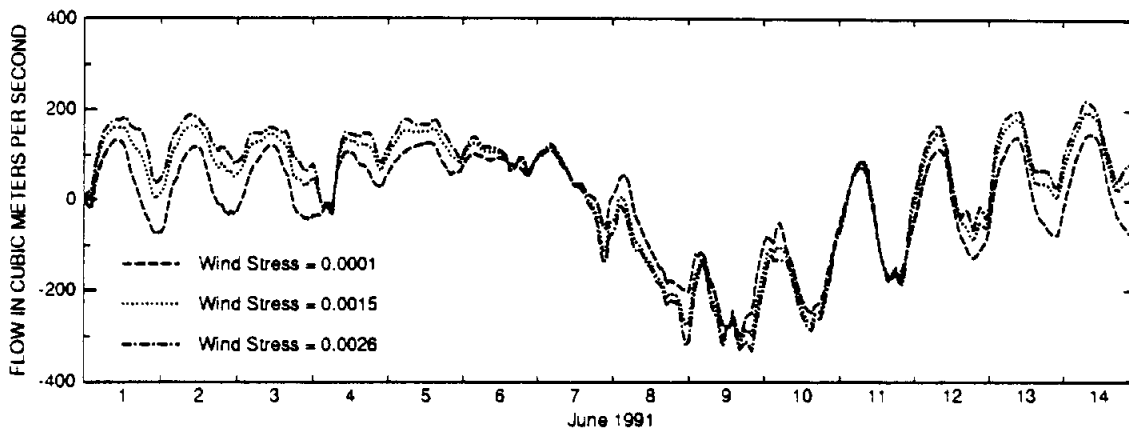


FIG. 40. Differences in Flow Due to the Wind Stress, GIWW at JFK Causeway

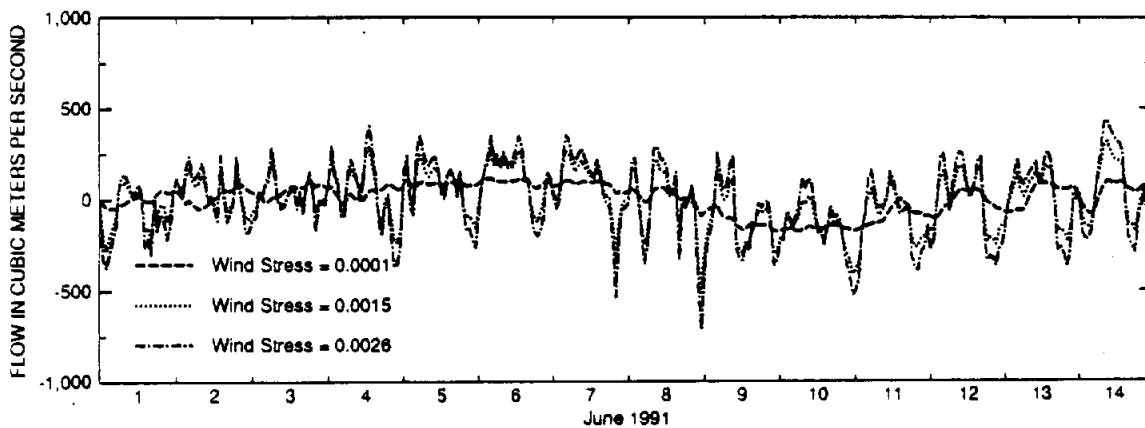


FIG. 41. Differences in Flow Due to the Wind Stress, Baffin Bay

Simulations with the 25 percent reduction in roughness and the constant value of 0.030 produced an increase in the magnitude of flow and velocity in both the positive and negative directions. The variations caused by changes in the roughness coefficient were on the same order of magnitude as those resulting from use of the 720 second time step. Variation of the n values had the greatest impact at the Humble Channel, GIWW at the JFK Causeway, and GIWW at Marker 199 stations. Velocities were improved slightly at these stations. Reduction of the roughness in the tidal flats and non-channel areas evidently caused the improvement. The use of a constant n value of 0.030 essentially increased the channel roughness and decreased the roughness in the tidal flats and other areas.

TABLE 13. Root Mean Squared Errors between Simulated and Observed Velocities for Simulations with Different Manning's Roughness Coefficients

Water Level Station	RMSE (meters per second)			
	Varied 0.025-0.040 (Calibrated)	-25%	+25%	Constant
Humble Channel	0.13	0.11	0.15	0.10
GIWW at the JFK Causeway	0.16	0.14	0.17	0.13
GIWW at Marker 199	0.19	0.17	0.20	0.17
North of Baffin Bay	0.10	0.09	0.10	0.09
Mouth of Baffin Bay	0.08	0.09	0.08	0.08
South of Baffin Bay-Middle	0.11	0.10	0.11	0.11
South of Baffin Bay-West	0.08	0.07	0.08	0.08
North Land Cut	0.12	0.11	0.13	0.11
Average	0.12	0.11	0.13	0.11

Manning's n

The values of the Manning's roughness coefficient in each of the model grid cells also exerts a strong influence on model simulations. Results for simulations with a range of n values are shown in Figs. 42 through 47 for the same observation stations discussed in the time step and wind stress sections. Tables 12 and 13 show the RMSE between simulated and observed water levels and velocities, respectively. Four scenarios were simulated in order to observe the influence of roughness on the computations. The calibrated model incorporated a spatially varied roughness which ranged from 0.025 in the GIWW to 0.040 on shallow tidal flats. The distribution of n values was similar to that used in the TxBLEND model. Scenarios two and three increased and decreased the spatially varied roughness at all points by 25% respectively. The fourth scenario employed a constant value of 0.030 in all computational grid cells.

The results of the sensitivity analysis appear to indicate that additional modifications of the roughness could improve the simulation. The use of a constant roughness produced the lowest average RMSE and improves the error at each water level station except for Packery Channel. The effects of the 25 percent reduction in the spatially varied roughness produced similar results. The greatest improvement was observed at the Yarborough Pass tide station.

TABLE 12. Root Mean Squared Errors between Simulated and Observed Water Levels for Simulations with Different Manning's Roughness Coefficients

Water Level Station	RMSE (meters)			
	Varied 0.025-0.040 (Calibrated)	-25%	+25%	Constant
Corpus Christi NAS	0.001	0.001	0.001	0.001
Packery Channel	0.043	0.048	0.040	0.048
Pita Island	0.036	0.038	0.036	0.035
South Bird Island	0.059	0.052	0.065	0.053
Yarborough Pass	0.067	0.060	0.072	0.055
Riviera Beach	0.124	0.120	0.128	0.118
El Toro Island	0.006	0.005	0.006	0.005
Average	0.048	0.046	0.050	0.045

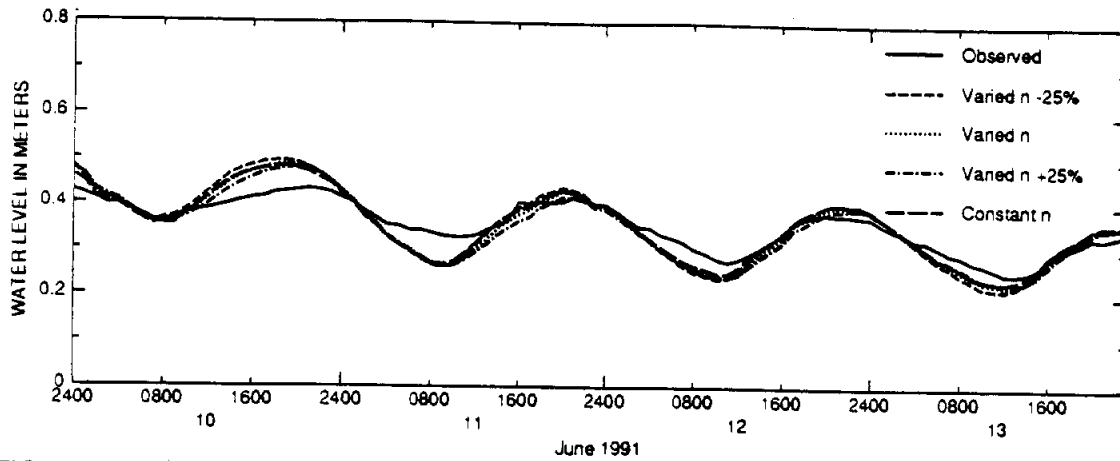


FIG. 42. Differences in Water Levels Due to Manning's n , Pita Island

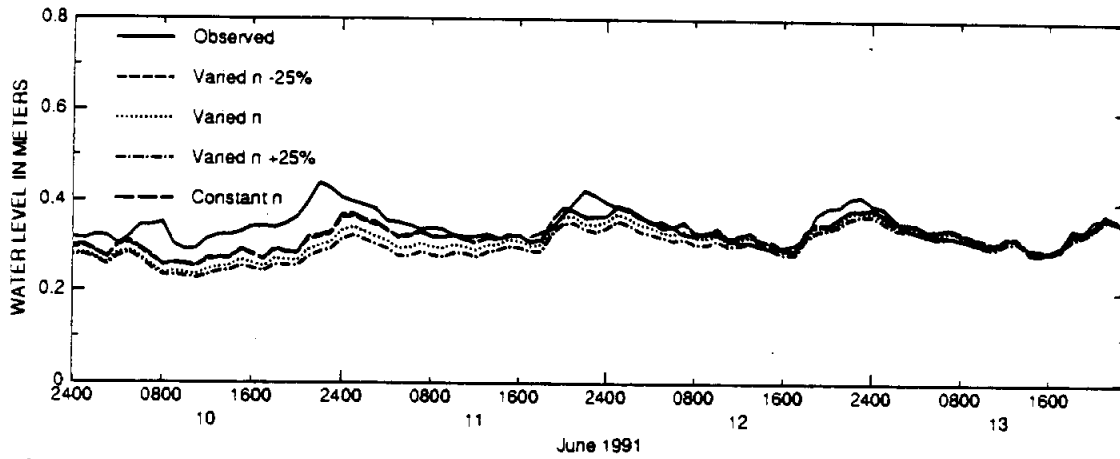


FIG. 43. Differences in Water Levels Due to Manning's n , Riviera Beach

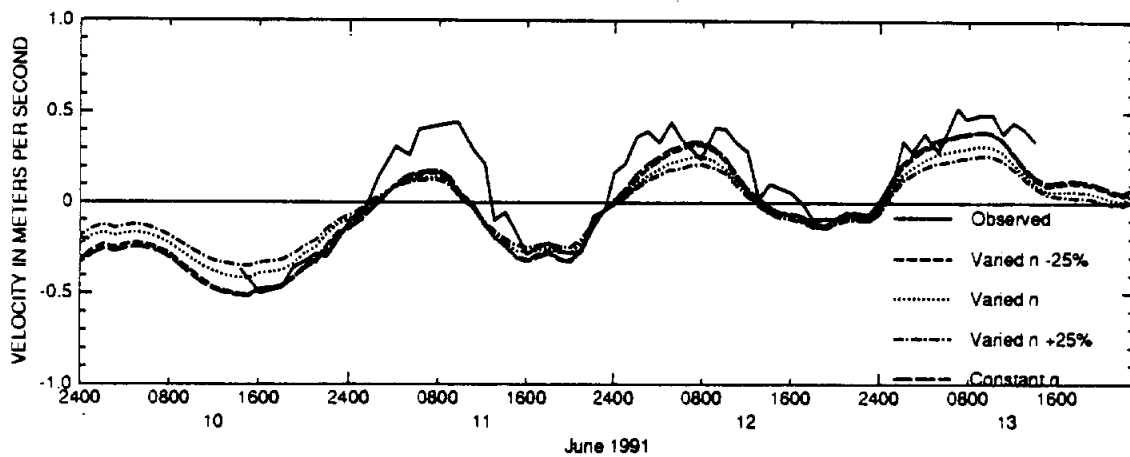


FIG. 44. Differences in Velocity Due to Manning's n , GIWW at JFK Causeway

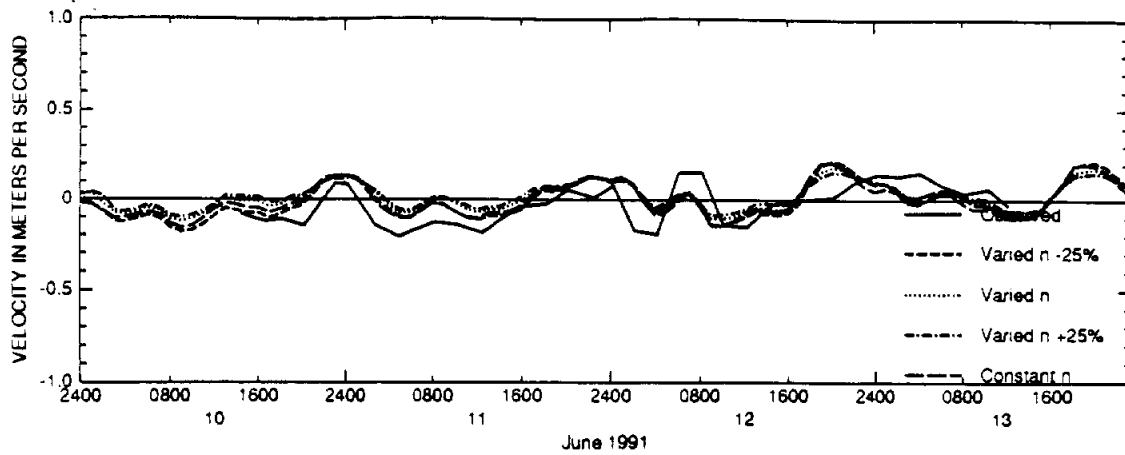


FIG. 45. Differences in Velocities Due to Manning's n , South of Baffin Bay-Middle

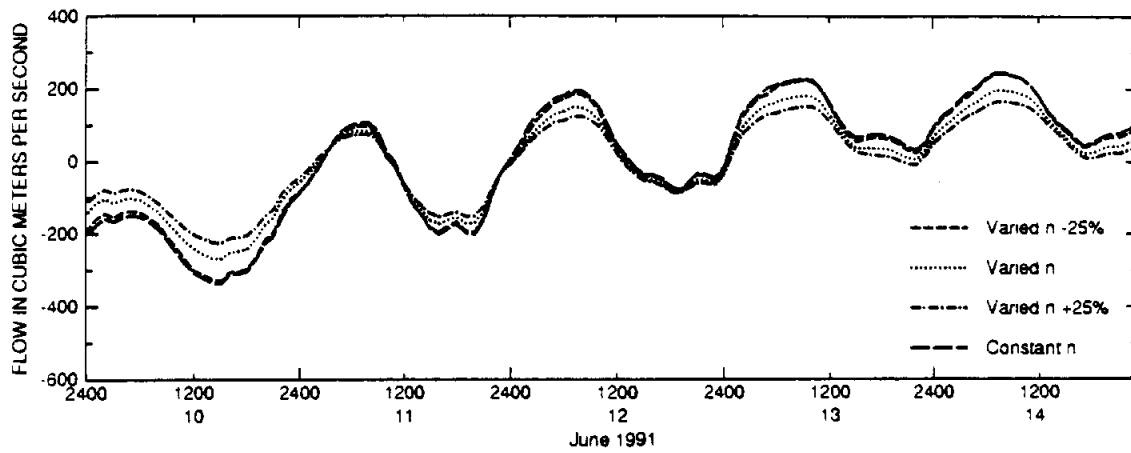


FIG. 46. Differences in Flow Due to Manning's n , GIWW at JFK Causeway

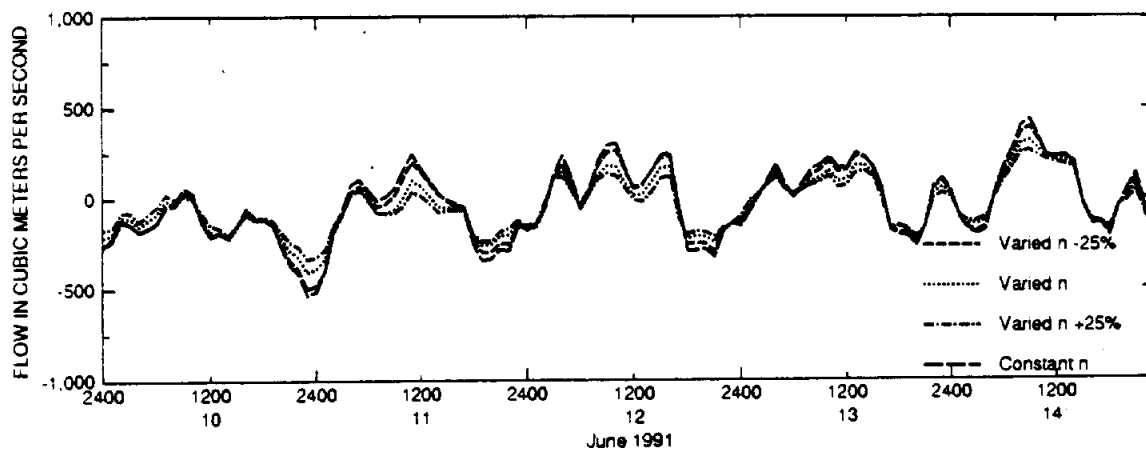


FIG. 47. Differences in Flow Due to Manning's n , Baffin Bay

Viscosity and Advection Option

Adjustments to the viscosity and advection option parameters had limited effects on the simulations. Variation of the vorticity related viscosity coefficient, k' in (14) produced no discernible change in the model simulation. A value of 1 meter was used for k' in the sensitivity runs. Variation of the spatially distributed viscosity coefficient, k_0 in (14), had a more noticeable effect. A viscosity coefficient larger than the maximum value of $10 \text{ m}^2/\text{s}$ used in the sensitivity analysis, however, would have been required to significantly affect the simulations. A viscosity coefficient of $10 \text{ m}^2/\text{s}$ generally tended to reduce the magnitudes of flows and velocities in both the positive and negative directions, as would be expected from a more viscous fluid. Lee et al. (1994) used $1.9 \text{ m}^2/\text{s}$ and 3.0 meters for k_0 and k' , respectively. The effects of the viscosity coefficient on velocity and flow are shown in Figs. 48 and 49.

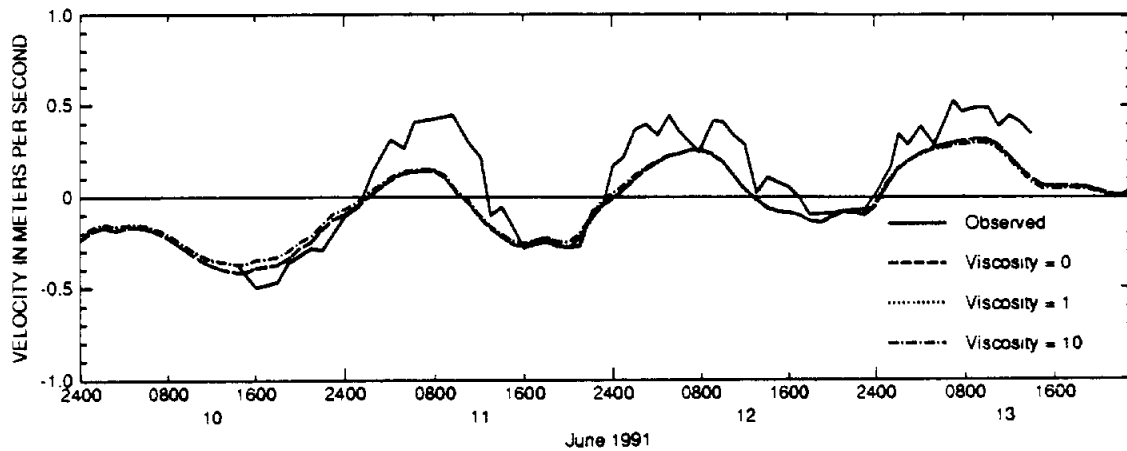


FIG. 48. Differences in Velocity Due to Viscosity, GIWW at JFK Causeway

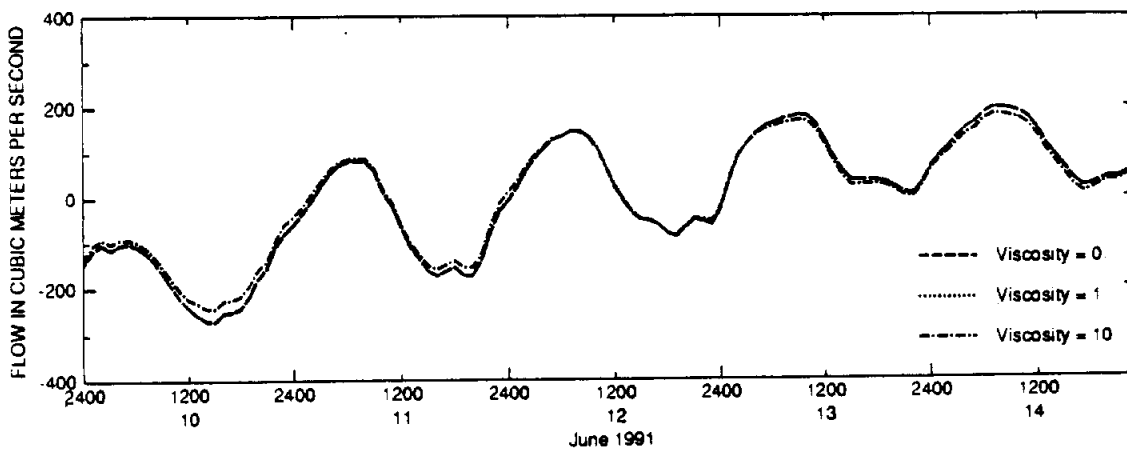


FIG. 49. Differences in Flow Due to Viscosity, GIWW at JFK Causeway

The selection of the three different advection options had a negligible effect on the simulations. At all observation stations the results for the Arakawa and Leendertse options were essentially identical. The simulation run without the advection term in the momentum equation produced slight differences in flow at the North Land Cut station shown in Fig. 50.

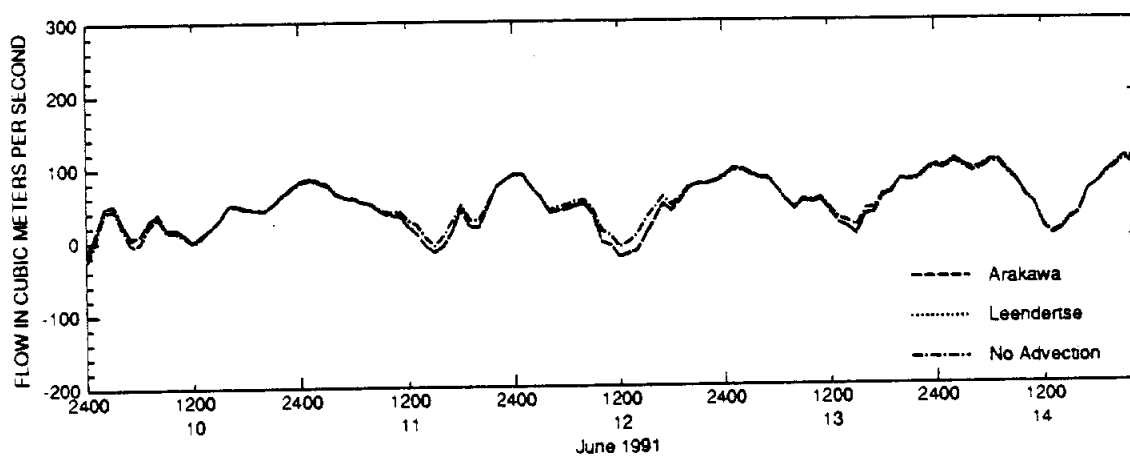


FIG. 50. Differences in Flow Due to the Advection Option, LM at North Land Cut

Wetting and Drying

SWIFT2D accounts for flooding and drying on tidal flats by considering grid points to be dry at depths less than a given marginal depth. When the water level at a cross section between two grid points becomes half the value of the marginal depth, the two points are taken out of the computation. The time interval to check for flooding and drying is specified in the SWIFT2D input file. The calibrated model used a marginal depth of 0.2 meter and a time interval to check for flooding and drying of 30 minutes. A summary of the total number of times that cells flooded and dried and the total area that actually flooded and dried during a 15 day simulation is shown in Table 14. The number of times that cells flooded and dried in the simulation is not necessarily equal since cells that dried at some point in the simulation may not have flooded again before the end of the simulation. The grid was checked for flooding and drying every thirty minutes of simulated time.

TABLE 14. Summary of the Wetting and Drying of Grid Cells during the 15 Day Sensitivity Analysis Simulations

Parameter Changed for the Sensitivity Runs	Number of Times Cells Dry in the Simulation	Number of Times Cells Flood in the Simulation	Maximum Dry Area in the Simulation (km ²)	Dry Area as a Percentage of Total Area (%)
Calibrated	8075	7923	22.6	3.9
Time Step (Low)	8328	8179	22.6	3.9
Time Step (High)	6063	5924	23.6	4.1
Wind Stress (Low)	1537	1460	16.8	2.9
Wind Stress (High)	18701	18257	41.8	7.2
Manning's n (Low)	10017	9792	26.0	4.5
Manning's n (High)	9062	8874	25.4	4.4
Manning's n (Constant)	7368	7230	20.5	3.5
Viscosity (Low)	8071	7920	22.7	3.9
Viscosity (High)	8119	7967	21.6	3.7
Arakawa Advection	8066	7913	23.0	4.0
No Advection	8172	8009	23.2	4.0
0.4 m Marginal Depth	10020	10010	33.9	5.9

The viscosity coefficient and the advection option had very little effect on the number of cells that were involved in flooding and drying. The 180 second (Low) and 360 second (Calibrated) time steps produced almost the same amount of wetting and drying in the simulations, which indicates that the use of 360 second time step instead of a slightly more accurate smaller time step was justified. The 720 second (High) time step produced significantly smaller amounts of flooding and drying. The wind stress coefficient had the greatest effect on cell wetting and drying. The use of a negligible wind stress reduced the amount of wetting and drying by approximately 80%. A wind stress coefficient of 0.0026 produced approximately a 230% increase in the amount of wetting and drying. The effects of wind stress on wetting and drying were much larger than the effects of changes in the roughness coefficient. The two-fold decrease in the marginal depth used to test for wetting and drying did not increase wetting and drying as much as the use of a high wind stress coefficient. The majority of the shallow grid cells are located at the south end and along the eastern side of the upper Laguna Madre. The predominant south and south easterly winds tend to dry the cells along the southern and eastern tidal margins.

VI COMPARISON WITH TXBLEND RESULTS

TXBLEND MODEL APPLICATION

The TxBLEND model used for comparison with SWIFT2D incorporated the entire Corpus Christi Bay and Upper Laguna Madre systems. The ultimate goal of the TWDB is to integrate the Corpus Christi Bay system and the Upper and Lower portions of the Laguna Madre Estuary into a single model. This combination will allow the model to be driven entirely by tides and water quality (salinity) measured in the Gulf of Mexico. As a result, less data will be required for planning level simulations. Although the external driving conditions were different in the two models, the representations of the upper portion of the Laguna Madre were similar.

Final calibration of the TxBLEND model for the Laguna Madre Estuary, Corpus Christi Bay, and Copano Bay system was not complete at the date of this study. The simulation results discussed in this study are based on the partially calibrated TxBLEND model as of May, 1996. The TWDB had not fully investigated the effects of the wind stress coefficient on the simulation. However, the calibration was sufficiently complete to allow a reasonable comparison between the TxBLEND and SWIFT2D models. The TxBLEND model results used in the following comparisons covered the period from May 15, 1991 through the end of the intensive inflow survey on June 14, 1991. The TWDB model incorporated salinity, however, the calibration of salinity was considered to be at an early stage and was not evaluated in this report. Salinity was not simulated in the application of the SWIFT2D model. A value of 0.3 inches per day of evaporation was included in the simulation. Hourly wind data at the Corpus Christi NAS was used as the driving wind.

TxBLEND provides several parameters which aid in the definition of the initial conditions of water levels, concentrations, and inflows. The initial water levels were set to zero (mean water level) at the start of the simulation. One parameter used in the model provides a six hour warm-up operation. The warm-up period allows for a smooth transition from zero water levels to the actual conditions in the estuary at the start of the simulation period. This option serves to reduce the possibility of numerical instabilities at start-up and eliminates the need to specify a starting water surface elevation at each mesh node. A similar option for a six hour build-up of inflows was implemented in the model. The six hour period allows river inflows to start at zero and increase to the actual value at the start of the simulation. Seven inflow points were included in the TxBLEND model. Only one, San Fernando Creek, flows directly into the upper Laguna Madre (Baffin Bay). The San Fernando Creek inflow was small during the time period of the simulation and its absence in the SWIFT2D model did not appear to affect the results. A third parameter, which allows repetition of the

first day of simulation, was not invoked. The start date of the simulation was approximately 28 days prior to the period of observed velocities. This time was considered sufficient to smooth out any residual effects of the initial conditions. The initial water surface elevation for the SWIFT2D model was set to the average water surface elevation observed at each of the tide stations in the estuary. The water surface elevations were fairly consistent at each station, therefore, the SWIFT2D model quickly reached equilibrium with the actual conditions. The initial velocities in both models were set to zero at start-up. The warm-up times allowed the velocities to approximate the actual velocities well before the times when observed velocities were reached.

COMPARISON OF MODELS

The complete TxBLEND model mesh used for the comparisons was comprised of 8,187 linear, triangular elements. The portion of the model which included the same area as the SWIFT2D model was comprised of approximately 3,562 elements. The overall sizes and shapes of the computational SWIFT2D grid and TxBLEND mesh were similar. Both representations of the bathymetry were derived from the NOAA nautical charts. Comparisons of the SWIFT2D finite difference grid and the TxBLEND finite element mesh is shown in Table 15.

TABLE 15. Geometric Characteristics of the SWIFT2D Finite Difference Grid and the TxBLEND Finite Element Mesh

Characteristic	SWIFT2D Grid	TxBLEND Upper Laguna Madre Mesh	TxBLEND Complete Mesh
Number of computational cells	~15,000	3,562	8,187
Minimum cell depth (m)	0.10	0.55	0.46
Maximum cell depth (m)	5.0	10.8	17.9
Average cell depth (m)	1.03	1.58	2.81
Area weighted, average cell depth (m)	1.03	1.18	3.90
Minimum cell area (m ²)	40,000	1,634	1,634
Maximum cell area (m ²)	40,000	1,395,481	1,758,784
Average cell area (m ²)	40,000	140,401	222,712
Total area (km ²)	577.4	511.4	1,823
Total volume below mean water level (m ³)	5.92x10 ⁸	5.87x10 ⁸	7.11x10 ⁹

The gross parameters of total area, total volume, and average depth are similar between the SWIFT2D grid and the portion of the TxBLEND mesh which covers the upper Laguna Madre. The area at mean water level was 13% greater in the SWIFT2D grid, while the volume at mean water level was 1% greater in the SWIFT2D grid. The difference in the size of the two computational areas is primarily due to the inclusion in the SWIFT2D grid of the feature called "the Hole" at the southern end of the estuary. The smaller difference between the volumes can be explained by the average depths in the two representations of the bathymetry. The area weighted cell depth weights the average depth in each cell by the corresponding area of that cell. The total of these weighted depths was divided by the total area to produce an estimate of the average depths in the two meshes. The TxBLEND mesh was, on average, 15% deeper than the SWIFT2D grid. The disparity in depth is due primarily to the estimation of depths along the shallow, eastern side of the estuary. The nautical charts provided very little data in this area. The estimated depths were greater in the TxBLEND mesh, which produced a greater average depth in the finite element mesh. The portions of the meshes which conduct most of the circulation in the estuary were reasonably similar. Figs. 51 and 52 show the complete TxBLEND mesh and an enlarged area of the mesh in the vicinity of the JFK Causeway respectively.

The advantage of variable cell sizes is readily apparent from a comparison of the number of computational cells required for each model. The TxBLEND model is able to simulate the entire upper Laguna Madre, Corpus Christi Bay, and Copano Bay system with 55% fewer cells than were required to simulate the upper Laguna Madre alone with SWIFT2D. The continuity questions discussed in Chapter III place an upper limit on the size of triangular elements, however, the finite element mesh is still able to provide a substantial reduction in the number of cells required to represent the estuary. Note the high resolution in the vicinity of the GIWW and other channels and the larger element sizes in the wide areas with shallow or uniform depths.

The computational advantage of the TxBLEND model is also manifested in the model run times. A one month simulation with the TxBLEND model took approximately 2.5 hours with a 300 second time step (5 minutes). A corresponding one month simulation with the 200 meter grid SWIFT2D model took approximately 4.6 hours with a 360 second (6 minute) time step. The TxBLEND model was run on a Sun SPARCstation 20 while the SWIFT2D model was run on a Data General AViiON 8500 dual cpu server. The difference in hardware platforms could not account for the significant difference between the run times.

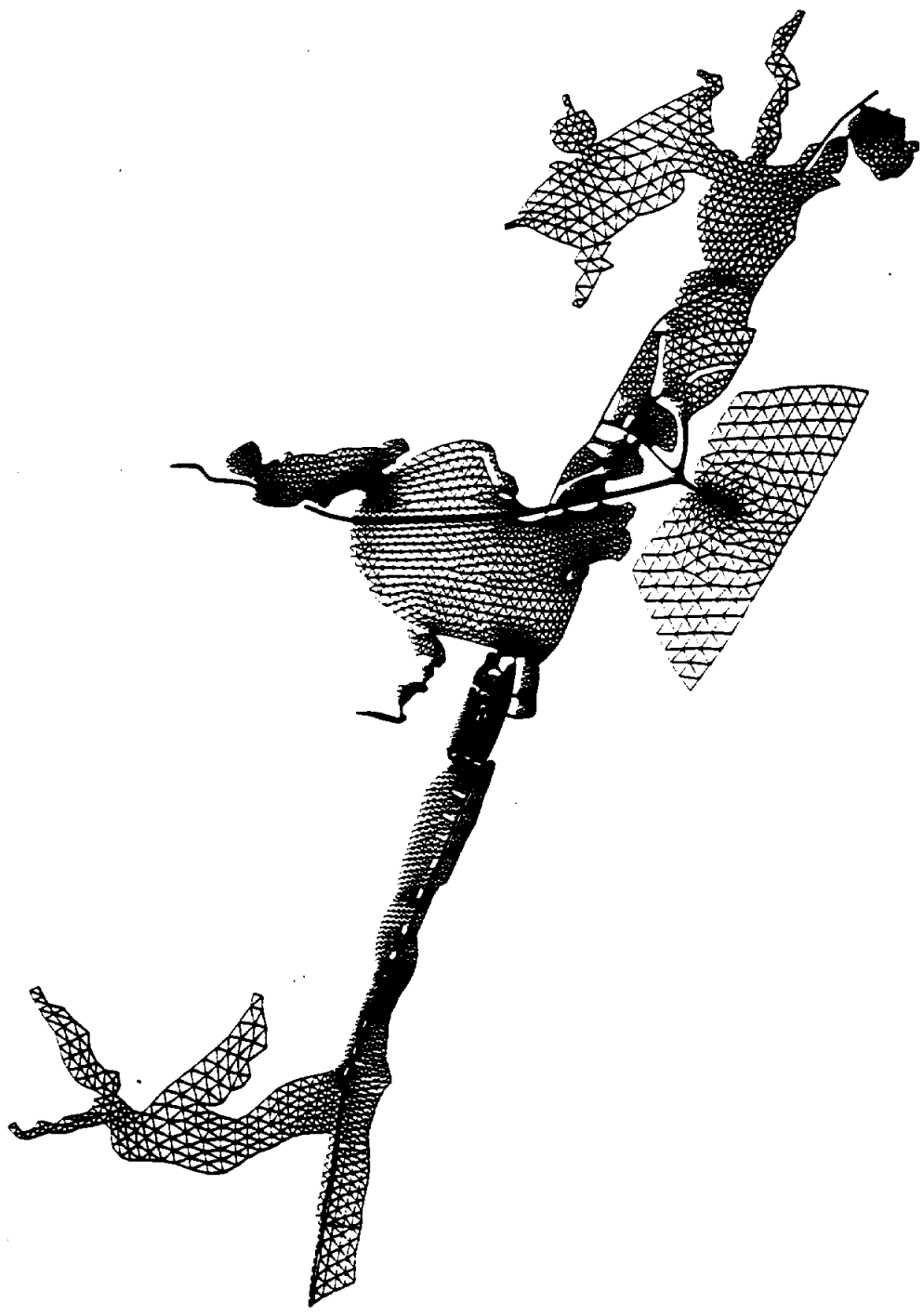


FIG. 51. TxBLEND Finite Element Mesh for the Upper Laguna Madre Estuary, Corpus Christi Bay, and Copano Bay System

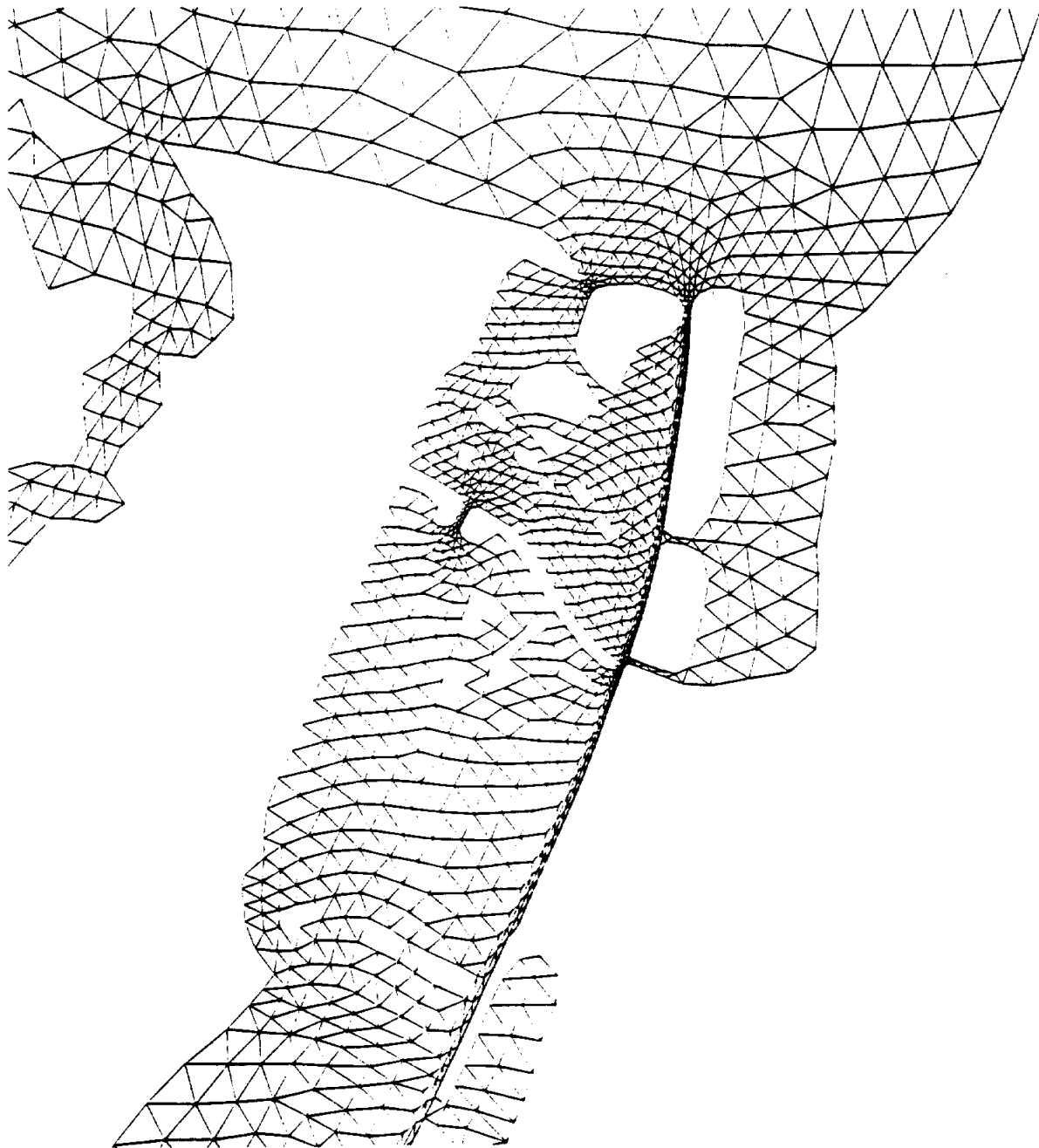


FIG. 52. Close-up of the TxBLEND Mesh in the Vicinity of the JFK Causeway

The large portion of time involved in the development of both models is taken up by the creation of the bathymetry data. The use of a GIS system in the development of the SWIFT2D model facilitated rapid creation of model grids, however, the grids required further editing outside of the GIS. In addition, the learning curve for inexperienced GIS users is steep. An experienced GIS user with data already in digital format could produce a model grid in a matter of days. The final editing of the grid outside of the GIS may take several days or weeks. The TxBLEND mesh was developed with the aid of a mesh generation program, however, a majority of the mesh development required hand editing. Abridged examples of the SWIFT2D and TxBLEND input files are included in Appendix B.

COMPARISON OF RESULTS

Despite significant differences between the two models, the results were in good agreement. The SWIFT2D and TxBLEND simulations were evaluated at each of the water level, velocity, and flow stations described in regard to the SWIFT2D results and sensitivity analysis. The water level, velocity, and flow stations are shown in Figs. 12, 13 and 14 respectively. The differences in the tidal driving conditions were a major concern, however, the TxBLEND simulated water levels at the Corpus Christi NAS gage closely matched the observed values, which were used as the driving tides in the SWIFT2D model. Therefore, comparisons between tide and velocity stations internal to the upper Laguna Madre were considered valid. The model results were compared with both time series plots of water levels, velocities, and flows and a set of velocity vector plots. The vector plots allowed for a comparison of the overall circulation patterns in the estuary.

Water Levels

Water levels simulated by the two models were in good agreement, especially for the stations nearest the NAS driving tide. The largest discrepancies were probably due to the slightly different representations of the bathymetry in the models. The differences observed in simulated water levels were rarely greater than 0.1 meters and more often were within 0.05 meters. The average RMSE between simulated and observed water levels was 4.8 centimeters for the SWIFT2D model and 5.4 centimeters for the TxBLEND model. The results were considered good given the fact that different techniques were used to generate the bathymetry data for the models. Comparisons of water level at the seven tide station locations are shown in Figs. 53 through 59.

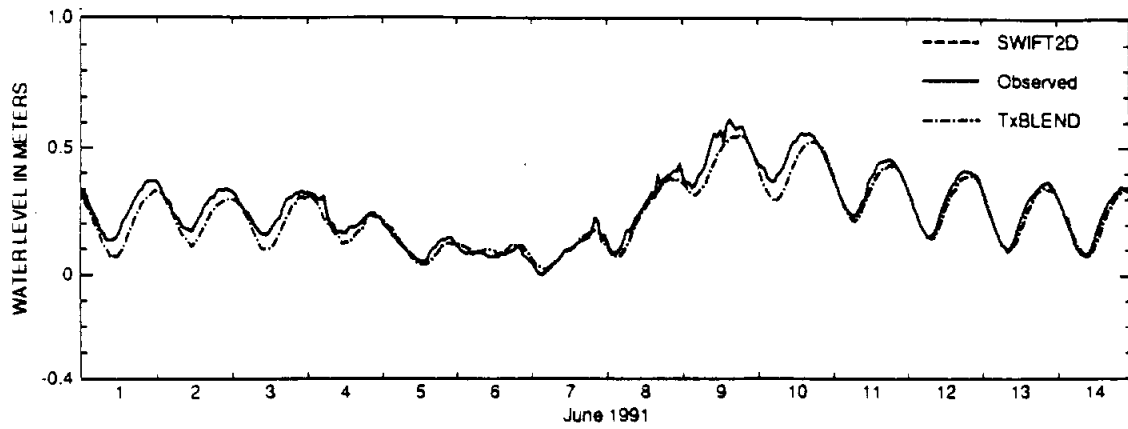


FIG. 53. Comparison of Water Levels at the Corpus Christi Naval Air Station Tide Station

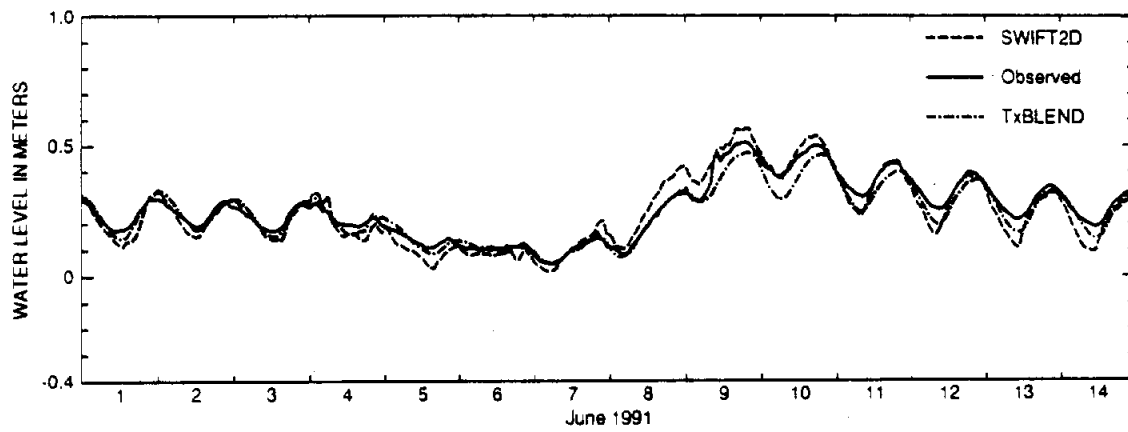


FIG. 54. Comparison of Water Levels at the Packery Channel Tide Station

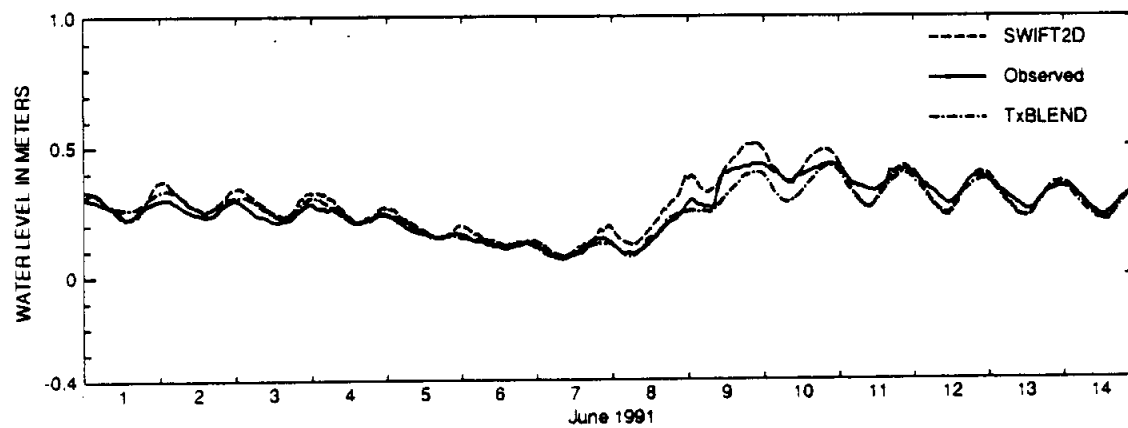


FIG. 55. Comparison of Water Levels at the Pita Island Tide Station

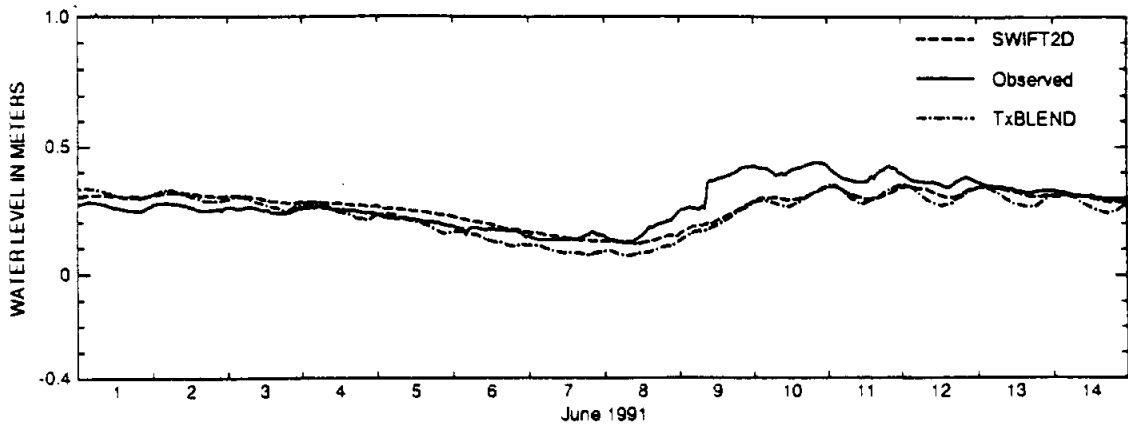


FIG. 56. Comparison of Water Levels at the South Bird Island Tide Station

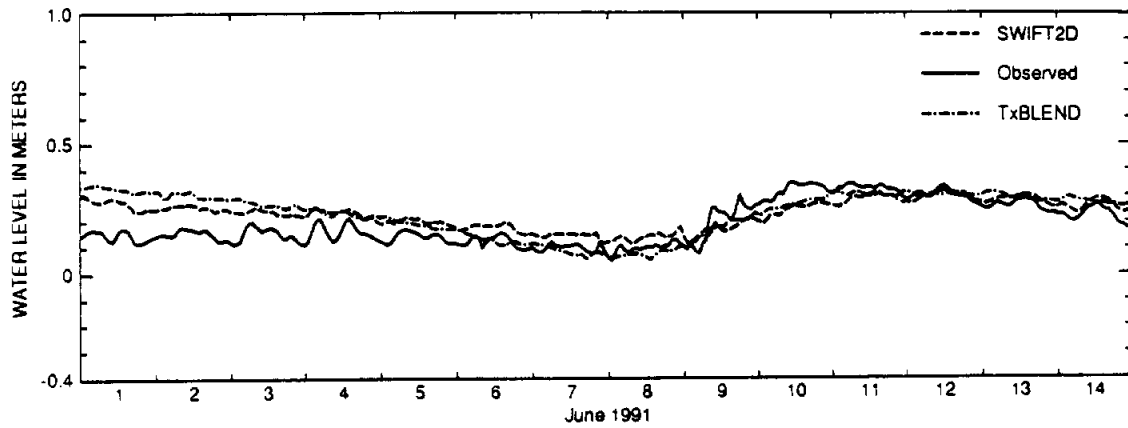


FIG. 57. Comparison of Water Levels at the Yarborough Pass Tide Station

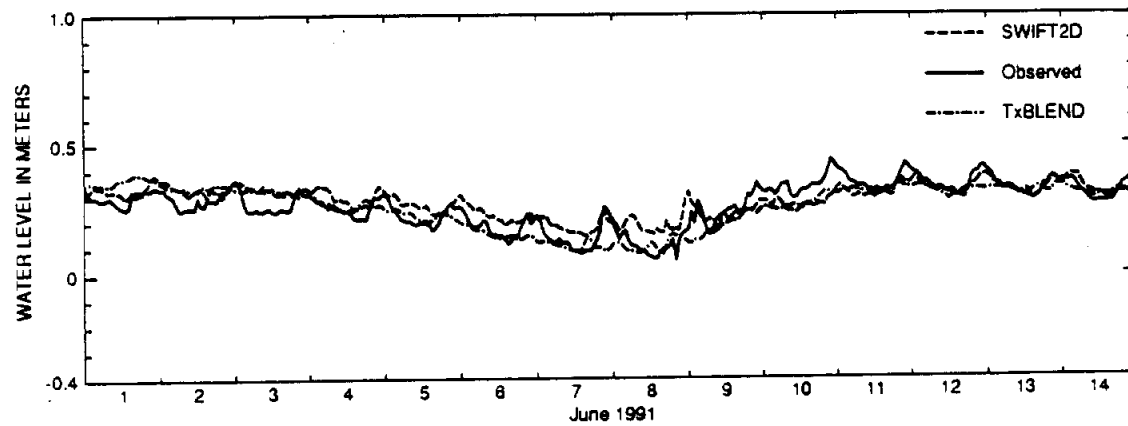


FIG. 58. Comparison of Water Levels at the Riviera Beach Tide Station

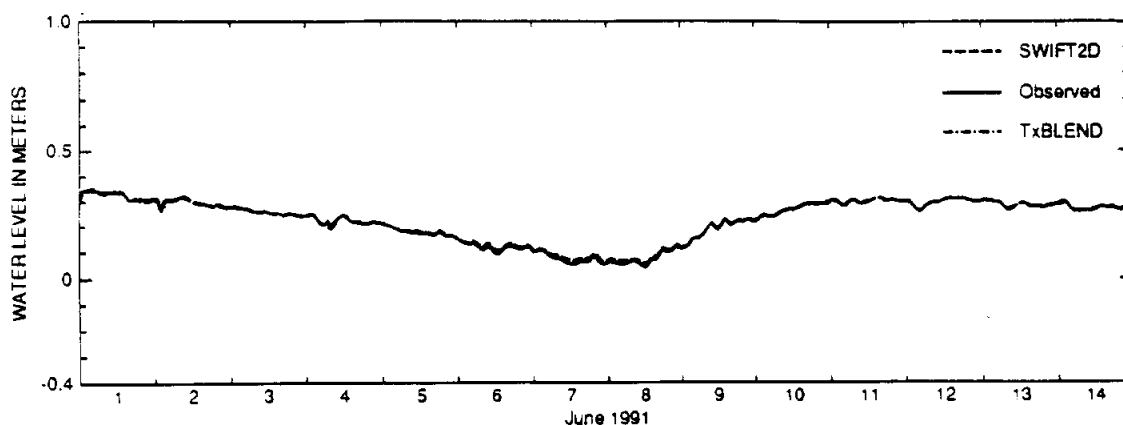


FIG. 59. Comparison of Water Levels at the El Toro Island Tide Station

Table 16 shows the RMSE's between simulated and observed water levels for both the SWIFT2D and TxBLEND simulations. Water levels at the Yarborough Pass and Riviera Beach stations did not match as well as the water levels at the northern tide stations. The differences seem to arise from the simulated wind effects in the models. The influence of wind appears to be smaller in the TxBLEND model. The RMSE's from the TxBLEND results were larger at the South Bird Island, Yarborough Pass and Riviera Beach stations, while the TxBLEND errors were smaller for the Packery Channel and Pita Island Stations. Additional adjustments of the wind stress factor in the TxBLEND model will probably improve the simulation of the lower three internal station. The effects of wind on the simulations are discussed further in the sections which describe the velocity and flow comparisons.

TABLE 16. Root Mean Squared Errors between SWIFT2D and TxBLEND Simulated Water Levels and Observed Water Levels

Water Level Station	RMSE (meters)	
	SWIFT2D	TxBLEND
Corpus Christi NAS	0.001	0.039
Packery Channel	0.043	0.032
Pita Island	0.036	0.029
South Bird Island	0.059	0.068
Yarborough Pass	0.067	0.081
Riviera Beach	0.124	0.128
El Toro Island	0.006	0.004
Average	0.048	0.054

Velocity

The velocities simulated by SWIFT2D also were comparable to those from the TxBLEND simulations, however, a consistent phase shift was observed in the timing of velocities at stations distant from the NAS driving tide. Figs. 60 through 67 show comparisons of simulated velocities at the eight locations shown in Fig. 13. The simulated velocities at the Humble Channel and GIWW at the JFK Causeway stations matched well in regard to both phase and amplitude. These stations are located near the NAS driving tide and are not significantly affected by wind. The phase of the SWIFT2D simulated velocities show a noticeable lag in comparison to TxBLEND velocities at stations south of the GIWW at Marker 199 station. The phase shift is consistent at around six hours. This shift is even more noticeable in comparisons of simulated flows discussed in the following section of this report. Velocities at these southern locations are strongly dependent on the influence of wind. The observed phase shift was discovered to be the result of a simple problem in the input of wind data in the two models. The tide data used in the simulation was referenced to Greenwich Mean Time (GMT) while the wind data received from the National Climatic Data Center (NCDC) was referenced to Local Standard Time (LST). LST for the Laguna Madre study area can be obtained by subtracting six hours from the GMT. All tidal and wind inputs in the SWIFT2D model were adjusted to GMT. The TxBLEND model used GMT for the tide data, however, LST was evidently used for the wind data. The resulting six hour difference corresponds directly to the observed phase shift observed in the velocities and flows.

Velocities simulated by the two models were very similar. Table 17 show the RMSE's between simulated and observed velocities for the SWIFT2D and TxBLEND models. The average difference between simulated and observed velocities was 0.12 for SWIFT2D and 0.13 for TxBLEND.

TABLE 17. Root Mean Squared Errors between SWIFT2D and TxBLEND Simulated Velocities and Observed Velocities

Water Level Station	RMSE (meters per second)	
	SWIFT2D	TxBLEND
Humble Channel	0.13	0.14
GIWW at the JFK Causeway	0.16	0.15
GIWW at Marker 199	0.19	0.19
North of Baffin Bay	0.10	0.09
Mouth of Baffin Bay	0.08	0.09
South of Baffin Bay-Middle	0.11	0.14
South of Baffin Bay-West	0.08	0.10
North Land Cut	0.12	0.13
Average	0.12	0.13

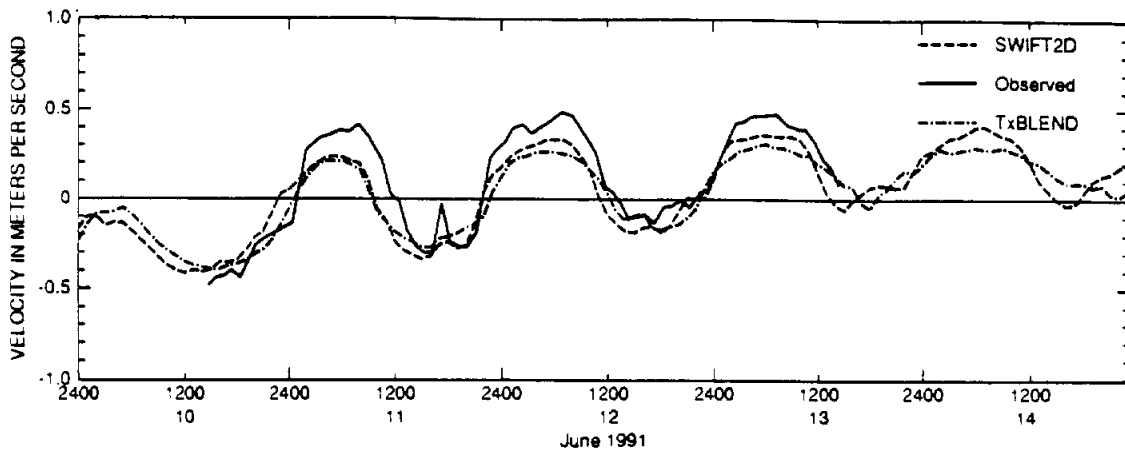


FIG. 60. Comparison of Velocity at the Humble Channel Station

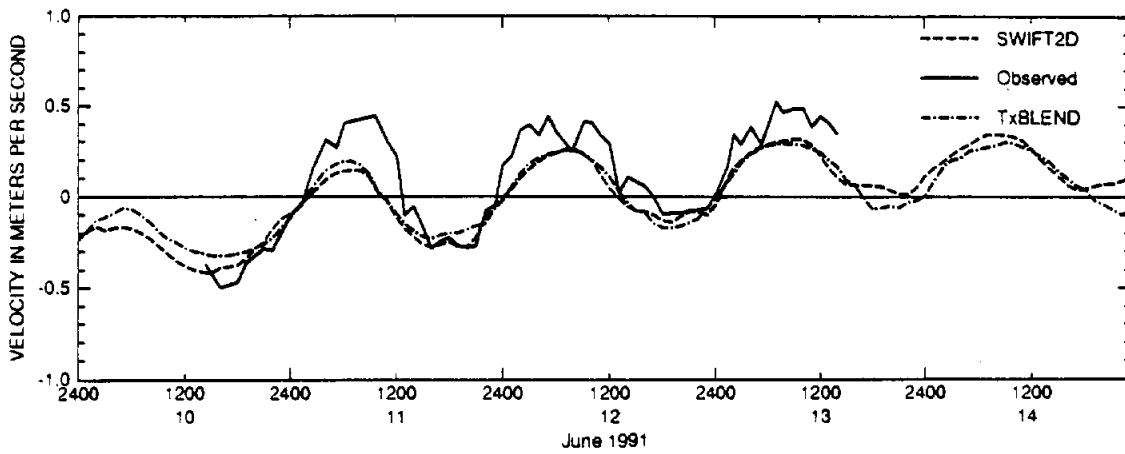


FIG. 61. Comparison of Velocity at the GIWW at JFK Causeway Station

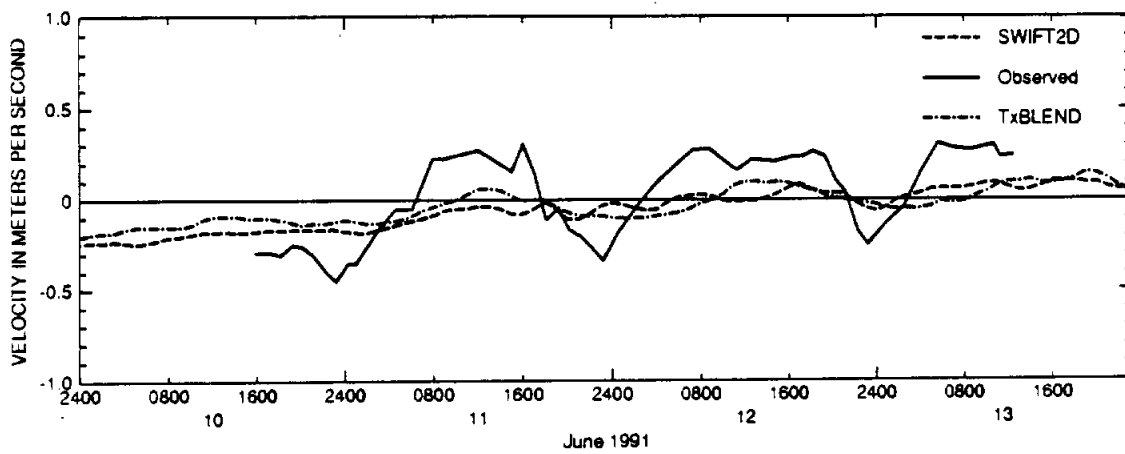


FIG. 62. Comparison of Velocity at the GIWW Marker 199 Station

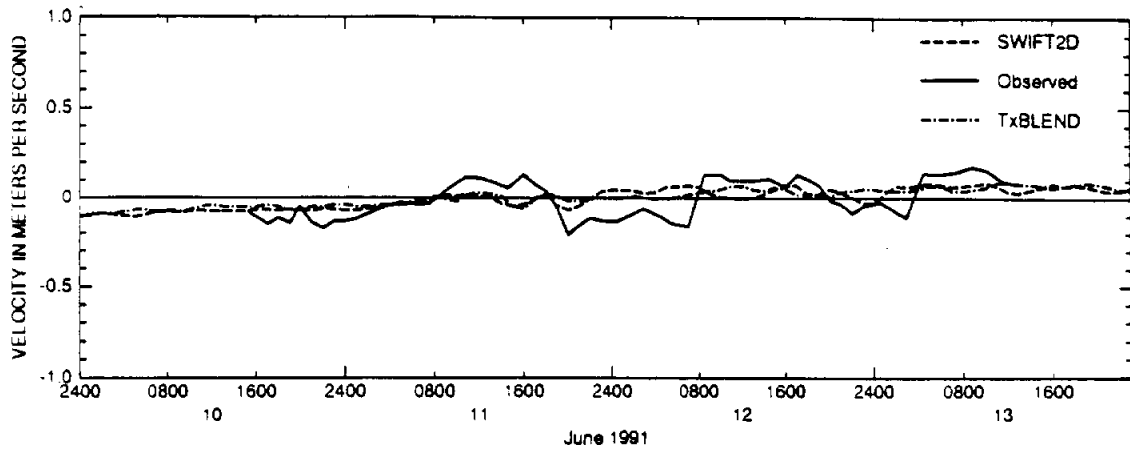


FIG. 63. Comparison of Velocity at the North of Baffin Bay Station

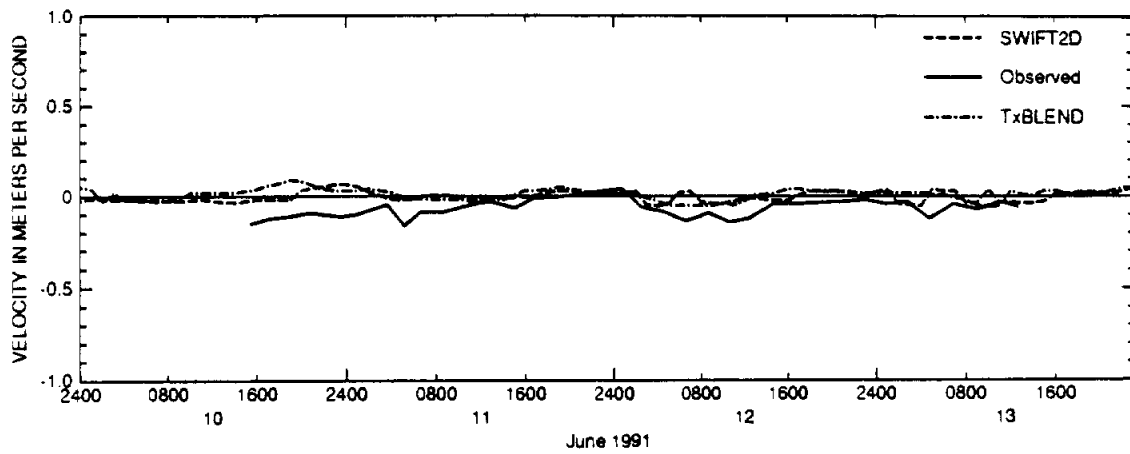


FIG. 64. Comparison of Velocity at the Mouth of Baffin Bay Station

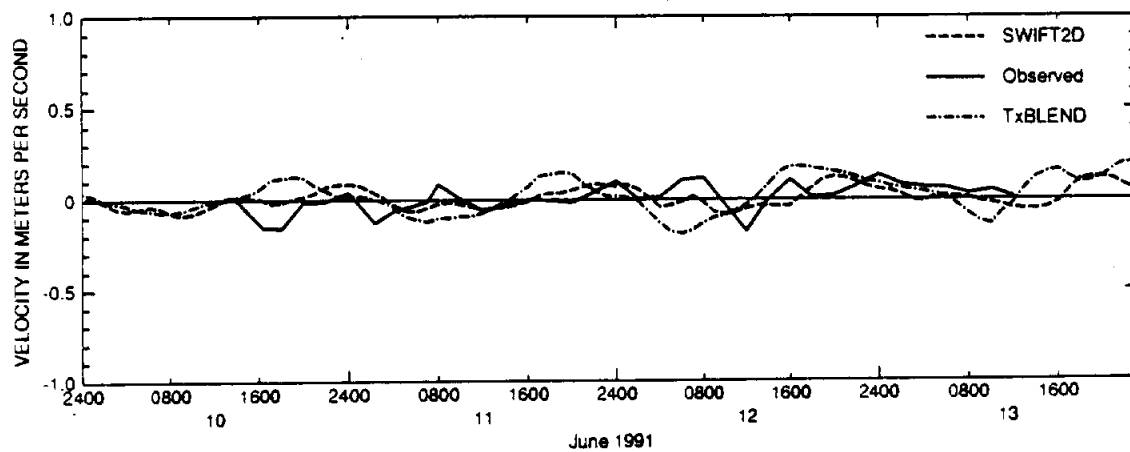


FIG. 65. Comparison of Velocity at the South of Baffin Bay-Middle Station

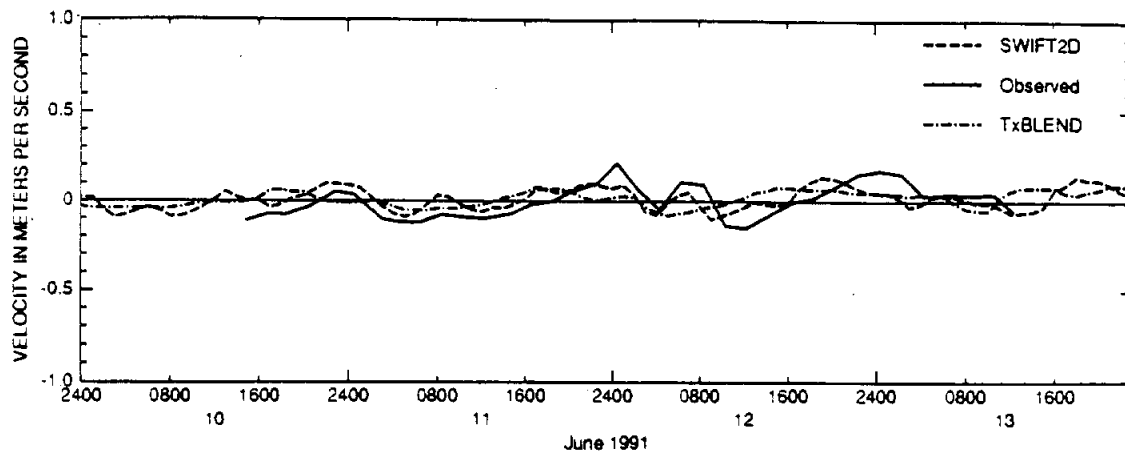


FIG. 66. Comparison of Velocity at the South of Baffin Bay-West Station

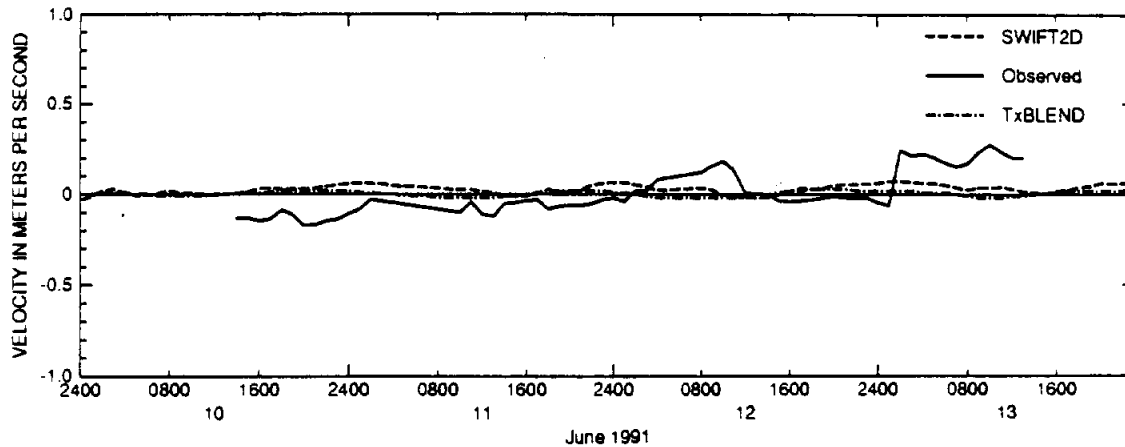


FIG. 67. Comparison of Velocity at the North Land Cut Station

Flow

Simulated flows were compared at the eight cross sections shown in Fig 14. There were no measured flow data available for these cross sections during the time period of the simulations, therefore, the comparisons are based solely on a comparison of the flows simulated by the SWIFT2D and TxBLEND models. Figs. 68 through 78 show the SWIFT2D and TxBLEND simulated flows at the eight cross sections.

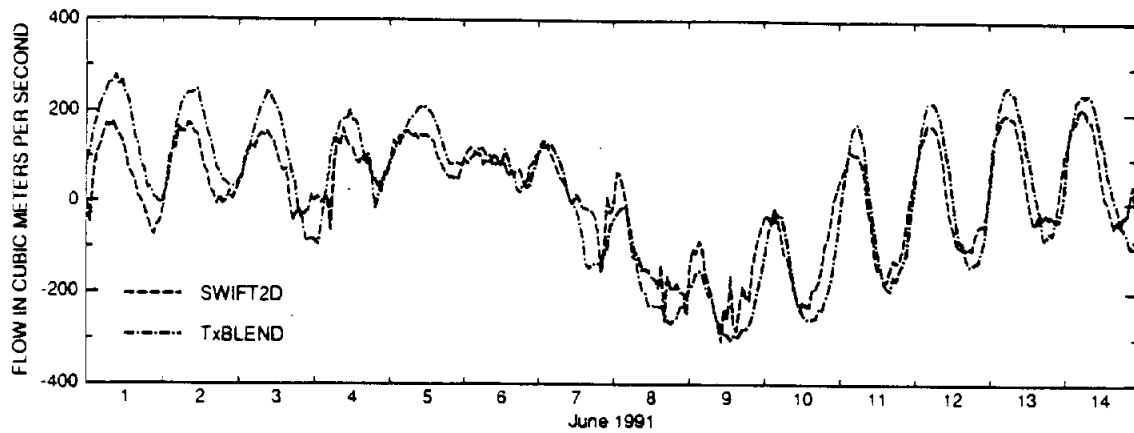


FIG. 68. Comparison of Flow at the GIWW at Corpus Christi Cross Section

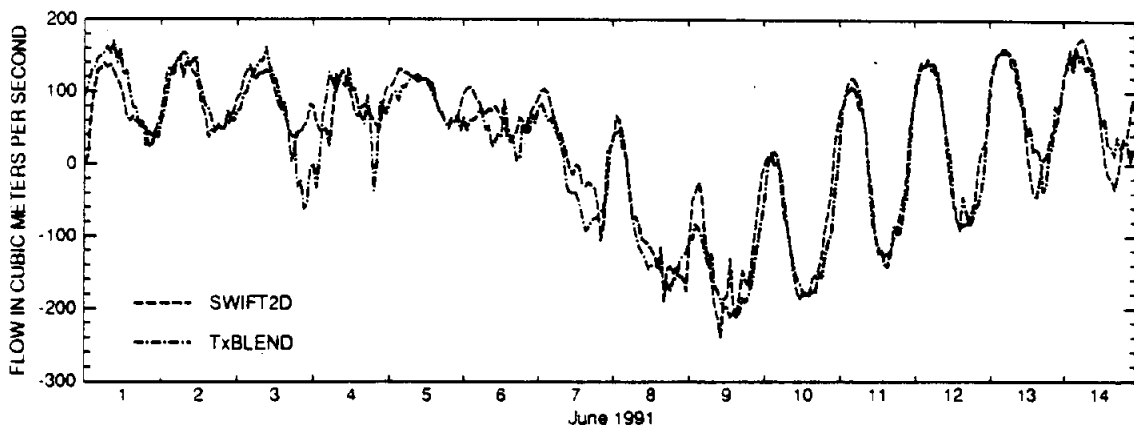


FIG. 69. Comparison of Flow at the Corpus Christi NAS Cross Section

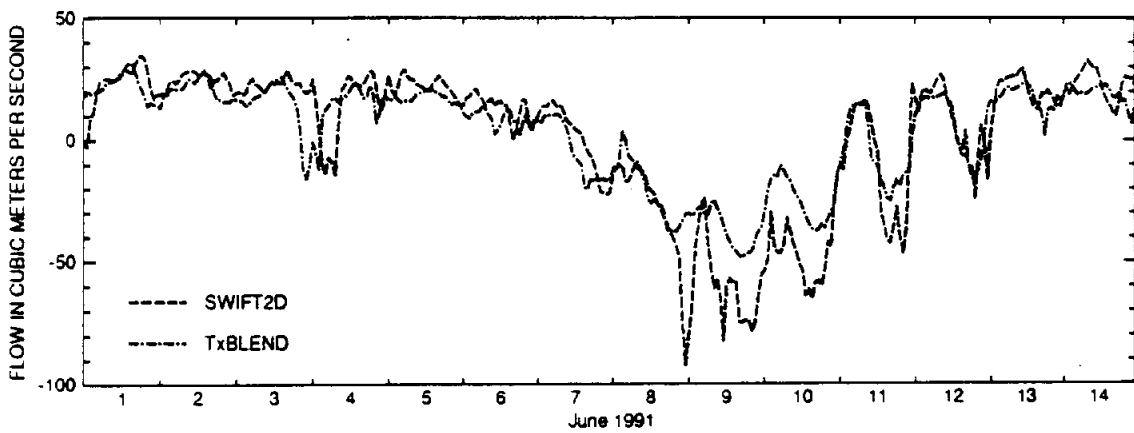


FIG. 70. Comparison of Flow at the Packery Channel Cross Section

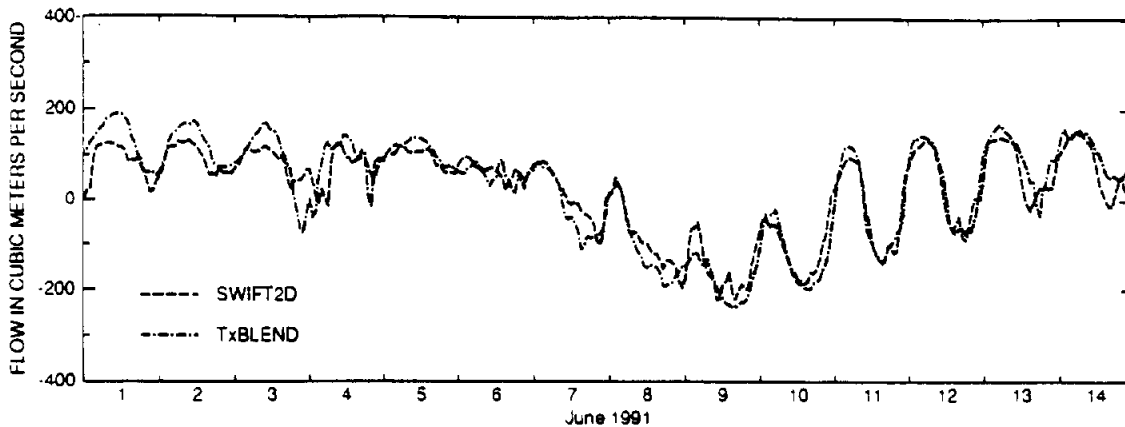


FIG. 71. Comparison of Flow at the Humble Channel Cross Section

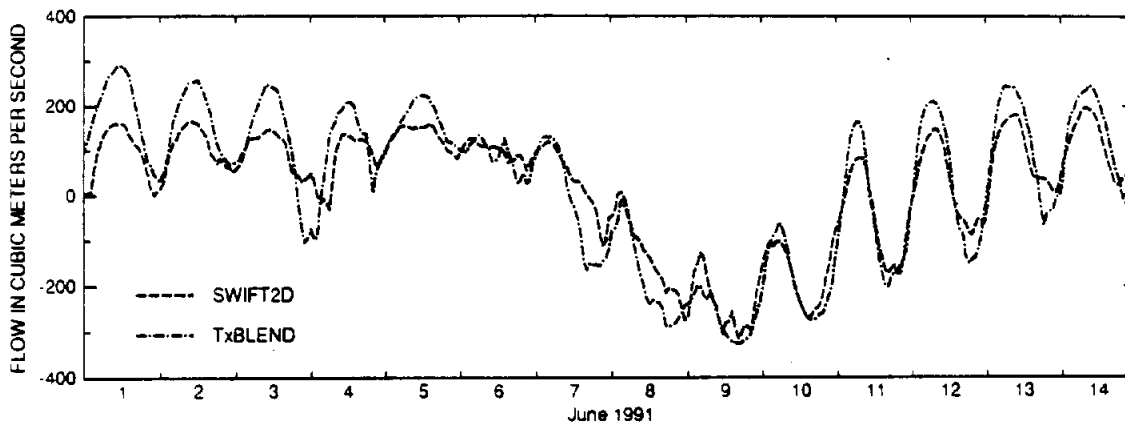


FIG. 72. Comparison of Flow at the GIWW at JFK Causeway Cross Section

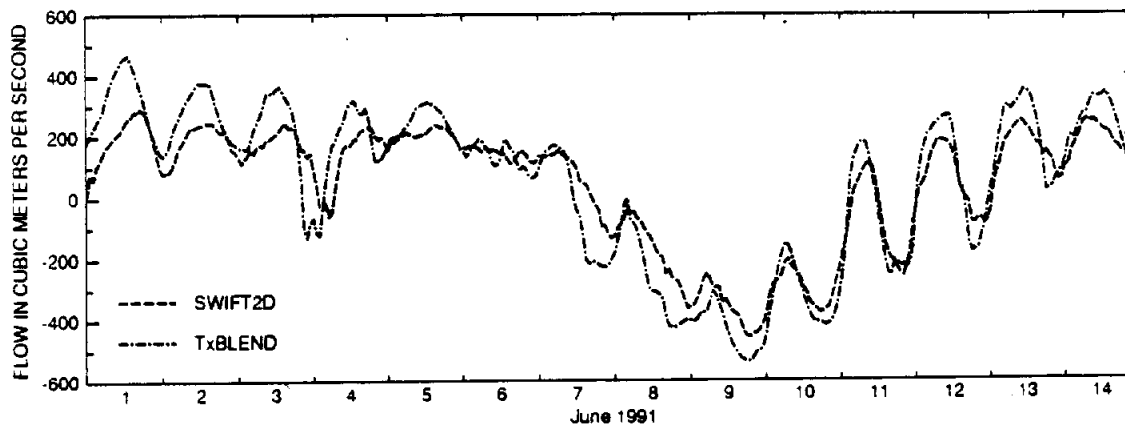


FIG. 73. Comparison of Flow at the Laguna Madre at Pta Island Cross Section

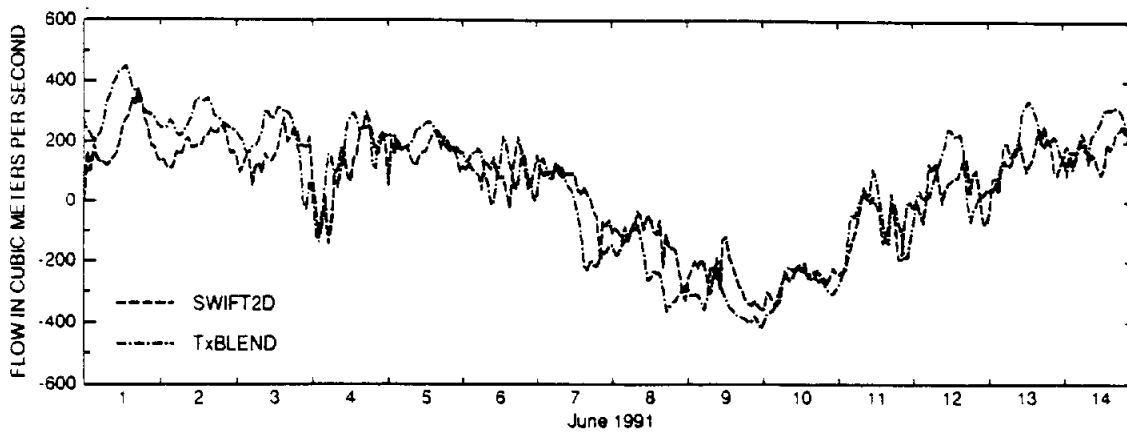


FIG. 74. Comparison of Flow at the Laguna Madre at South Bird Island Cross Section

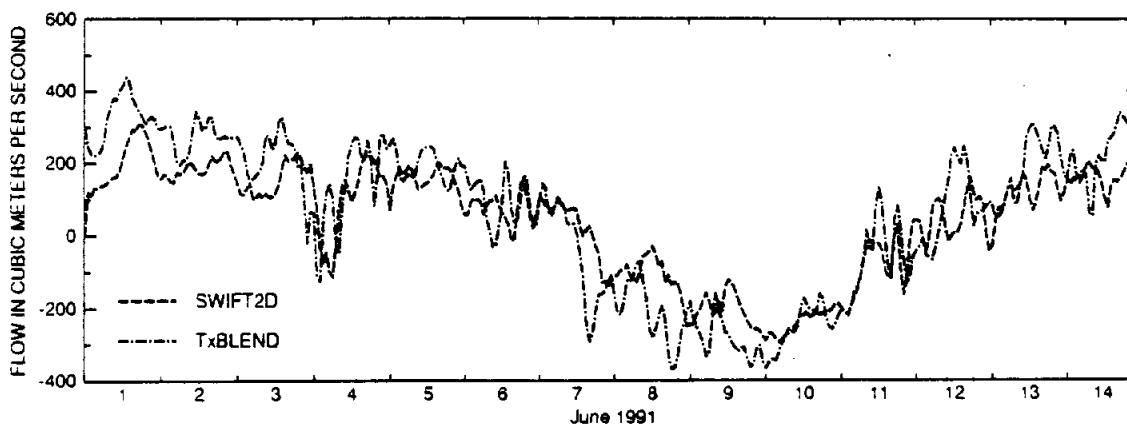


FIG. 75. Comparison of Flow at the Laguna Madre at Green Hill Cross Section

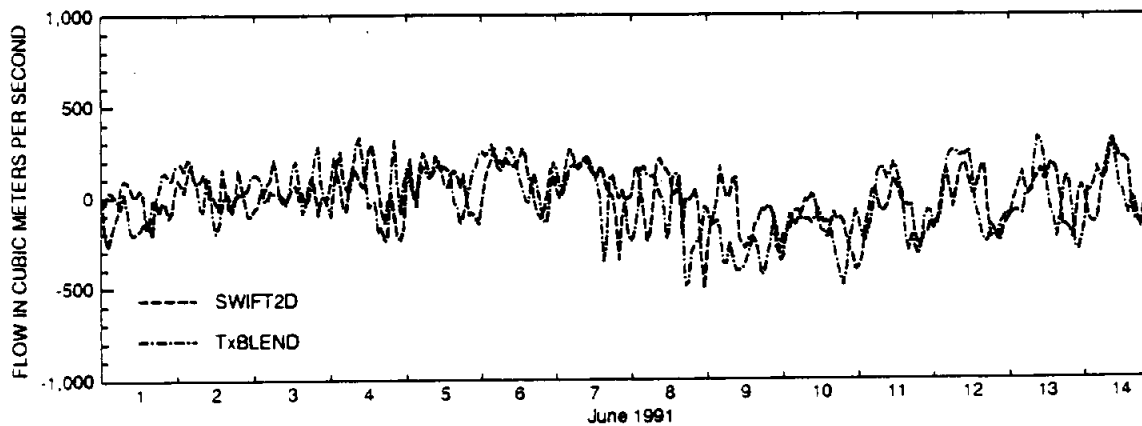


FIG. 76. Comparison of Flow at the Baffin Bay Cross Section

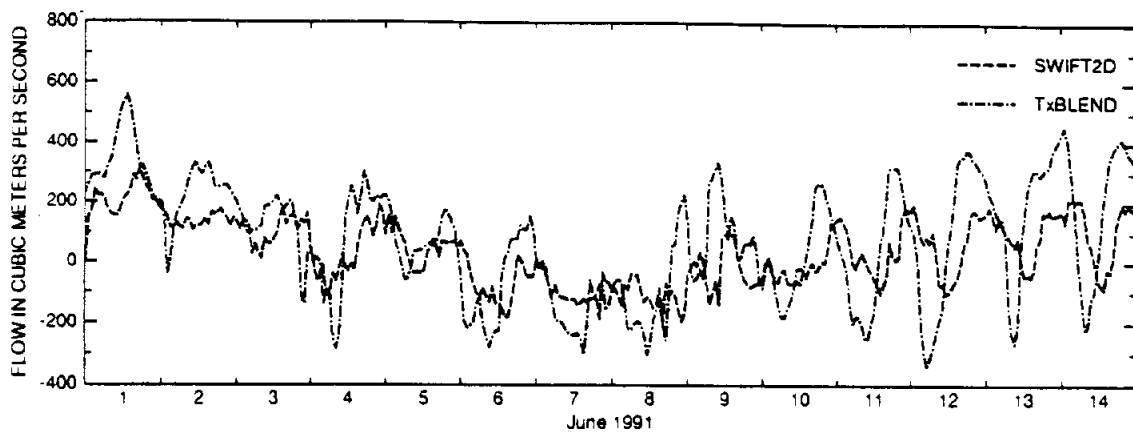


FIG. 77. Comparison of Flow at the Laguna Madre at Yarborough Pass Cross Section

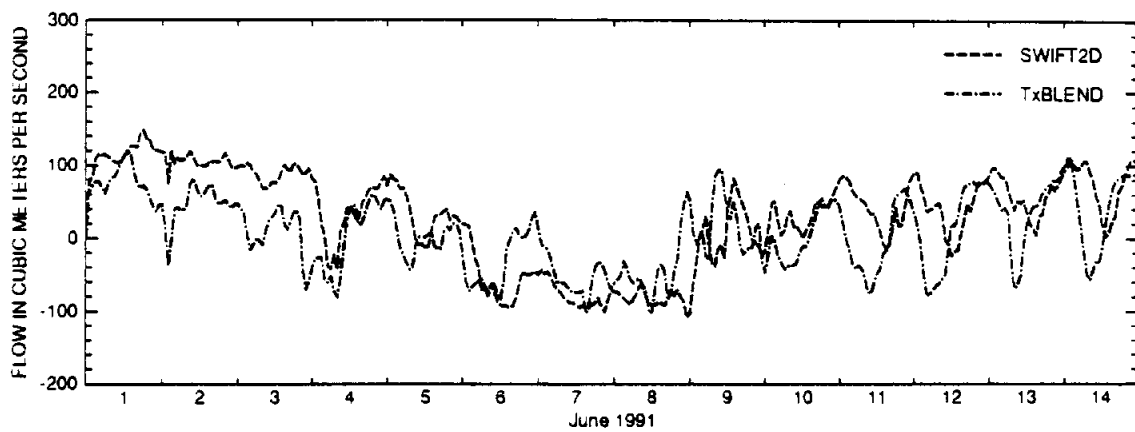


FIG. 78. Comparison of Flow at the Laguna Madre at North Land Cut Cross Section

The magnitudes of the SWIFT2D simulated flows are generally smaller than the corresponding TxBLEND flows. The discrepancy is probably attributable to the differences in the bathymetry of the two models. On average, the TxBLEND mesh is deeper, which would tend to produce larger flows. The RMSE's between the SWIFT2D and TxBLEND simulated flows are shown in Table 18. The largest differences were observed at the Yarborough Pass and North Land Cut cross sections. One contributing factor to the flow differences at the southern end of the upper Laguna Madre may have been the inclusion of the feature called "the Hole in the SWIFT2D model grid. The Hole, which is a shallow arm of the estuary with depths of less than two feet, was not included in the TxBLEND mesh. The Hole extends into the sand flats south of Yarborough Pass.

TABLE 18. Root Mean Squared Errors between SWIFT2D and TxBLEND Simulated Flows

Water Level Station	RMSE (cubic meters per second)
GIWW at Corpus Christi	62.4
Corpus Christi NAS	32.2
GIWW at the JFK Causeway	61.8
Humble Channel	38.6
Packery Channel	13.6
Pita Island	94.8
South Bird Island	100.4
Green Hill	104.8
Baffin Bay	177.2
Yarborough Pass	168.6
North Land Cut	58.5
Average	83.0

The six hour phase lag caused by the problems with the wind data in the models is even more apparent in the simulated flows than in the velocities. Once again, the effect is more noticeable at the southern cross sections which are strongly influenced by wind. Flows at the northern cross sections were dominated by the tidal signal and did not exhibit the phase lag.

Circulation Patterns

Velocity vector plots were used to evaluate the overall circulation patterns simulated by the SWIFT2D and TxBLEND models. Plots of velocity vectors simulated by the two models at periods of high tide, slack tide, and low tide are shown in Figs. 79 through 87. The high, low, and slack tide conditions are referenced to the tide at the Bob Hall Pier tide station (Gulf of Mexico tide). The corresponding high, low, and slack tides near the JFK Causeway are lagged two to three hours due to the travel time of the tide signal across Corpus Christi Bay. High tide occurred around 09:00 on June 10, while slack tide occurred around 18:00 on June 10, and low tide occurred around 00:00 on June 11. Figs. 81, 84, and 87 show the velocity vectors on an enlarged view of the SWIFT2D grid near the JFK Causeway area. The largest velocities were observed in the GIWW and in other, smaller channels near the JFK Causeway. Visual inspection of the velocity patterns simulated by the two models showed no major differences in the northern part of the estuary near the JFK Causeway. Flow into Baffin Bay in Figs. 82, 83, 85, and 86, however, appears to be lagged by six hours in the SWIFT2D model. This corresponds to the six hour lag discussed in conjunction with the simulated velocities and flows. A full set of velocity vector plots at three hour time intervals from 06:00 on June 10, to 12:00 on June 11, can be found in Appendix C.

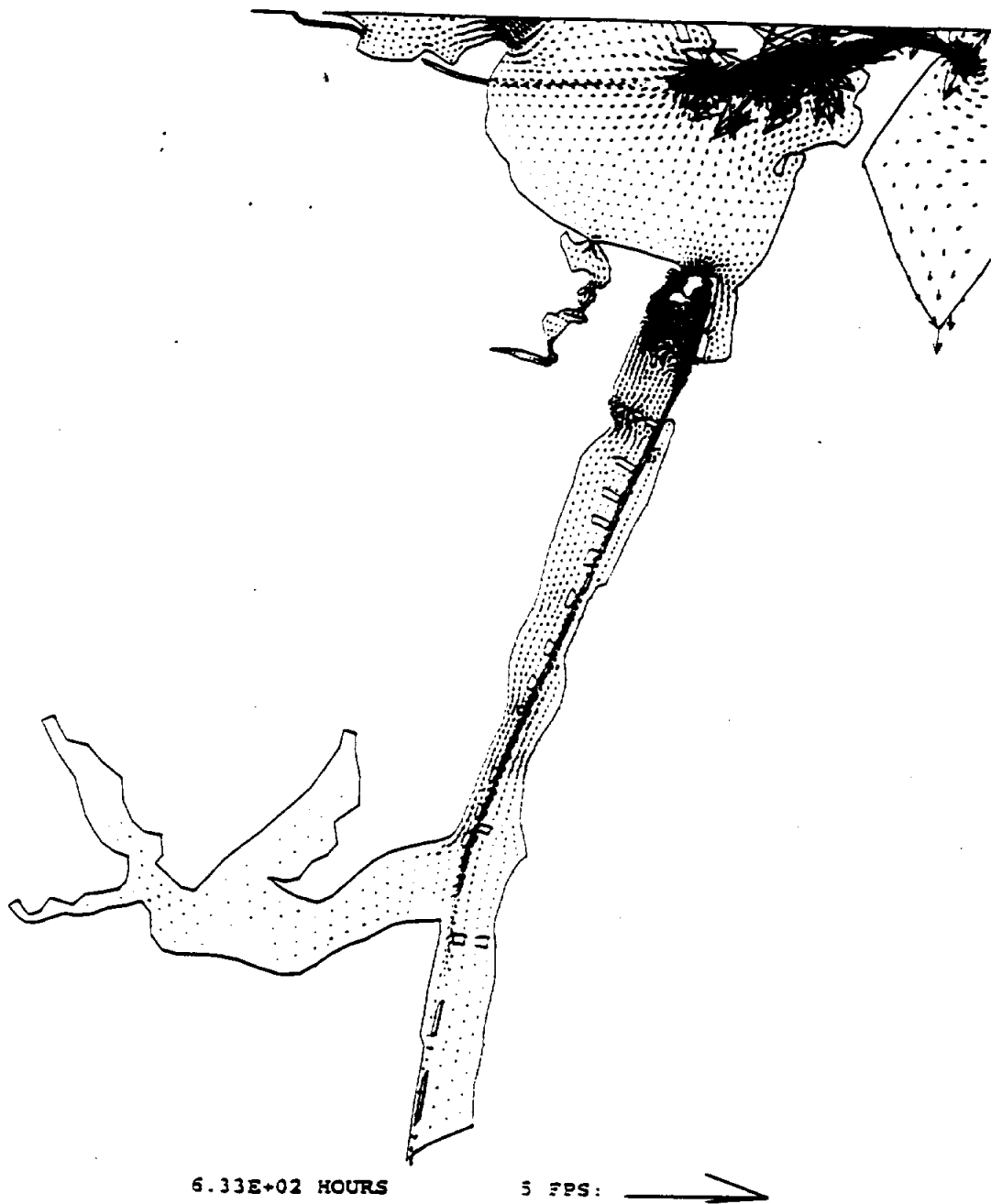


FIG. 79. TxBLEND Simulated Velocity Vectors, June 10, 09:00

VELOCITY AT TIME 13500 GRID SIZE 290 BY 401

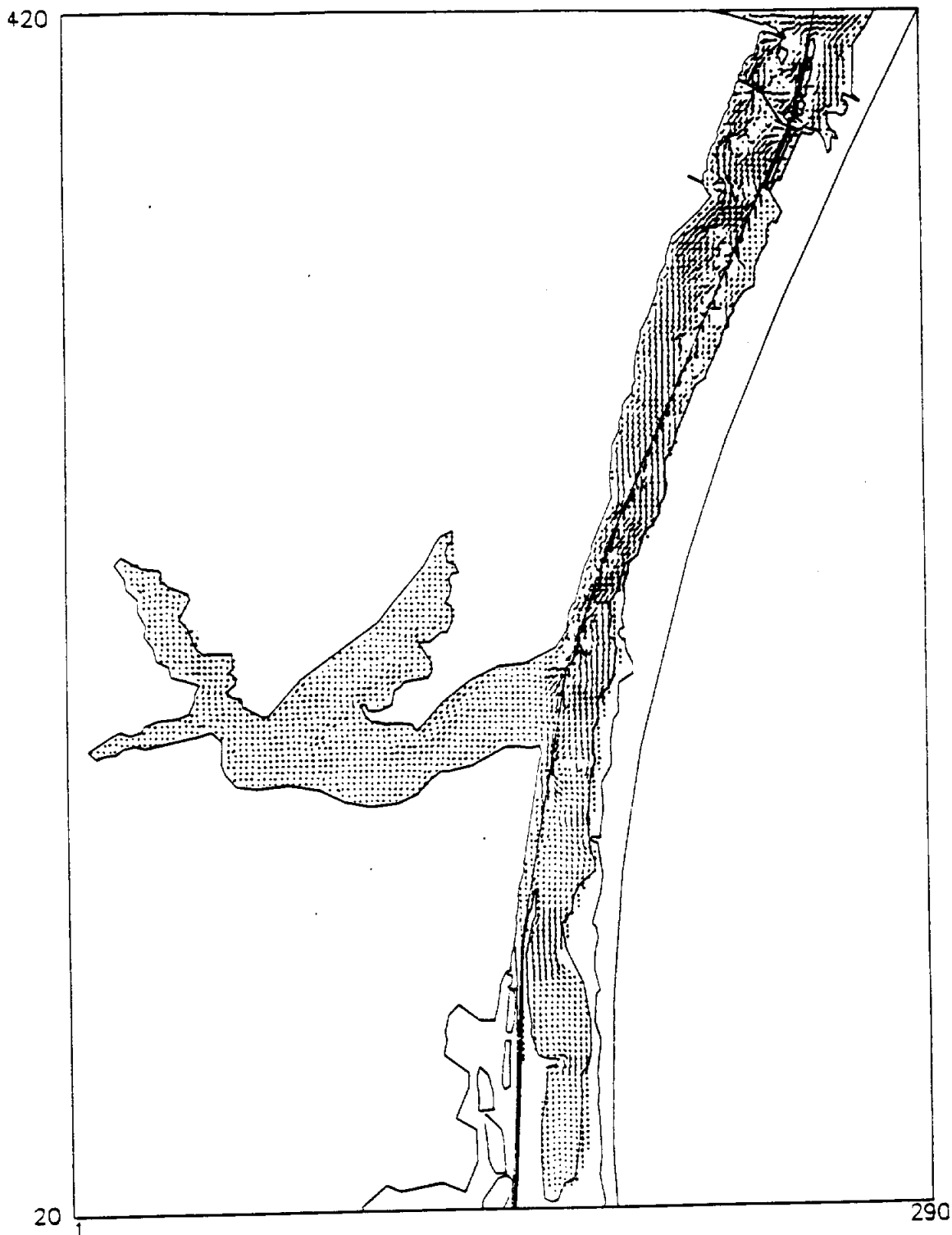


FIG. 80. SWIFT2D Simulated Velocity Vectors, June 10, 09:00

VELOCITY AT TIME 13500 GRID SIZE 76 BY 107

426

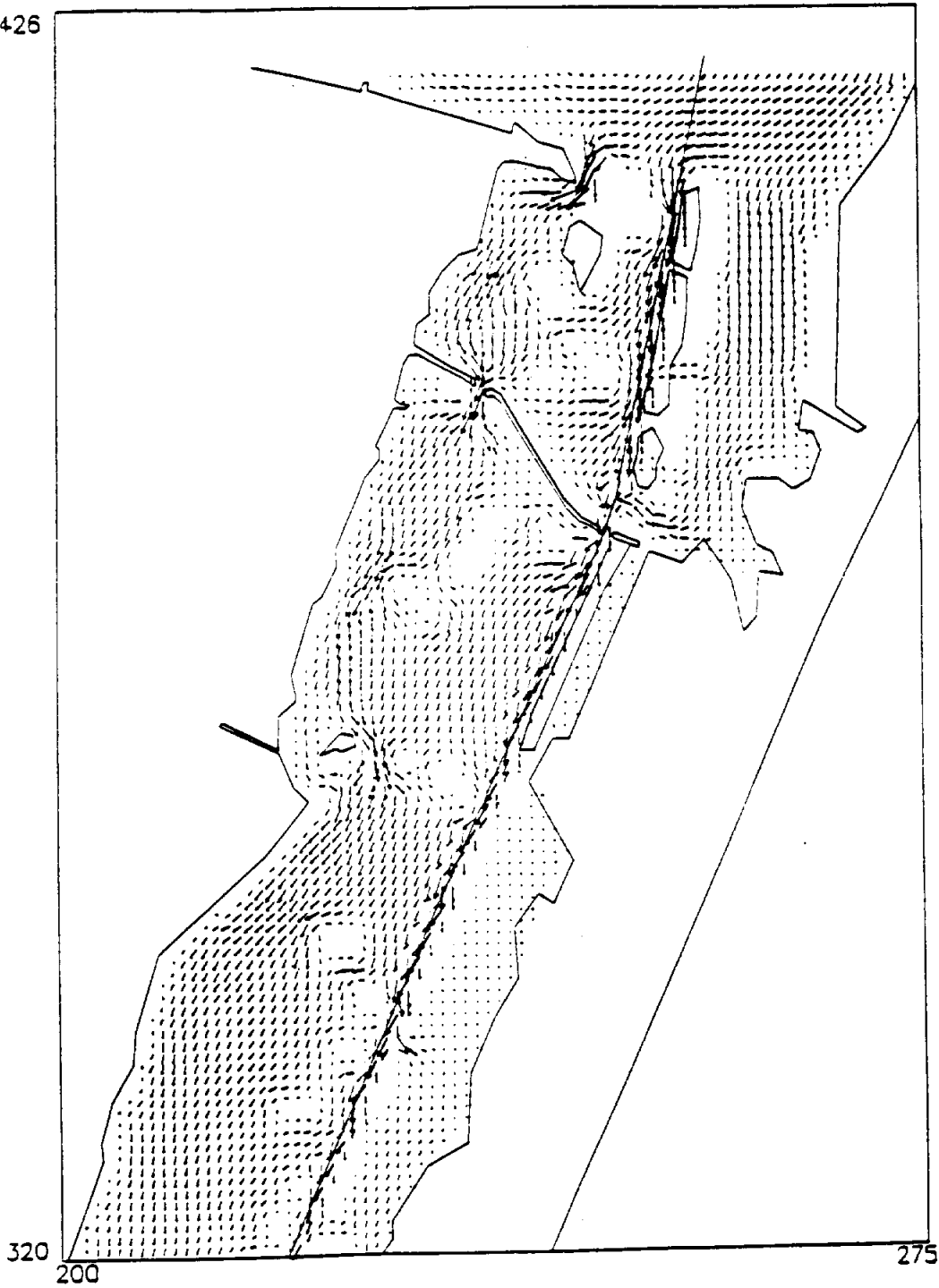


FIG. 81. SWIFT2D Simulated Velocity Vectors near the John F. Kennedy Causeway, June 10, 09:00

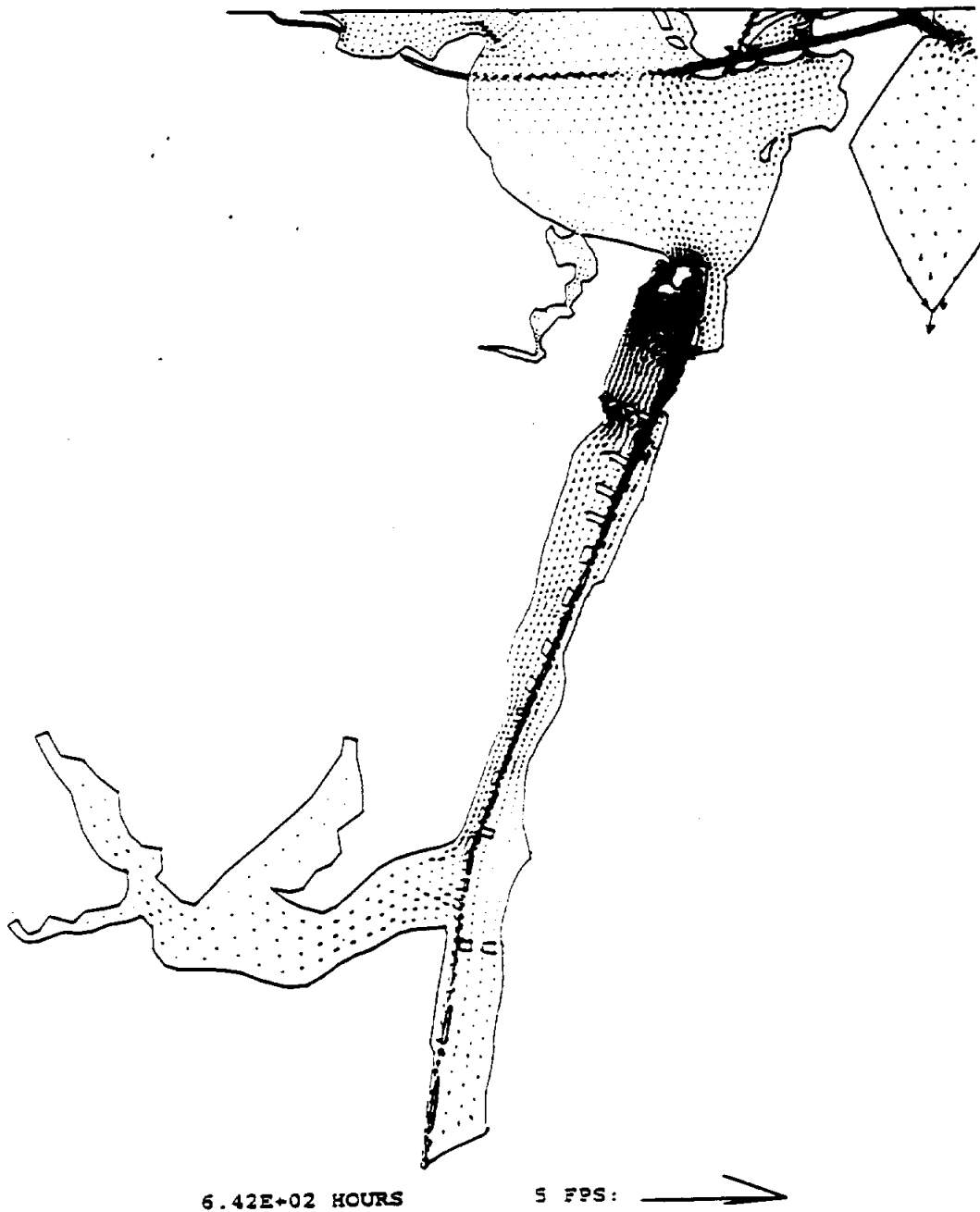


FIG. 82. TxBLEND Simulated Velocity Vectors, June 10, 18:00

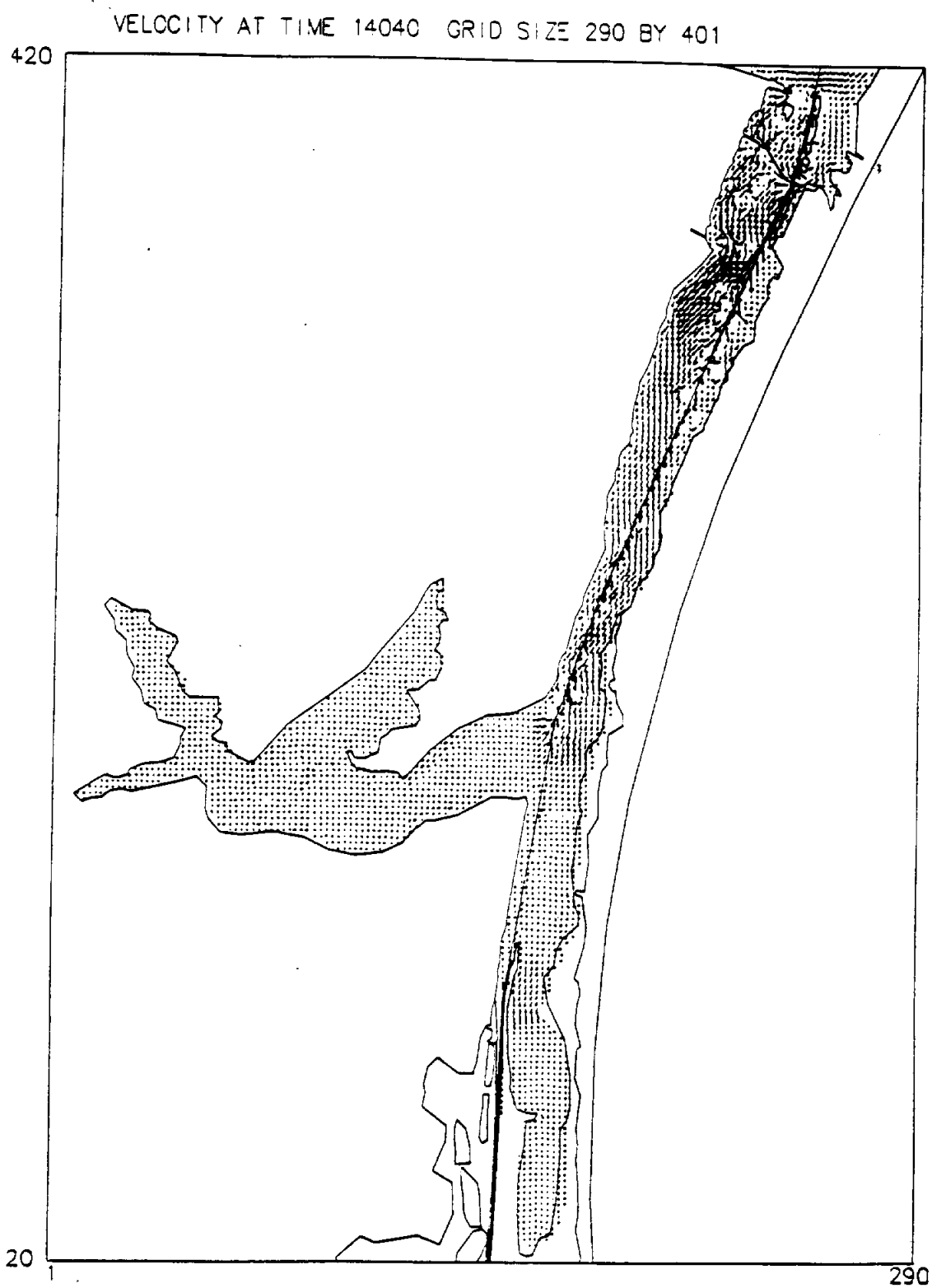


FIG. 83. SWIFT2D Simulated Velocity Vectors, June 10, 18:00

VELOCITY AT TIME 14040 GRID SIZE 76 BY 107

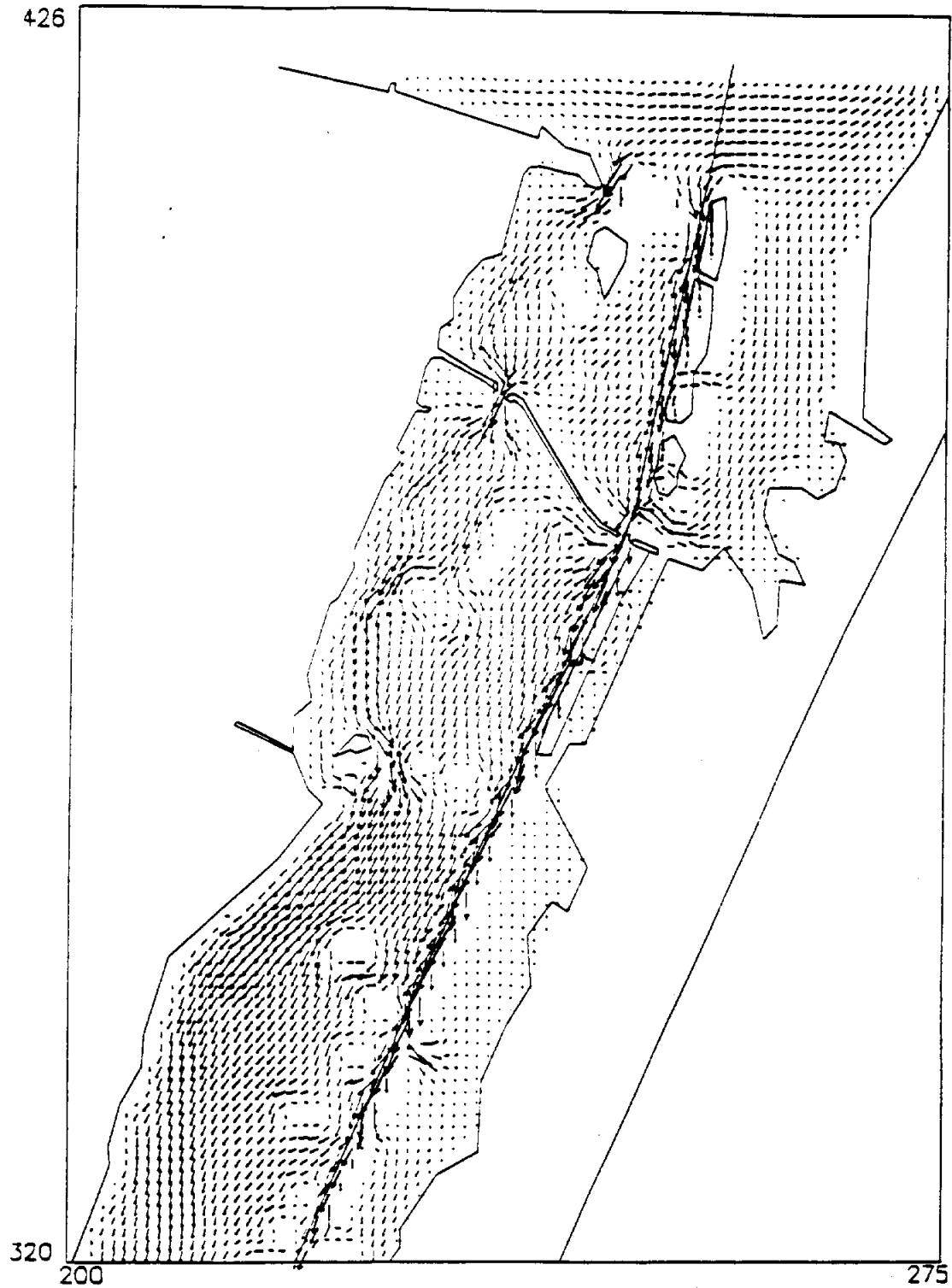


FIG. 84. SWIFT2D Simulated Velocity Vectors near the John F. Kennedy Causeway, June 10, 18:00

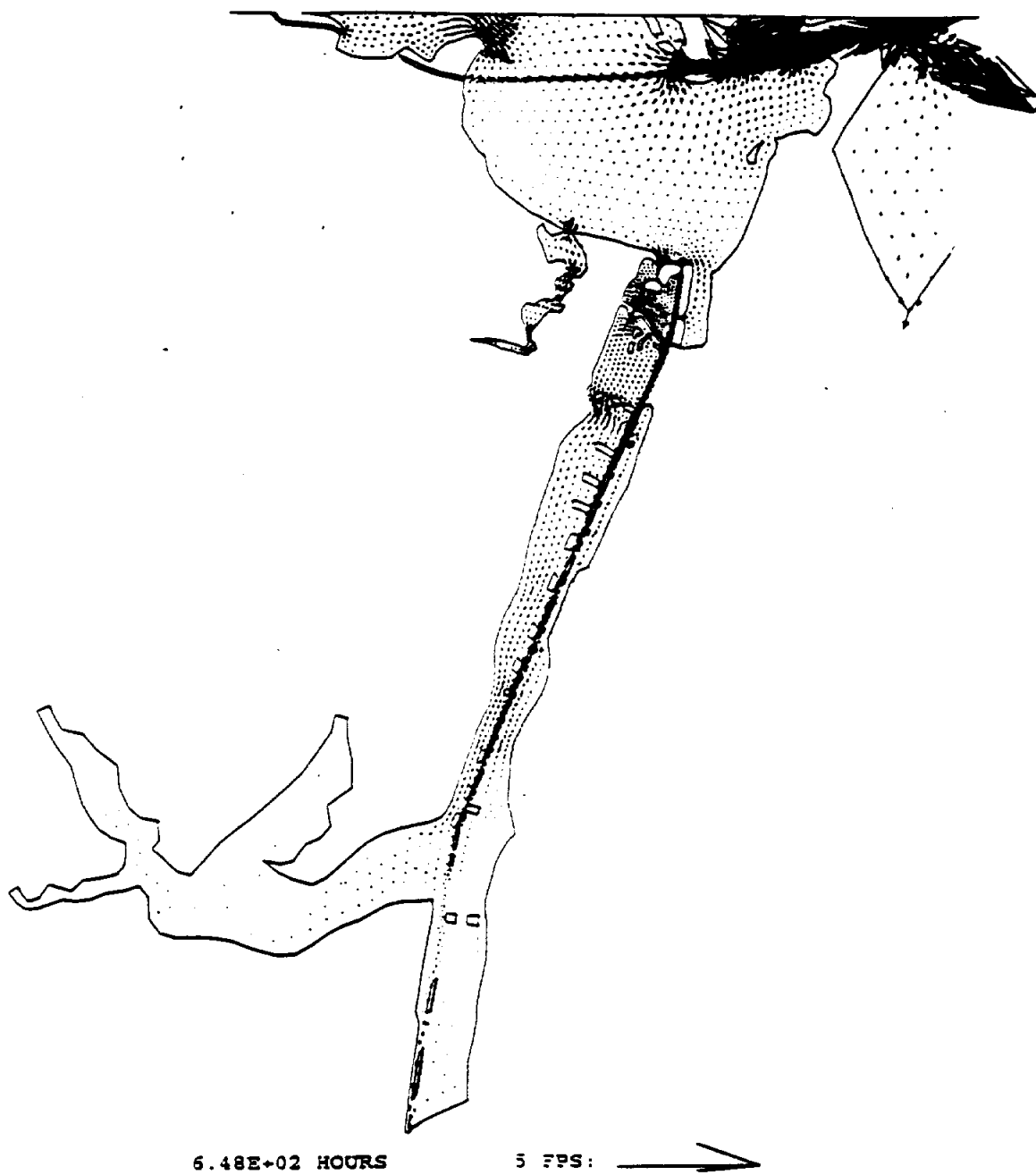


FIG. 85. TxBLEND Simulated Velocity Vectors, June 11, 00:00

VELOCITY AT TIME 14400 GRID SIZE 290 BY 401

420

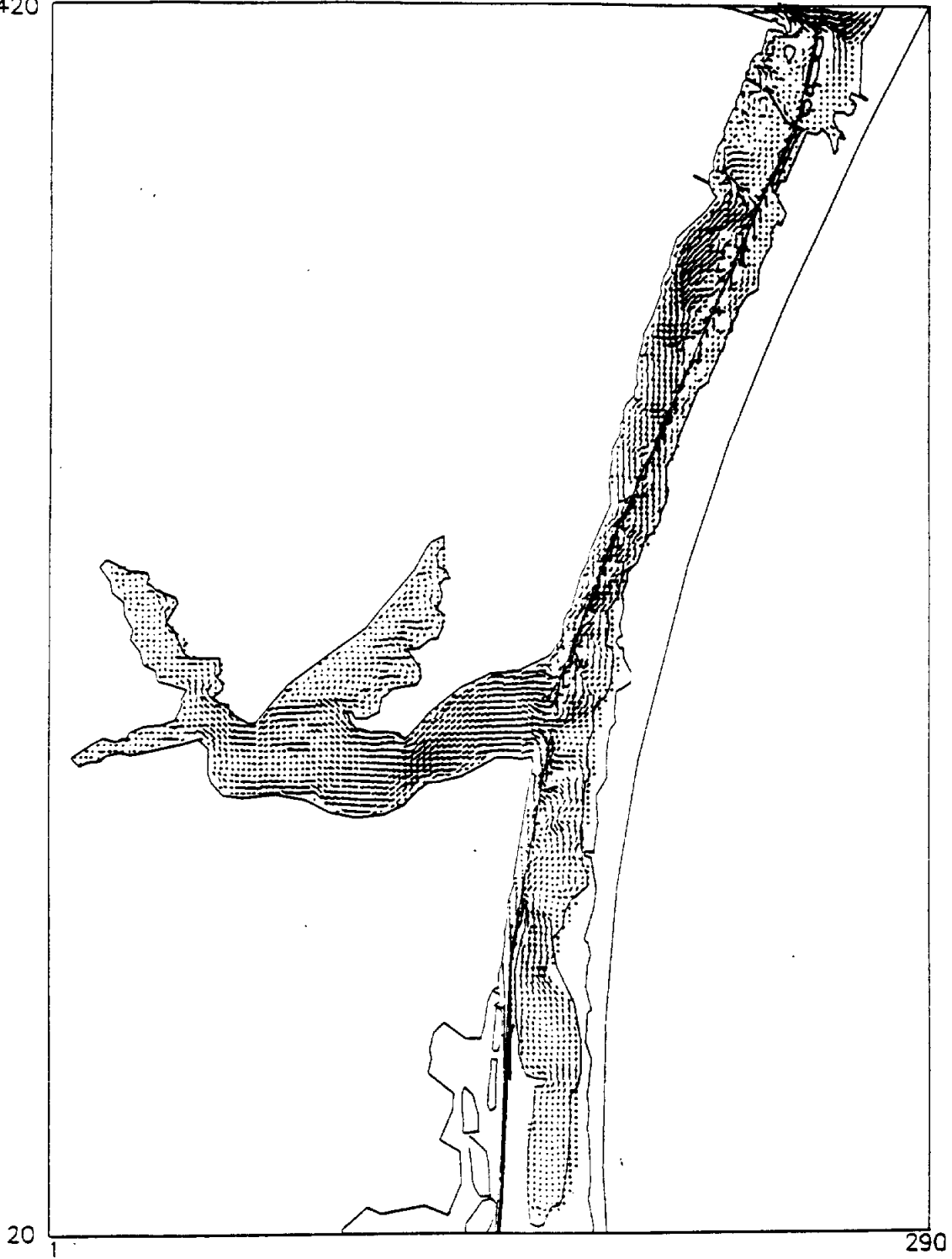


FIG. 86. SWIFT2D Simulated Velocity Vectors, June 11, 00:00

VELOCITY AT TIME 14400 GRID SIZE 76 BY 107

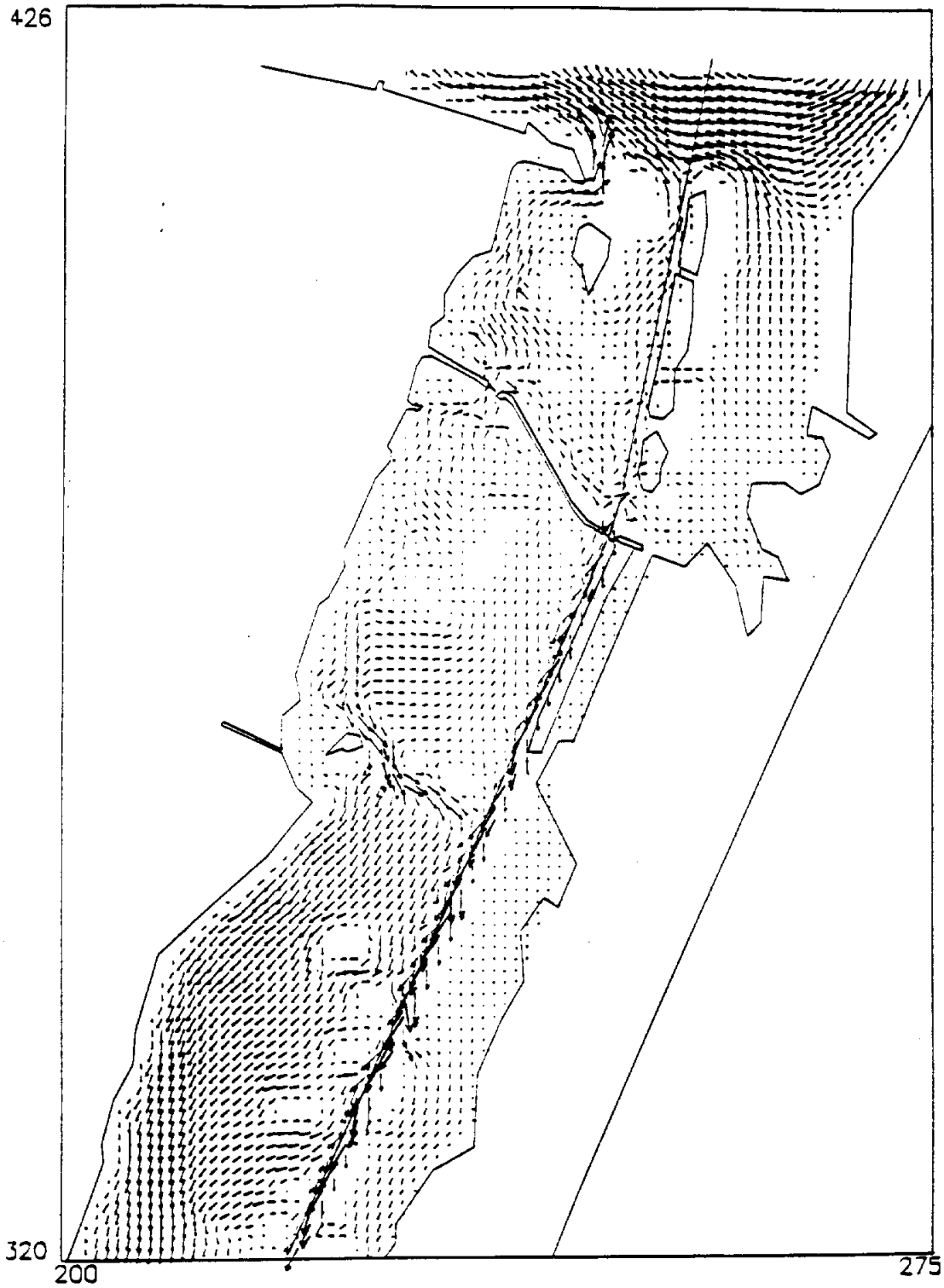


FIG. 87. SWIFT2D Simulated Velocity Vectors near the John F. Kennedy Causeway, June 11, 00:00

VII SUMMARY AND CONCLUSIONS

SUMMARY

The U.S. Geological Survey Surface Water Flow and Transport Model in Two-Dimensions (SWIFT2D) model was applied to the northern half of the Laguna Madre Estuary. SWIFT2D is a two-dimensional hydrodynamic and transport model for well-mixed estuaries, coastal embayments, harbors, lakes, rivers, and inland waterways. The model numerically solves finite difference forms of the vertically integrated equations of mass and momentum conservation in conjunction with transport equations for heat, salt, and constituent fluxes. The finite difference scheme in SWIFT2D is based on a spatial discretization of the water body as a grid of equal sized, square cells. The model includes the effects of wetting and drying, wind, inflows and return flows, flow barriers, and hydraulic structures.

The results of the SWIFT2D model were compared to results from an application of the TxBLEND model by Texas Water Development Board to the same part of the estuary. TxBLEND is a two-dimensional hydrodynamic model based on the finite element method. The model employs triangular elements with linear basis functions and solves the generalized wave continuity formulation of the shallow water equations. TxBLEND is an expanded version of the BLEND model to which the TWDB has added a number of important features. These features include the coupling of the density and momentum equations, the inclusion of evaporation and direct precipitation, and the addition tributary inflows. The TxBLEND model simulations discussed in this study were performed by personnel at the TWDB.

The SWIFT2D finite difference grid was developed using the raster based capabilities of a Geographic Information System (GIS). The bathymetry data used in both the SWIFT2D model and the TxBLEND model was derived from the set of National Ocean Service nautical charts which cover the Laguna Madre area. The bathymetry data was digitized into the GIS and used to create the SWIFT2D grid. A newer and more extensive set of hydrographic survey data became available during the study, however, the new data was not used in order to maintain consistency between the two models. The SWIFT2D computational grid contained approximately 15,000 cells, while the TxBLEND finite element mesh was comprised of 8,187 triangular elements. The TxBLEND mesh included the Corpus Christi and Copano Bay systems in addition to the upper Laguna Madre.

The two models were calibrated to a June 1991 data set from a TWDB intensive inflow survey of the Laguna Madre. Velocity and water quality data were available for the three days of the survey. Tide data for a much longer period were available from TCOON network stations. Results of the two models were compared at seven tide stations, eight velocity stations, and eleven flow cross sections.

The simulated results were generally in good agreement with observed data and between models. Calculations of RMSE's and time series plots were used to determine the quality of the model calibration.

CONCLUSIONS

The SWIFT2D and TxBLEND models offer substantially different approaches to the problem of hydrodynamic modeling in shallow estuaries. The contrasting characteristics of the models led to a several conclusions.

1. Despite the major differences in solution schemes applied by the two models, both do an adequate job of reproducing the observed water level, velocity, and flow patterns in the Laguna Madre Estuary. The errors between simulated and observed water levels were very similar at the tide stations in the northern portion of the upper Laguna Madre. SWIFT2D provided smaller errors between simulated and observed water levels at the stations south of Bird Island. These stations appeared to be strongly affected by the presence of wind. SWIFT2D more accurately simulated the large daily variations in water level caused by wind, however, subsequent adjustments of the wind stress parameter in the TxBLEND model may improve results. The simulated velocities followed the same pattern observed in the water levels. Both models produced equivalent results at the velocity stations nearest the Corpus Christi NAS driving tide. Velocities at the southern stations were small and, therefore, difficult to compare. The largest discrepancies between the two models were observed in the simulated flows. The magnitude of flows simulated by SWIFT2D were consistently smaller than those simulated by TxBLEND. The differences were probably the result of the representation of the bathymetry in the two models. The coarse grid size used in the SWIFT2D model did not allow an accurate representation of the true shape of channels.

2. Wind was observed to have a dominant effect on conditions in much of the upper Laguna Madre. High frequency (diurnal or shorter) oscillations in water level in the southern portion of the upper Laguna Madre are almost completely due to wind. Comparisons between SWIFT2D model runs with large and negligible wind stress coefficients illustrated the influence of wind on the circulation patterns. Variations in water levels at the Yarrowborough Pass and Riviera Beach tide stations simulated without the presence of wind were driven by low frequency oscillations, which could possibly represent the lunar tidal cycle. Water levels at the stations nearest the JFK Causeway were more dependent of the daily tidal cycle in the Gulf of Mexico. Simulated velocities at stations south to the GIWW at Marker 199 station were essentially zero. The single wind station used in the simulation appears to be

sufficient for atmospheric driving, however, the use of additional sites with the wind input grid option in SWIFT2D might produce even more accurate results.

3. The unusual characteristics of the Laguna Madre stretched the capabilities of the SWIFT2D model. The limitation of a fixed cell size forced the use of an excessive number of computational cells in order to accurately simulate the GIWW. A grid size on the order of 50 meters would be required to more accurately represent the channels. Such a grid size would force unacceptable simulation times. The ability to vary the element size in the TxBLEND mesh allows for a more efficient representation of actual bathymetry. Small elements were used in the vicinity of the GIWW and other channels, while larger elements were used to represent areas with constant depths. The TWDB was able to simulate the entire Corpus Christi Bay and upper Laguna Madre Estuary system with fewer elements than were required for simulation of the upper Laguna Madre alone with SWIFT2D. The possibility of adding routines to SWIFT2D to allow variable cell sizes should be explored if the model is to be used for other systems with areas on the order of that of the Laguna Madre. Currently, the model is applicable to smaller systems or systems where small features such as the GIWW are not dominant.

4. The TxBLEND model provided several computational advantages over the SWIFT2D model. The flexibility of the finite element mesh resulted in a much smaller number of computational cells than the finite difference mesh. A simulation of the entire upper Laguna Madre, Corpus Christi Bay, and Copano Bay system for a period of one month takes approximately 2.5 hours (5 minute time step) on a Sun SPARCstation 20. A SWIFT2D simulation (200 meter grid size) for a period of one month on the upper Laguna Madre alone takes approximately 4.6 hours (6 minute time step) on a DG AViiON 8500 dual cpu server. The difference in platforms does not account for the for the longer run times with SWIFT2D.

5. The ADI effect was observed to reduce the accuracy of the SWIFT2D simulations at large time step. The stair step nature of the finite difference grid representation of channels appears to cause much of the error associated with the ADI effect. The large number of spoil islands in the Laguna Madre could also have contributed to the errors.

6. The SWIFT2D results could potentially be improved with additional adjustment of the roughness coefficient. The roughness coefficient, in addition to the time step and wind stress, exerted the greatest influence of any of the model parameters on the simulated results.

7. The influence of wetting and drying was not extensively investigated in the current study, however, a simple comparison of the number of cells which flooded and dried indicated potentially significant effects. A large number of cells along the southern and eastern tidal margins were subject to wetting and drying. The influence of wind was found to have the largest impact on the number of cells subject to flooding and drying during the simulation.

RECOMMENDATIONS FOR FUTURE STUDY

1. Evaporation and direct precipitation are important considerations, especially in the Laguna Madre Estuary. The Laguna Madre is subject to large evaporation rates, which are the primary cause of the hypersaline nature of the estuary. In contrast to evaporation, direct precipitation accounts for more than half of the freshwater inflow to the estuary. These source and sink terms are included in the TxBLEND model. The addition of these terms to the SWIFT2D model would be fairly simple and probably should be done if the model is to be used for salinity modeling of the Laguna Madre. The addition of evaporation and precipitation terms would improve the ability of the SWIFT2D model for any future applications to estuaries in warm climates with small freshwater inflows.

2. Data from the hydrographic survey of the Laguna Madre completed in 1995 offers an order of magnitude increase in the number of depths points. The coverage of the new data extends to the shallow eastern side of the estuary where information is almost non-existent on the nautical charts. The use of the newer data would eliminate many of the assumptions and much of the manual editing which can lead to substantial differences between grids and meshes developed by different parties. Comparisons should be made between the models with bathymetry defined by the nautical charts and by the newer hydrographic survey. The ability of both models to accurately simulate observed conditions should improve with the addition of the new data.

REFERENCES

- Akanbi, A.A., and Katopodes, N.D. (1988). "Model for flood propagation on initially dry land." *J. Hydraulic Engrg.*, ASCE, 114(7), 689-706.
- ARC/INFO User's Guide 6.0: Cell-based Modeling with GRID. (1991a). Environmental Systems Research Institute, Inc., Redlands, CA.
- ARC/INFO User's Guide 6.0: Surface Modeling with TIN. (1991b). Environmental Systems Research Institute, Inc., Redlands, CA.
- Austria, P.M., and Aldama, A.A. (1990). "Adaptive mesh scheme for free surface flows with moving boundaries." *Proc. of the Eighth Int. Conf. On Comp. Methods in Water Resources*, ed. By G. Gambolati, A. Rinaldo, C.A. Brebbia, W.G. Gray, and G.F. Pinder, Springer-Verlag, Berlin, 455-460.
- Bales, J.D. (1990). "Data collection program for Pamlico River estuary model calibration and verification." *Proc. International Estuarine and Coastal Modeling Conf.*, Spaulding, M.L., ed., ASCE, New York, NY, 492-501.
- Bales, J.D., and Douglas, J.M. (1991). "Application of a geographic information system to estuarine hydrodynamic modeling." *Proc., National Conference on Hydraulic Engineering*, ASCE, New York, NY, 870-875.
- Brown, C.A., Militello, A. and Kraus, N.C. (1995). "Hydrodynamic assessment for elevation of the J.F.K. Causeway, Corpus Christi, Texas." *TAMU-CC-CBI-95-07*, Center for Coastal Studies, Texas A&M University-Corpus Christi, Corpus Christi, TX.
- Bureau, J.R., and Chang, R.T. (1989). "A general method for generating bathymetric data for hydrodynamic computer models." U.S. Geological Survey Open-File Report 89-28, 45p.
- Cartwright, G. (1996). "Eerie canal." *Texas Monthly*, 83-89; 104-106.
- Casulli, V., and Cheng, R.T. (1990). "Stability analysis of Eulerian-Lagrangian methods for the one-dimensional shallow water equations." *Appl. Math. Modeling*, 14(3), 122-131.
- Duke, J.H. (1990). "Upper Laguna Madre modeling study in the vicinity of the John F. Kennedy Causeway, Corpus Christi, Texas." Report for Texas General Land Office, Austin, TX.
- Giese, G.L. and Bales, J. D. (1992). "Two-dimensional circulation modeling of the Pamlico River Estuary, North Carolina." *Proc. 2nd International Estuarine and Coastal Modeling Conf.*, Spaulding, M. L., ed., ASCE, New York, NY, 607-619.
- Gray, W.G. (1987). "Fast linear element explicit in time triangular finite element models for tidal circulation: User's manual." University of Notre Dame, Notre Dame, IN, 39 p.

- Grenier, R.R., Jr., Luettich, R.A., Jr., and Westerink, J.J. (1993). "Comparison of 2d and 3d models for computing shallow water tides in a friction dominated tidal embayment." *Proc. 3rd International Estuarine and Coastal Modeling Conf.*, ASCE, New York, NY, 58-70.
- Jeffress, G., Michaud, P., Thurlow, C. and Aston, L. (1995). "The Texas coastal ocean observation network." *Proc., Texas Water '95*, Texas Section ASCE, Austin, TX, 53-60.
- Jenter, H.L., and Signell, R.P. (1992). "NetCDF: A public-domain-software solution to data-access problems for numerical modelers." *Proc. 2nd International Estuarine and Coastal Modeling Conf.*, ASCE, New York, NY, 72-82.
- Jones, N.L. and Richards, D.R. (1992) "Mesh generation for estuarine flow modeling." *J. Wtrwy., Port, Coast., and Oc. Div.*, ASCE, 120(6), 599-613.
- Kinnmark, I.P.E. and Gray, W.G. (1984). "An implicit wave equation model for the shallow water equations." *Advances in Water Resources*, 7(4), 168-171.
- Kjerfve, B., Ed. (1987). *Hydrodynamics of Estuaries, Volume II, Estuarine Case Studies*, CRC Press, Boca Raton, FL.
- Lee, J.K., Schaffranek, R.W. and Baltzer, R.A. (1994). "Simulating effects of highway embankments on estuarine circulation." *J. Wtrwy., Port, Coast., and Oc. Div.*, ASCE, 120(3), 199-218.
- Leendertse, J.J. (1987). "Aspects of SIMSYS2D, A system for two-dimensional flow computation." R-3572-USGS, RAND Corp., Santa Monica, CA, 80 p.
- Longley, W.L. ed. (1994). *Freshwater inflows to Texas estuaries: Ecological relationships and methods for the determination of needs*. Texas Water Development Board, Austin, TX, 386 p.
- Luettich, R.A. Jr., Westerink, J.J., and Scheffner, N.W. (1992). "ADCIRC: An advanced three-dimensional circulation model of shelves, coasts and estuaries, Report I: Theory and Methodology of ADCIRC-2DDI and ADCIRC-3DL", DRP Technical Report, U.S. Army Corps of Engineers Waterways Experiment Station, Vicksburg, MS.
- Lynch, D.R. and Gray, W.G. (1979). "A wave equation model for finite element tidal computations." *Computers and Fluids*, 7, 207-228.
- Masch, F.D. and Associates. (1971). "Tidal hydrodynamic and salinity models for the San Antonio & Matagorda Bays, Texas." [333.9/M37T], Report to the Texas Water Development Board. Austin, TX, 130p.
- Matsumoto, J. (1991). "Simulation analysis of changes in flow exchange in the upper Laguna Madre with removal of portions of the John F. Kennedy Causeway. Part II. Study of the opening of the John F. Kennedy Causeway." Report for Texas General Land Office, Asset Management Program, Austin, TX.

- Matsumoto, J. (1992). "Mathematical description of the FETEX model based on a generalized finite difference method." *Proc. IX International Conference on Computational Methods in Water Resources*, Elsevier, New York, NY, (1) 299-305.
- Matsumoto, J. (1993). "User's manual for the Texas Water Development Board's hydrodynamic and salinity model: TxBLEND." Texas Water Development Board, Austin, TX, unpublished, 142 p.
- Militello, A. and Kraus, N.C. (1994). "Reconnaissance investigation of the current and sediment movement in the lower Laguna Madre between Port Isabel and Port Mansfield, Texas." *TAMU-CC-CBI-94-04*, Center for Coastal Studies, Texas A&M University-Corpus Christi, Corpus Christi, TX, 39 p.
- Navon, I.M., and deVillers, R. (1987). "The application of the Turkel-Zwas explicit large time-step scheme to a hemispheric barotropic model with constraint restoration." *Mon. Weather Rev.*, 115(5), 1036-1051.
- Regan, R.S. and Schaffranek, R.W. (1993). "Users Manual: SWIFT2D - - A computer program for simulating two-dimensional, surface water flow and transport for well-mixed estuaries, coastal seas and inland waterways." U.S. Geological Survey Water-Resources Investigations Report, unpublished, 136 p.
- Schaffranek, R.W. (1986). "Hydrodynamic simulation of the upper Potomac Estuary." *Proc., Water Forum '86: World Water Issues in Evolution*, ASCE, New York, NY, Vol. II, 1572-1581.
- Sheng, Y.P., Lee, H.K., and Wang, K.H. (1990). "On numerical strategies of estuarine and coastal modeling." *Proc. International Estuarine and Coastal Modeling Conf.*, Spaulding, M.L., ed., ASCE, New York, NY, 492-501.
- Siden, G.L.D., and Lynch, D.R. (1988). "Wave equation hydrodynamics on deforming elements." *Int. J. Num. Meth. in Fluids*, 8, 1071-1093.
- Solis, R.S. (1991). "Simulation analysis of changes in flow exchange in the upper Laguna Madre with removal of portion of the John F. Kennedy Causeway. Part 1. Identification and analysis of problems with model runs for the Texas General Land Office." Report for Texas General Land Office, Asset Management Program, Austin, TX.
- Stelling, G.S., Wiersma, A.K., and Willemse, J.M.T.M. (1986). "Practical aspects of accurate tidal computations." *J. of Hydraulic Engineering*, ASCE, 112(9), 802-817.
- Texas Department of Water Resources. (1983). "Laguna Madre estuary: a study of the influence of freshwater inflows." *LP-182*, Austin, TX. 265 p.
- U.S. Department of Commerce, National Ocean Service, "Texas, Intracoastal Waterway, Laguna Madre, Chubby Island to Stover Point, including the Arroyo Colorado." Nautical Chart 11303, Edition 17, Washington DC, August, 1992.

- U.S. Department of Commerce, National Ocean Service, "Texas, Intracoastal Waterway, Laguna Madre, Stover Point to Port Brownsville, including Brazos Santiago Pass." Nautical Chart 11303, Edition 24, Washington DC, March 19, 1994.
- U.S. Department of Commerce, National Ocean Service, "Texas, Intracoastal Waterway, Redfish Bay to Middle Ground, including Baffin Bay." Nautical Chart 11308, Edition 18, Washington DC, April 16, 1994.
- U.S. Department of Commerce, National Ocean Service, "Texas Intracoastal Waterway, Carlos Bay to Redfish Bay including Copano Bay." Nautical Chart 11314, Edition 18, Washington DC, July, 1994.
- U.S. Department of Commerce, National Ocean Service, "Texas, Intracoastal Waterway, Laguna Madre, Middle Ground to Chubby Island." Nautical Chart 11306, Edition 18, Washington DC, October 15, 1994.
- Westerink, J.J., and Gray, W.G. (1991). "Progress in surface water modeling." *U.S. National Report to International Union of Geodesy and Geophysics 1987-1990, Reviews of Geophysics, Supplement*, American Geophysical Union, 210-217.

APPENDIX A

SENSITIVITY ANALYSIS

EFFECT OF CHANGES IN THE TIME STEP ON SWIFT2D SIMULATION RESULTS

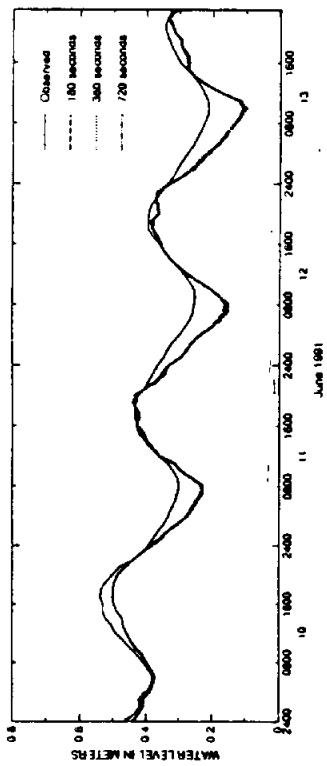


FIG. A-1: Differences in Water Levels Due to the Time Step, Peckery Channel

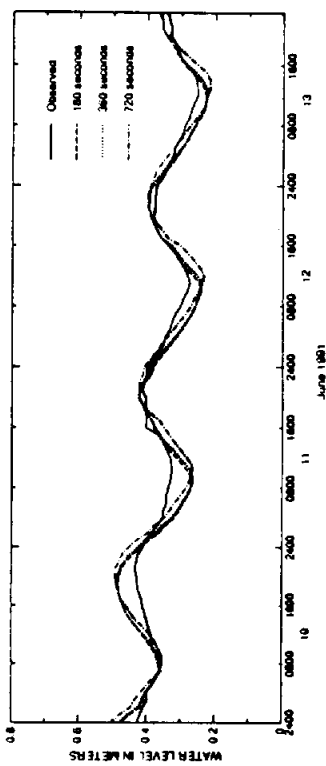


FIG. A-2: Differences in Water Levels Due to the Time Step, Pita Island

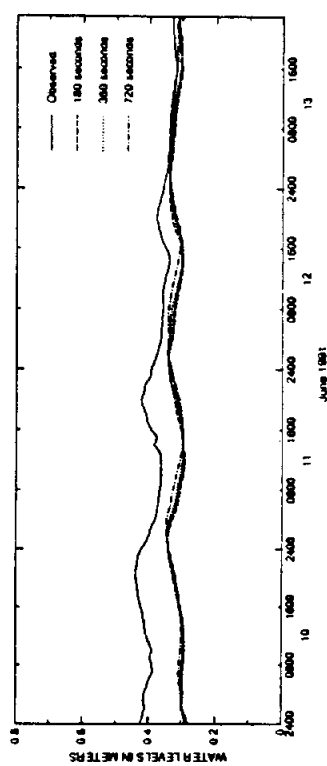


FIG. A-3: Differences in Water Levels Due to the Time Step, South Bird Island

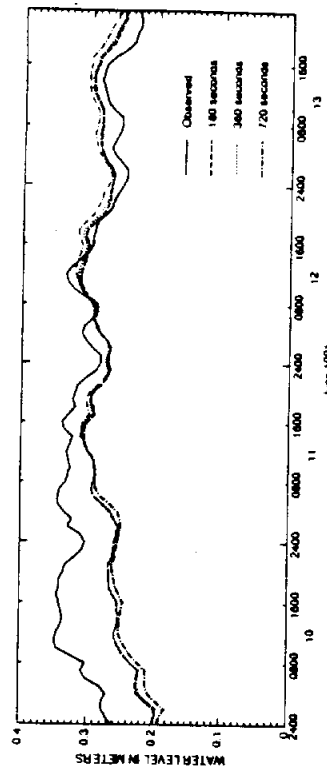


FIG. A-4: Differences in Water Levels Due to the Time Step, Yarbrough Pass

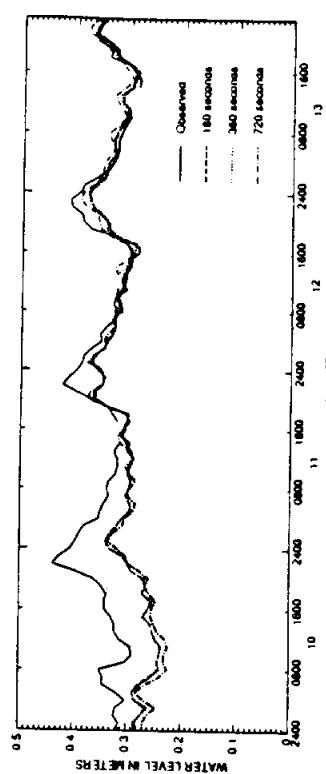


FIG. A-5: Difference in Water Levels Due to the Time Step, Riviera Beach

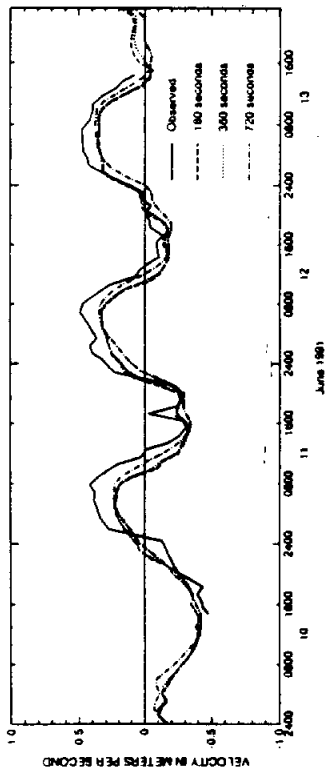


FIG. A-6: Difference in Velocity Due to the Time Step, Humble Channel

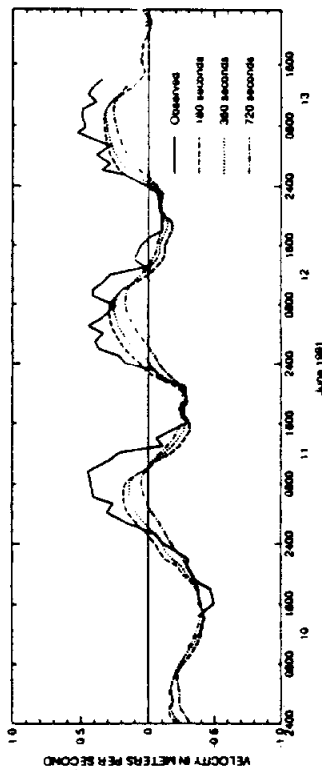


FIG. A-7: Differences in Velocity Due to the Time Step, GIWW at JFK Causeway

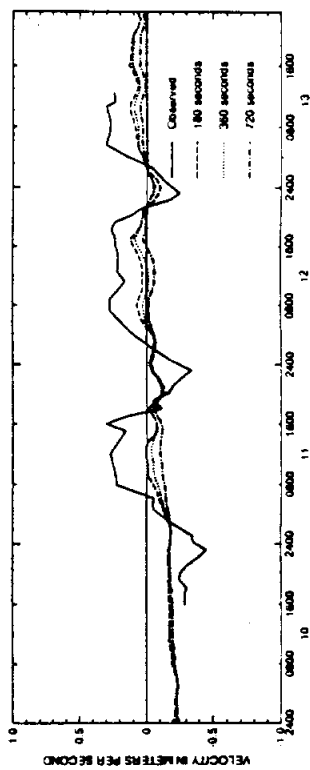


FIG. A-8: Differences in Velocity Due to the Time Step, GIWW Marker 199

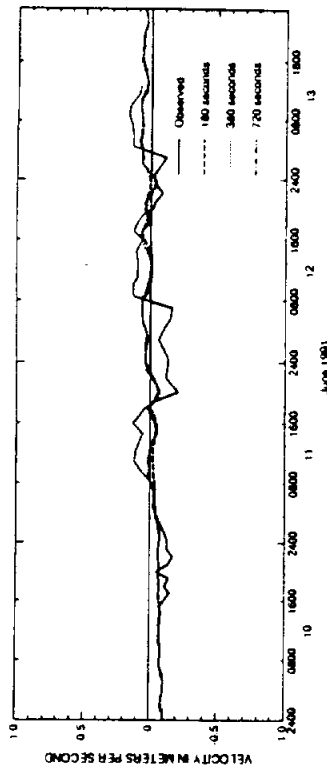


FIG. A-9: Difference in Velocity Due to the Time Step, North of Baffin Bay

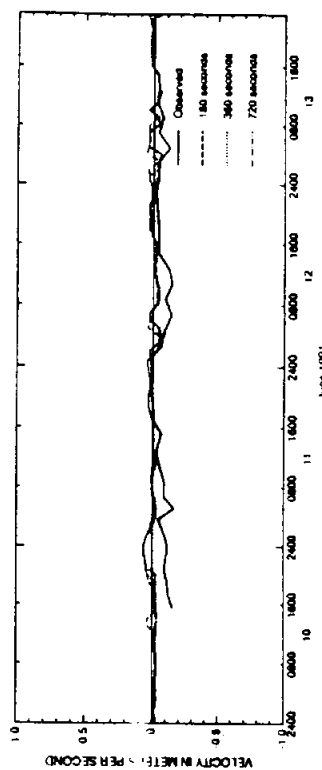


FIG. A-10: Differences in Velocity Due to the Time Step, Mouth of Baffin Bay

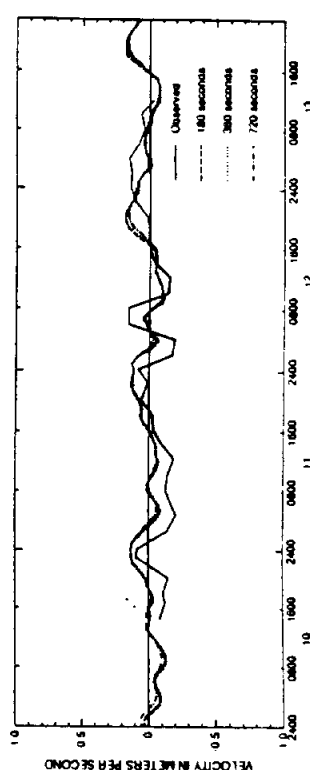


FIG. A-11: Differences in Velocity Due to the Time Step, South of Baffin Bay-Middle

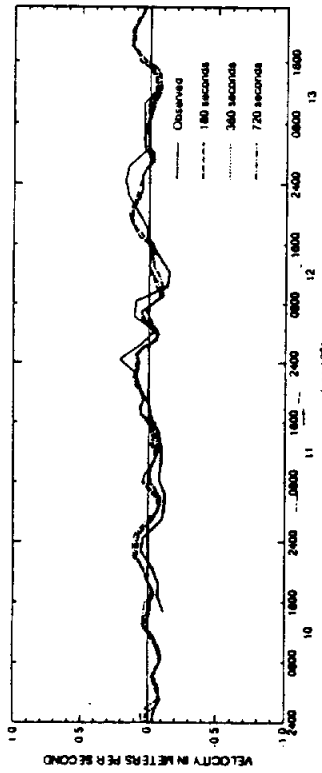


FIG. A-12: Difference in Velocity Due to the Time Step, South of Baffin Bay-West

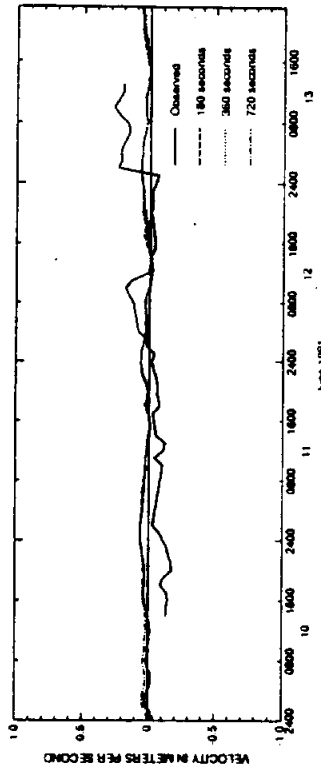


FIG. A-13: Differences in Velocity Due to the Time Step, North Land Cut

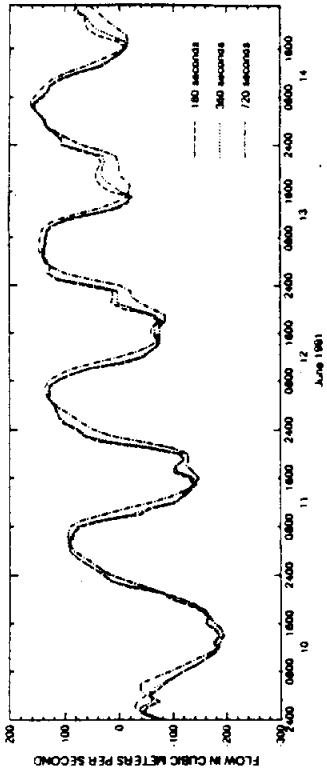


FIG. A-17: Differences in Flow Due to the Time Step, Humble Channel

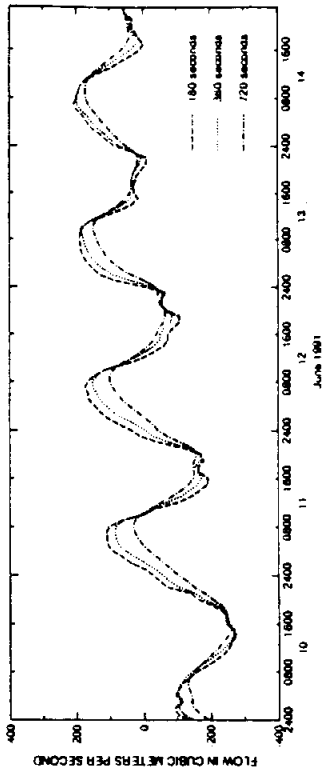


FIG. A-18: Differences in Flow Due to the Time Step, GIWW at JFK Causeway

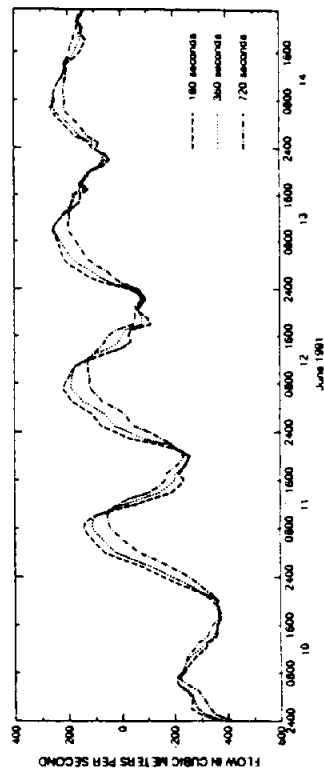


FIG. A-19: Differences in Flow Due to the Time Step, LM at Pita Island

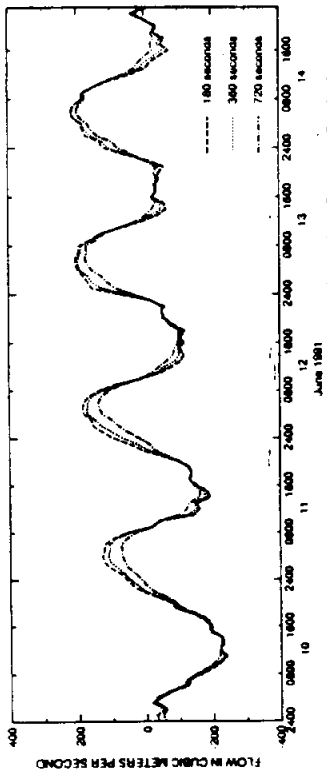


FIG. A-14: Differences in Flow Due to the Time Step, GIWW at Corpus Christi

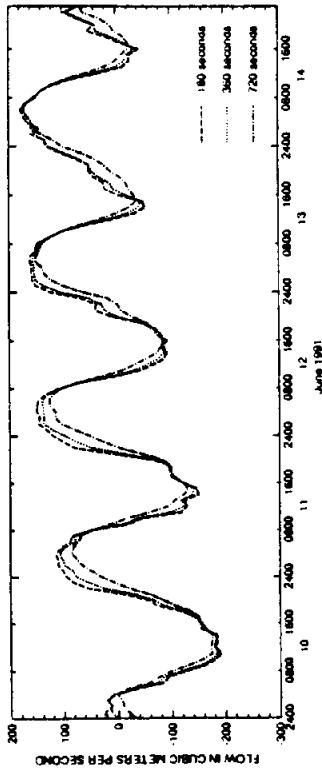


FIG. A-15: Differences in Flow Due to the Time Step, Corpus Christi NAS

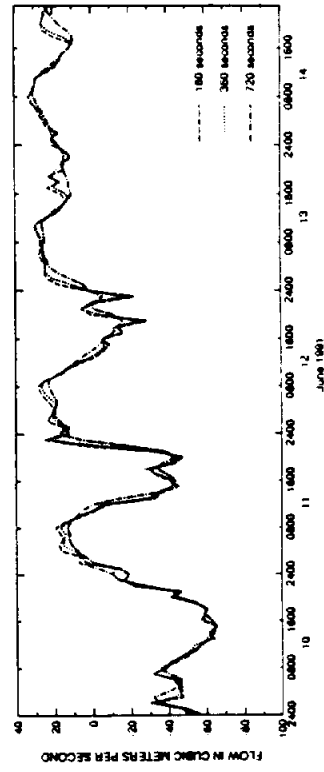


FIG. A-16: Differences in Flow Due to the Time Step, Packery Channel

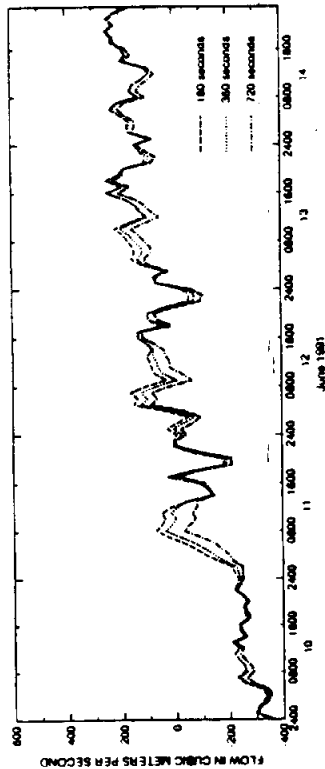


FIG. A-20: Differences in Flow Due to the Time Step, LM at South Bird Island

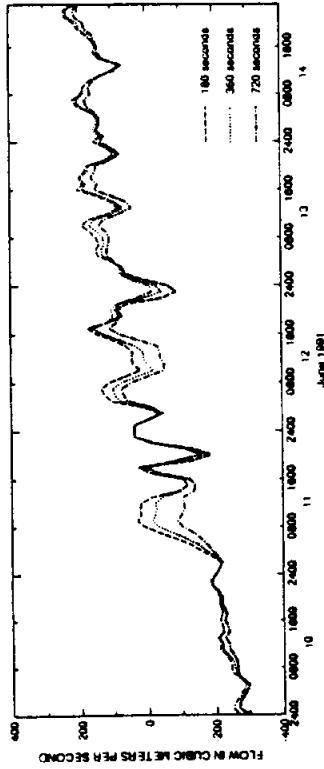


FIG. A-21: Differences in Flow Due to the Time Step, LM at Green Hill

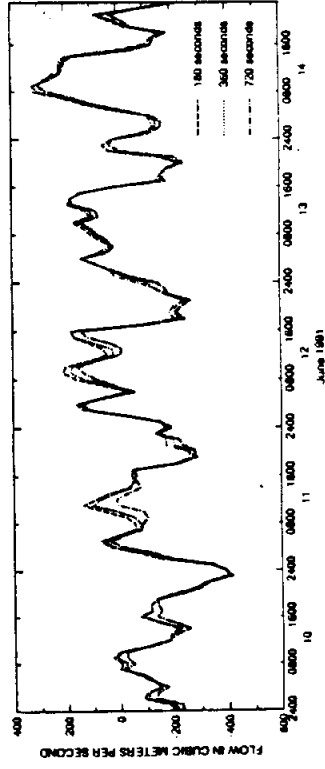


FIG. A-22: Differences in Flow Due to the Time Step, Baffin Bay

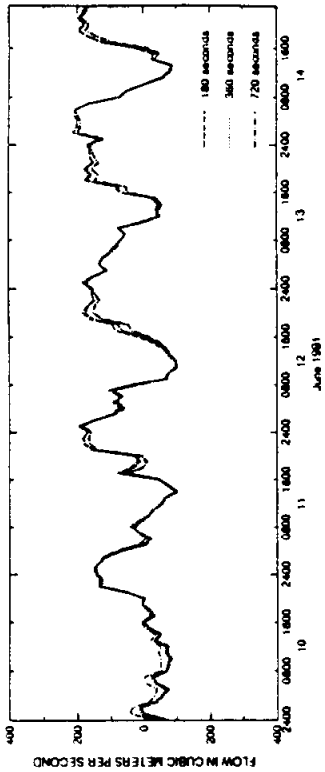


FIG. A-23: Differences in Flow Due to the Time Step, LM at Yarborough Pass

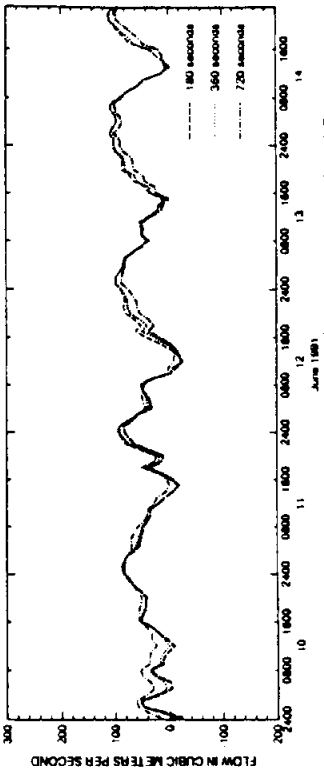


FIG. A-24: Differences in Flow Due to the Time Step, LM at North Land Cut

EFFECT OF CHANGES IN THE WIND STRESS COEFFICIENT ON SWIFT2D SIMULATION RESULTS

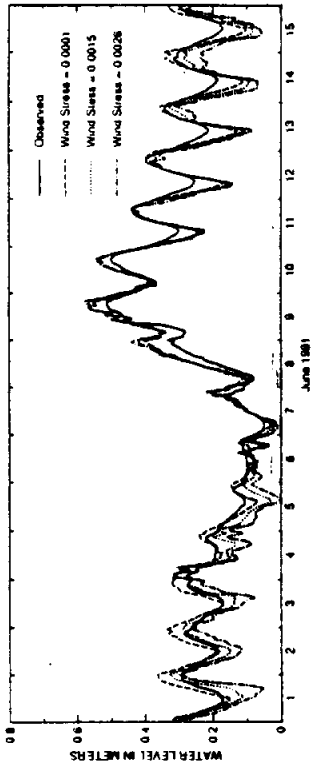


FIG. A-25: Differences in Water Levels Due to the Wind Stress, Packery Channel

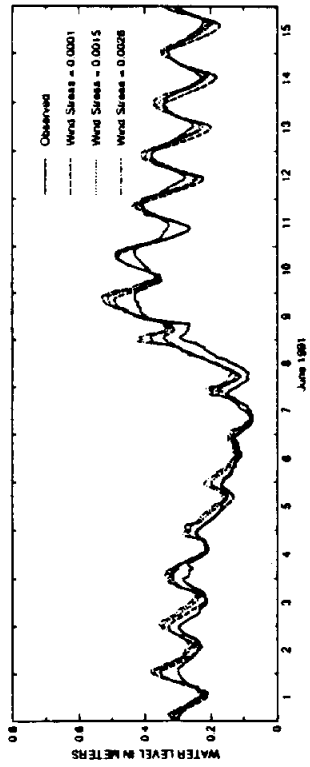


FIG. A-26: Differences in Water Levels Due to the Wind Stress, Pita Island

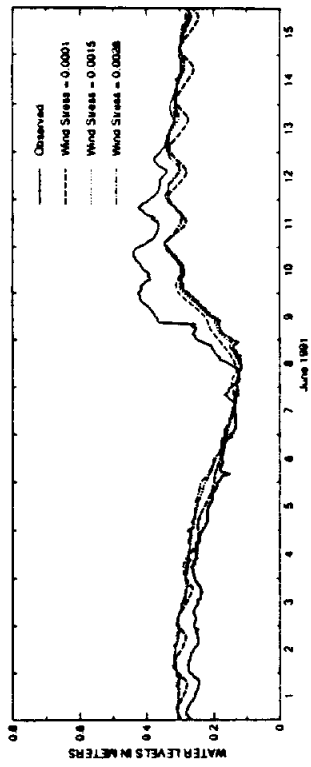


FIG. A-27: Differences in Water Levels Due to the Wind Stress, South Bird Island

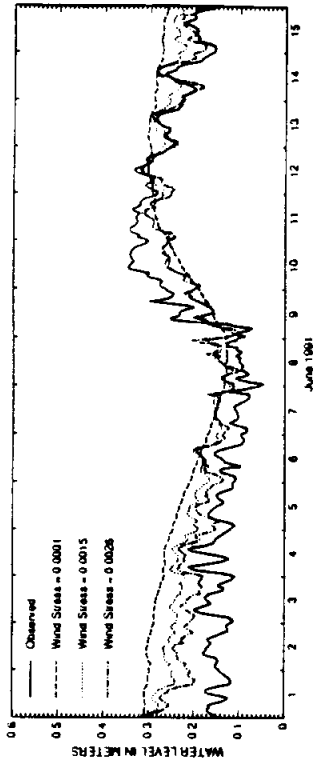


FIG. A-28: Differences in Water Levels Due to the Wind Stress, Yorborough Pass

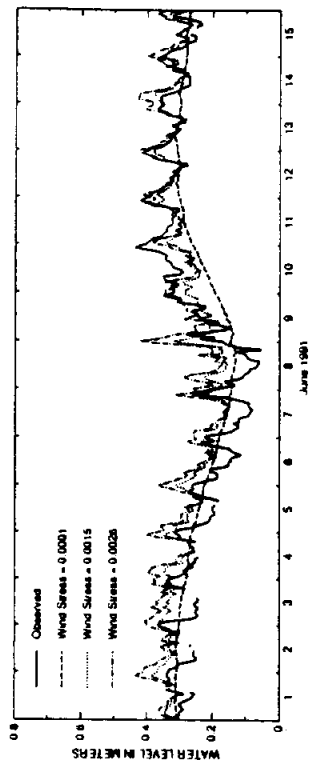


FIG. A-29: Differences in Water Levels Due to the Wind Stress, Riviera Beach

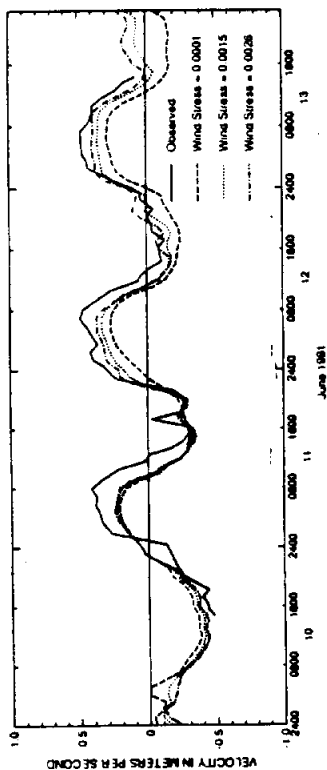


FIG. A-30: Difference in Velocity Due to the Wind Stress, Humble Channel

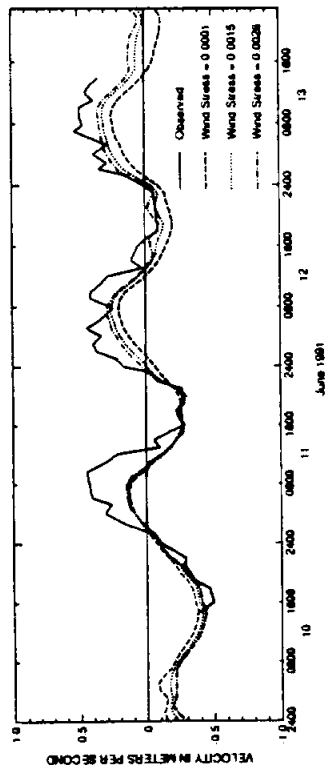


FIG. A-31: Differences in Velocity Due to the Wind Stress, GIWW at JFK Causeway

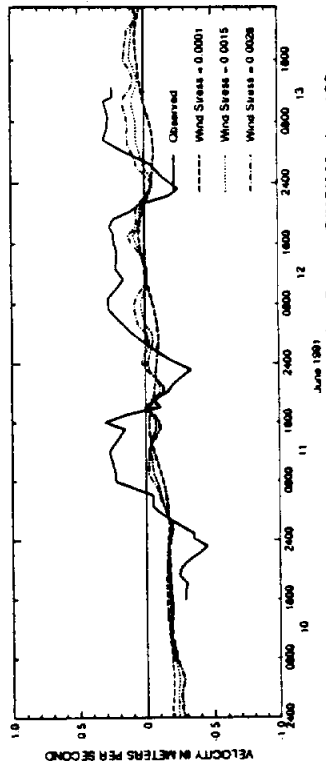


FIG. A-32: Differences in Velocity Due to the Wind Stress, GIWW Marker 199

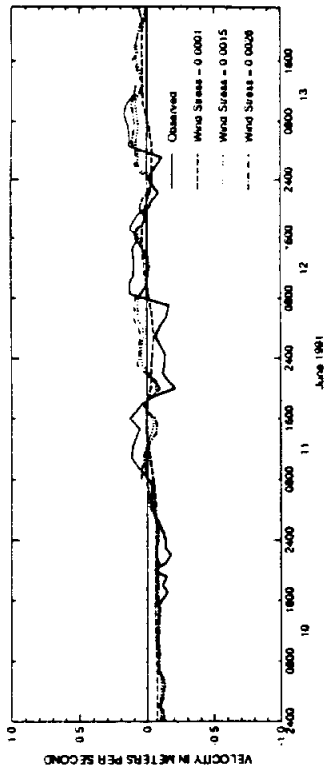


FIG. A-33: Difference in Velocity Due to the Wind Stress, North of Baffin Bay

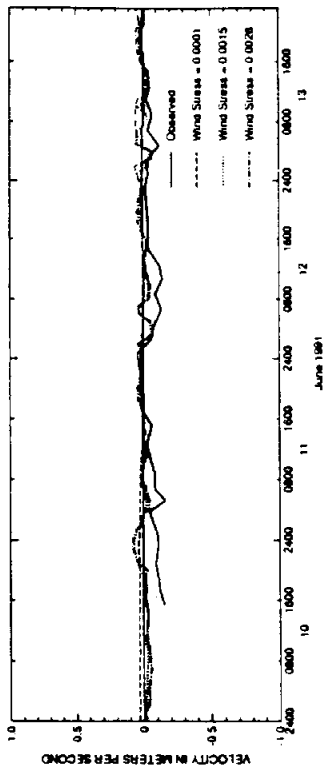


FIG. A-34: Differences in Velocity Due to the Wind Stress, Mouth of Baffin Bay

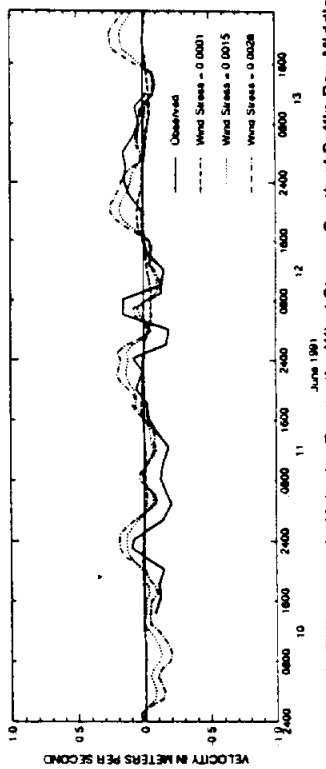


FIG. A-35: Differences in Velocity Due to the Wind Stress, South of Baffin Bay-Middle

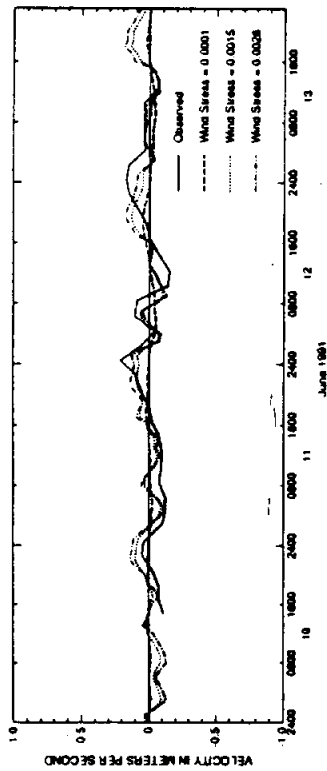


FIG. A-36: Difference in Velocity Due to the Wind Stress, South of Baffin Bay-West

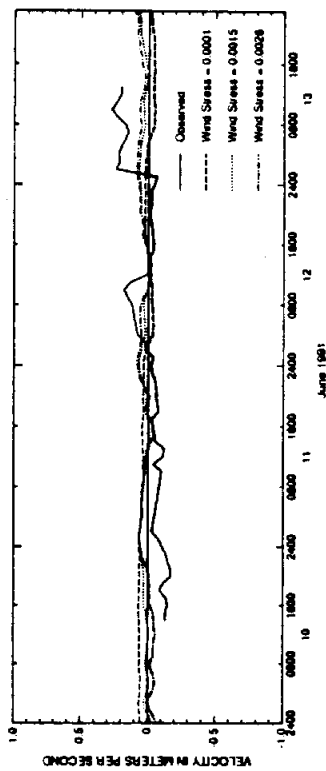


FIG. A-37: Differences in Velocity Due to the Wind Stress, North Land Cut

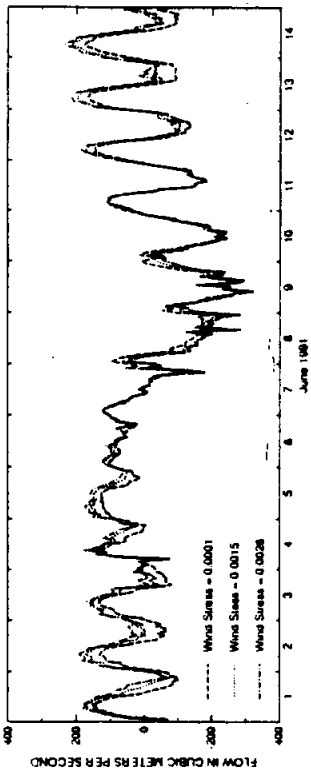


FIG. A-38: Differences in Flow Due to the Wind Stress, GIWW at Corpus Christi

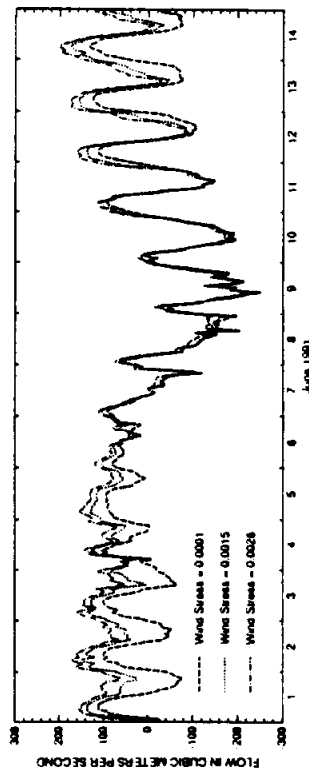


FIG. A-39: Differences in Flow Due to the Wind Stress, Corpus Christi NAS

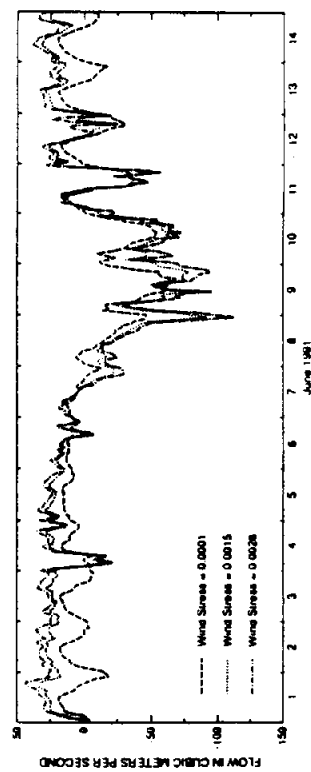


FIG. A-40: Differences in Flow Due to the Wind Stress, Packery Channel

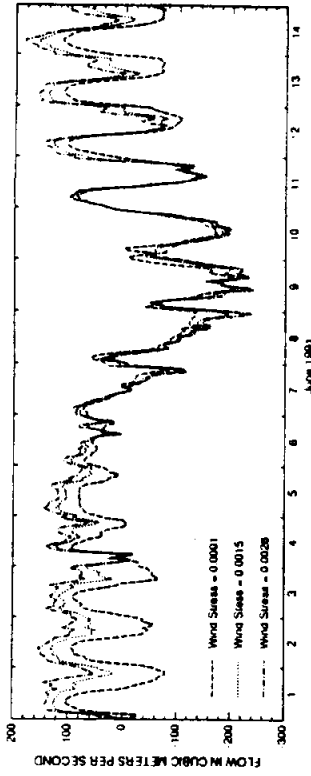


FIG. A-41: Differences in Flow Due to the Wind Stress, Humble Channel

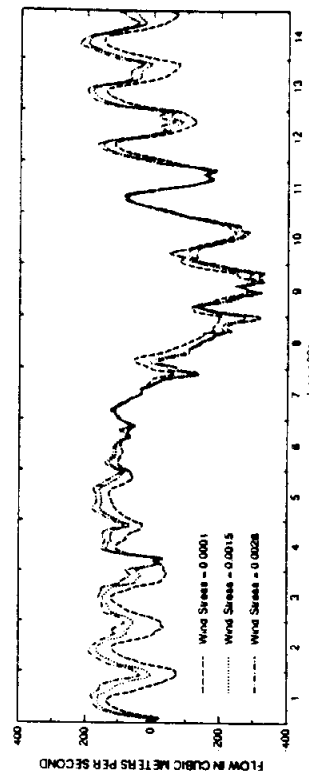


FIG. A-42: Differences in Flow Due to the Wind Stress, GIWW at JFK Causeway

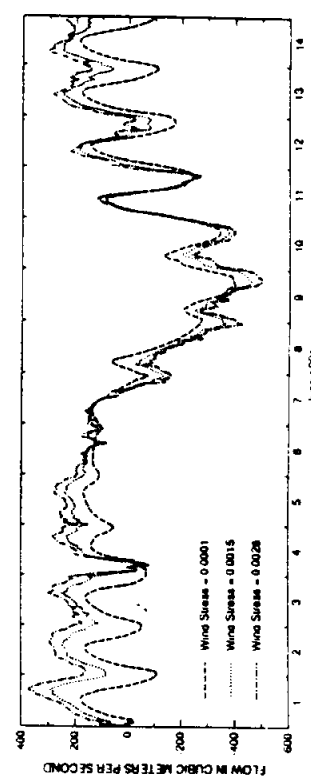


FIG. A-43: Differences in Flow Due to the Wind Stress, LM at Pita Island

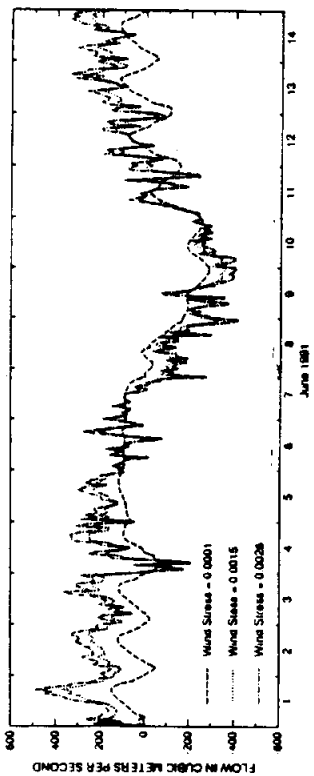


FIG. A-44: Differences in Flow Due to the Wind Stress, LM at South Bird Island

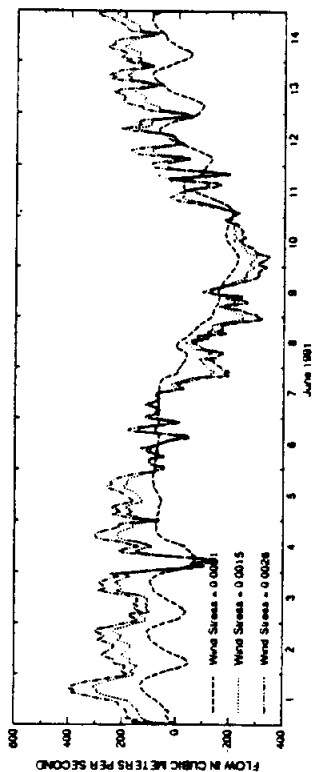


FIG. A-45: Differences in Flow Due to the Wind Stress, LM at Green Hill

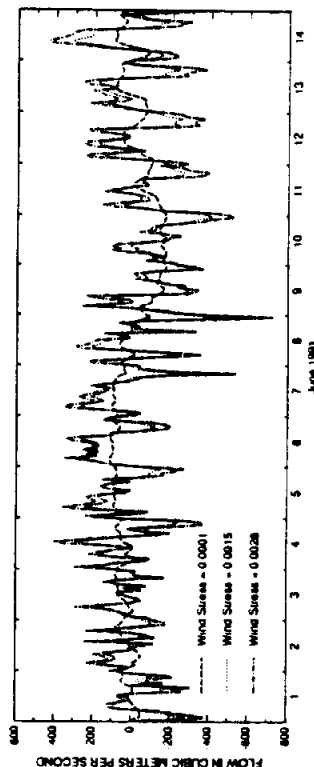


FIG. A-46: Differences in Flow Due to the Wind Stress, Beffin Bay

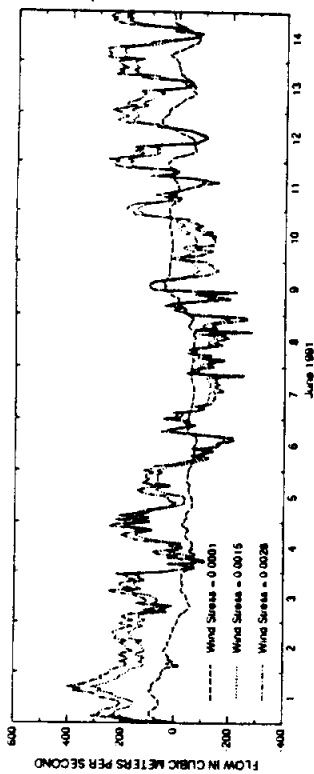


FIG. A-47: Differences in Flow Due to the Wind Stress, LM at Yarborough Pass

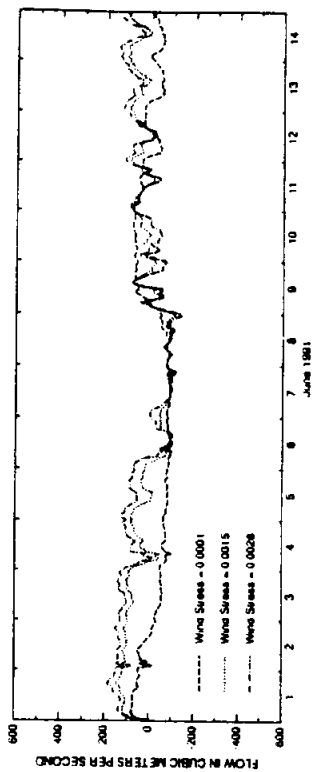


FIG. A-48: Differences in Flow Due to the Wind Stress, LM at North Land Cut

EFFECT OF CHANGES IN MANNING'S N ON SWIFT2D SIMULATION RESULTS

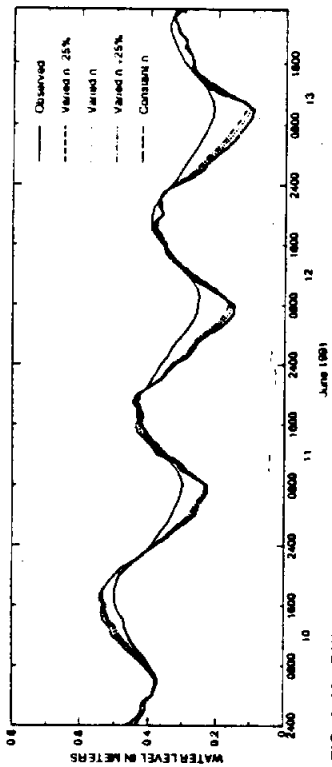


FIG. A-49: Differences in Water Levels Due to Manning's n, Packery Channel

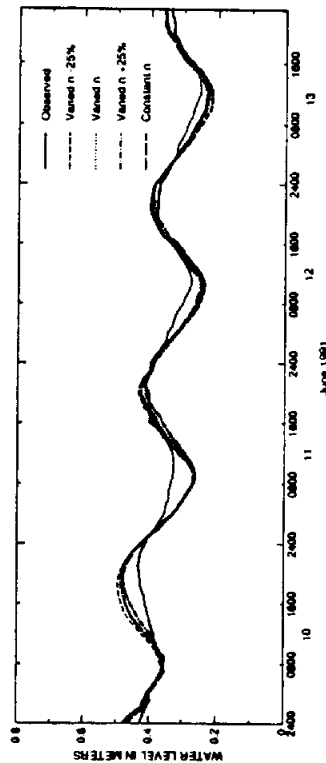


FIG. A-50: Differences in Water Levels Due to Manning's n, Piva Island

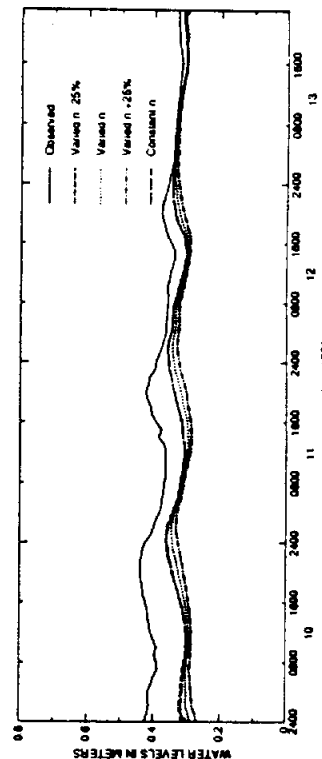


FIG. A-51: Differences in Water Levels Due to Manning's n, South Bird Island

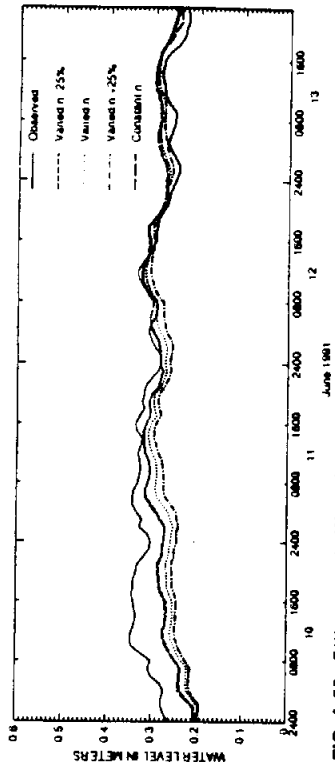


FIG. A-52: Differences in Water Levels Due to Manning's n, Yarborough Pass

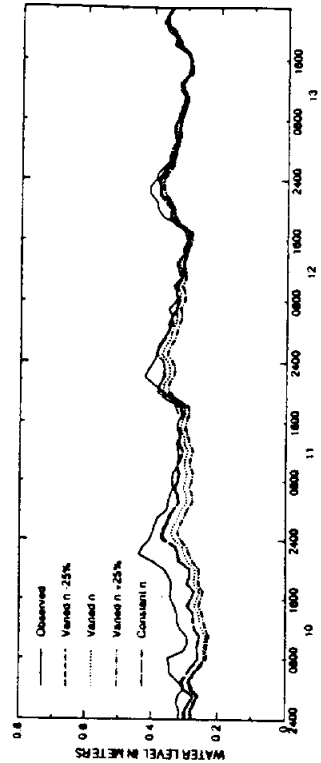


FIG. A-53: Differences in Water Levels Due to Manning's n, Riviera Beach

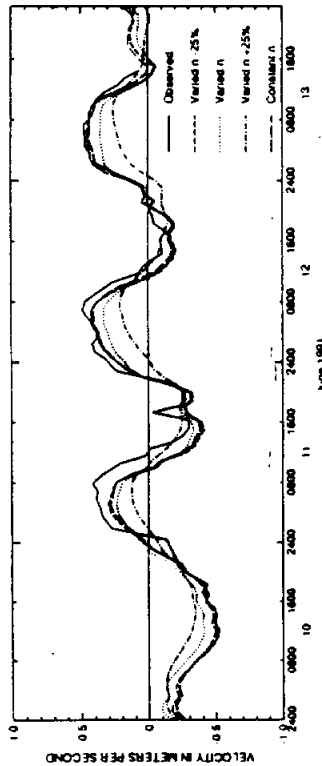


FIG. A-54: Difference in Velocity Due to Manning's n, Humble Channel

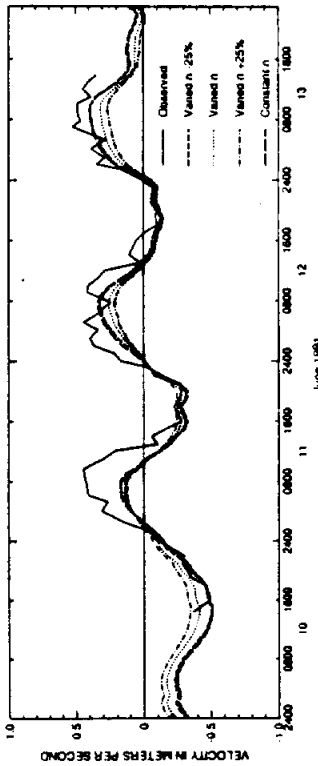


FIG. A-55: Differences in Velocity Due to Manning's n, GIWW at JFK Causeway

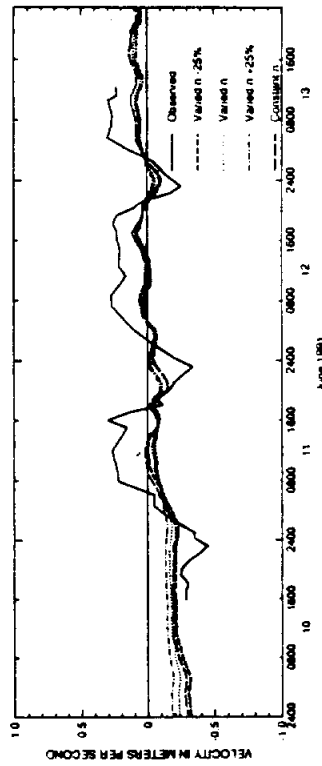


FIG. A-56: Differences in Velocity Due to Manning's n, GIWW Marker 199

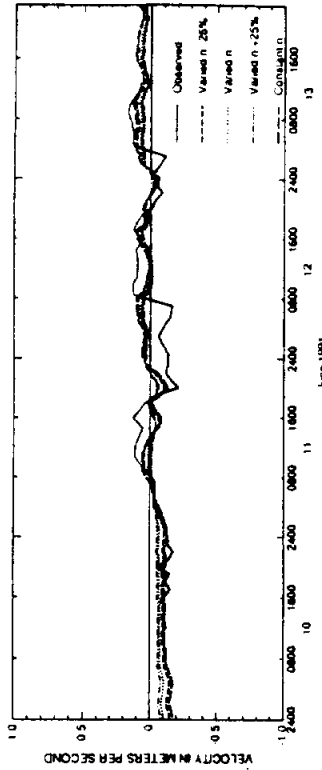


FIG. A-57: Difference in Velocity Due to Manning's n, North of Batfin Bay

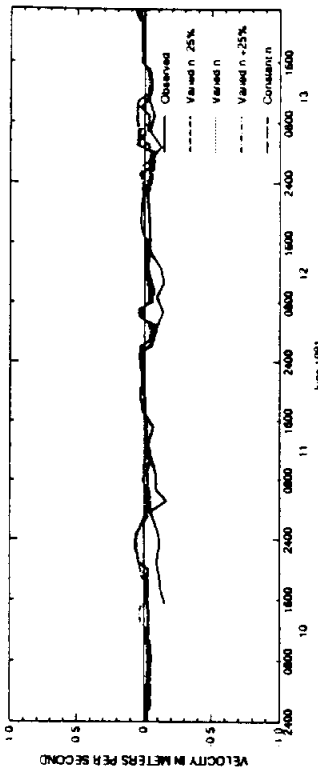


FIG. A-58: Differences in Velocity Due to Manning's n, Mouth of Batfin Bay

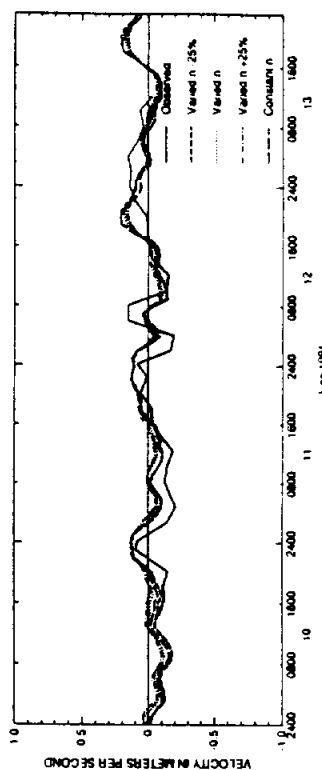


FIG. A-59: Differences in Velocity Due to Manning's n, South of Batfin Bay-Middle

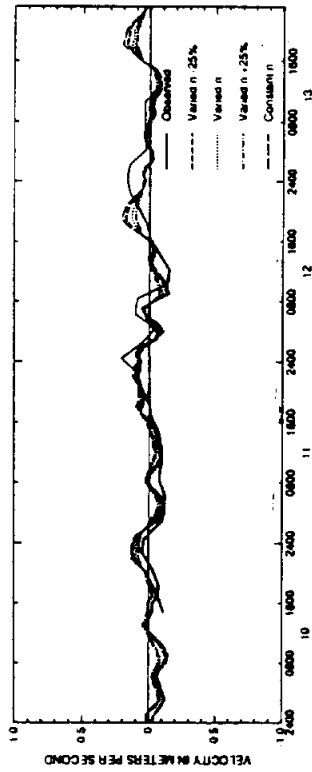


FIG. A-60: Difference in Velocity Due to Manning's n, South of Baffin Bay-West

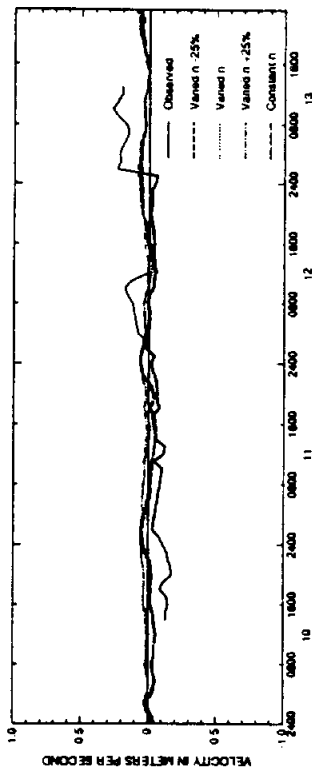


FIG. A-61: Differences in Velocity Due to Manning's n, North Land Cut

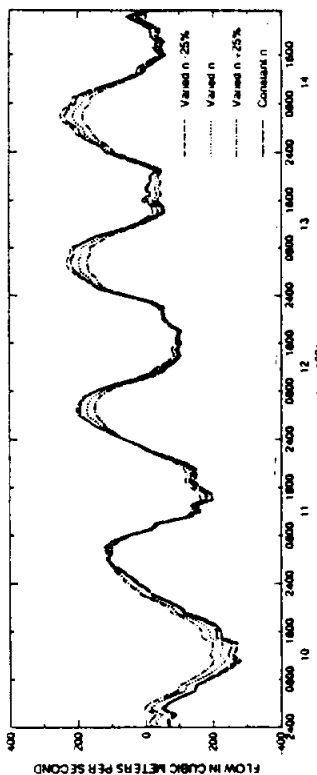


FIG. A-62: Differences in Flow Due to Manning's n, GIWW at Corpus Christi

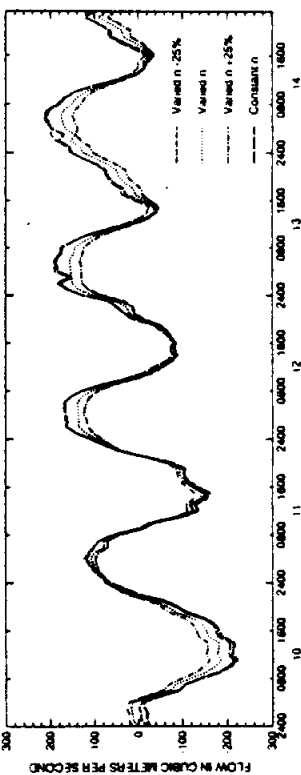


FIG. A-63: Differences in Flow Due to Manning's n, Corpus Christi NAS

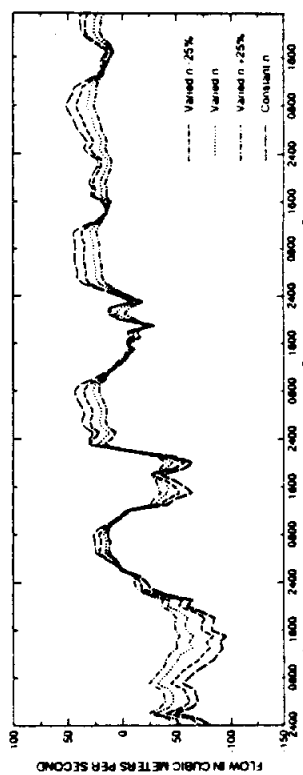


FIG. A-64: Differences in Flow Due to Manning's n, Packery Channel

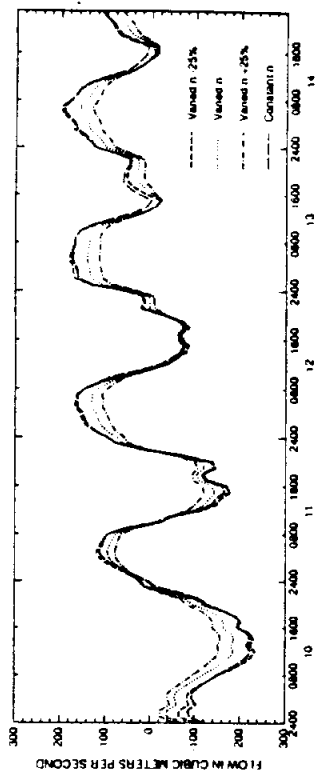


FIG. A-65: Differences in Flow Due to Manning's n, Humble Channel

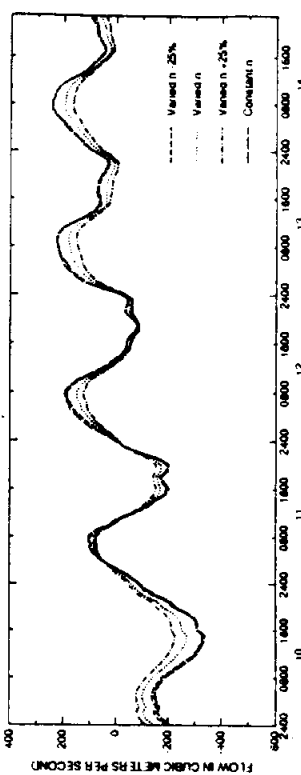


FIG. A-66: Differences in Flow Due to Manning's n, GIWW at JFK Causeway

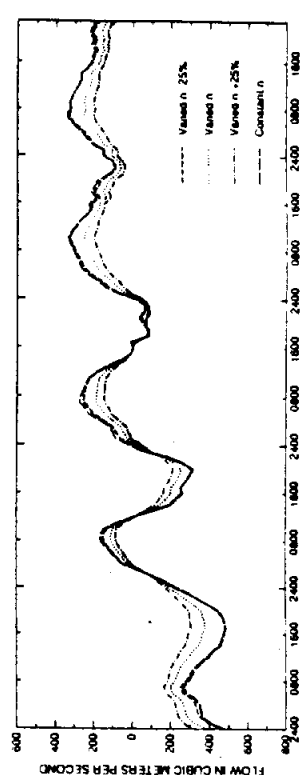


FIG. A-67: Differences in Flow Due to Manning's n, LM at Pita Island

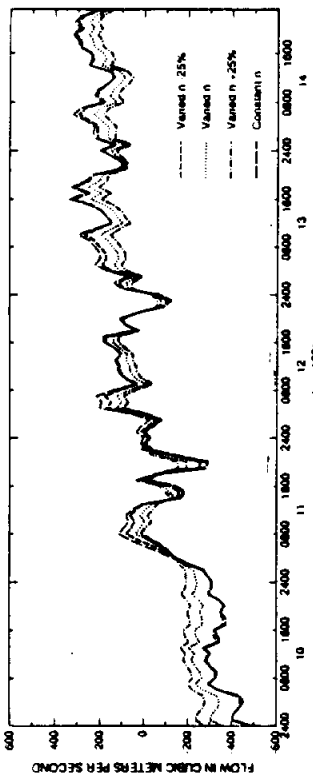


FIG. A-68: Differences in Flow Due to Manning's n, LM at South Bird Island

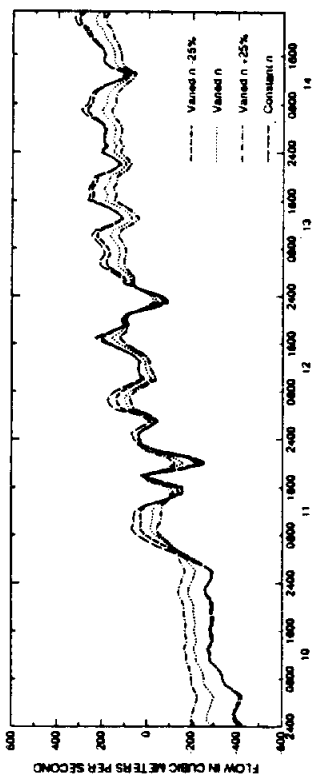


FIG. A-69: Differences in Flow Due to Manning's n, LM at Green Hill

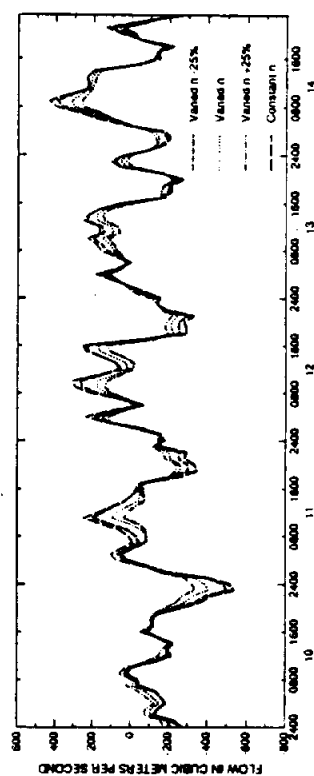


FIG. A-70: Differences in Flow Due to Manning's n, Baffin Bay

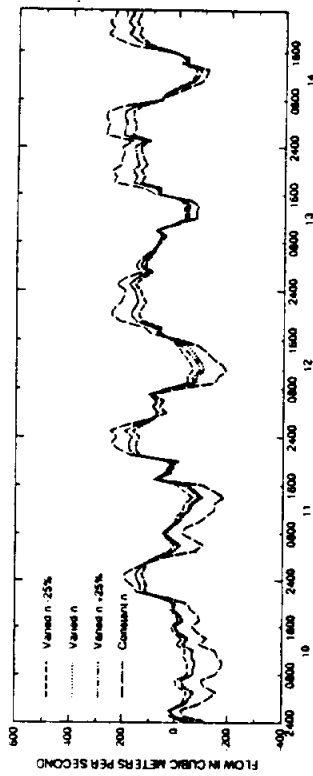


FIG. A-71: Differences in Flow Due to Manning's n, LM at Yarborough Pass

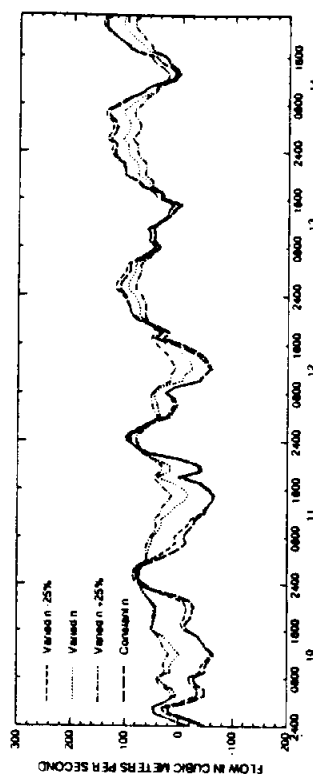


FIG. A-72: Differences in Flow Due to Manning's n, LM at North Land Cut

EFFECT OF CHANGES IN VISCOSITY ON SWIFT2D SIMULATION RESULTS

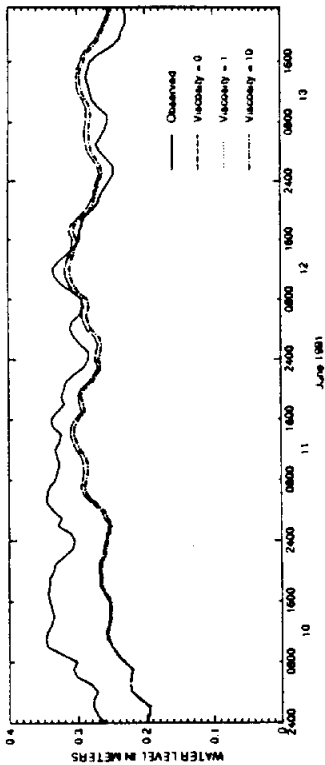


FIG. A-76: Differences in Water Levels Due to Viscosity, Yaborough Pass

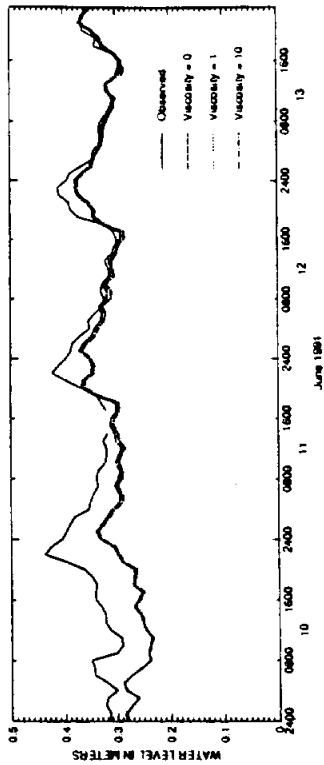


FIG. A-77: Difference in Water Levels Due to Viscosity, Riviera Beach

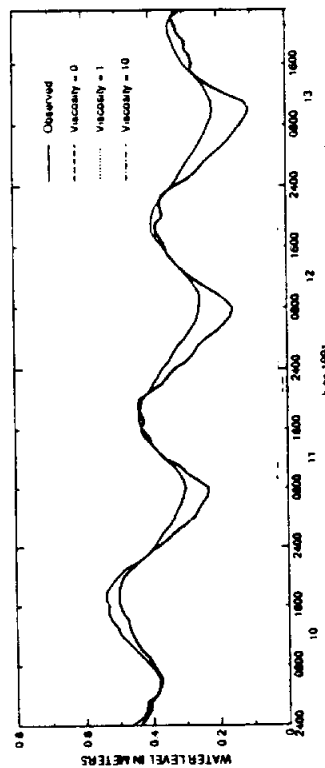


FIG. A-73: Differences in Water Levels Due to Viscosity, Peckery Channel

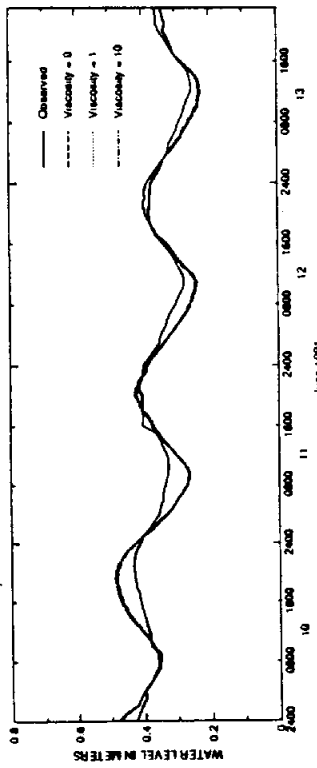


FIG. A-74: Differences in Water Levels Due to Viscosity, Pita Island

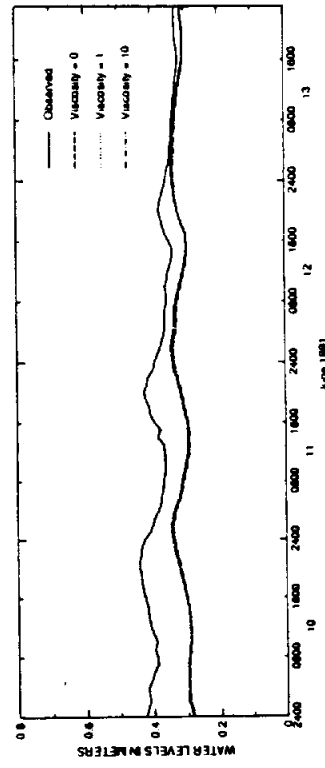


FIG. A-75: Differences in Water Levels Due to Viscosity, South Bird Island

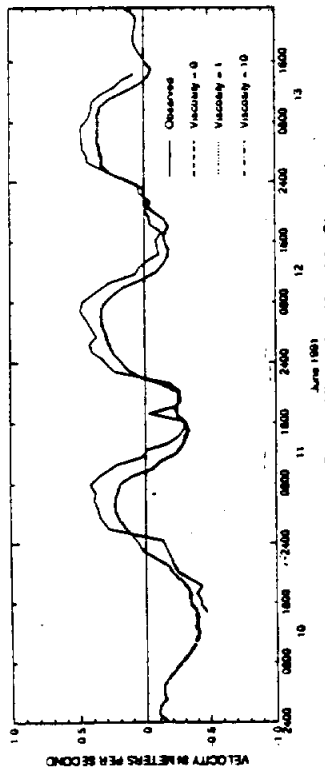


FIG. A-78: Difference in Velocity Due to Viscosity, Humble Channel

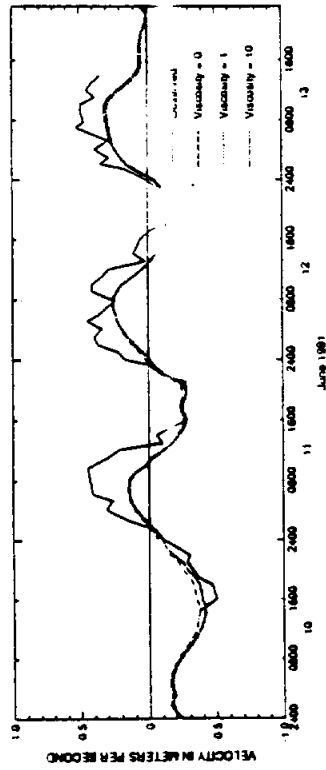


FIG. A-79: Differences in Velocity Due to Viscosity, JFK Causeway

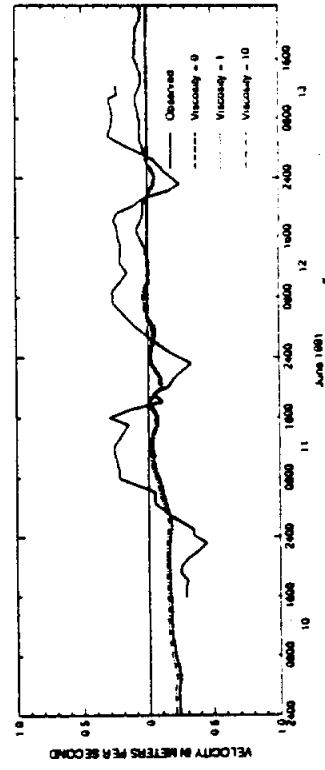


FIG. A-80: Differences in Velocity Due to Viscosity, GIWW Marker 199

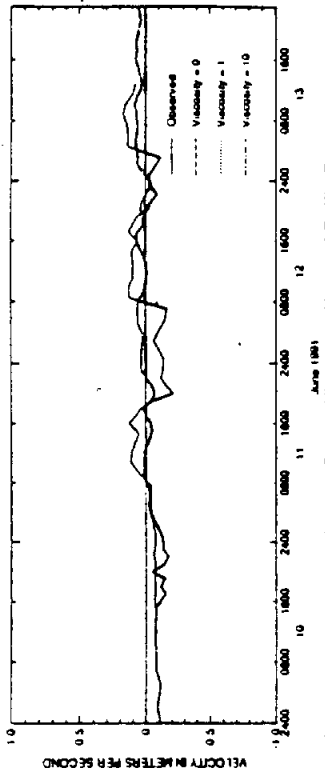


FIG. A-81: Difference in Velocity Due to Viscosity, North of Baffin Bay

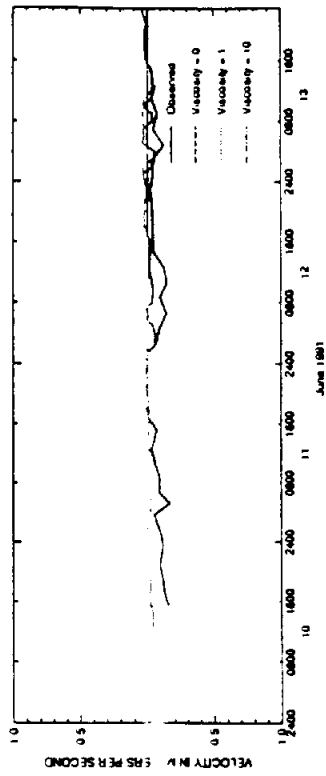


FIG. A-82: Differences in Velocity Due to Viscosity, Mouth of Baffin Bay

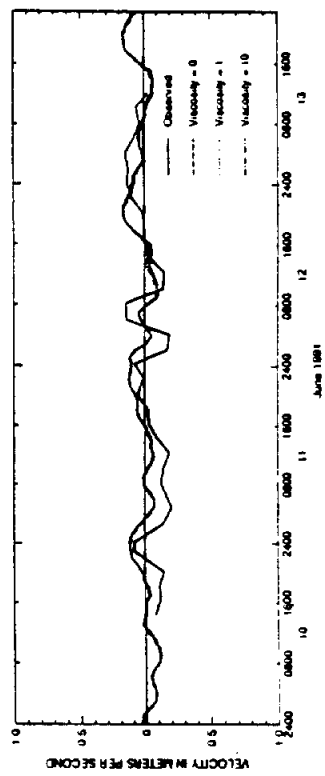


FIG. A-83: Differences in Velocity Due to Viscosity, South of Baffin Bay-Middle

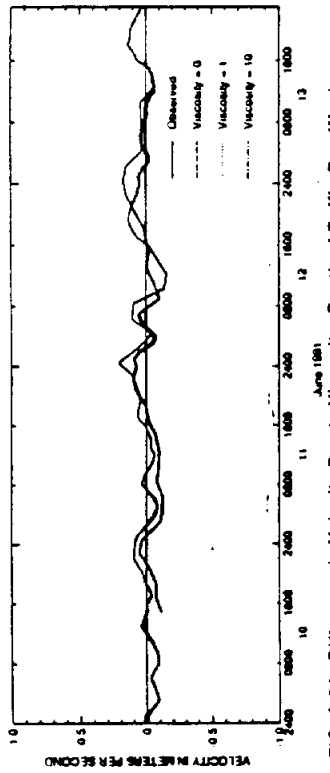


FIG. A-94: Difference in Velocity Due to Viscosity, South of Baffin Bay-West

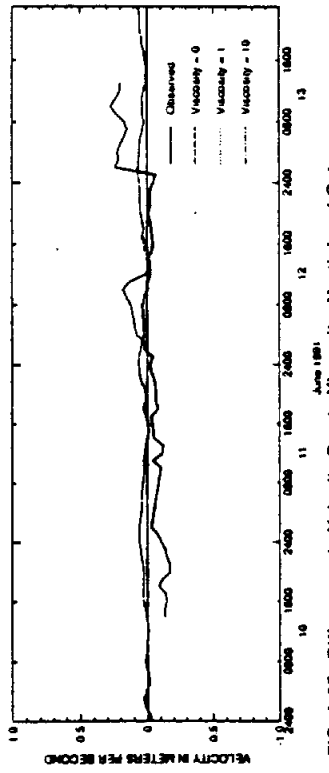


FIG. A-95: Differences in Velocity Due to Viscosity, North Land Cut

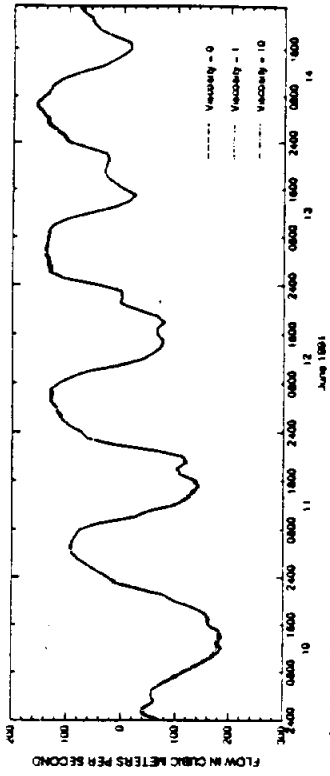


FIG. A-89: Differences in Flow Due to Viscosity, Humble Channel

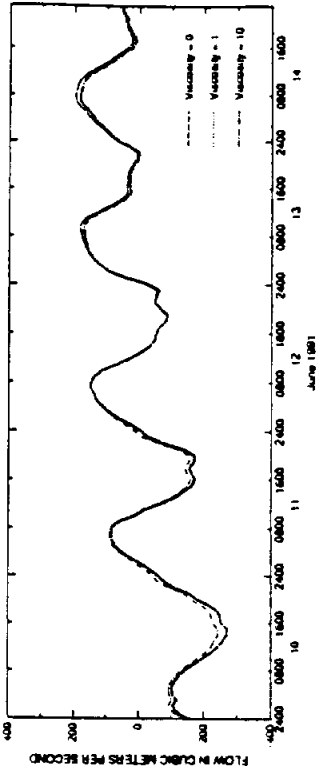


FIG. A-90: Differences in Flow Due to Viscosity, GIWW at JFK Causeway

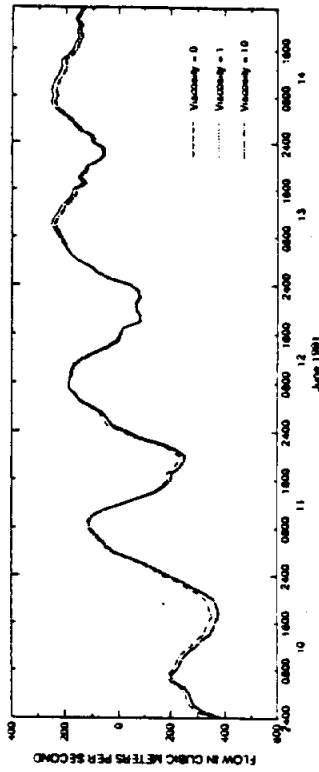


FIG. A-91: Differences in Flow Due to Viscosity, LM at Pita Island

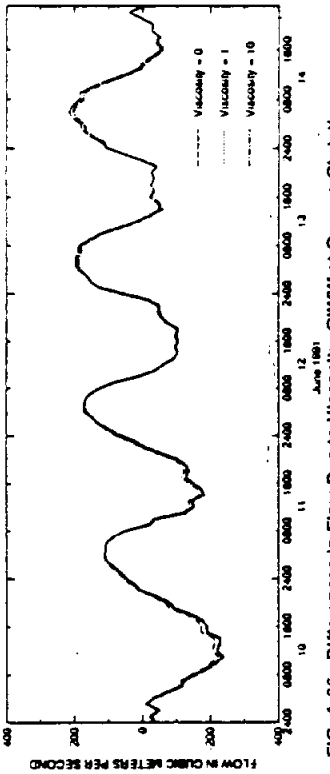


FIG. A-96: Differences in Flow Due to Viscosity, GIWW at Corpus Christi

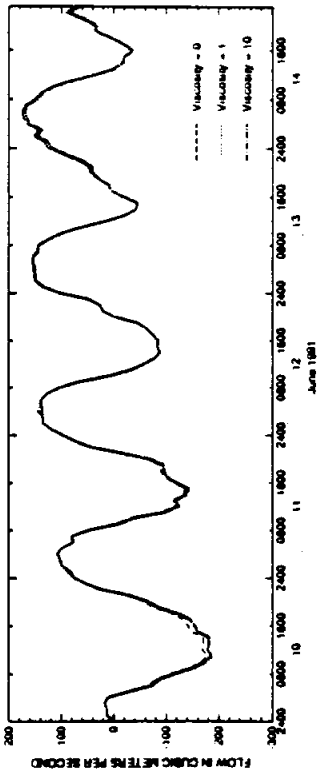


FIG. A-97: Differences in Flow Due to Viscosity, Corpus Christi NAS

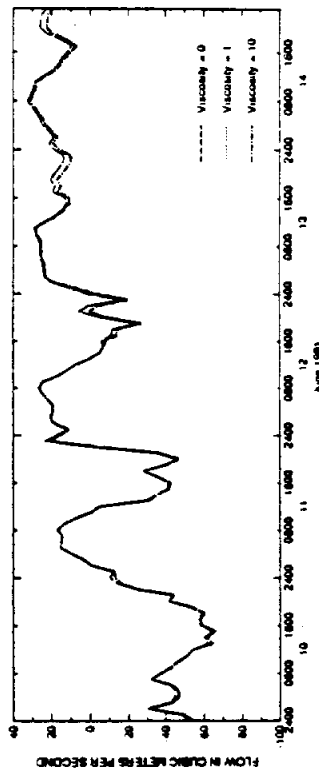


FIG. A-98: Differences in Flow Due to Viscosity, Packery Channel

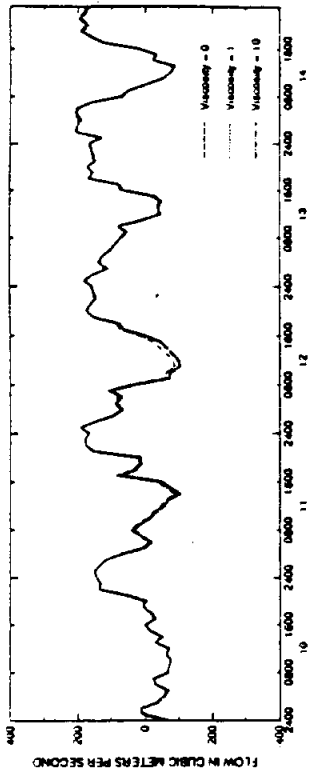


FIG. A-95: Differences in Flow Due to Viscosity, LM at Yarborough Pass

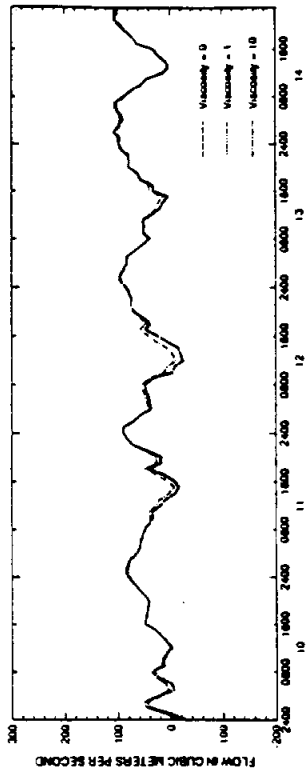


FIG. A-96: Differences in Flow Due to Viscosity, LM at North Land Cut

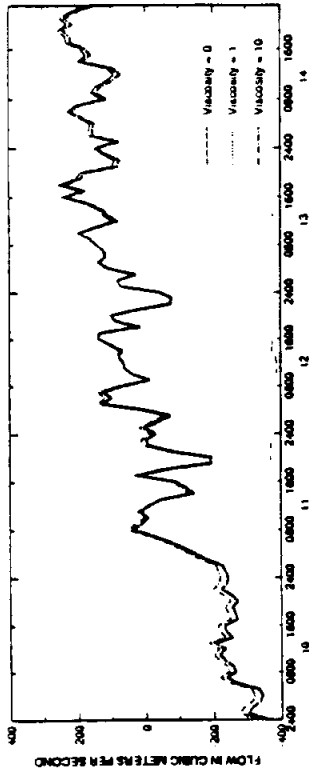


FIG. A-92: Differences in Flow Due to Viscosity, LM at South Bird Island

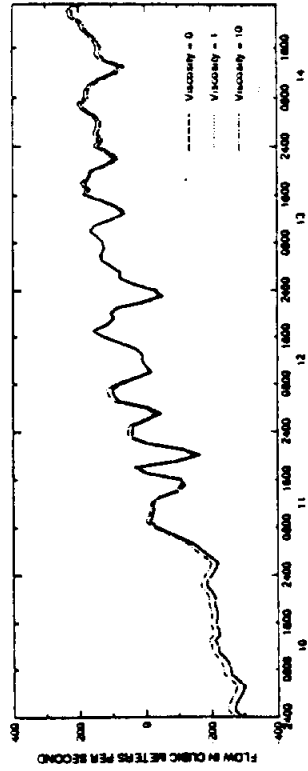


FIG. A-93: Differences in Flow Due to Viscosity, LM at Green Hill

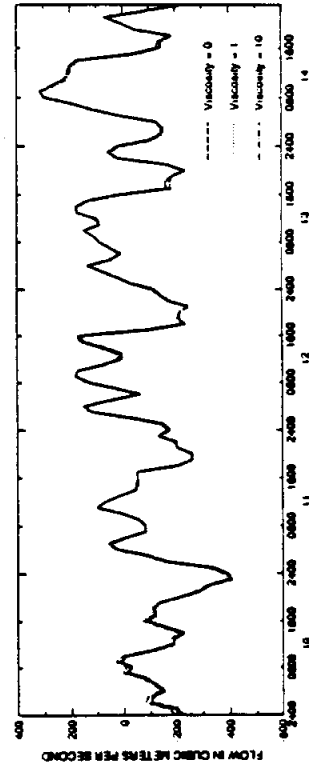


FIG. A-94: Differences in Flow Due to Viscosity, Baffin Bay

**EFFECT OF CHANGES IN THE ADVECTION OPTION ON SWIFT2D SIMULATION
RESULTS**

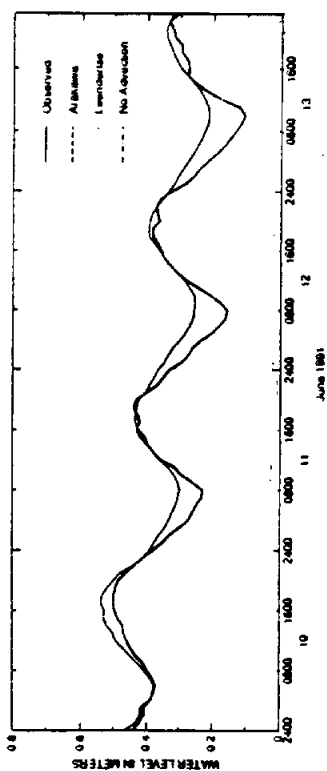


FIG. A-97: Differences in Water Levels Due to the Advection Option, Packery Channel

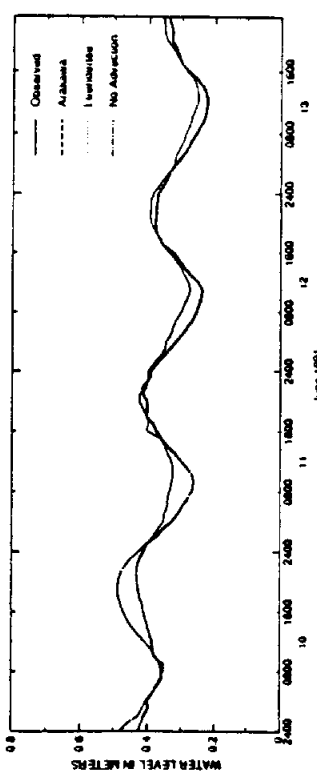


FIG. A-98: Differences in Water Levels Due to the Advection Option, Pita Island

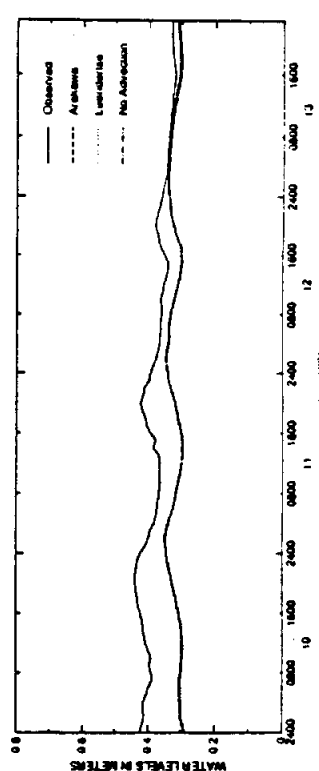


FIG. A-99: Differences in Water Levels Due to the Advection Option, South of Bird Island

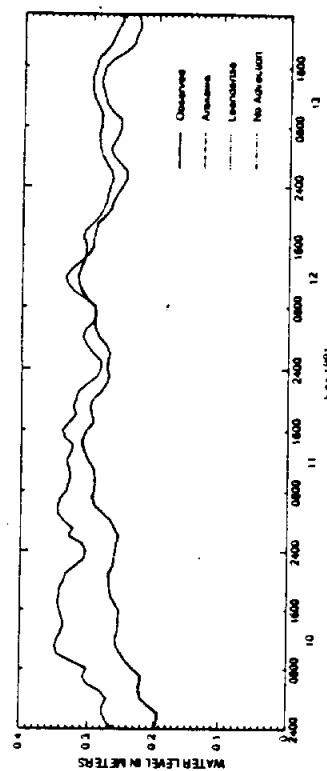


FIG. A-100: Differences in Water Levels Due to the Advection Option, Yarbrough Pass

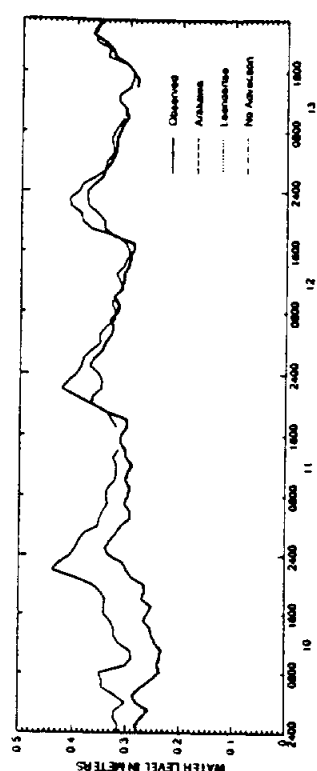


FIG. A-101: Differences in Water Levels Due to the Advection Option, Riviera Beach

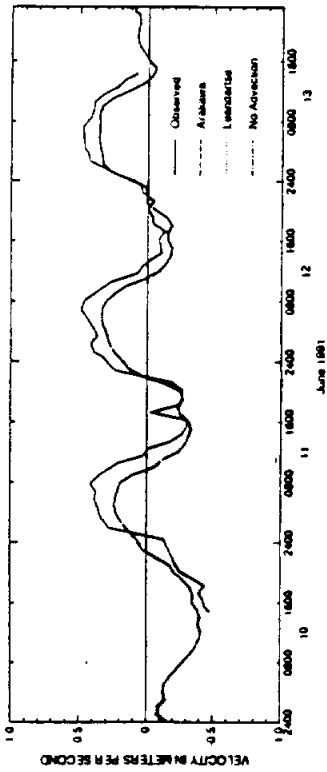


FIG. A-102: Difference in Velocity Due to the Advection Option, Humble Channel

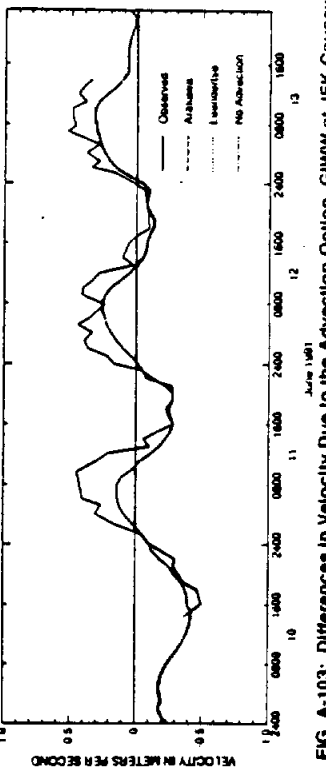


FIG. A-103: Differences in Velocity Due to the Advection Option, JFK Causeway

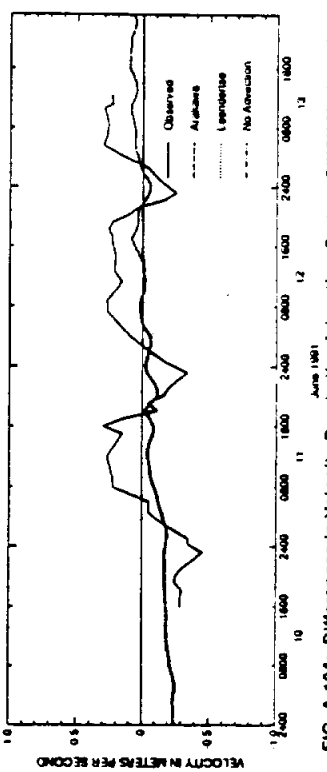


FIG. A-104: Differences in Velocity Due to the Advection Option, GIWW Marker 199

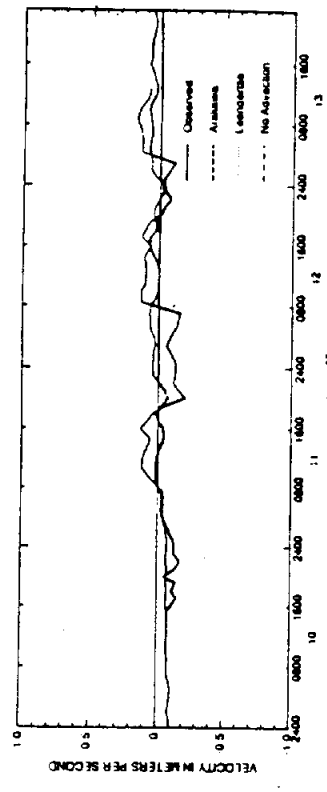


FIG. A-105: Difference in Velocity Due to the Advection Option, North of Baffin Bay

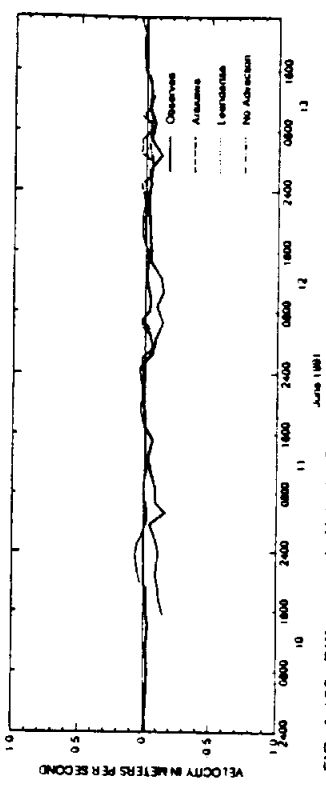


FIG. A-106: Differences in Velocity Due to the Advection Option, Mouth of Baffin Bay

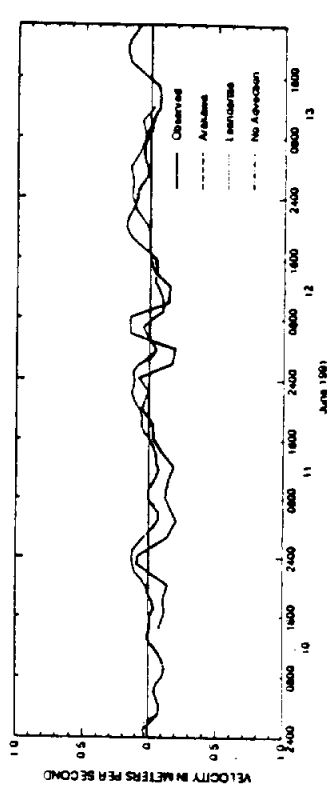


FIG. A-107: Differences in Velocity Due to the Advection Option, South of Baffin Bay-M

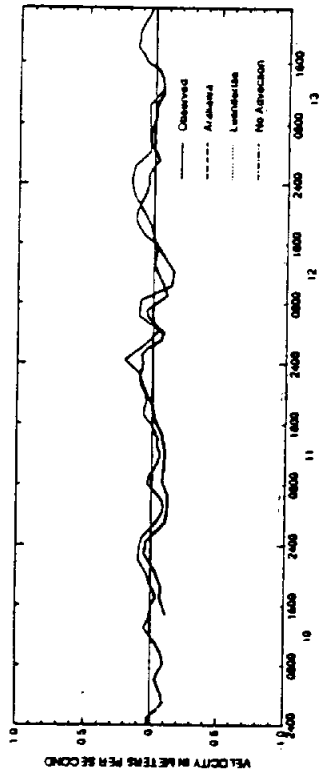


FIG. A-108: Difference in Velocity Due to the Advection Option, South of Baffin Bay-W

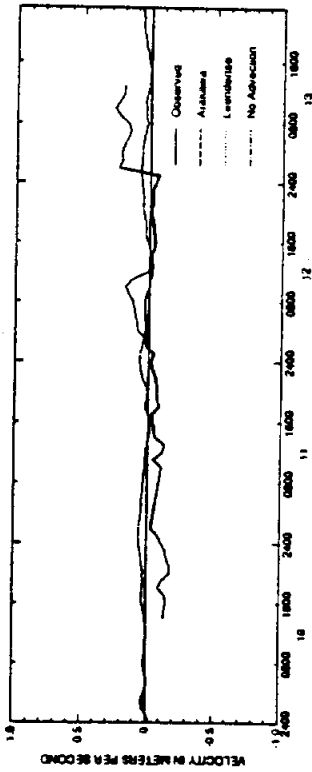


FIG. A-109: Differences in Velocity Due to the Advection Option, North Land Cut

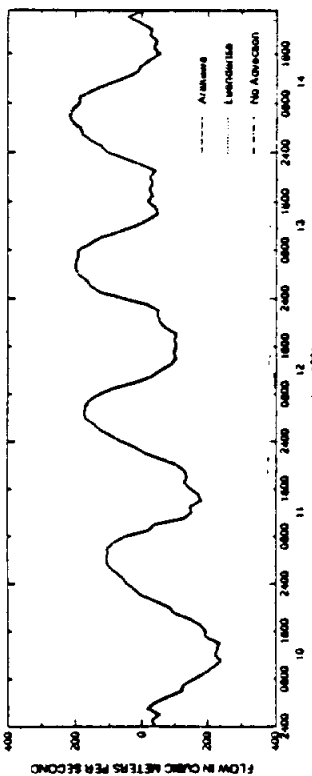


FIG. A-110: Differences in Flow Due to the Advecton Option, GIWW at Corpus Christi

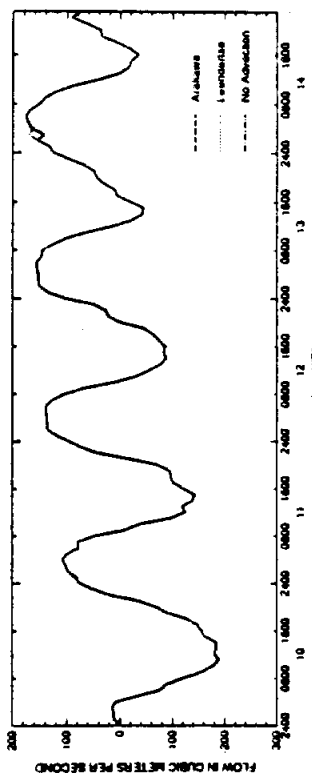


FIG. A-111: Differences in Flow Due to the Advecton Option, Corpus Christi NAS

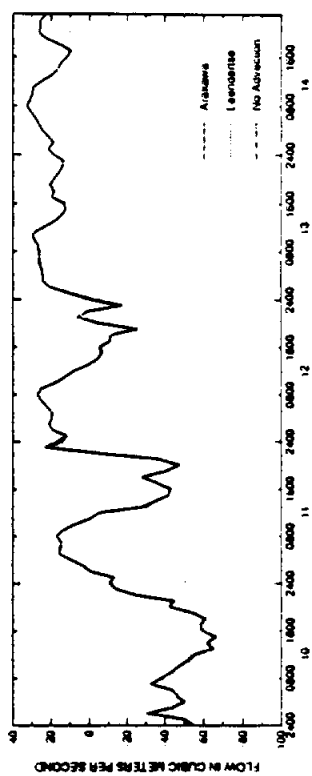


FIG. A-112: Differences in Flow Due to the Advecton Option, Peacery Channel

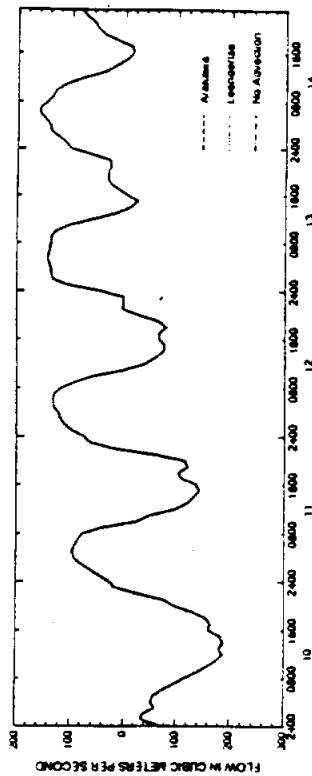


FIG. A-113: Differences in Flow Due to the Advecton Option, Humble Channel

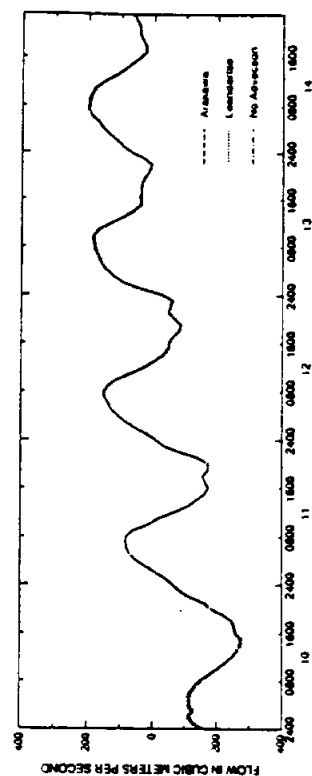


FIG. A-114: Differences in Flow Due to the Advecton Option, GIWW at JFK Causeway

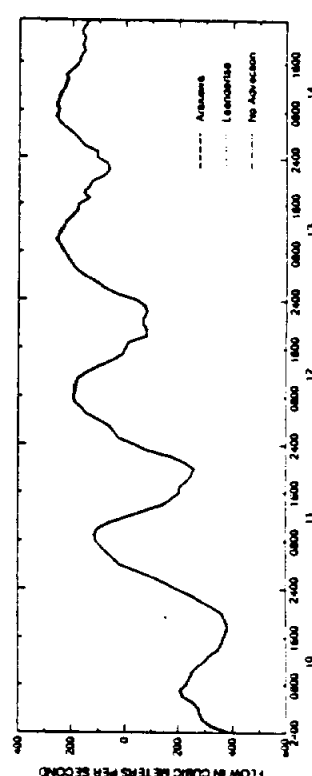


FIG. A-115: Differences in Flow Due to the Advecton Option, LM at Pitts Island

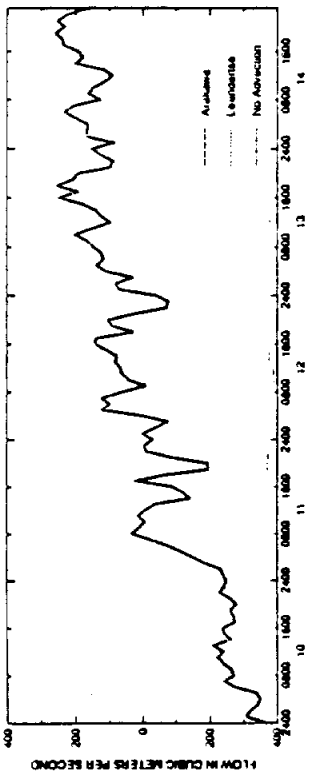


FIG. A-116: Differences in Flow Due to the Advection Option, LM at South Bird Island

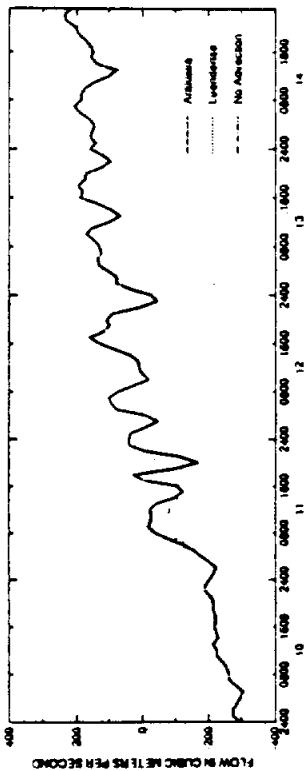


FIG. A-117: Differences in Flow Due to the Advection Option, LM at Green Hill

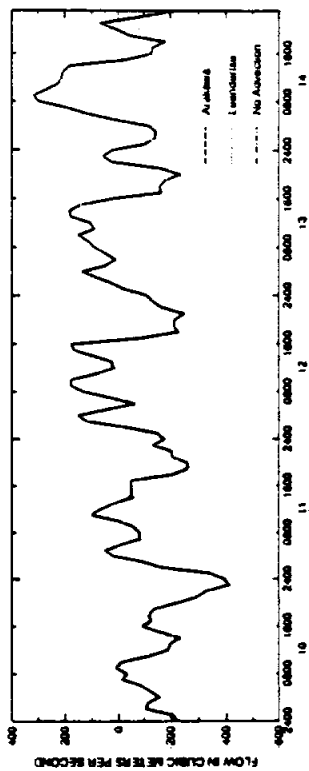


FIG. A-118: Differences in Flow Due to the Advection Option, Batfin Bay

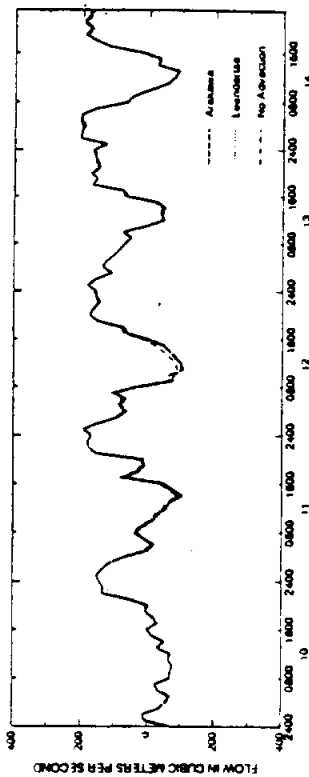


FIG. A-119: Differences in Flow Due to the Advection Option, LM at Yarrowbough Pass

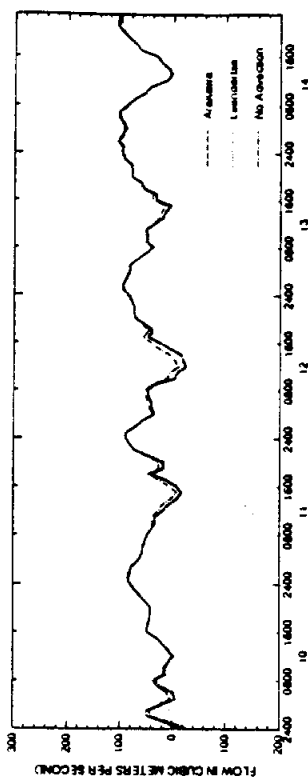


FIG. A-120: Differences in Flow Due to the Advection Option, LM at North Land Cut

APPENDIX B**ABBRIDGED INPUT FILES FOR SWIFT2D AND TXBLEND**

EXAMPLE INPUT FILE FOR SWIFT2D (FILE.IDP)

Lines that begin with an * are comment lines added for clarity.

```

DGUX
SWIFT2D MODEL RUN BY KARL MCARTHUR
U.S. GEOLOGICAL SURVEY, AUSTIN, TX
END HEAD
PRINT LSEPA=1, LHDIV=0, LINP=60, NCO=133, LFICH=0, NOPLU=0, MCKOUT=00000000
      UPPER LAGUNA MADRE SWIFT2D DATA FILE
      200M GRID : RUNS FOR WATER LEVEL CALIBRATION
      SIMULATION RUN ul200c: 2 TIDES, 1 WIND
END NOTE
UL200C
UPPER LAGUNA MADRE : 200M GRID
LAGUNA MADRE 01 JUN '91
*
* Time control, input, and output parameters
*
      3 60 0 0 15840 12960 60 60
99999 99999 99999 60 24 30 99999 0 180 12960 15840 0
      0 0 0 1 0 5 1 1 0 1 1 0
      7 7 7 7 7 7 7
      7 7 7 7 7 7 7
      0 0 0 0 0 0 0 0 0
      0 0 0 0 0 0 0 0
12966 13266 13566 13866 14166 14466 14766 15066 15366 15666 15966 16266
16566 16866 17166 17466 17766 18066 18366 18666 18966 19266 19566 19866
*
* Grid parameters and numerical constants
*
      296 426 0 7 10 0 0 2 9 2 0 0
      0 0 0 0 0 0 0 0 0 0 0
      0.0 0.0 0.0 0 0 0 0 0 0 0
27.333 0.0 200 0.304 1 0.2 1.0 1.0 0.5 1.0 35.0 0
      9.81 0.0015 0.00119 1.011 0.5144 14.3 1000.0 0.97 0.0023
FR80 35SPRO 1.0 1.0
      32 1 0.0 15 30 10.0 M/S 0.75 5
      0.0 0.0 1.5 0.0 0.0 1.0 0.75 0.75
      1.0 2.0 2.0 2.0 2.0 0.00 0.00 0.5 0.5
      1 1 2 1.5 50.0 -0.40 -0.40 0.25 1.0 0.0 1 1
99999 99999
      25.0 1.0000 0.698
*
* Description of tide, velocity, and flow stations and cross sections
*
      1 230 421 CORPUS CHRISTI NAS
      2 255 381 PACKERY CHANNEL
      3 221 366 PITA ISLAND
      4 210 300 SOUTH BIRD ISLAND
      5 156 123 YARBOROUGH
      6 19 179 RIVIERA BEACH
      7 151 75 EL TORO ISLAND
      1 237 394 HUMBLE CHANNEL
      2 248 383 GIWW JFK CAUSEWAY
      3 174 214 GIWW MARKER199
      4 170 214 N OF BAFFIN BAY
      5 162 184 M OF BAFFIN BAY
      6 165 171 S OF BAFFIN BAY E
      7 164 170 S OF BAFFIN BAY M
      8 163 170 S OF BAFFIN BAY W
      9 161 170 S OF BAFFIN BAY FRW
      10 151 69 NORTH LANDCUT
      1 156 170 208 BAFFIN BAY
      2 252 382 386 PACKERY CHANNEL
      1 412 251 256 GIWWLM/CC
      2 413 230 248 NAS
      3 383 247 249 GIWW/JFK
      4 394 236 238 HUMBLE CHANNEL
      5 358 215 245 LM-PITA ISLAND

```

6 291 185 220 LM-BIRD ISLAND
 7 225 168 195 LM-GREEN HILL
 8 124 145 180 LM-YARBOROUGH
 9 75 149 153 LM-LAND CUT

REC 6
 REC 6
 REC 6
 REC 6

* Initial wind speed and direction
 11 160

REC 8

* Descriptions of tidal boundaries

1 6225422277422 1 70.0 CORPUS CHRISTI NAS
 2 8150 69152 69 1 70.0 EL TORO ISLAND

REC 12
 REC 12
 REC 13
 REC 13
 R 23
 1000. R 24
 1.0 R 25
 REC 26

1 0.335
 2 0.338
 0.05 0.10 0.20 0.5 1.0 2.0 5.0
 1.0 2.0 5. 10. 50. 100. 200. 500.
 -0.5 -0.2 -0.1 -0.05 0.001 0.1 0.2 0.5
 2 0 0
 216.4 422.0

. ** Land boundary outlines **

146.2 1.2

999999999.

REC 26

0 0 0 0 0 0 0 0 0 0 0 0 0 0 0 0

. ** Bathymetry data **

-10 -10 0 0 0 0 0 0 0 0 0 0 0 0 0 0
 -11 -11 -10 -10 0 0 0 0 0 0 0 0 0 0 0 0
 -11 -11 -11 -11 -10 -10 0 0 0 0 0 0 0 0 0 0
 -11 -11 -11 -11 -11 -10 -10 0 0 0 0 0 0 0 0 0
 -10 -10 -11 -11 -11 -11 -11 -10 -10 0 0 0 0 0 0 0
 -10 -10 -10 -11 -11 -11 -11 -11 -11 -10 -10 0 0 0 0 0
 -10 -10 -10 -10 -11 -11 -11 -11 -11 -11 -11 -10 -10 -10 0
 3 3 3 -10 -10 -10 -10 -11 -11 -11 -11 -11 -11 -11 -11 -10
 2 2 2 3 3 2 -10 -10 -10 -11 -11 -11 -11 -11 -11
 2 2 2 4 3 3 3 3 -10 -10 -10 -11 -11 -11 -11
 3 3 3 3 3 3 3 3 3 2 -10 -10 -10 -10 -11 -11
 15 15 15 15 15 15 15 15 15 15 15 4 6 2 -10 -10
 3 3 3 3 3 3 3 3 15 3 3 3 4 1 3 3
 2 2 2 2 2 2 2 2 3 15 15 3 3 2 1 5 6
 2 2 2 2 2 2 2 2 3 3 15 15 15 3 2 3 15
 2 2 2 2 2 2 2 2 2 2 3 3 10 15 15 15 15
 2 2 2 2 2 2 2 2 2 -10 2 10 10 3 3 3
 2 2 2 2 2 2 2 2 2 2 15 2 10 2 2 2 1 1
 2 2 2 2 2 2 2 -10 10 10 15 10 2 2 2 1 1
 2 2 2 2 2 2 2 2 10 10 3 15 15 15 2 1 1
 2 2 2 2 2 2 2 3 3 3 -10 -10 3 2 2 15 15
 2 2 2 2 2 3 3 3 3 3 -10 -10 3 2 3 3
 2 2 2 2 3 3 3 3 3 3 3 -10 -10 -10 -10 3
 2 3 3 3 3 3 3 3 2 3 3 3 3 3 3 -10 2
 3 3 3 3 3 3 3 3 3 3 3 3 3 3 3 3
 3 3 3 3 3 3 3 3 3 3 3 3 3 3 3 3
 4 4 4 3 3 3 3 3 3 3 3 3 3 3 3 3
 30 30 4 4 4 3 3 3 3 3 3 3 3 3 3 15
 -10 30 30 30 4 4 4 4 3 3 3 3 3 -10 15 15
 -10 -10 3 30 30 30 30 4 4 4 3 3 -10 15 15 3
 3 3 3 -10 -10 -10 30 30 30 4 4 3 15 15 3 -10
 2 3 3 3 3 -10 -10 -10 30 31 32 4 15 3 -10 -10
 2 2 2 3 3 3 3 3 7 -10 35 38 42 5 5 15
 -11 -10 -10 2 3 3 3 3 7 -10 -10 -10 45 48 50 48
 -11 -11 -11 -10 -10 2 3 3 7 7 3 -10 -10 -10 -10 46
 -11 -11 -11 -11 -11 -10 -10 2 3 7 7 -10 -10 -10 5 8
 -11 -11 -11 -11 -11 -11 -11 -11 -10 3 7 -10 -10 5 8 8
 -11 -11 -11 -11 -11 -11 -11 -11 -11 -11 -10 5 8 8 5
 -11 -11 -11 -11 -11 -11 -11 -11 -11 -11 -11 -10 5 8 5 -10
 -11 -11 -11 -11 -11 -11 -11 -11 -11 -11 -10 8 8 8 5 4
 -11 -11 -11 -11 -11 -11 -11 -11 -11 -11 -10 8 5 4 4 4
 -11 -11 -11 -11 -11 -11 -11 -11 -11 -11 -11 8 5 5 5 5
 -11 -11 -11 -11 -11 -11 -11 -11 -11 -11 8 8 5 5 5 5

```

-11 -11 -11 -11 -11 -11 -11 -11 -11 -11 8 4 4 4 4 4
-11 -11 -11 -11 -11 -11 -11 -11 -11 -10 8 3 3 3 3 3
-11 -11 -11 -11 -10 -11 -11 -11 -11 -10 4 6 3 3 2 2 2
-11 -11 -11 -11 -11 -11 -11 -11 2 2 3 3 2 2 -10 -10
-11 -11 -11 -11 -11 -11 -11 -11 -10 -10 2 2 2 -10 -11 -11
-10 -11 -11 -11 -11 -11 -11 -11 -11 -10 2 2 -10 -11 -11 -11
-11 -11 -11 -11 -11 -11 -11 -11 -10 -10 -10 -10 -11 -11 -11
-10 -10 -10 -11 -11 -11 -11 -11 -11 -11 -11 -11 -11 -11 -11
-10 -10 -10 -10 -10 -11 -11 -11 -11 -11 -11 -11 -11 -11 -11
-10 -10 -10 -10 -10 -10 -10 -10 -11 -11 -11 -11 -11 -11 -11
-10 -10 -10 -10 -10 -10 -10 -10 -10 -11 -11 -11 -11 -11 -11
-10 -10 -10 -10 -10 -10 -10 -10 -10 -10 -10 -10 -11 -11 -11
-10 -10 -10 -10 -10 -10 -10 -10 -10 -10 -10 -10 -10 -10 -10
-10 -10 -10 -10 -10 -10 -10 -10 -10 -10 -10 -10 -10 -10 -10
0 0 -10 -10 -10 -10 -10 -10 -10 -10 -10 -10 -10 -10 -10
0 0 0 0 -10 -10 -10 -10 -10 -10 -10 -10 -10 -10 -10

```

. ** Bathymetry data **

```

. 0 0 0 0 0 0 0 0 0 0 0 0 0 0 0
0.005
20.00
0.040
147 3 9 0.025 0.025 0.025 0.025 0.025 0.025 0.025

```

REC 28
REC 29
REC 30
REC 31
REC 32

. ** Spatially distributed Manning's n

```

. 274 415 421 0.040 0.040 0.040 0.040 0.040 0.040 0.031
0.0

```

REC 33
REC 34
REC 35
REC 36

```

235 393 1.0 1.0 HUMBLE CHANNEL
257 382 1.0 1.0 PACKERY CHANNEL
211 300 1.0 1.0 SOUTH BIRD ISLAND
60 175 1.0 1.0 BAFFIN BAY
19 123 1.0 1.0 RIVIERA BEACH
156 123 1.0 1.0 YARBOROUGH PASS
146 10 1.0 1.0 NORTH LAND CUT
249 381 1.0 1.0 GIWW AT JFK CAUSEWAY
228 422 1.0 1.0 CORPUS CHRISTI NAS

```

REC 37
REC 37
REC 37
REC 37
REC 37
REC 37
REC 37
REC 37

225 422

REC 39

. ** Computational grid enclosure **

. 225 422 1

REC 39

A 1 1 0 6 0.335 0.317 0.289 0.259 0.237 0.210

. ** Corpus Christi NAS hourly tide data **

```

A 1301800 6 0.262 0.280 0.289 0.295 0.295 0.295
A 2 1 0 6 0.338 0.344 0.347 0.350 0.353 0.344

```

. ** El Toro Island hourly tide data **

```

A 2301800 6 0.125 0.109 0.121 0.133 0.130 0.124
F 1 0 16

```

. ** Corpus Christi NAS wind speed data **

```

F 302300 14
G 1 0 140

```

. ** Corpus Christi NAS wind direction data **

G 302300 150

BLANK
BLANK

EXAMPLE INPUT FILE FOR TXBLEND

BOTH ; north end channel inflows, 1/5/96; no inflow but open;4/17/96
 Corpus Christi/Laguna Madre; Corpus.geo.5; June 1991 FieldStudy
 Model: TxBLEND:S1.

NN	NE	NH	NLIN	NV	NVEL	NTRT	NOPT	NCON	NMOM	ITW	INEW	NTRN	NHC		
4913	8187	29	1	1750	0	1	0	1	3	0	1	2	35		
	TSTRT		TIME		DELT		ITMAX		NFRST		NCUT		NCARD		NPLOT
	000.0		0744.0		300.		07992		007560		0036		01		00
	COR		TWGT		LMPC		LMPM		BCLUMP		THETA		ALPHA		WIMP
	29.6		0.5		1.0		1.0		1.0		1.0		0.5		1.0
	TWGT		LMPTL		LMPTR		DISX		DISY		DISXY				
	1.0		01.0		01.0		0.0		0.0		0000.0				

INCIDENCE LISTS

1	1	21	22
2	2	1	22

8186	4910	4912	4913
8187	4910	4913	4911

NODAL LOCATION

1	685672.8	3115812.0	3.28	3.28
2	687424.3	3115090.8		

4912	624965.6	3017874.2
4913	624306.2	3017444.2

SET DEPTH NODES

1497	1470	1443	1412	1413	1377				
1378	1379	1380	1346	1311	1312	1275	1276	1277	1313
1314	1347	1381	1414	1444					
4869	4857	4870	4871	4872	4861	4845	4846		

SPECIFIED NORMAL

21	62	104	145	186	226	265	266	304	340
341	305	267	268	269	231	232	191	148	192

1298	1299	1336	1372	1409	1441	1469	1415	1383
1350	1318	1283	1245	1246				

KNOWN VELOCITIES

DIRECTION ANGLE

21	1	62
62	21	104

1246	1245	1210
1210	1246	1175

SPECIAL EDGES

BATHYMETRIES

1	2.40
2	6.00

4912	2.02
4913	2.02

INITIAL HEIGHTS

HEIGHTS AT T-DT

VELOCITIES

T-DT VELOCITIES

NORMAL VELOCITY

MANNINGS N VALUE

1 0.0287
2 0.0287

4912 0.0401
4913 0.0401

CONCENTRATIONS

1 5.00
2 5.00

4912 23.81
4913 23.81

FIXED QUALITY

1497 1470
1443 1412 1413 1377 1378 1379 1380 1346 1311 1312
1275 1276 1277 1313 1314 1347 1381 1414 1444
340 341
483 484
3831 3851
3708 3709
4908 4909
519 543
354 355

DISPERSION COEFS

1 203.
2 203.

4912 3000.
4913 3000.

ANISOTROPIC DISP

XXXX: end of BLEND input data

TWDB input parameters

1,0.2, idens: 1 to calculate the density terms

1, imix : 1 to call subr POLUTE

1, iwarm: zero means no warmup

0, irepeat: number of repetition days at the simulation start

0.001,2,0.50, 0.55,0.6,0.67, 0.5, pictim, itpics, wt2: Picard iteration parameters

1, iwantp: 0 to suppress intermediate printouts for u,v,h,c

3600., printime: TWDB printout interval(for outflw1 file), in seconds

3600.,3, flwtime, iflwunit: print interval in sec(for outflw2); 1 in cfs;2 in 1000

6., buildtime: initial river inflow build-up time, in hours

0, irestrt: 1 to restart

720, iwrite: write interval in hours for restart data; 0 no write

0, ievap: 0 to use constant meteo data; 1 to use daily data

0.3, evap0: constant evaporation rate in inches per day

1.0, evpfac: evaporation effect adjustment factor

3, iwind: 0 for constant wind; 1 for 3-hourly wind; 2 for daily wind;3:hourly

0,150, wnd0 and wndd0: constant wind vel(mph) and direction

0.8, 1.0, wndfac: wind stress adjustment factor

1, 3, iwave: 1 to read tide data;2 to use sine wave starting 0 elev;3 at middle

2, ntids: number of tidal locations

```

0,0,0, 1.5,24,0, tidal amplitude and period(hours); 0,0 to read input tidal data
0,0,0, 1.5,24,0, tidal amplitude and period(hours); 0,0 to read input tidal data
0, isumq: 0 not to calculate residual flows
0,0, strtaq,endaq: for residual flow calculation
DIFCON
1,5000, 50000,
0,0,0 to stop difcon section
constant DISPERSION
0, idisprsn: 0 for constant dispersion coeff;1 for variable(i.e. use DIFCON)
0,0,0, to stop idisp section
1., convfac:convective term adjuster
0,1000., idiff,tdiff
0,.95,.95, ialph,prcnt,prcnt2
0.2,0.5, 0.0, nlnfac
bigG section
100.,0.01,, H1,G1
-10.,0.03,, H2,G2
Manning's N
0,0,0, to stop manN section
*****
Nueces River
0, number of months in the record
5,15,1991, starting date of simulation
6,16,1991, ending date of simulation
7, number of inflow locations
0, 1: variable inflows, 0: constant inflows
3831,3851, 100.,, Nueces
3708,3709,10.,, Oso Crk
483,484,10.,, Aransas Rvr
340,341,10.,, Mission Rvr
354,355,10.,, Copano Crk
519,543,10.,, Salt/Cavasso Crk
4908,4909,10.,, SanFernando Crk(BaffinBay)
**Tide Data**
BobHall tides (actid.BobH2; 0% adjustment); data start 0th hour
32, number of days in the tide record
2, number of tidal locations
21, number of nodes in the 1st location (Gulf at Corpus)
3, number of nodes in the 2nd location (South end of CCBNEP)
1, tidal location number (Gulf at Corpus)
  5 15 -0.48 -0.82 -0.61 0.25 1.21 1.80 1.83 1.85 1.53 1.06 1.00 0.43
  5 16 -0.34 -0.93 -0.93 -0.34 0.50 1.61 1.94 2.03 1.95 1.57 1.52 1.09
  5 17 0.48 -0.25 -0.36 -0.72 -0.56 1.67 0.99 1.75 1.71 1.52 1.46 1.08
  5 18 0.61 -0.06 -0.49 -0.49 -0.11 0.62 1.69 1.69 2.00 1.70 1.73 1.83
  5 19 0.98 1.03 0.00 -0.06 0.13 0.66 1.52 1.91 2.01 1.82 1.62 1.49
  5 20 1.37 1.41 0.84 0.50 0.44 0.81 1.34 1.81 2.08 1.84 1.76 1.57
  5 21 1.50 1.53 1.33 1.06 0.90 0.81 1.18 1.48 1.65 1.47 1.21 1.09
  5 22 1.03 1.25 1.35 1.30 1.22 1.08 1.26 1.54 1.66 1.45 1.11 0.92
  5 23 0.90 1.23 1.49 1.98 1.79 2.21 2.01 1.95 2.12 1.90 1.55 1.27
  5 24 1.24 1.29 1.83 2.32 2.10 2.10 1.88 1.71 1.67 1.44 1.12 0.72
  5 25 0.47 0.55 1.08 1.72 1.94 1.85 1.81 1.40 1.55 1.51 1.04 0.68
  5 26 0.21 0.24 0.74 1.37 1.83 1.98 1.85 1.60 1.49 1.25 0.90 0.41
  5 27 -0.15 -0.24 0.09 0.74 1.32 1.51 1.55 1.30 1.22 1.13 0.74 0.29
  5 28 -0.12 -0.26 -0.06 0.73 1.27 1.77 1.76 1.64 1.41 1.24 1.00 0.42
  5 29 -0.04 -0.33 -0.25 0.39 1.02 1.66 1.69 1.54 1.41 1.27 1.15 0.63
  5 30 -0.04 -0.32 -0.24 0.08 0.90 1.58 1.72 1.56 1.46 1.21 1.14 0.67
  5 31 0.24 -0.18 -0.23 -0.04 0.48 1.16 1.54 1.50 1.45 1.19 1.01 0.66
  6 1 0.21 -0.18 -0.47 -0.15 0.46 0.85 1.31 1.41 1.46 1.27 1.21 0.95
  6 2 0.67 0.22 -0.08 -0.02 0.32 0.81 1.46 1.23 1.24 1.02 0.99 0.80
  6 3 0.62 0.35 0.00 -0.20 0.14 0.76 1.11 1.42 1.35 1.21 1.05 0.94
  6 4 0.59 0.44 0.06 0.29 0.49 0.65 0.88 1.09 1.07 0.84 0.47 0.54
  6 5 0.44 0.27 0.02 0.07 -0.09 0.29 0.36 0.71 0.60 0.46 0.17 0.24
  6 6 0.34 0.30 0.41 0.37 0.43 0.28 0.29 0.73 0.44 0.33 -0.20 -0.19
  6 7 -0.01 0.16 0.44 0.44 0.79 0.08 0.90 0.61 0.51 0.53 0.12 -0.19
  6 8 0.14 0.56 0.98 1.93 1.31 1.53 1.44 1.47 1.69 1.37 0.98 0.89
  6 9 0.80 1.22 1.91 2.31 2.60 2.28 2.06 1.91 1.83 1.48 0.95 0.30
  6 10 0.08 0.55 1.31 1.98 2.53 2.60 2.22 2.01 1.87 1.31 0.88 0.03
  6 11 -0.27 -0.34 0.34 1.28 2.00 1.96 2.17 1.71 1.64 1.14 0.81 0.07
  6 12 -0.42 -0.76 -0.10 0.68 1.55 2.00 2.10 1.74 1.52 1.30 0.99 0.30
  6 13 -0.61 -1.00 -0.76 0.03 1.18 1.60 1.95 1.64 1.55 1.20 0.99 0.52
  6 14 -0.39 -0.76 -0.91 -0.20 0.71 1.38 1.84 1.76 1.65 1.46 1.21 0.94
  6 15 0.21 -0.66 -0.98 -0.72 0.18 0.86 1.46 1.46 1.47 1.09 1.16 1.10

```

2, tidal location number (South end) actid.ElToro2

5 15	0.92	0.98	0.98	0.98	0.96	0.94	0.92	0.92	0.94	0.96	0.97	0.97
5 16	0.92	0.96	0.94	0.94	0.92	0.94	0.94	0.93	0.90	0.90	0.90	0.93
5 17	0.94	0.88	0.87	0.84	0.58	0.98	1.03	0.78	0.84	0.89	0.87	0.93
5 18	0.88	0.80	0.82	0.80	0.77	0.77	0.80	0.77	0.74	0.74	0.76	0.82
5 19	0.80	0.80	0.77	0.76	0.78	0.76	0.72	0.72	0.74	0.79	0.84	0.86
5 20	0.82	0.81	0.81	0.84	0.83	0.82	0.80	0.84	0.85	0.85	0.83	0.89
5 21	0.92	0.89	0.89	0.92	0.95	0.95	0.93	0.93	0.95	0.99	0.98	0.99
5 22	1.01	1.00	0.98	1.00	1.02	1.02	1.02	1.00	0.99	0.99	1.02	1.01
5 23	0.98	0.99	1.02	1.02	1.01	1.04	1.04	1.05	1.07	1.08	1.08	1.08
5 24	1.08	1.09	1.11	1.11	1.12	1.13	1.14	1.15	1.18	1.20	1.22	1.20
5 25	1.24	1.26	1.22	1.21	1.24	1.20	1.21	1.25	1.18	1.29	1.25	1.25
5 26	1.24	1.25	1.24	1.22	1.21	1.19	1.16	1.17	1.19	1.19	1.22	1.22
5 27	1.22	1.22	1.19	1.16	1.15	1.17	1.18	1.16	1.16	1.12	1.14	1.14
5 28	1.13	1.12	1.10	1.09	1.07	1.07	1.05	1.07	1.07	1.06	1.06	1.06

6 15 0.91 0.91 0.90 0.88 0.81 0.85 0.85 0.84 0.85 0.83 0.86 0.87

Flow Exchange*

CCBNEP flow exchange locations

35, number of passes or cross-sections (at most 48)

02,NuecesRiver, 1 (watch for I2,1X,A8; nodes on section at most 15)

3851 3831

02,NuecesR2 2

3751 3728

02,NuecesR3 3

3504 3503

02,NuecesR4 4

3339 3338

04,CCchnUTMSI 5

973 955 935 911

04,CCchnB&R 6

996 995 970 969

04,CCchnIngleside 7

1449 1418 1417 1416

02,CCchnTurnBasin 8

2490 2436

08,NuecesCauseway 9

2361,2362,2363,2364,2365,2366,2430,2486,2487,2488

03,PtMustang 1

1437 1438 1408

03,PelicanIsland 11

1452 1482 1483

02,icwwIngCut 1

1420 1421

03,LydiaAnn 1

790 789 788

02,AransPas 1

980 879

03,Morris1

968 967 943

02,Morris2

915 914

02,CCBayou

760 759

02,icwwCoveHarbor 18

630 608

04,CopanoBridge 1

74 33 7 36

02,AyresDugout 2

615 591

02,Icww/Refugi 2

547 548

02,Icww/BludworthIsl 22

330 331

02,CedarDugout 2

393 394

03,OscBridge 2

2337 2338 2284

04,icwwLM/CC 2

2469 2416 2417 2356

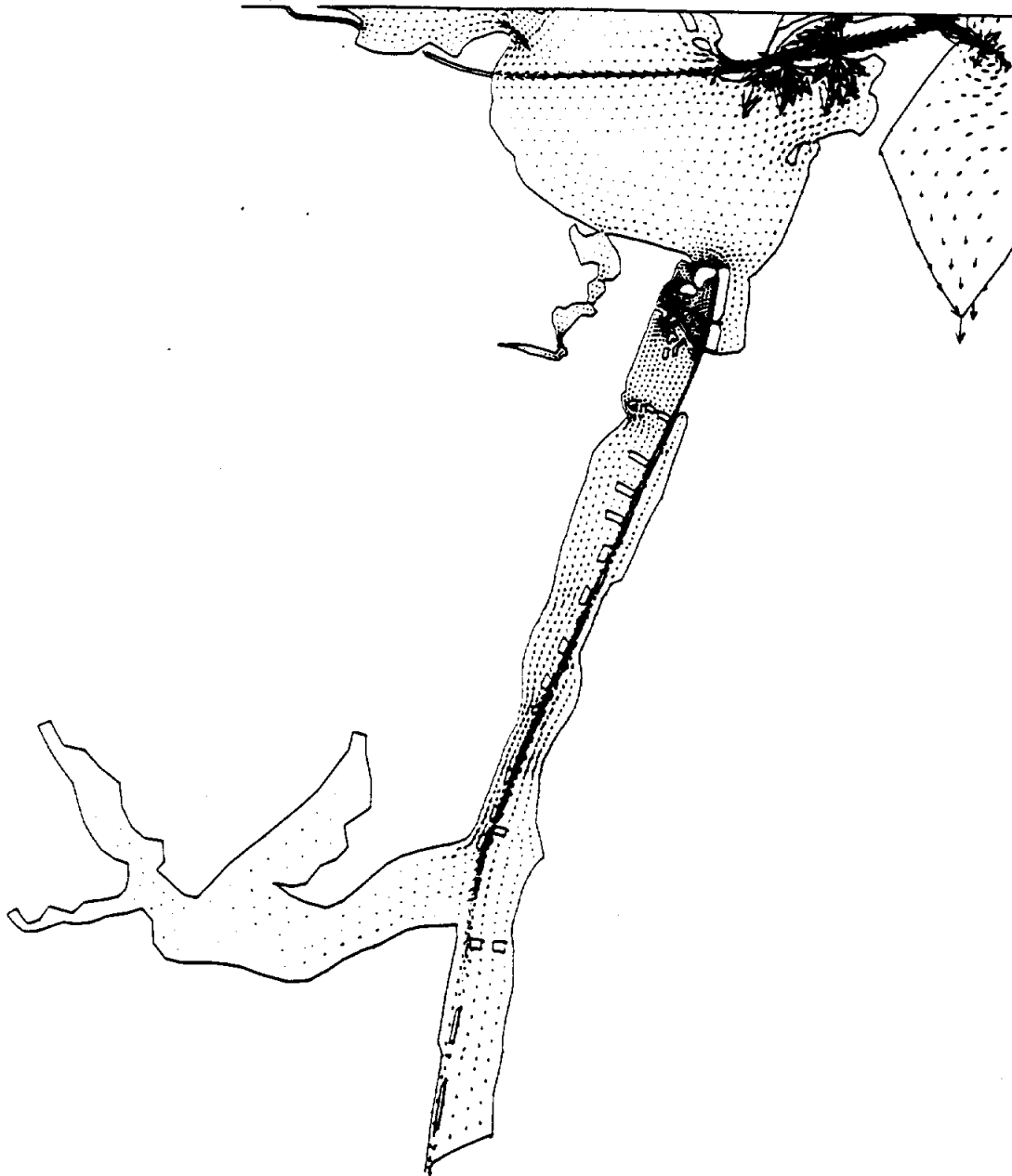

```

04,NAS
  2285 2344 2406 2468
04,icwJFK
  3209 3173 3174 3133
03,HumbleChannel 28
  3191 3192 3193
02,PackeryChannel 29
  2986 2933
10,LM-PitaIsland 30
  3781 3758 3736 3737 3738 3721 3702 3703 3704 3686
10,LM-BirdIsl 3
  4076 4065 4066 4067 4068 4083 4096 4097 4110 4111
10,LM-GreenHill 35
  4334 4335 4336 4349 4350 4364 4365 4377 4378 4390
08,Baffin
  4602 4583 4566 4550 4535 4521 4506 4492
08,LM-Yarborough 33
  4770 4771 4791 4792 4812 4794 4776 4798
03,LM-LandCut 3
  4869 4857 4870
***Check Nodes***
40, number of check nodes(at most 40)
01, 3831, Nueces River inflow point
02, 2363, Nueces Causeway-2 (spoil), 3231, mid Nueces River
03, 3271, Nueces River Mouth
04, 3333, upper Nueces Bay
05, 2841, mid Nueces Bay
06, 2486, Nueces Causeway at the Channel
07, 3691, B.Davis PwrPlnt, 6, 2831, Nueces Power
08, 2490, CCchn near COE (or Turning Basin)
09, 1693, mid Corpus at RangeTower(Datasonde site)
10, 1418, CCchannel near Ingleside
11, 970, CCchannel near B&R
12, 935, CCchannel near UTMSI
13, 1311, Tidal Boundary
14, 789, Lydia Ann Channel
15, 2416, icwLM/CC
16, 3174, icw/JFK
17, 2344, NAS
18, 3192, Humble Channel
19, 2338, Oso Bridge
20, 535, AransasBay
21, 33, CopanoBridge
22, 3752, Pita Island, 378, Bayside
23, 4096, BirdIsland
24, 2986, PackeryChannel(tide)
25, 4857, SouthEnd
26, 4447, LM-RockyPt-B(icw)
27, 4444, LM-RockyPt
28, 3726, icwLM/PitaIsl
29, 4621, So of BaffinBay-A
30, 4639, So of BaffinBay-C(icw)
31, 4771, YarboroughPass(tide)
32, 485, RockPort(tide)
33, 858, Aransas(shrimp) Channel
34, 914, Morris and Cummings Cut
35, 944, Redfish Cut
36, 4567, BaffinBay(mouth)
37, 972, PortAransaa(tide)
38, 3136, WhitePoint(tide, Nueces Bay)
39, 4852, Riviera Beach, 39,2544, Flourbluff-1
40, 1260, Gulf beach for BobHall
*****
Variable Boundary concentrations
0, IBCONC: 0 not to invoke this option
***end of input*****
365, ndaycn
1, nconls

```

APPENDIX C

VELOCITY VECTOR PLOTS FOR JUNE 10, 1991 06:00 TO JUNE 11, 1991 12:00



6.30E+02 HOURS

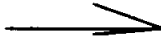
5 FPS: 

FIG. B-1. TxBLEND Simulated Velocity Vectors, June 10, 06:00

VELOCITY AT TIME 13320 GRID SIZE 290 BY 401

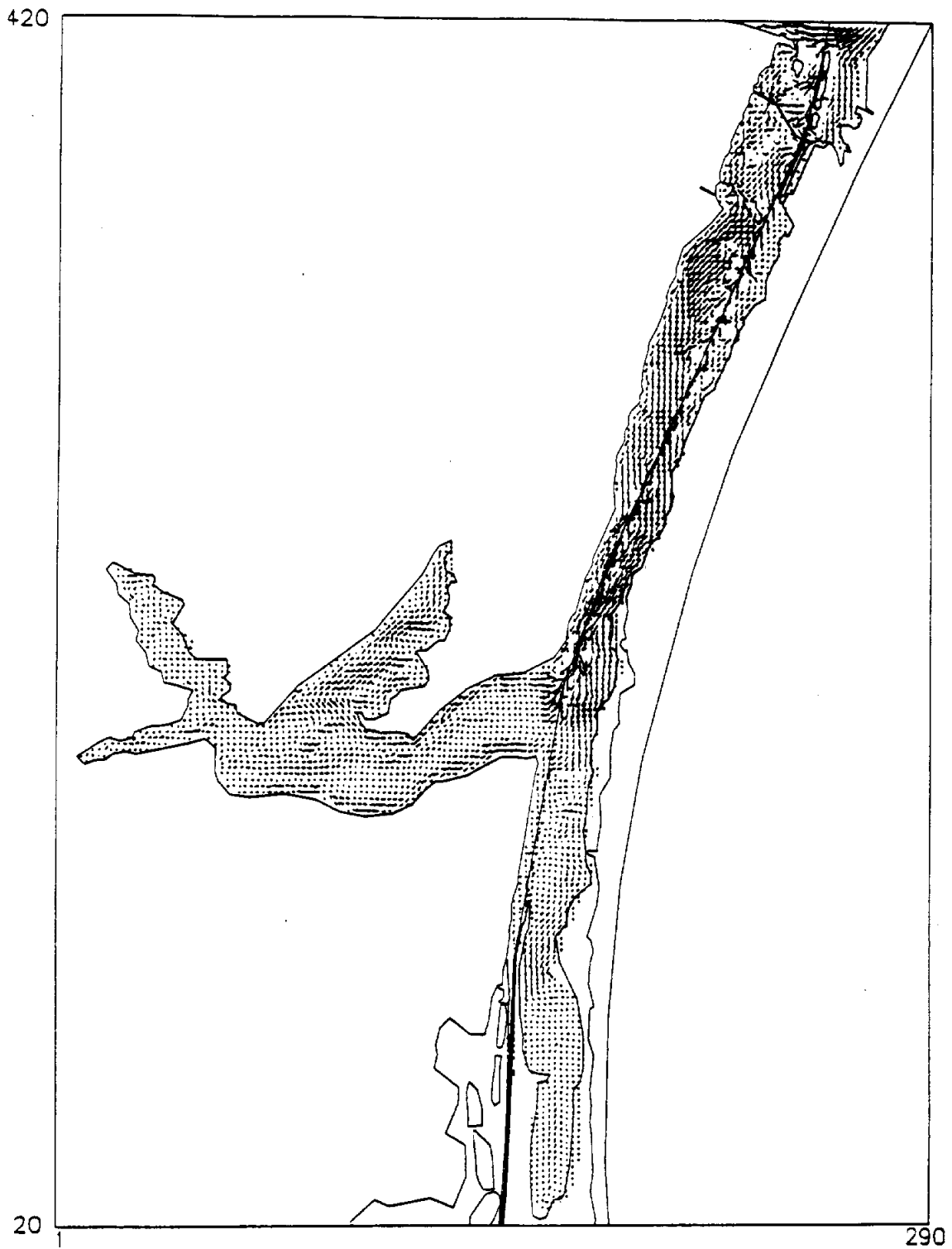


FIG. B-2. SWIFT2D Simulated Velocity Vectors, June 10, 06:00

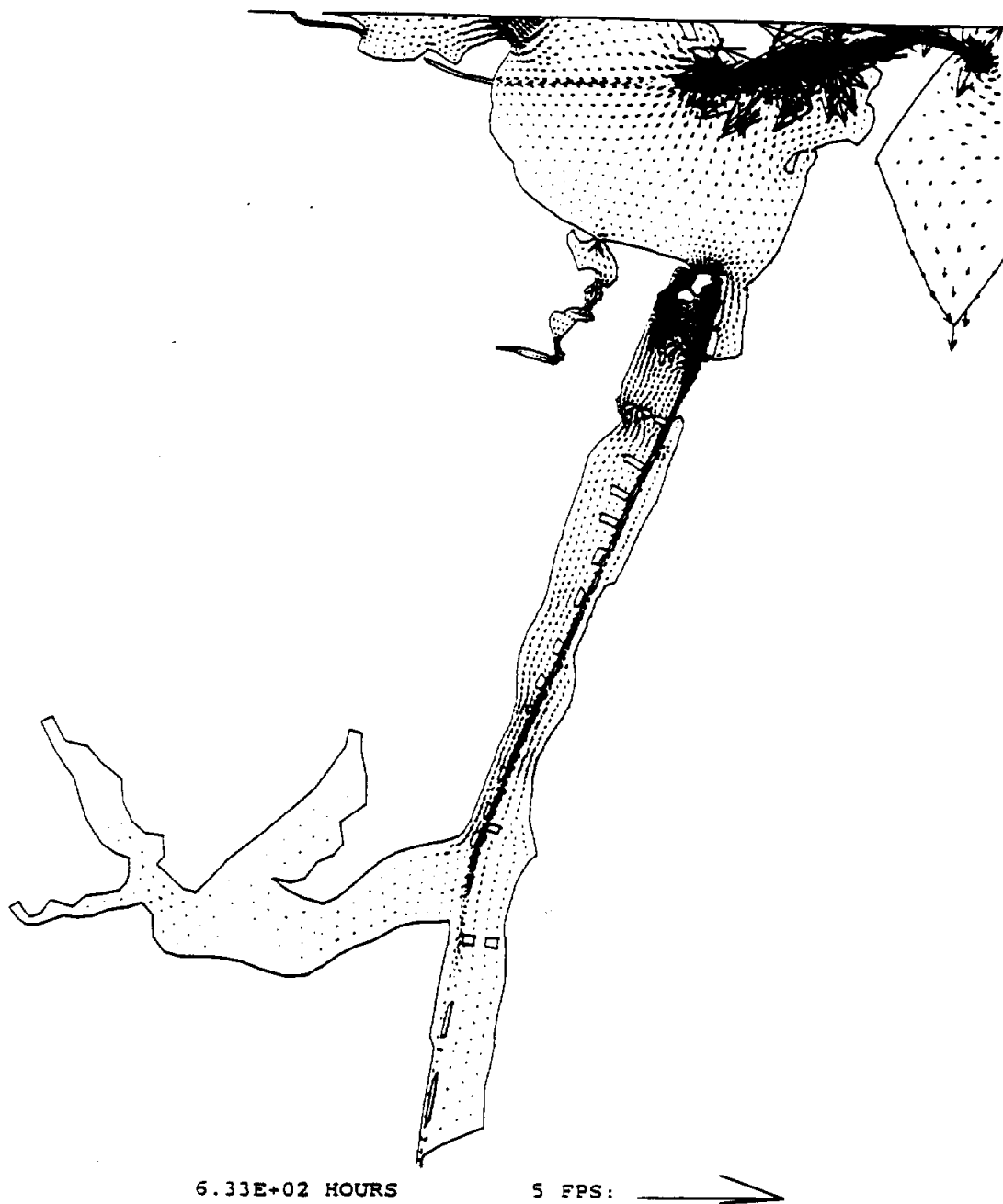


FIG. B-3. TxBLEND Simulated Velocity Vectors, June 10, 09:00

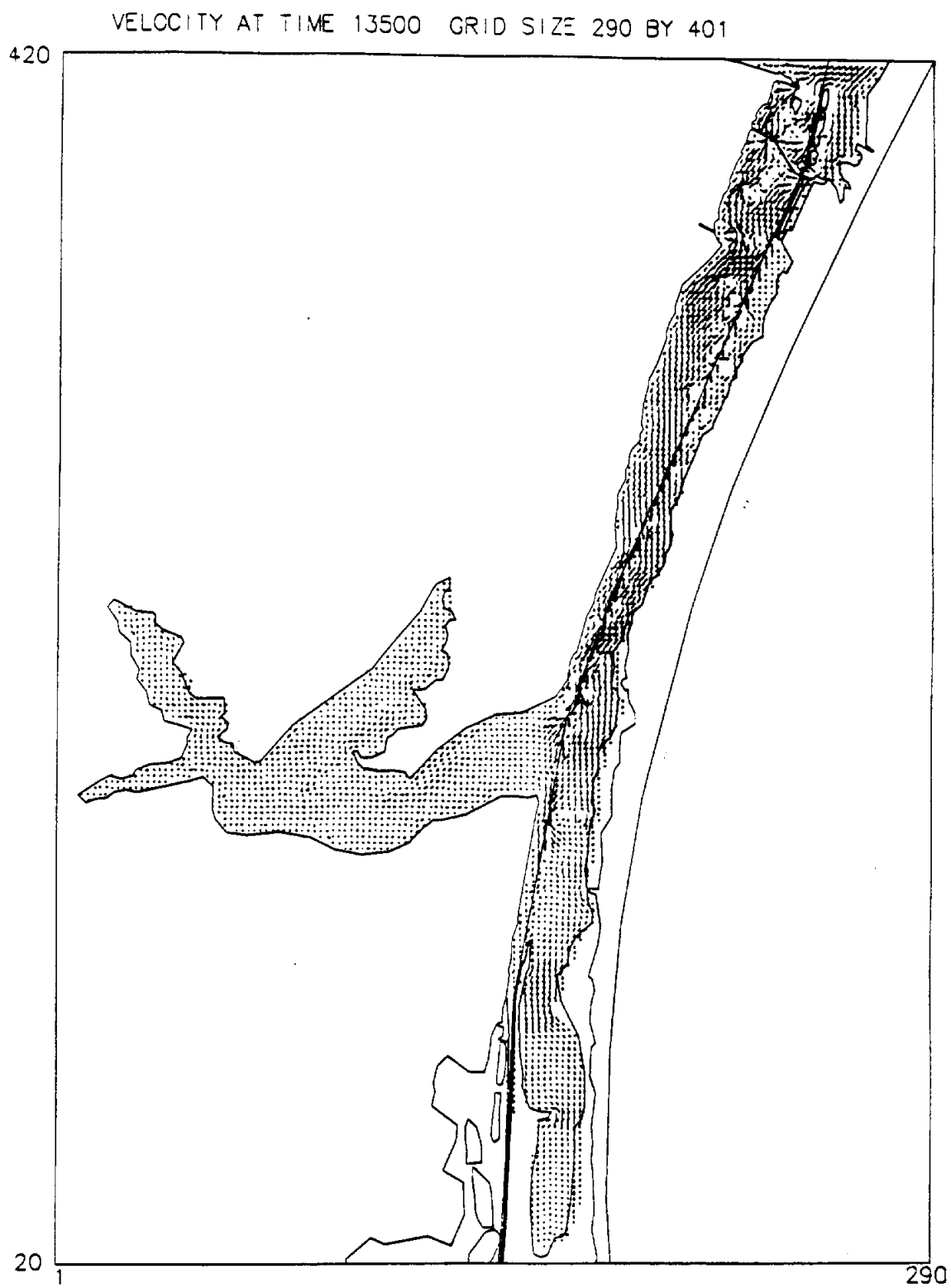


FIG. B-4. SWIFT2D Simulated Velocity Vectors, June 10, 09:00

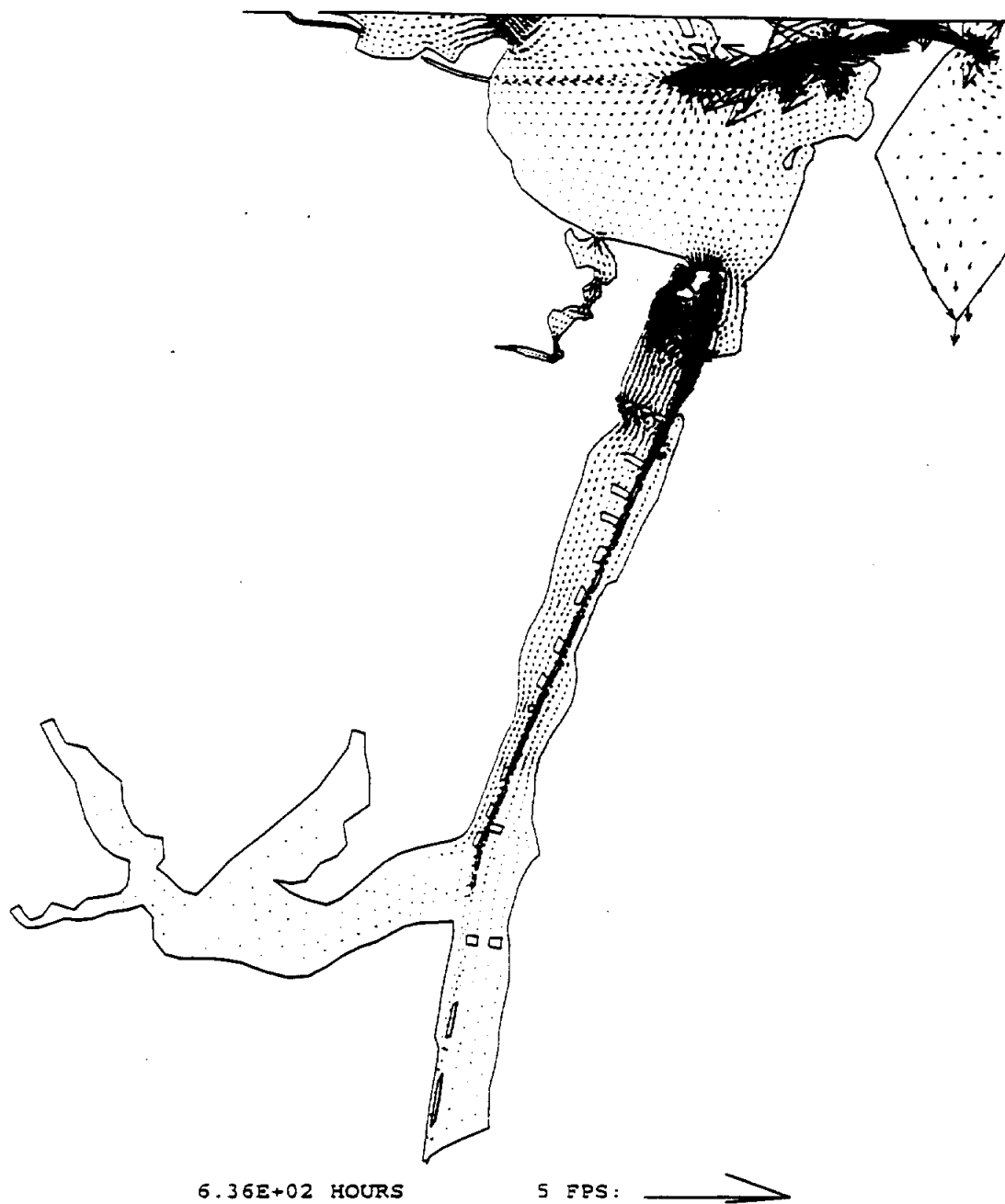


FIG. B-5. TxBLEND Simulated Velocity Vectors, June 10, 12:00

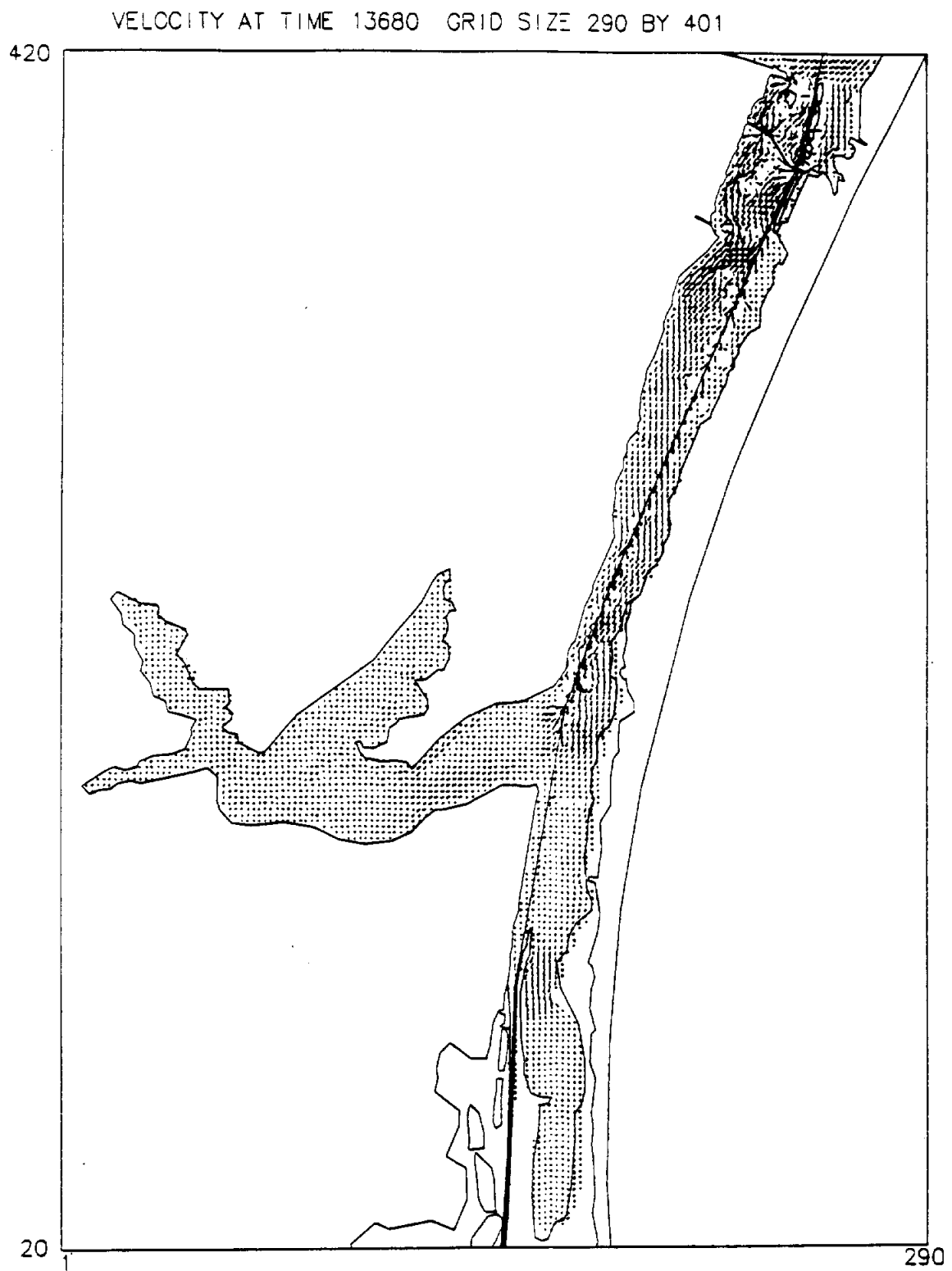


FIG. B-6. SWIFT2D Simulated Velocity Vectors, June 10, 12:00

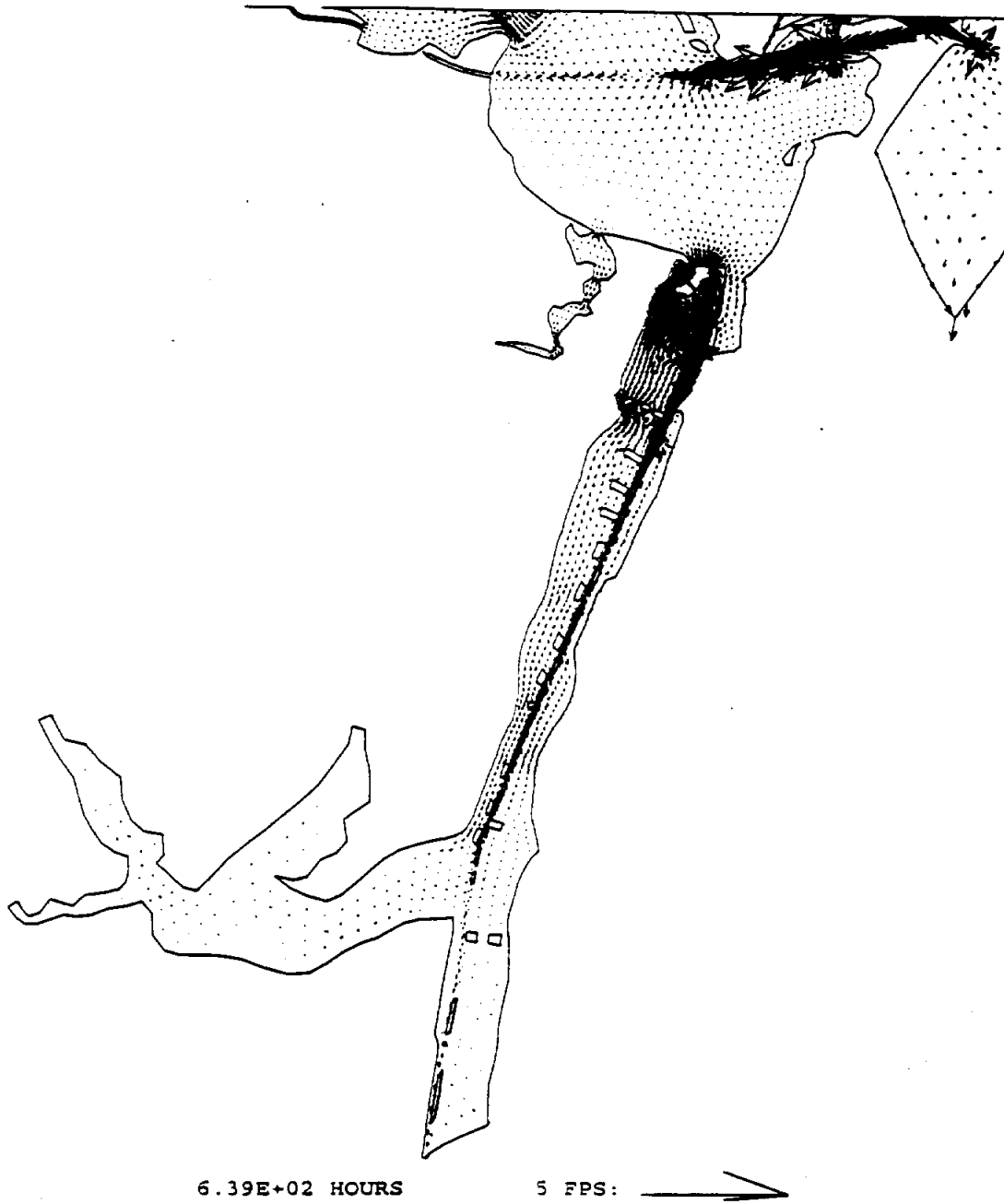


FIG. B-7. TxBLEND Simulated Velocity Vectors, June 10, 15:00

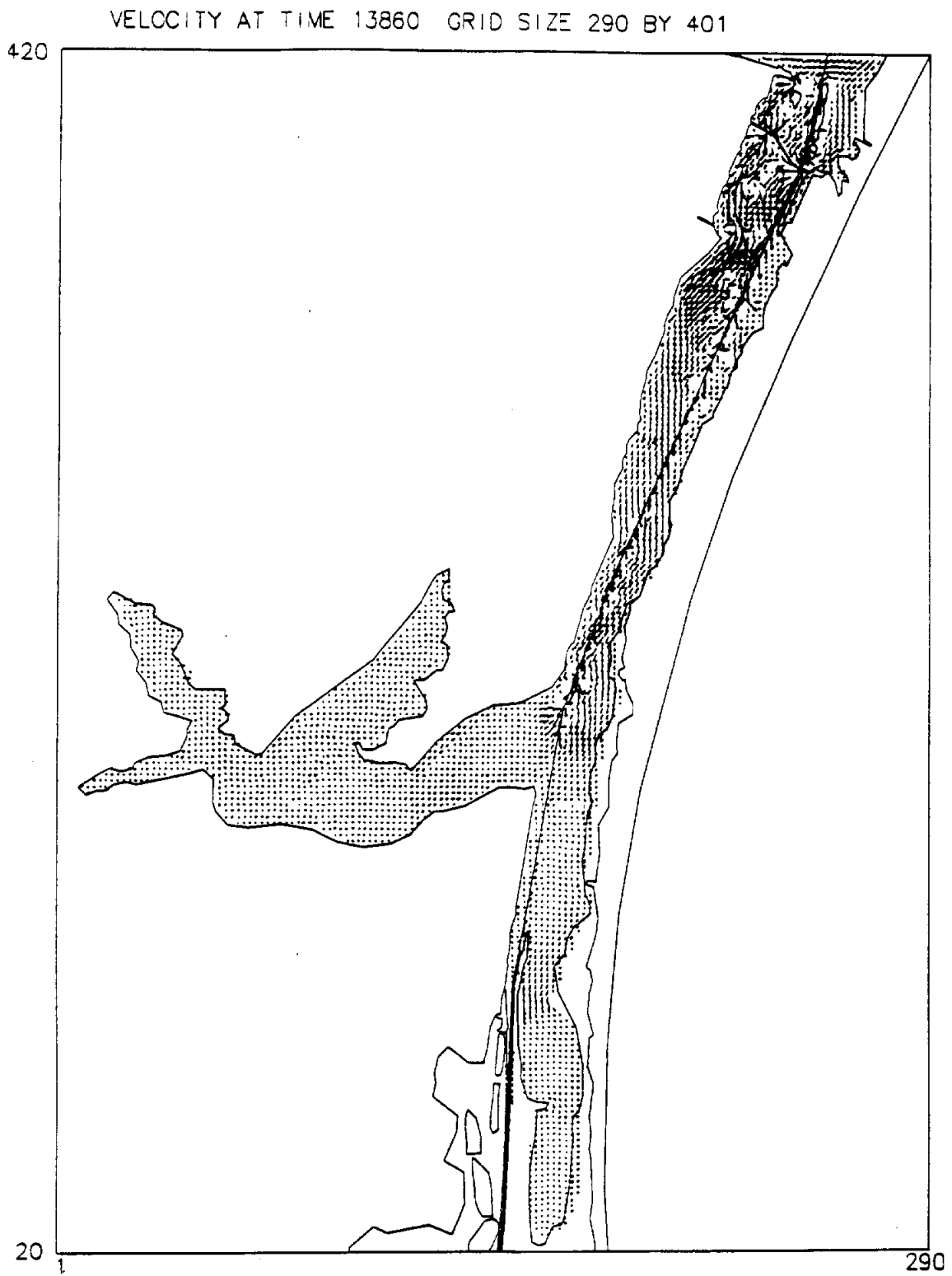
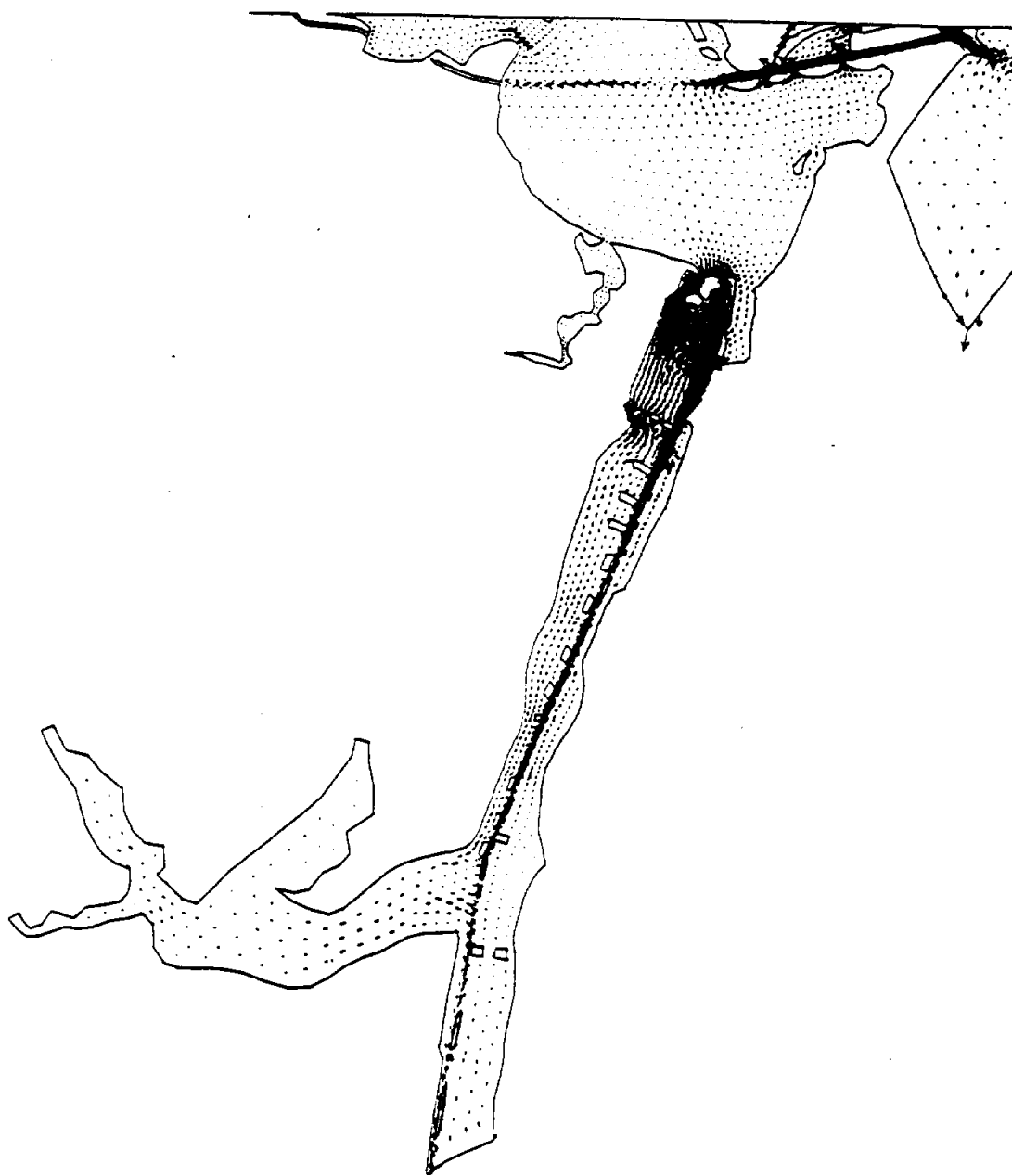


FIG. B-8. SWIFT2D Simulated Velocity Vectors, June 10, 15:00



6.42E+02 HOURS

5 FPS: 

FIG. B-9. TxBLEND Simulated Velocity Vectors, June 10, 18:00

VELOCITY AT TIME 14040 GRID SIZE 290 BY 401

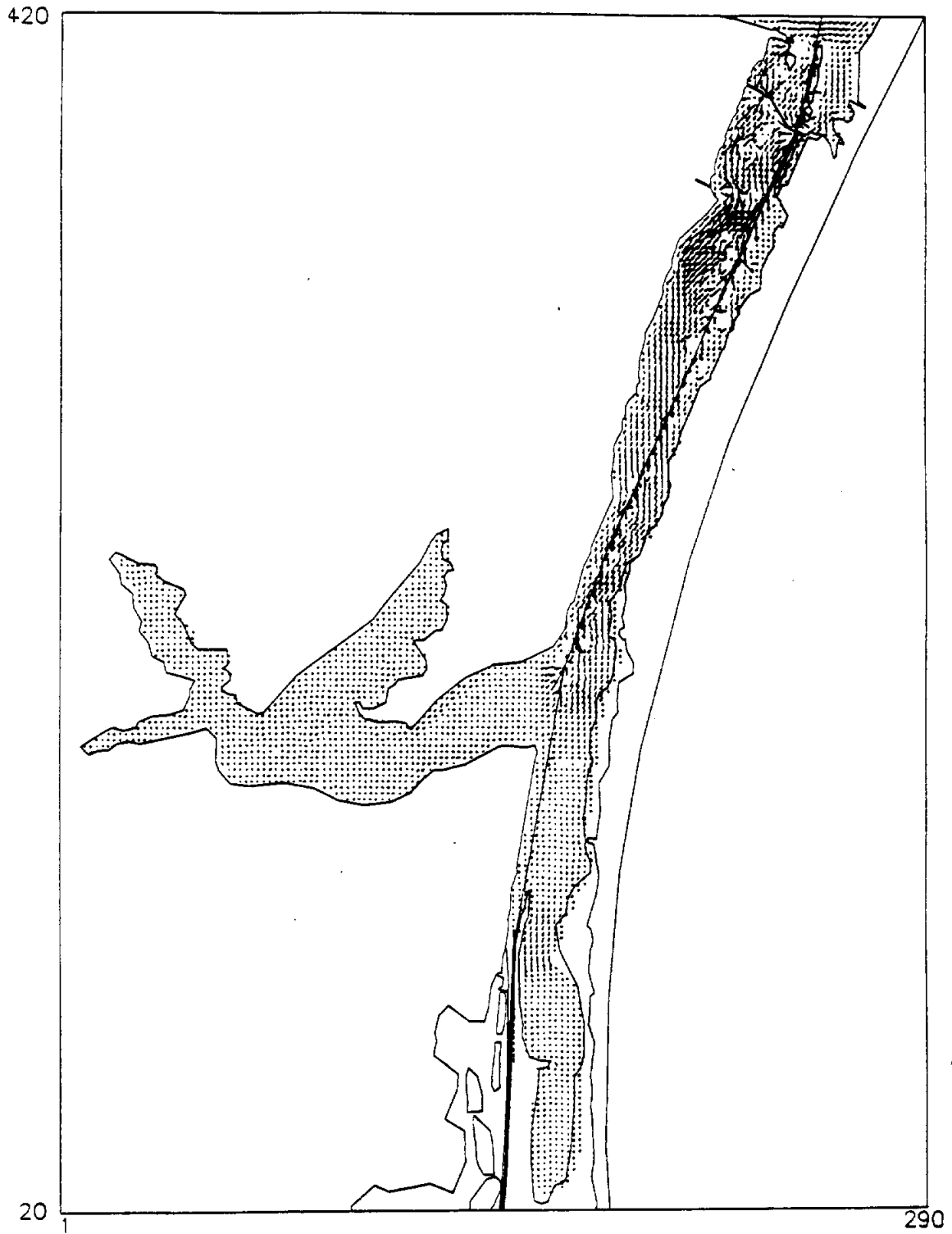


FIG. B-10. SWIFT2D Simulated Velocity Vectors, June 10, 18:00

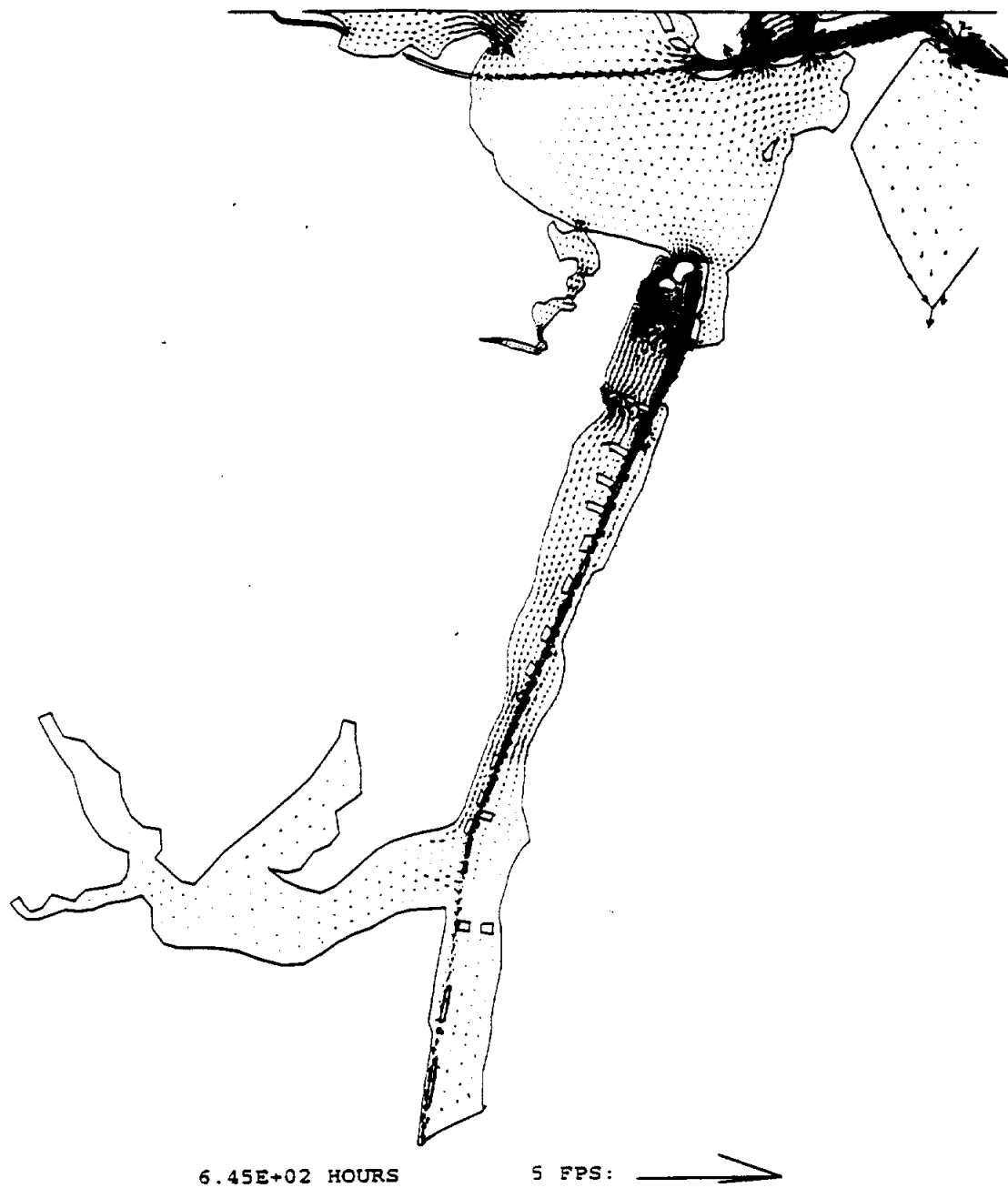


FIG. B-11. TxBLEND Simulated Velocity Vectors, June 10, 21:00

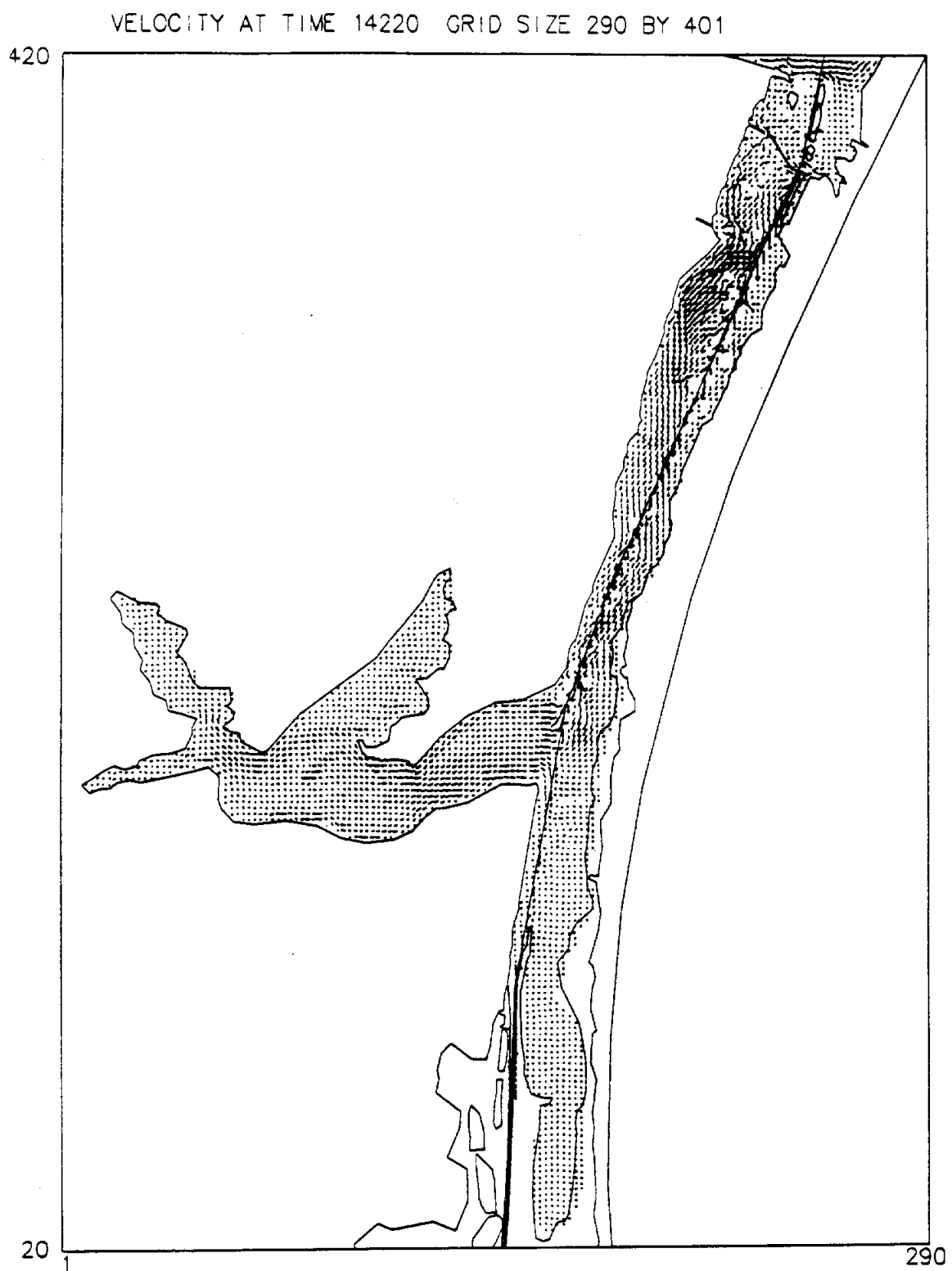


FIG. B-12. SWIFT2D Simulated Velocity Vectors, June 10, 21:00

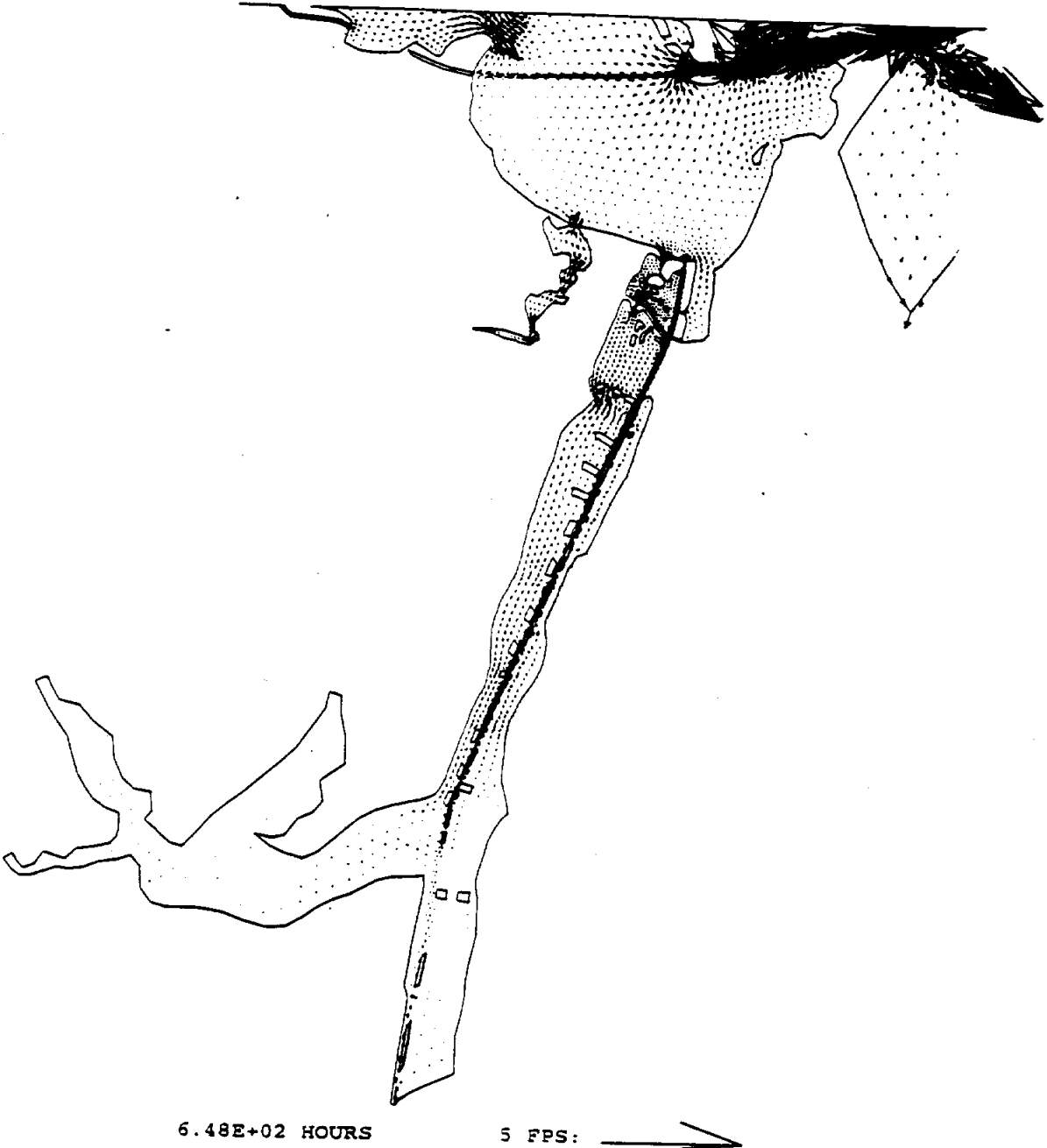


FIG. B-13. TxBLEND Simulated Velocity Vectors, June 11, 00:00

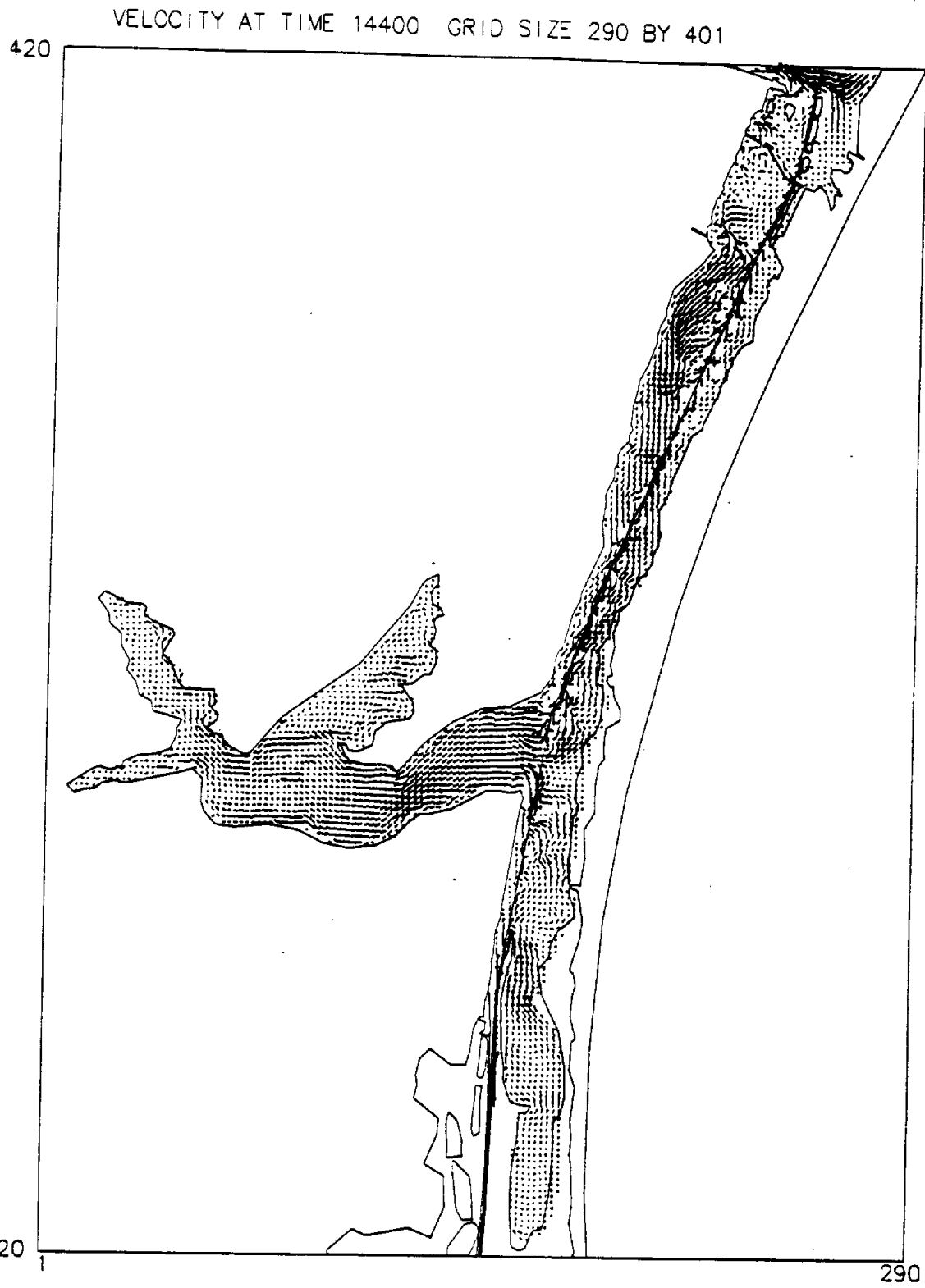
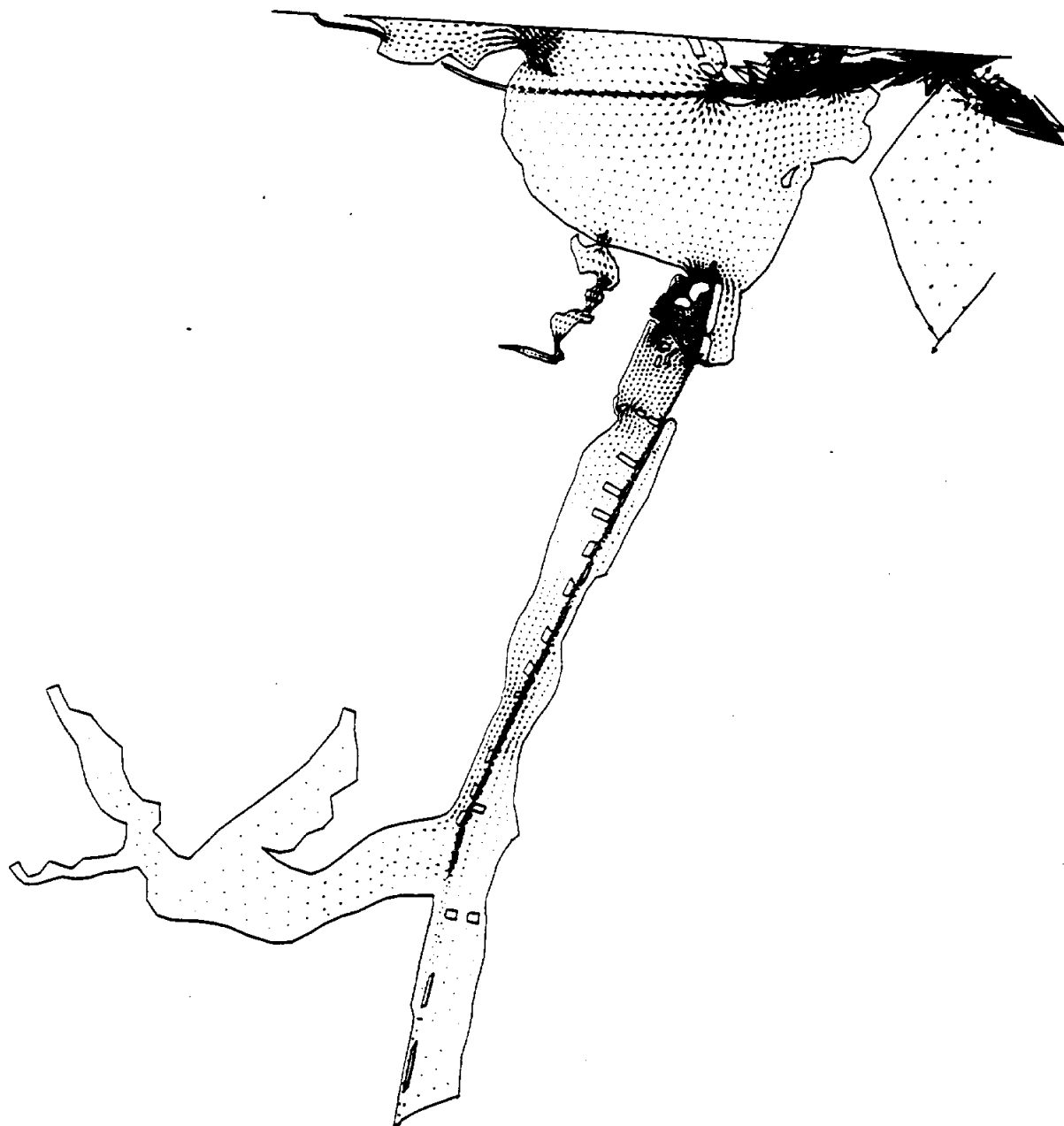


FIG. B-14. SWIFT2D Simulated Velocity Vectors, June 11, 00:00



6.51E+02 HOURS


5 FPS: 

FIG. B-15. TxBLEND Simulated Velocity Vectors, June 11, 03:00

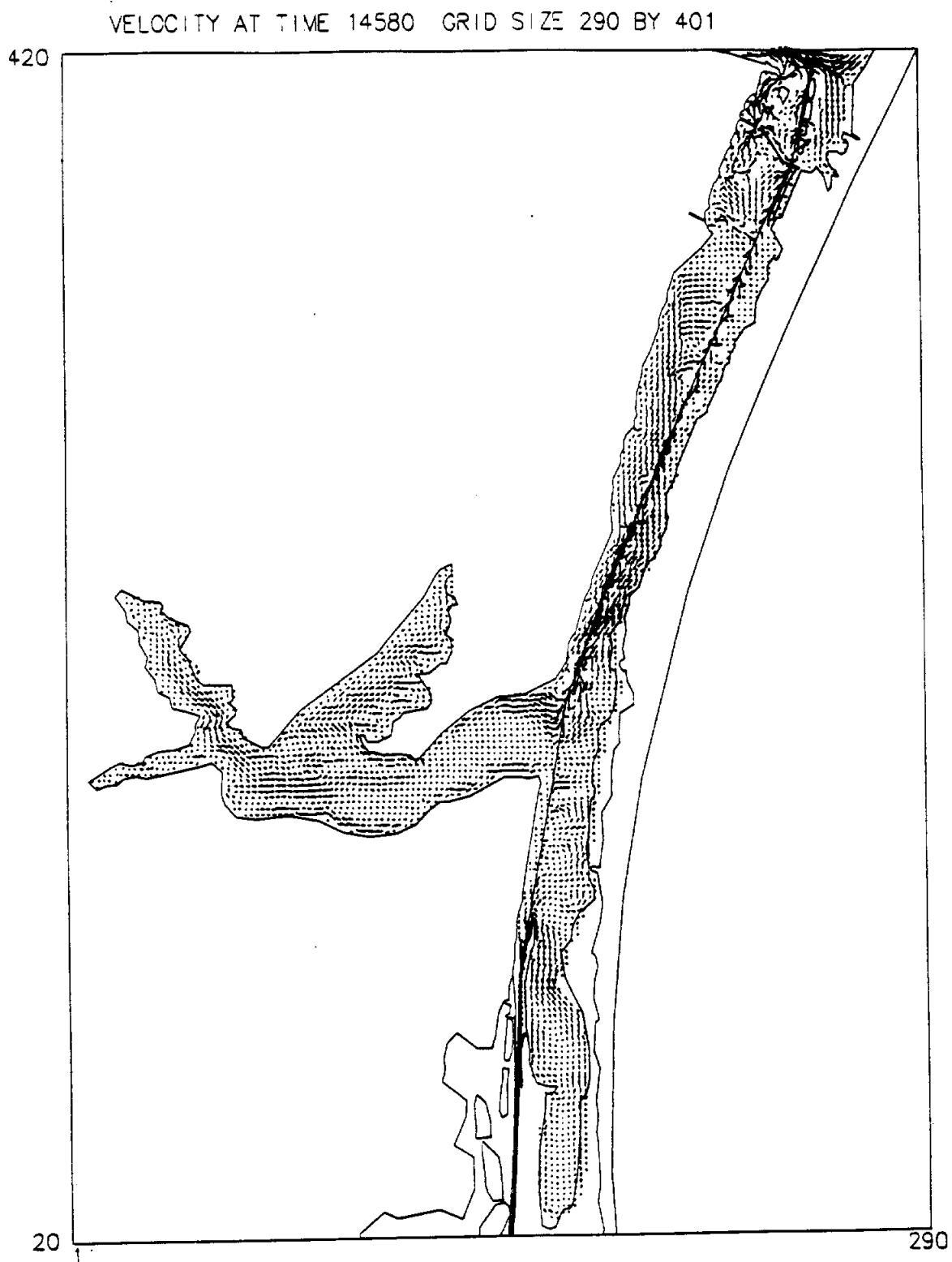


FIG. B-16. SWIFT2D Simulated Velocity Vectors, June 11, 03:00

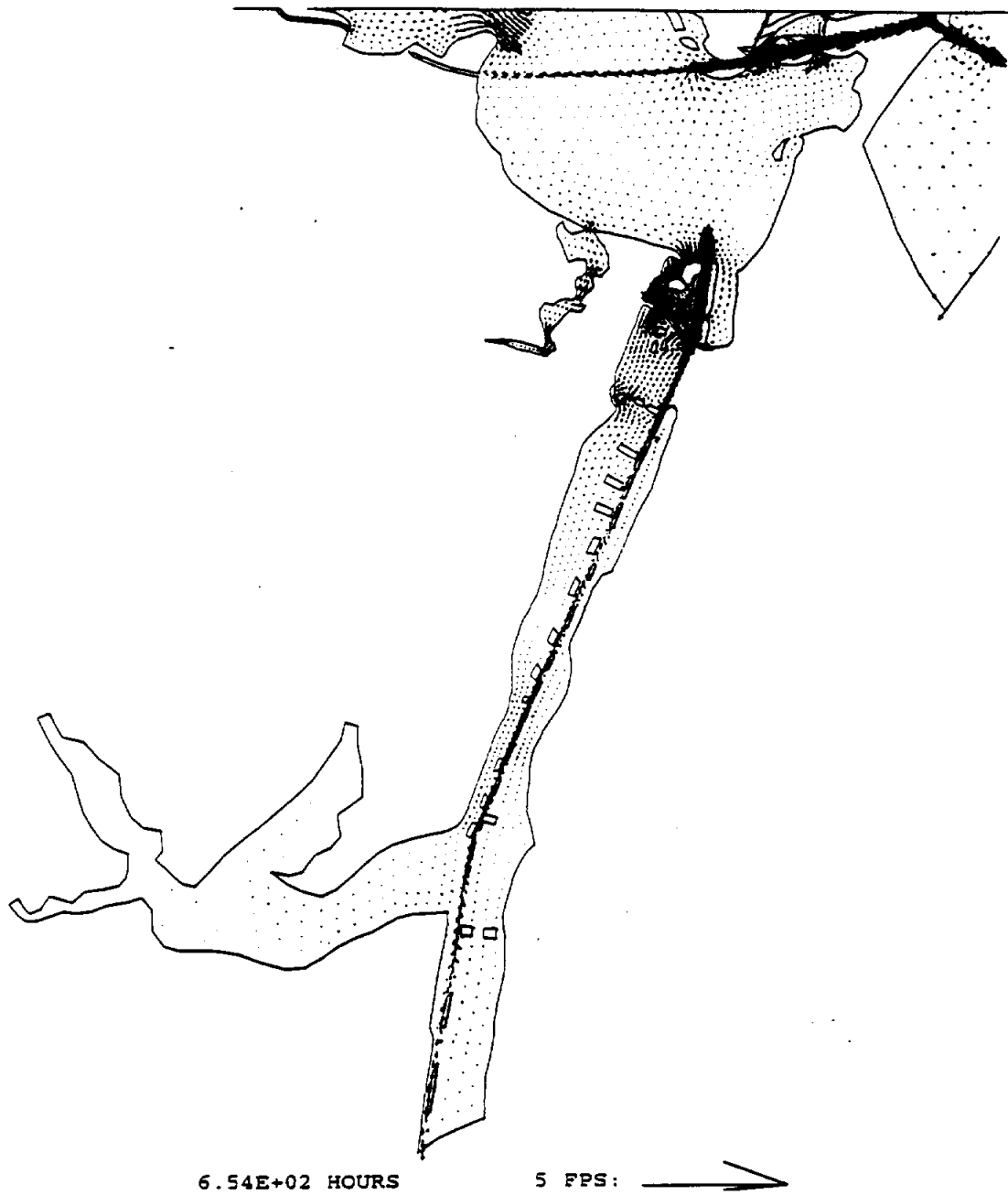


FIG. B-17. TxBLEND Simulated Velocity Vectors, June 11, 06:00

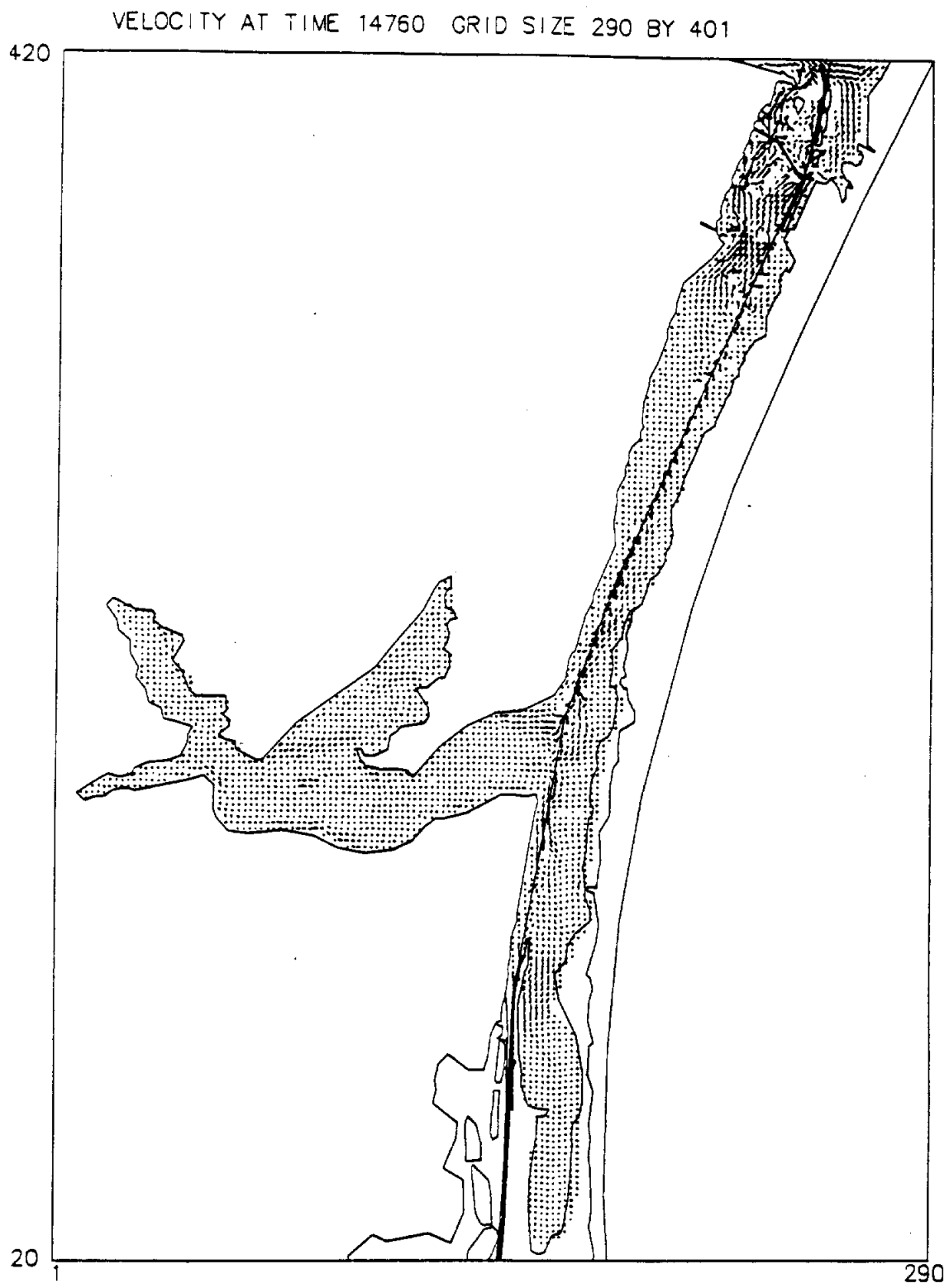


FIG. B-18. SWIFT2D Simulated Velocity Vectors, June 11, 06:00

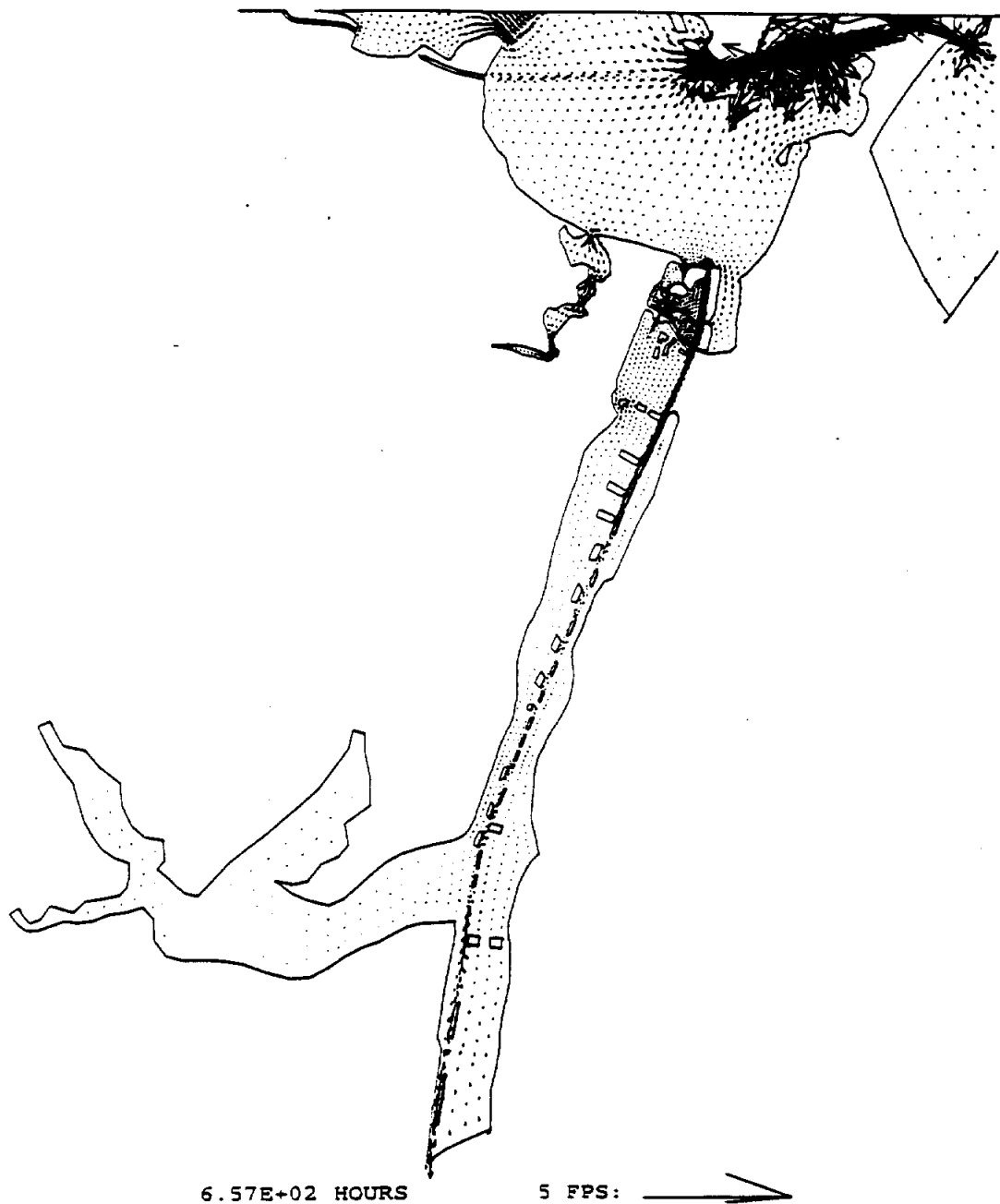


FIG. B-19. TxBLEND Simulated Velocity Vectors, June 11, 09:00

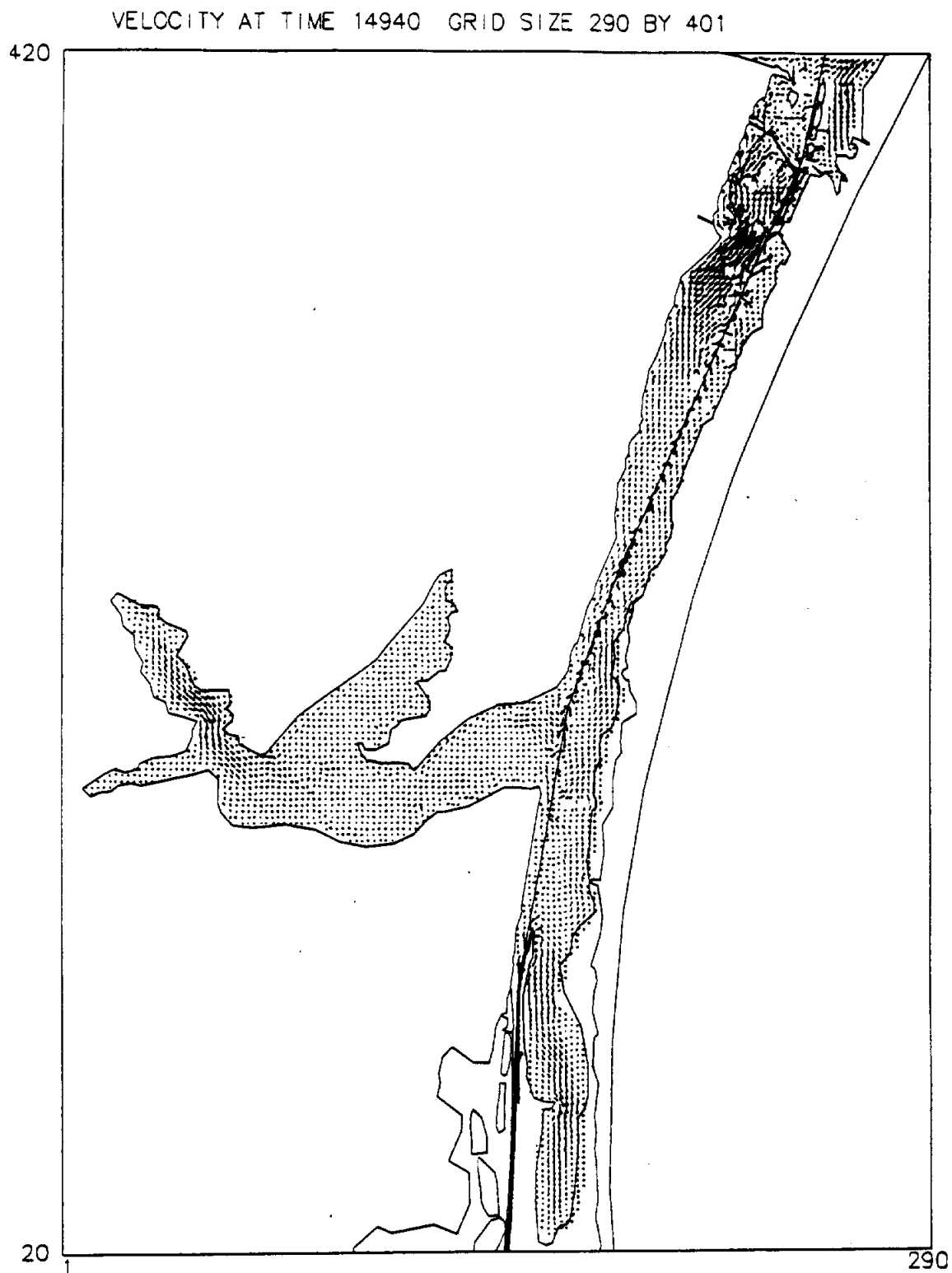


FIG. B-20. SWIFT2D Simulated Velocity Vectors, June 11, 09:00

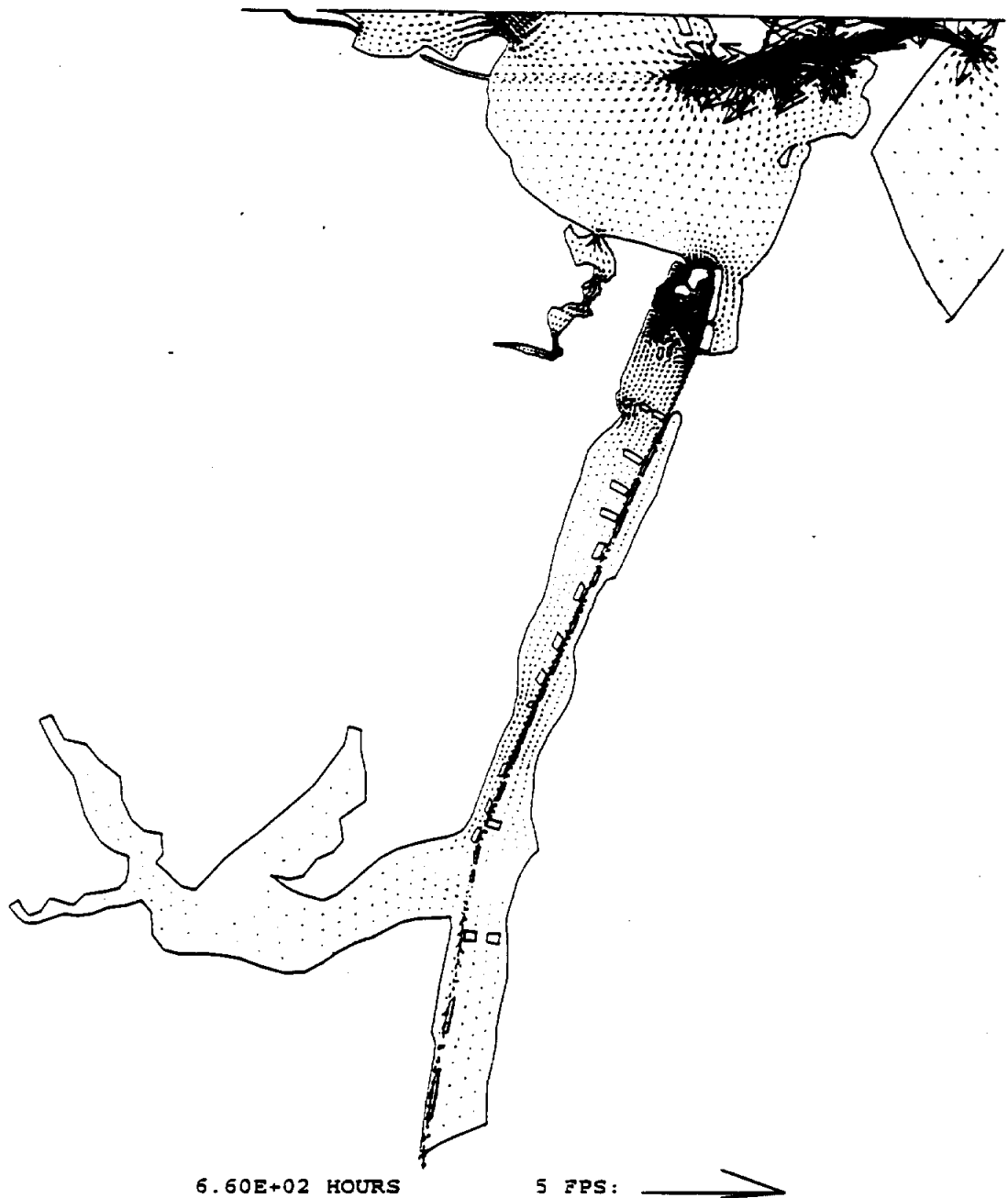


FIG. B-21. TxBLEND Simulated Velocity Vectors, June 11, 12:00

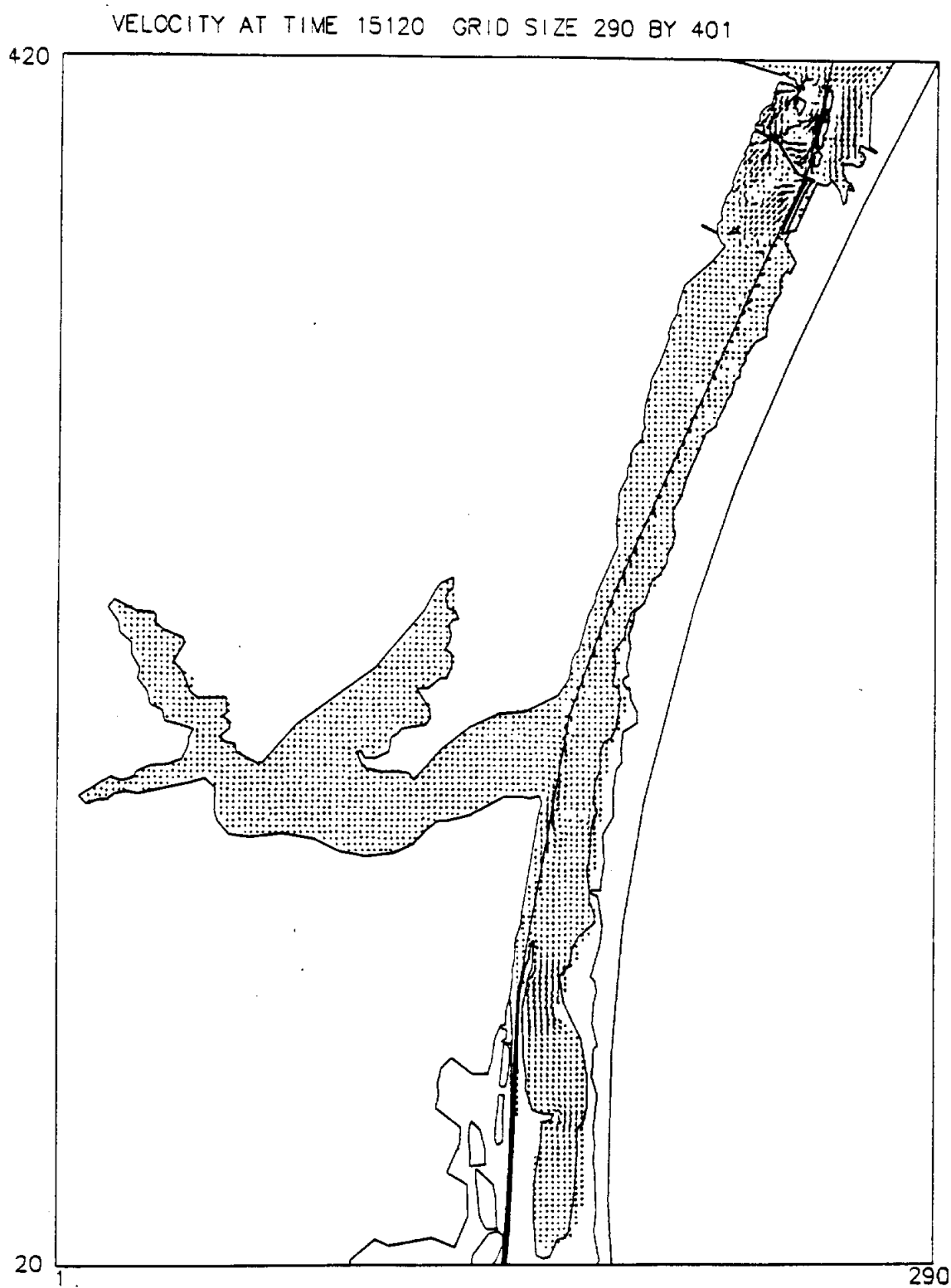


FIG. B-22. SWIFT2D Simulated Velocity Vectors, June 11, 12:00

VITA

Karl Edward McArthur was born to Roland and Peggy McArthur on April 27, 1971 in San Angelo Texas. He graduated as the salutatorian from Rusk High School in 1989. He furthered his education at the University of Texas at Austin, where he was a member of the Tau Beta Pi and Chi Epsilon engineering honor societies and was president of the student chapter of the American Society of Civil Engineers. He received the Bachelor of Science degree with high honors in Civil Engineering in May 1994. In August 1994 he enrolled in the graduate program at Texas A&M University and will receive the Master of Science degree in Civil Engineering in December 1996.

Mr. McArthur worked as an undergraduate and graduate coop student with the United States Geological Survey from January 1992 to September 1996. Upon completion of the Master's program, he will hold a position with Espey, Huston & Associates in Austin, Texas. Karl Edward McArthur can be reached through his parents, Roland and Peggy McArthur, 1209 Dan Way Ave., Rockdale, TX 76567.

**SIMULATION OF THE
LOWER LAGUNA MADRE ESTUARY
WITH SWIFT2D**

By Karl McArthur

U.S. GEOLOGICAL SURVEY

OCTOBER 9, 1996

TABLE OF CONTENTS

	Page
TABLE OF CONTENTS	ii
LIST OF FIGURES	iii
LIST OF TABLES	iv
OVERVIEW	1
BATHYMETRY AND GEOMETRY	5
SIMULATION RESULTS	8
APPENDIX A: PLOTS OF RESULTS	12
Calibrated Simulation.....	13
Velocity Vector Plots for the Calibrated Model with the Hydrographic Survey Data.....	22
Velocity Vector Plots for the Calibrated Model with the Nautical Chart Data	37
Manning's n Variation Simulation	52
Wind Stress Variation 1 Simulation.....	60
Wind Stress Variation 2 Simulation.....	68
Time Step Variation Simulation	76
APPENDIX B: LIST OF FILES FOR DELIVERY	84

LIST OF FIGURES

	Page
1. Locations of Tide Stations in the Lower Laguna Madre	2
2. Locations of Velocity Station in the Lower Laguna Madre.....	3
3. Locations of Flow Cross Sections in the Lower Laguna Madre.....	4
4. 200 Meter Grid from Nautical Chart Data.....	6
5. 200 Meter Grid from Hydrographic Survey Data	7
6. Location of Grid Cells Which Dried During the Simulation (Nautical Chart Grid).....	11
7. Location of Grid Cells Which Dried During the Simulation (Hydrographic Survey Data Grid).....	12

LIST OF TABLES

	Page
1. Geometric Characteristics of the Nautical Chart and Hydrographic Survey Grids	8
2. Root Mean Squared Errors (meters) between Simulated and Observed Water Levels	10
3. Root Mean Squared Errors (square meters) between Simulated and Observed Water Levels.....	10

OVERVIEW

The lower Laguna Madre Estuary from the south end of the Land Cut to South Bay was simulated with the SWIFT2D model. The lower half of the Laguna Madre has two openings to the Gulf of Mexico. Port Mansfield Channel and the Brazos-Santiago Pass at Port Isabel. The lower Laguna is connected to the upper Laguna Madre by the Gulf Intracoastal Waterway (GIWW) through the Land Cut. The most significant source of fresh-water inflow into the estuary is the Arroyo Colorado, which flows into the estuary between Port Mansfield and Port Isabel.

The SWIFT2D simulations of the estuary were performed for the month of June, 1991, which corresponded to the June 10 through June 14, 1991 intensive inflow survey performed by the Texas Water Development Board (TWDB). Simulations were performed for water levels, velocities, and circulation patterns (hydrodynamics only). Salinity was not considered in the simulations. Inflows from the Arroyo Colorado were also not considered. Three tide signals were used to drive the model at the South Land Cut, Port Mansfield Channel, and Brazos-Santiago Pass. The driving tides at the South Land Cut were provided by the tide station at El Toro Island. Tide records were available at Port Mansfield and Port Isabel, however, these stations were internal to the model.

In order to provide an external (Gulf of Mexico) driving tide, the tide signal from the Bob Hall Pier tide stations was used. The Bob Hall tidal signal was applied on the Gulf side of Padre Island at the Port Mansfield Channel and Brazos-Santiago Pass. The Bob Hall Pier tide station is located just south of Corpus Christi on the Gulf side of Padre Island. The Bob Hall tide was compared to the tidal signal at the Port Mansfield and Port Isabel stations to determine whether a phase shift would be required. The three tide signals were determined to be in phase, therefore, the unaltered Bob Hall tide was used to drive the model at both locations.

The simulation results were compared to observed data at four tide stations and twelve velocity stations. These stations are shown in Figures 1 and 2 respectively. Results for flow were also output at the ten cross sections shown in Figure 3.

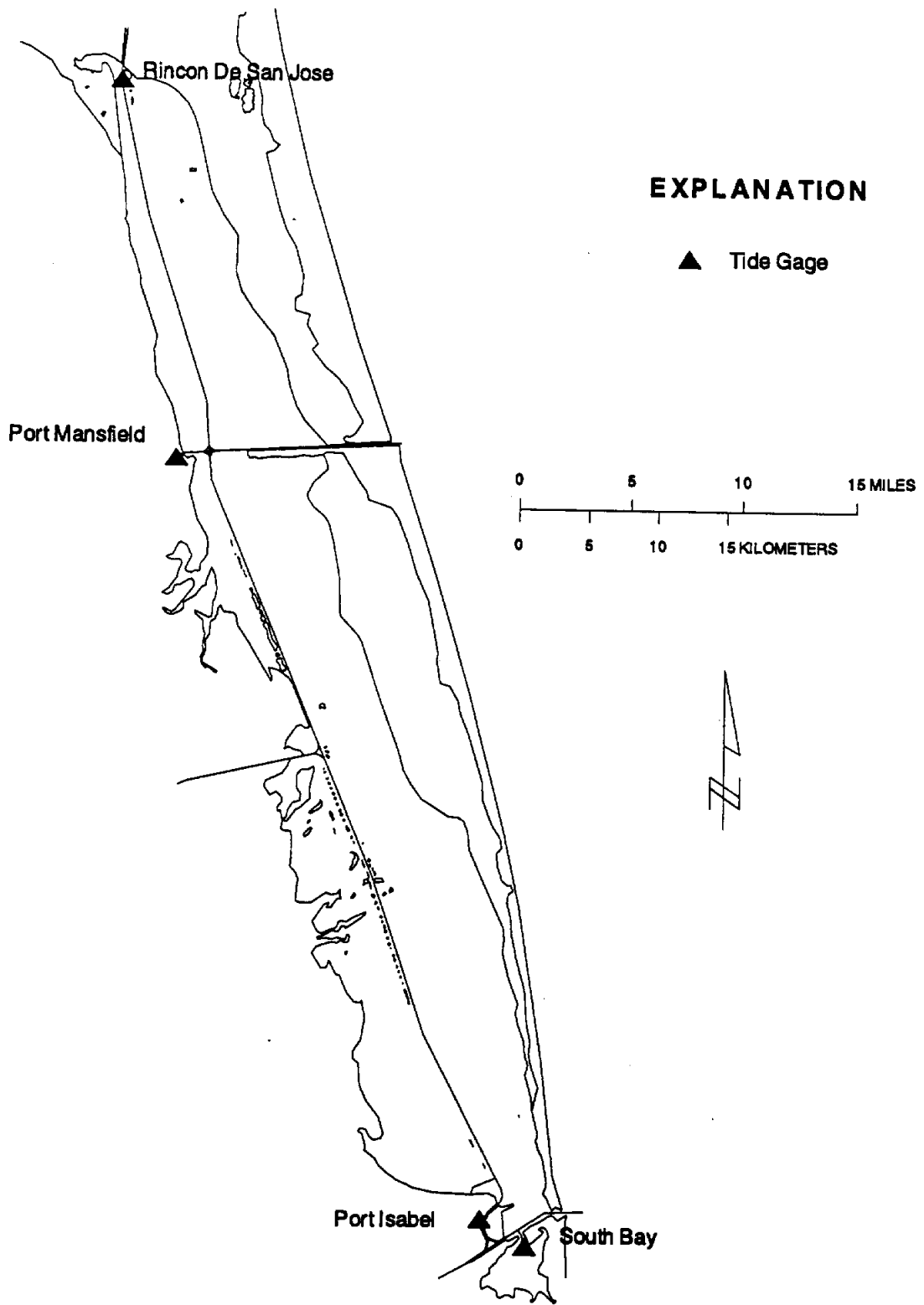


Figure 1. Locations of Tide Stations in the Lower Laguna Madre

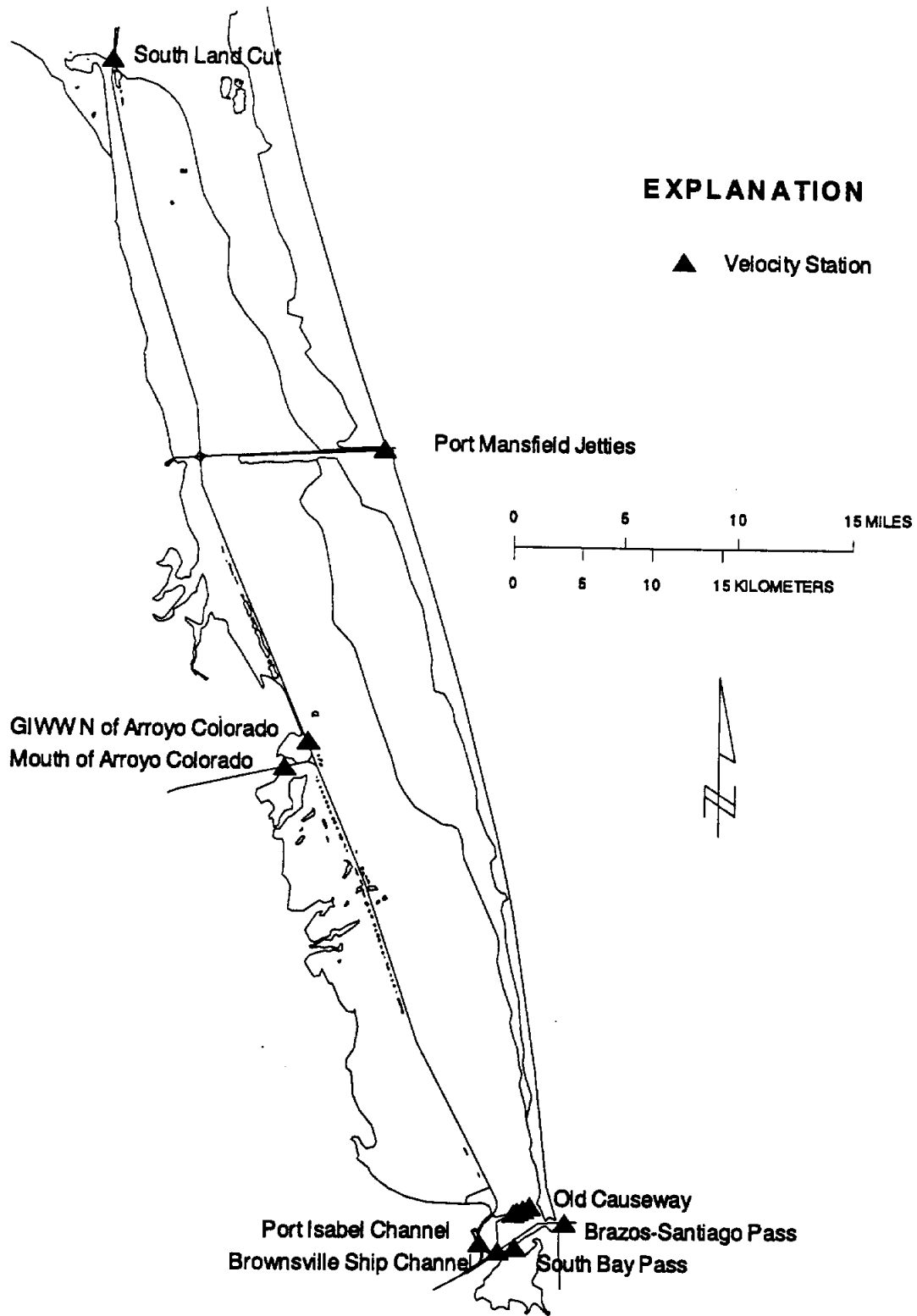


Figure 2. Locations of Velocity Stations in the Lower Laguna Madre

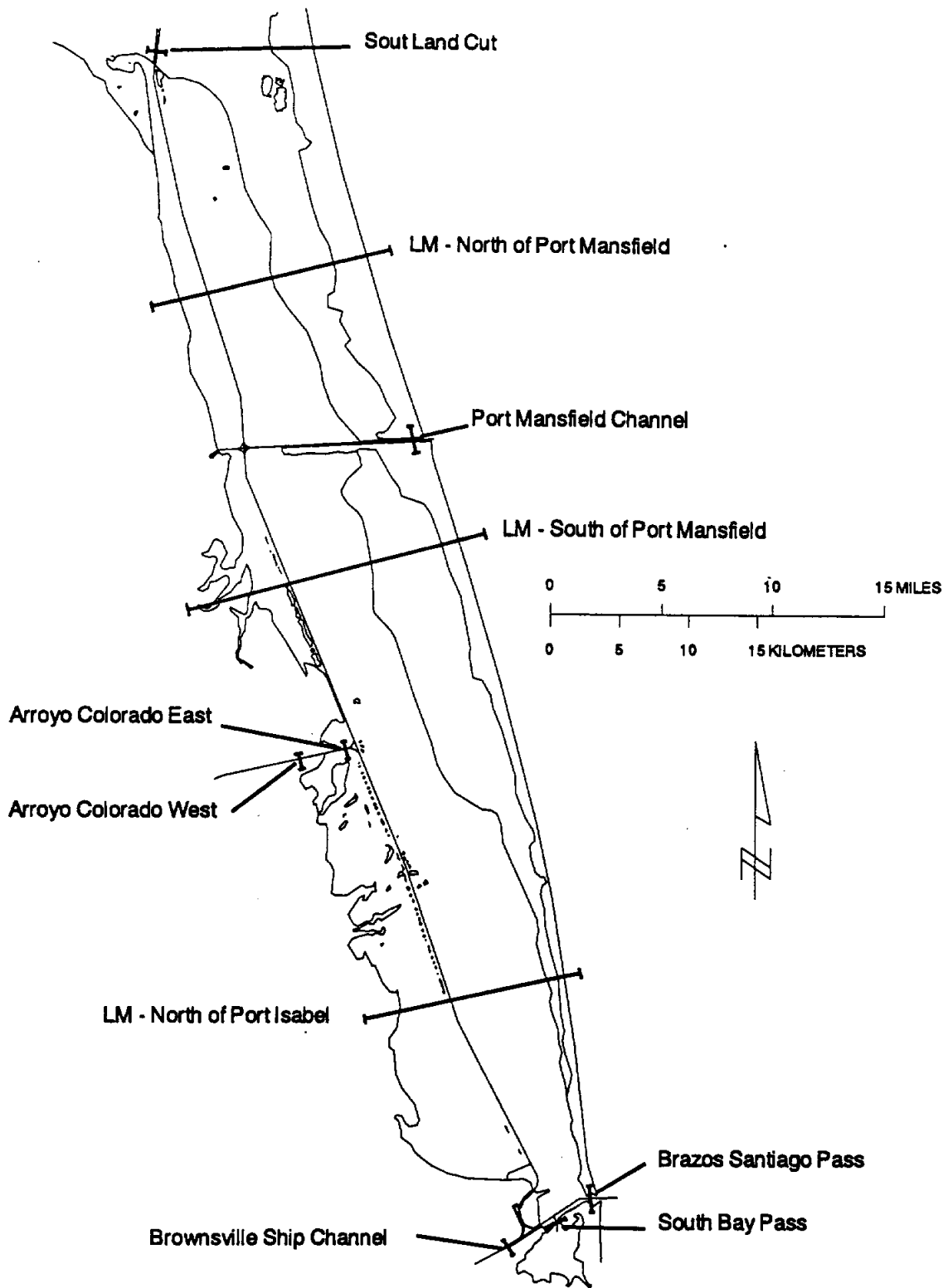


Figure 3. Locations of Flow Cross Sections in the Lower Laguna Madre

Observed tide data for the period of simulation was obtained from the Texas Coastal and Ocean Observation Network (TCOON) through the Conrad Blucher Institute. Observed velocities were obtained from the TWDB intensive inflow survey. The tidal datums were referenced to the mean tide level observed at each station.

BATHYMETRY AND GEOMETRY

Two sources were used to generate the bathymetry for the SWIFT2D model grid. The first set of data was derived from the three, 1:40,000 scale NOAA/NOS nautical charts which cover the lower Laguna Madre. The three maps are titled as follows: 1. Texas Intracoastal Waterway, Laguna Madre: Middle Ground to Chubby Island; 2. Texas Intracoastal Waterway, Laguna Madre: Chubby Island to Stover Point Including the Arroyo Colorado; 3. Texas Intracoastal Waterway, Laguna Madre: Stover Point to Brownsville Including the Brazos Santiago Pass. The second set of data consisted of the recent hydrographic survey data for the Laguna Madre obtained from the U.S. Army Corps of Engineers, Waterways Experiment Station. USGS 1:100,000 scale digital line graphs were used to form the boundary of the estuary.

The ARC/INFO geographic information system was used to process the bathymetry data and create the required information for the SWIFT2D model grids. Separate grids were created for the nautical chart data and the hydrographic survey data. The nautical chart grid was derived from 1080 points digitized from the charts, while the hydrographic survey grid was derived from 28,059 points. The hydrographic survey data obviously provides a more extensive set of points for the definition of bathymetry. Both grids were rotated 13 degrees clockwise to reduce the extent of the grid required to define the study area. The resulting grids were 125 cells wide by 505 cells tall. The grid size used was 200 meters. The specifics of the two grids are compare in Table 1.

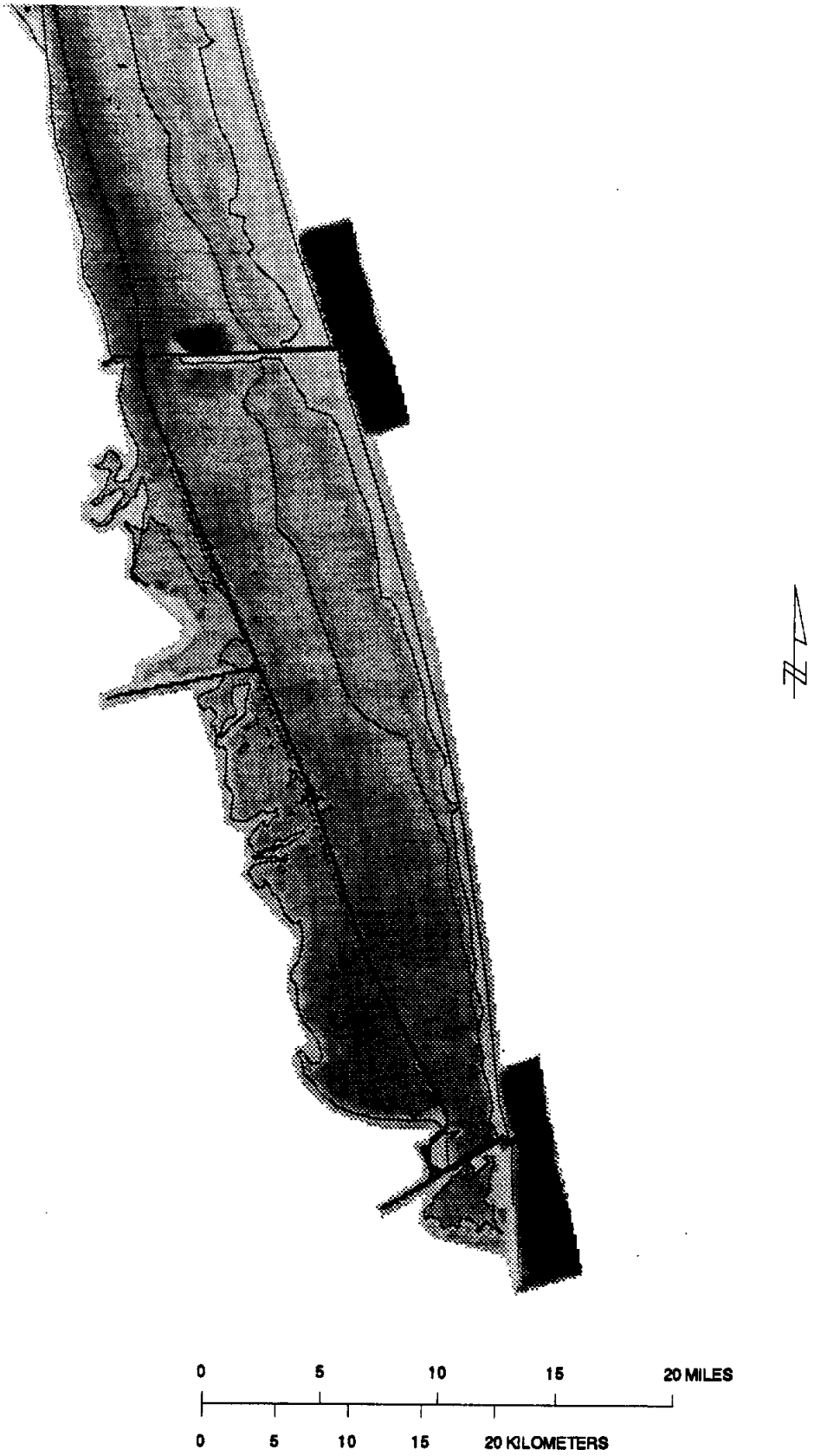


Figure 4. 200 Meter Grid from Nautical Chart Data

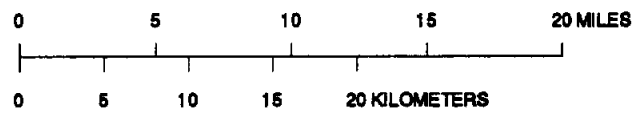
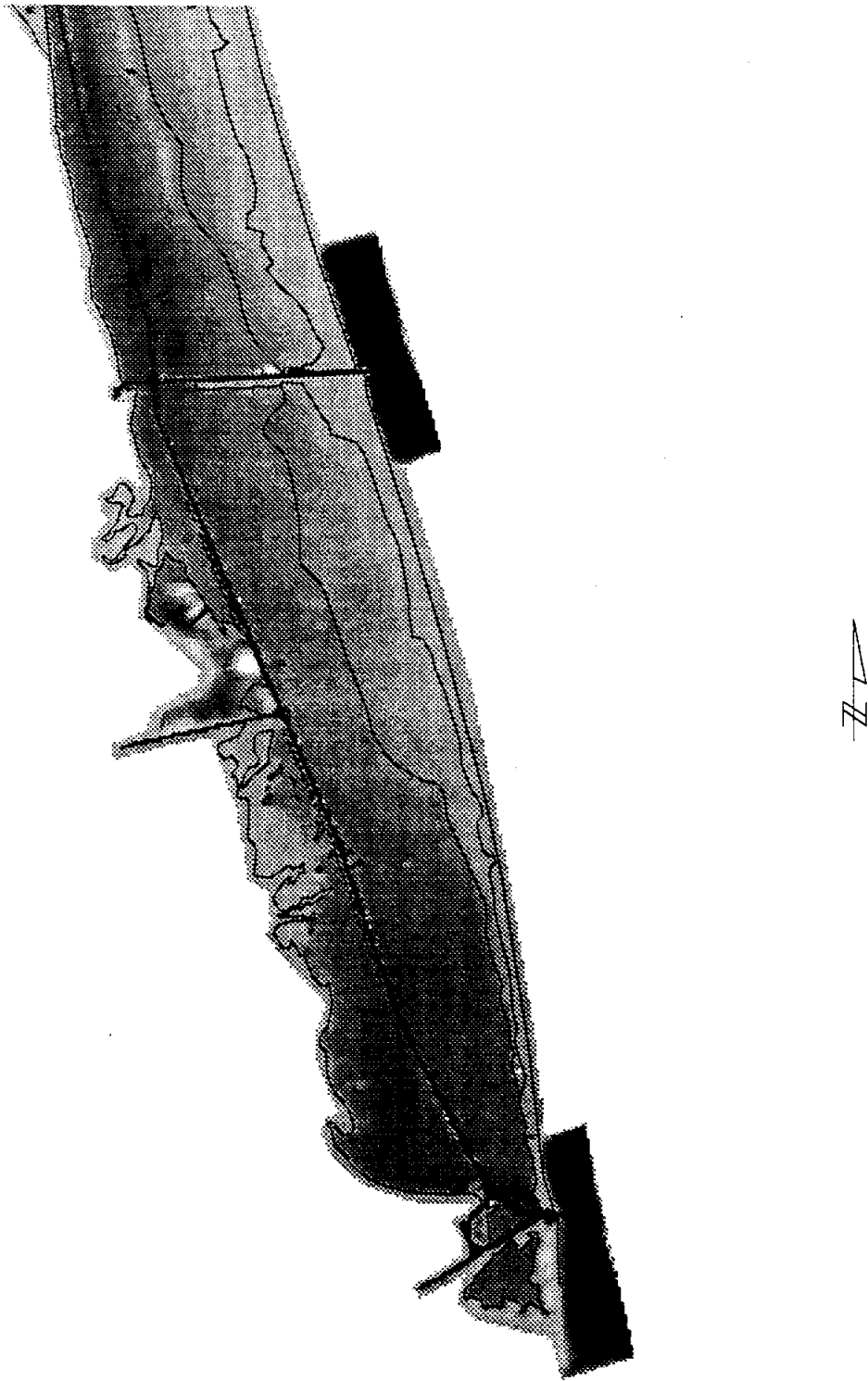


Figure 5. 200 Meter Grid from Hydrographic Survey Data

Table 1. Geometric Characteristics of the Nautical Chart and Hydrographic Survey Grids

Characteristic	Nautical Chart Grid	Hydrographic Survey Grid
Number of cells with depth below MWL	26729	19439
Minimum cell depth (m)	0.1	0.1
Maximum cell depth (m)	14.5	14.3
Average cell depth (m)	1.35	1.65
Total area of cells with depth below MWL (km ²)	1,069	777.6
Total volume below mean water level (m ³)	1.44x10 ⁹	1.28x10 ⁹

The nautical chart grid has a larger area of shallow depth along the east side of the estuary than the hydrographic survey grid. These areas are slightly above mean water level (MWL) in the hydrographic survey grid.

SIMULATION RESULTS

The SWIFT2D model was calibrated to the data measured during the 1991 intensive inflow survey performed by the TWDB. Several problems remain in the final model. The primary areas of difficulty are in the vicinity of the channels between the Laguna Madre and the Gulf of Mexico. Instabilities in the model solution were observed in the vicinity of the Port Mansfield Jetties in the sensitivity analysis. The model also was unable to accurately simulate the magnitude of the tidal signal at the Port Isabel and South Bay tide stations. A majority of the inflow from the Brazos-Santiago Pass appears flow northward into the estuary instead of into the Laguna Madre Channel and South Bay Pass. The calibration for the lower Laguna Madre could be improved with additional work on the finite element grid and calibration parameters.

The roughly calibrated SWIFT2D model produced fairly good matches between simulated and observed water levels at the Rincon del San Jose and Port Mansfield stations. Results at the Port Isabel and South Bay stations were not as good. Simulated water levels at these sites matched in phase, however, were smaller in amplitude. The fit could probably be improved by adjustments to the model grids.

Additional simulations were performed to test the robustness of the model. The Manning's n values for the calibrated model were 0.025 in channels, 0.075 in the vicinity of the old Queen Isabel Causeway, and 0.035 elsewhere. A sensitivity simulation was performed with a constant n value of 0.030. Sensitivity runs were also performed for wind stress coefficients of 0.0001 and 0.0026 in addition to the calibration value of 0.0015. The calibrated model used a time step of 6 minutes. A time step of 12 minutes was used in a sensitivity run. The larger time step created instabilities in the vicinity of the Port Mansfield jetties in the hydrographic survey model. Complete results of the simulations are shown in the section at the end of this report. Tables 2 and 3 show the root mean square errors between simulated and observed values for both models.

Figures 6 and 7 show the extent of grid cells that dried at some point in the simulation. The hydrographic survey grid produced a substantially larger number of dry cells. The difference was a result of the shallower bathymetry along the east side of the estuary in the hydrographic survey grid.

Table 2. Root Mean Squared Errors (meters) between Simulated and Observed Water Levels

Water Level Stations	Calibrated		Constant n-value		No Wind Stress		High Wind Stress		12 Minute Time Step	
	NC	HS	NC	HS	NC	HS	NC	HS	NC	HS
Rincon Del San Jose	0.260	0.255	0.264	0.256	0.242	0.241	0.279	0.269	0.262	0.257
Port Mansfield	0.098	0.098	0.099	0.099	0.104	0.102	0.106	0.120	0.098	0.214
Port Isabel	0.146	0.142	0.144	0.135	0.129	0.133	0.158	0.148	0.144	0.138
South Bay	0.116	0.107	0.118	0.177	0.113	0.107	0.121	0.111	0.137	0.127

Table 3. Root Mean Squared Errors (square meters) between Simulated and Observed Water Levels

Velocity Stations	Calibrated		Constant n-value		No Wind Stress		High Wind Stress		12 Min. Time Step	
	NC	HS	NC	HS	NC	HS	NC	HS	NC	HS
South Land Cut	0.226	0.251	0.244	0.261	0.204	0.244	0.248	0.259	0.212	0.244
Port Mansfield Jetties	0.698	0.731	0.772	0.768	0.691	0.685	0.692	0.725	0.783	0.809
Mouth of Arroyo Colorado	0.096	0.105	0.096	0.107	0.098	0.102	0.094	0.107	0.096	0.102
GIWW North of Arroyo Colorado	0.151	0.137	0.153	0.137	0.162	0.154	0.144	0.132	0.147	0.135
Old Causeway (Eastern)	0.208	0.198	0.208	0.194	0.192	0.191	0.222	0.204	0.257	0.233
Old Causeway (Mid East)	0.175	0.143	0.191	0.156	0.161	0.134	0.186	0.149	0.231	0.198
Old Causeway (Mid West)	0.315	0.327	0.294	0.342	0.315	0.326	0.317	0.329	0.361	0.417
Old Causeway (Far West)	0.202	0.172	0.183	0.182	0.202	0.172	0.203	0.174	0.217	0.234
Port Isabel Channel	0.193	0.190	0.191	0.193	0.190	0.185	0.196	0.194	0.273	0.246
Brownsville Ship Channel	0.259	0.249	0.252	0.247	0.252	0.247	0.263	0.251	0.281	0.264
South Bay Pass	0.289	0.261	0.288	0.261	0.283	0.255	0.291	0.249	0.293	0.262

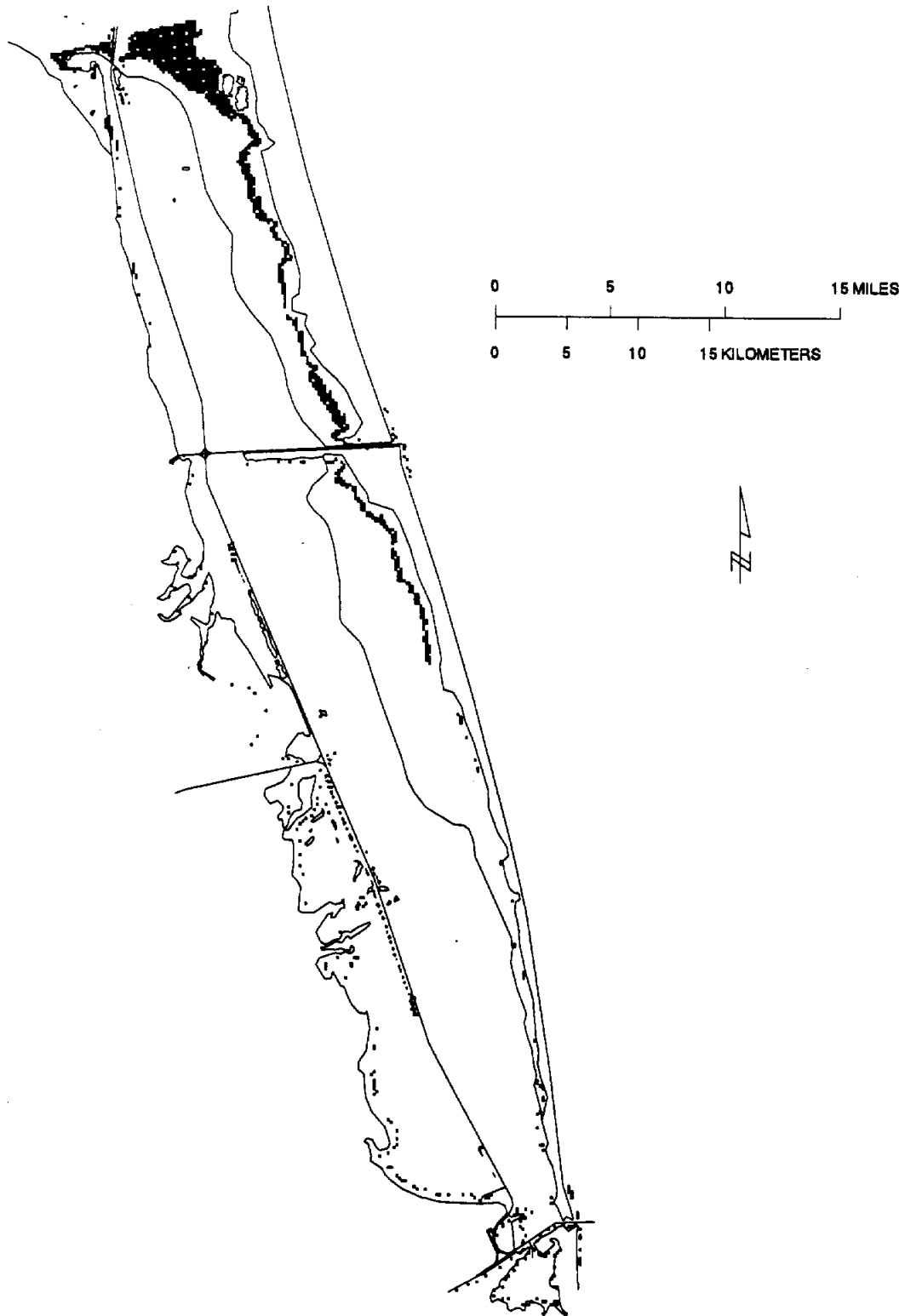


Figure 6. Location of Grid Cells Which Dried During the Simulation (Nautical Chart Grid).

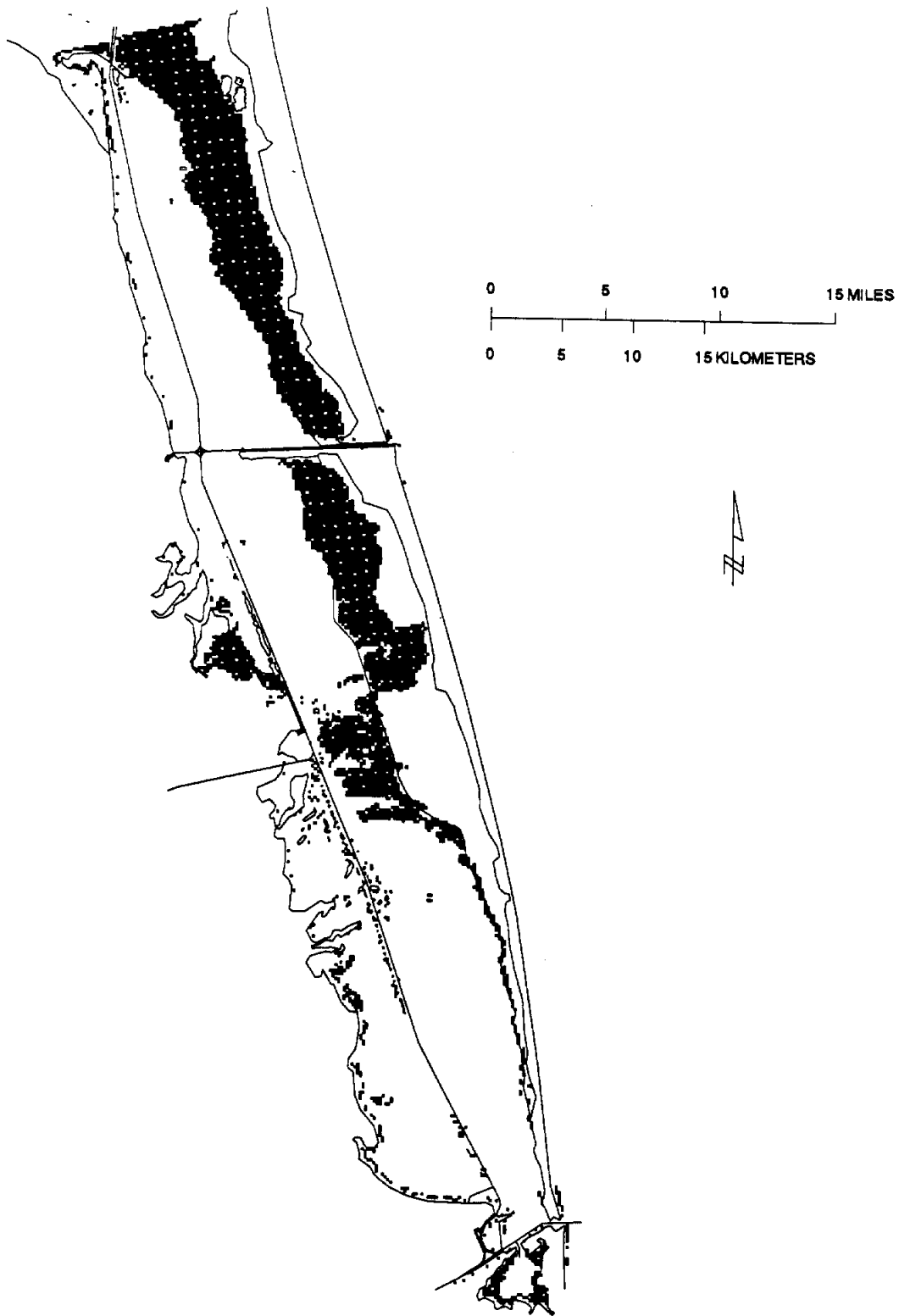


Figure 7. Location of Grid Cells Which Dried During the Simulation (Hydrographic Survey Data Grid).

APPENDIX A
PLOTS OF RESULTS

SWIFT2D SIMULATIONS

Calibrated Simulation

Manning's n = 0.025 in navigation channels
= 0.075 in the vicinity of the old Queen Isabel Causeway
= 0.035 elsewhere

Wind Stress = 0.0015

Time Step = 6 minutes

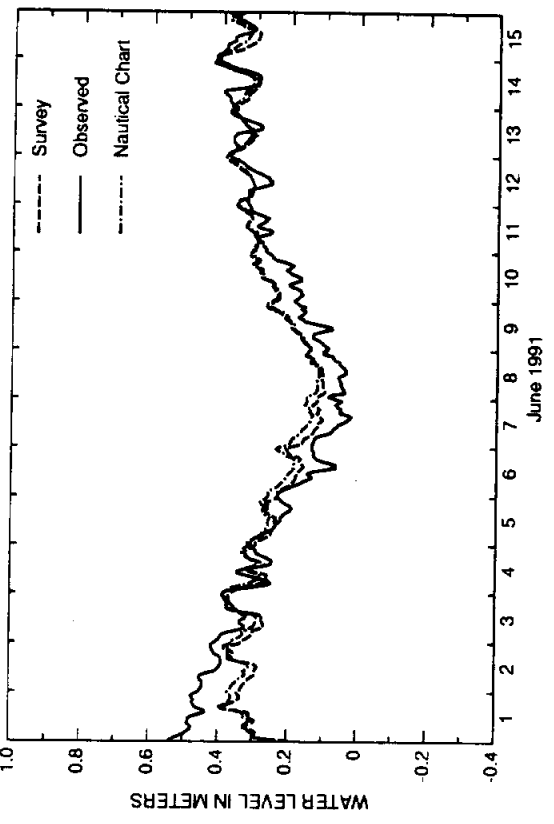


FIG. 1. Rincon Del San Jose Tide Station

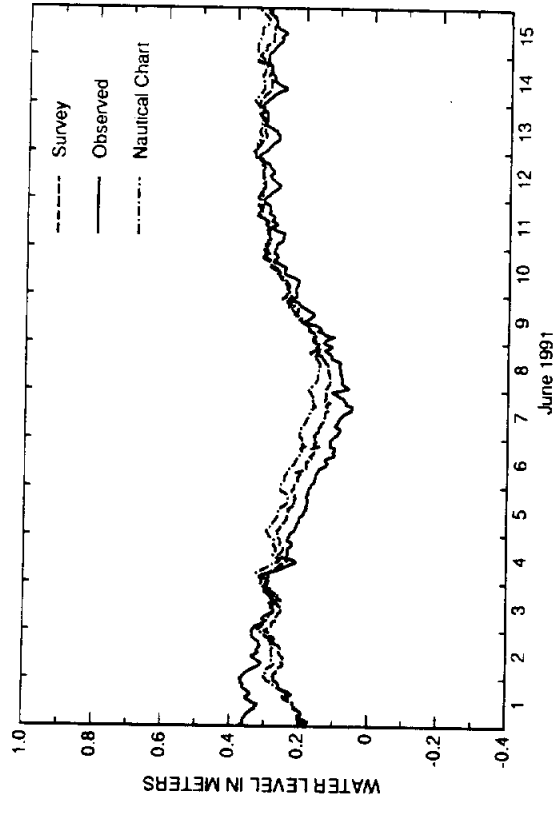


FIG. 2. Port Mansfield Tide Station

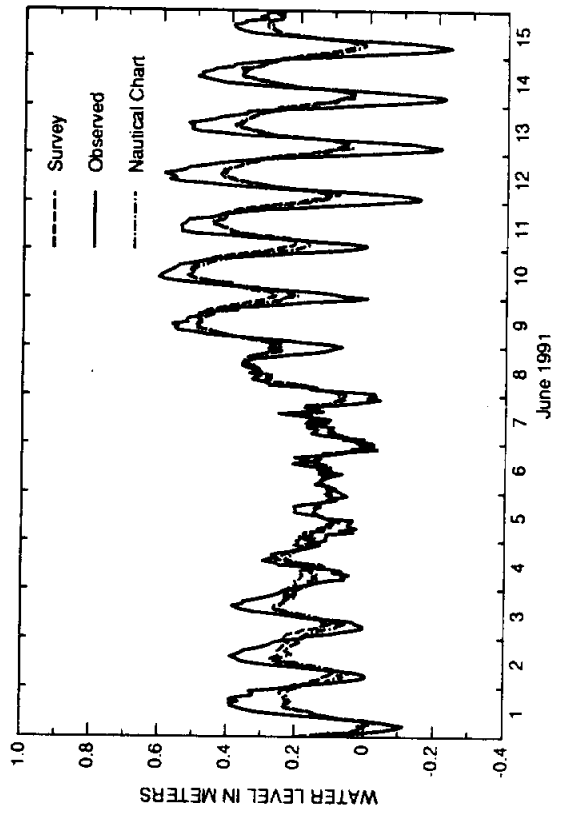


FIG. 3. Port Isabel Tide Station

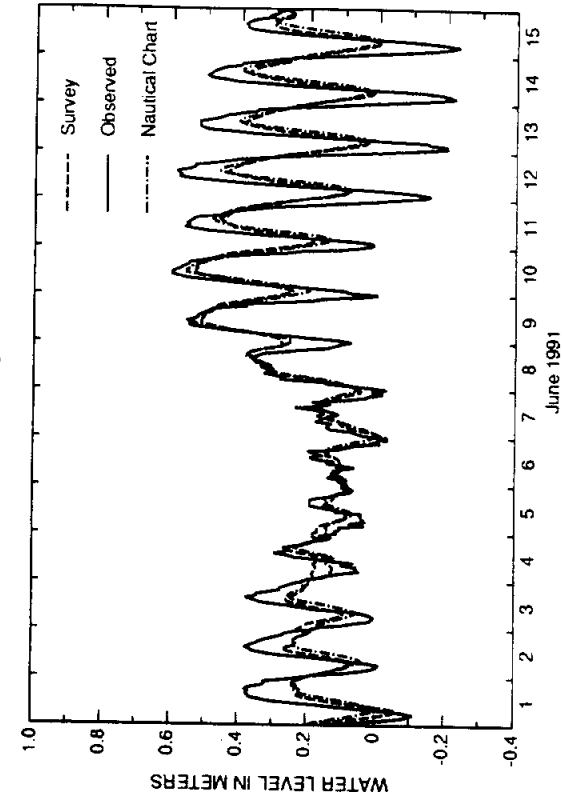


FIG. 4. South Bay Tide Station.

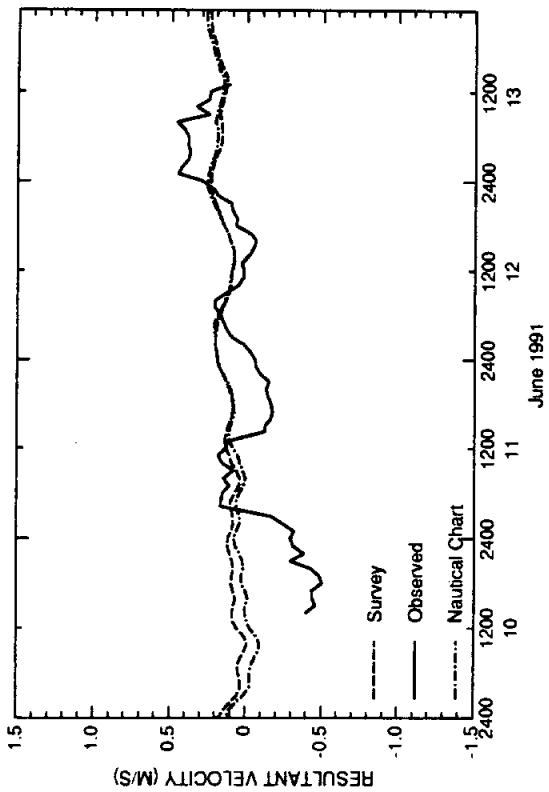


FIG. 1. South Land Cut

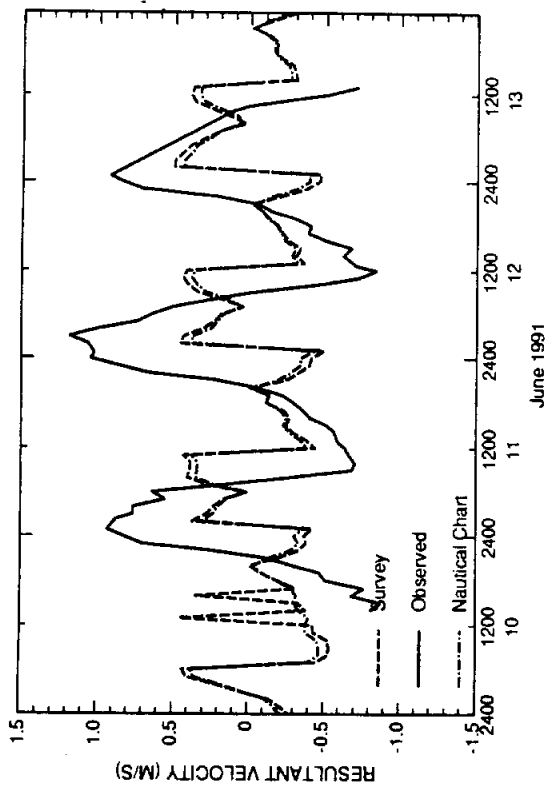


FIG. 2. Port Mansfield Jetties

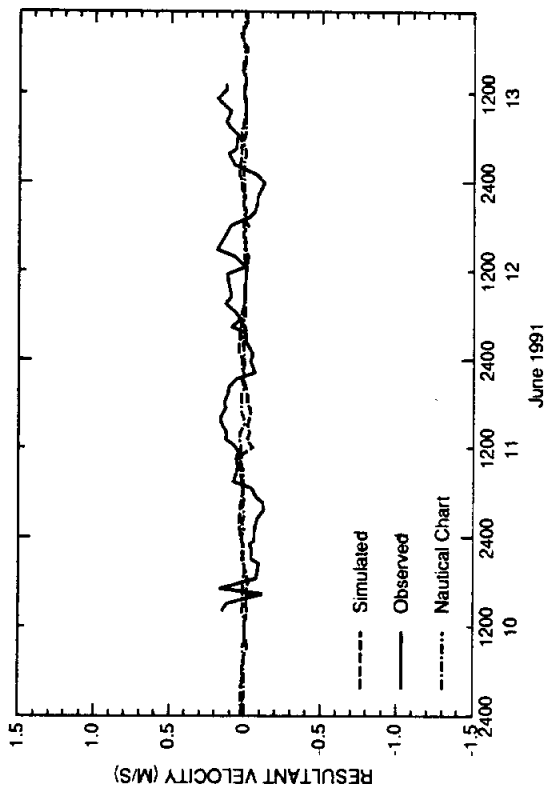


FIG. 3. Mouth of Arroyo Colorado

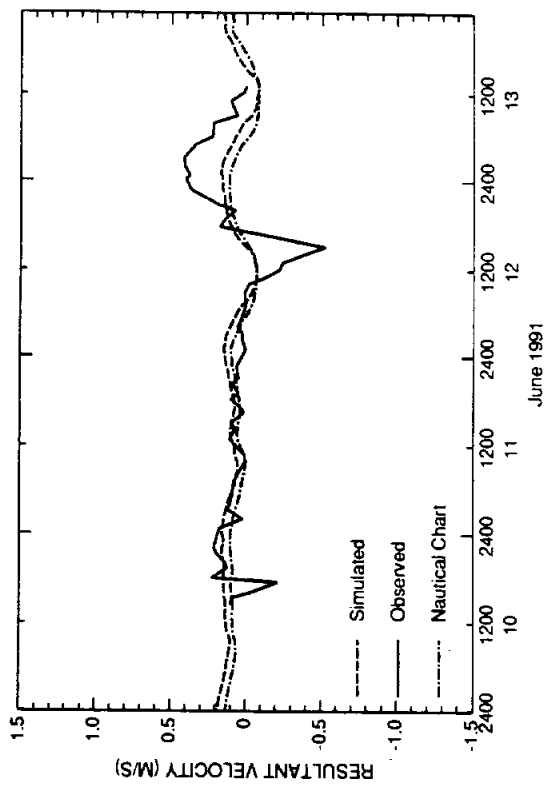


FIG. 4. GIWW North of Arroyo Colorado

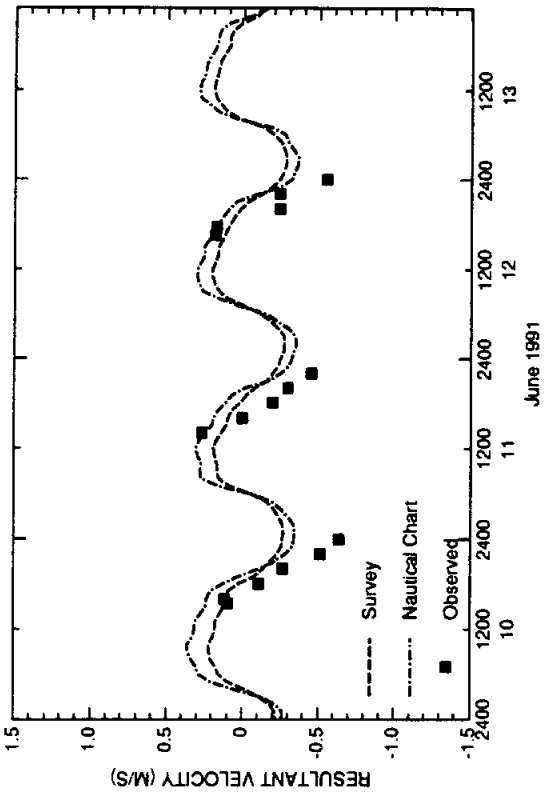


FIG. 5. Old Causeway (Eastern)

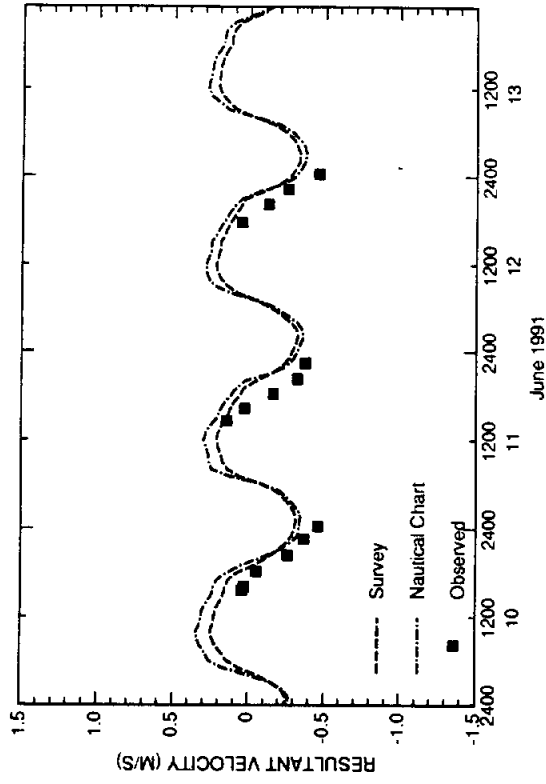


FIG. 6. Old Causeway (Mid East)

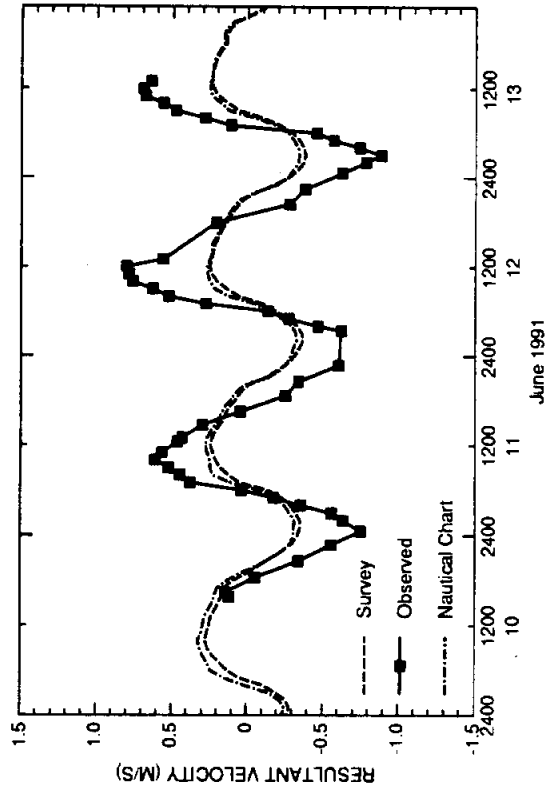


FIG. 7. Old Causeway (Mid West)

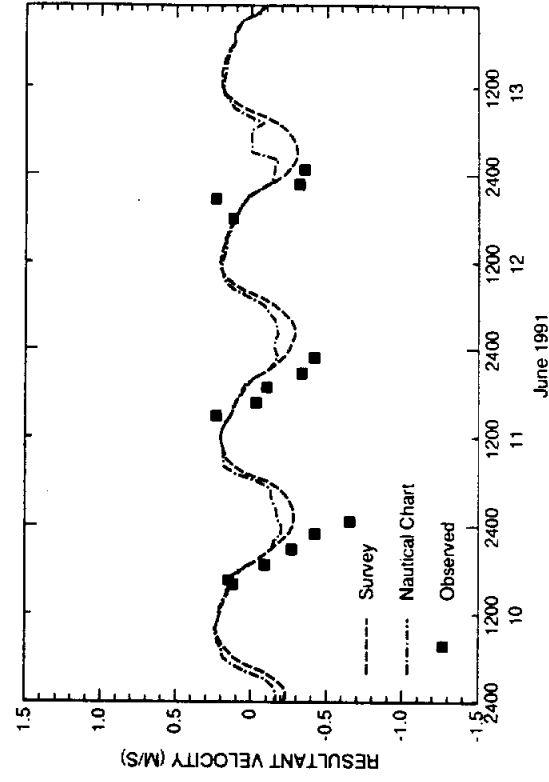


FIG. 8. Old Causeway (Western)

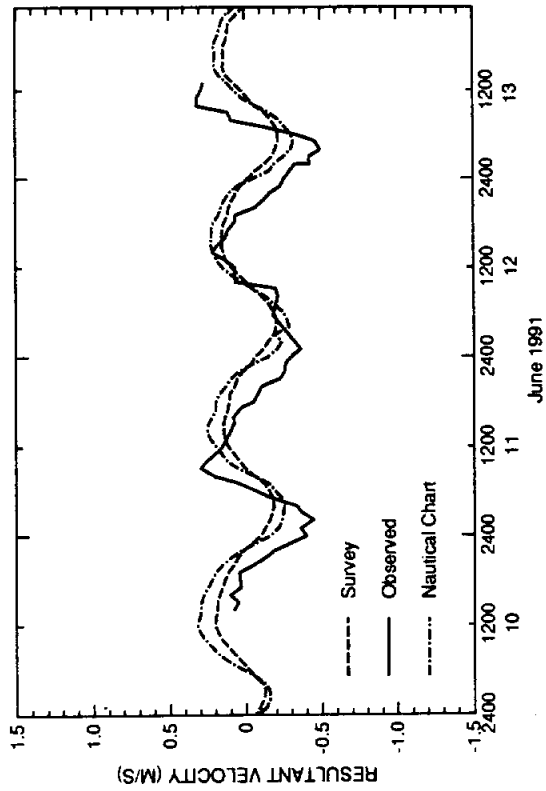


FIG. 9. Port Isabel Channel

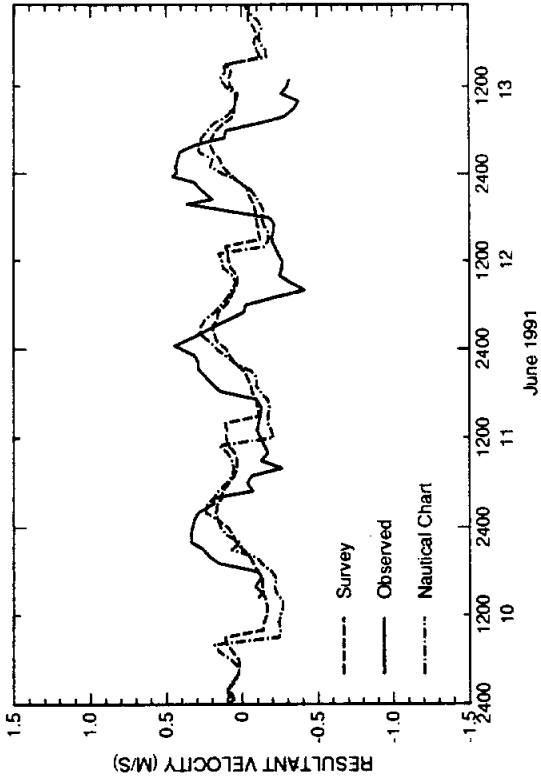


FIG. 10. Brownsville Ship Channel

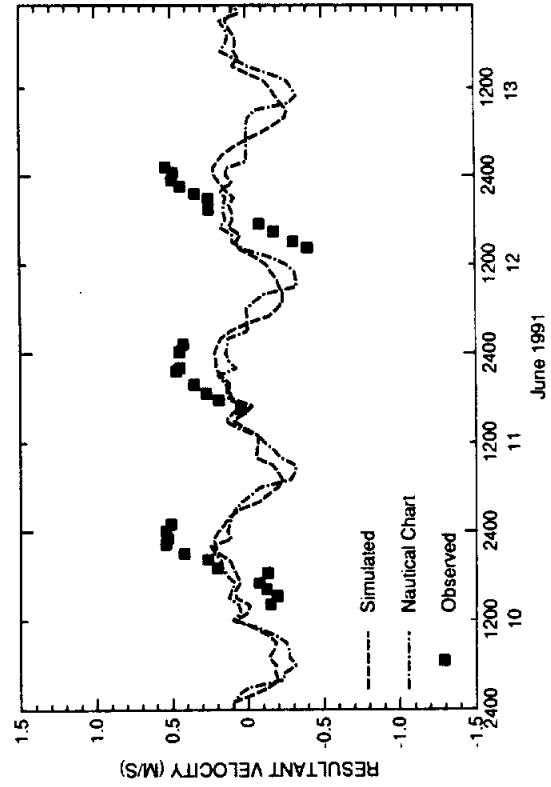


FIG. 11. South Bay Pass

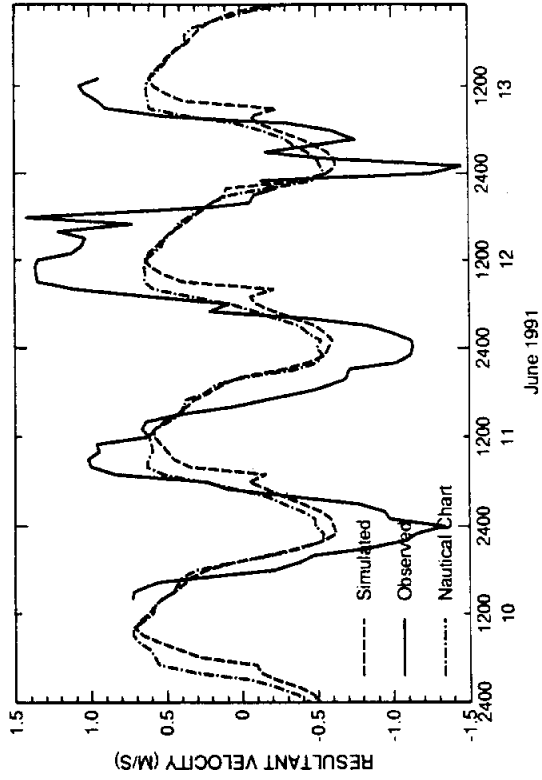


FIG. 12. Brazos Santiago Pass

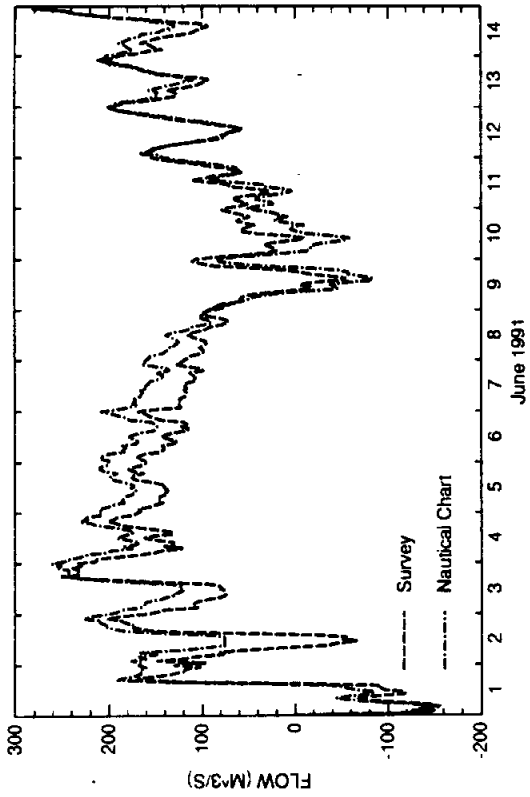


FIG. 1. South Land Cut

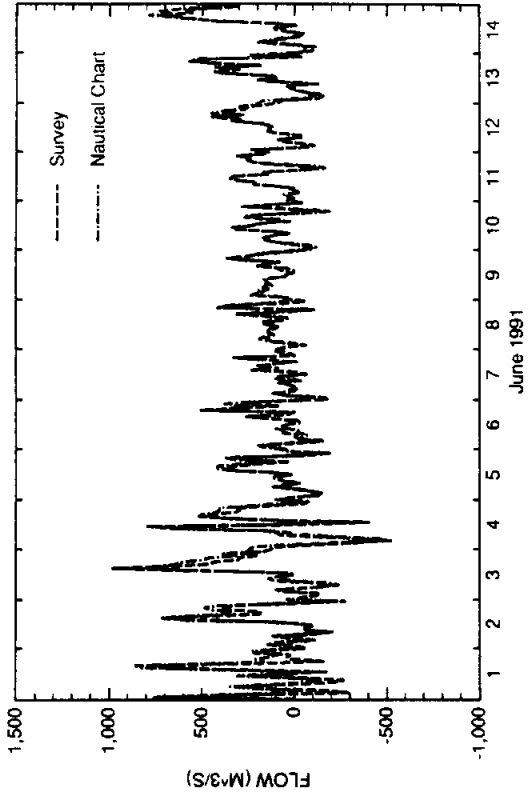


FIG. 2. Laguna Madre North of Port Mansfield

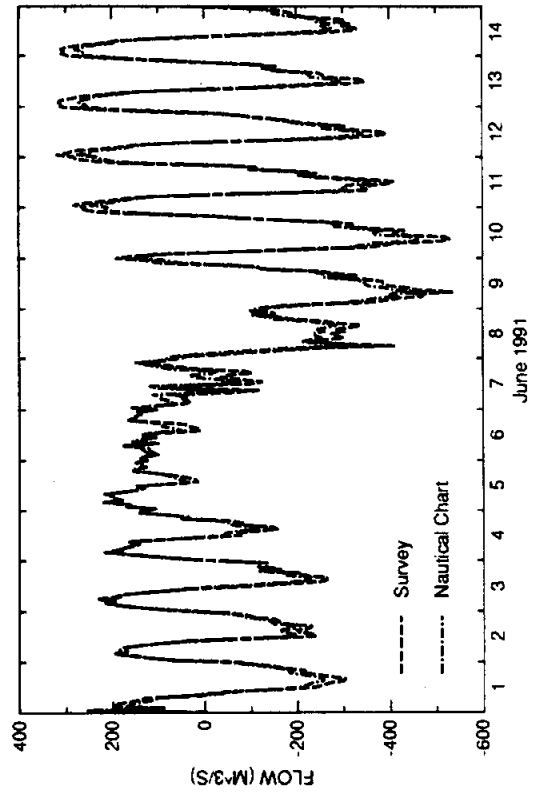


FIG. 3. Port Mansfield Channel

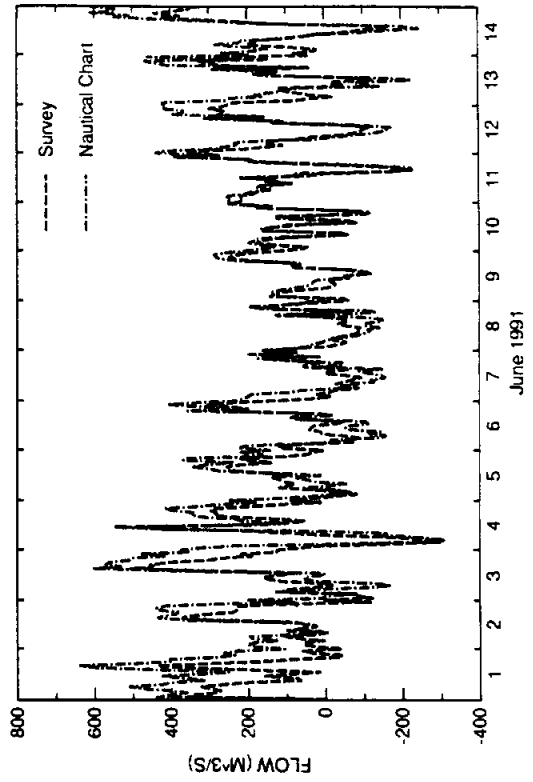


FIG. 4. Laguna Madre South of Port Mansfield

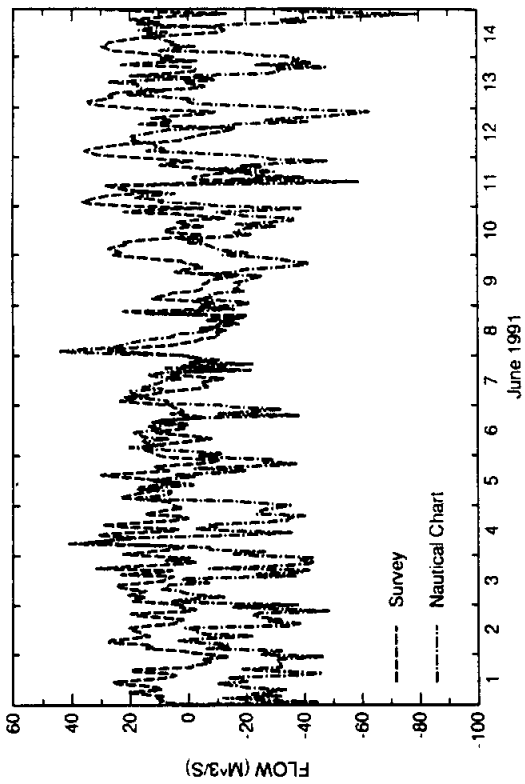


FIG. 6. Arroyo Colorado East of Laguna Atascosa

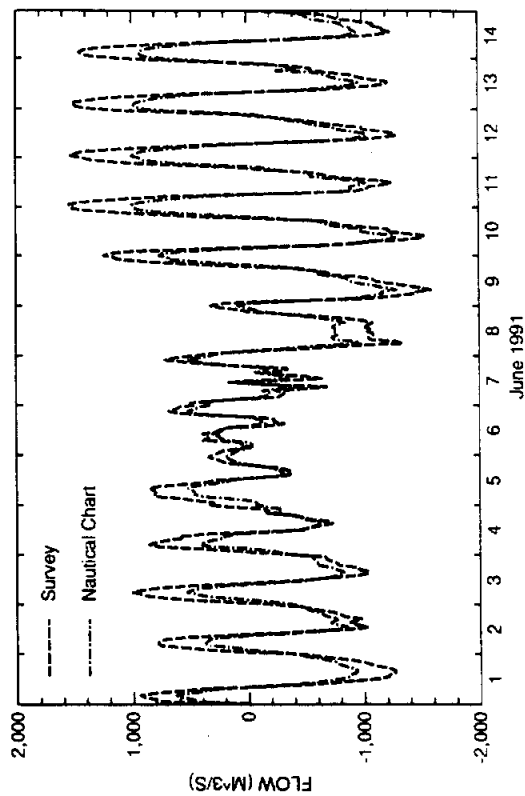


FIG. 8. Brazos-Santiago Pass

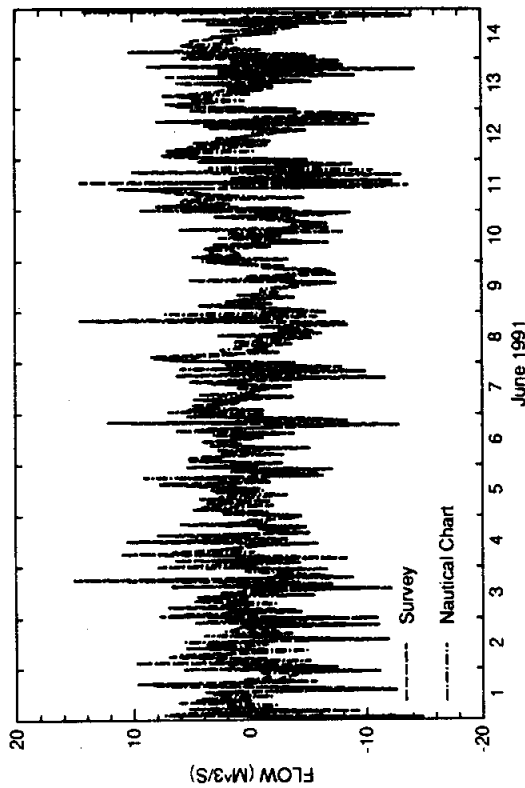


FIG. 5. Arroyo Colorado West of Laguna Atascosa

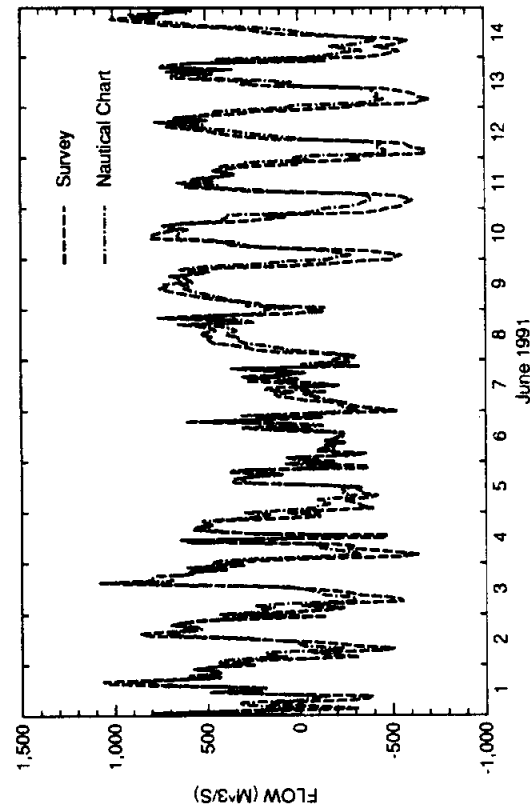


FIG. 7. Laguna Madre North of Port Isabel

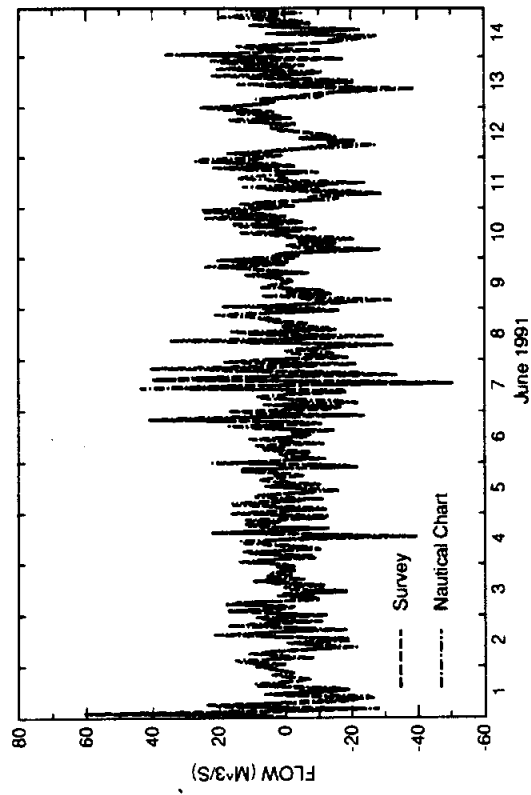


FIG. 9. Brownsville Ship Channel

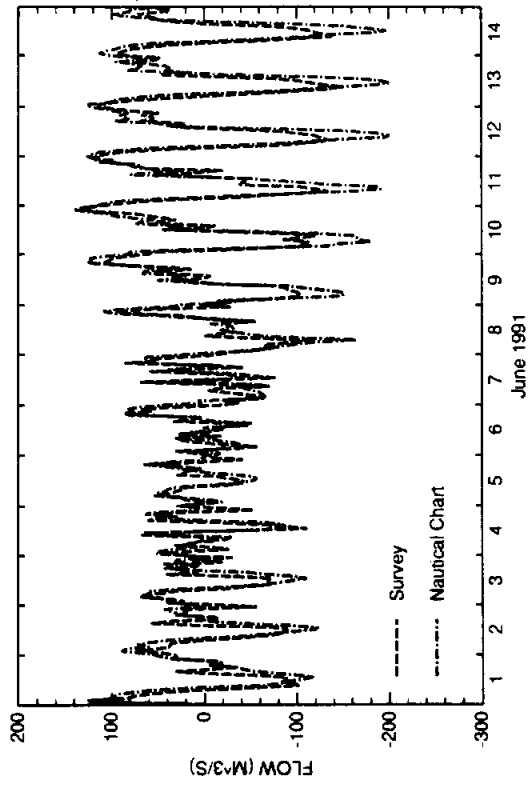
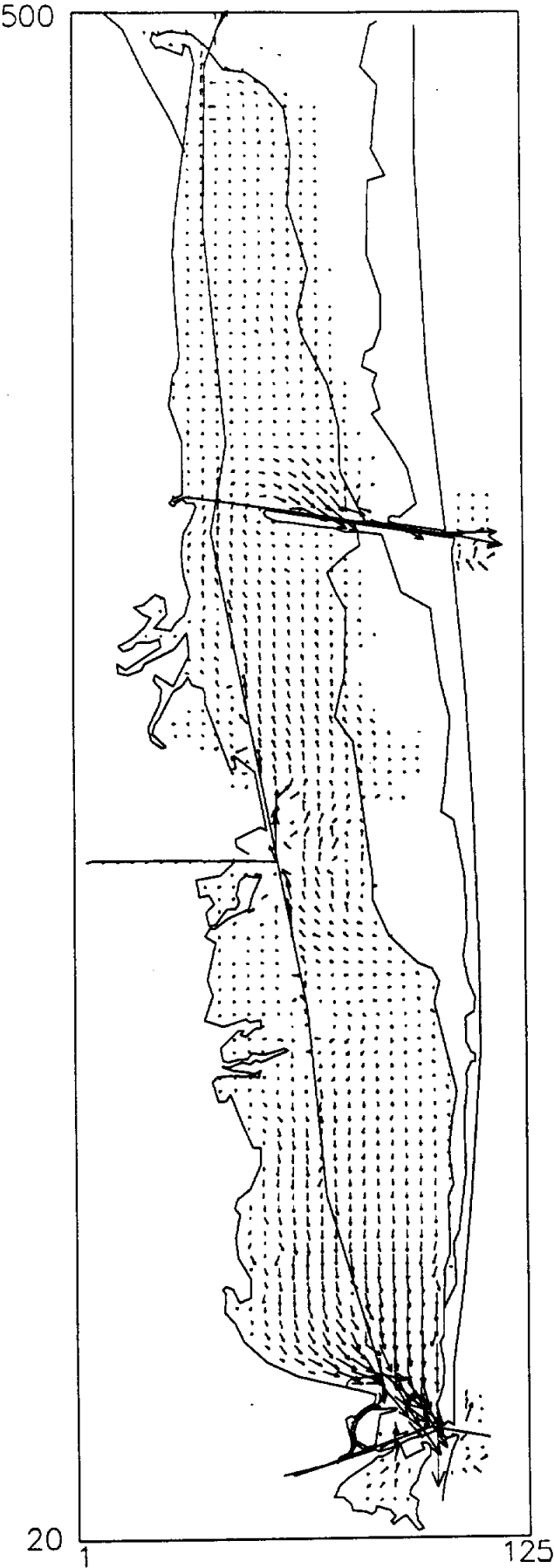


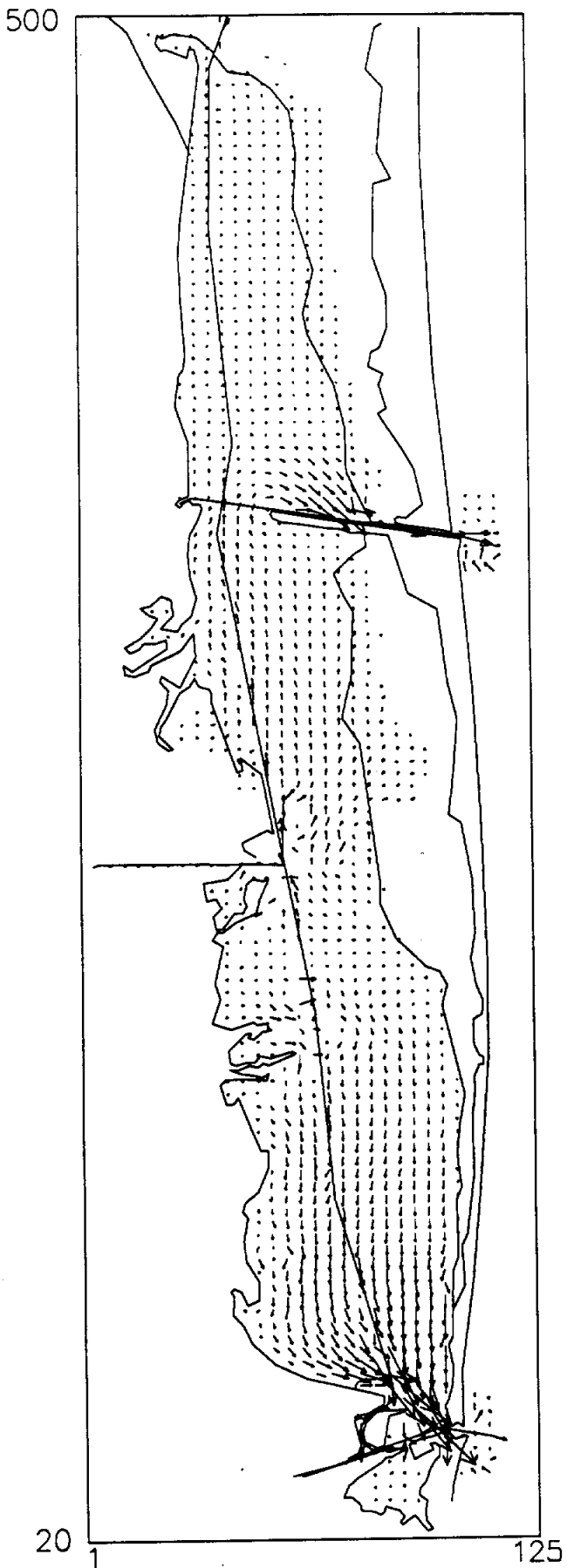
FIG. 10. South Bay Pass

**Velocity Vector Plots for the Calibrated Model
with the Hydrographic Survey Data**

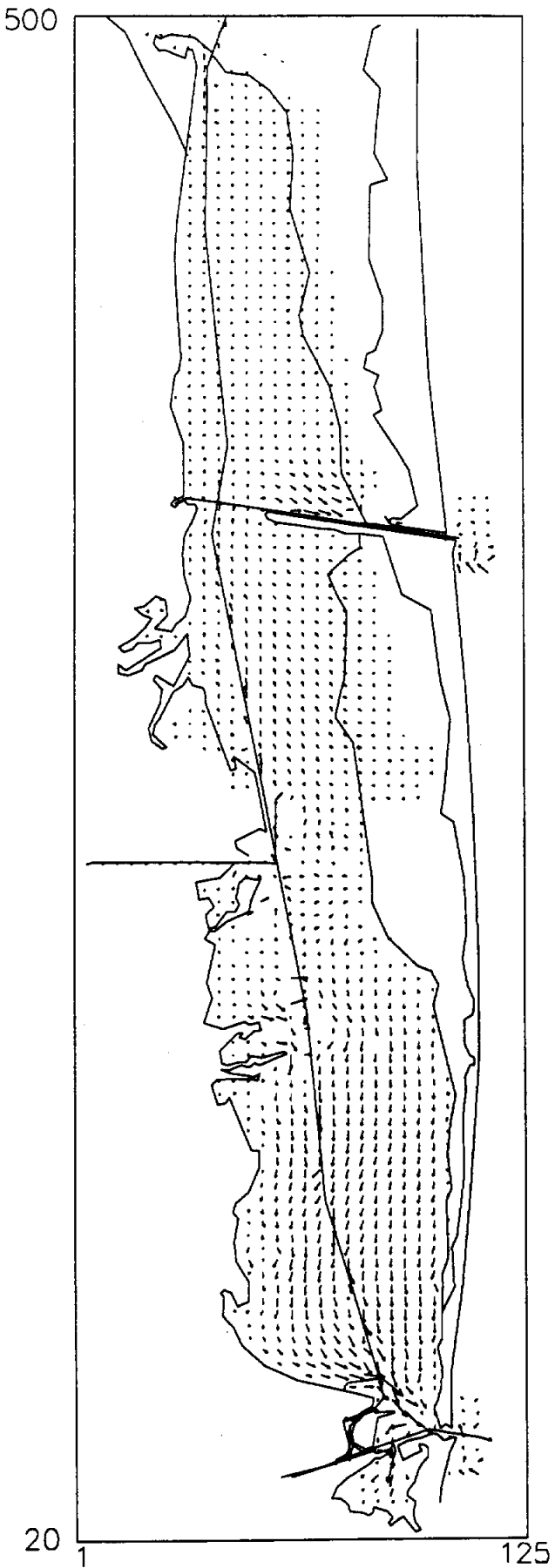
VELOCITY AT TIME 14400 GRID SIZE 125 BY 481



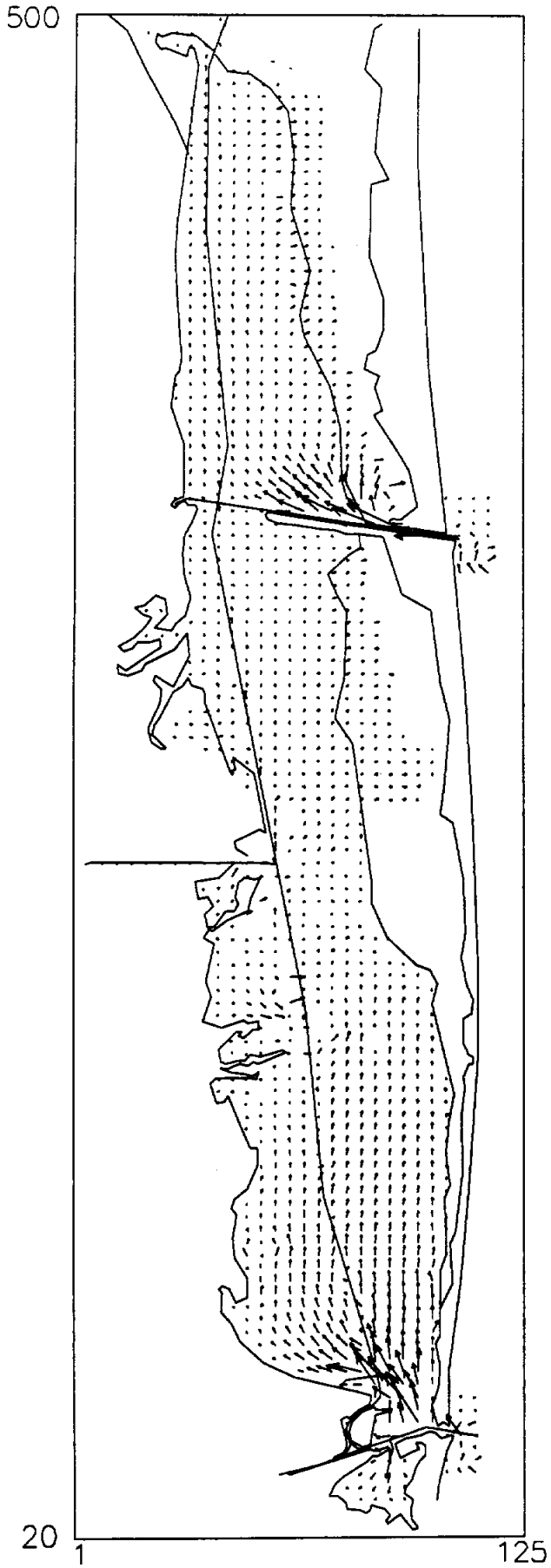
VELOCITY AT TIME 14580 GRID SIZE 125 BY 481



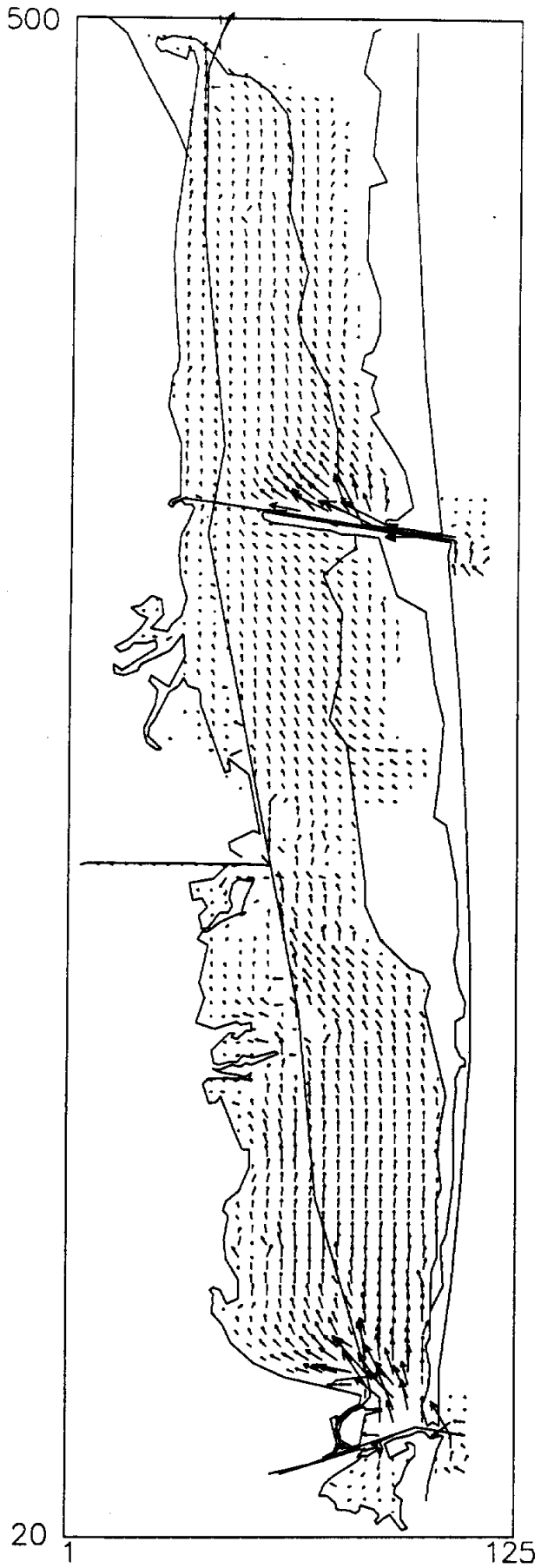
VELOCITY AT TIME 14760 GRID SIZE 125 BY 481



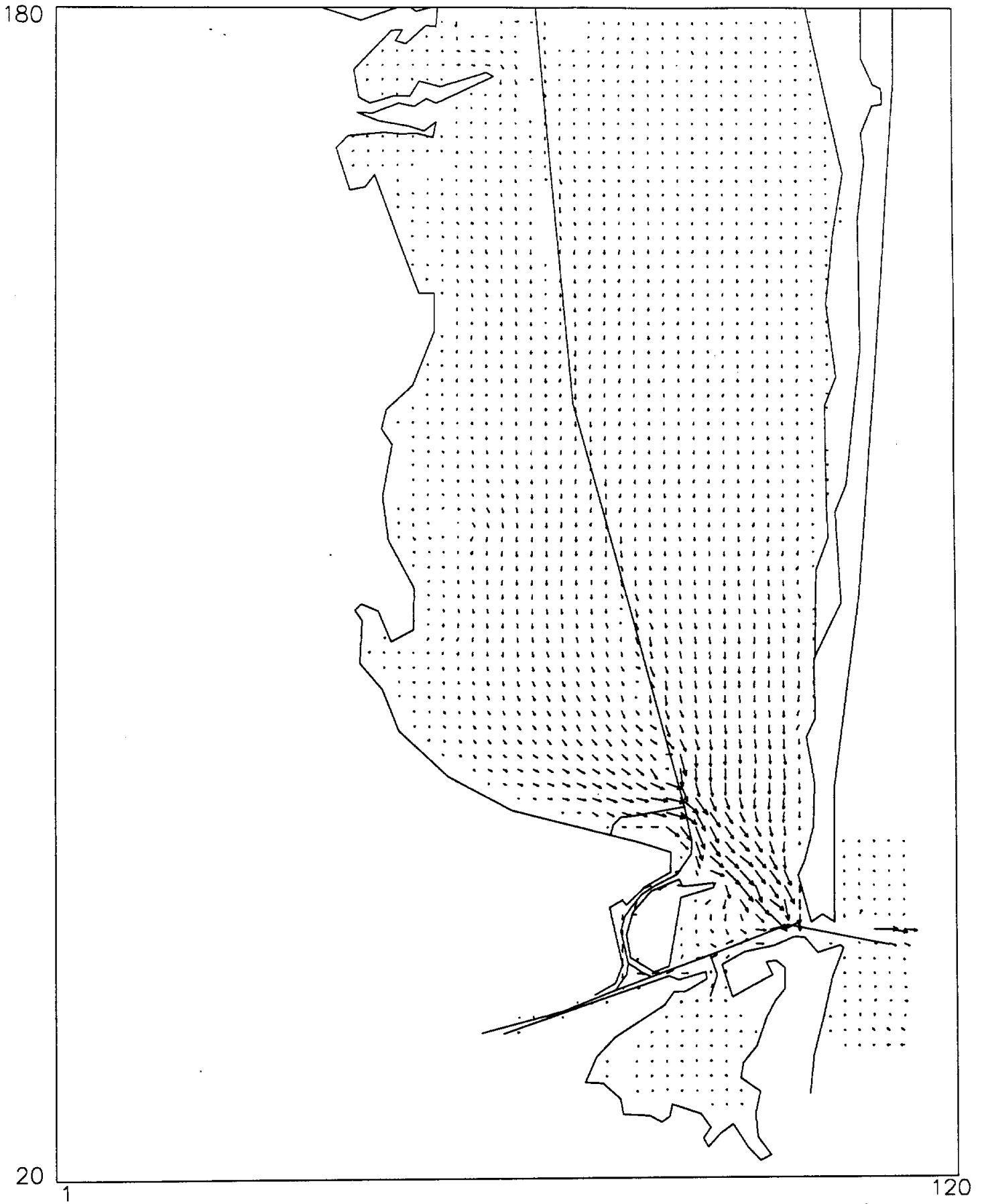
VELOCITY AT TIME 14940 GRID SIZE 125 BY 481



VELOCITY AT TIME 15120 GRID SIZE 125 BY 481



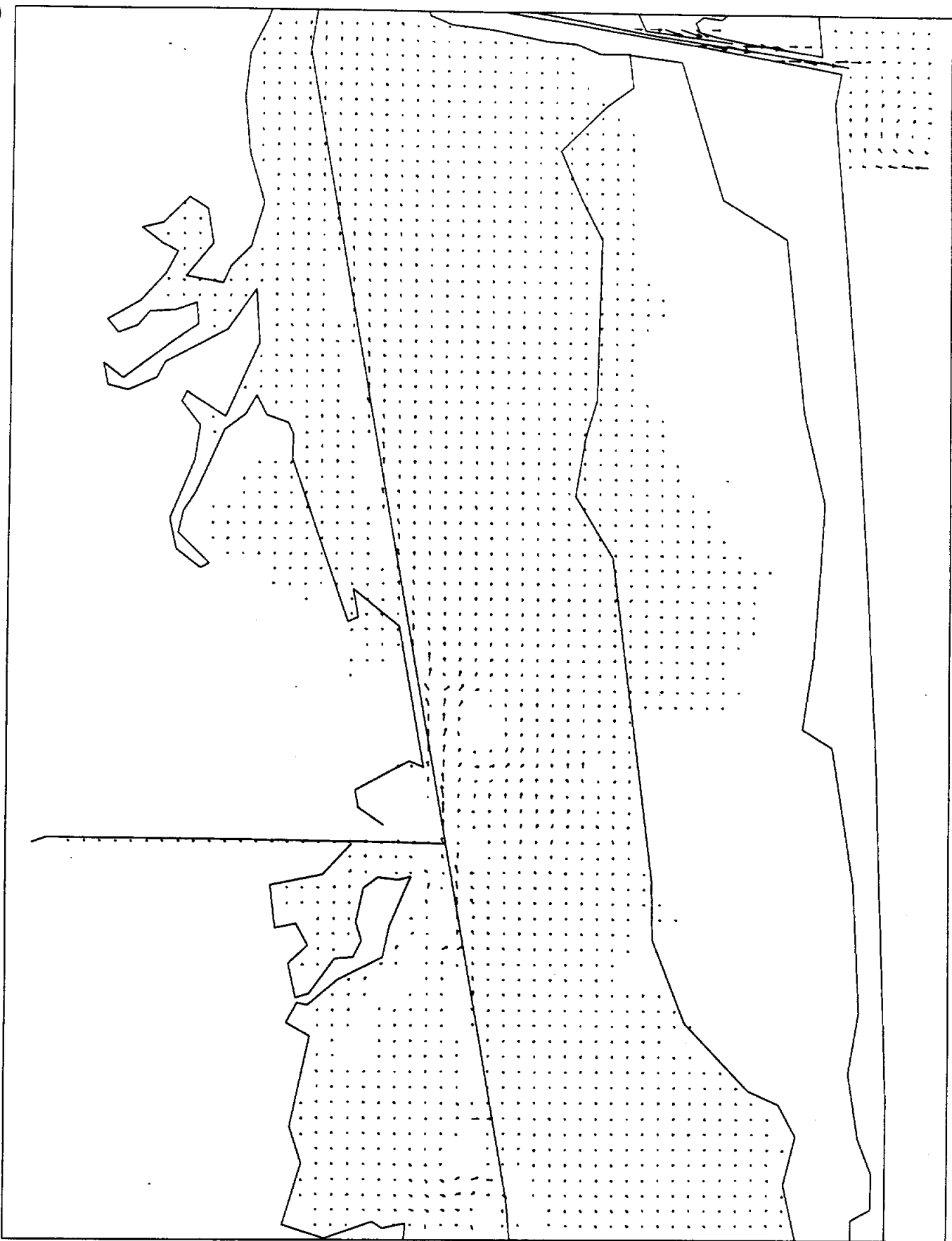
VELOCITY AT TIME 14580 GRID SIZE 120 BY 161



VELOCITY AT TIME 14580 GRID SIZE 120 BY 161

340

180



120

VELOCITY AT TIME 14580 GRID SIZE 120 BY 161

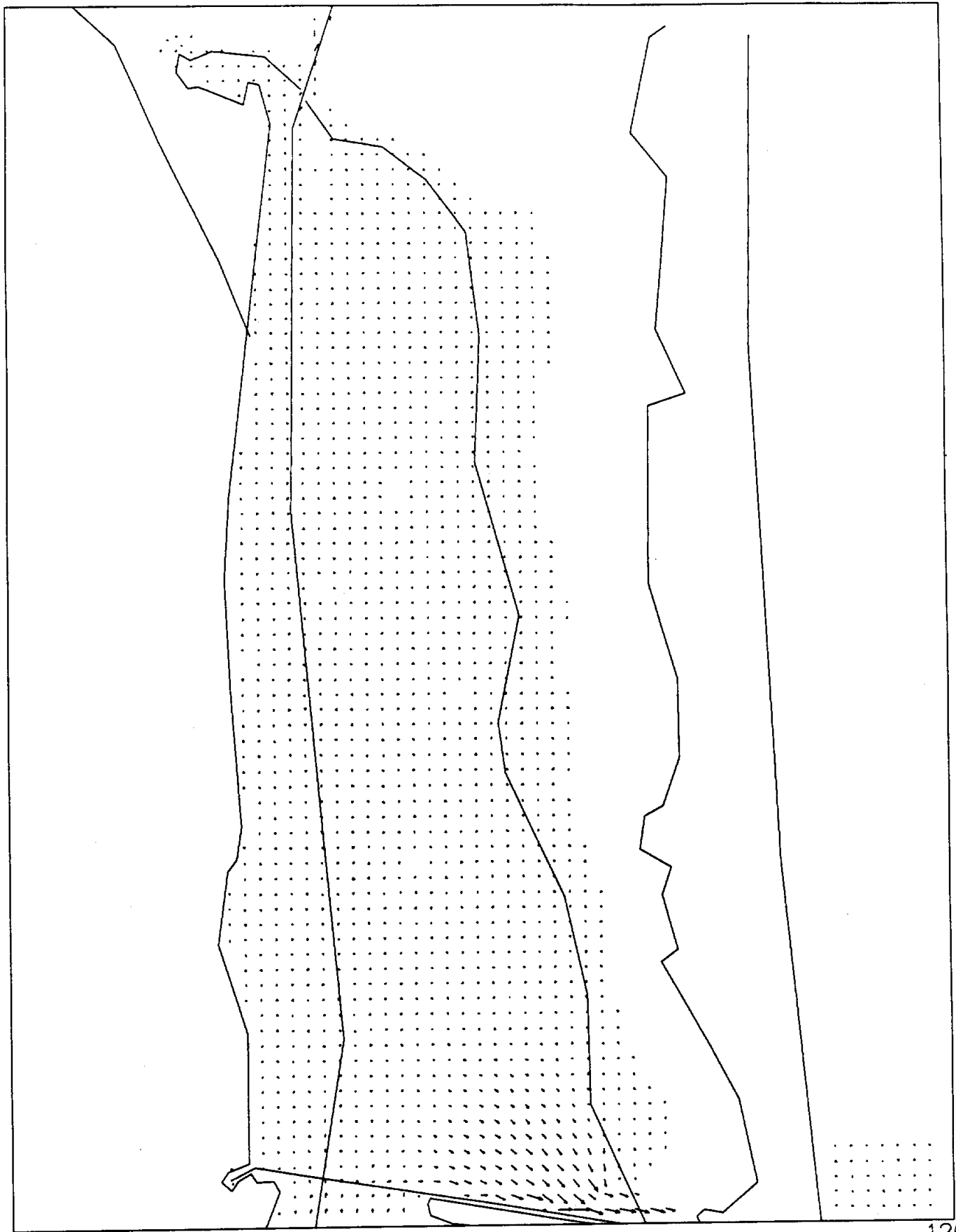
500

340

1

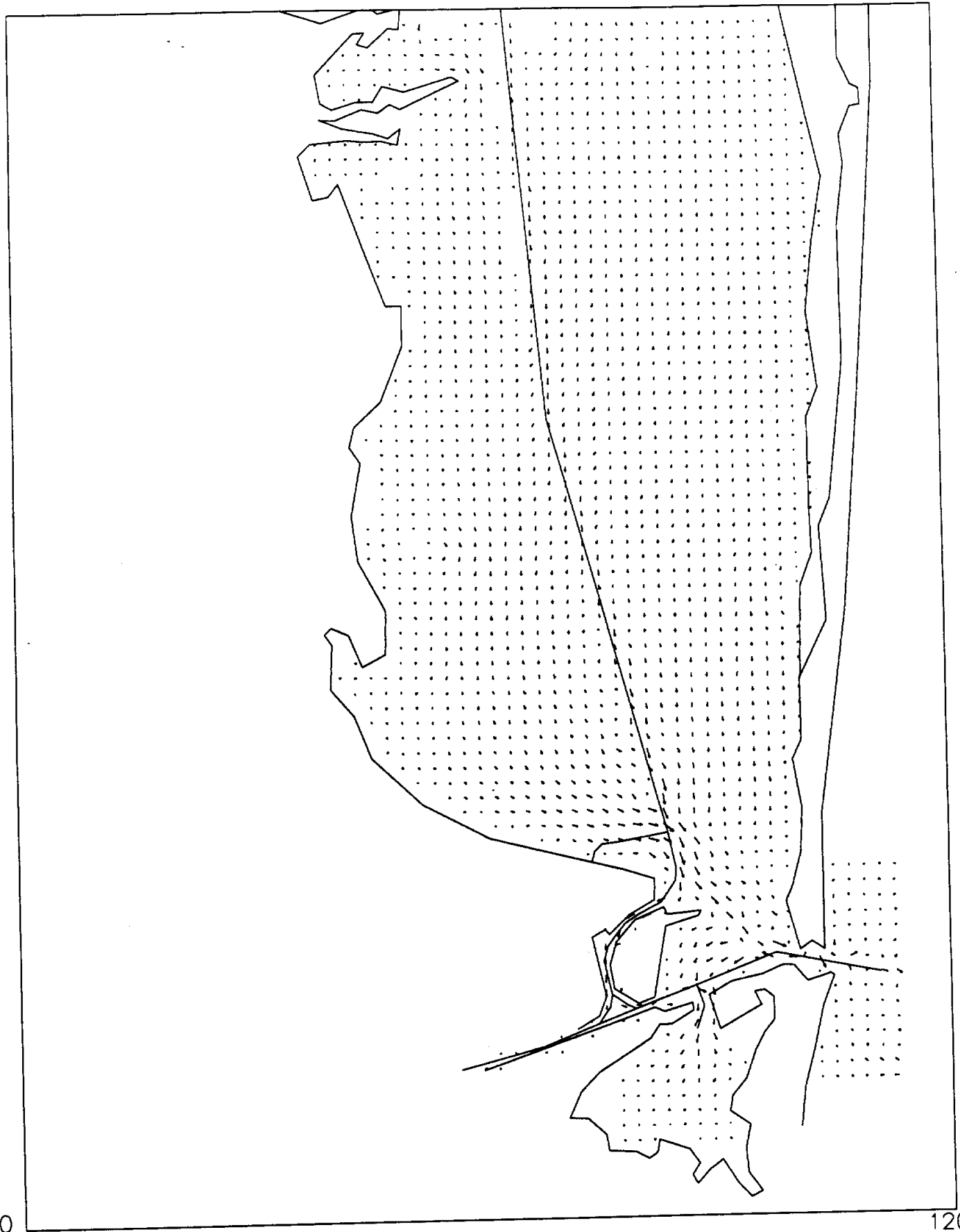
120

30



VELOCITY AT TIME 14760 GRID SIZE 120 BY 161

180

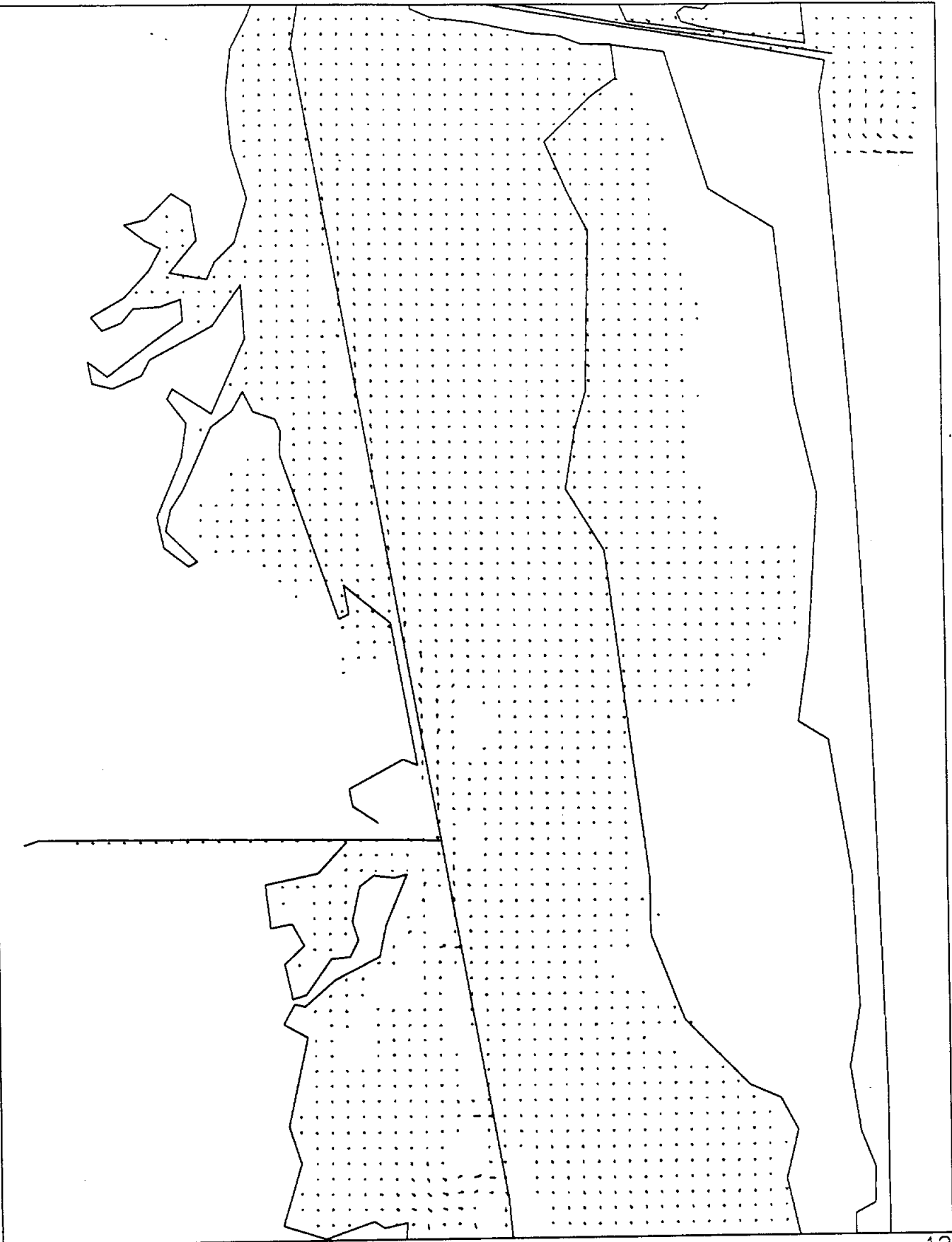


20

120

VELOCITY AT TIME 14760 GRID SIZE 120 BY 161

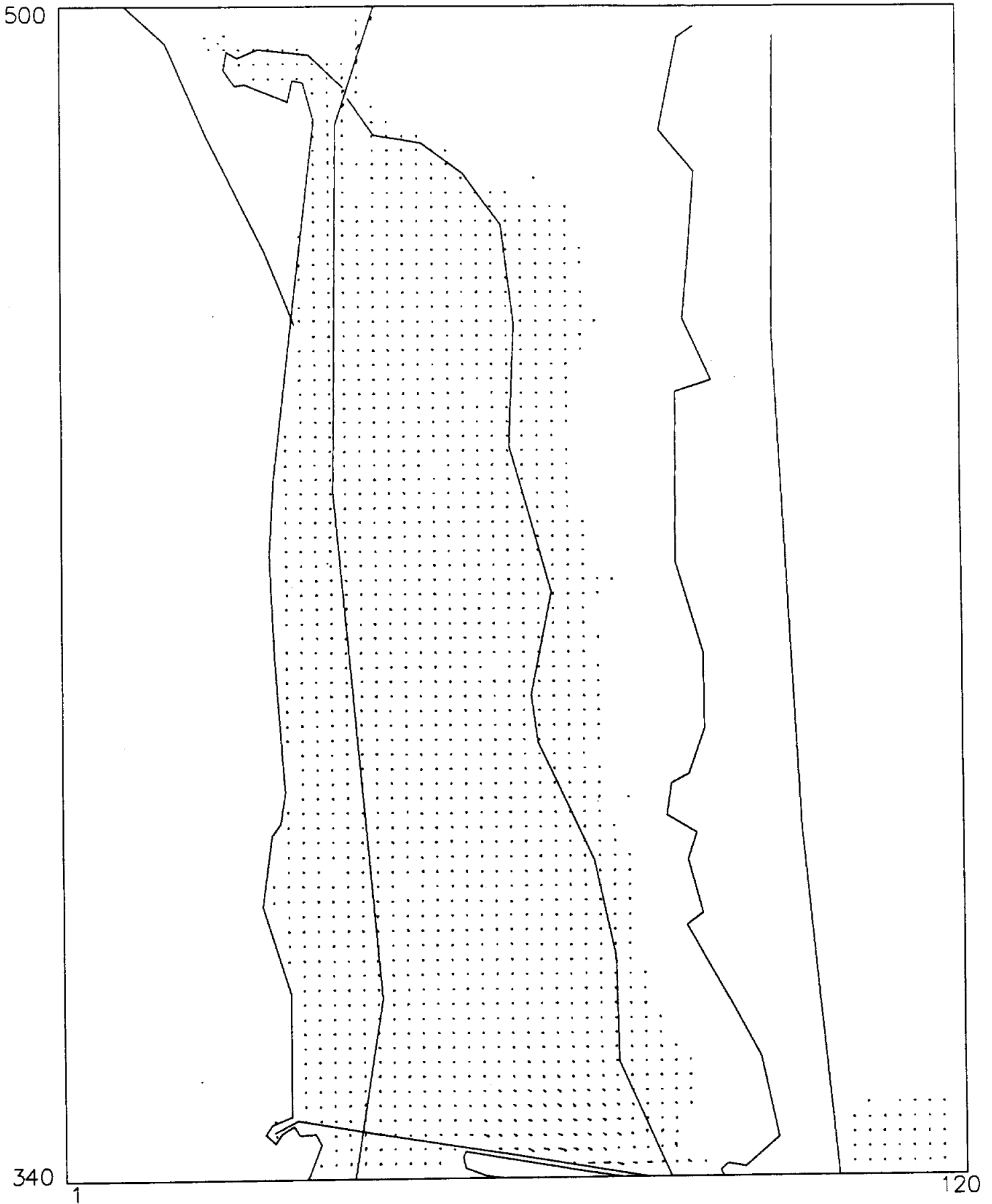
340



180

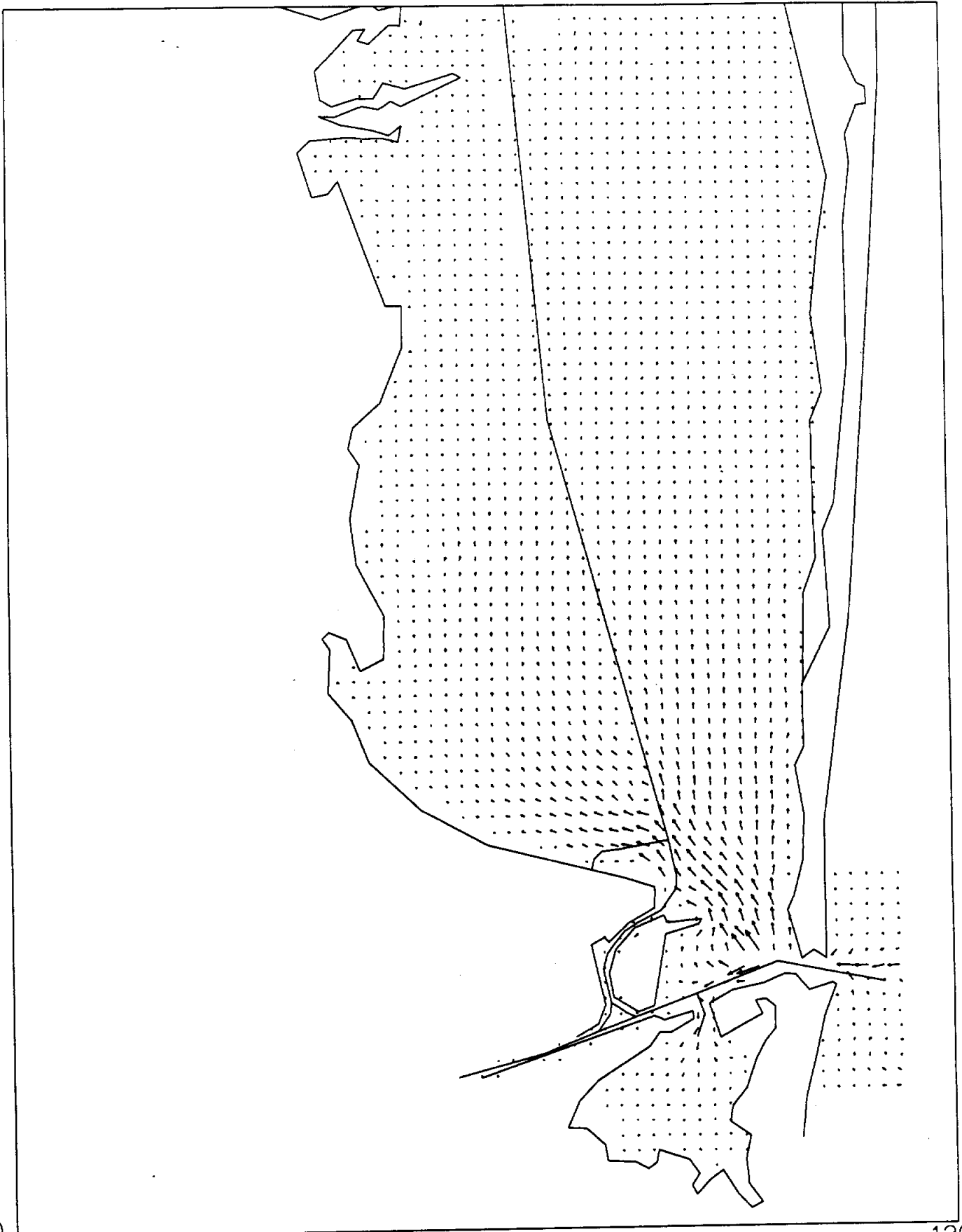
120

VELOCITY AT TIME 14760 GRID SIZE 120 BY 161



VELOCITY AT TIME 14940 GRID SIZE 120 BY 161

180



20

120

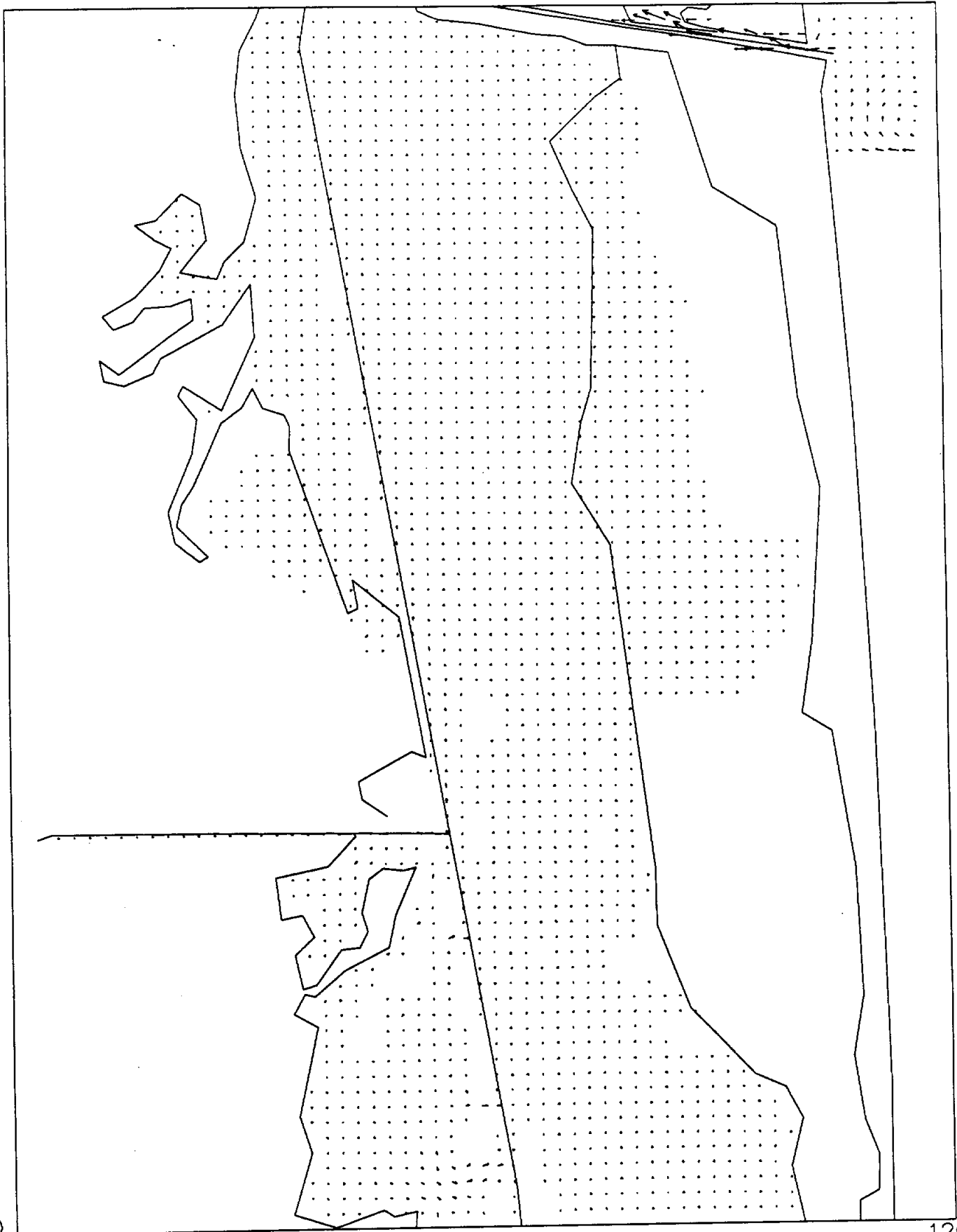
VELOCITY AT TIME 14940 GRID SIZE 120 BY 161

340

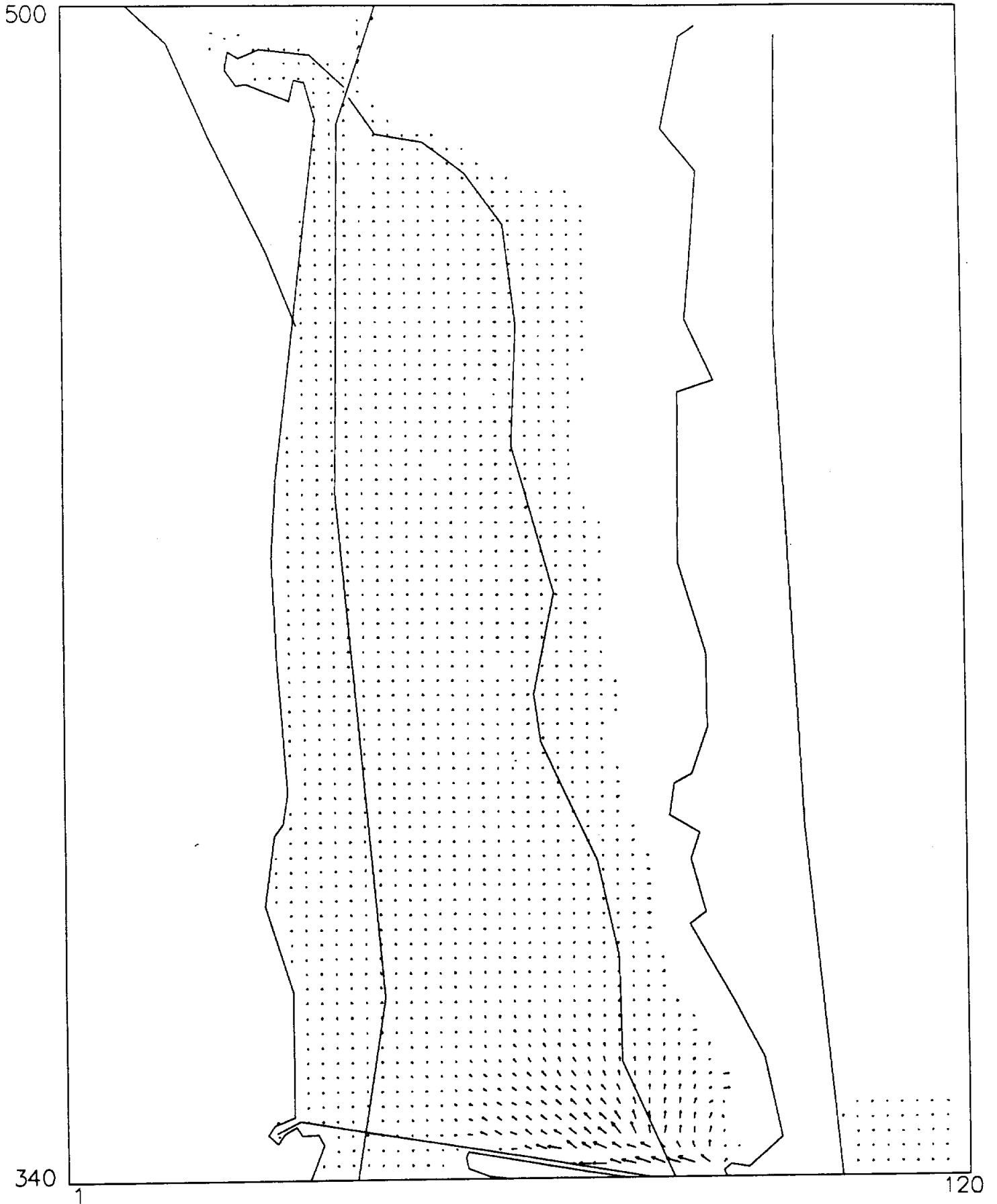
180

120

35

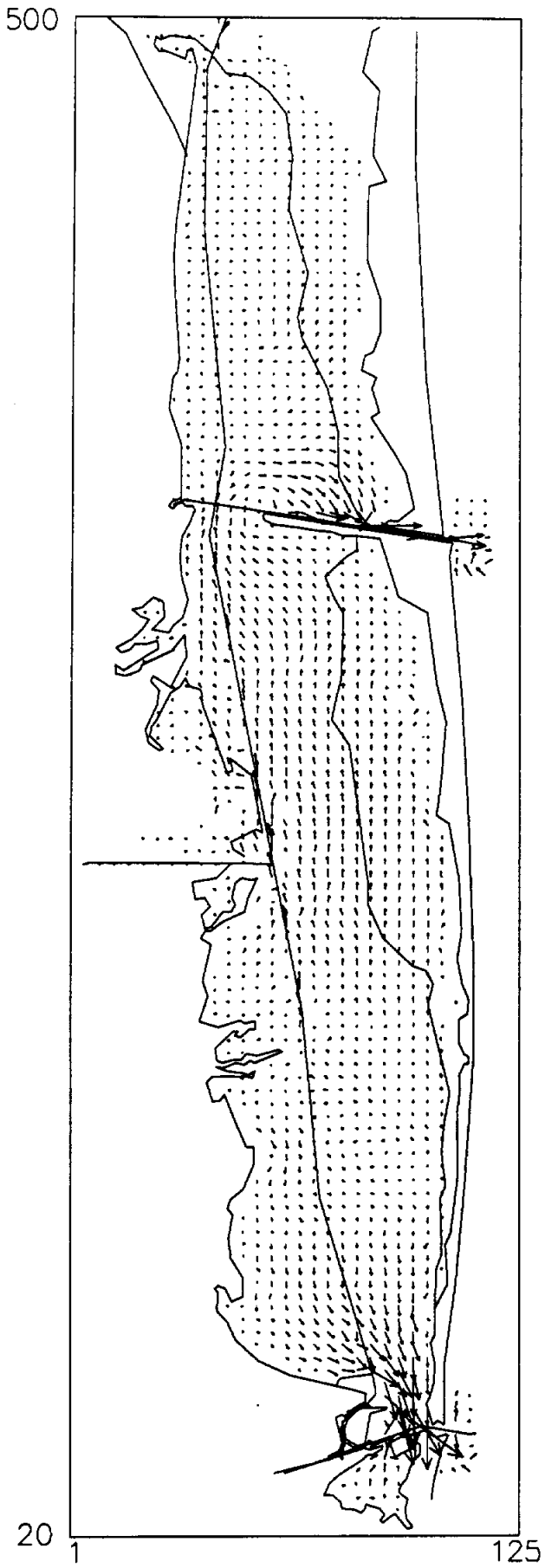


VELOCITY AT TIME 14940 GRID SIZE 120 BY 161

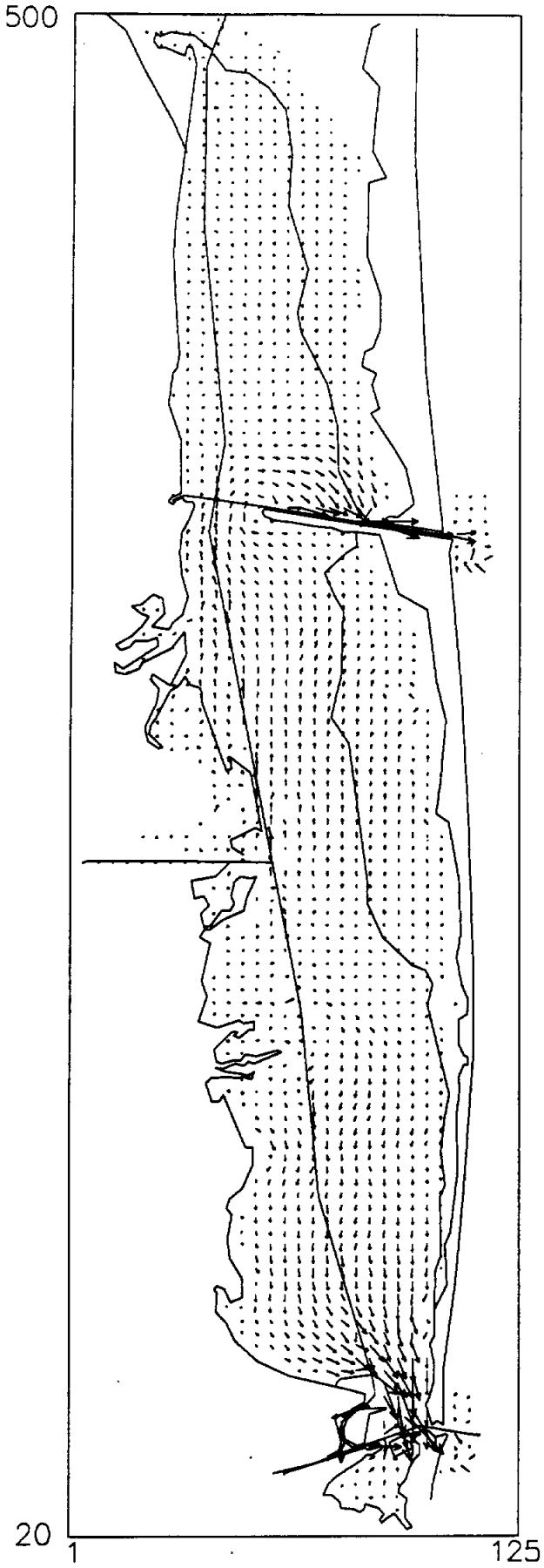


**Velocity Vector Plots for the Calibrated Model
with the Nautical Chart Data**

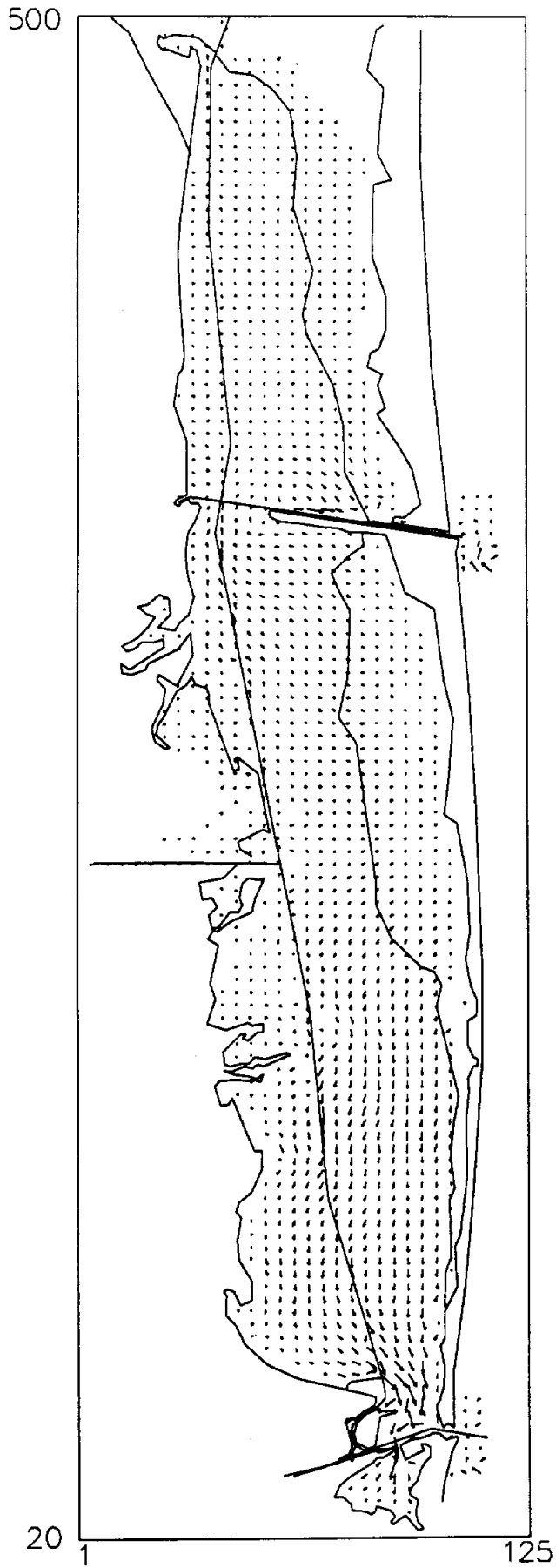
VELOCITY AT TIME 14400 GRID SIZE 125 BY 481



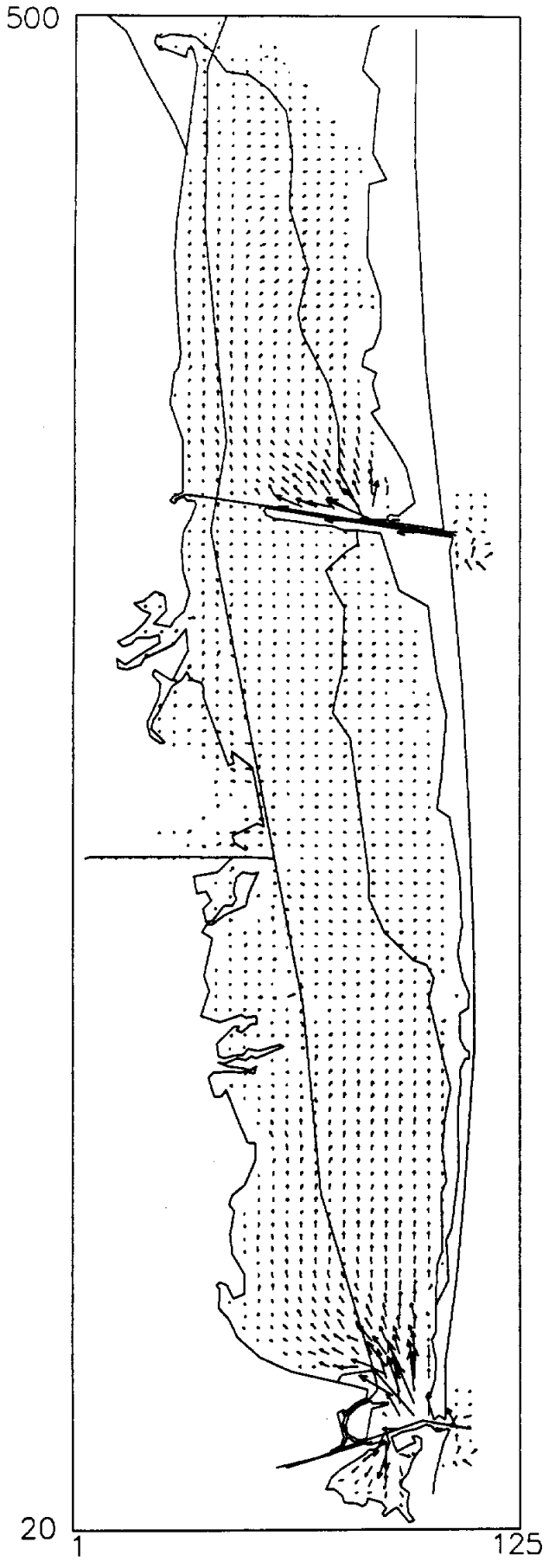
VELOCITY AT TIME 14580 GRID SIZE 125 BY 481



VELOCITY AT TIME 14760 GRID SIZE 125 BY 481

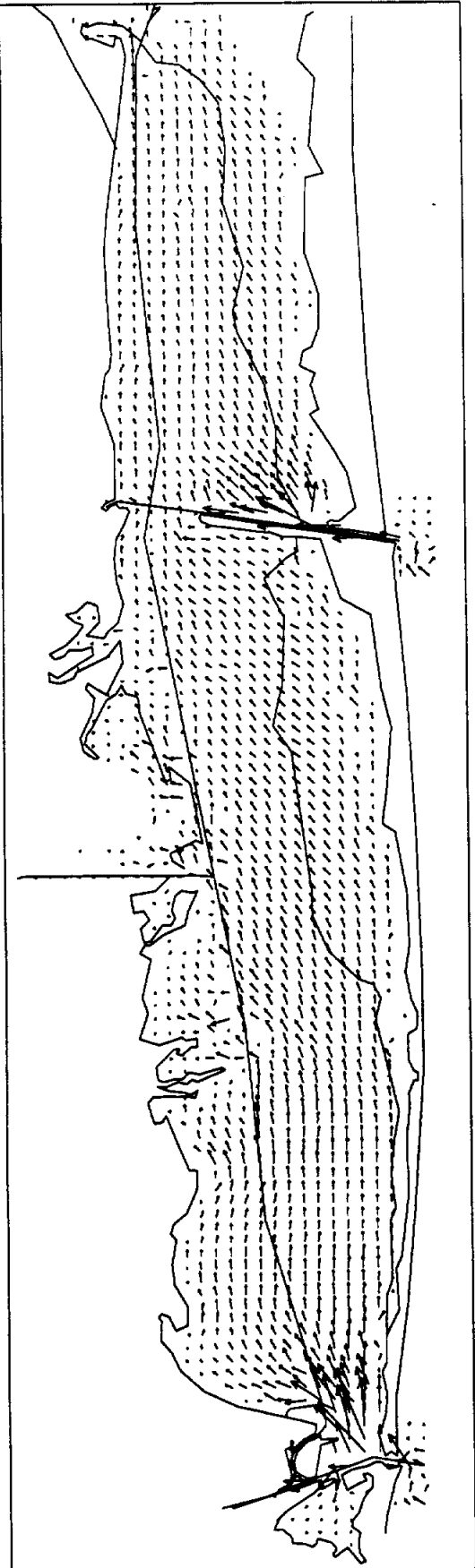


VELOCITY AT TIME 14940 GRID SIZE 125 BY 481



VELOCITY AT TIME 15120 GRID SIZE 125 BY 481

500

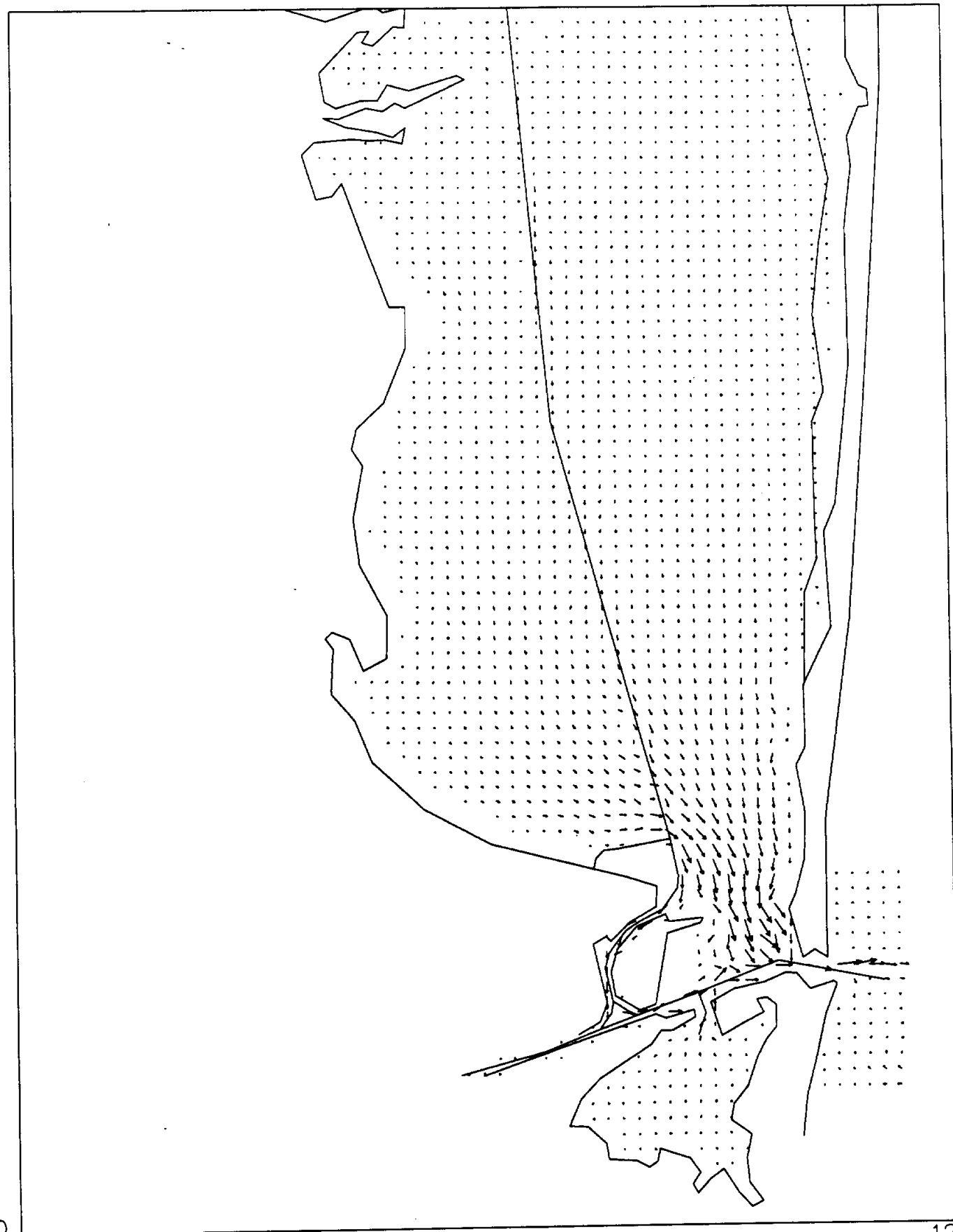


20

125

VELOCITY AT TIME 14580 GRID SIZE 120 BY 161

180



20

120

43

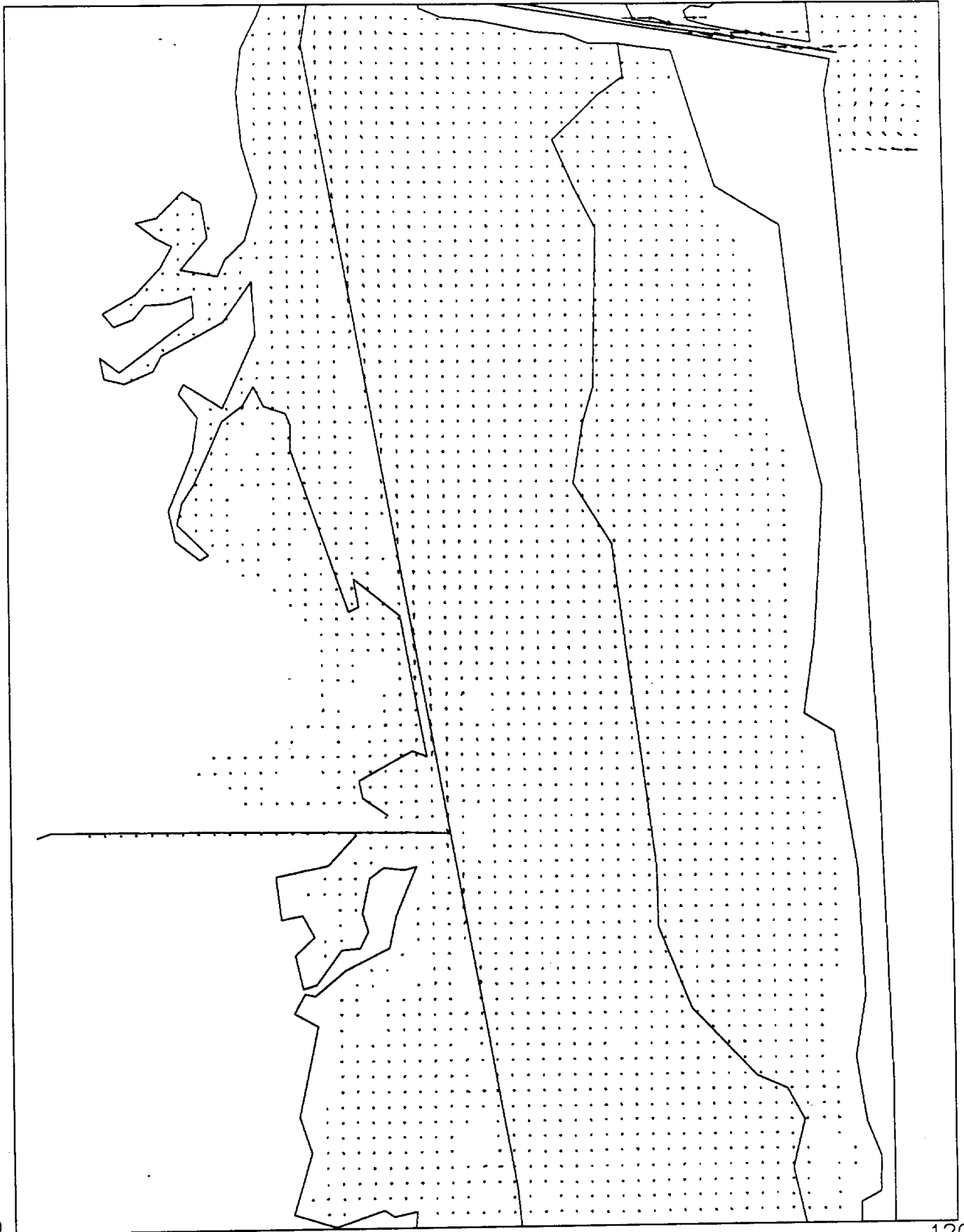
VELOCITY AT TIME 14580 GRID SIZE 120 BY 161

340

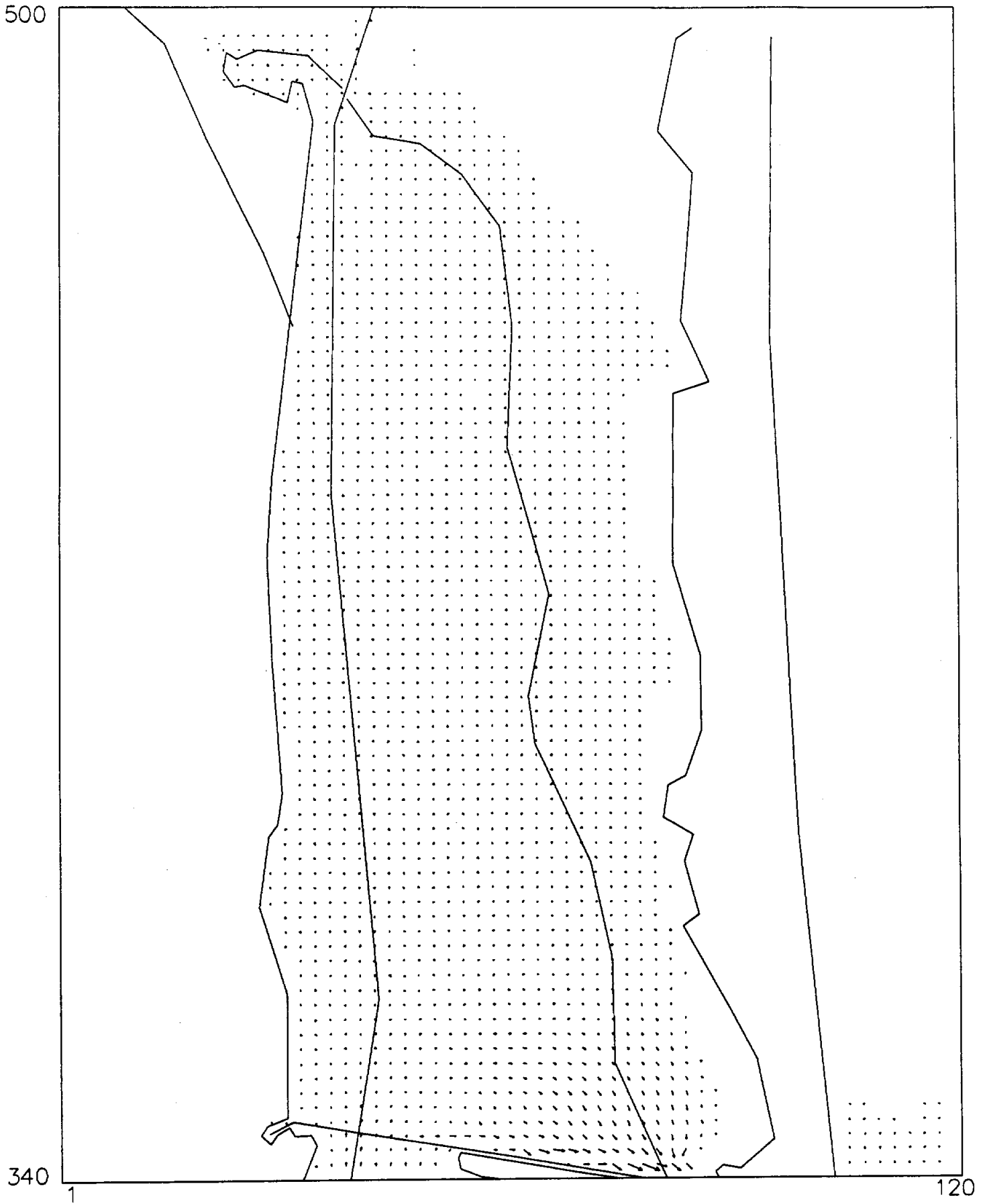
180

120

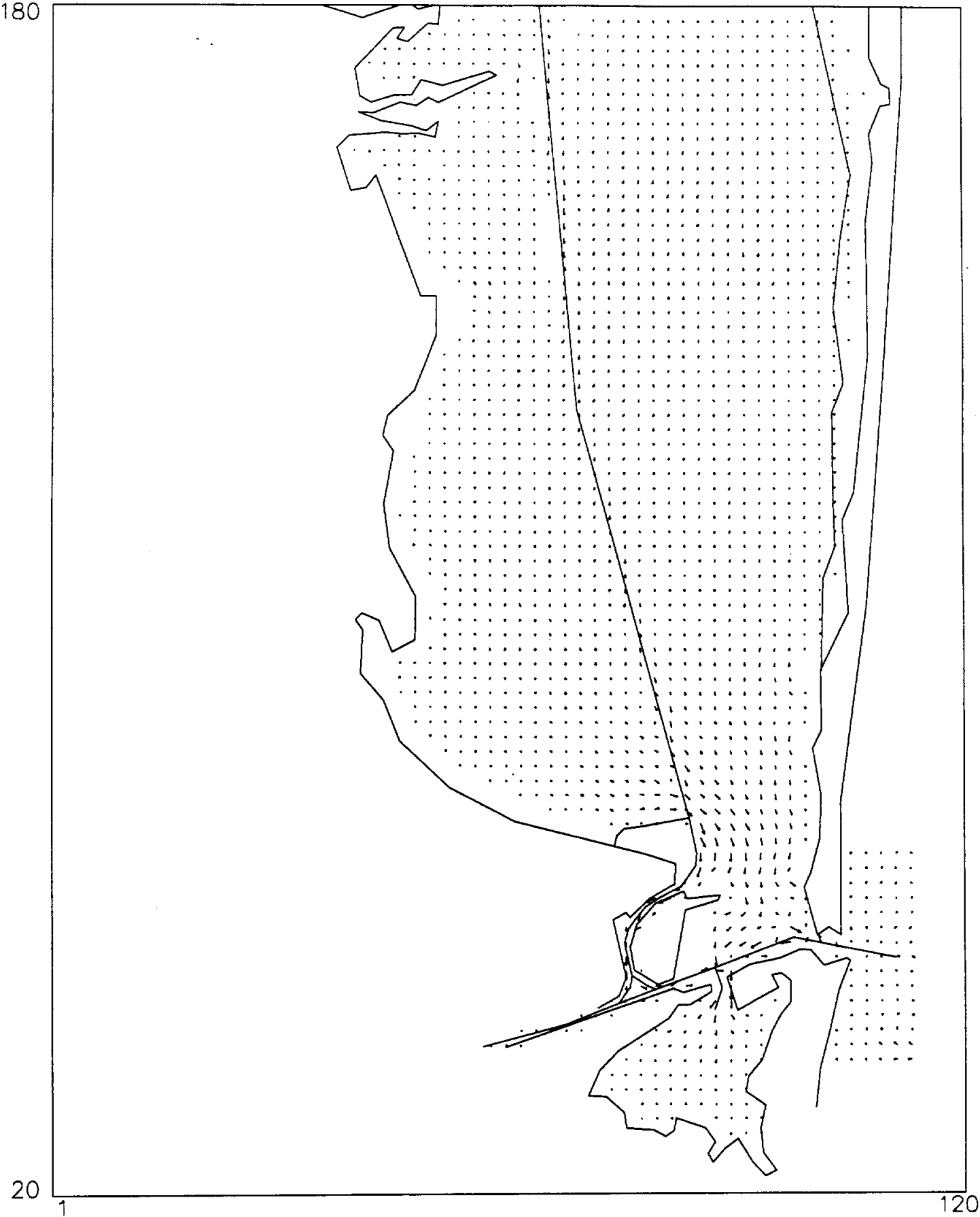
44



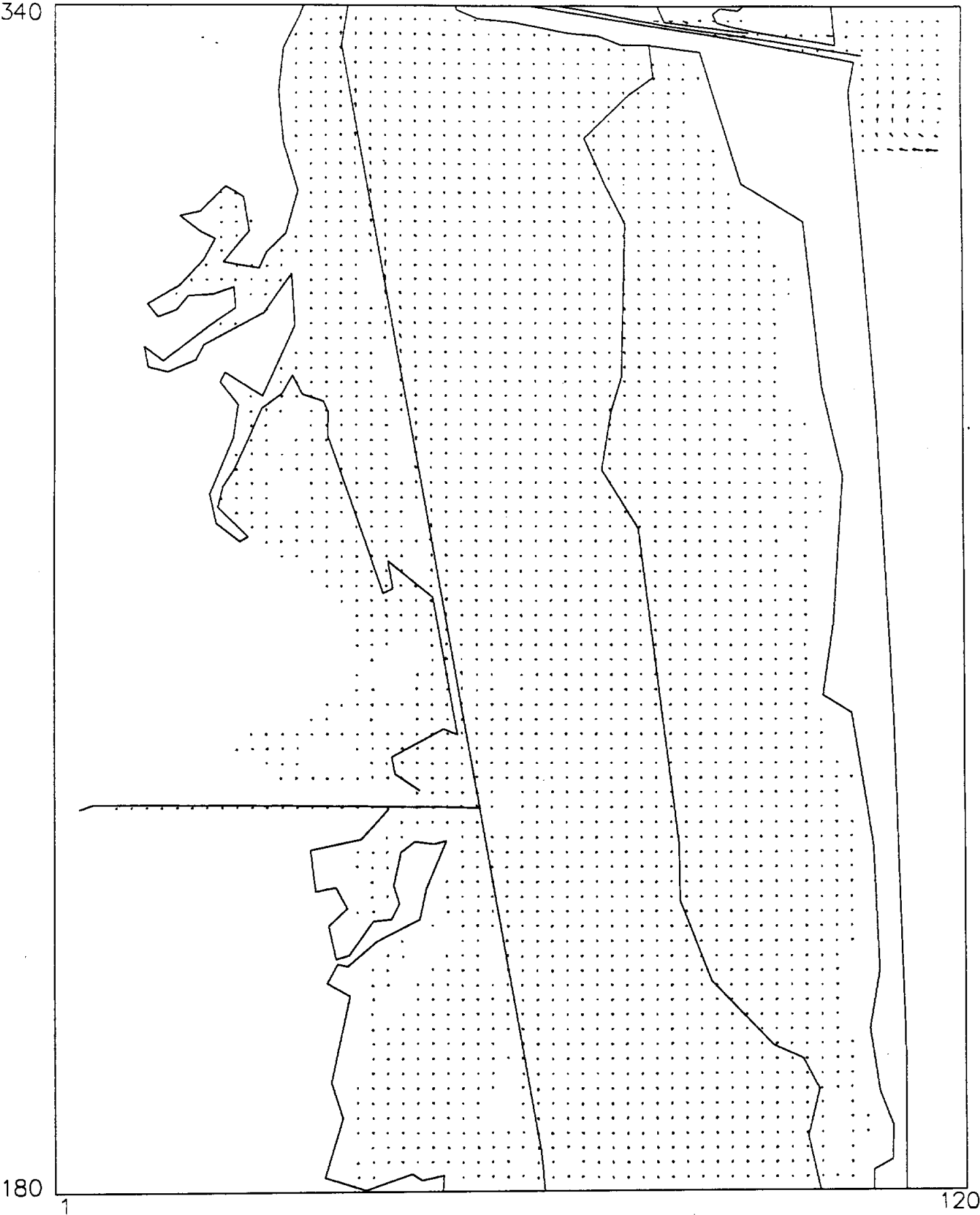
VELOCITY AT TIME 14580 GRID SIZE 120 BY 161



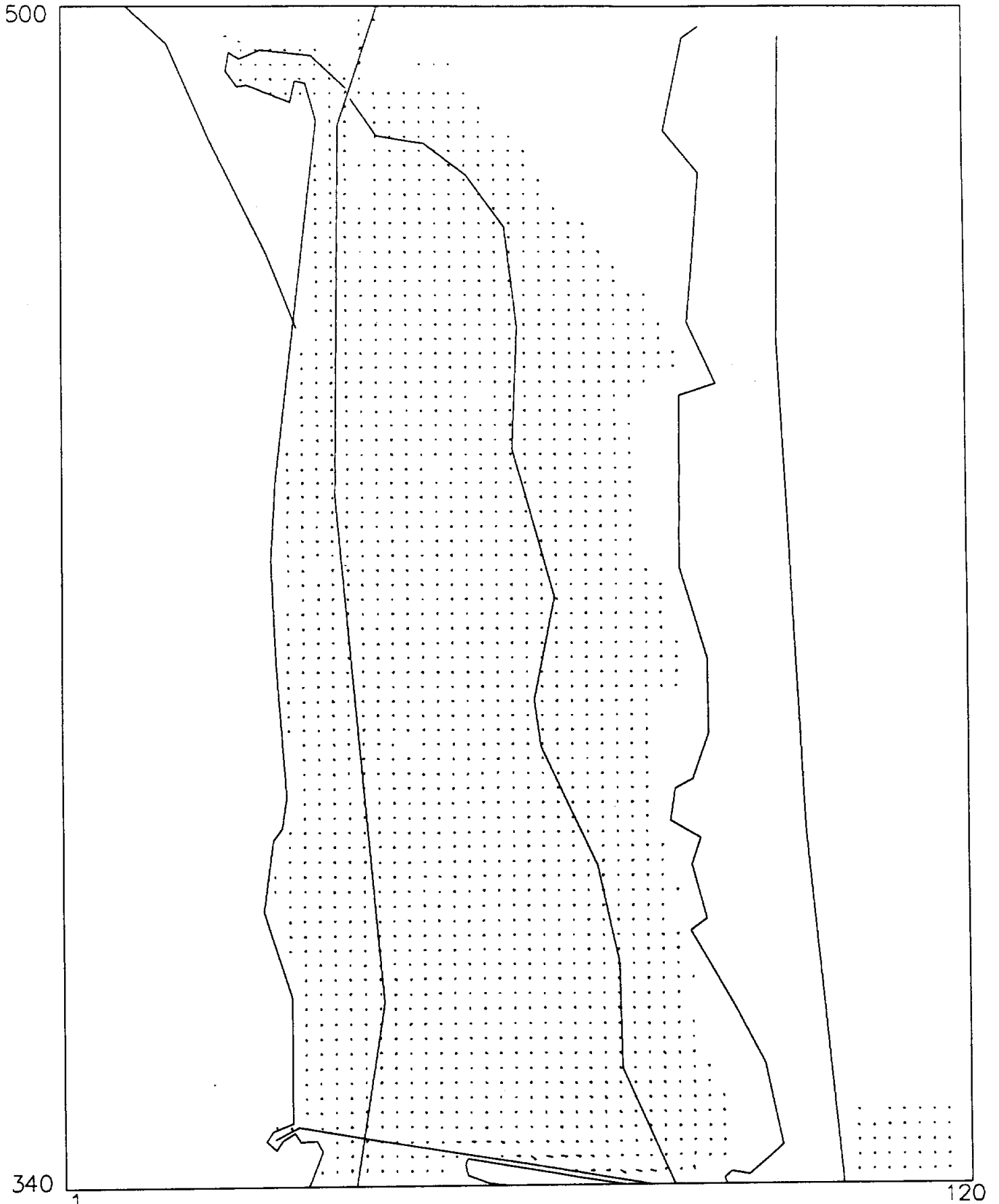
VELOCITY AT TIME 14760 GRID SIZE 120 BY 161



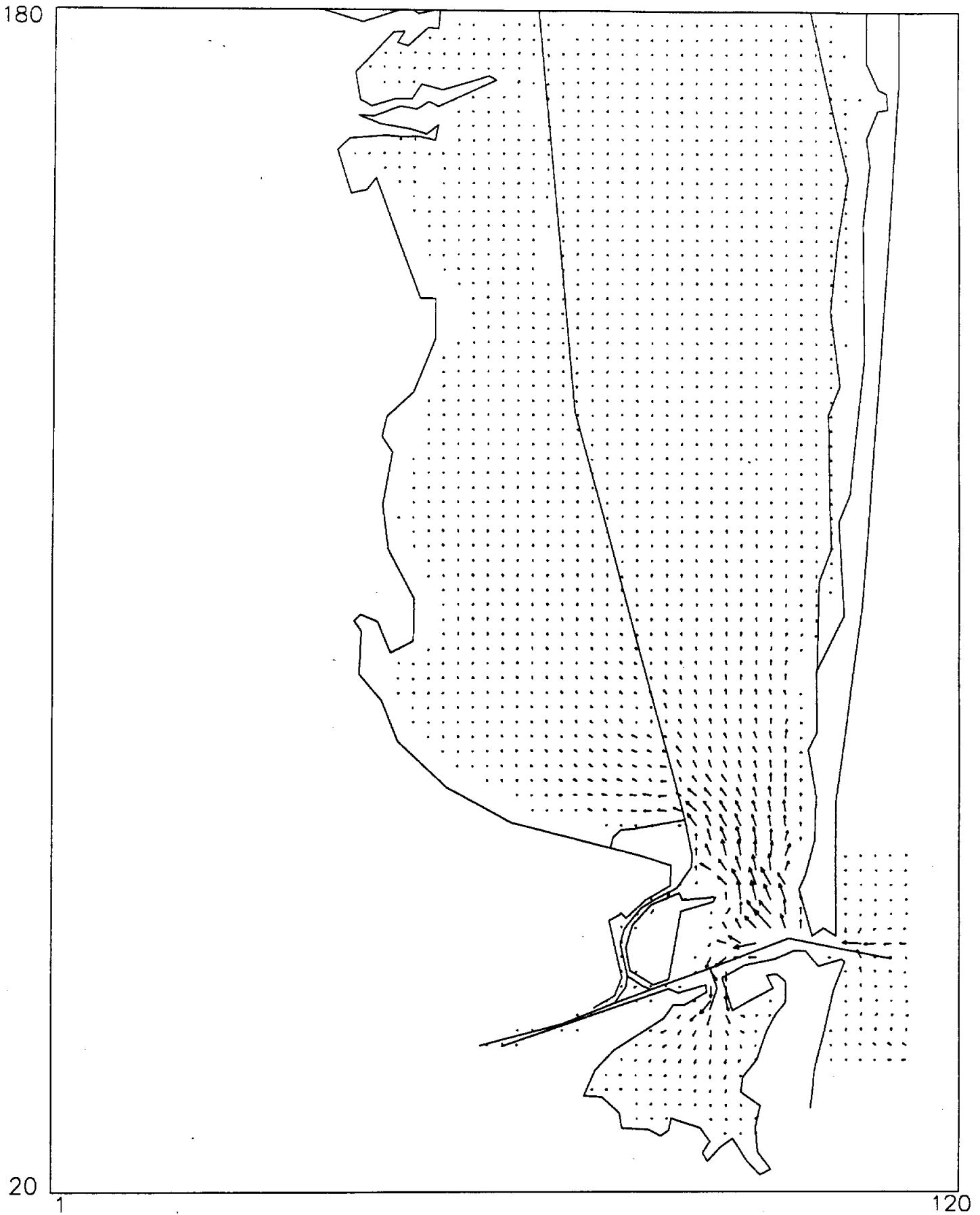
VELOCITY AT TIME 14760 GRID SIZE 120 BY 161



VELOCITY AT TIME 14760 GRID SIZE 120 BY 161

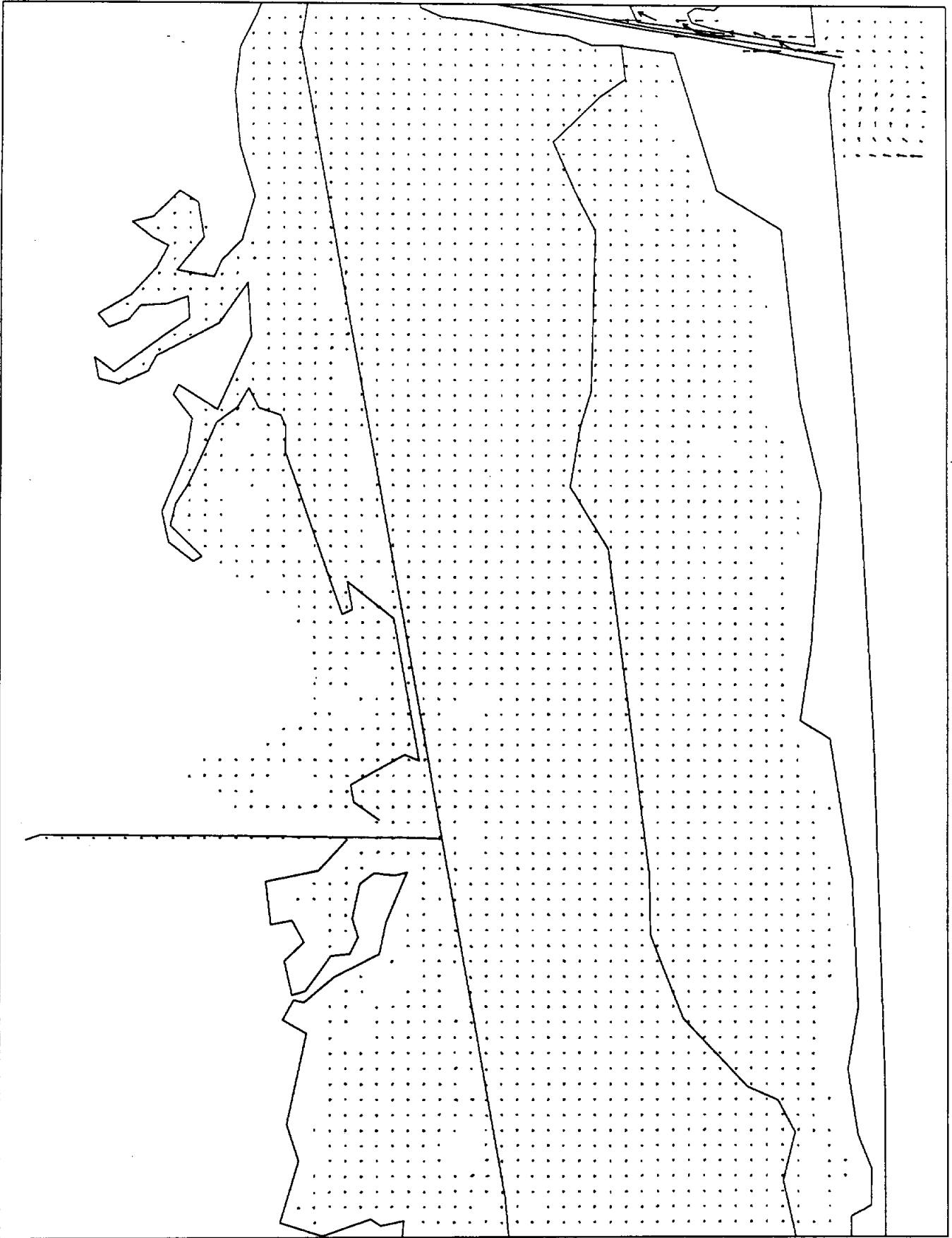


VELOCITY AT TIME 14940 GRID SIZE 120 BY 161



VELOCITY AT TIME 14940 GRID SIZE 120 BY 161

340

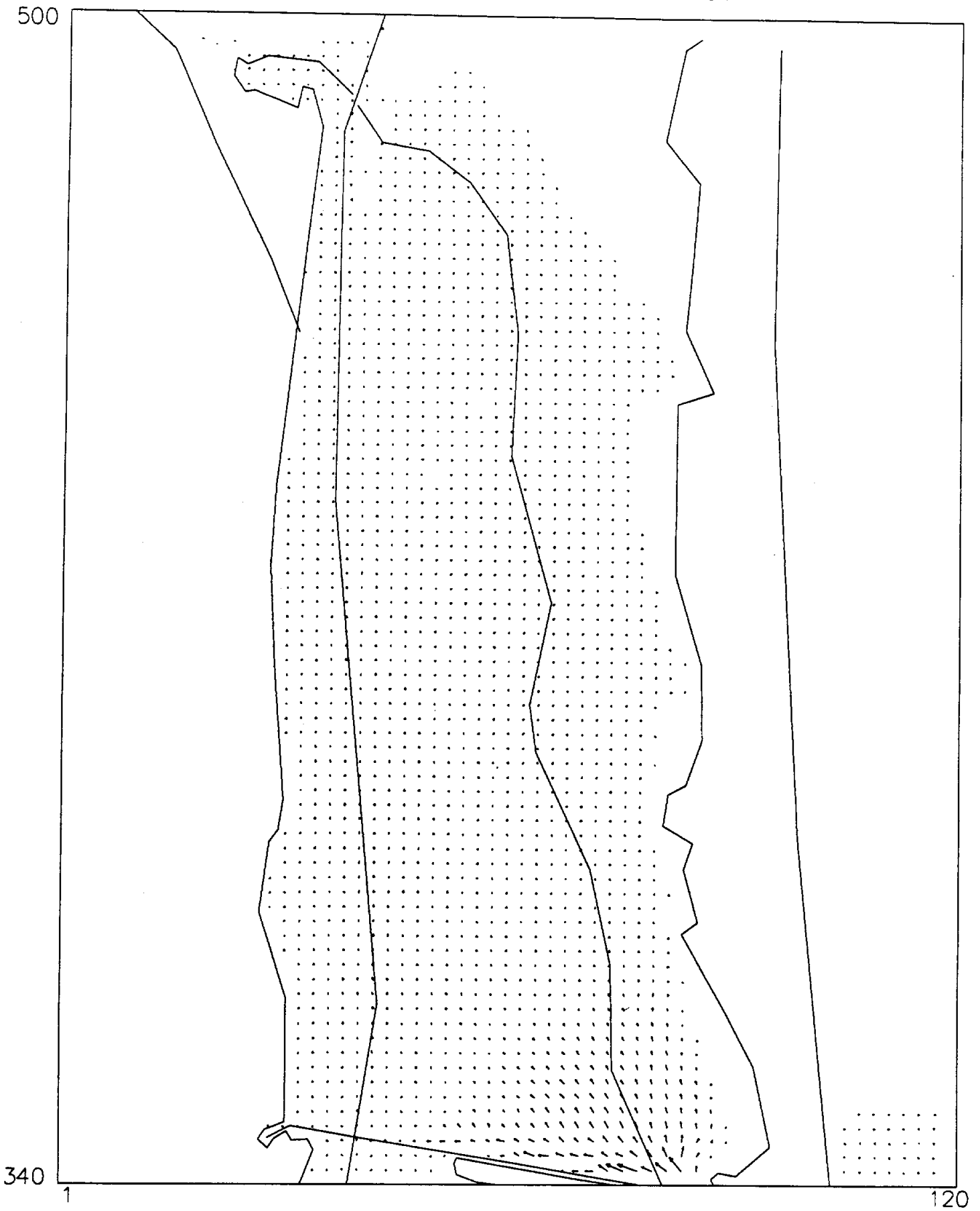


180

1

120

VELOCITY AT TIME 14940 GRID SIZE 120 BY 161



SWIFT2D SIMULATIONS

Manning's n Variation Simulation

Manning's n = 0.030 throughout the model

Wind Stress = 0.0015

Time Step = 6 minutes

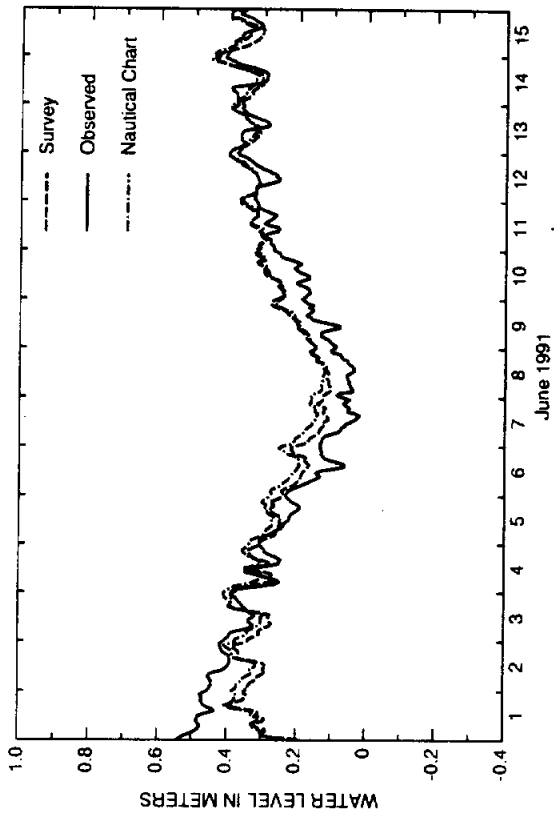


FIG. 1. Rincon Del San Jose Tide Station

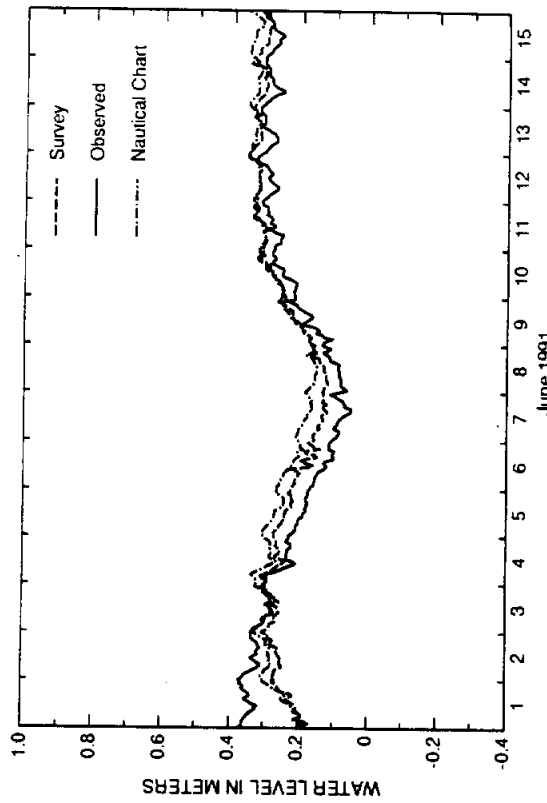


FIG. 2. Port Mansfield Tide Station

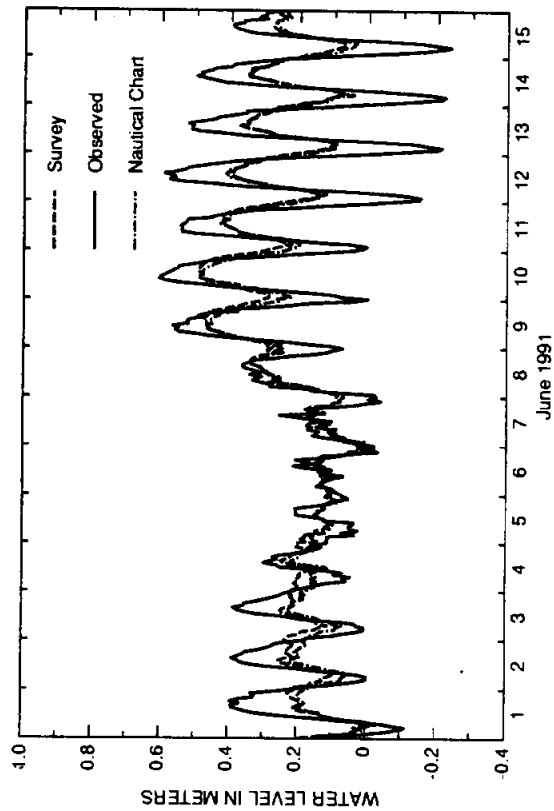


FIG. 3. Port Isabel Tide Station

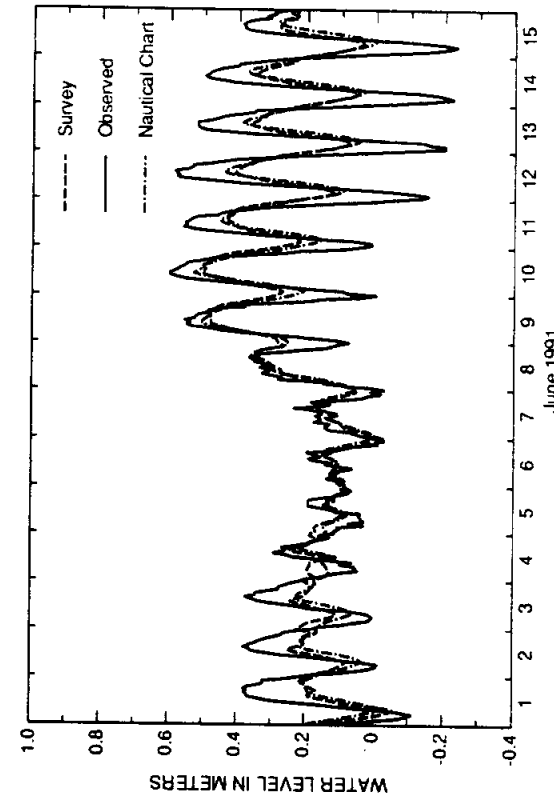


FIG. 4. South Bay Tide Station.

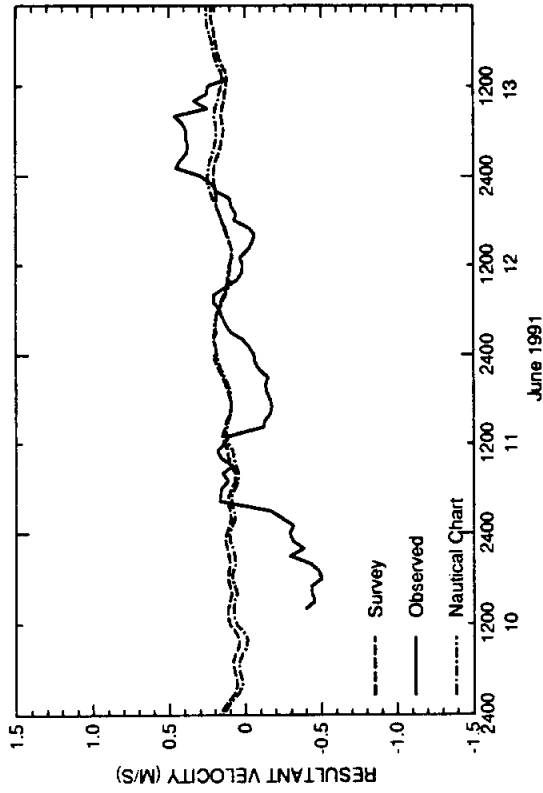


FIG. 1. South Land Cut

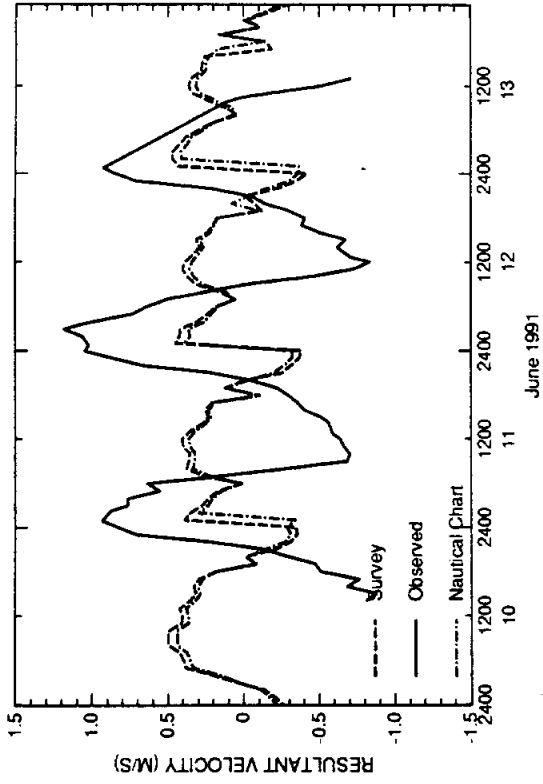


FIG. 2. Port Mansfield Jetties

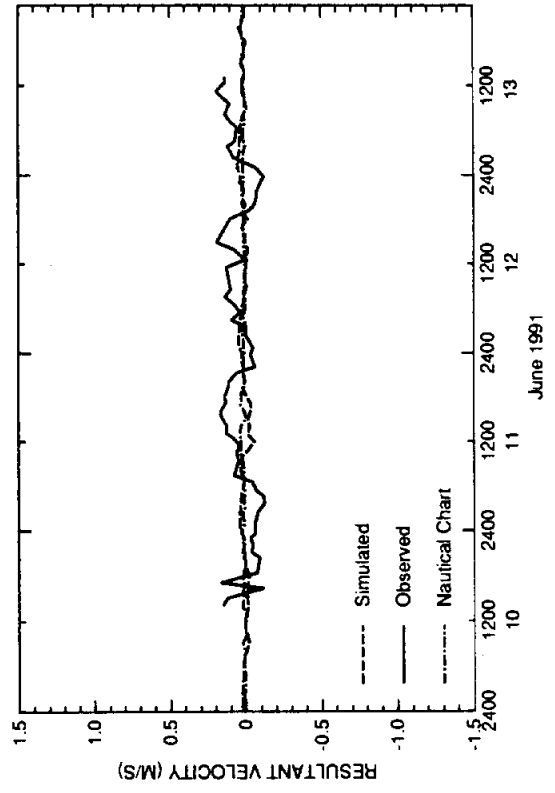


FIG. 3. Mouth of Arroyo Colorado

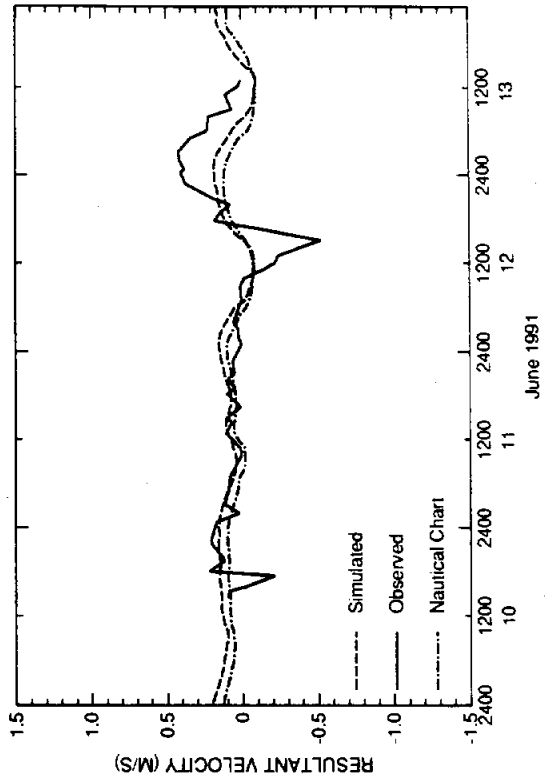


FIG. 4. GIWW North of Arroyo Colorado

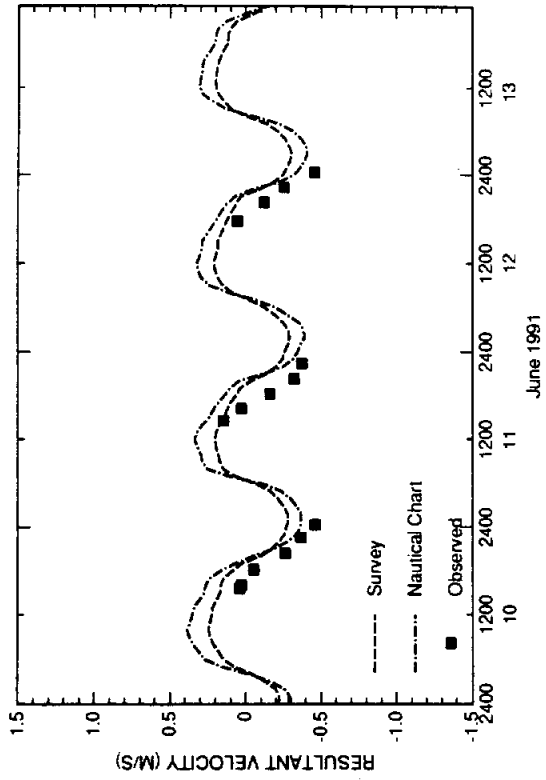


FIG. 6. Old Causeway (Mid East)

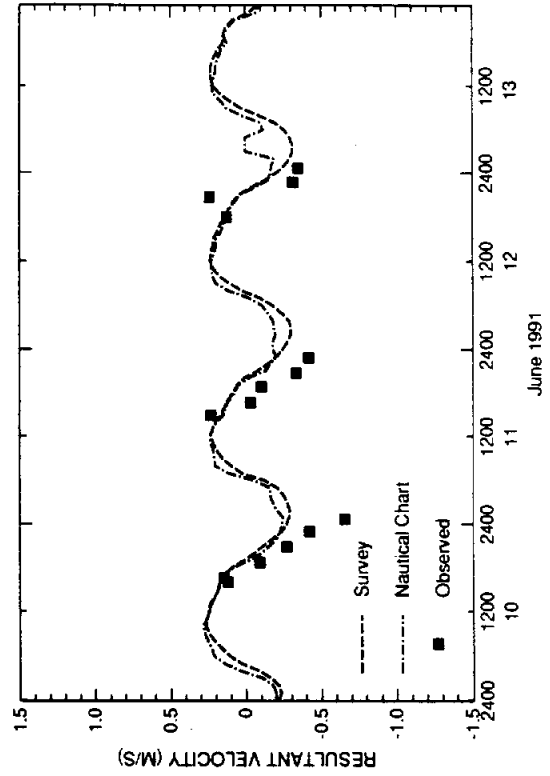


FIG. 8. Old Causeway (Western)

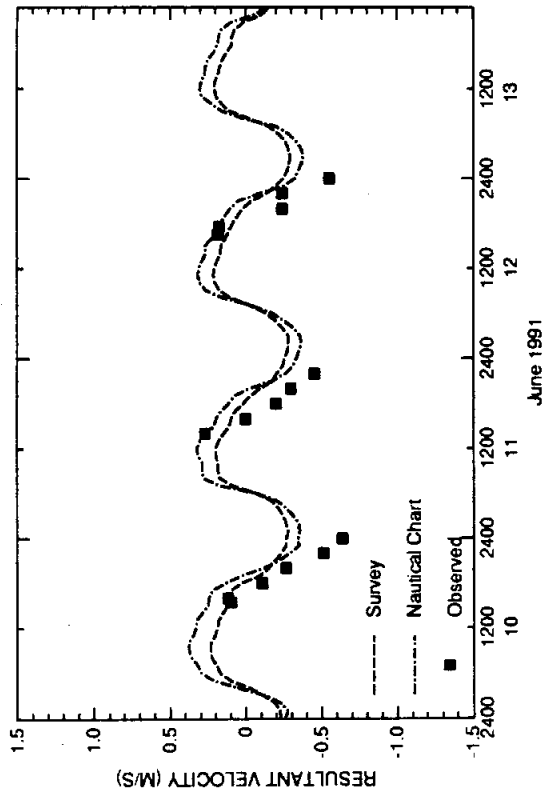


FIG. 5. Old Causeway (Eastern)

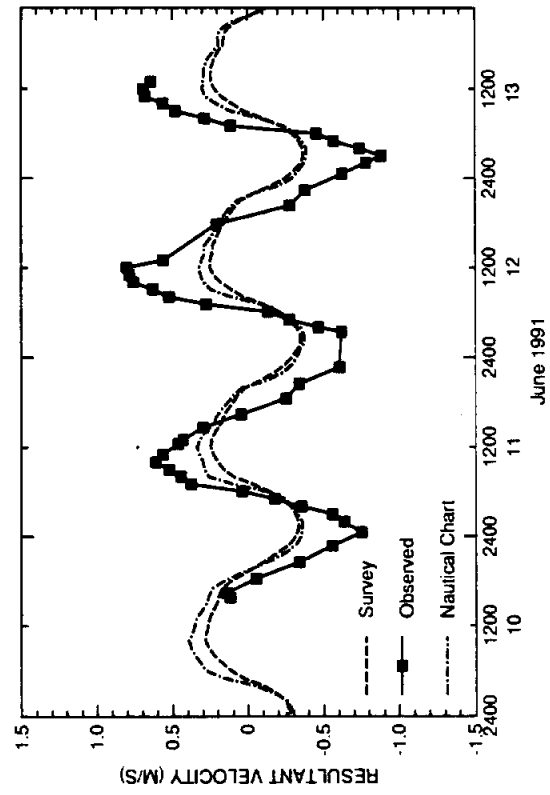


FIG. 7. Old Causeway (Mid West)

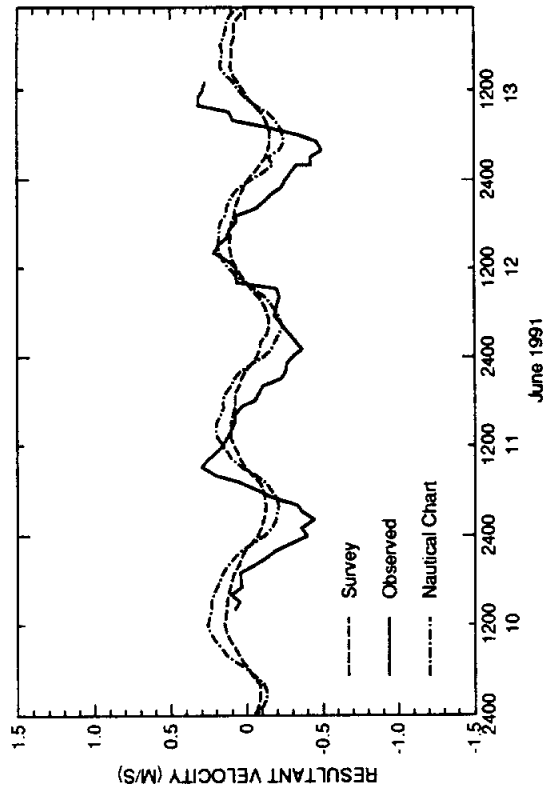


FIG. 9. Port Isabel Channel

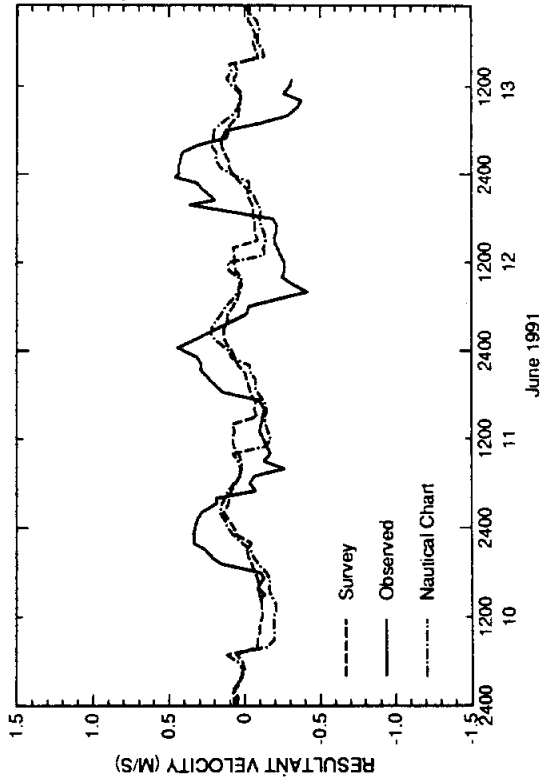


FIG. 10. Brownsville Ship Channel

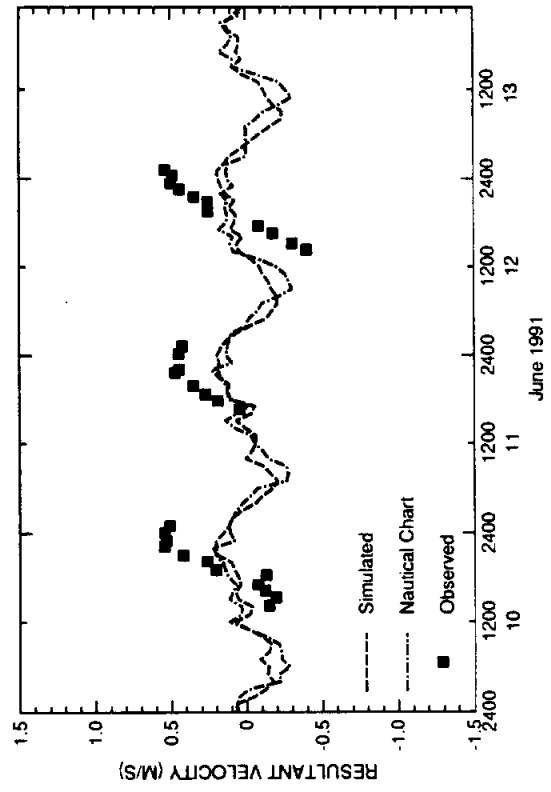


FIG. 11. South Bay Pass

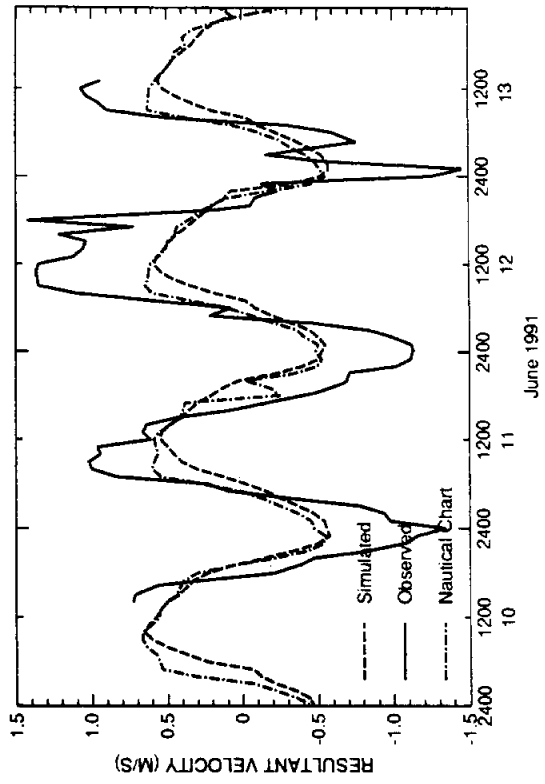


FIG. 12. Brazos Santiago Pass

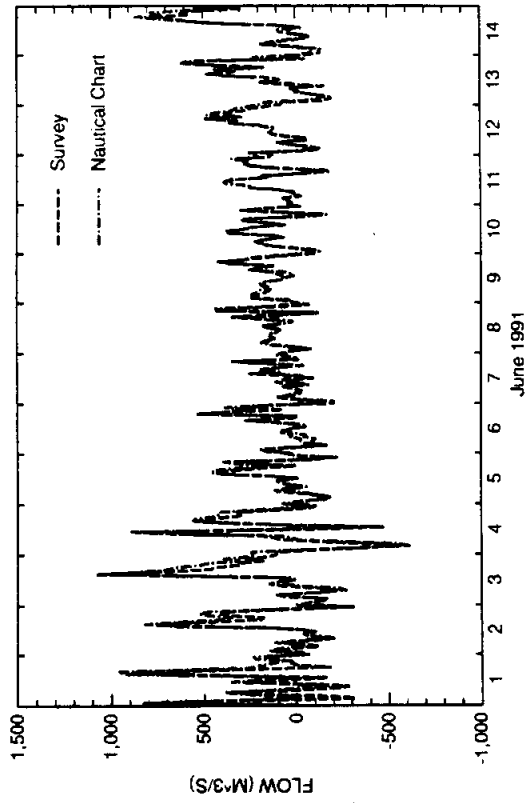


FIG. 2. Laguna Madre North of Port Mansfield

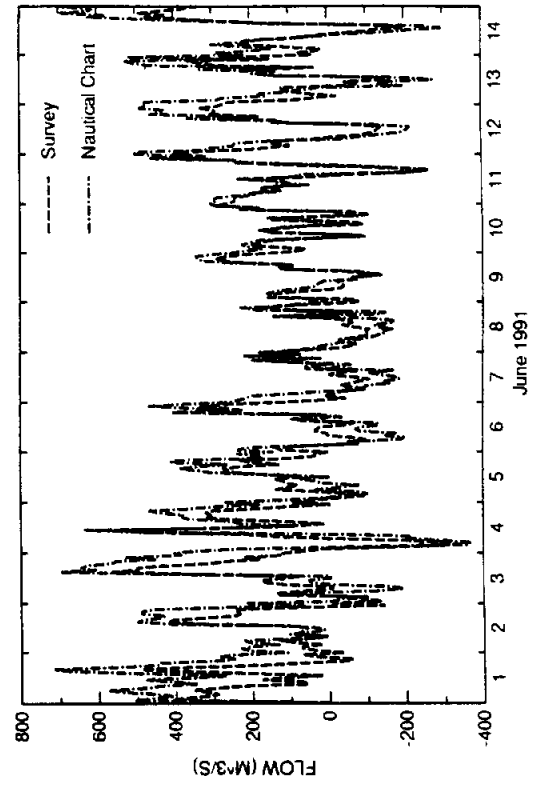


FIG. 4. Laguna Madre South of Port Mansfield

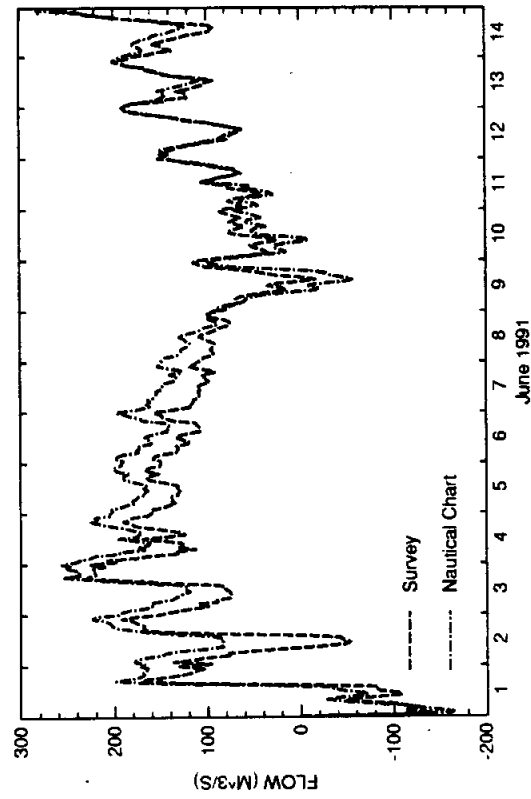


FIG. 1. South Land Cut

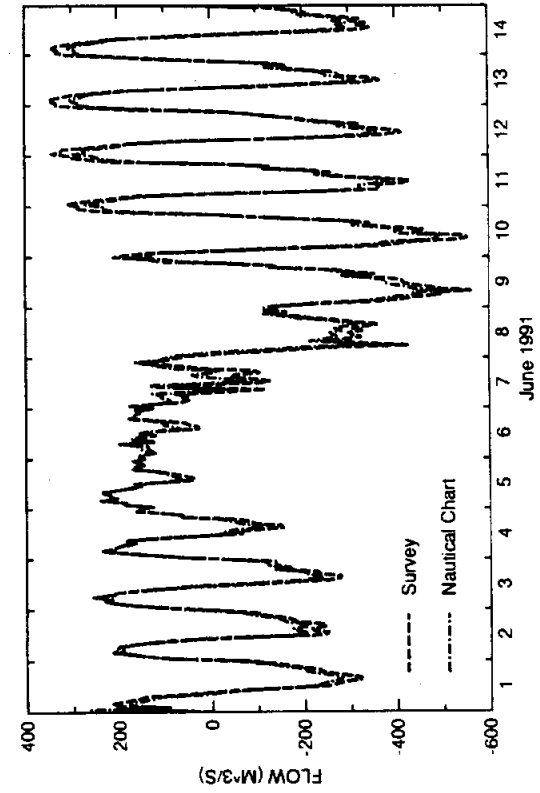


FIG. 3. Port Mansfield Channel

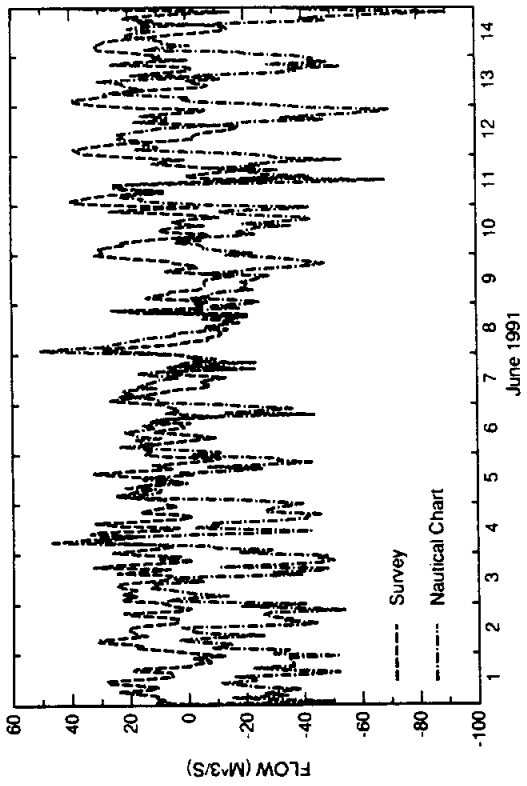


FIG. 6. Arroyo Colorado East of Laguna Atascosa

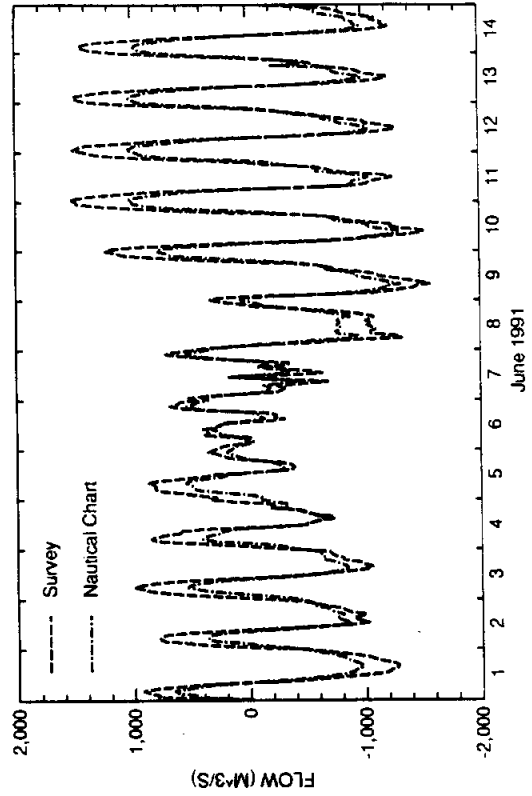


FIG. 8. Brazos-Santiago Pass

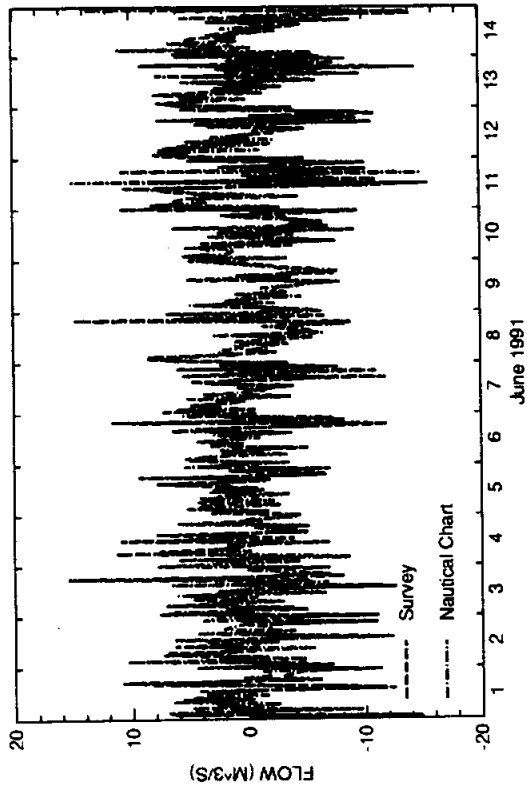


FIG. 5. Arroyo Colorado West of Laguna Atascosa

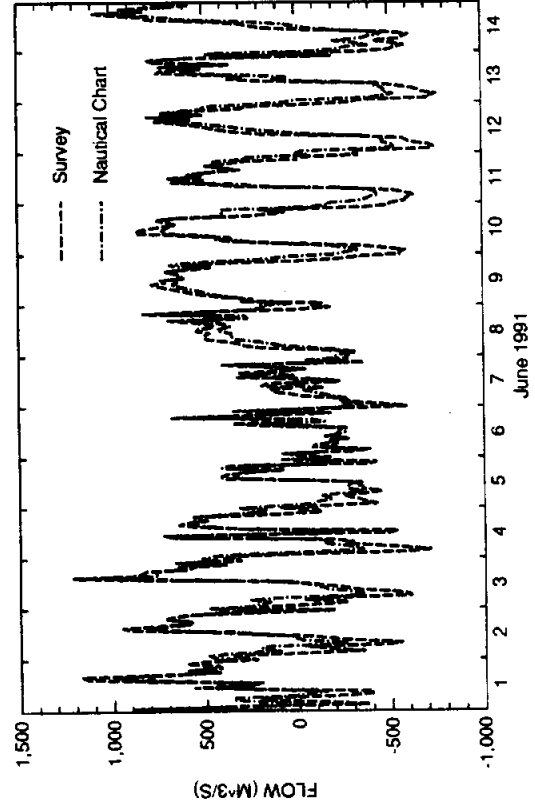


FIG. 7. Laguna Madre North of Port Isabel

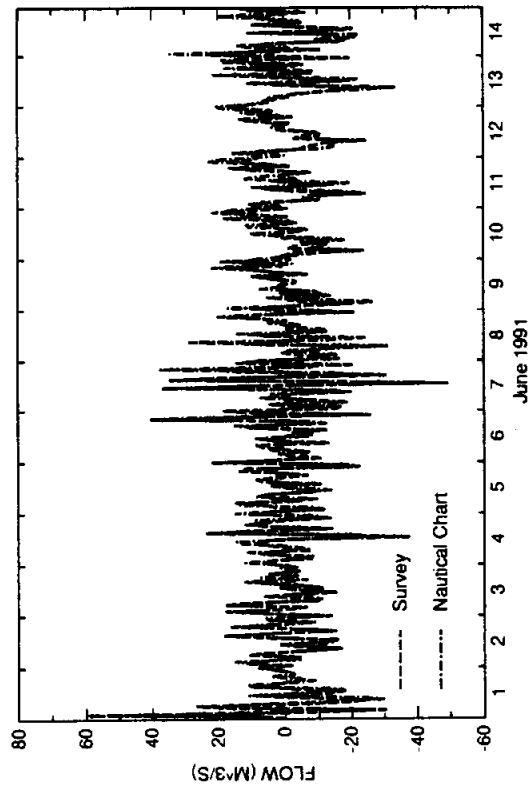


FIG. 9. Brownsville Ship Channel

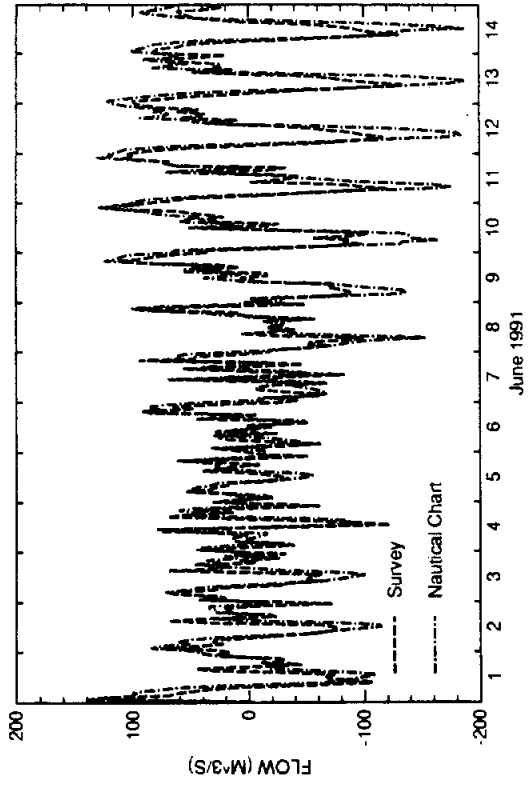


FIG. 10. South Bay Pass

SWIFT2D SIMULATIONS

Wind Stress Variation 1 Simulation

Manning's n = 0.025 in navigation channels
= 0.075 in the vicinity of the old Queen Isabel Causeway
= 0.035 elsewhere

Wind Stress = 0.0001

Time Step = 6 minutes

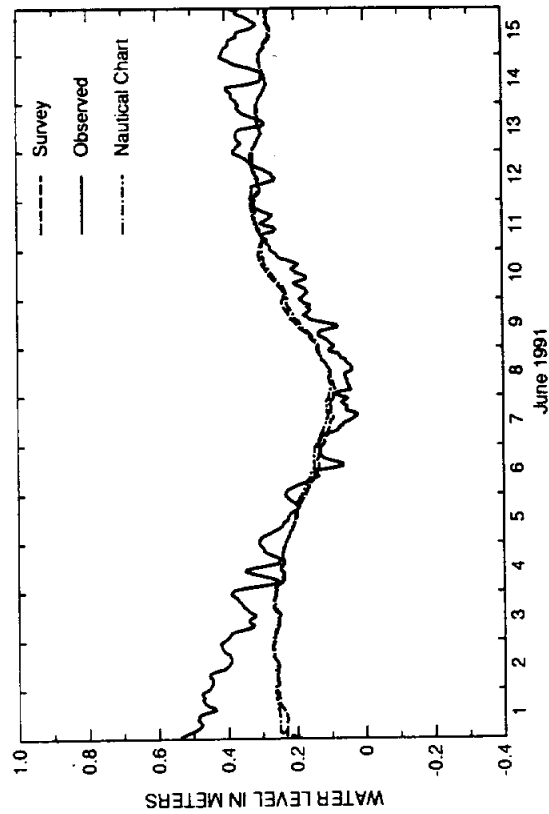


FIG. 1. Rincon Del San Jose Tide Station

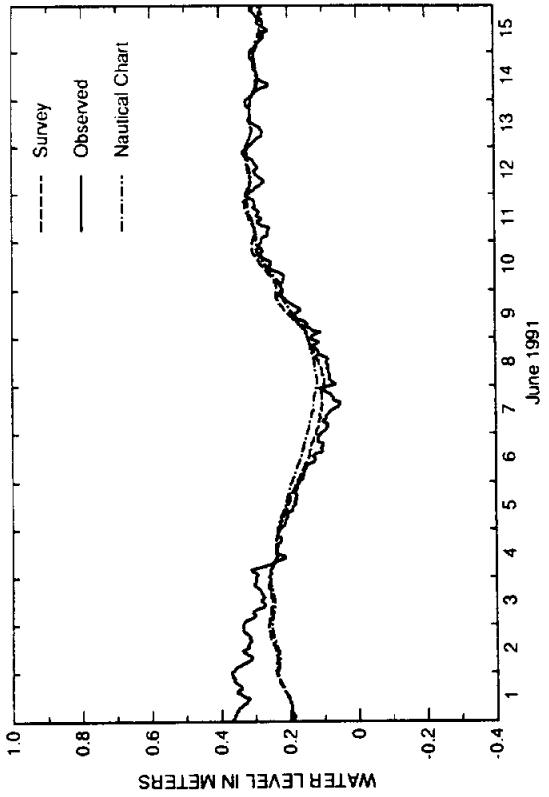


FIG. 2. Port Mansfield Tide Station

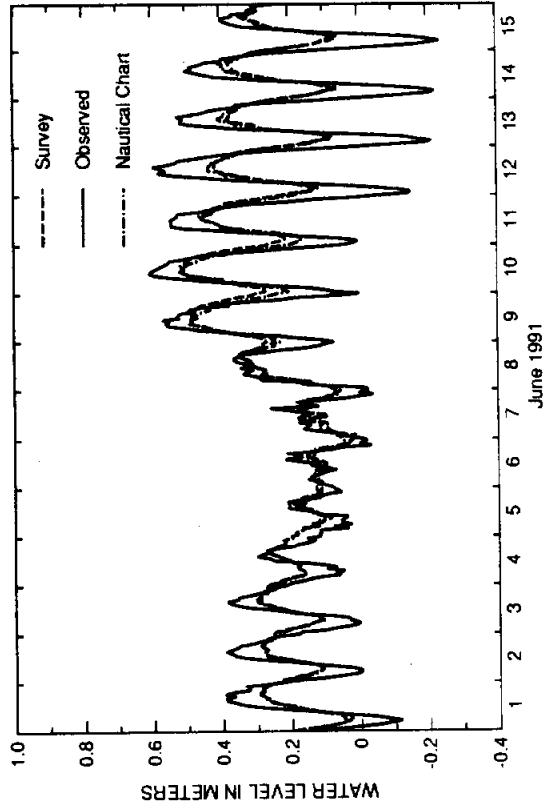


FIG. 3. Port Isabel Tide Station

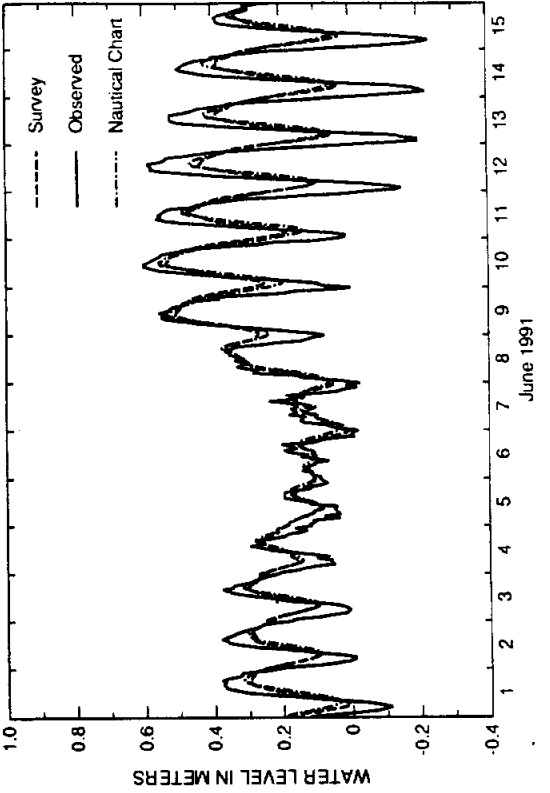


FIG. 4. South Bay Tide Station.

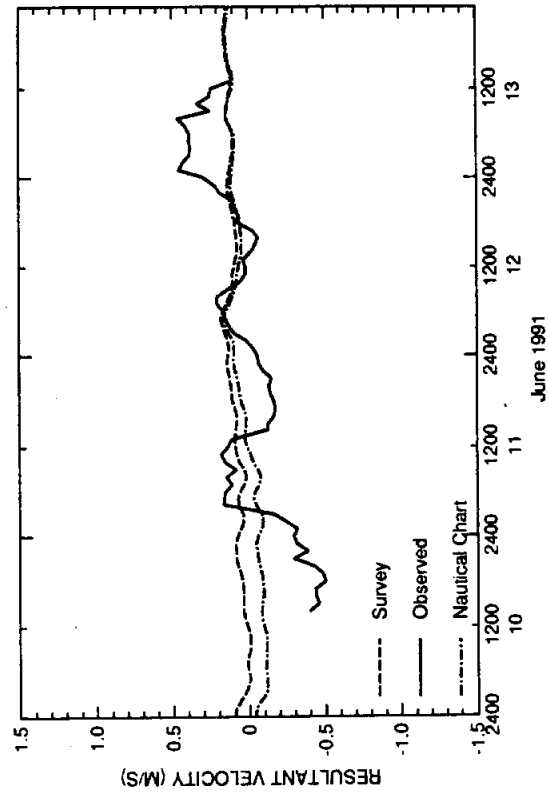


FIG. 1. South Land Cut

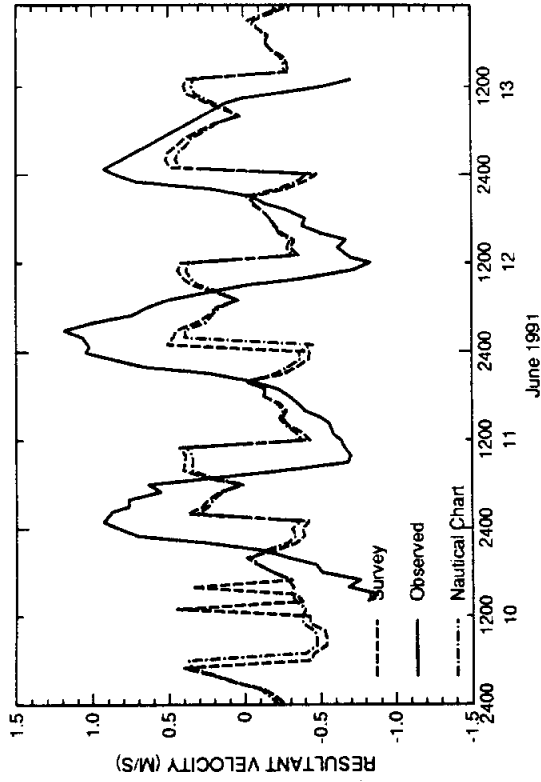


FIG. 2. Port Mansfield Jetties

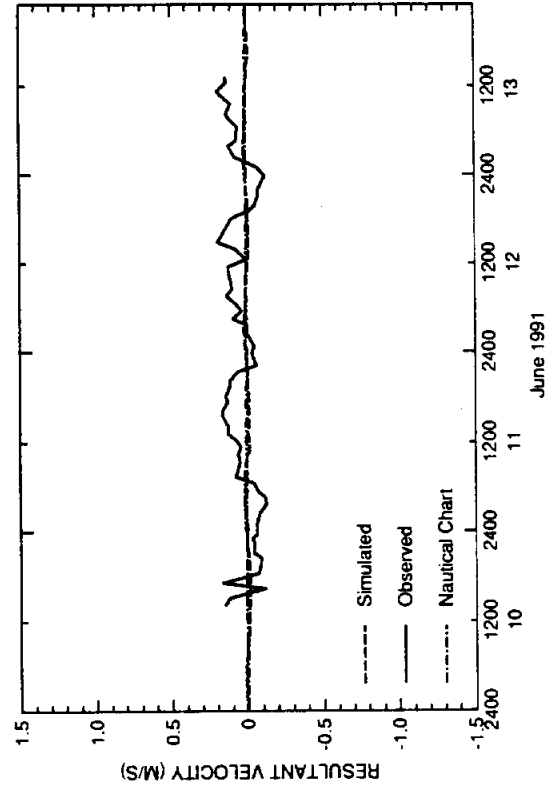


FIG. 3. Mouth of Arroyo Colorado

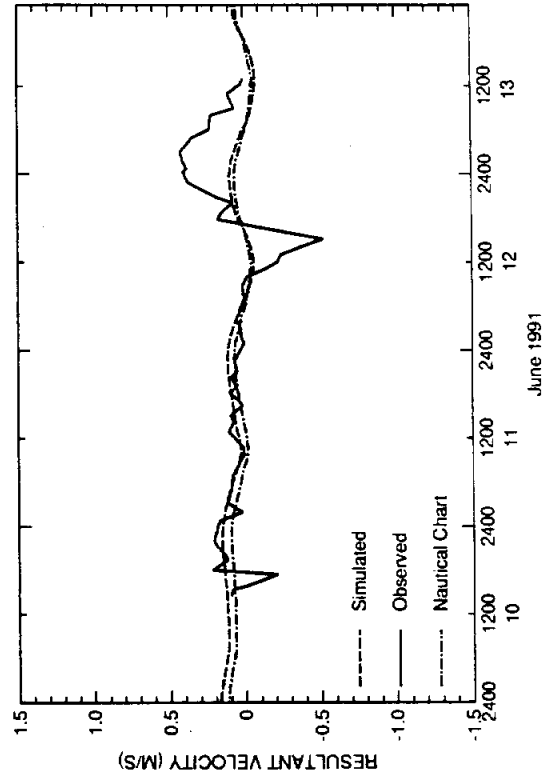


FIG. 4. GIWW North of Arroyo Colorado

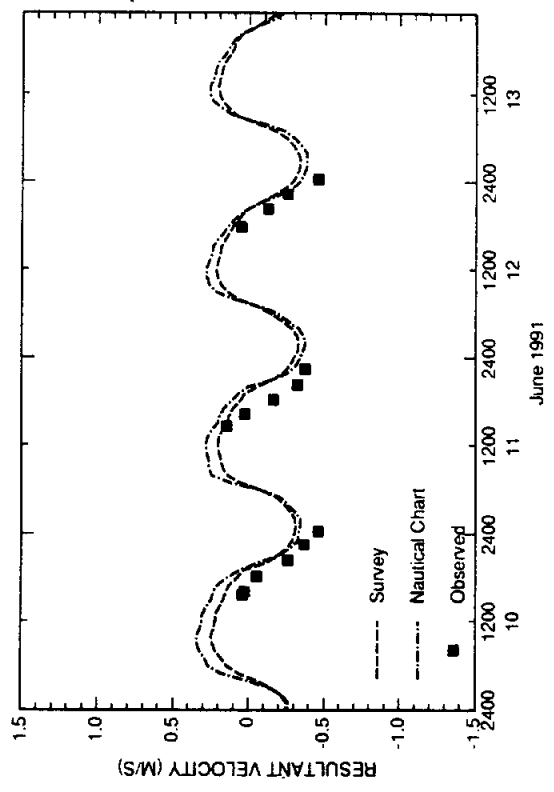


FIG. 6. Old Causeway (Mid East)

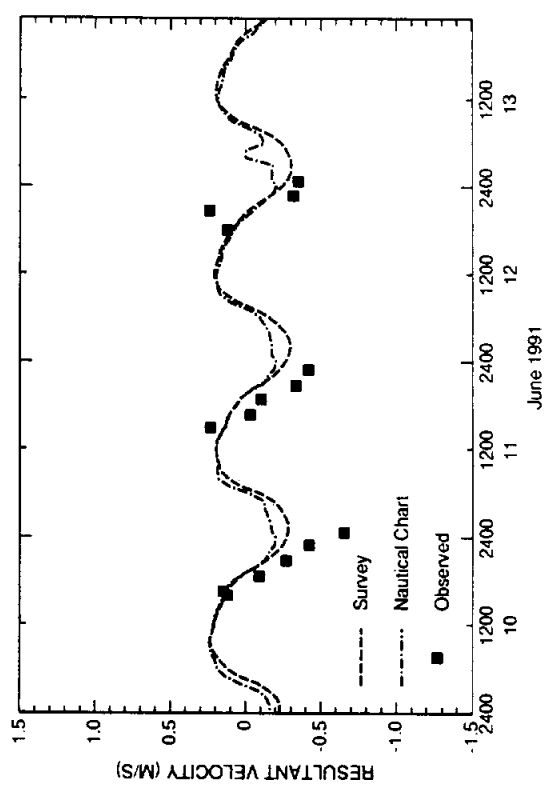


FIG. 8. Old Causeway (Western)

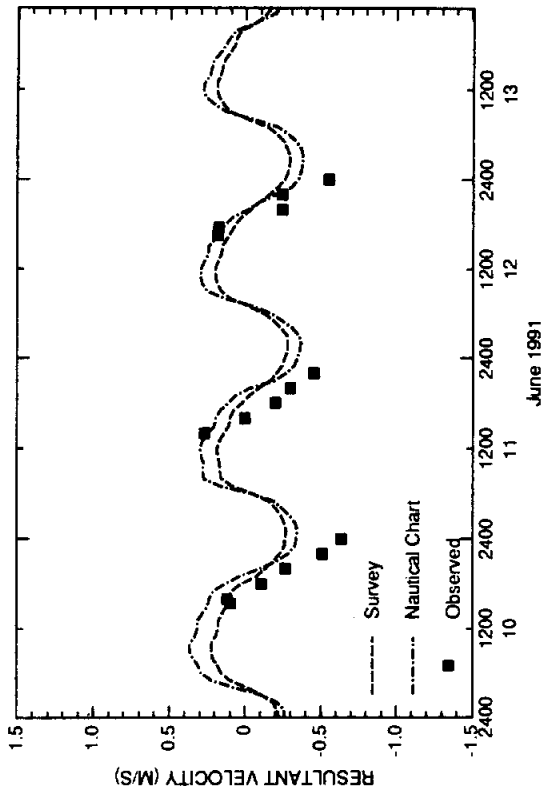


FIG. 5. Old Causeway (Eastern)

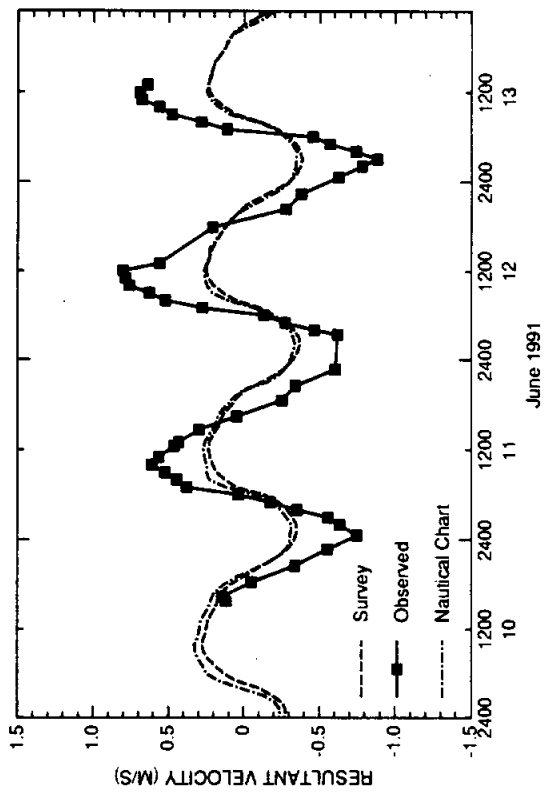


FIG. 7. Old Causeway (Mid West)

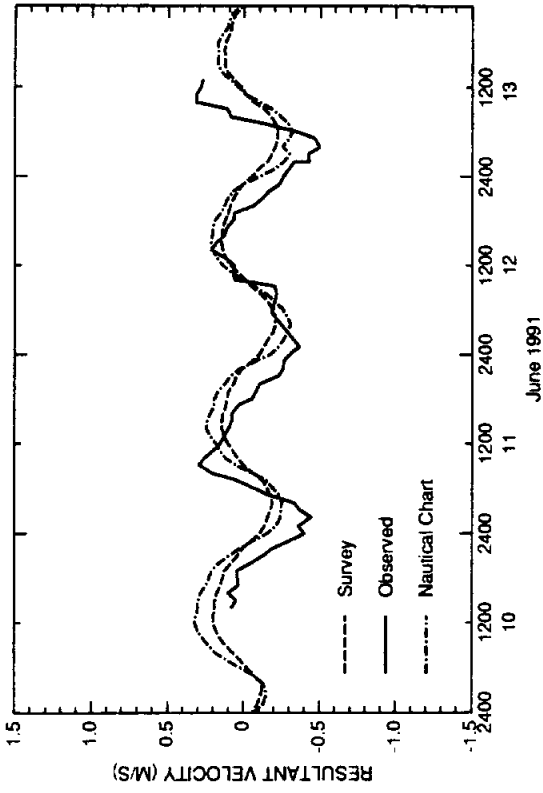


FIG. 9. Port Isabel Channel

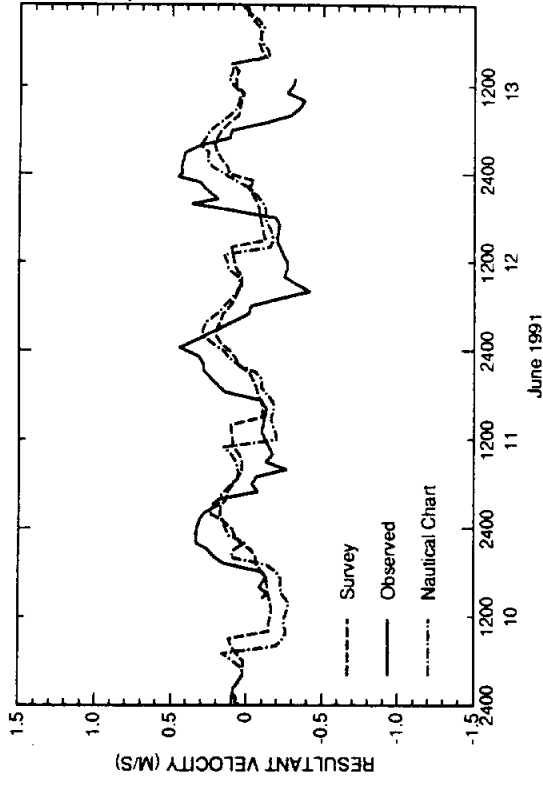


FIG. 10. Brownsville Ship Channel

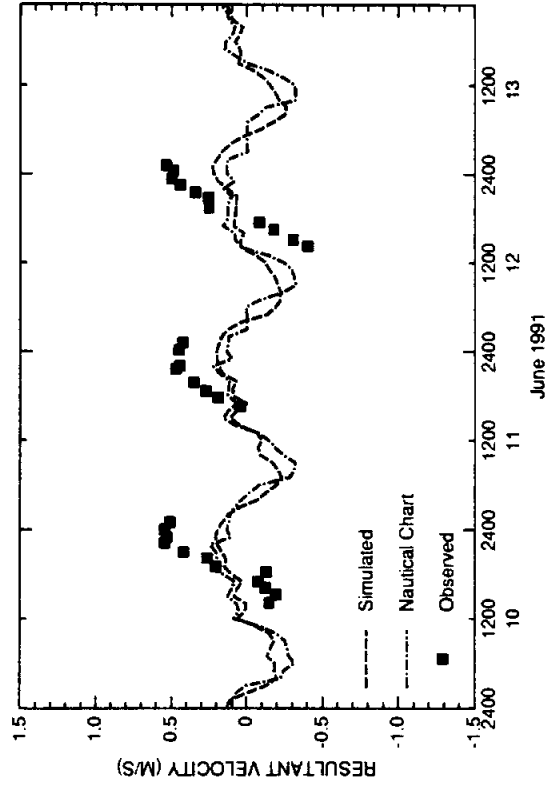


FIG. 11. South Bay Pass

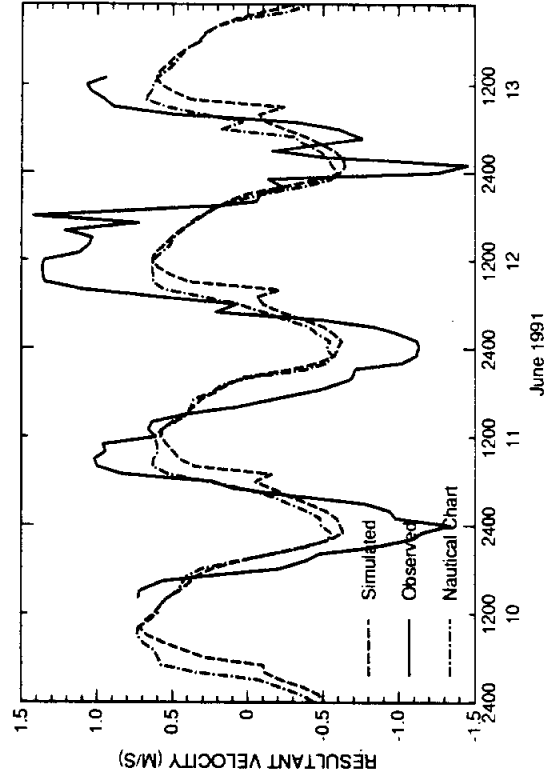


FIG. 12. Brazos Santiago Pass

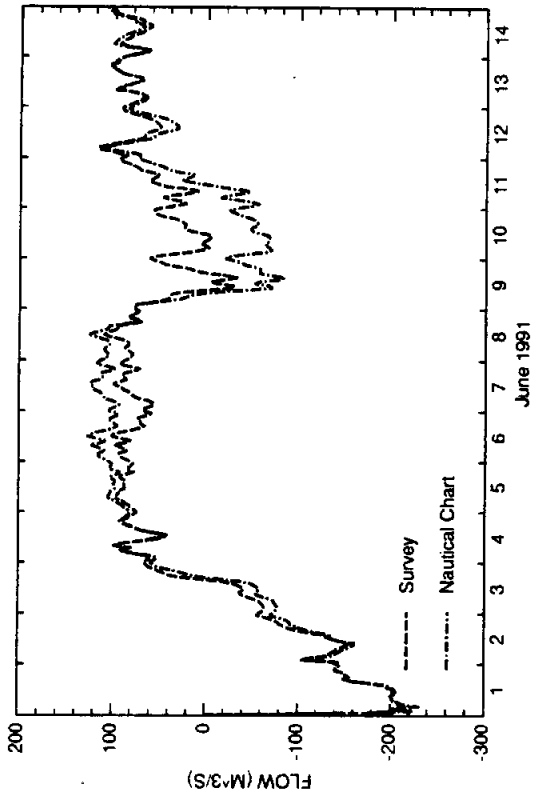


FIG. 1. South Land Cut

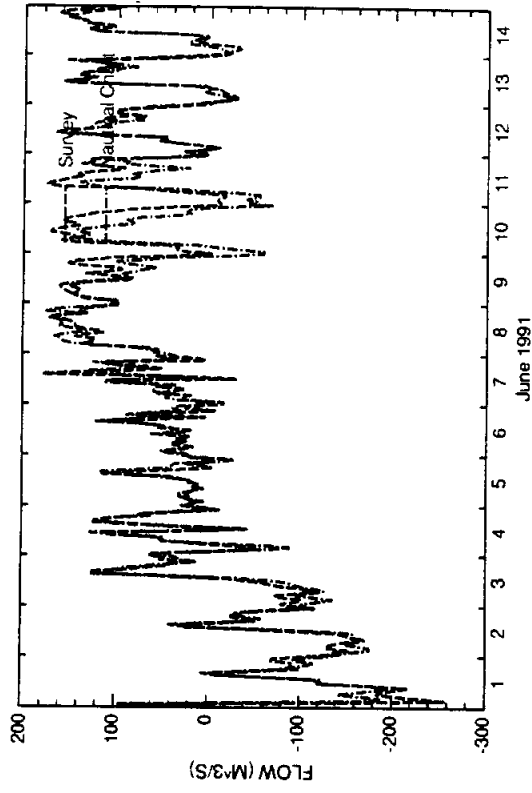


FIG. 2. Laguna Madre North of Port Mansfield

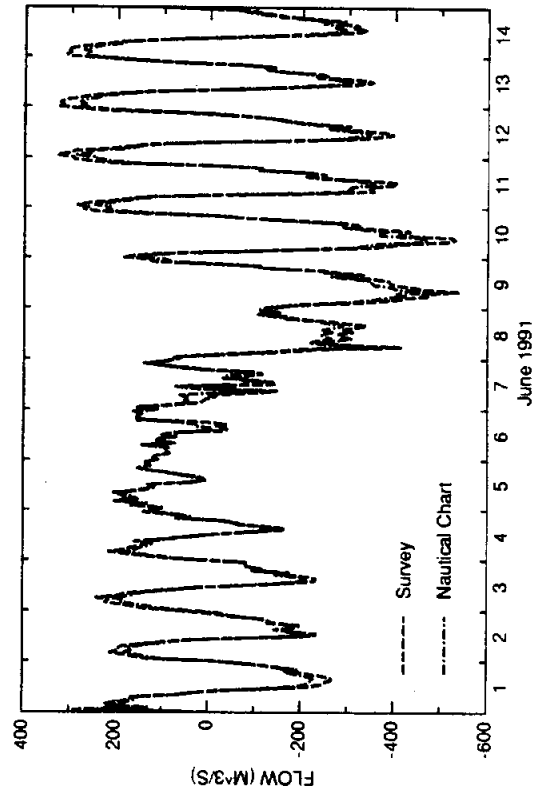


FIG. 3. Port Mansfield Channel

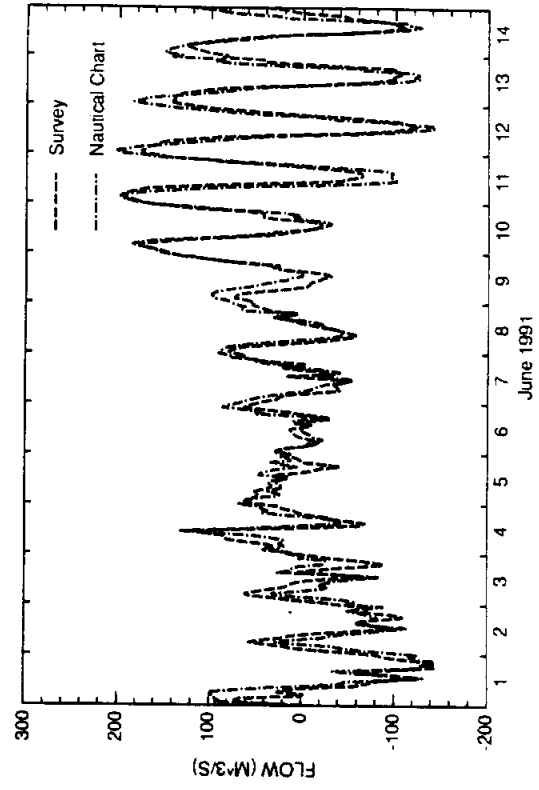


FIG. 4. Laguna Madre South of Port Mansfield

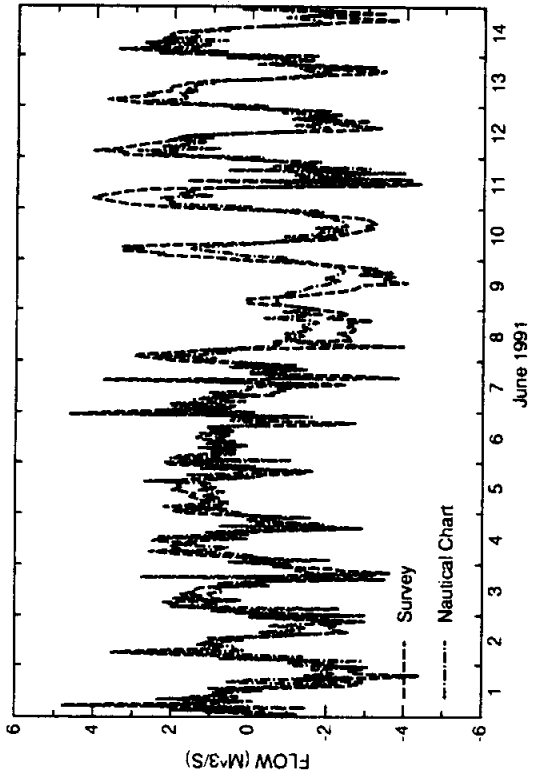


FIG. 5. Arroyo Colorado West of Langua Atascosa

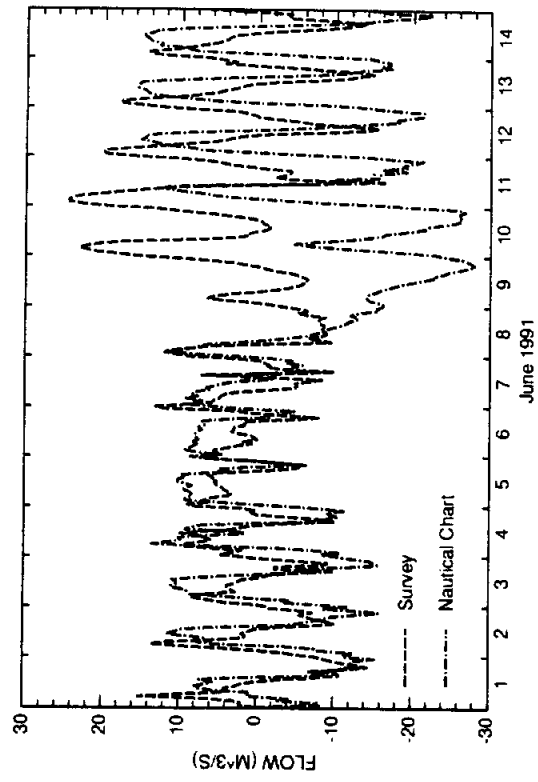


FIG. 6. Arroyo Colorado East of Laguna Atascosa

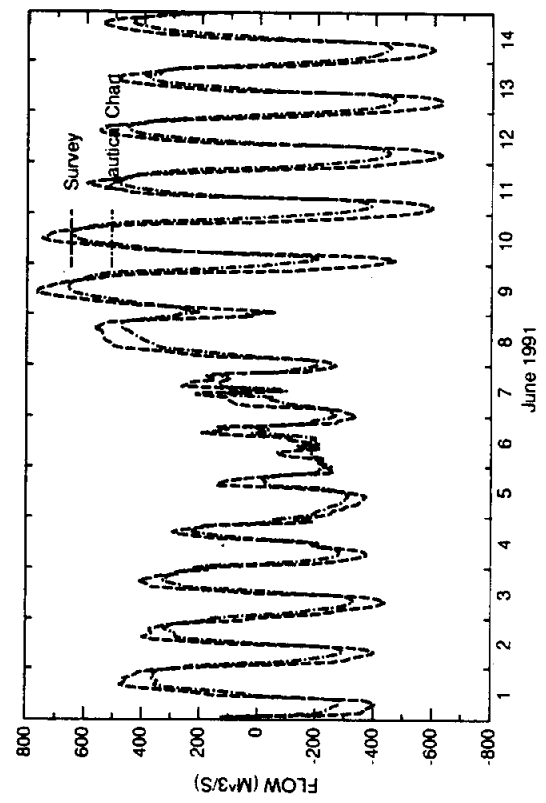


FIG. 7. Laguna Madre North of Port Isabel

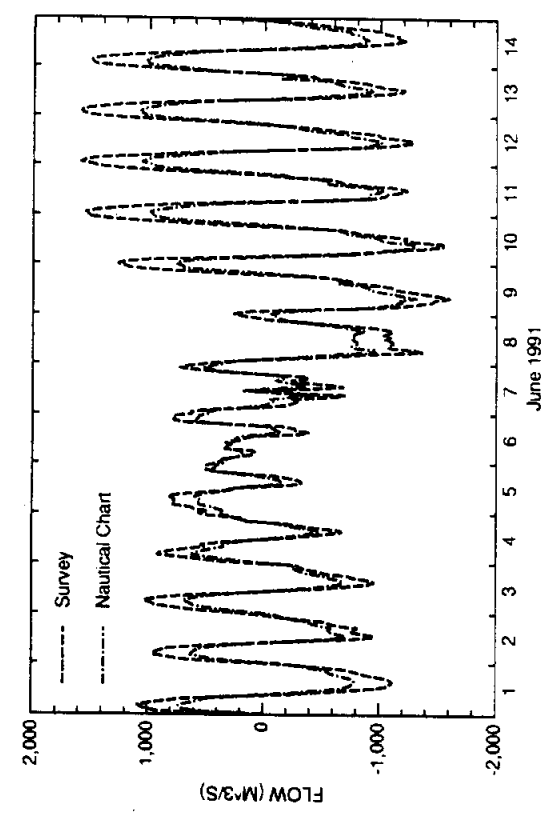


FIG. 8. Brazos-Santiago Pass

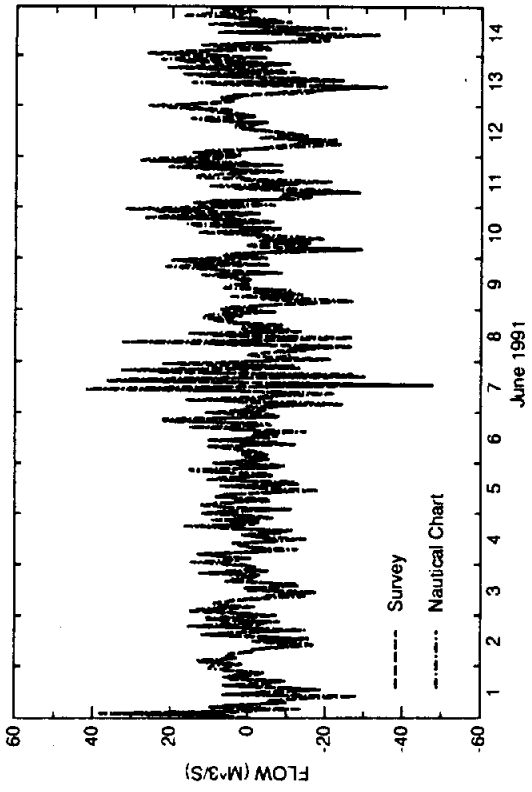


FIG. 9. Brownsville Ship Channel

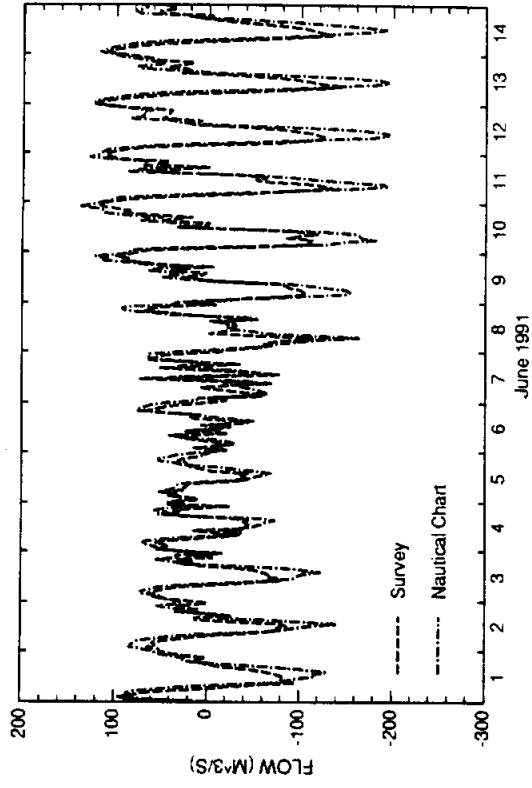


FIG. 10. South Bay Pass

SWIFT2D SIMULATIONS

Wind Stress Variation 2 Simulation

Manning's n = 0.025 in navigation channels
= 0.075 in the vicinity of the old Queen Isabel Causeway
= 0.035 elsewhere

Wind Stress = 0.0026

Time Step = 6 minutes

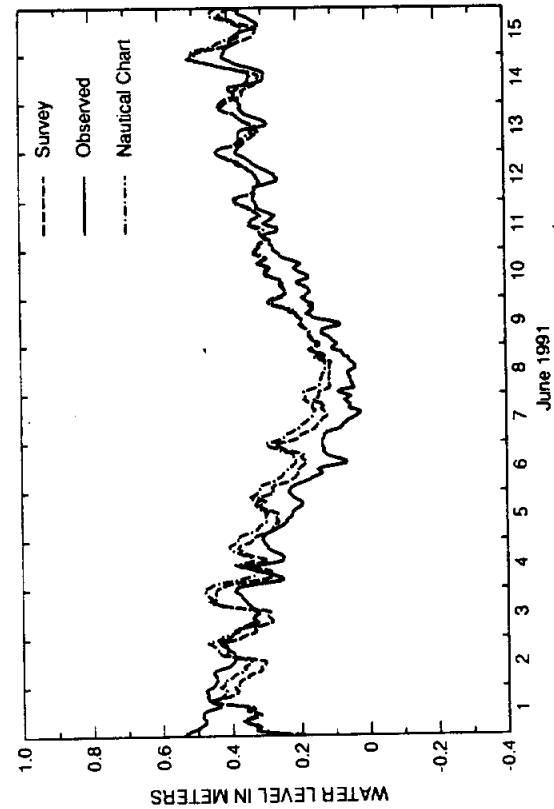


FIG. 1. Rincon Del San Jose Tide Station

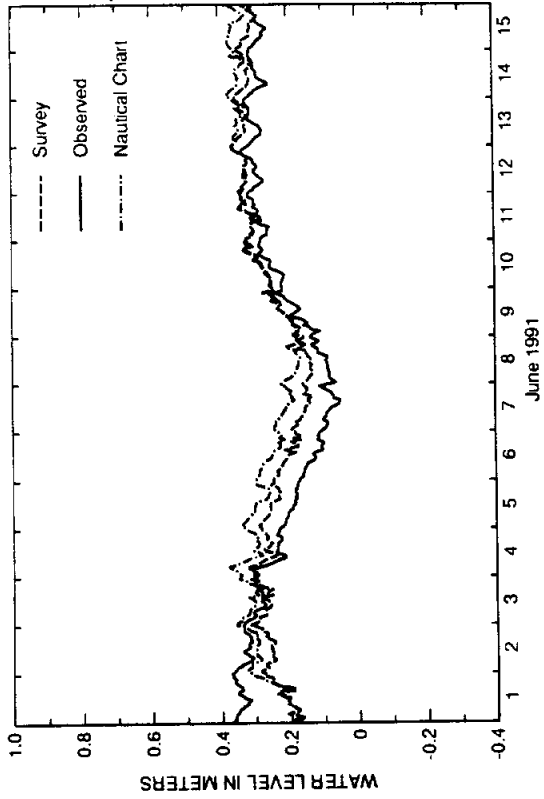


FIG. 2. Port Mansfield Tide Station

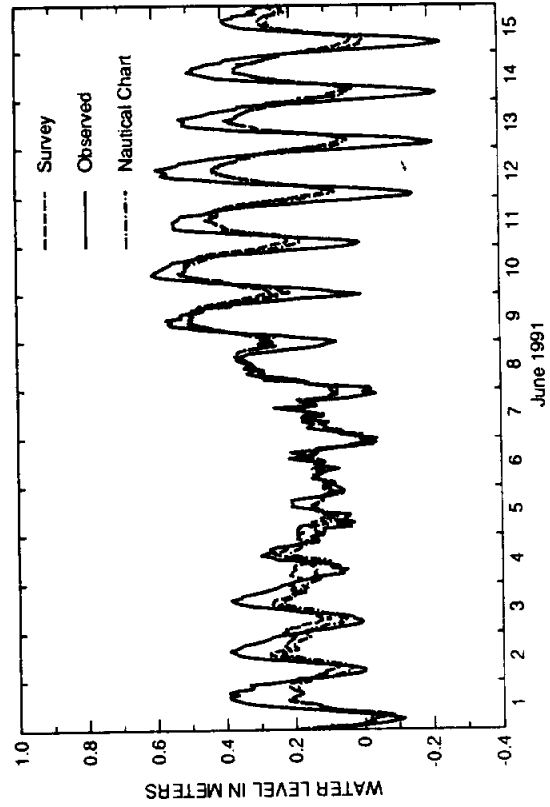


FIG. 3. Port Isabel Tide Station

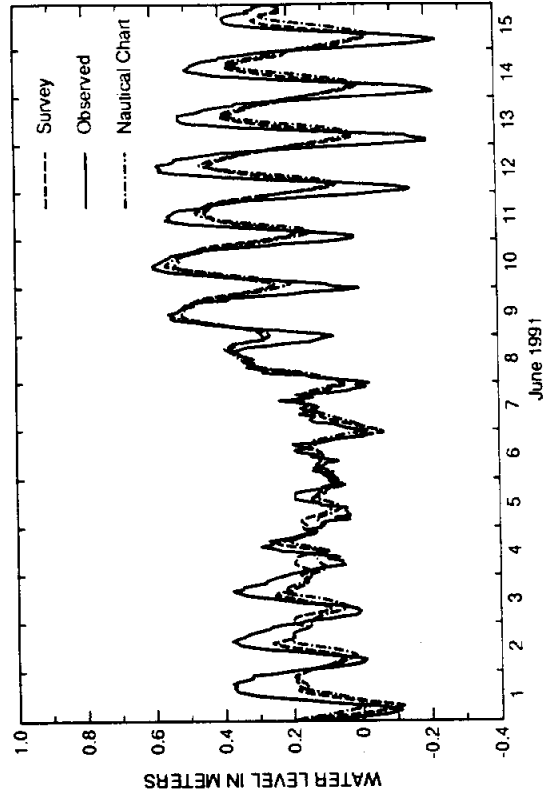


FIG. 4. South Bay Tide Station.

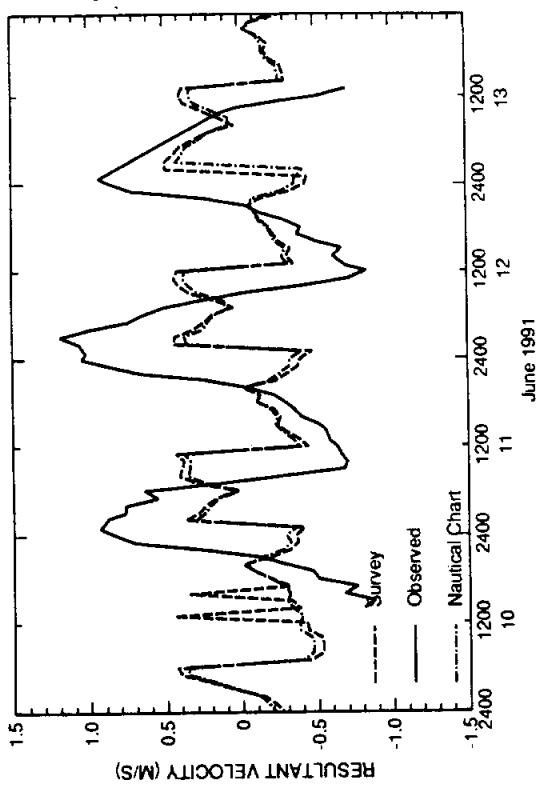


FIG. 2. Port Mansfield Jetties

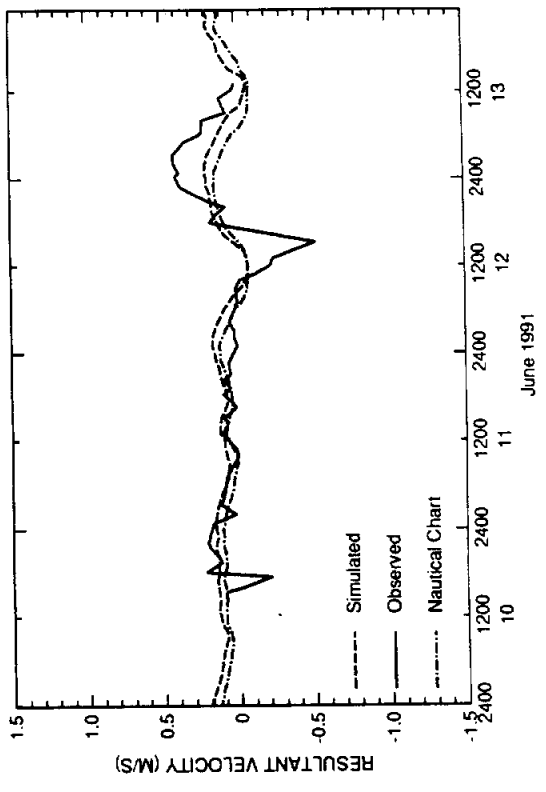


FIG. 4. GIWW North of Arroyo Colorado

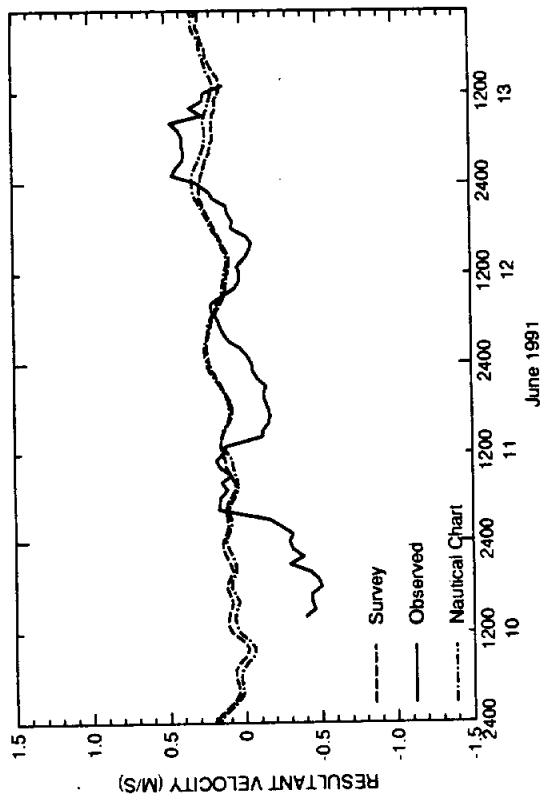


FIG. 1. South Land Cut

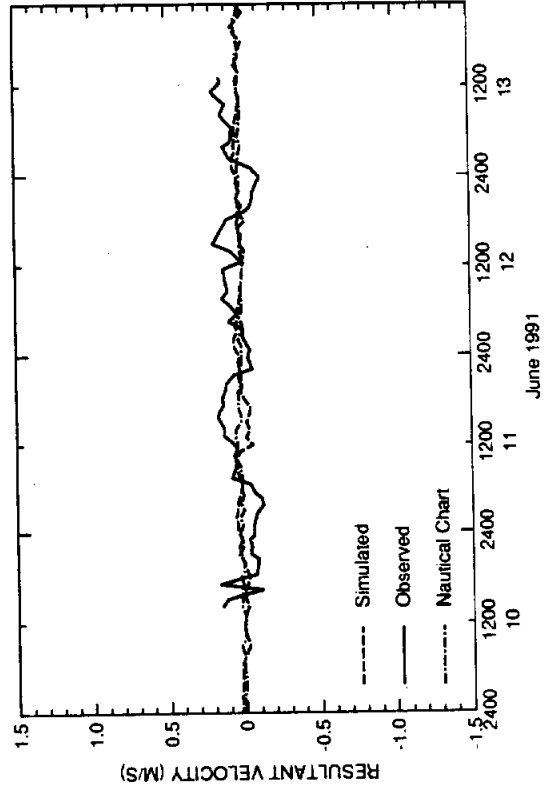


FIG. 3. Mouth of Arroyo Colorado

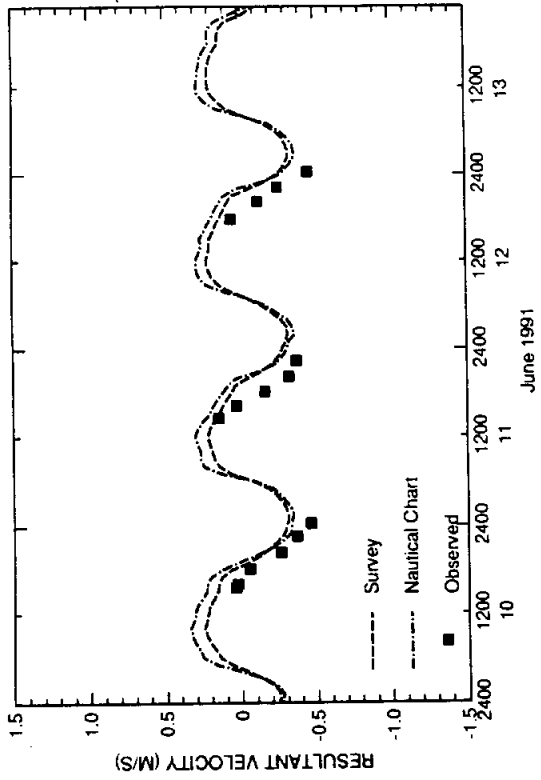


FIG. 6. Old Causeway (Mid East)

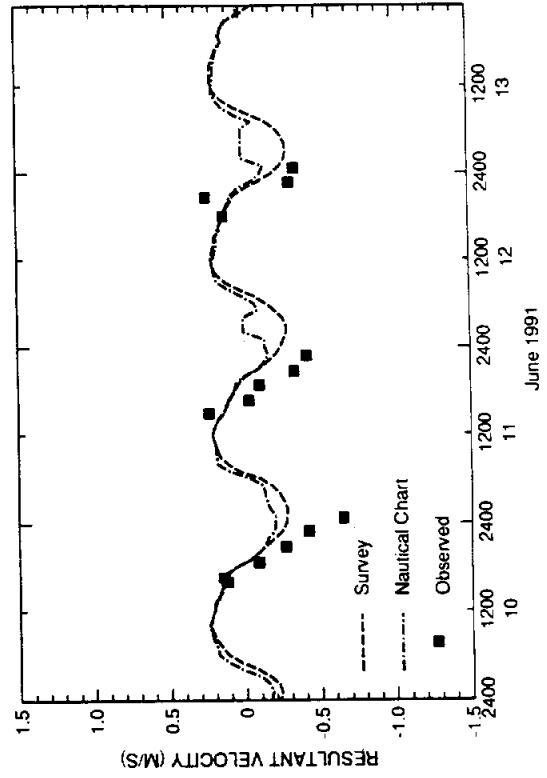


FIG. 8. Old Causeway (Western)

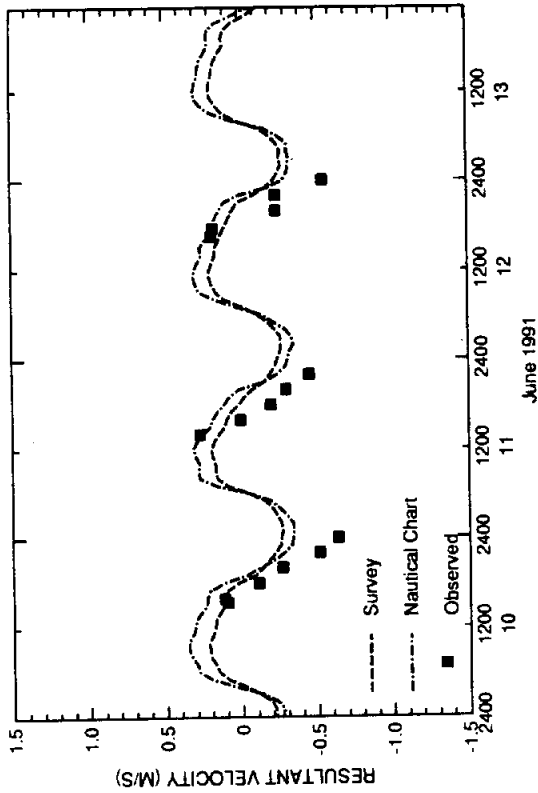


FIG. 5. Old Causeway (Eastern)

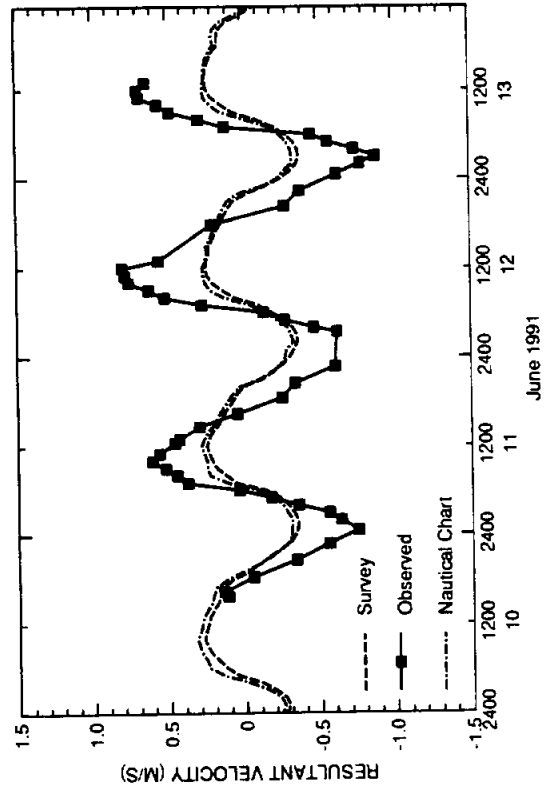


FIG. 7. Old Causeway (Mid West)

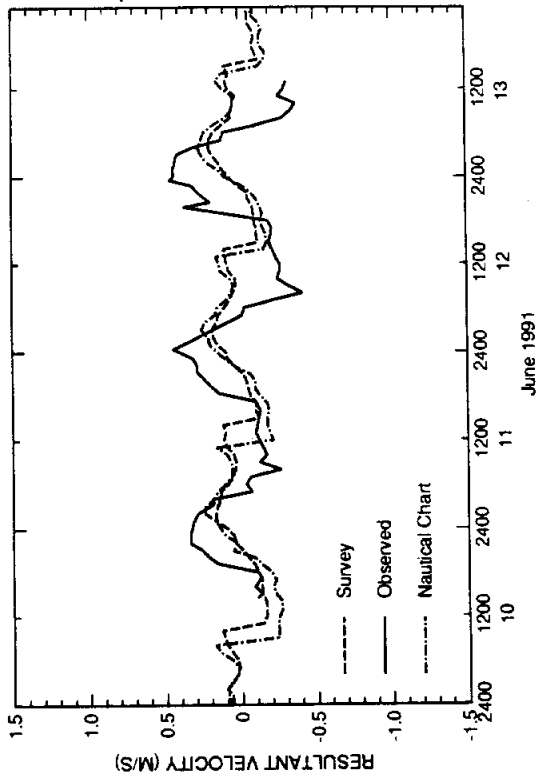


FIG. 10. Brownsville Ship Channel

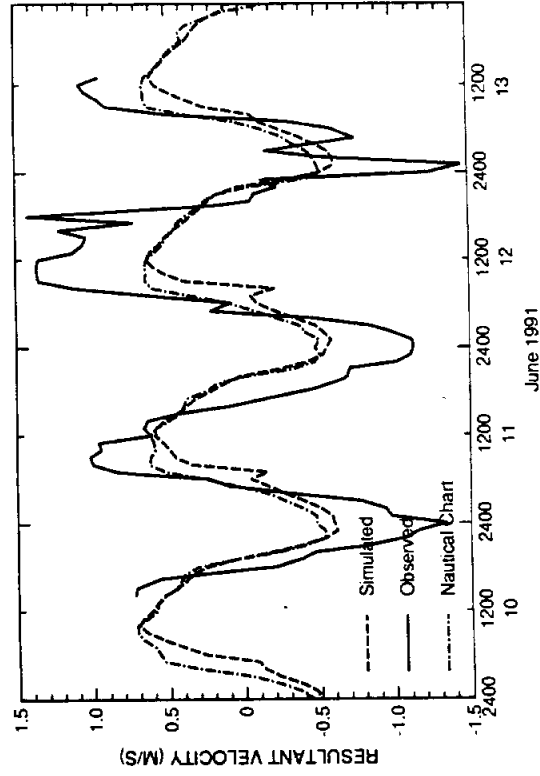


FIG. 12. Brazos Santiago Pass

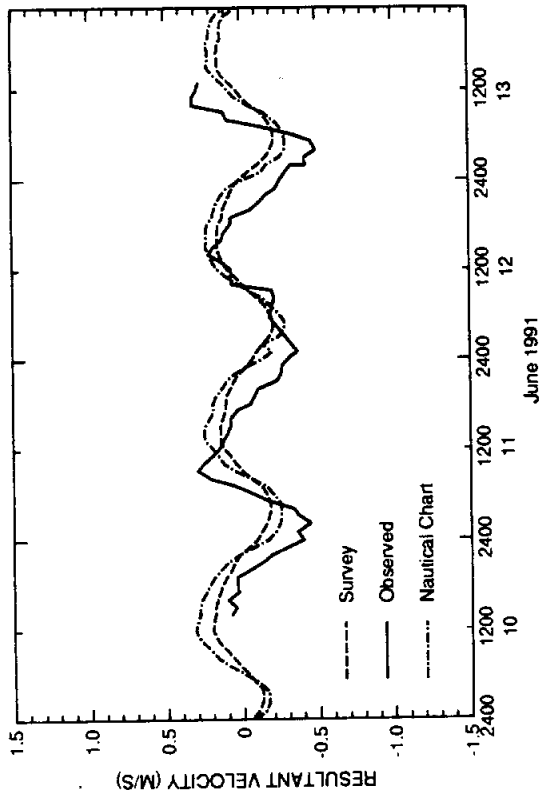


FIG. 9. Port Isabel Channel

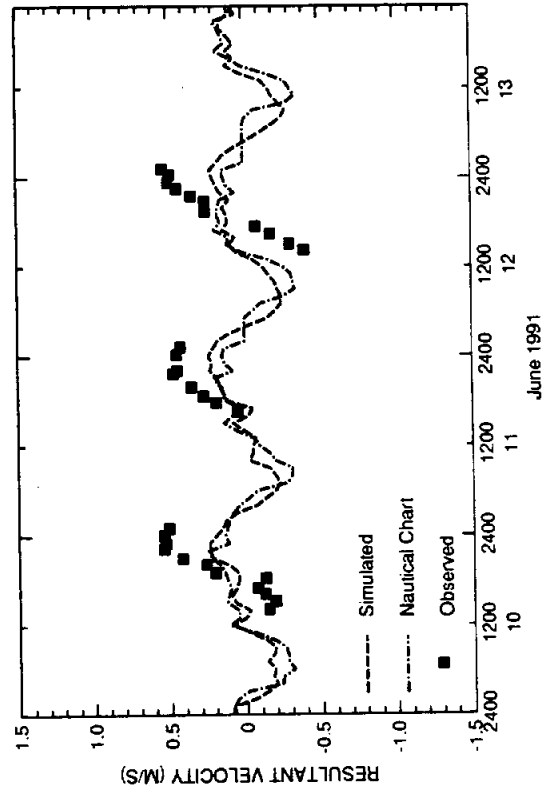


FIG. 11. South Bay Pass

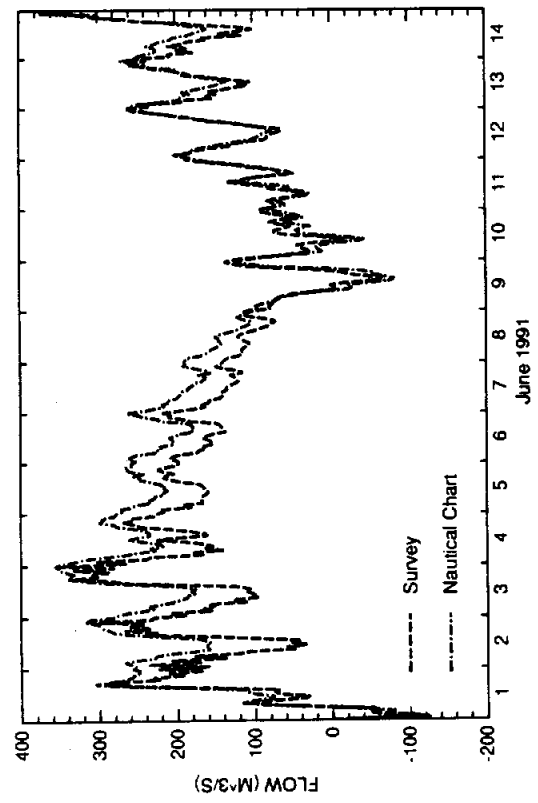


FIG. 1. South Land Cut

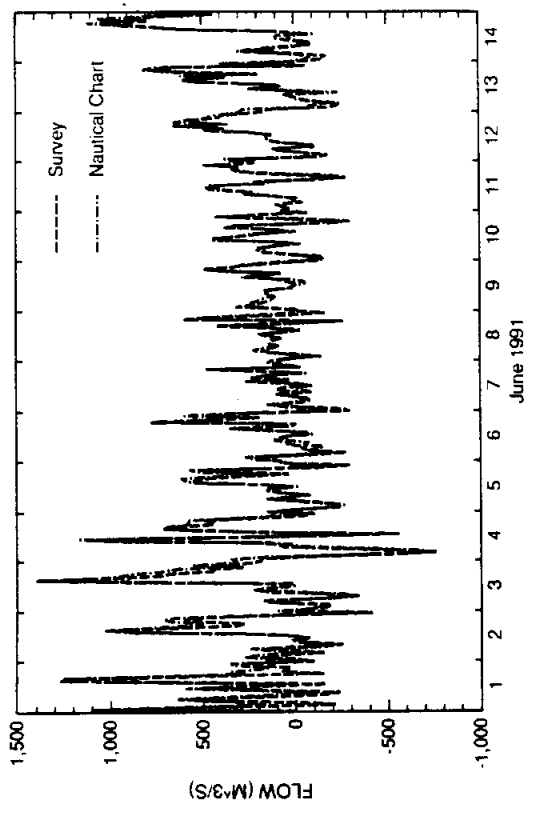


FIG. 2. Laguna Madre North of Port Mansfield

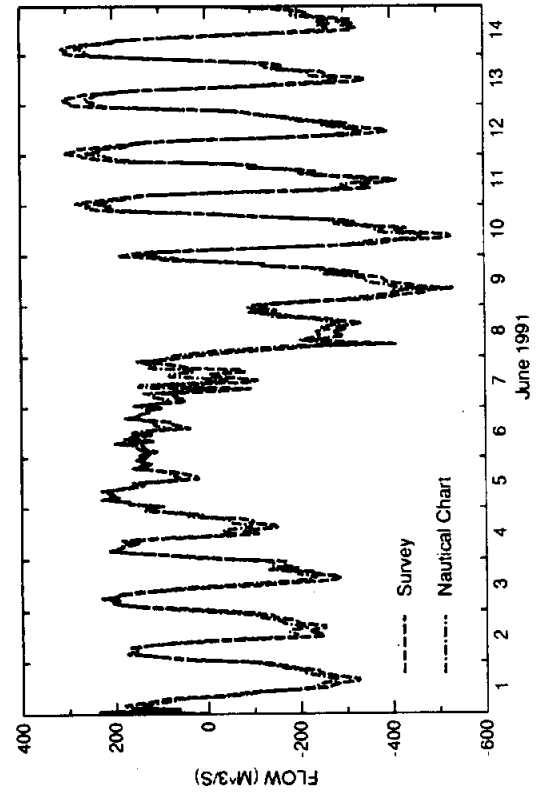


FIG. 3. Port Mansfield Channel

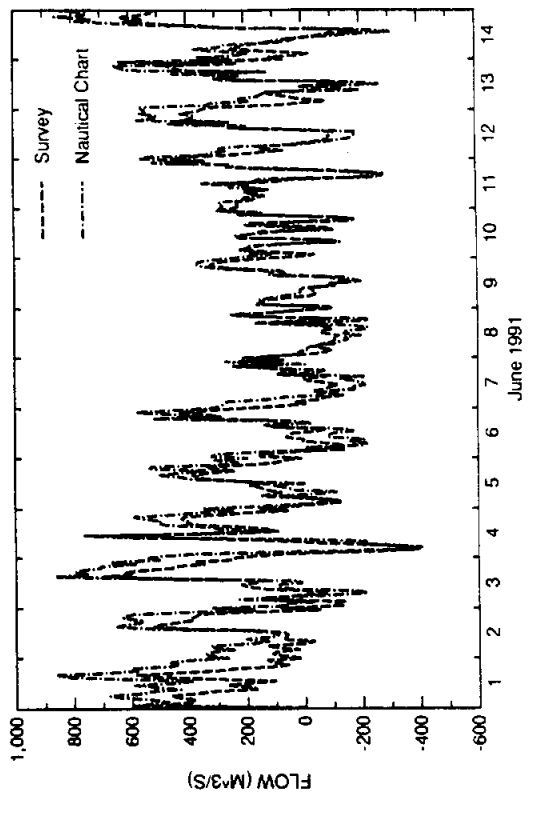


FIG. 4. Laguna Madre South of Port Mansfield

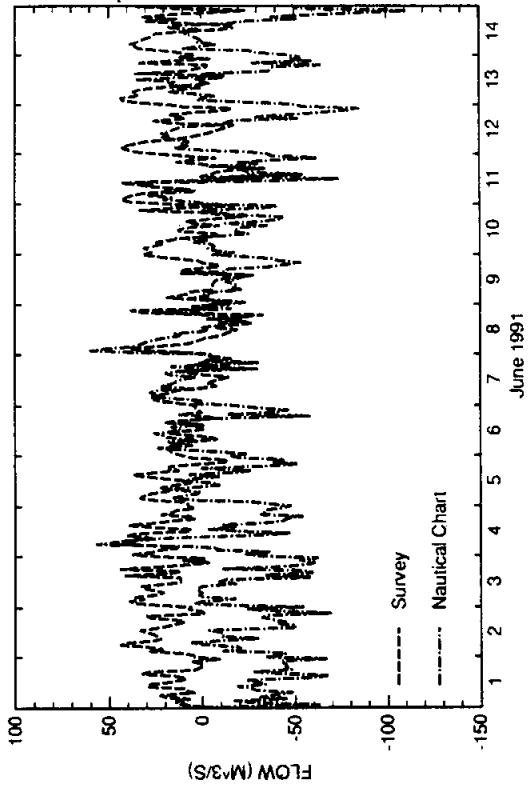


FIG. 6. Arroyo Colorado East of Laguna Atascosa

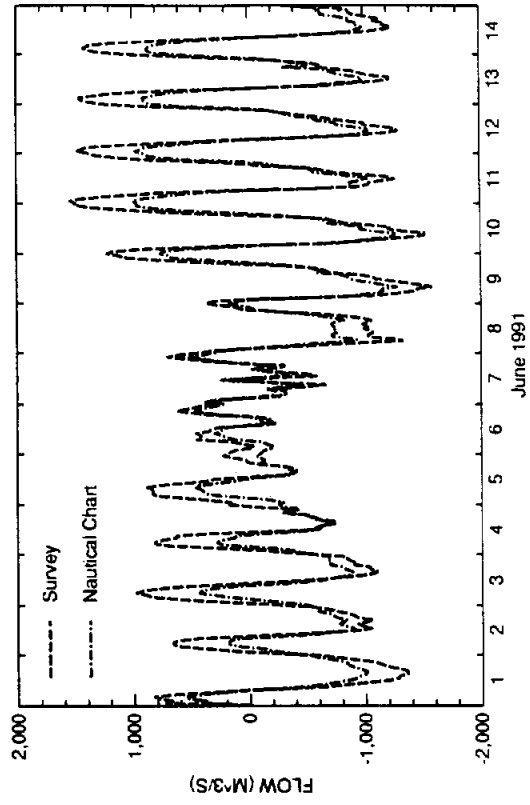


FIG. 8. Brazos-Santiago Pass

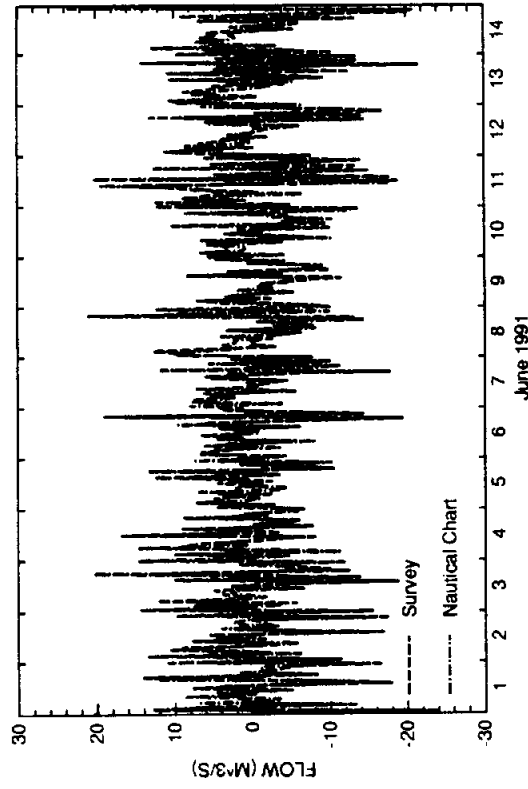


FIG. 5. Arroyo Colorado West of Laguna Atascosa

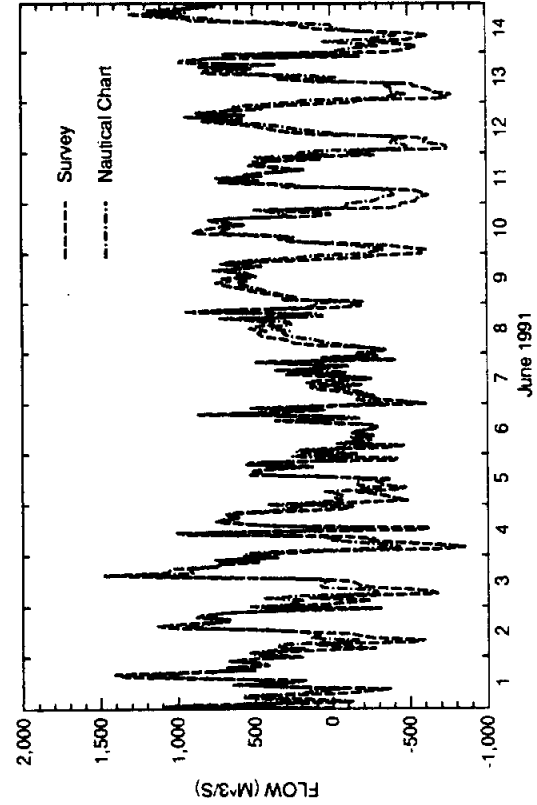


FIG. 7. Laguna Madre North of Port Isabel

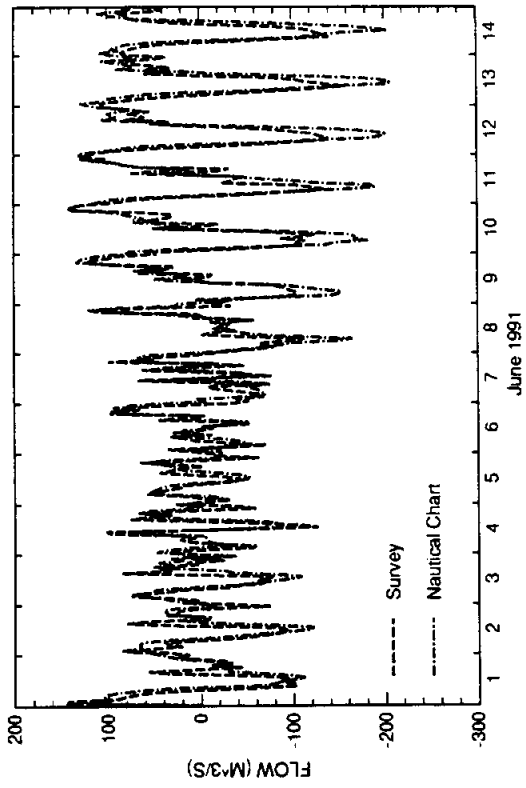


FIG. 10. South Bay Pass

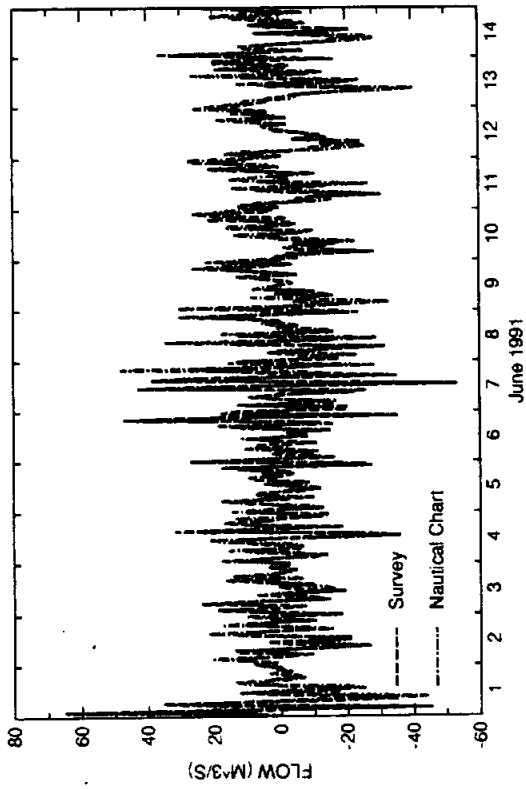


FIG. 9. Brownsville Ship Channel

SWIFT2D SIMULATIONS

Time Step Variation Simulation

Manning's n = 0.025 in navigation channels
= 0.075 in the vicinity of the old Queen Isabel Causeway
= 0.035 elsewhere

Wind Stress = 0.0015

Time Step = 12 minutes

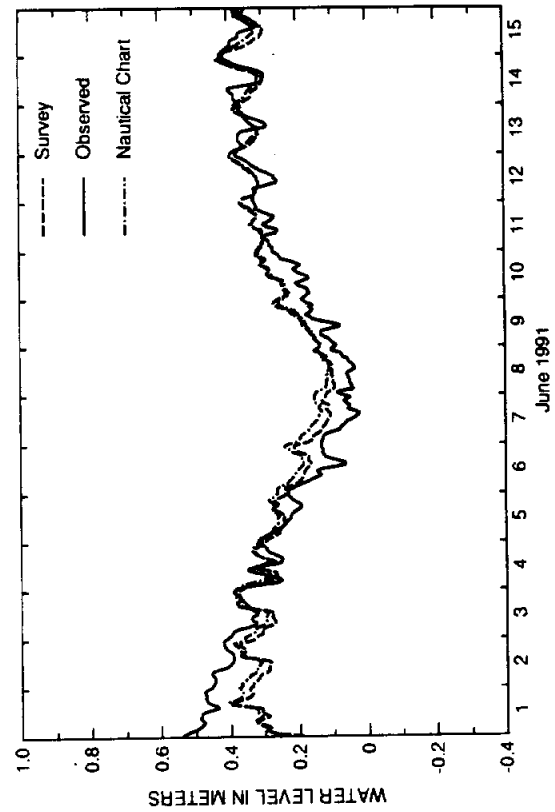


FIG. 1. Rincon Del San Jose Tide Station

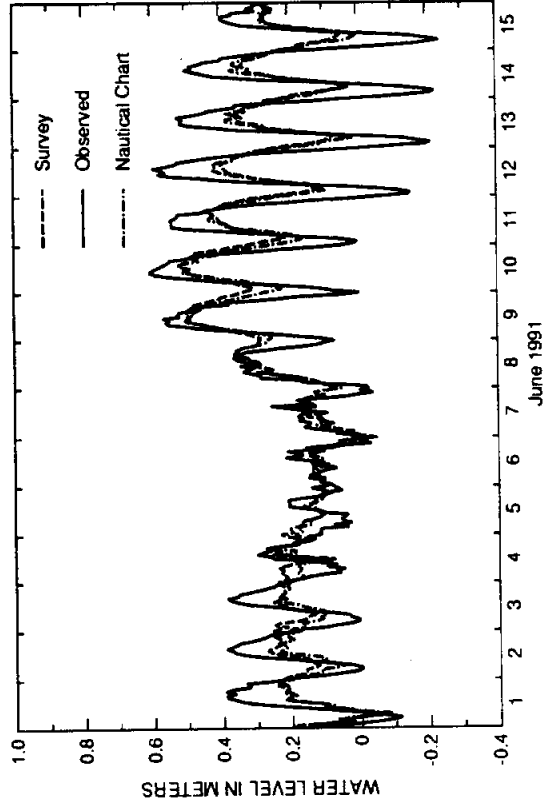


FIG. 3. Port Isabel Tide Station

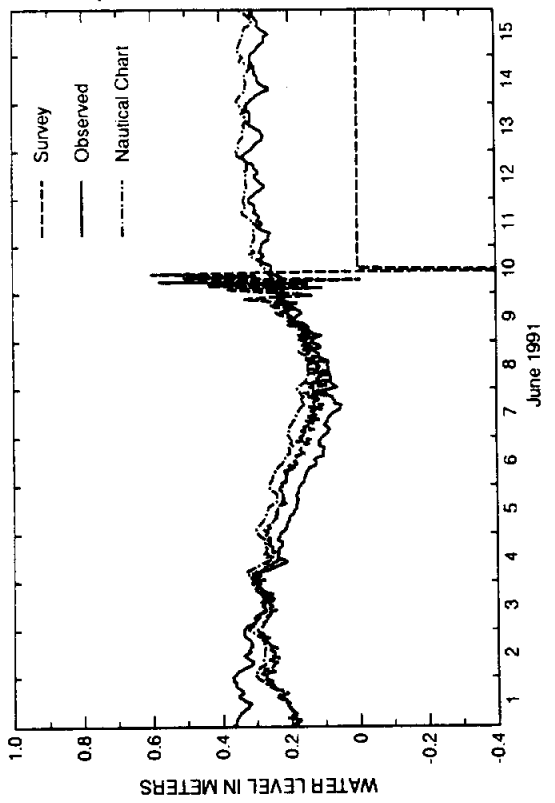


FIG. 2. Port Mansfield Tide Station

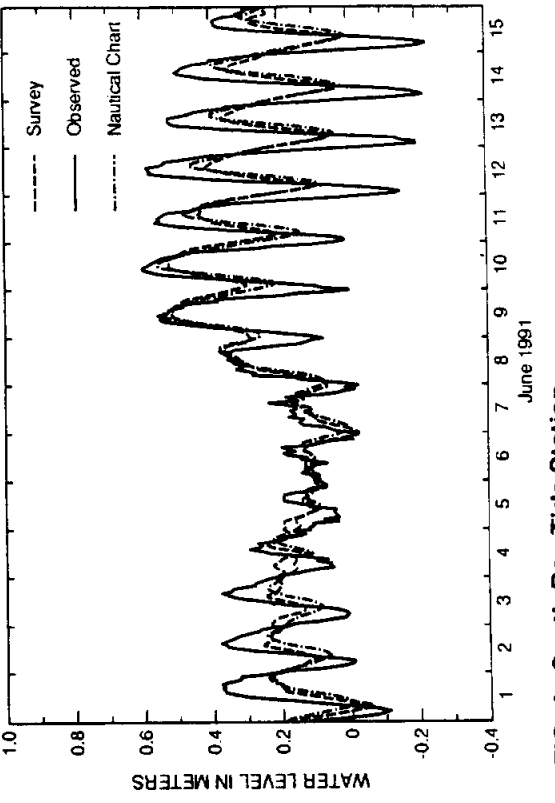


FIG. 4. South Bay Tide Station

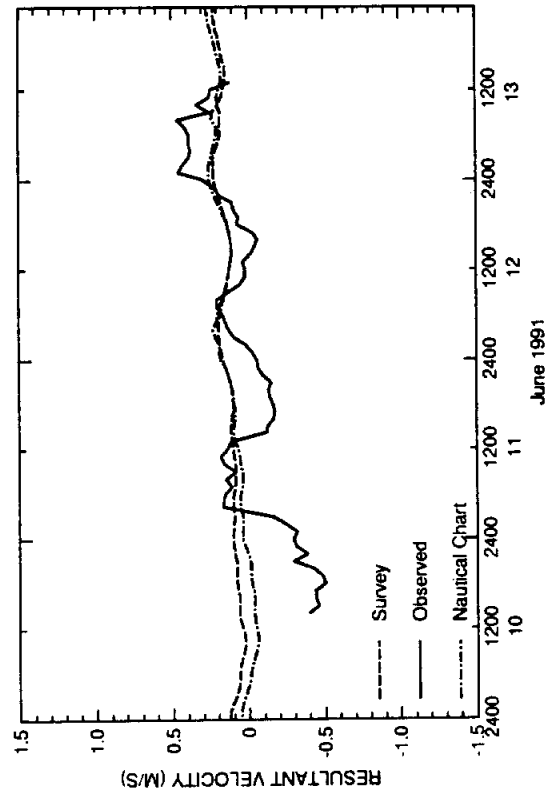


FIG. 1. South Land Cut

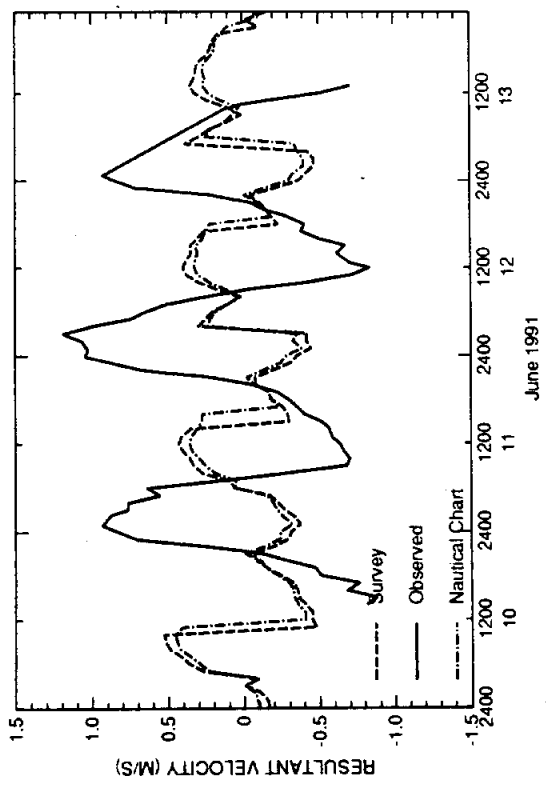


FIG. 2. Port Mansfield Jetties

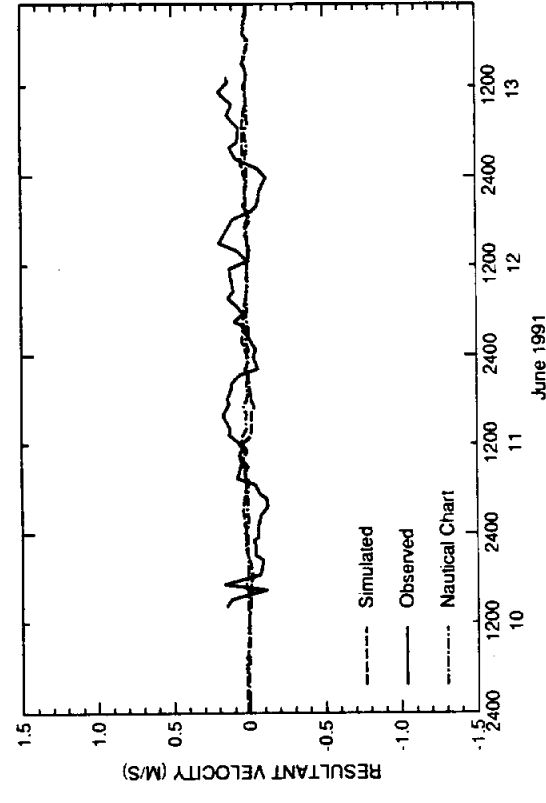


FIG. 3. Mouth of Arroyo Colorado

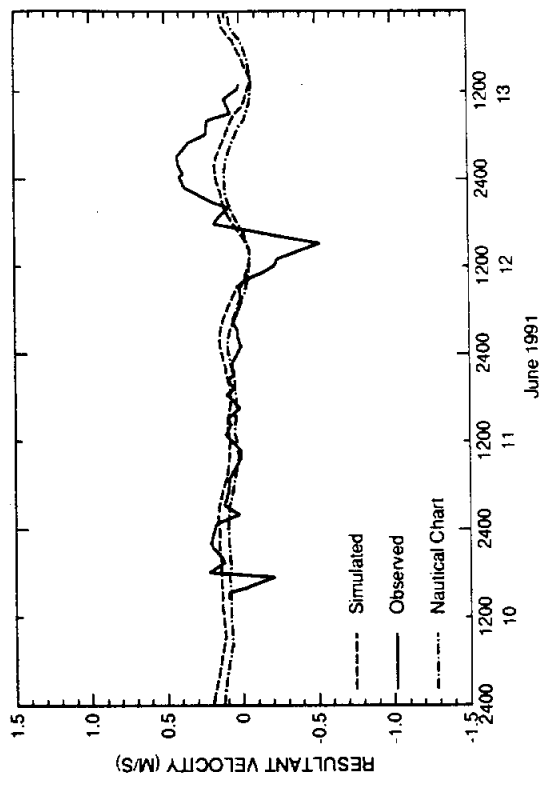


FIG. 4. GIWW North of Arroyo Colorado

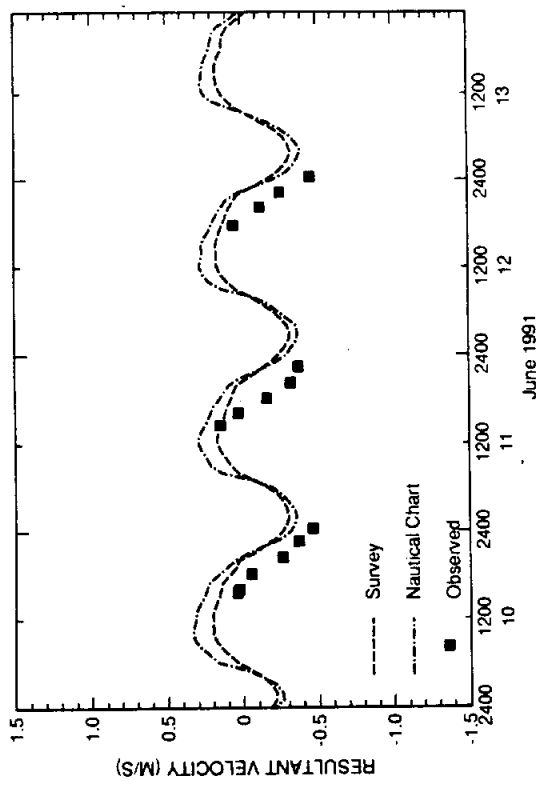


FIG. 6. Old Causeway (Mid East)

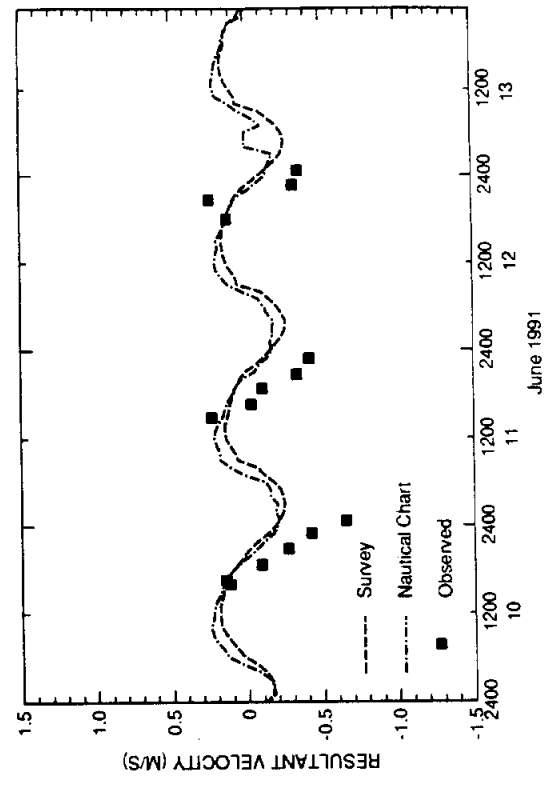


FIG. 8. Old Causeway (Western)

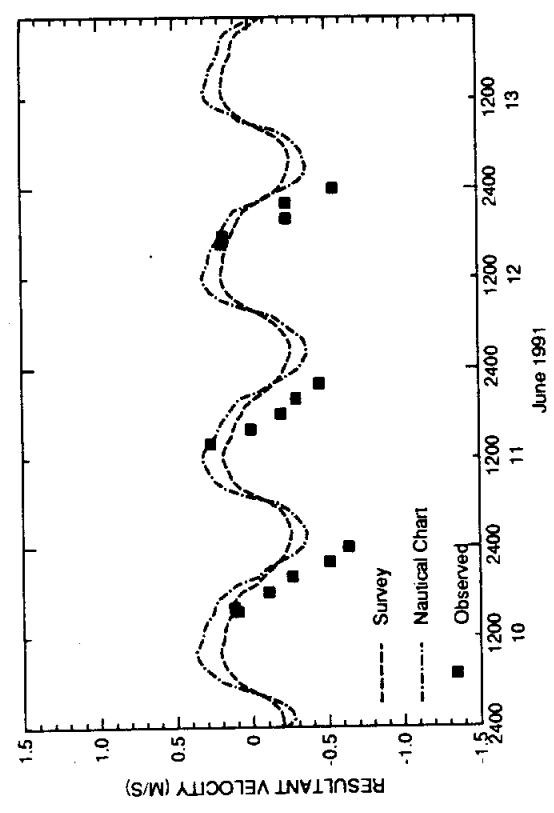


FIG. 5. Old Causeway (Eastern)

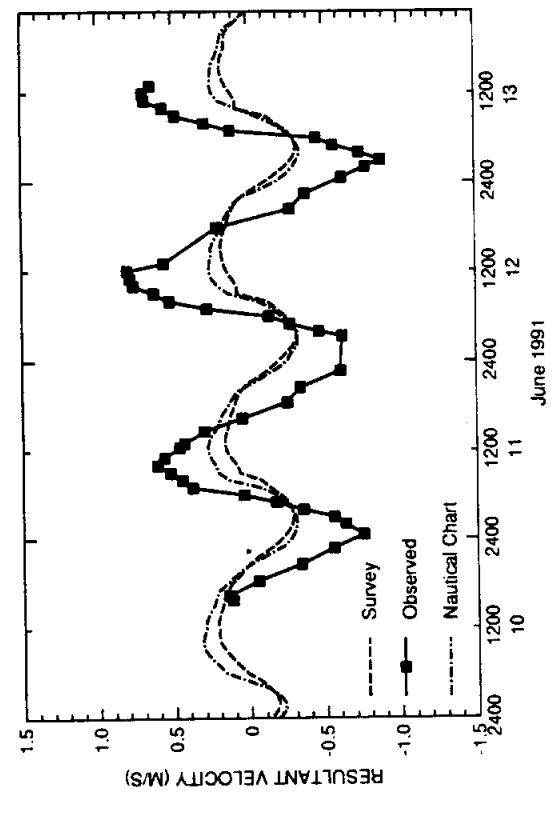


FIG. 7. Old Causeway (Mid West)

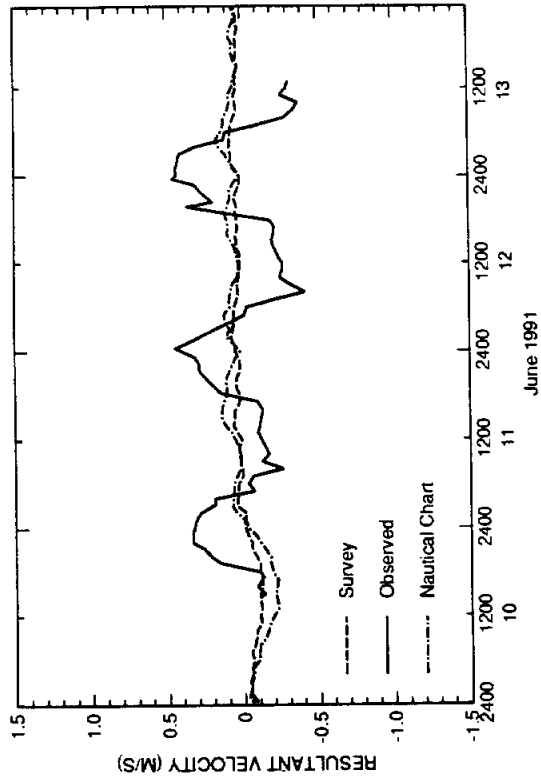


FIG. 10. Brownsville Ship Channel

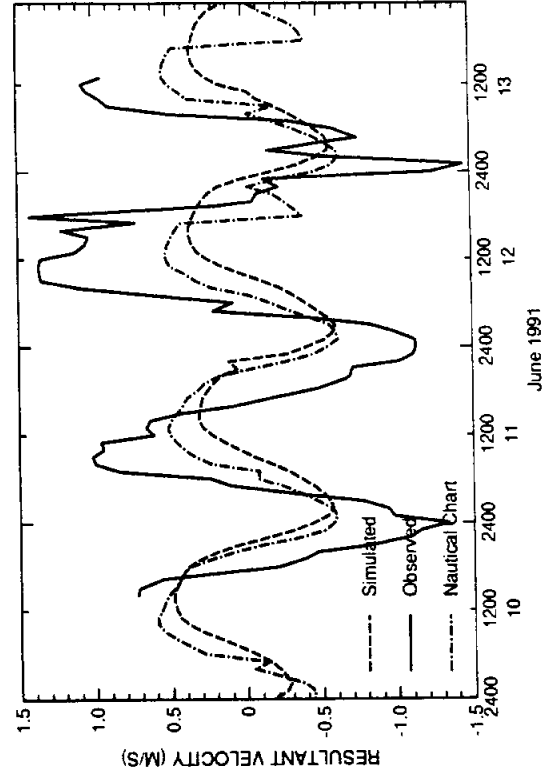


FIG. 12. Brazos Santiago Pass

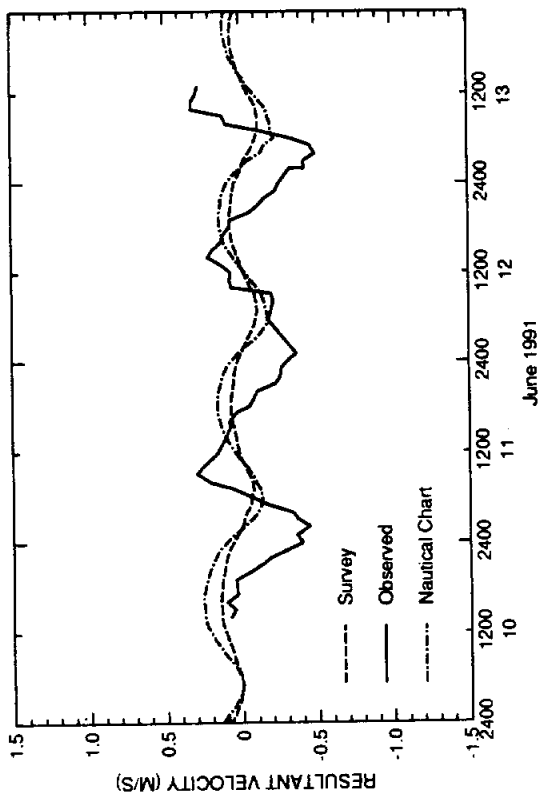


FIG. 9. Port Isabel Channel

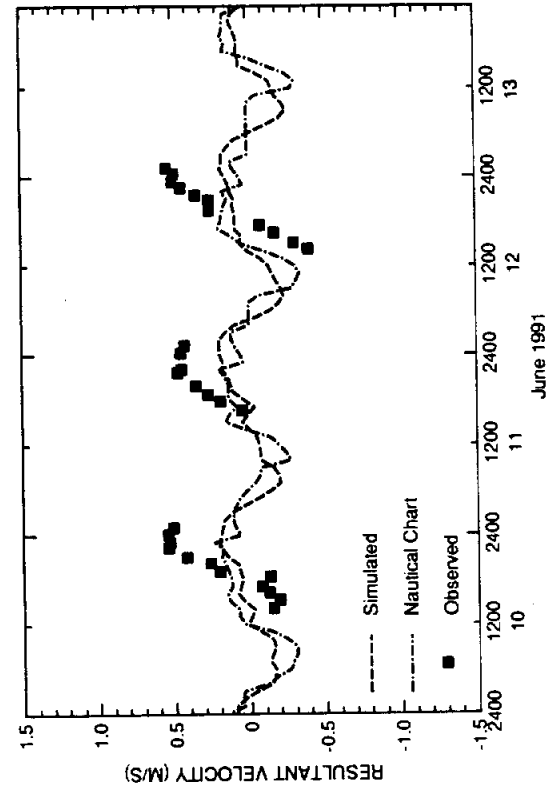


FIG. 11. South Bay Pass

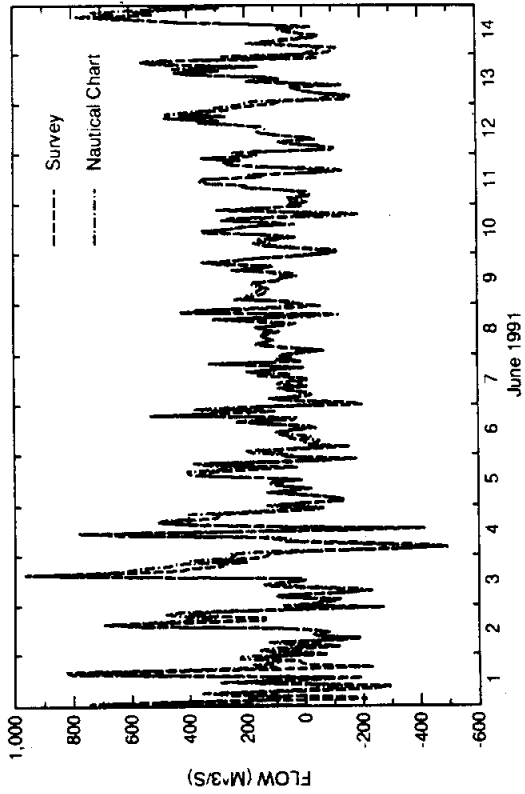


FIG. 2. Laguna Madre North of Port Mansfield

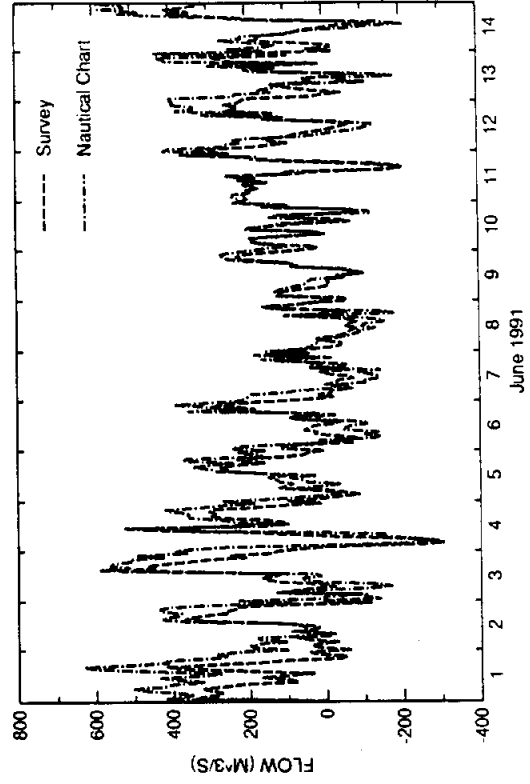


FIG. 4. Laguna Madre South of Port Mansfield

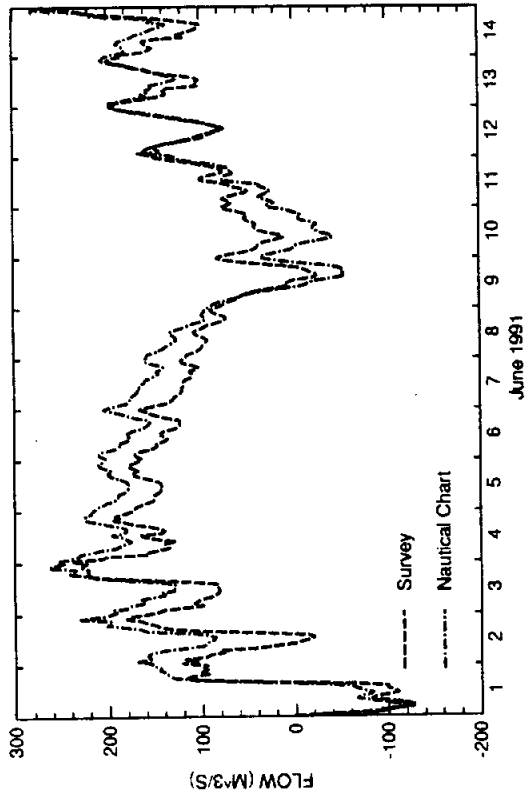


FIG. 1. South Land Cut

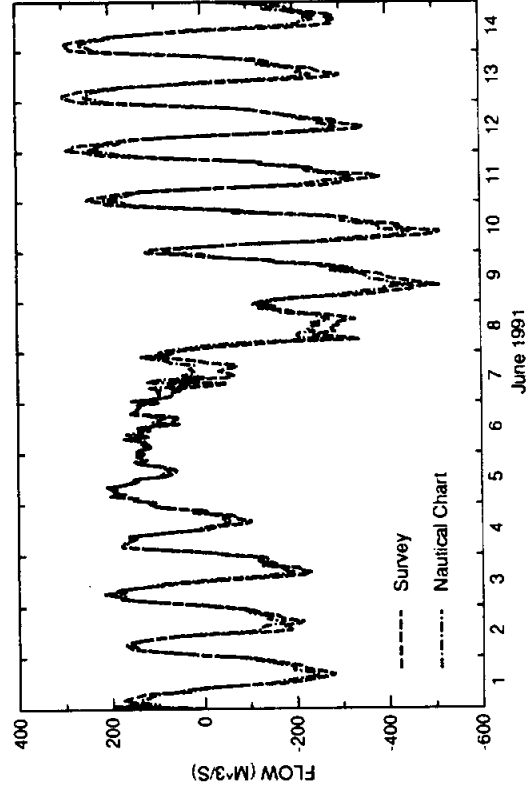


FIG. 3. Port Mansfield Channel

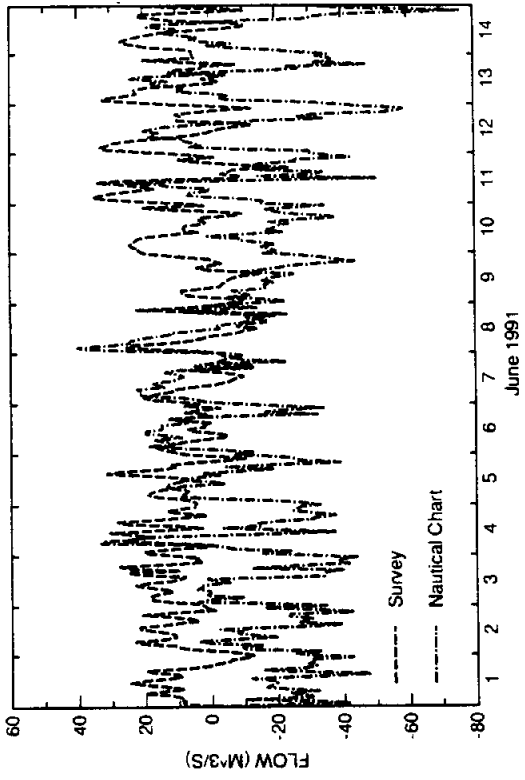


FIG. 6. Arroyo Colorado East of Laguna Atascosa

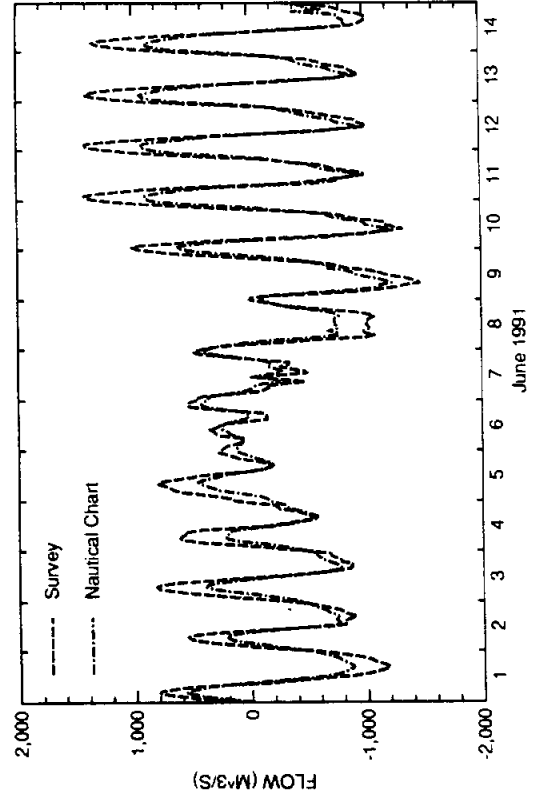


FIG. 8. Brazos-Santiago Pass

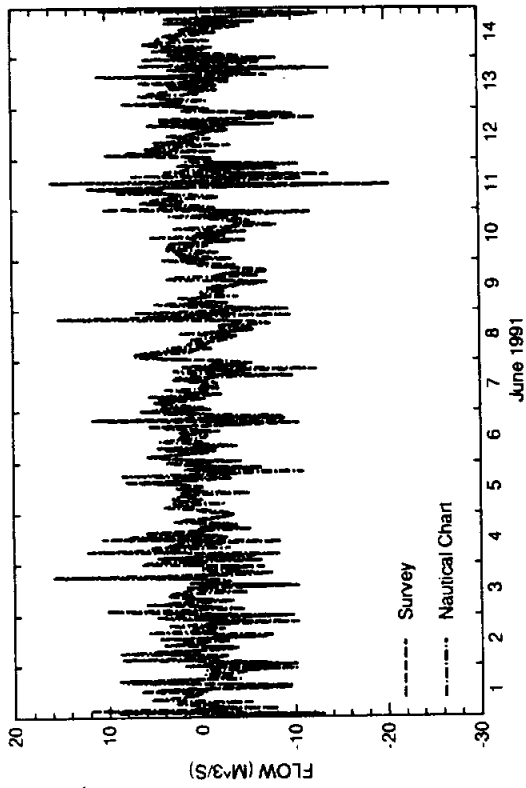


FIG. 5. Arroyo Colorado West of Laguna Atascosa

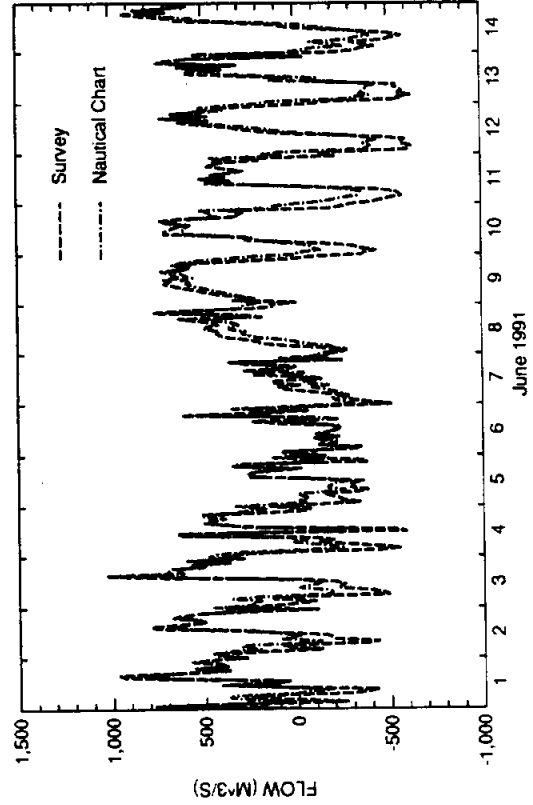


FIG. 7. Laguna Madre North of Port Isabel

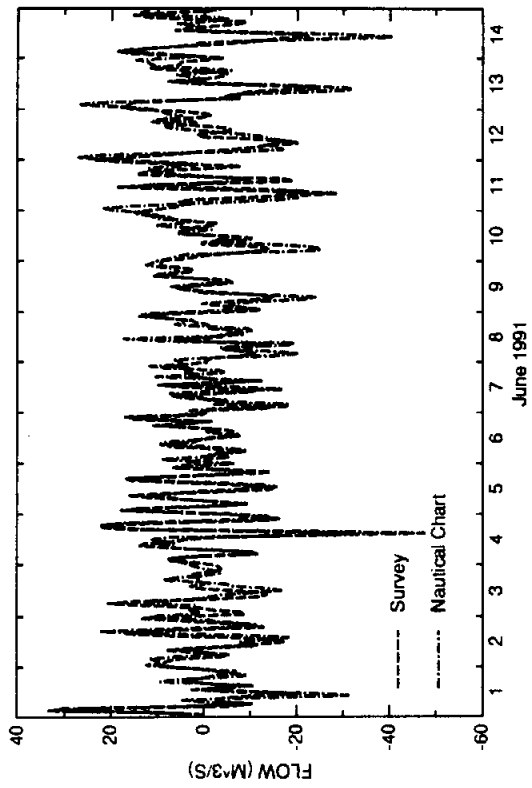


FIG. 9. Brownsville Ship Channel

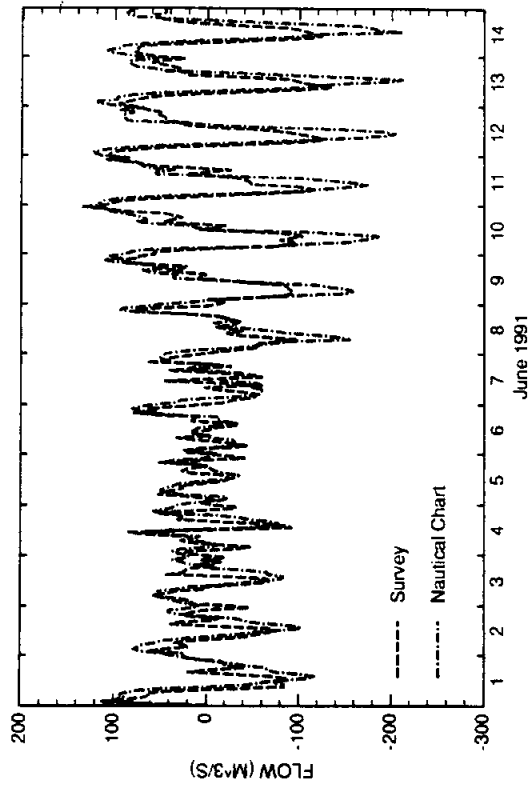


FIG. 10. South Bay Pass

APPENDIX B

LIST OF FILES FOR DELIVERY

INDEX

This file

For all coverages with elevation data the item SPOT represents the elevation (depth) in meters, while the item HOLD represents the elevation (depth) in feet. All coverages are in UTM coordinates with NAD27.

USGS 1:100,000 scale digital line graphs (DLG)

The DLG's were used to develop the boundaries of the mode grids.

baffin_b.hys.e00.Z	Baffin Bay DLG
brownsville.hys.e00.Z	Brownsville DLG
cchristi.hys.e00.Z	Corpus Christi DLG
harlingen.hys.e00.Z	Harlingen DLG
p_mansfld.hys.e00.Z	Port Mansfield DLG
laguna_hys.e00.Z	Combination of DLG's which cover the Laguna Madre

USGS 1:250,000 scale Digital Elevation Model (DEM)

The DEM's could be used to add elevation points on land.

demread	Simple shell script to format DEM data for use in ARC/INFO.
dugdem.txt	Description of demread
brownsville-w.Z	Brownsville DEM
corpus_christi-w.Z	Corpus Christi DEM
port_isabel-w.Z	Port Isabel DEM

Coverages derived from the NOAA/NOS Nautical Charts.

laguna_c.e00.Z	Channels
laguna_con.e00.Z	Contour lines
laguna_d.e00.Z	Depth points
laguna_sd.e00.Z	Supplemental depth points adde by hand

Coverages, grids, amls, etc. used to derive the model grids for the lower Laguna Madre. The grid used in the model was rotated 13 degree in order to reduce the size of the grid needed to represent the estuary. All coverages needed to create the grids are listed below.

r1195grd.aml	AML used to generate the rotated 200 meter grid from the hydrographic survey data (HSD)
r11cgrd.aml	AML used to generate the rotated 200 meter grid from the nautical chart data (NCD)
l1195grd.aml	AML used to generate an unrotated grid from the HSD
l11cgrd.aml	AML used to generate an unrotated grid from the NCD
l120095_grd.e00.Z	Unrotated 200 meter grid from HSD
l1200c_grd.e00.Z	Unrotated 200 meter grid from NCD
l1195sup_d.e00.Z	HSD supplemental depth coverage
llaguna_c.e00.Z	NCD channel coverage
llaguna_d.e00.Z	NCD depth coverage
llaguna_i.e00.Z	NCD island coverage
llaguna_sd.e00.Z	NCD supplemental depth coverage
l1m95_d.e00.Z	HSD depth coverage
l1m95_land.e00.Z	HSD land boundary outline
l1tin_clip.e00.Z	Clip coverage used to create tins
llaguna_land.e00.Z	NCD land boundary outline

Miscellaneous Coverages

lm95xy.e00.Z	Coverage of the HSD
stations.e00.Z	Coverage with locations of tide, wind, velocity, water quality, etc. stations
tx95.e00.Z	Coverage of the mesh points in the TXBLEND model

Coverages, grids, amls, etc. used to derive the model grids for the upper Laguna Madre. All coverages needed to create the grids are listed below.

ulgrid.aml	AML used to create the 200 meter grid (NCD) for the upper Laguna Madre
ul200_g.e00.Z	200 meter grid (NCD)
ul400_g.e00.Z	400 meter grid (NCD)
ulaguna_c2.e00.Z	Channel coverage
ulaguna_d.e00.Z	Depth point coverage
ulaguna_i2.e00.Z	Island coverage
ulaguna_sd.e00.Z	Supplemental depth points
ulland.e00.Z	Outline coverage
uloutnc.e00.Z	Outline coverage
ultin.e00.Z	TIN of the upper Laguna Madre
ultin_clip.e00.Z	Clip coverage used to create the TIN

Upper Laguna Madre TIN based on HSD

ulm95tin.aml	AML used to create the TIN
ulm95_d.e00.Z	HSD depth point coverage
ulm95_tin.e00.Z	TIN created from HSD

**SIMULATION OF THE
LOWER LAGUNA MADRE ESTUARY
WITH SWIFT2D**

By Karl McArthur

U.S. GEOLOGICAL SURVEY

OCTOBER 9, 1996

TABLE OF CONTENTS

	Page
TABLE OF CONTENTS	ii
LIST OF FIGURES	iii
LIST OF TABLES	iv
OVERVIEW	1
BATHYMETRY AND GEOMETRY	5
SIMULATION RESULTS	8
APPENDIX A: PLOTS OF RESULTS	12
Calibrated Simulation	13
Velocity Vector Plots for the Calibrated Model with the Hydrographic Survey Data	22
Velocity Vector Plots for the Calibrated Model with the Nautical Chart Data	37
Manning's n Variation Simulation	52
Wind Stress Variation 1 Simulation	60
Wind Stress Variation 2 Simulation	68
Time Step Variation Simulation	76
APPENDIX B: LIST OF FILES FOR DELIVERY	84

LIST OF FIGURES

	Page
1. Locations of Tide Stations in the Lower Laguna Madre	2
2. Locations of Velocity Station in the Lower Laguna Madre.....	3
3. Locations of Flow Cross Sections in the Lower Laguna Madre	4
4. 200 Meter Grid from Nautical Chart Data.....	6
5. 200 Meter Grid from Hydrographic Survey Data	7
6. Location of Grid Cells Which Dried During the Simulation (Nautical Chart Grid).....	11
7. Location of Grid Cells Which Dried During the Simulation (Hydrographic Survey Data Grid).....	12

LIST OF TABLES

	Page
1. Geometric Characteristics of the Nautical Chart and Hydrographic Survey Grids	8
2. Root Mean Squared Errors (meters) between Simulated and Observed Water Levels	10
3. Root Mean Squared Errors (square meters) between Simulated and Observed Water Levels.....	10

OVERVIEW

The lower Laguna Madre Estuary from the south end of the Land Cut to South Bay was simulated with the SWIFT2D model. The lower half of the Laguna Madre has two openings to the Gulf of Mexico. Port Mansfield Channel and the Brazos-Santiago Pass at Port Isabel. The lower Laguna is connected to the upper Laguna Madre by the Gulf Intracoastal Waterway (GIWW) through the Land Cut. The most significant source of fresh-water inflow into the estuary is the Arroyo Colorado, which flows into the estuary between Port Mansfield and Port Isabel.

The SWIFT2D simulations of the estuary were performed for the month of June, 1991, which corresponded to the June 10 through June 14, 1991 intensive inflow survey performed by the Texas Water Development Board (TWDB). Simulations were performed for water levels, velocities, and circulation patterns (hydrodynamics only). Salinity was not considered in the simulations. Inflows from the Arroyo Colorado were also not considered. Three tide signals were used to drive the model at the South Land Cut, Port Mansfield Channel, and Brazos-Santiago Pass. The driving tides at the South Land Cut were provided by the tide station at El Toro Island. Tide records were available at Port Mansfield and Port Isabel, however, these stations were internal to the model.

In order to provide an external (Gulf of Mexico) driving tide, the tide signal from the Bob Hall Pier tide stations was used. The Bob Hall tidal signal was applied on the Gulf side of Padre Island at the Port Mansfield Channel and Brazos-Santiago Pass. The Bob Hall Pier tide station is located just south of Corpus Christi on the Gulf side of Padre Island. The Bob Hall tide was compared to the tidal signal at the Port Mansfield and Port Isabel stations to determine whether a phase shift would be required. The three tide signals were determined to be in phase, therefore, the unaltered Bob Hall tide was used to drive the model at both locations.

The simulation results were compared to observed data at four tide stations and twelve velocity stations. These stations are shown in Figures 1 and 2 respectively. Results for flow were also output at the ten cross sections shown in Figure 3.

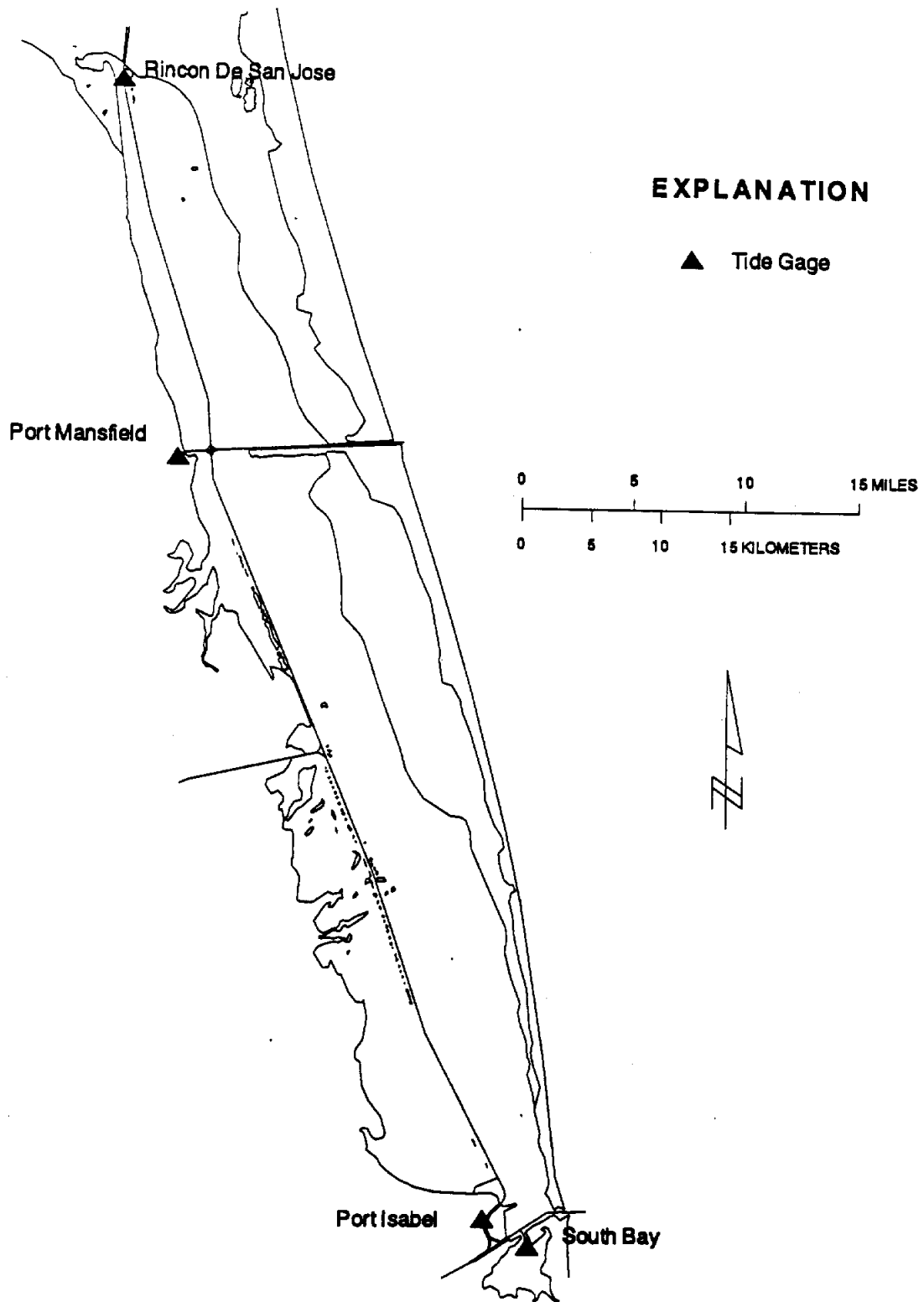


Figure 1. Locations of Tide Stations in the Lower Laguna Madre

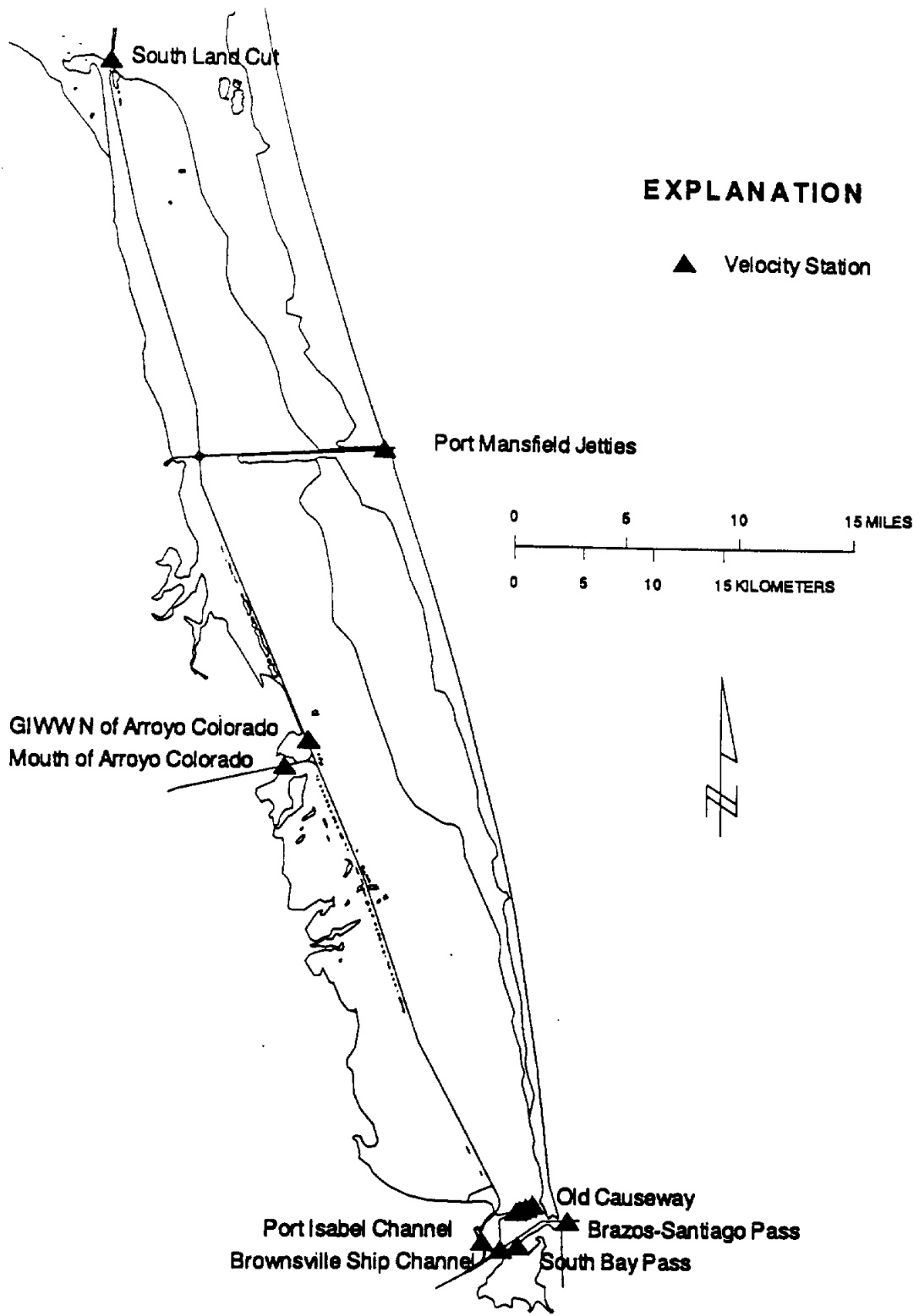


Figure 2. Locations of Velocity Stations in the Lower Laguna Madre

Observed tide data for the period of simulation was obtained from the Texas Coastal and Ocean Observation Network (TCOON) through the Conrad Blucher Institute. Observed velocities were obtained from the TWDB intensive inflow survey. The tidal datums were referenced to the mean tide level observed at each station.

BATHYMETRY AND GEOMETRY

Two sources were used to generate the bathymetry for the SWIFT2D model grid. The first set of data was derived from the three, 1:40,000 scale NOAA/NOS nautical charts which cover the lower Laguna Madre. The three maps are titled as follows: 1. Texas Intracoastal Waterway, Laguna Madre: Middle Ground to Chubby Island; 2. Texas Intracoastal Waterway, Laguna Madre: Chubby Island to Stover Point Including the Arroyo Colorado; 3. Texas Intracoastal Waterway, Laguna Madre: Stover Point to Brownsville Including the Brazos Santiago Pass. The second set of data consisted of the recent hydrographic survey data for the Laguna Madre obtained from the U.S. Army Corps of Engineers, Waterways Experiment Station. USGS 1:100,000 scale digital line graphs were used to form the boundary of the estuary.

The ARC/INFO geographic information system was used to process the bathymetry data and create the required information for the SWIFT2D model grids. Separate grids were created for the nautical chart data and the hydrographic survey data. The nautical chart grid was derived from 1080 points digitized from the charts, while the hydrographic survey grid was derived from 28,059 points. The hydrographic survey data obviously provides a more extensive set of points for the definition of bathymetry. Both grids were rotated 13 degrees clockwise to reduce the extent of the grid required to define the study area. The resulting grids were 125 cells wide by 505 cells tall. The grid size used was 200 meters. The specifics of the two grids are compare in Table 1.

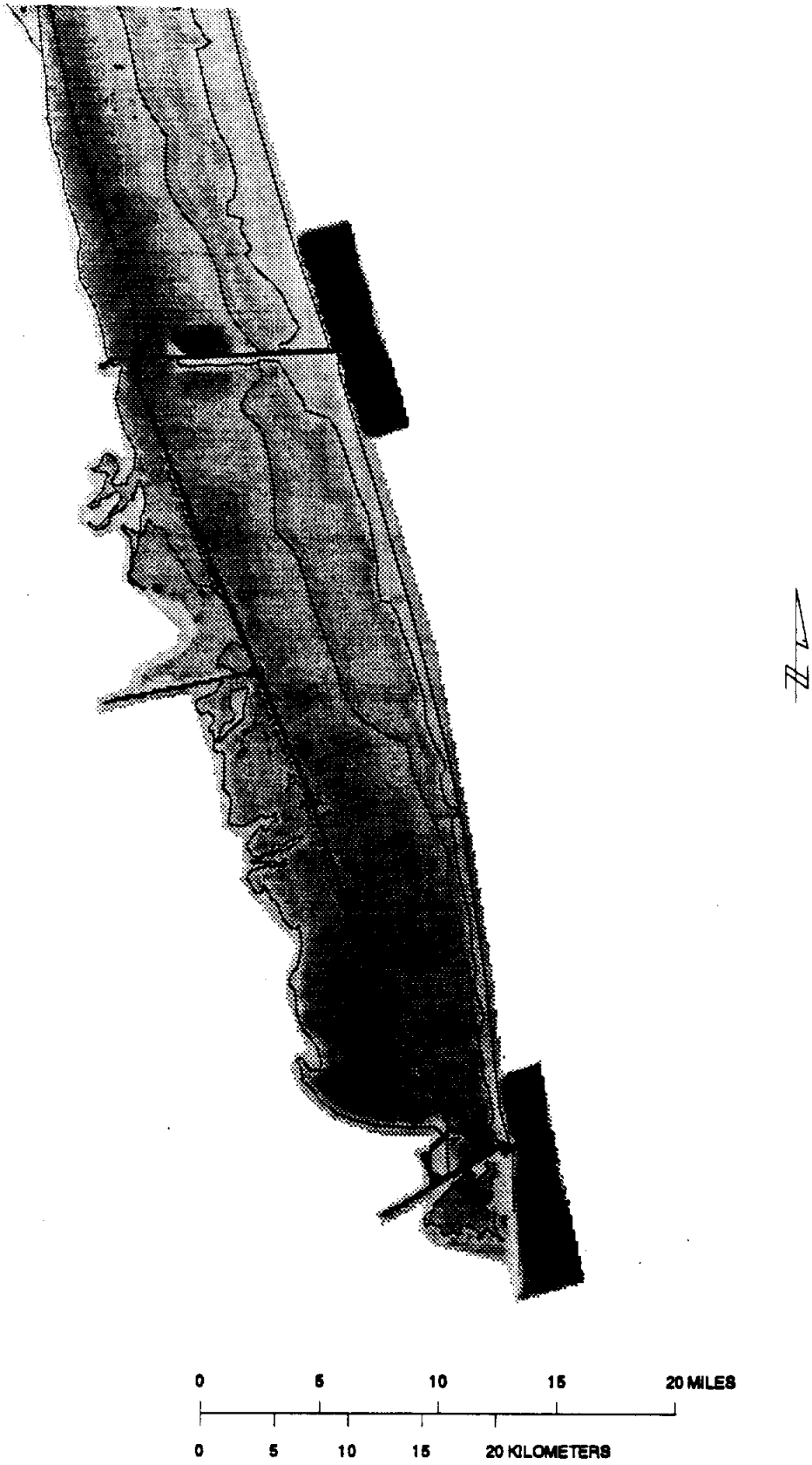


Figure 4. 200 Meter Grid from Nautical Chart Data

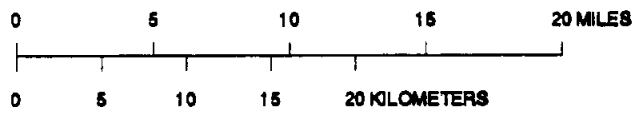
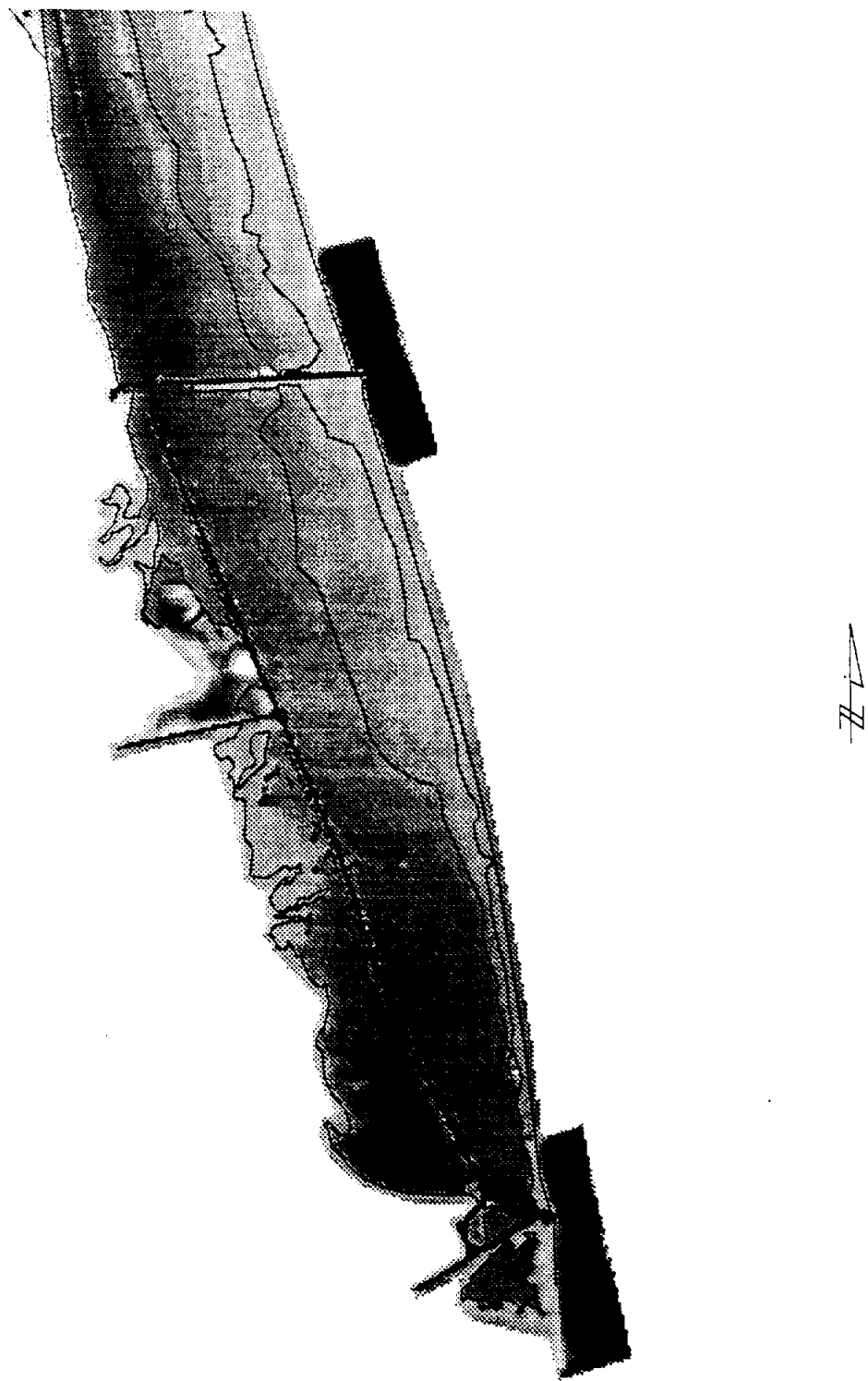


Figure 5. 200 Meter Grid from Hydrographic Survey Data

Table 1. Geometric Characteristics of the Nautical Chart and Hydrographic Survey Grids

Characteristic	Nautical Chart Grid	Hydrographic Survey Grid
Number of cells with depth below MWL	26729	19439
Minimum cell depth (m)	0.1	0.1
Maximum cell depth (m)	14.5	14.3
Average cell depth (m)	1.35	1.65
Total area of cells with depth below MWL (km ²)	1,069	777.6
Total volume below mean water level (m ³)	1.44x10 ⁹	1.28x10 ⁹

The nautical chart grid has a larger area of shallow depth along the east side of the estuary than the hydrographic survey grid. These areas are slightly above mean water level (MWL) in the hydrographic survey grid.

SIMULATION RESULTS

The SWIFT2D model was calibrated to the data measured during the 1991 intensive inflow survey performed by the TWDB. Several problems remain in the final model. The primary areas of difficulty are in the vicinity of the channels between the Laguna Madre and the Gulf of Mexico. Instabilities in the model solution were observed in the vicinity of the Port Mansfield Jetties in the sensitivity analysis. The model also was unable to accurately simulate the magnitude of the tidal signal at the Port Isabel and South Bay tide stations. A majority of the inflow from the Brazos-Santiago Pass appears flow northward into the estuary instead of into the Laguna Madre Channel and South Bay Pass. The calibration for the lower Laguna Madre could be improved with additional work on the finite element grid and calibration parameters.

The roughly calibrated SWIFT2D model produced fairly good matches between simulated and observed water levels at the Rincon del San Jose and Port Mansfield stations. Results at the Port Isabel and South Bay stations were not as good. Simulated water levels at these sites matched in phase, however, were smaller in amplitude. The fit could probably be improved by adjustments to the model grids.

Additional simulations were performed to test the robustness of the model. The Manning's n values for the calibrated model were 0.025 in channels, 0.075 in the vicinity of the old Queen Isabel Causeway, and 0.035 elsewhere. A sensitivity simulation was performed with a constant n value of 0.030. Sensitivity runs were also performed for wind stress coefficients of 0.0001 and 0.0026 in addition to the calibration value of 0.0015. The calibrated model used a time step of 6 minutes. A time step of 12 minutes was used in a sensitivity run. The larger time step created instabilities in the vicinity of the Port Mansfield jetties in the hydrographic survey model. Complete results of the simulations are shown in the section at the end of this report. Tables 2 and 3 show the root mean square errors between simulated and observed values for both models.

Figures 6 and 7 show the extent of grid cells that dried at some point in the simulation. The hydrographic survey grid produced a substantially larger number of dry cells. The difference was a result of the shallower bathymetry along the east side of the estuary in the hydrographic survey grid.

Table 2. Root Mean Squared Errors (meters) between Simulated and Observed Water Levels

Water Level Stations	Calibrated			Constant n-value			No Wind Stress			High Wind Stress			12 Minute Time Step		
	NC	HS		NC	HS		NC	HS		NC	HS		NC	HS	
		NC	HS		NC	HS		NC	HS		NC	HS			
Rincon Del San Jose	0.260	0.255	0.264	0.256	0.242	0.241	0.279	0.269	0.262	0.257	0.269	0.120	0.098	0.214	
Port Mansfield	0.098	0.098	0.099	0.099	0.104	0.102	0.106	0.120	0.098	0.214	0.106	0.148	0.144	0.138	
Port Isabel	0.146	0.142	0.144	0.135	0.129	0.133	0.158	0.148	0.144	0.138	0.158	0.148	0.144	0.138	
South Bay	0.116	0.107	0.118	0.177	0.113	0.107	0.121	0.111	0.137	0.127	0.121	0.111	0.137	0.127	

Table 3. Root Mean Squared Errors (square meters) between Simulated and Observed Water Levels

Velocity Stations	Calibrated			Constant n-value			No Wind Stress			High Wind Stress			12 Min. Time Step		
	NC	HS		NC	HS		NC	HS		NC	HS		NC	HS	
		NC	HS		NC	HS		NC	HS		NC	HS			
South Land Cut	0.226	0.251	0.244	0.261	0.204	0.244	0.248	0.259	0.212	0.244	0.248	0.259	0.212	0.244	
Port Mansfield Jetties	0.698	0.731	0.772	0.768	0.691	0.685	0.692	0.725	0.783	0.809	0.692	0.725	0.783	0.809	
Mouth of Arroyo Colorado	0.096	0.105	0.096	0.107	0.098	0.102	0.094	0.107	0.096	0.102	0.094	0.107	0.096	0.102	
GIWW North of Arroyo Colorado	0.151	0.137	0.153	0.137	0.162	0.154	0.144	0.132	0.147	0.135	0.144	0.132	0.147	0.135	
Old Causeway (Eastern)	0.208	0.198	0.208	0.194	0.192	0.191	0.222	0.204	0.257	0.233	0.222	0.204	0.257	0.233	
Old Causeway (Mid East)	0.175	0.143	0.191	0.156	0.161	0.134	0.186	0.149	0.231	0.198	0.186	0.149	0.231	0.198	
Old Causeway (Mid West)	0.315	0.327	0.294	0.342	0.315	0.326	0.317	0.329	0.361	0.417	0.317	0.329	0.361	0.417	
Old Causeway (Far West)	0.202	0.172	0.183	0.182	0.202	0.172	0.203	0.174	0.217	0.234	0.203	0.174	0.217	0.234	
Port Isabel Channel	0.193	0.190	0.191	0.193	0.190	0.185	0.196	0.194	0.246	0.246	0.196	0.194	0.246	0.246	
Brownsville Ship Channel	0.259	0.249	0.252	0.247	0.252	0.247	0.263	0.251	0.281	0.264	0.263	0.251	0.281	0.264	
South Bay Pass	0.289	0.261	0.288	0.261	0.283	0.255	0.291	0.249	0.293	0.262	0.291	0.249	0.293	0.262	

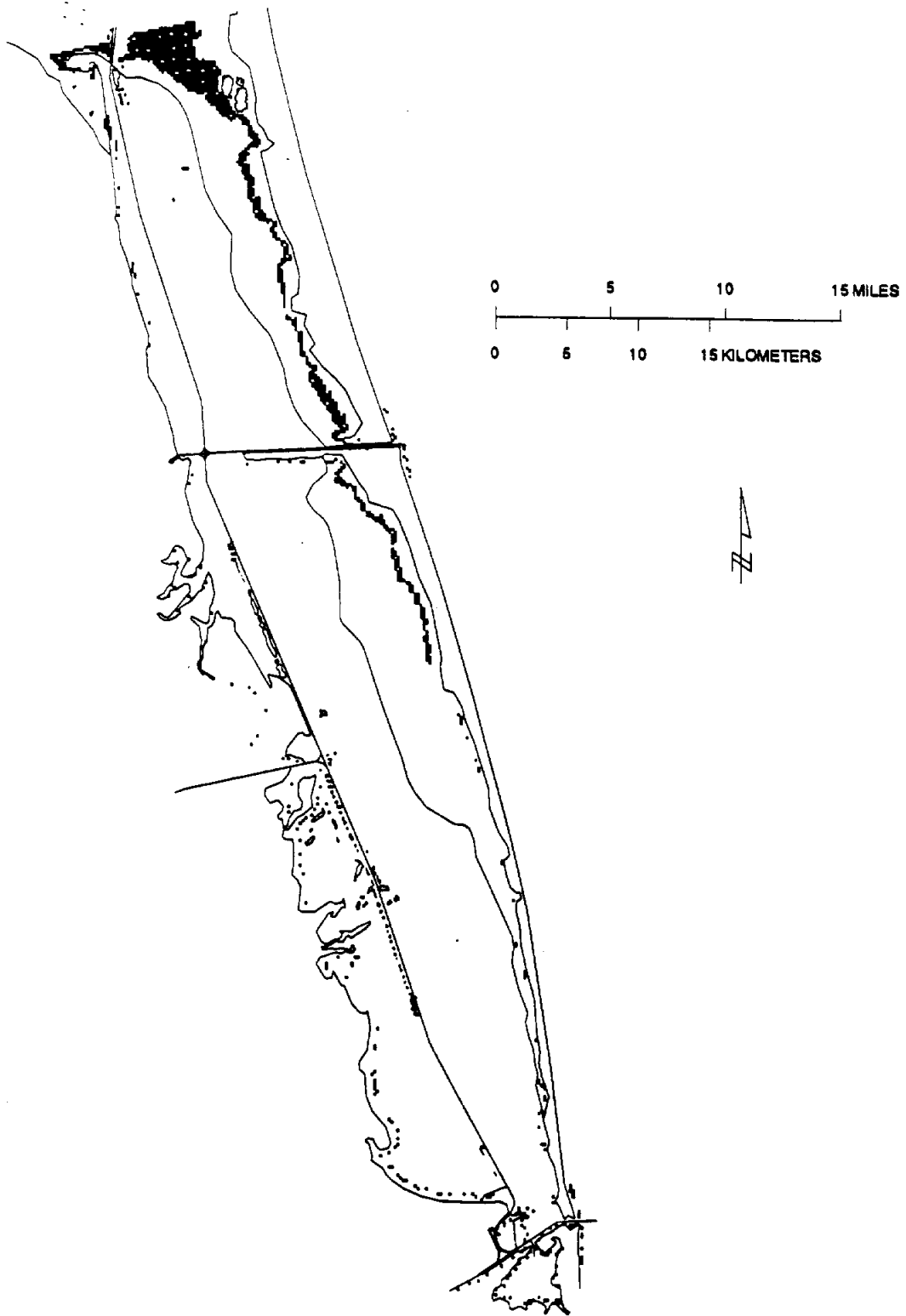


Figure 6. Location of Grid Cells Which Dried During the Simulation (Nautical Chart Grid).

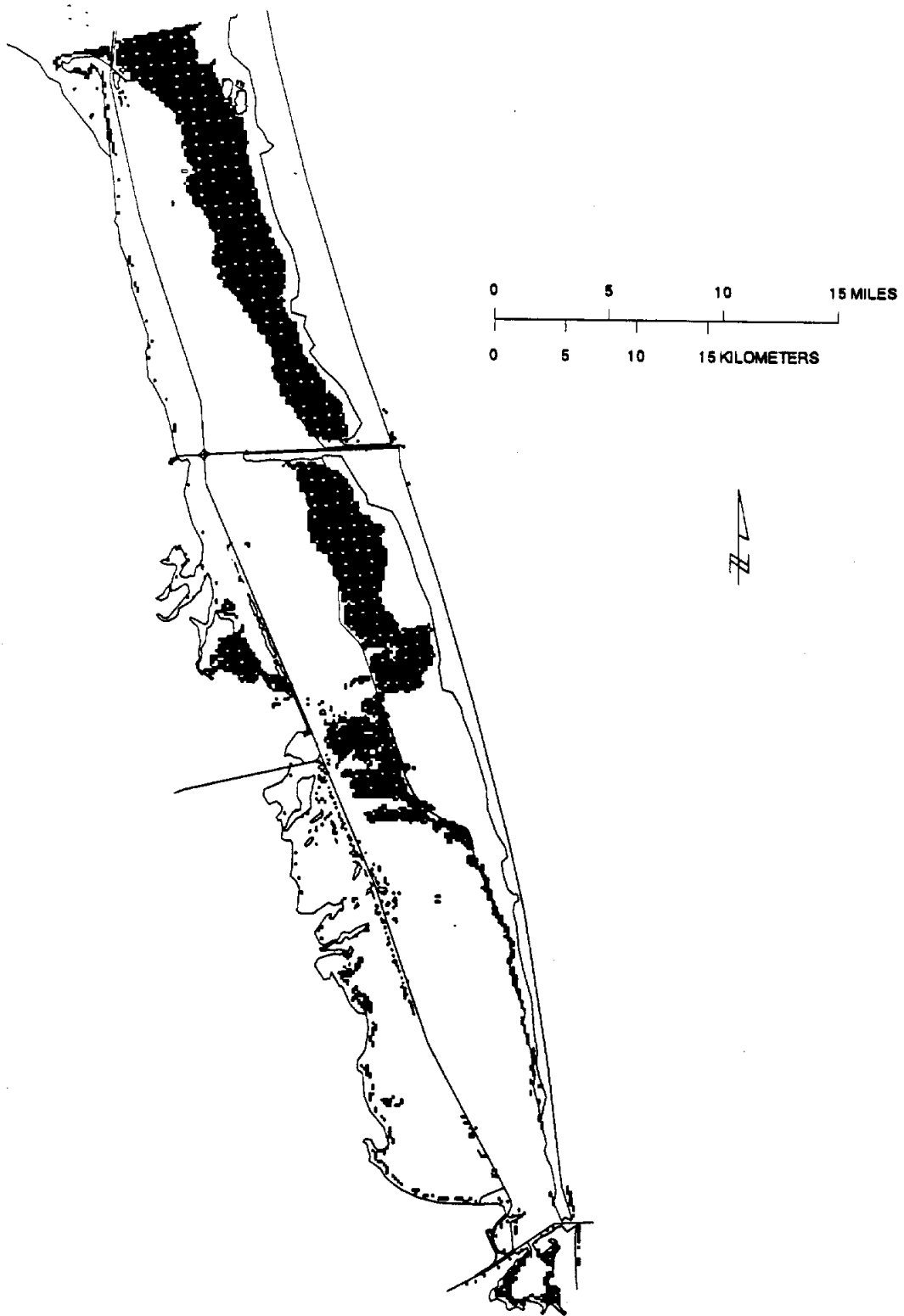


Figure 7. Location of Grid Cells Which Dried During the Simulation (Hydrographic Survey Data Grid).

APPENDIX A
PLOTS OF RESULTS

SWIFT2D SIMULATIONS

Calibrated Simulation

Manning's n = 0.025 in navigation channels
= 0.075 in the vicinity of the old Queen Isabel Causeway
= 0.035 elsewhere

Wind Stress = 0.0015

Time Step = 6 minutes

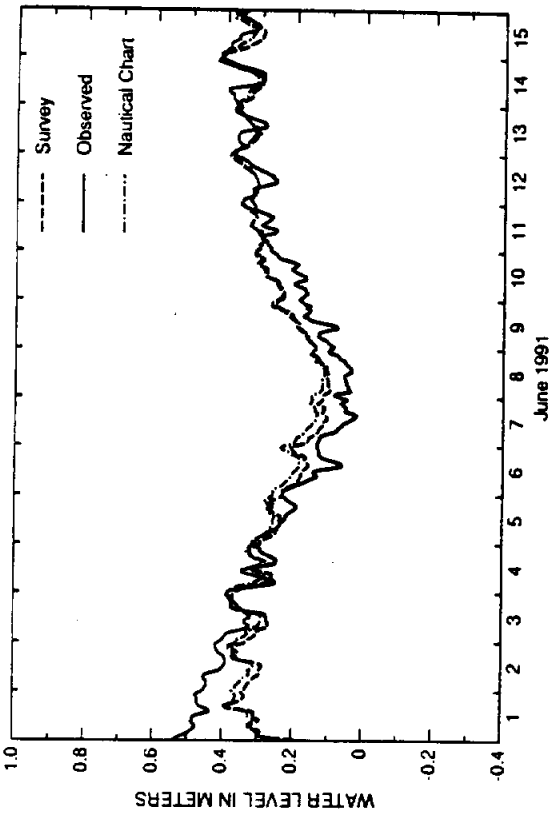


FIG. 1. Rincon Del San Jose Tide Station

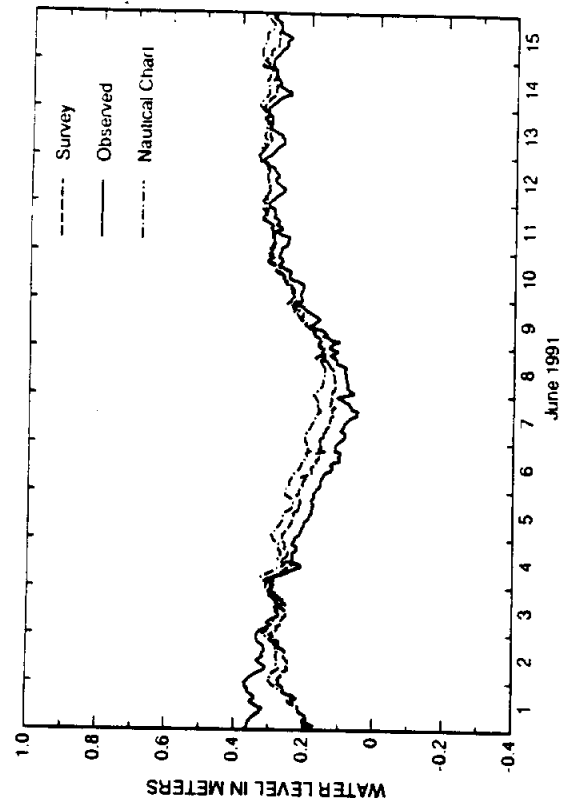


FIG. 2. Port Mansfield Tide Station

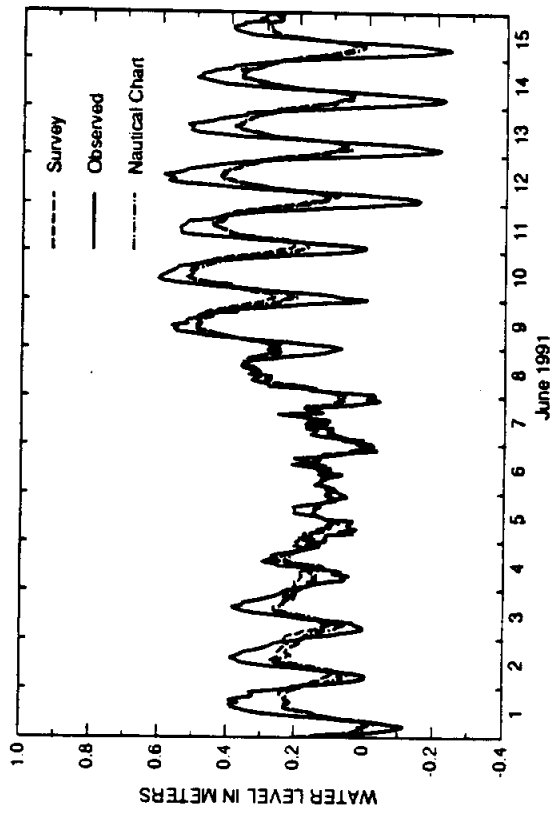


FIG. 3. Port Isabel Tide Station

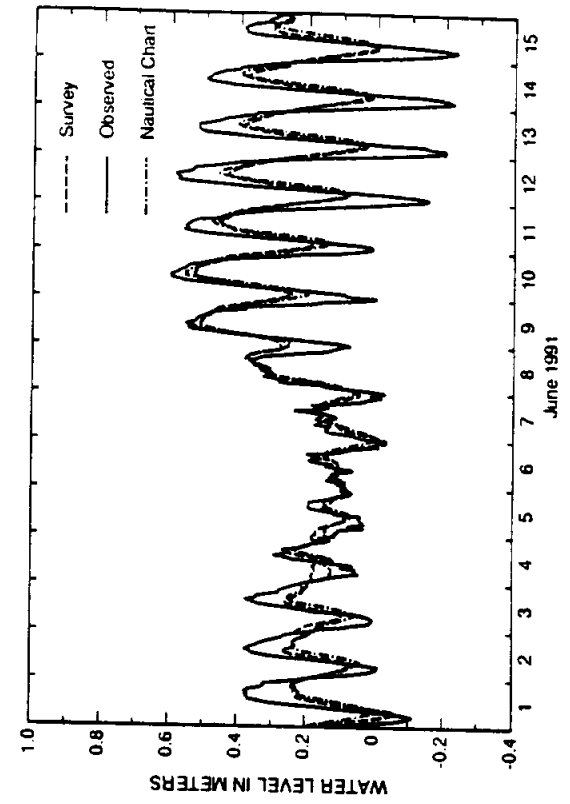


FIG. 4. South Bay Tide Station

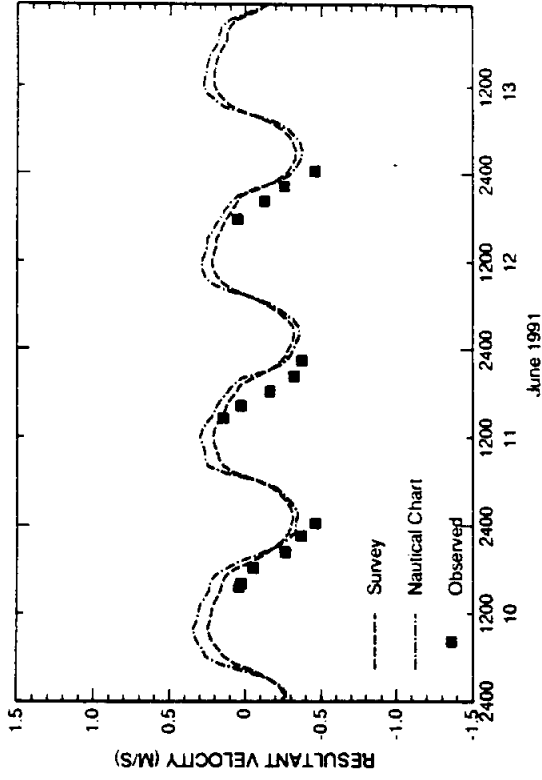


FIG. 6. Old Causeway (Mid East)

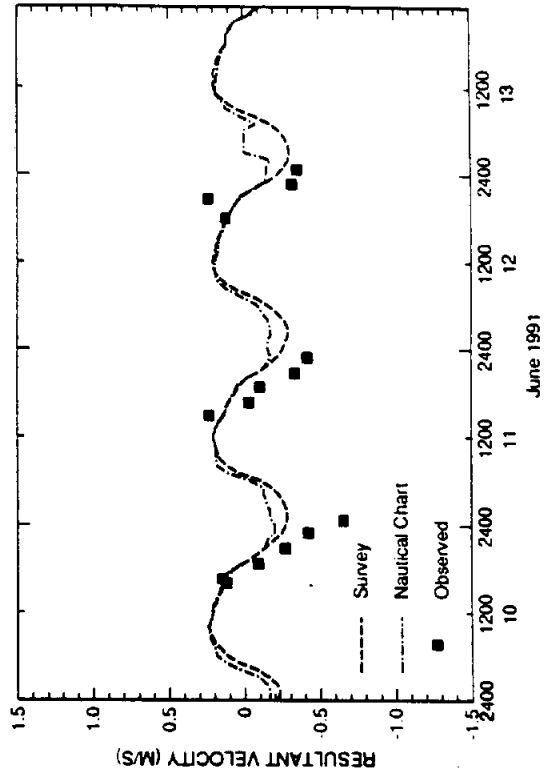


FIG. 8. Old Causeway (Western)

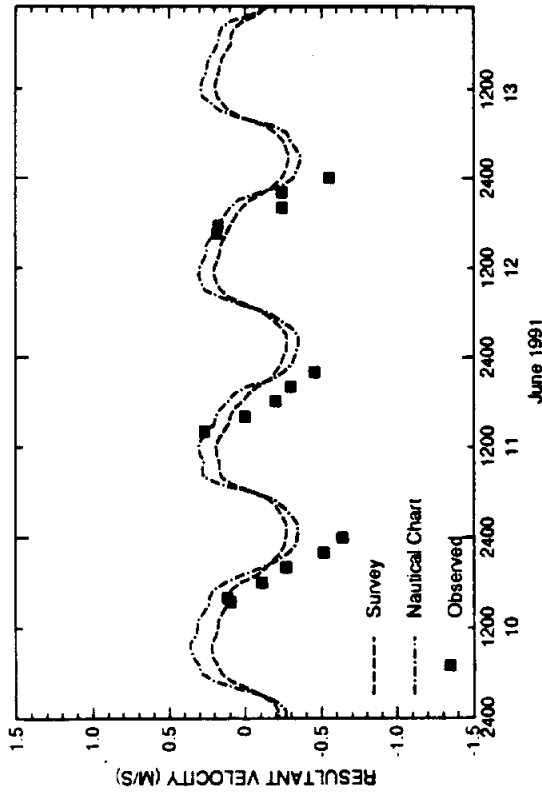


FIG. 5. Old Causeway (Eastern)

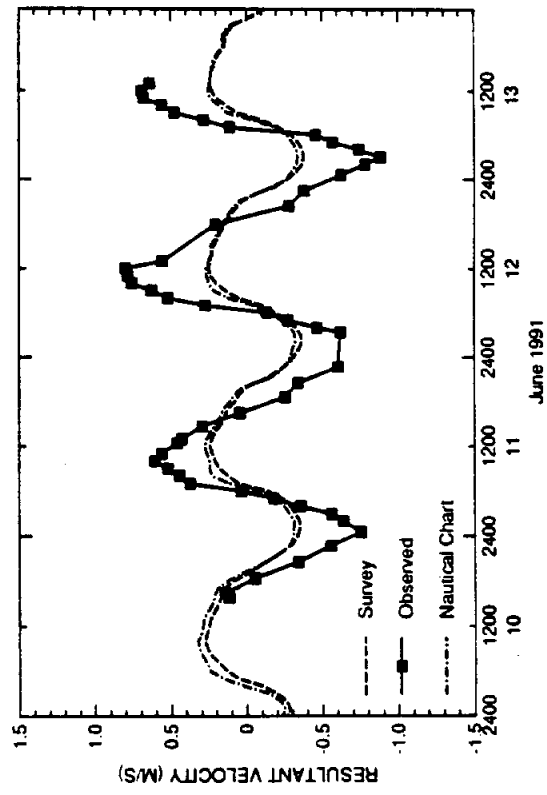


FIG. 7. Old Causeway (Mid West)

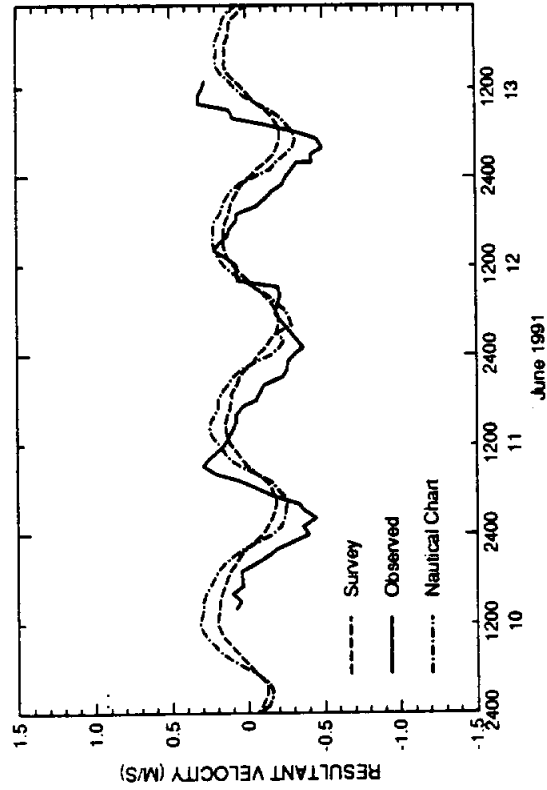


FIG. 9. Port Isabel Channel

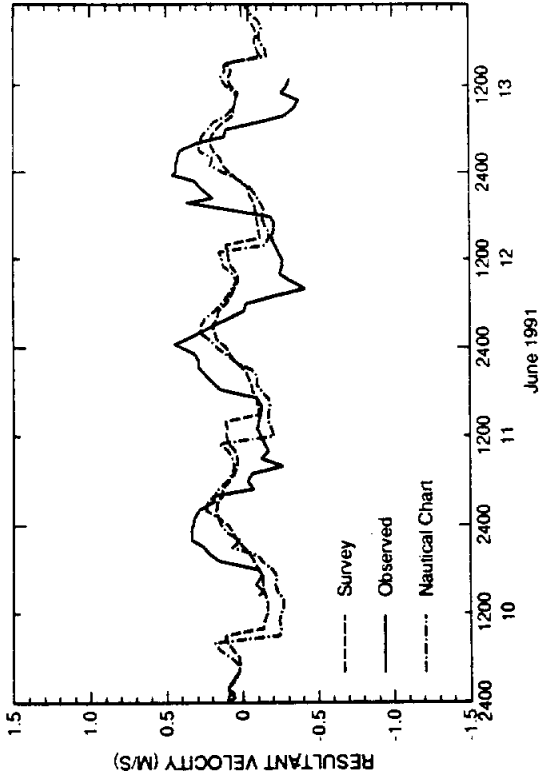


FIG. 10. Brownsville Ship Channel

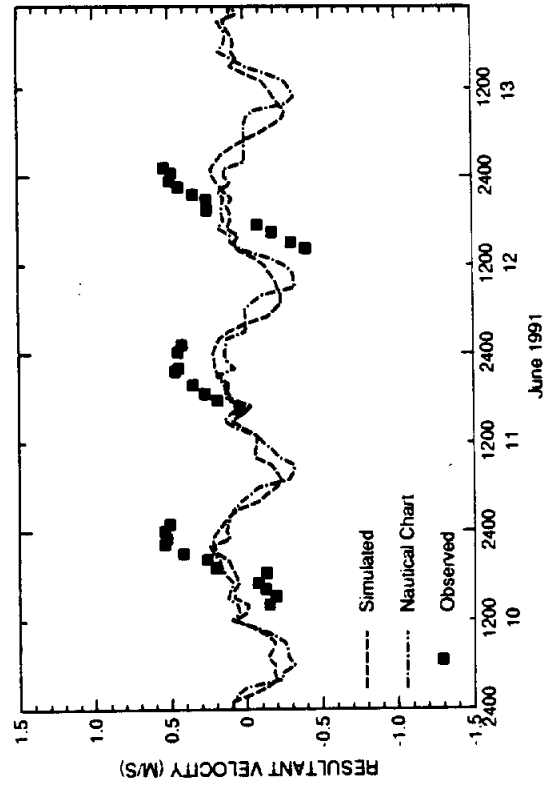


FIG. 11. South Bay Pass

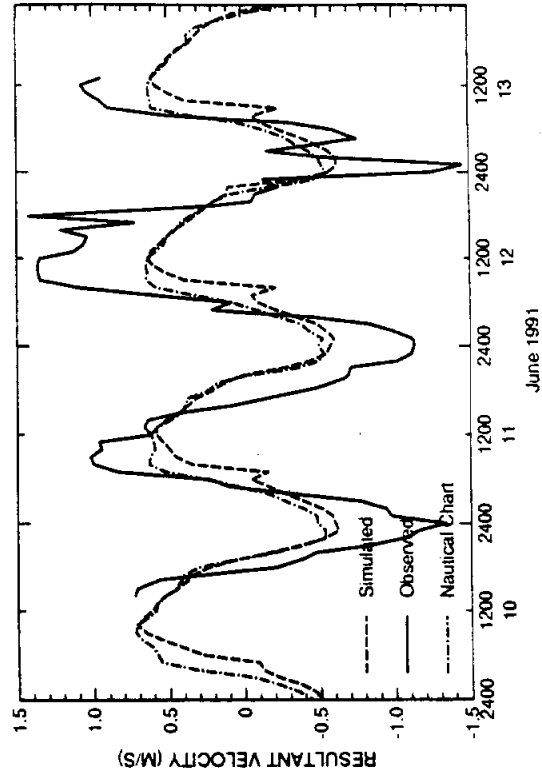


FIG. 12. Brazos Santiago Pass

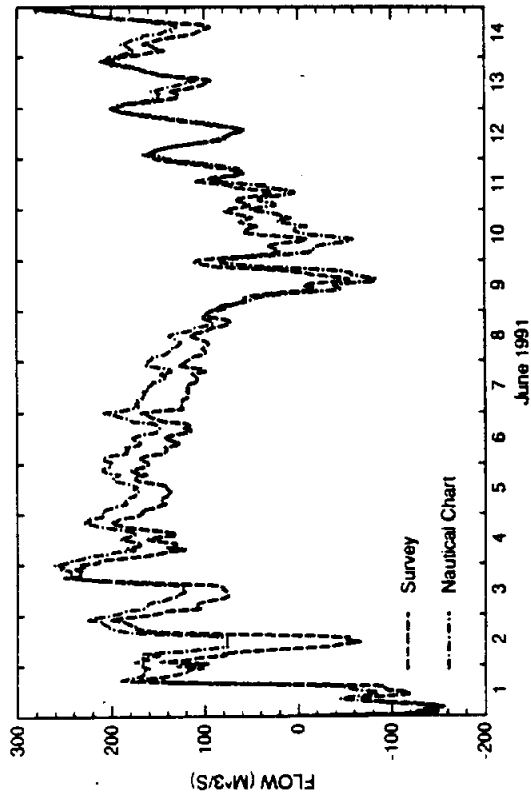


FIG. 1. South Land Cut

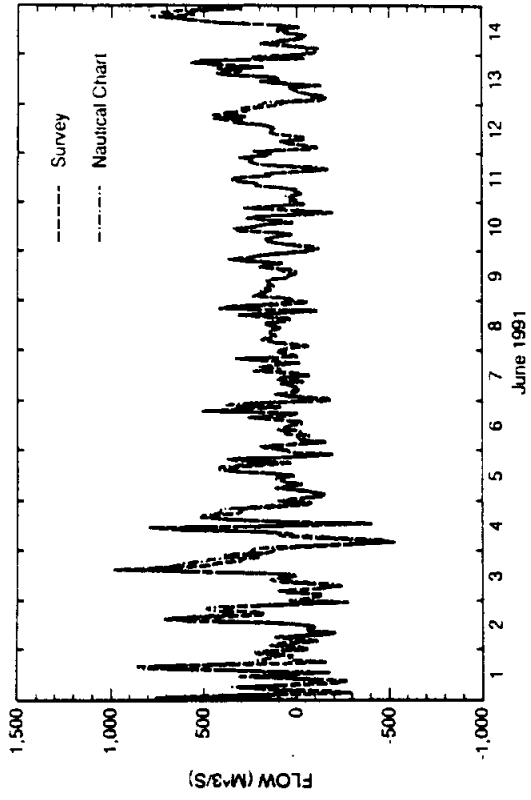


FIG. 2. Laguna Madre North of Port Mansfield

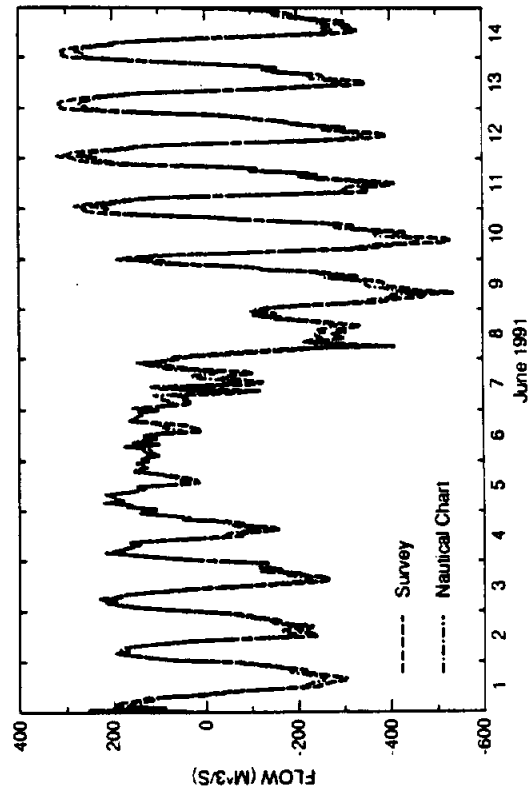


FIG. 3. Port Mansfield Channel

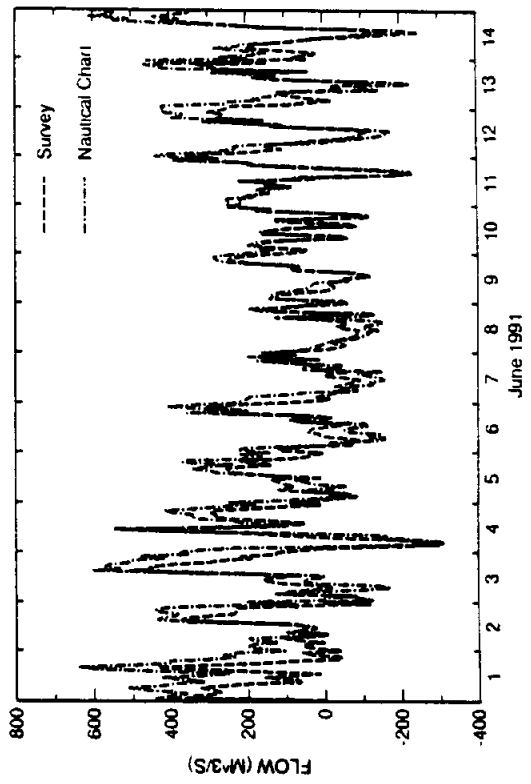


FIG. 4. Laguna Madre South of Port Mansfield

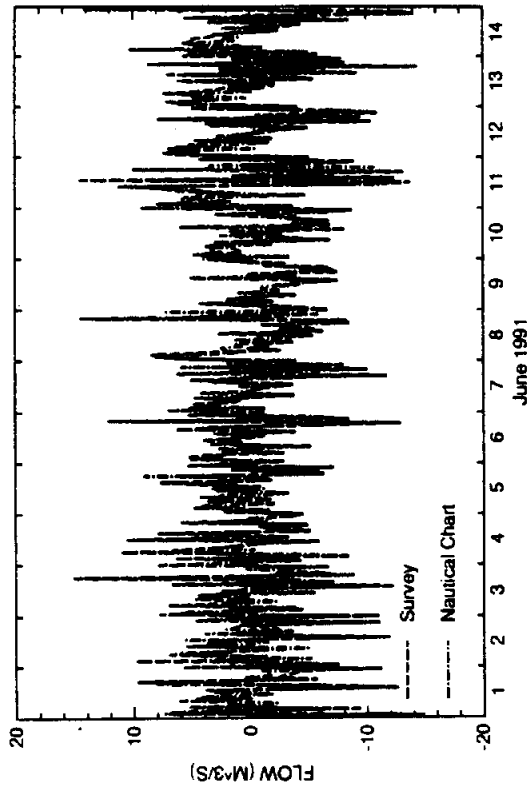


FIG. 5. Arroyo Colorado West of Laguna Atascosa

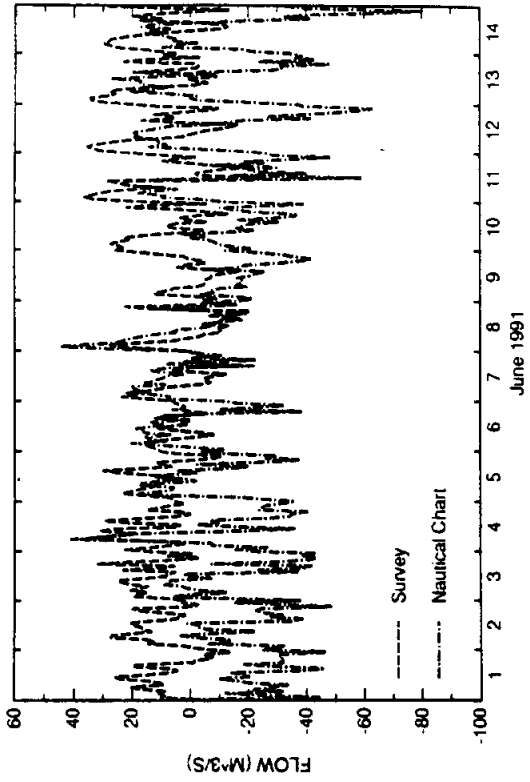


FIG. 6. Arroyo Colorado East of Laguna Atascosa

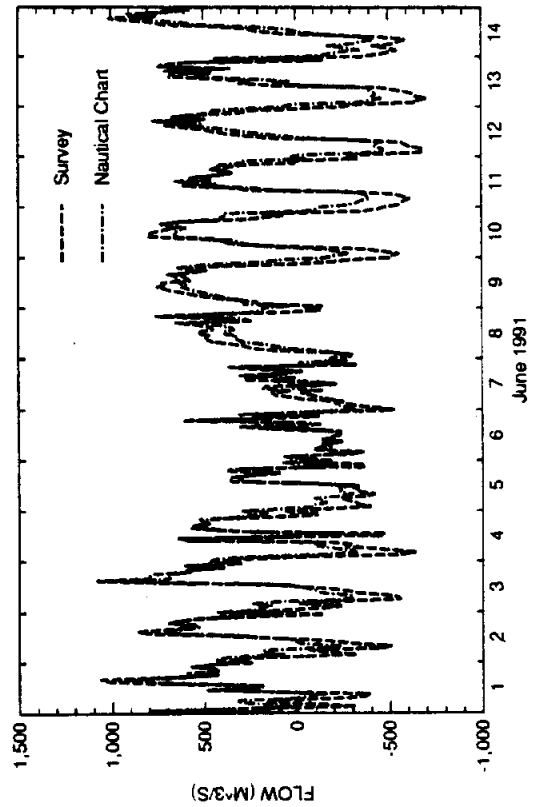


FIG. 7. Laguna Madre North of Port Isabel

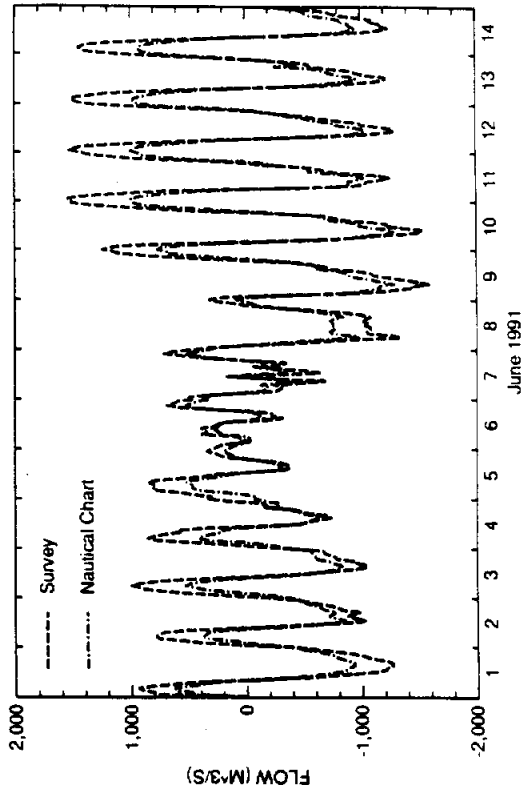


FIG. 8. Brazos-Santiago Pass

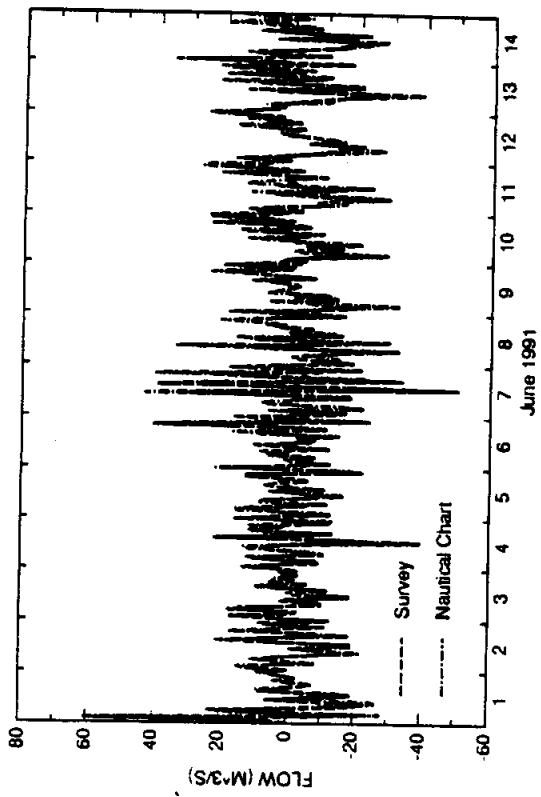


FIG. 9. Brownsville Ship Channel

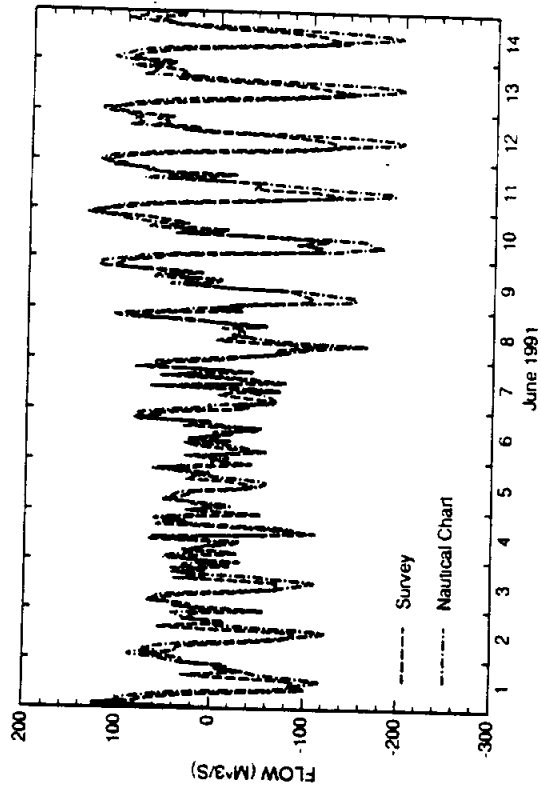
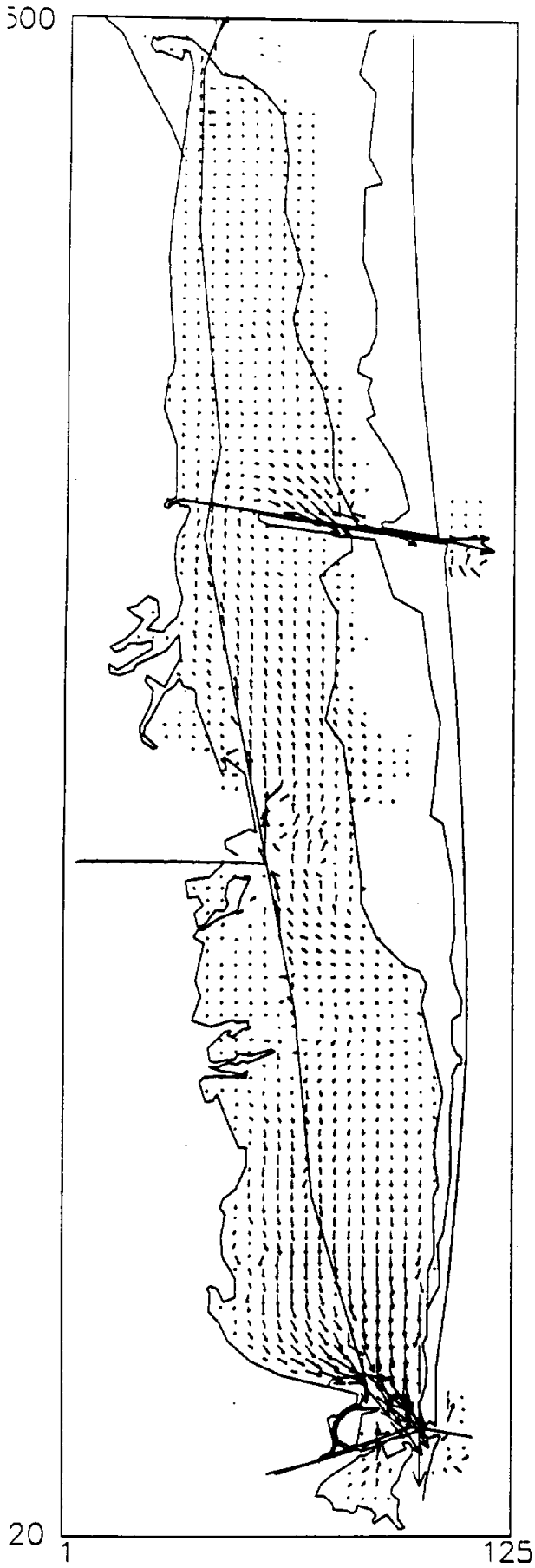


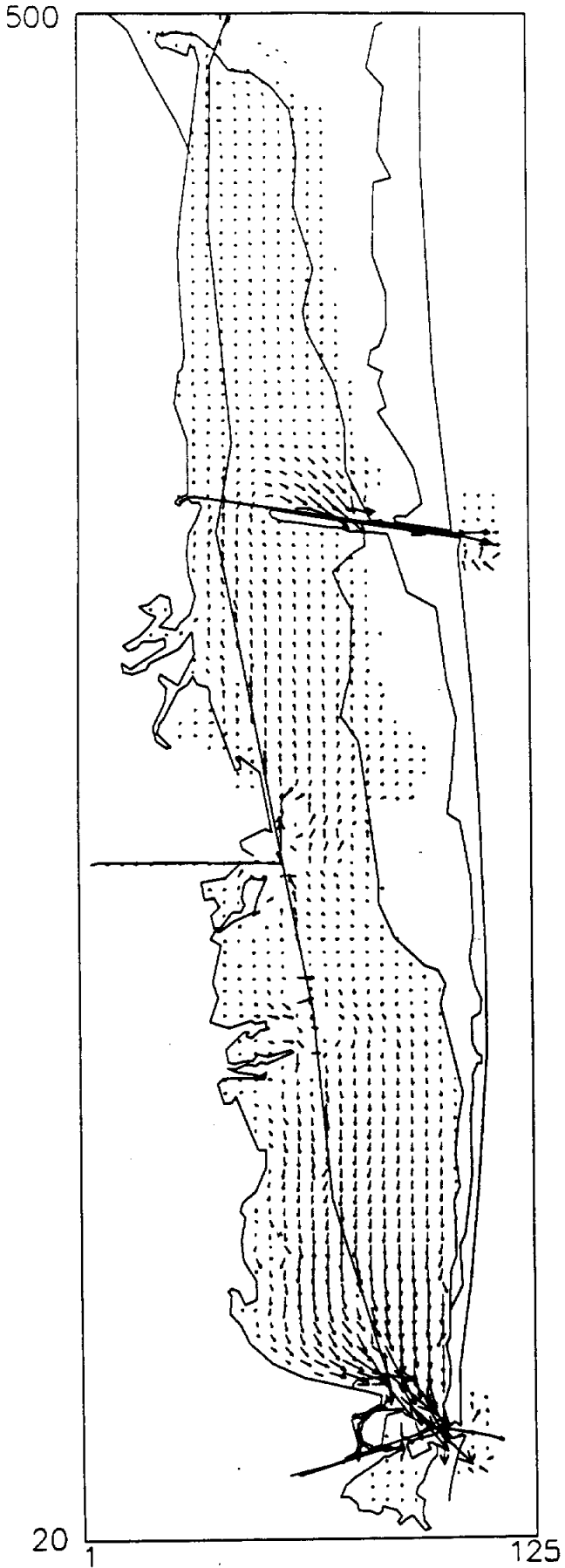
FIG. 10. South Bay Pass

**Velocity Vector Plots for the Calibrated Model
with the Hydrographic Survey Data**

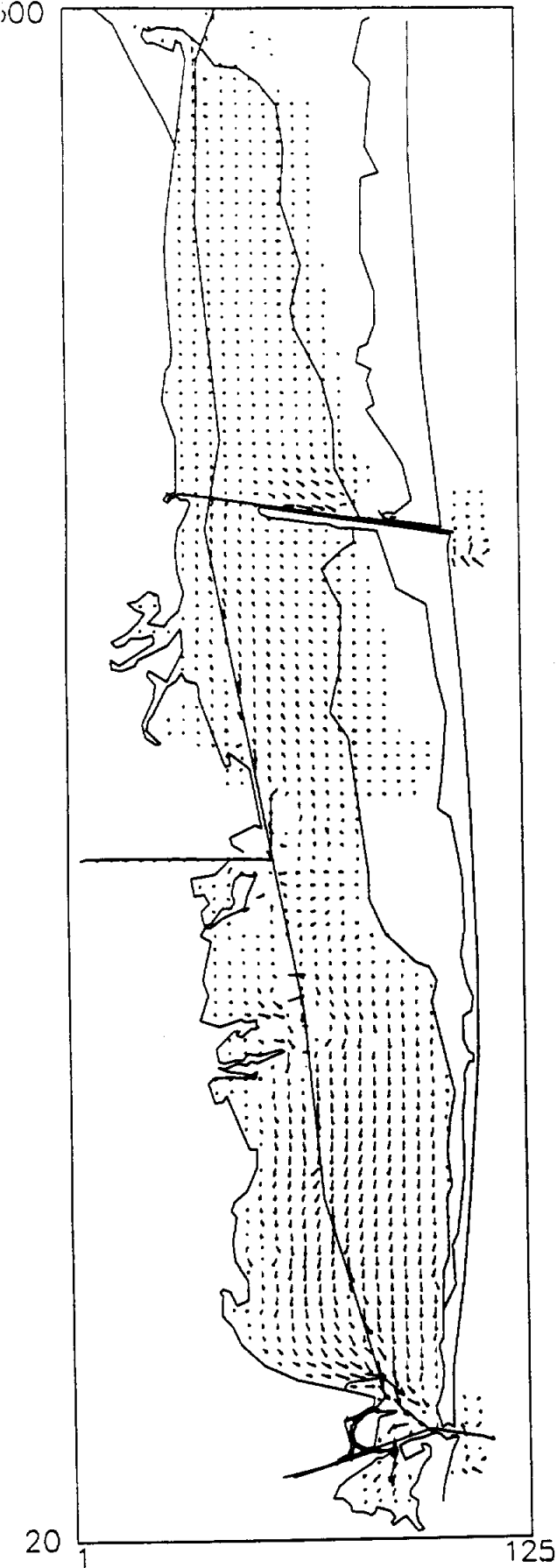
VELOCITY AT TIME 14400 GRID SIZE 125 BY 481



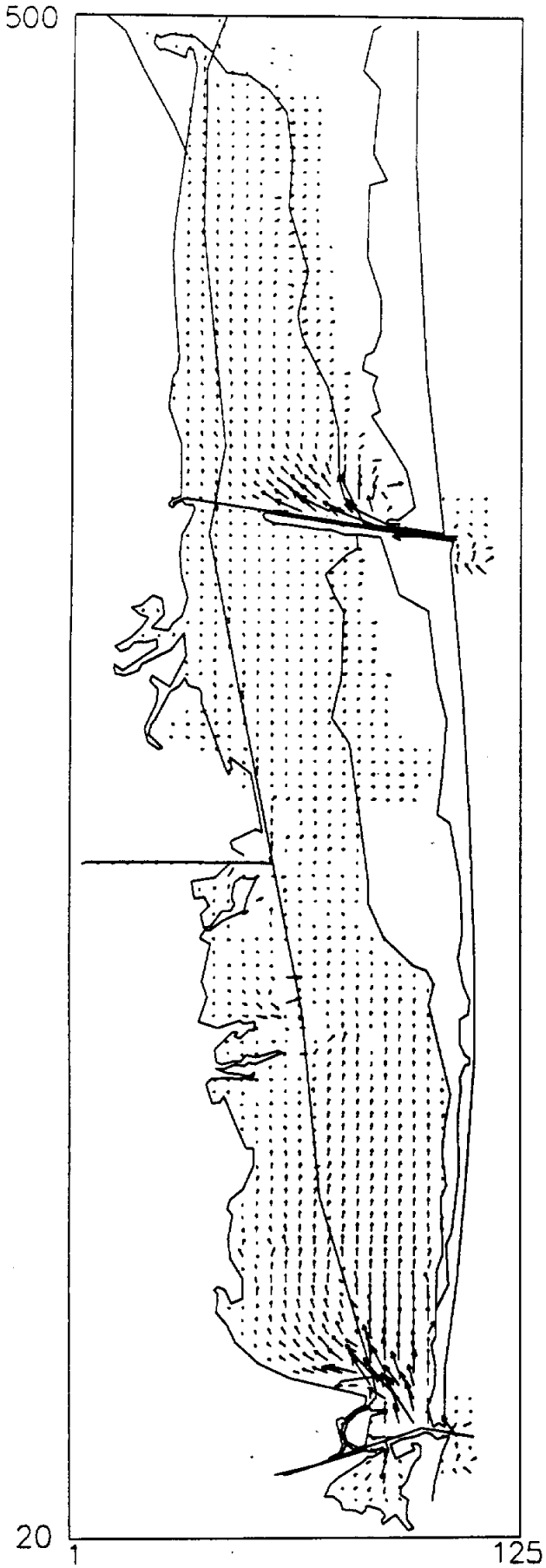
VELOCITY AT TIME 14580 GRID SIZE 125 BY 481



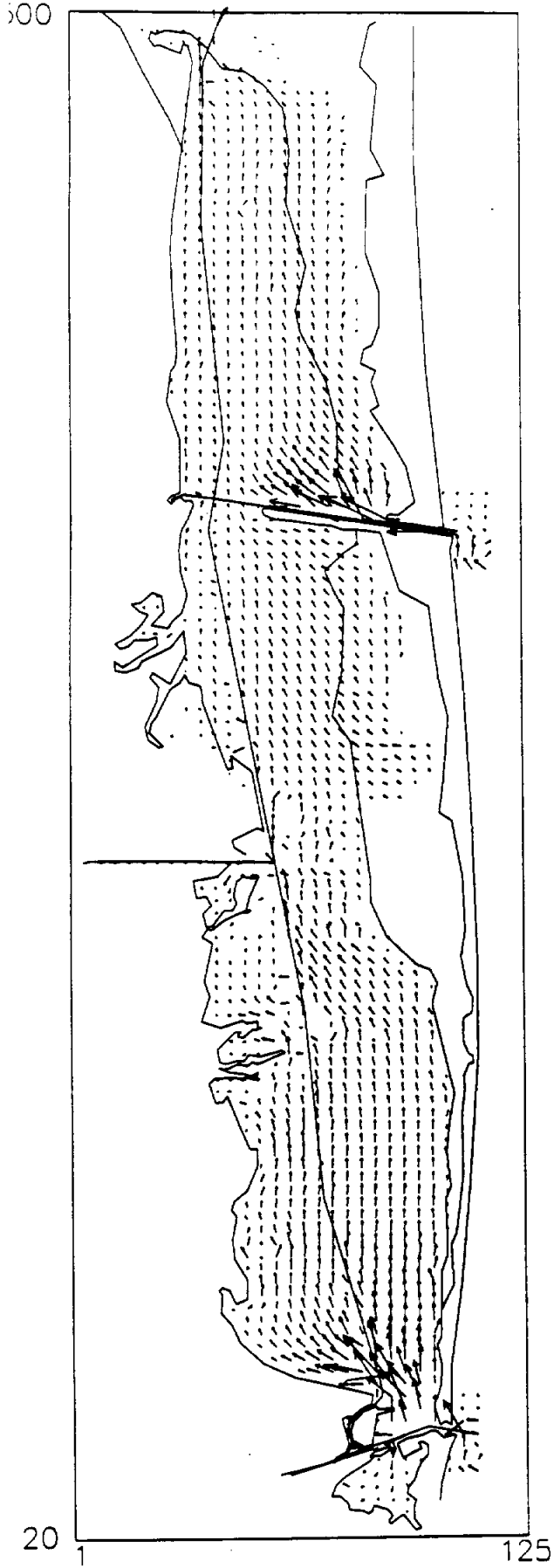
VELOCITY AT TIME 14760 GRID SIZE 125 BY 481



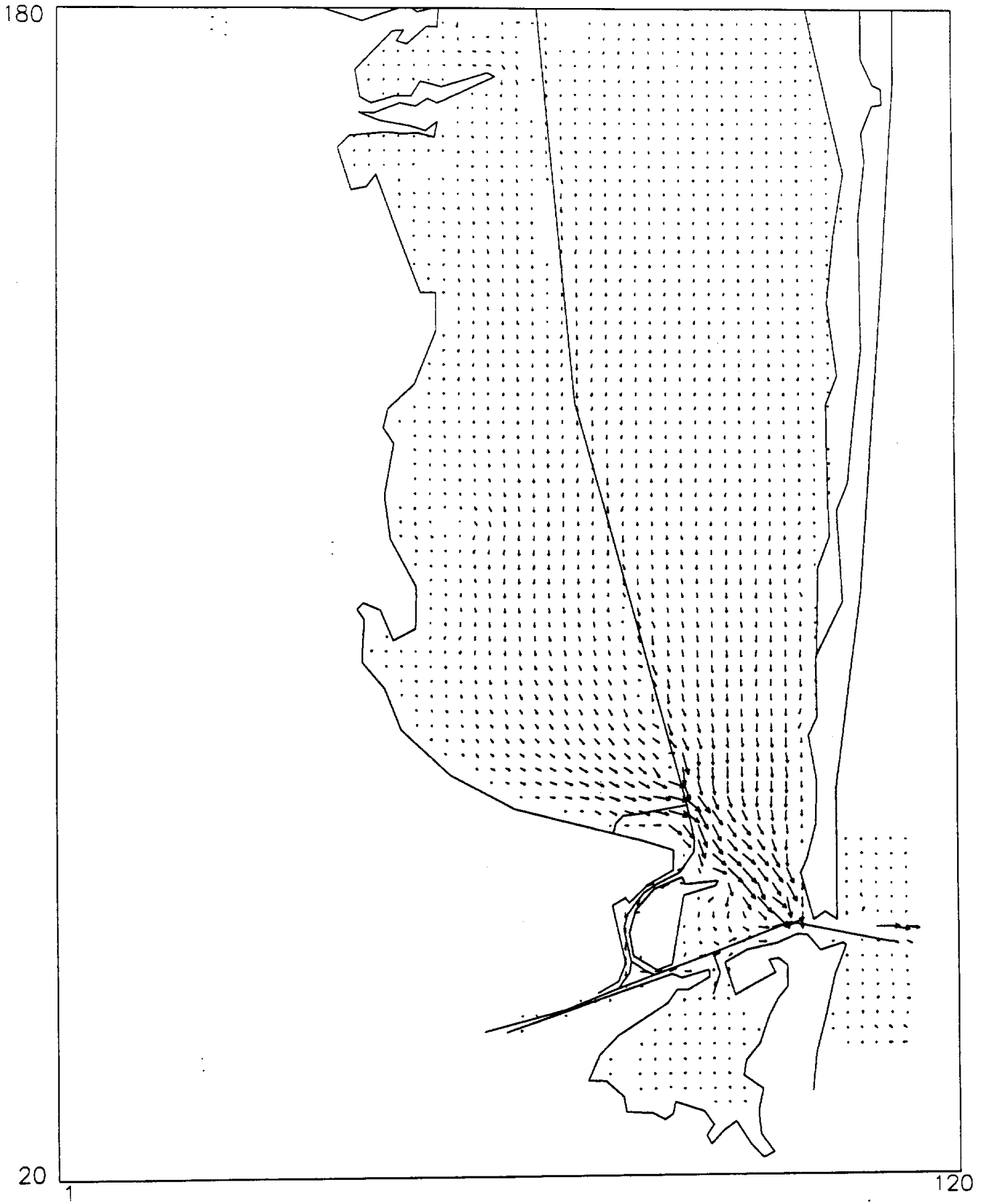
VELOCITY AT TIME 14940 GRID SIZE 125 BY 481



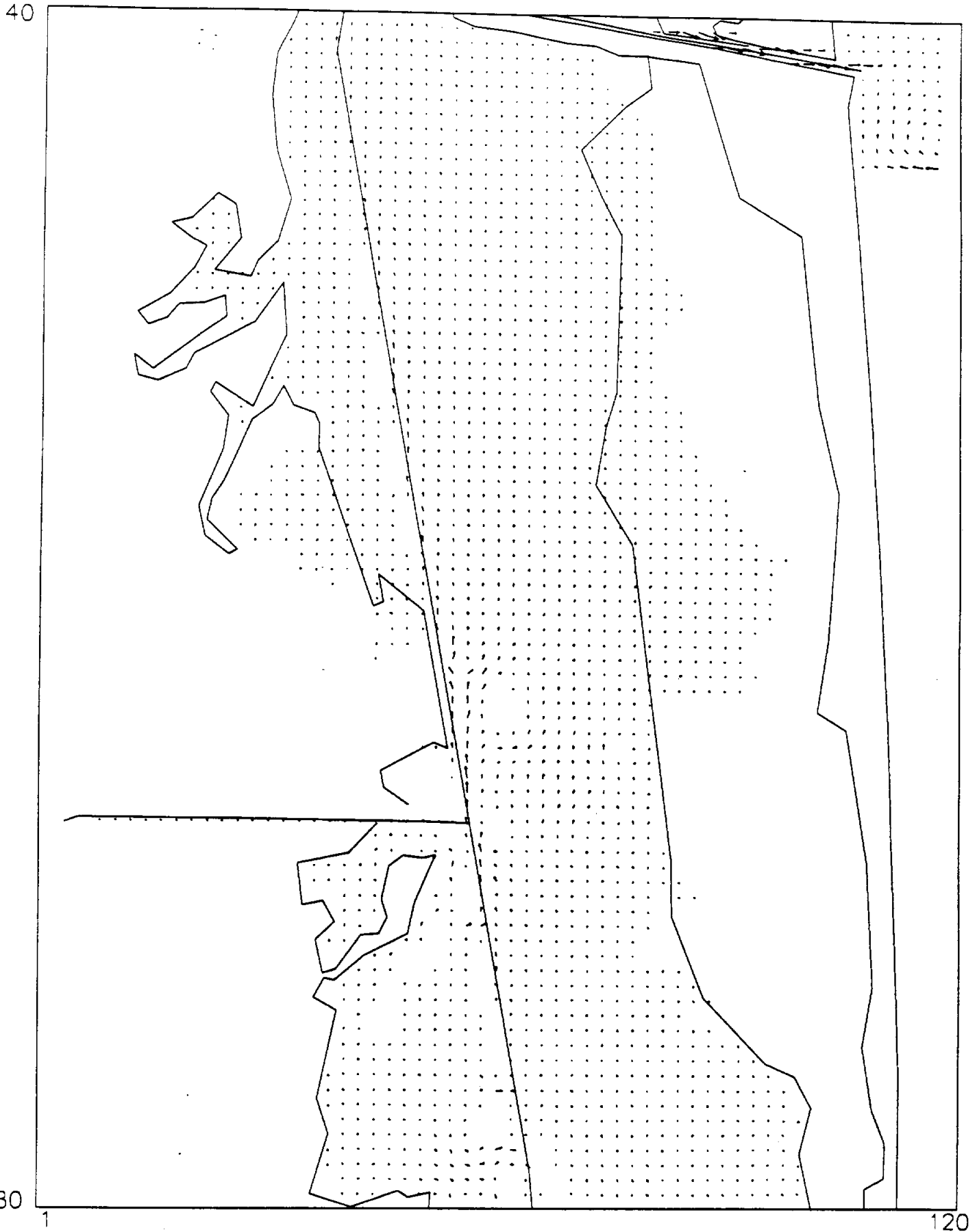
VELOCITY AT TIME 15120 GRID SIZE 125 BY 481



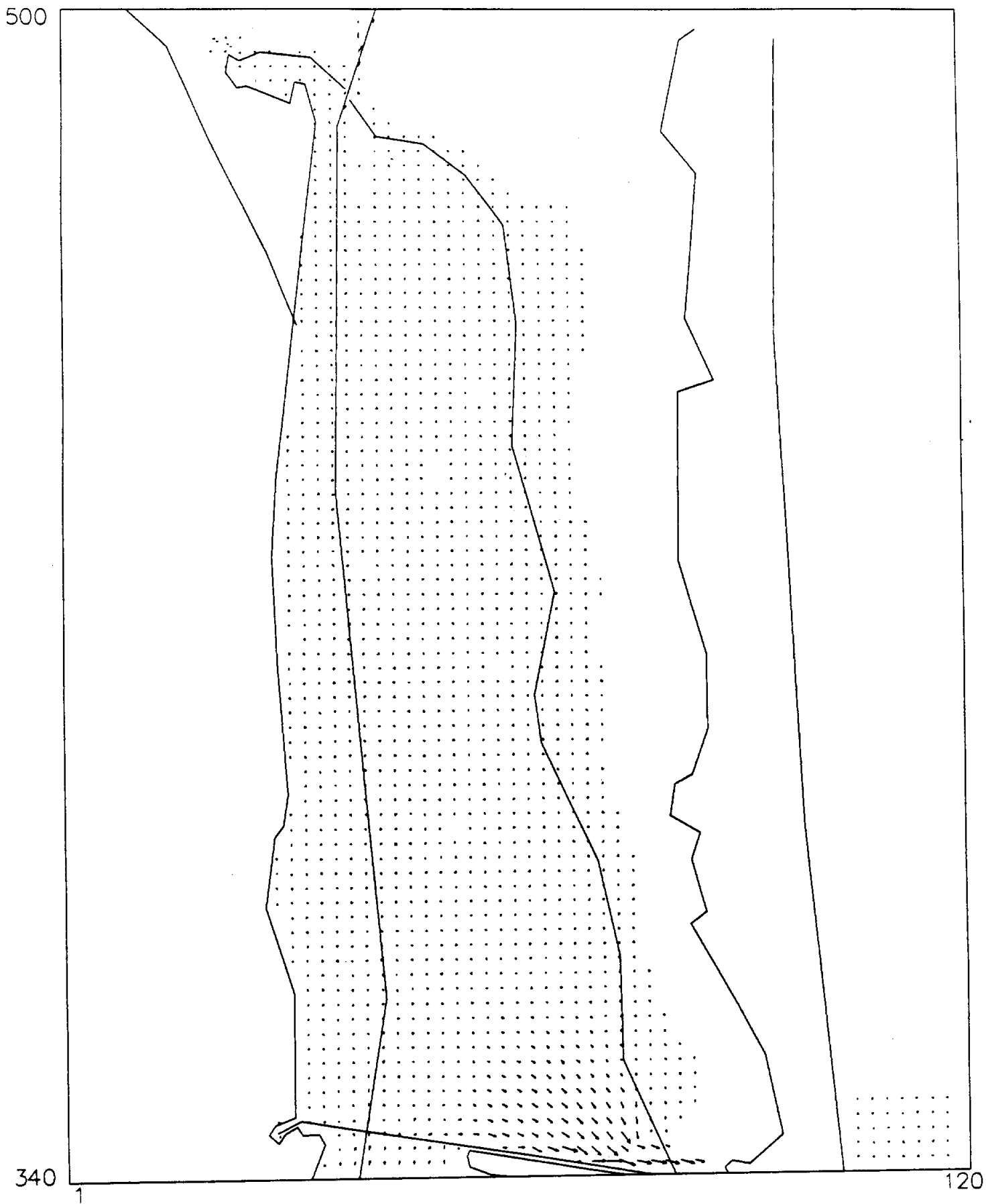
VELOCITY AT TIME 14580 GRID SIZE 120 BY 161



VELOCITY AT TIME 14580 GRID SIZE 20 BY 161

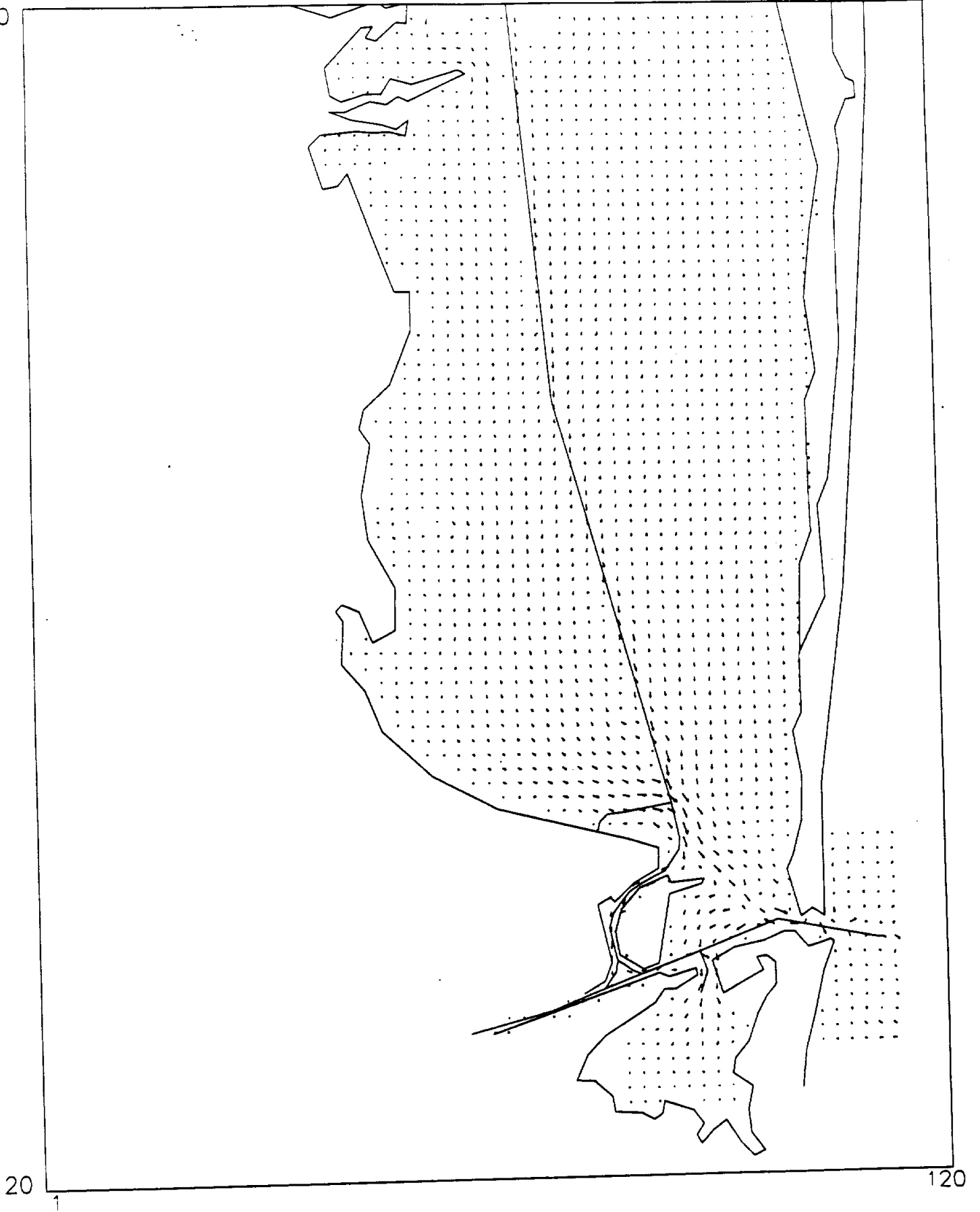


VELOCITY AT TIME 14580 GRID SIZE 120 BY 161



VELOCITY AT TIME 14760 GRID SIZE 120 BY 161

80



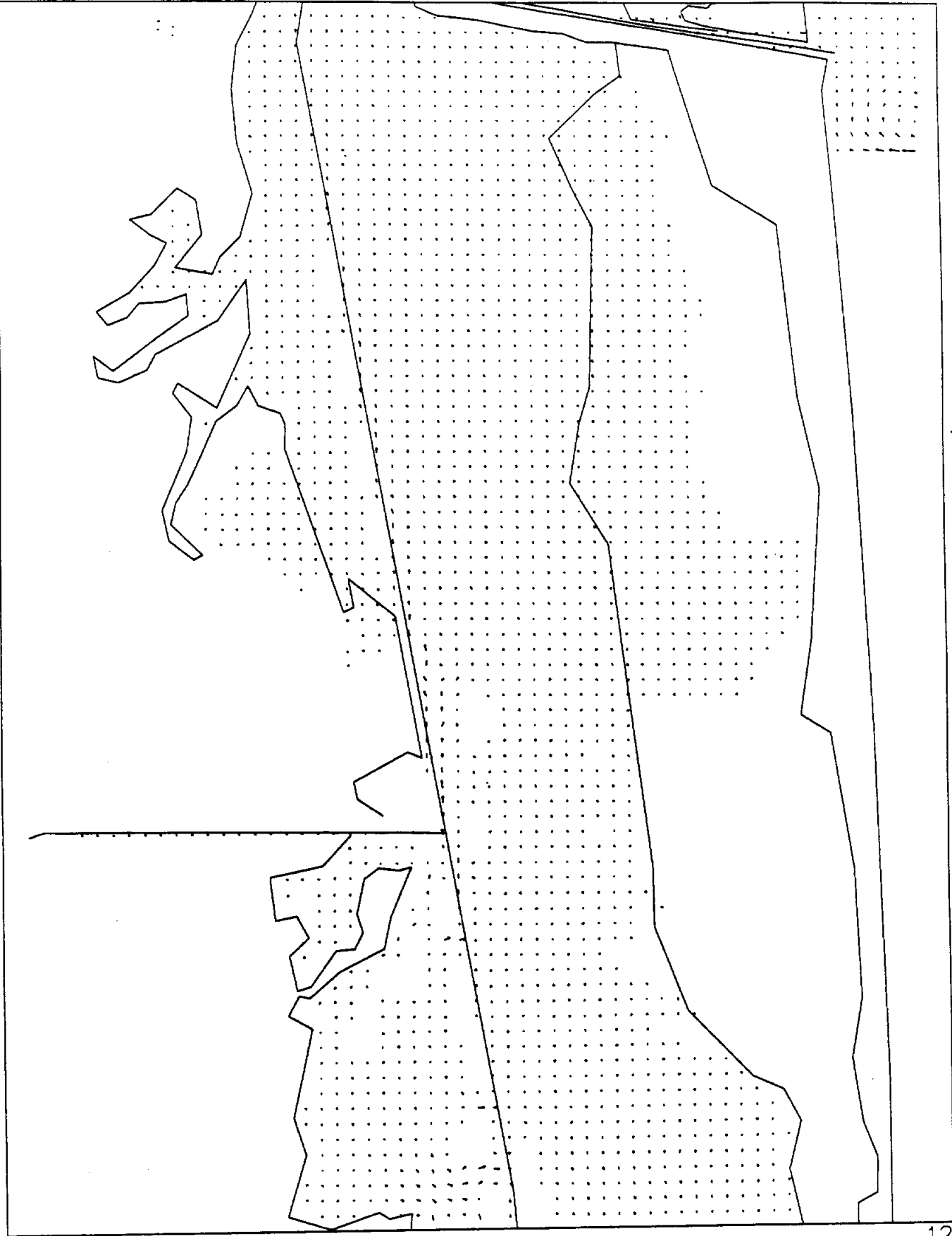
20

120

31

VELOCITY AT TIME 14760 GRID SIZE 120 BY 161

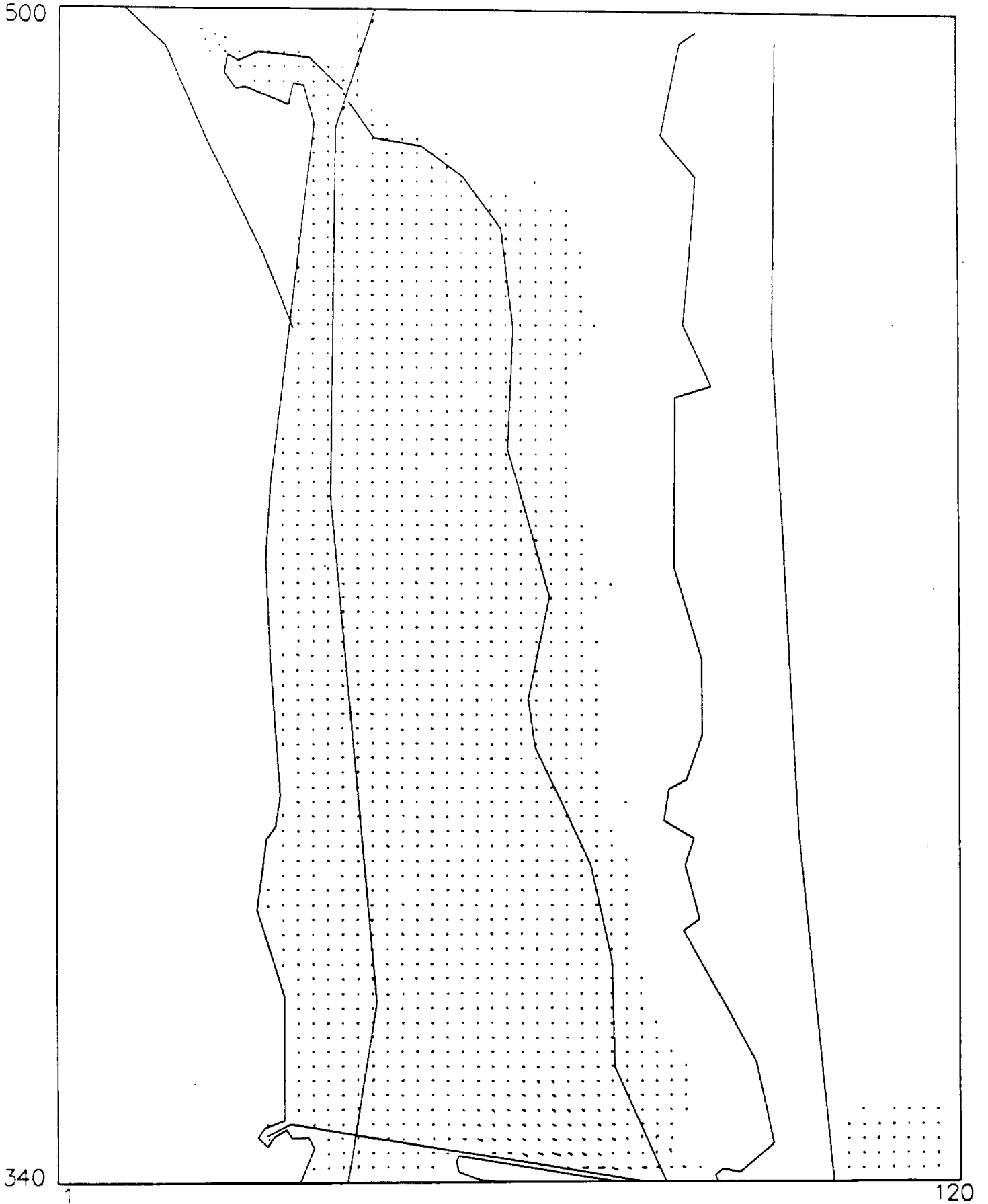
340



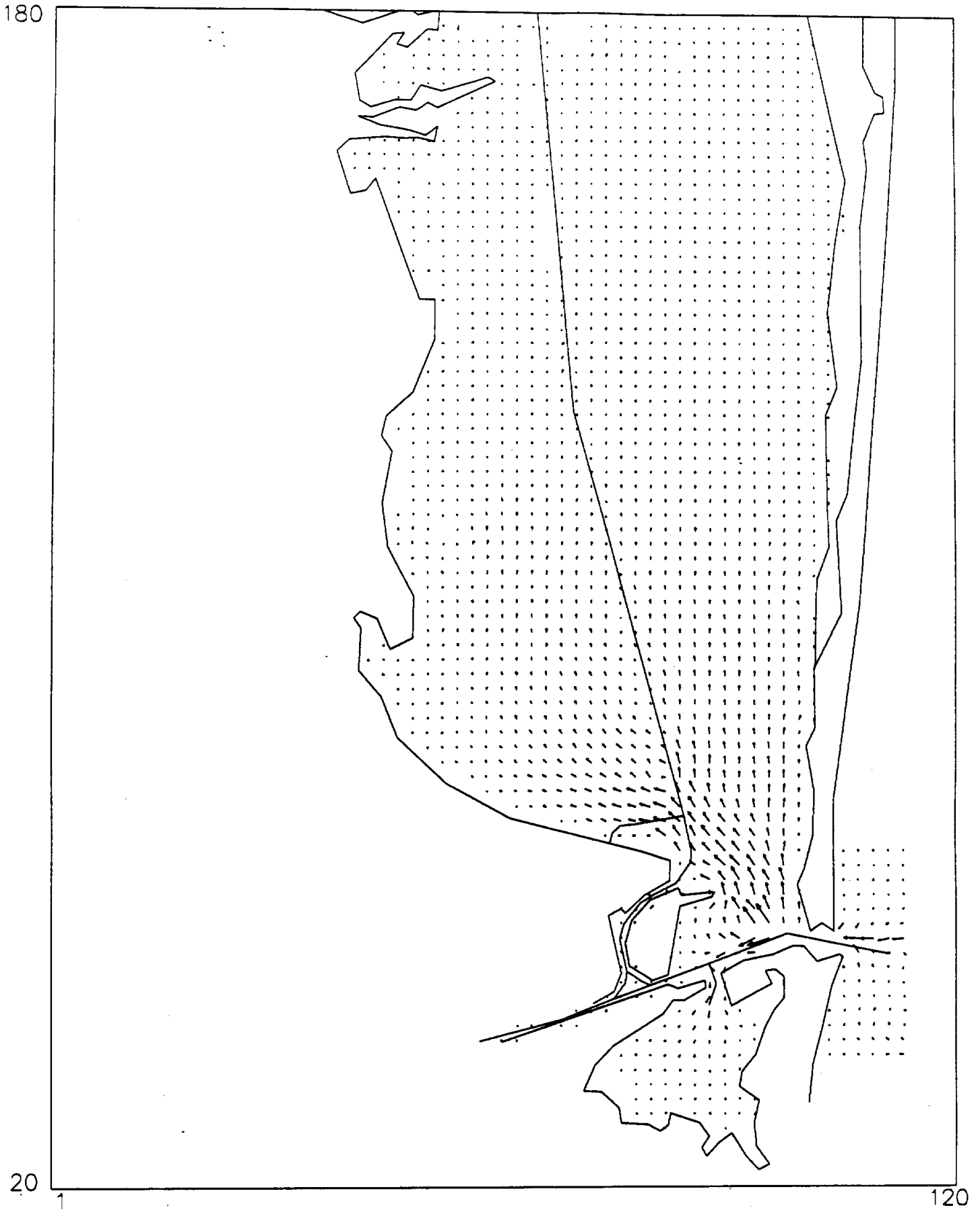
180

120

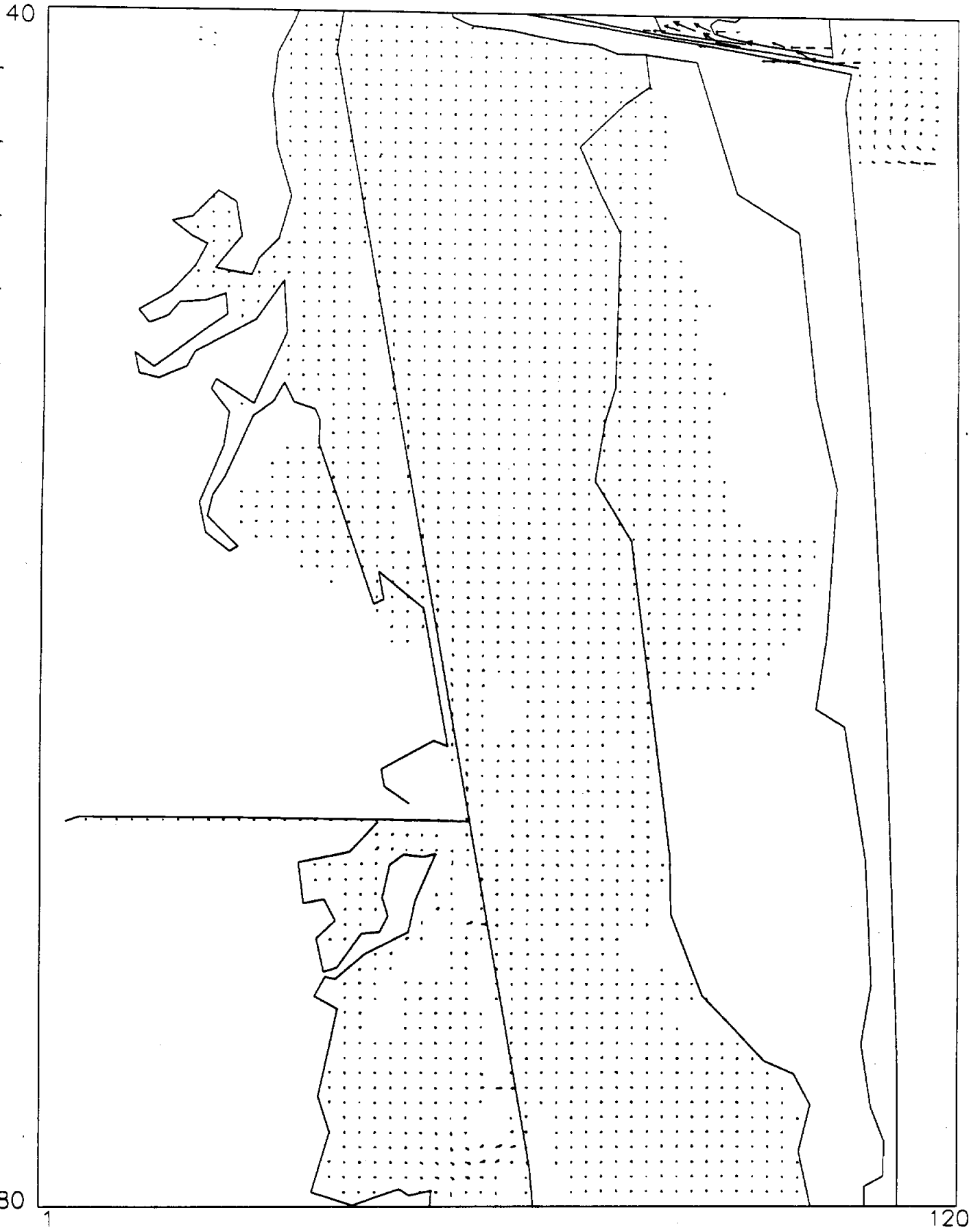
VELOCITY AT TIME 14760 GRID SIZE 120 BY 161



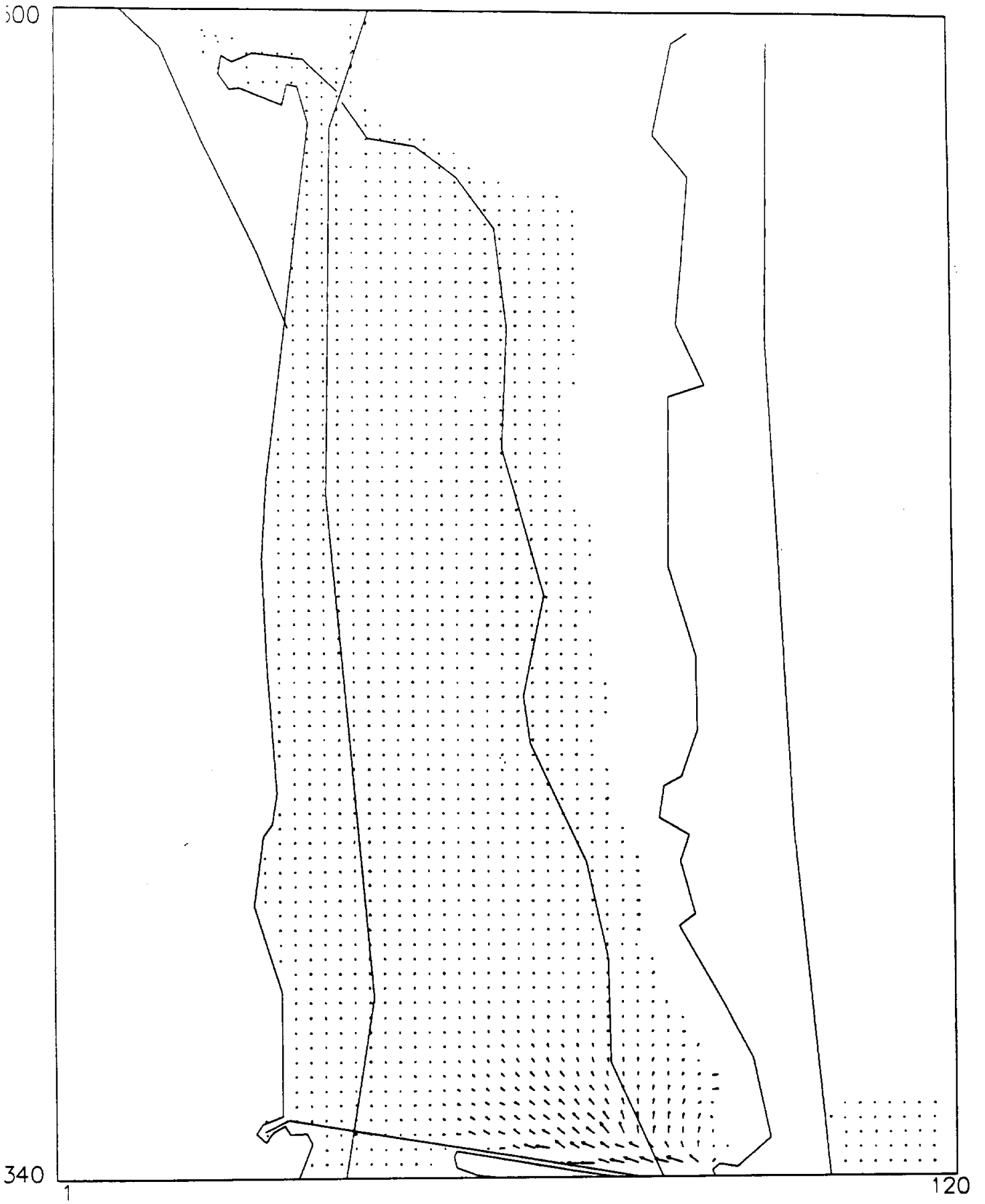
VELOCITY AT TIME 14940 GRID SIZE 120 BY 161



VELOCITY AT TIME 14940 GRID SIZE 120 BY 161

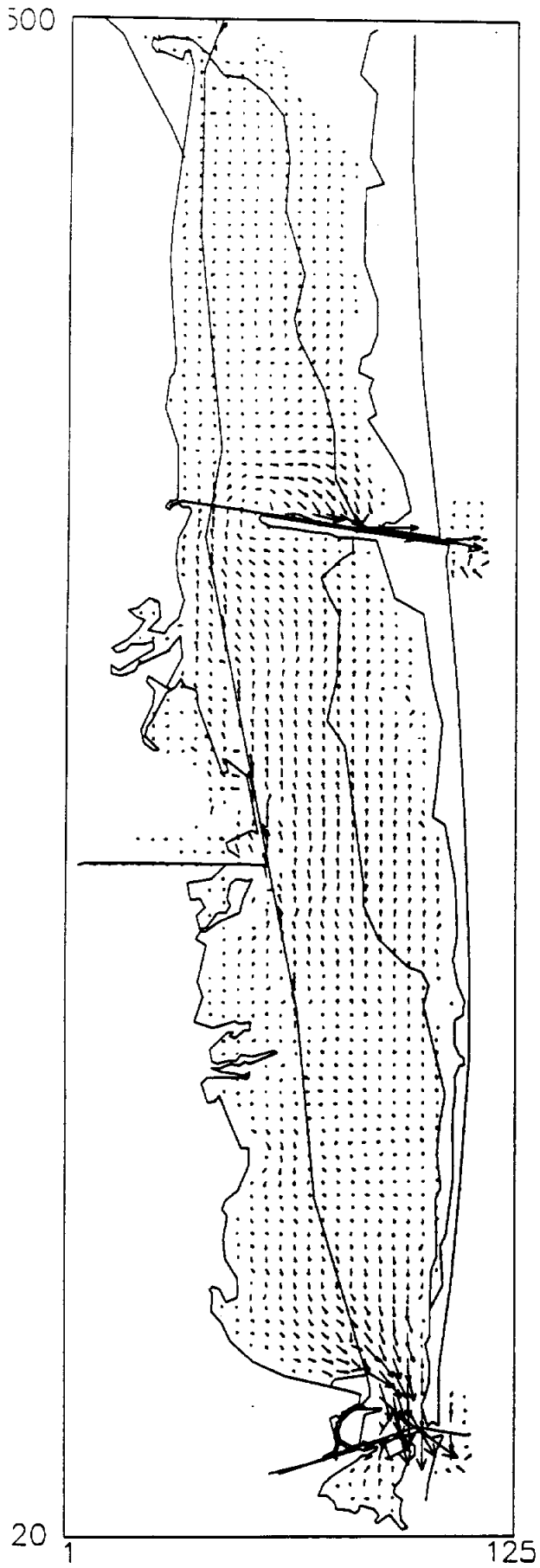


VELOCITY AT TIME 14940 GRID SIZE 120 BY 161

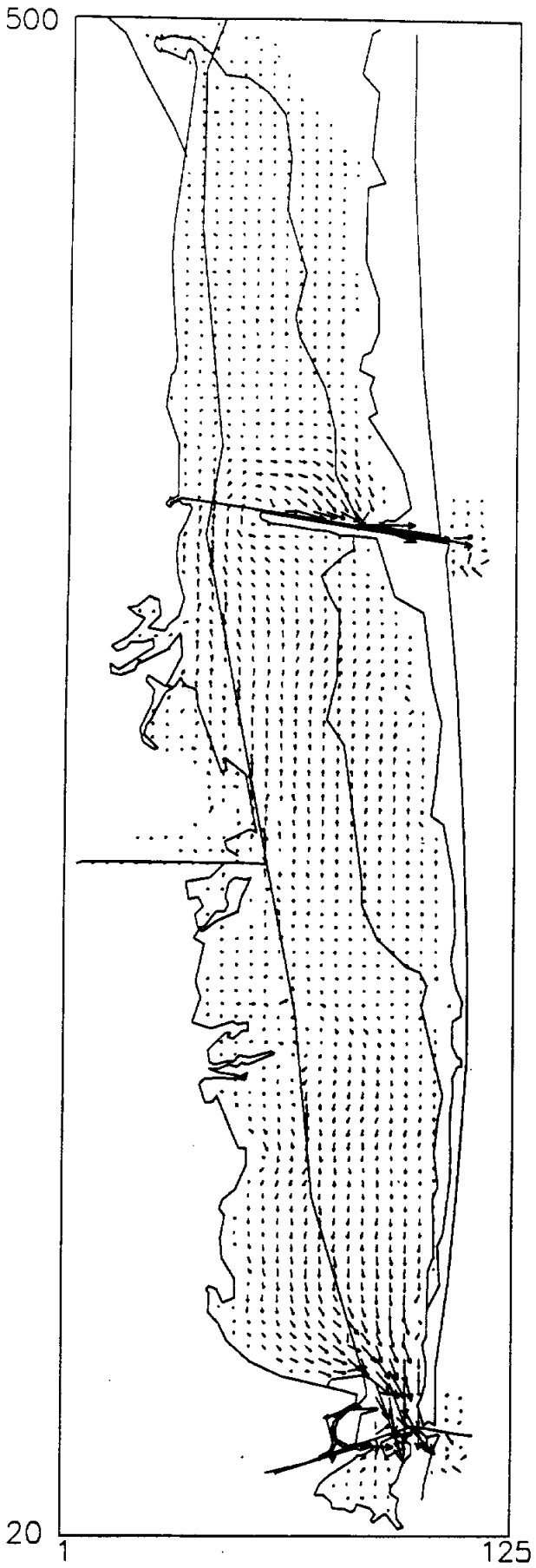


**Velocity Vector Plots for the Calibrated Model
with the Nautical Chart Data**

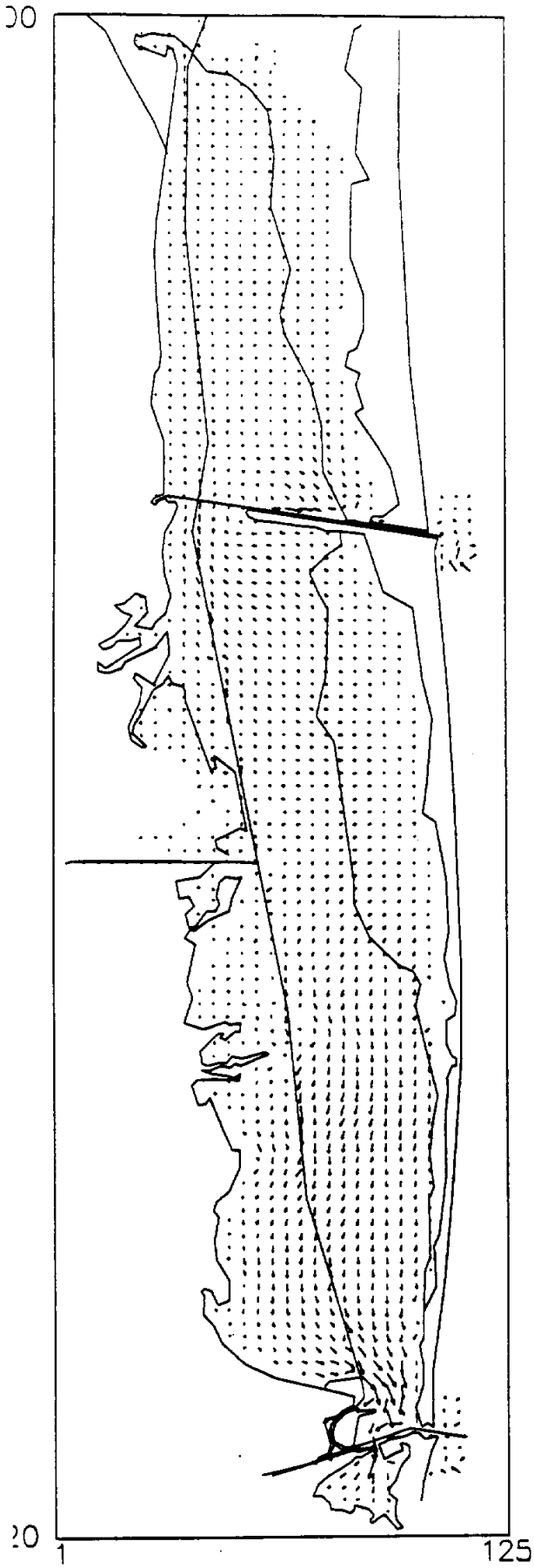
VELOCITY AT TIME 14400 GRID SIZE 125 BY 481



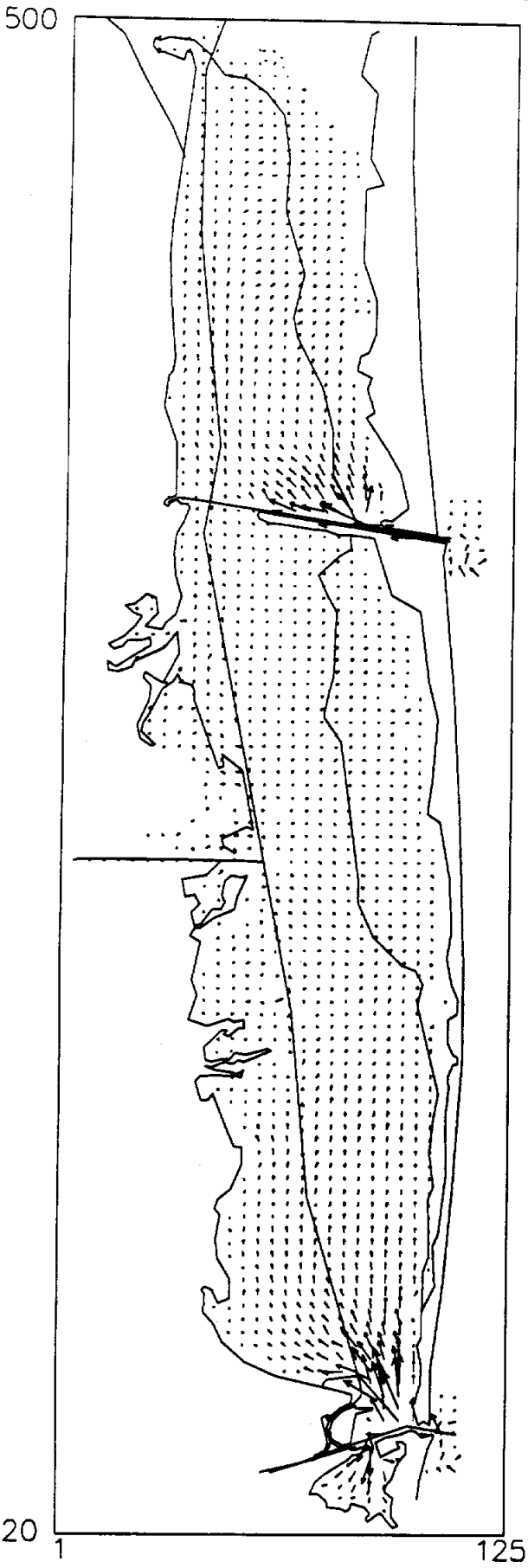
VELOCITY AT TIME 14580 GRID SIZE 125 BY 481



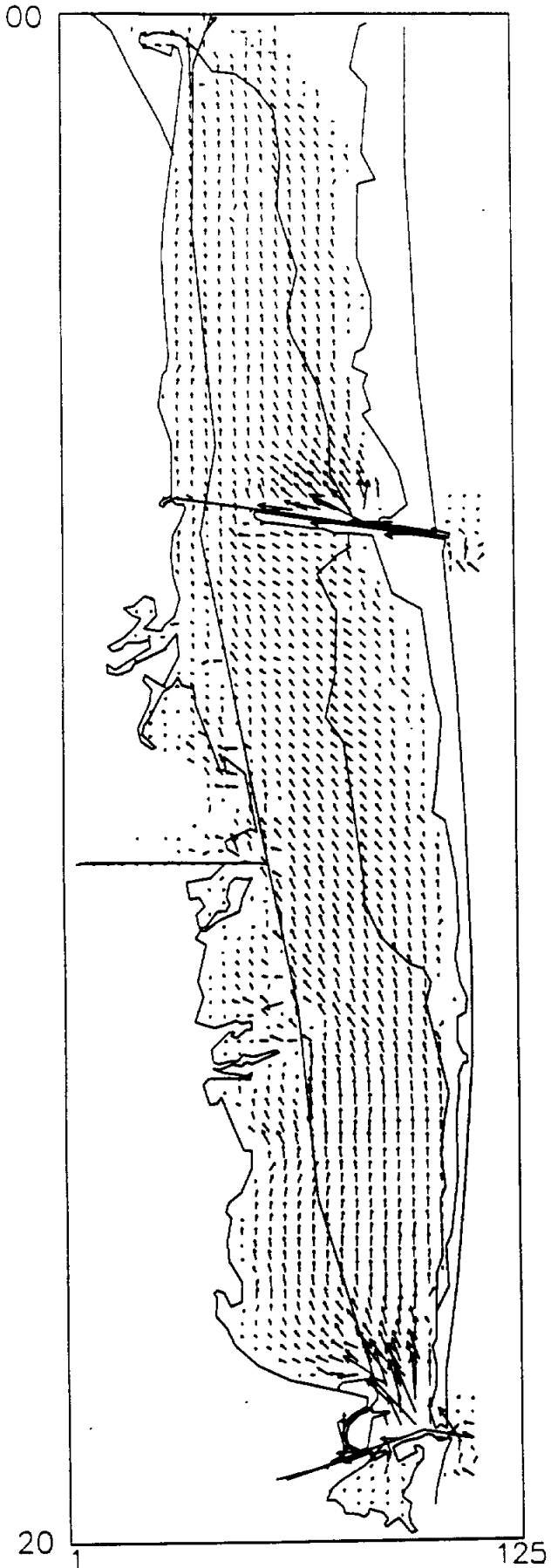
VELOCITY AT TIME 14760 GRID SIZE 125 BY 481



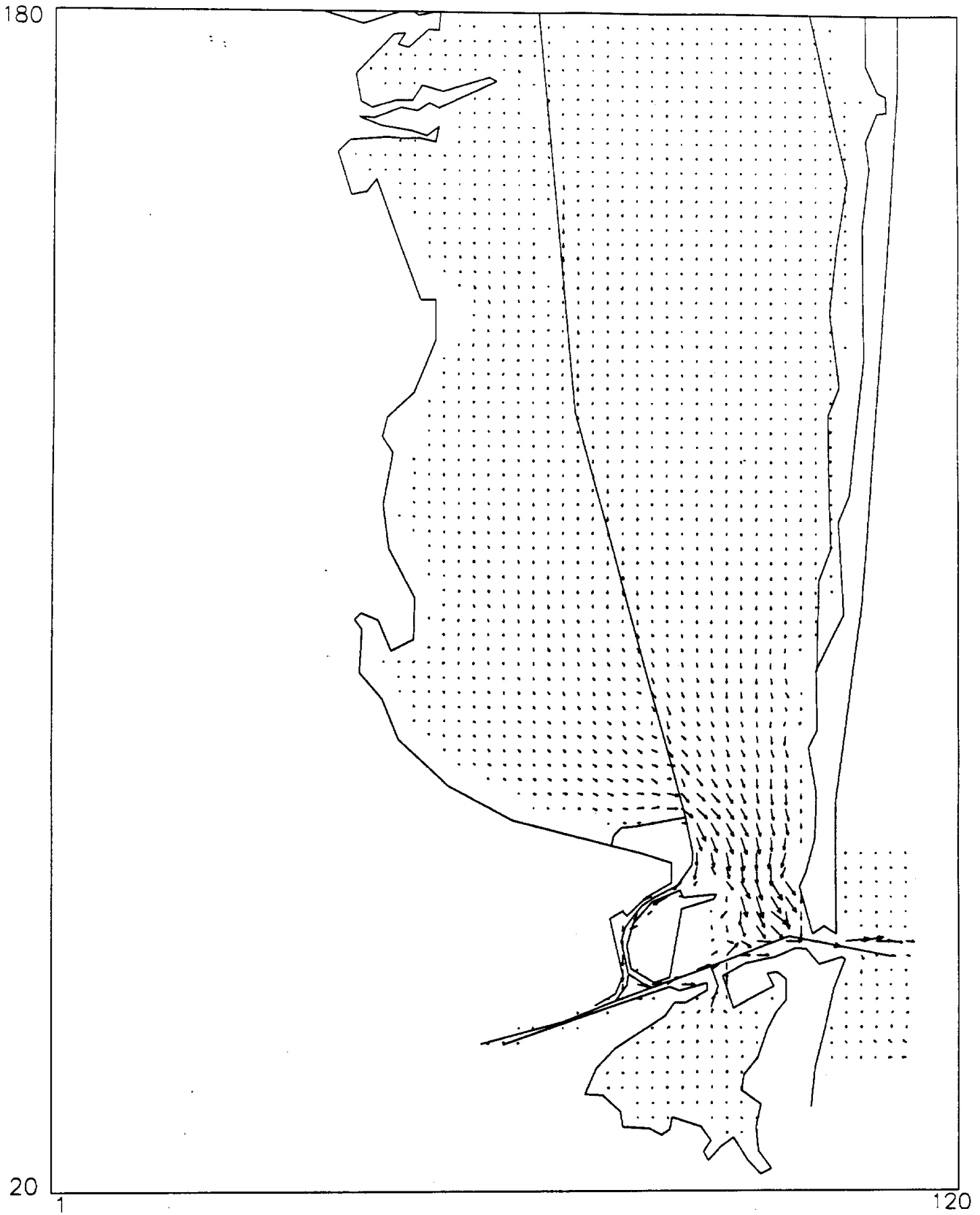
VELOCITY AT TIME 14940 GRID SIZE 125 BY 481



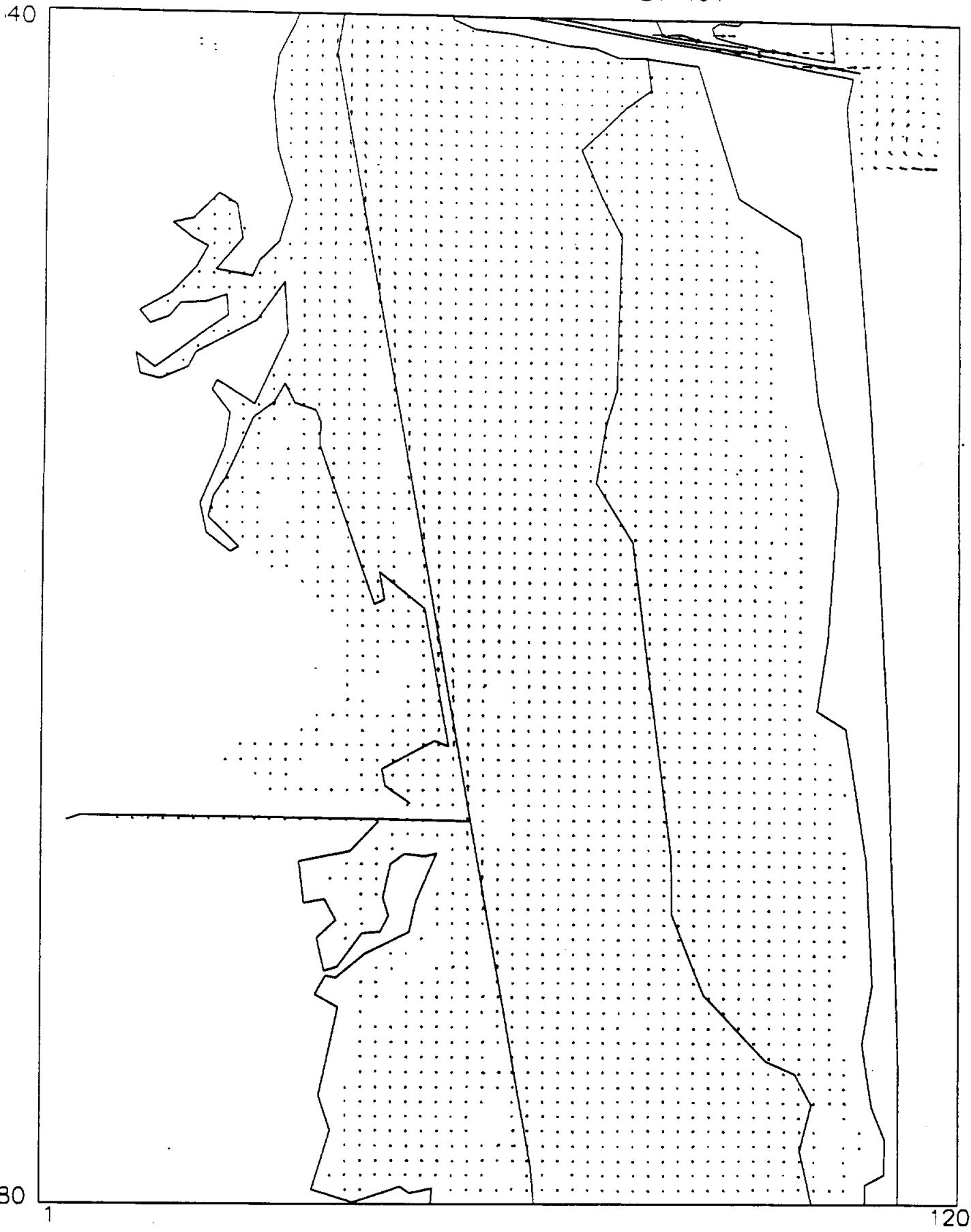
VELOCITY AT TIME 15120 GRID SIZE 125 BY 481



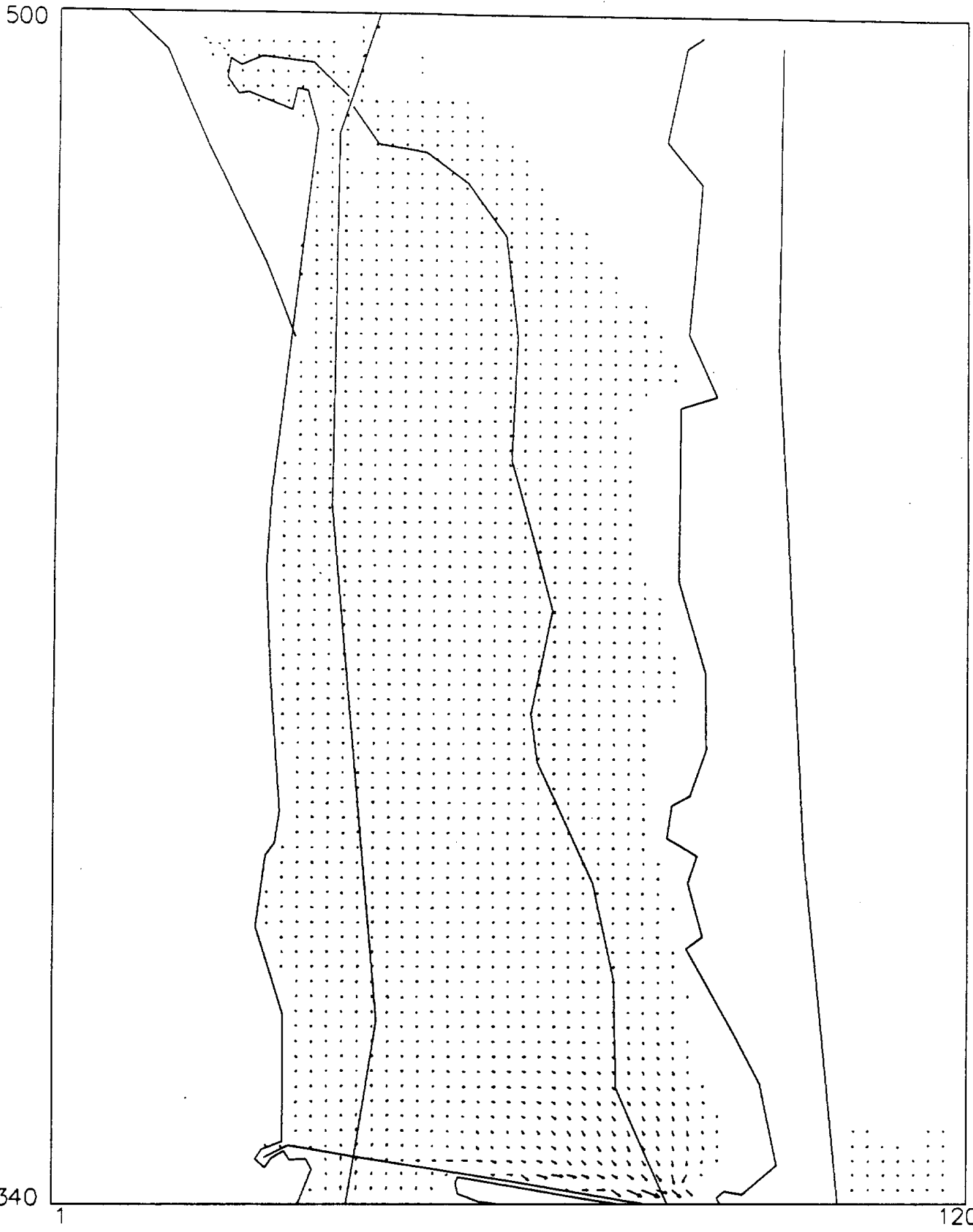
VELOCITY AT TIME 14580 GRID SIZE 120 BY 161



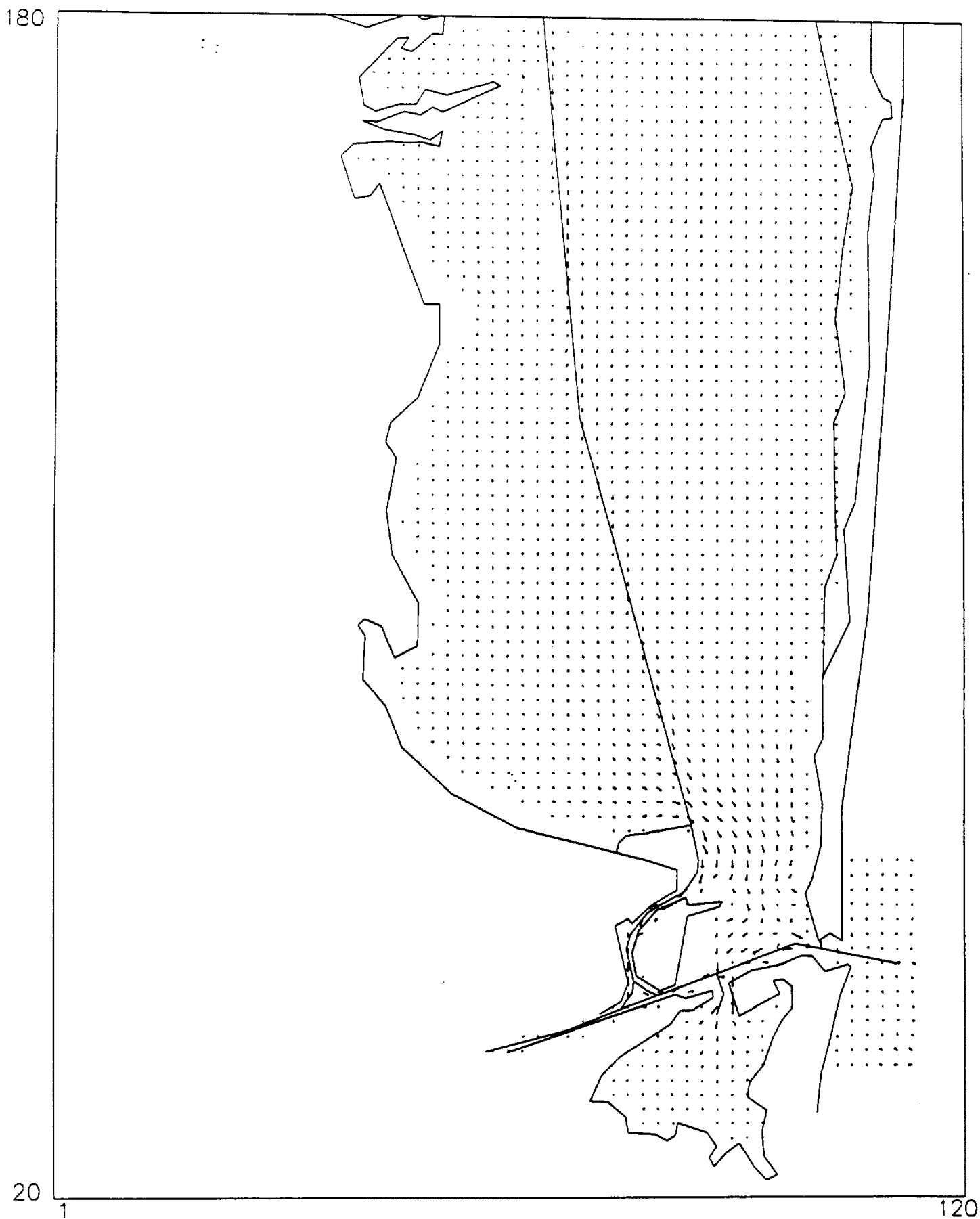
VELOCITY AT TIME 14580 GRID SIZE 120 BY 161



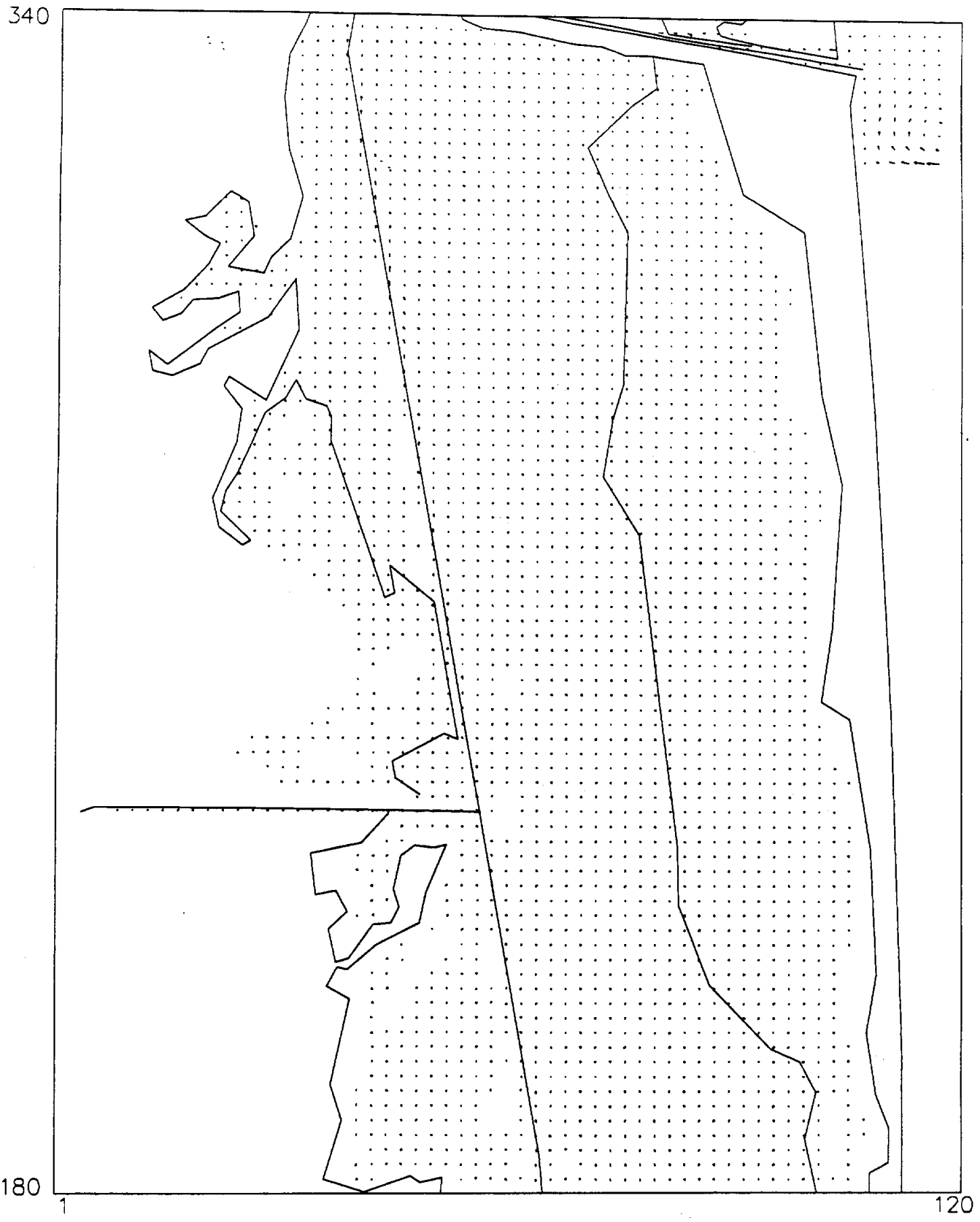
VELOCITY AT TIME 14580 GRID SIZE 120 BY 161



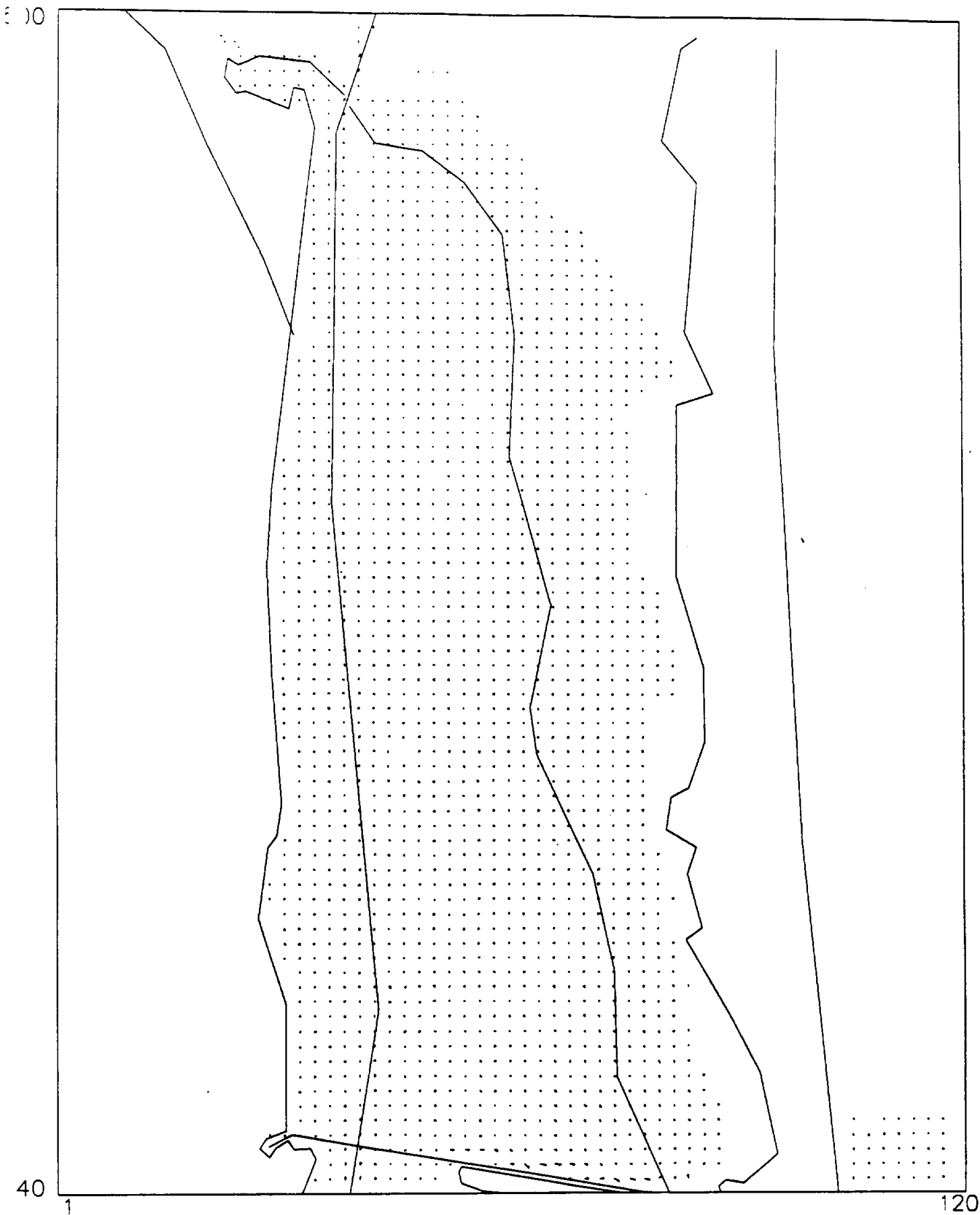
VELOCITY AT TIME 14760 GRID SIZE 120 BY 161



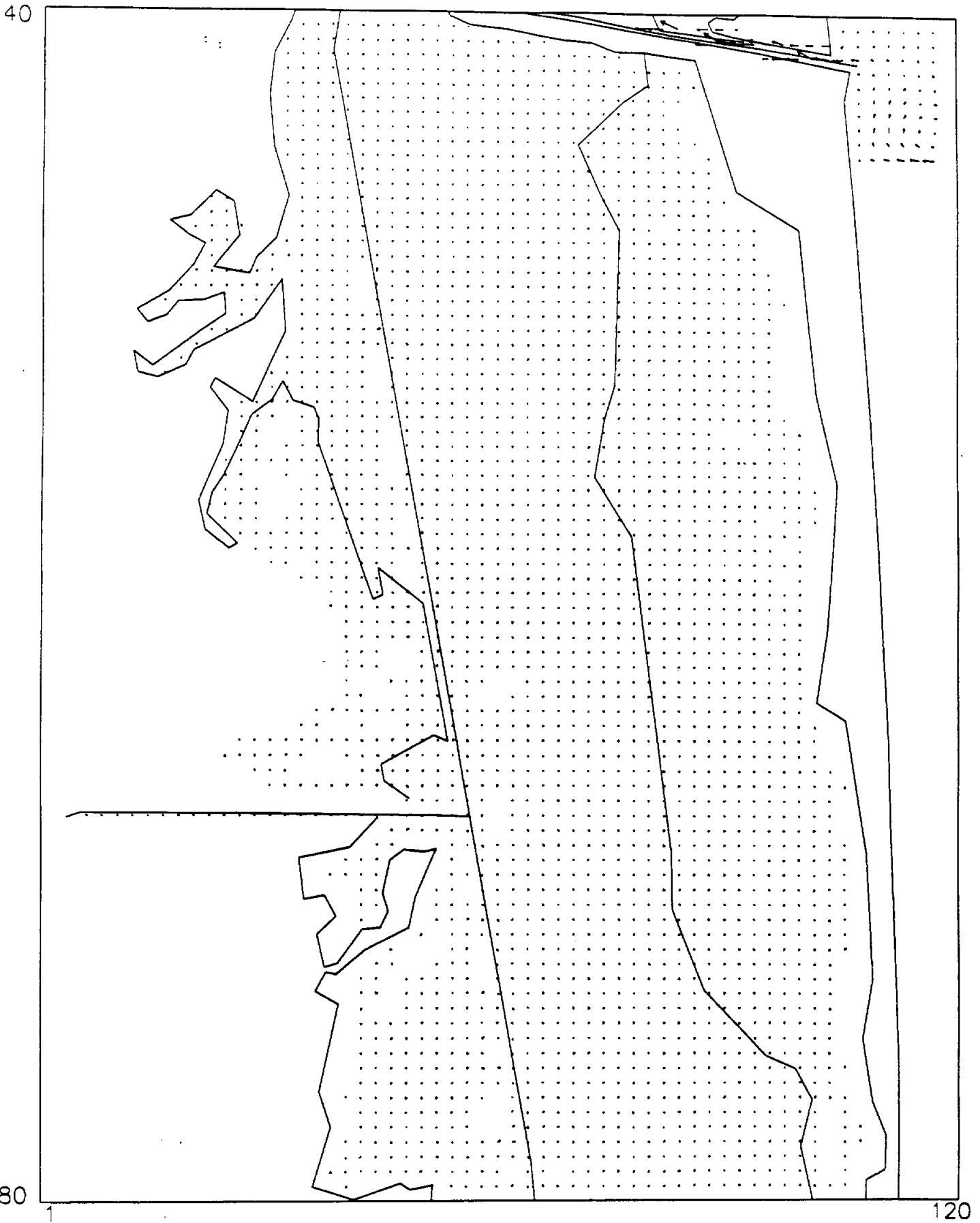
VELOCITY AT TIME 14760 GRID SIZE 120 BY 161



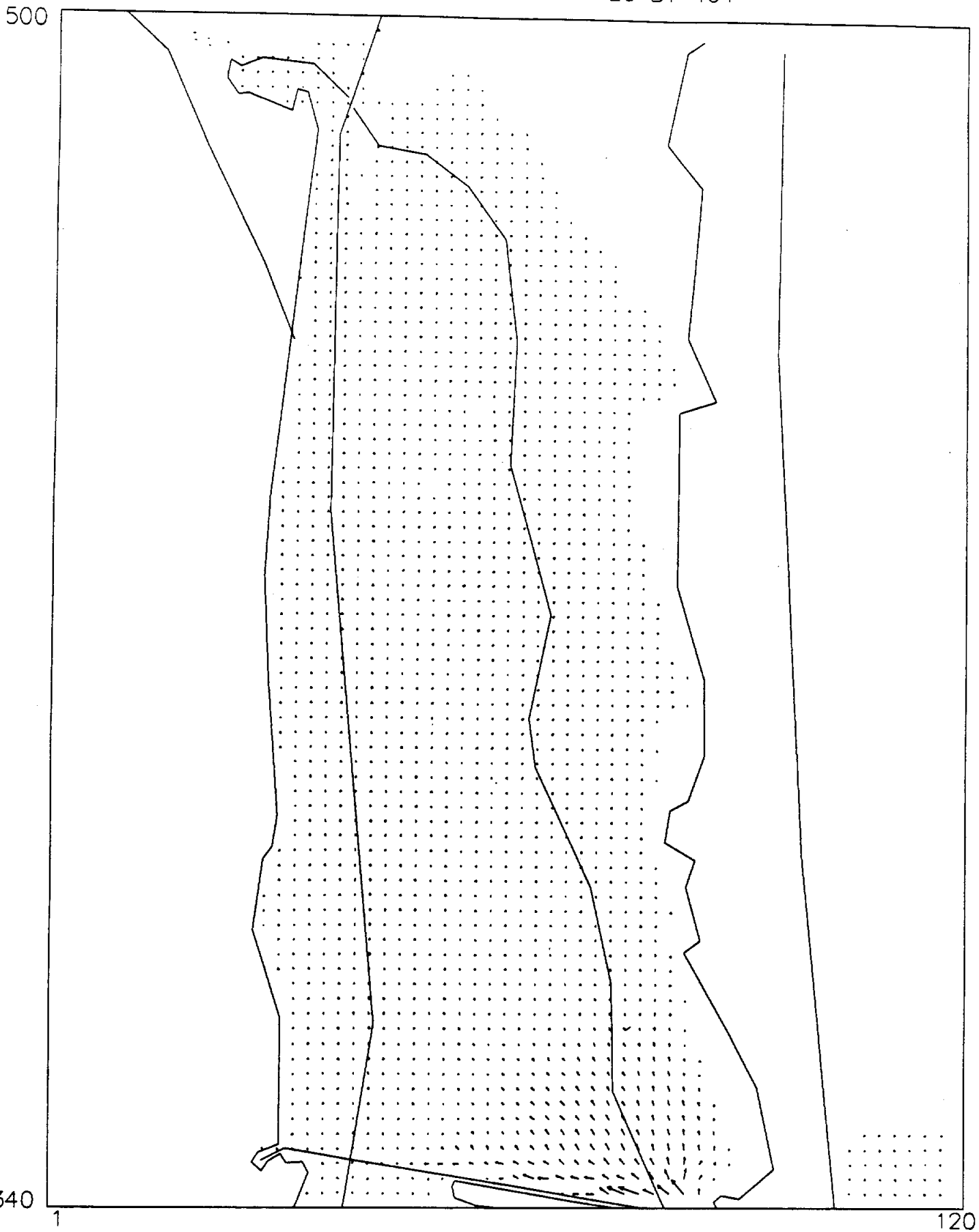
VELOCITY AT TIME 14760 GRID SIZE 120 BY 161



VELOCITY AT TIME 14940 GRID SIZE 120 BY 161



VELOCITY AT TIME 14940 GRID SIZE 120 BY 161



SWIFT2D SIMULATIONS

Manning's n Variation Simulation

Manning's n = 0.030 throughout the model

Wind Stress = 0.0015

Time Step = 6 minutes

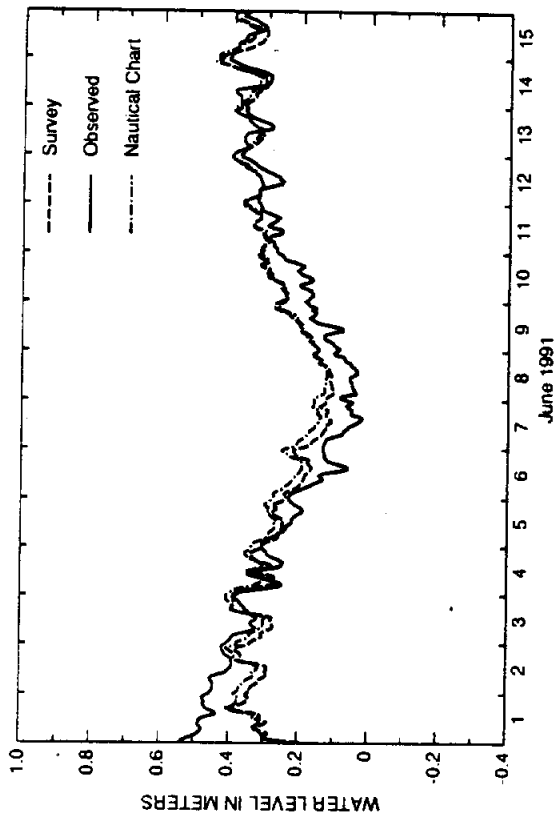


FIG. 1. Rincon Del San Jose Tide Station

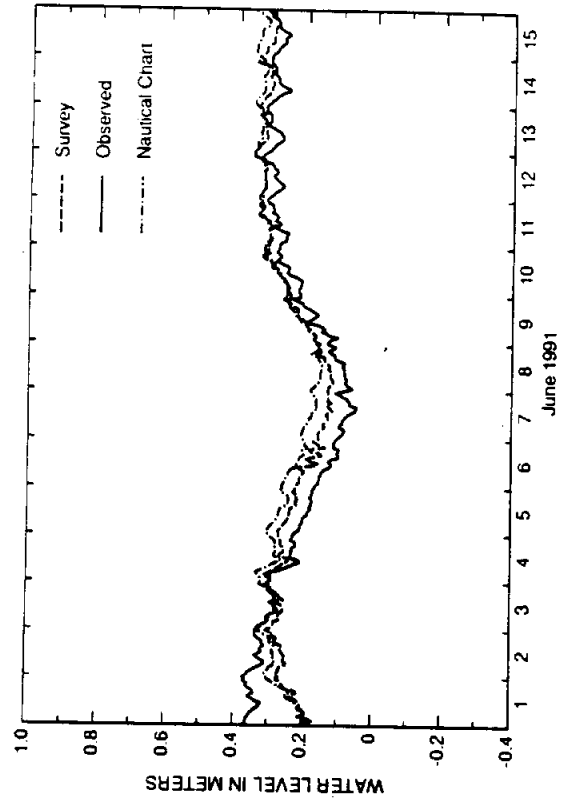


FIG. 2. Port Mansfield Tide Station

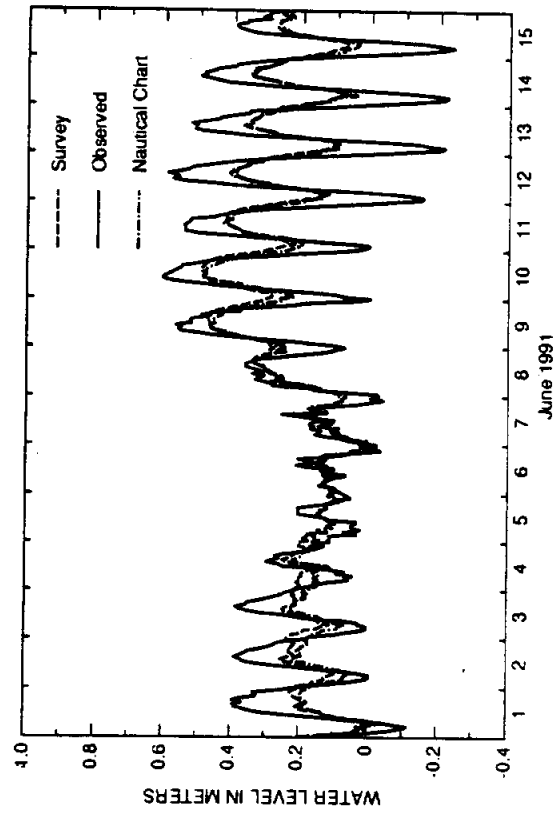


FIG. 3. Port Isabel Tide Station

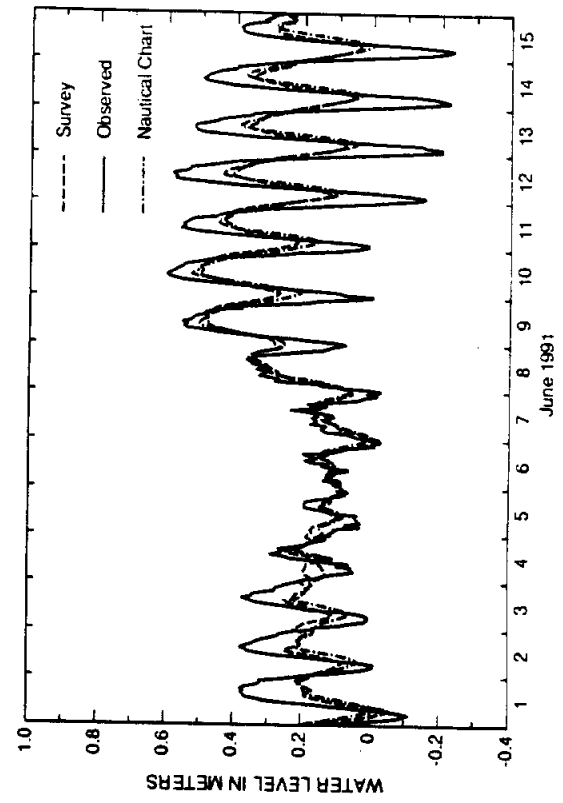


FIG. 4. South Bay Tide Station.

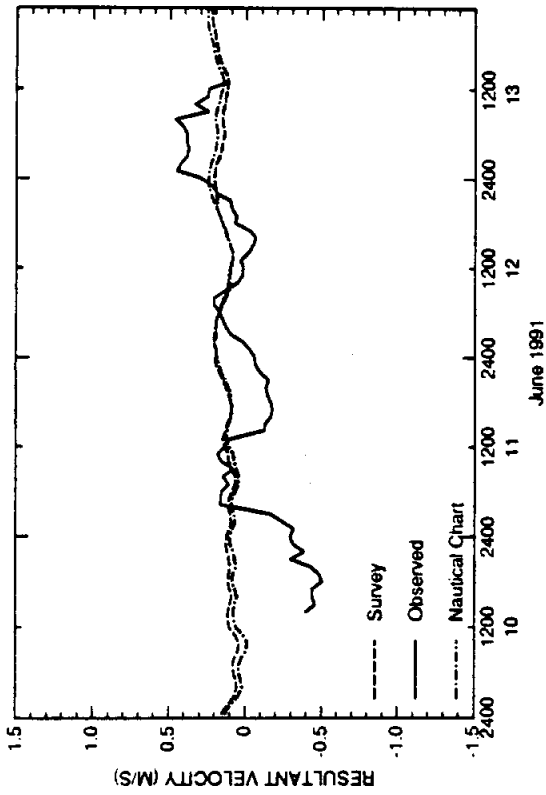


FIG. 1. South Land Cut

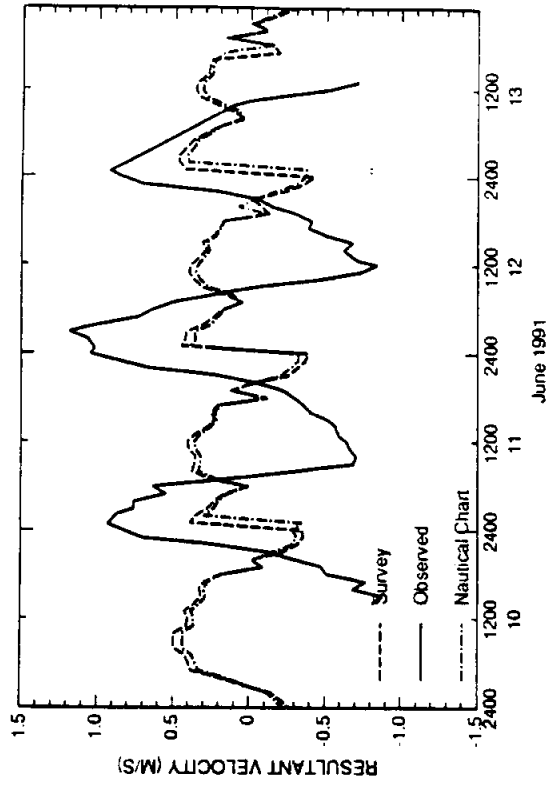


FIG. 2. Port Mansfield Jetties

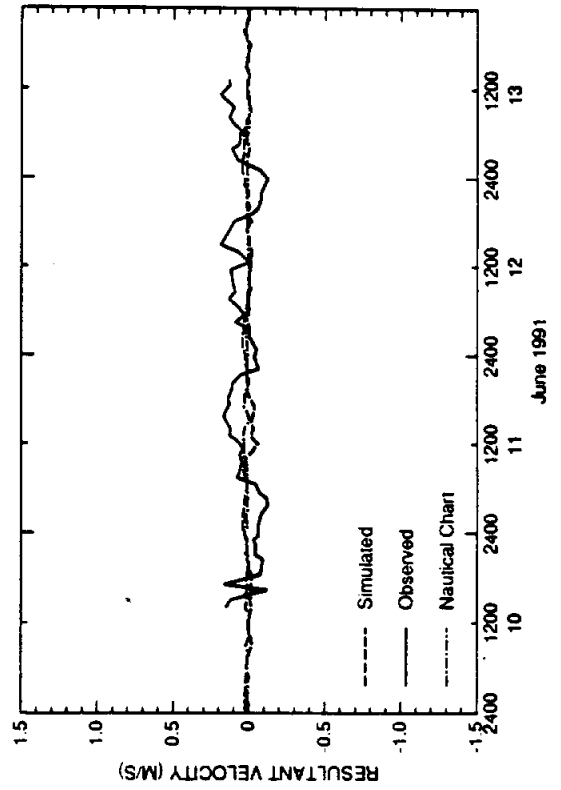


FIG. 3. Mouth of Arroyo Colorado

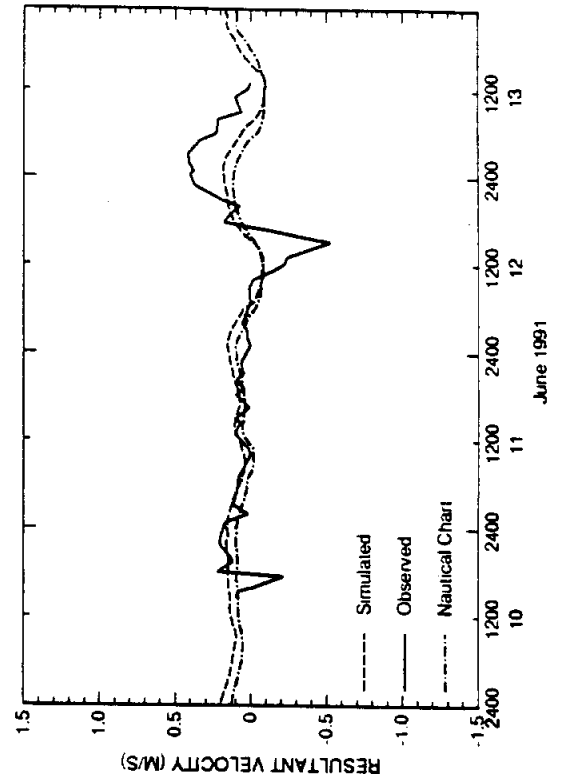


FIG. 4. GIWW North of Arroyo Colorado

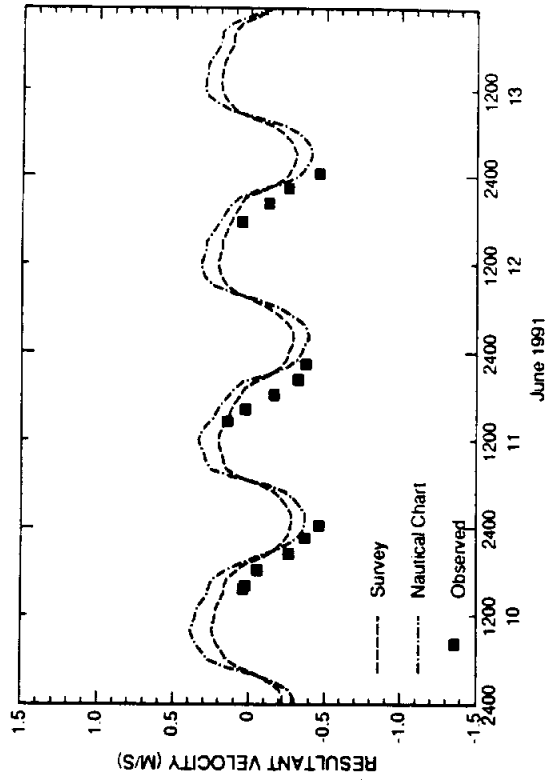


FIG. 6. Old Causeway (Mid East)

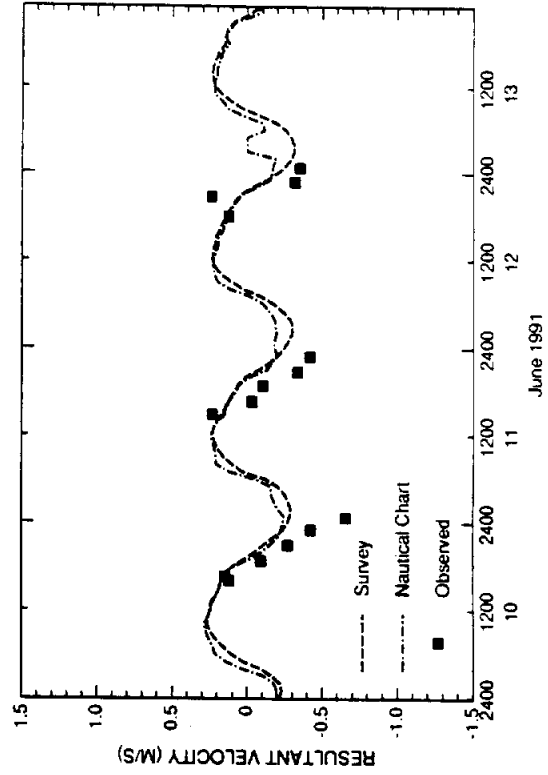


FIG. 8. Old Causeway (Western)

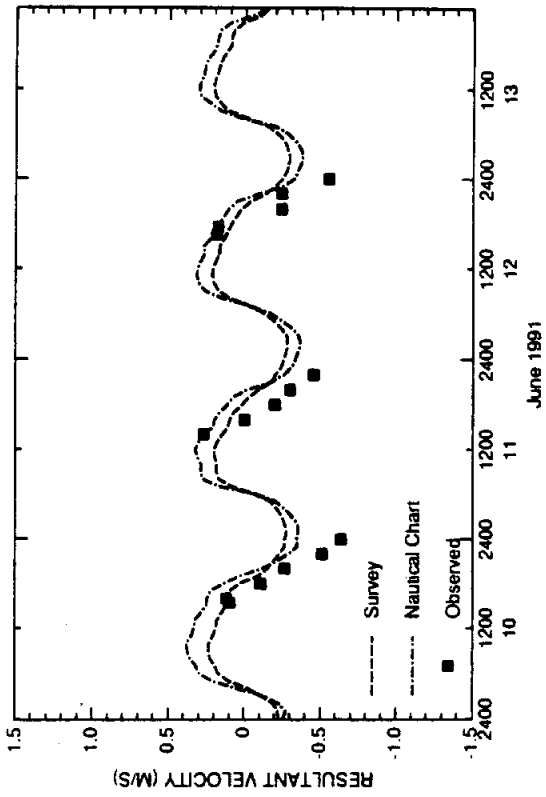


FIG. 5. Old Causeway (Eastern)

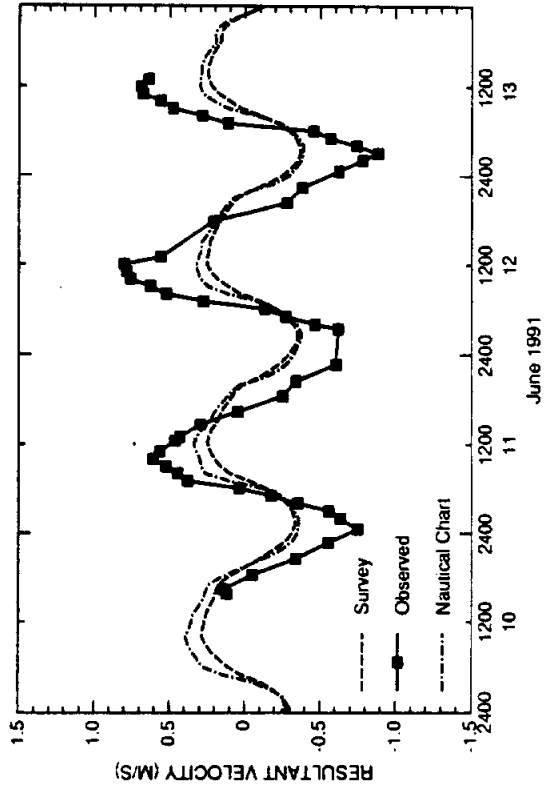


FIG. 7. Old Causeway (Mid West)

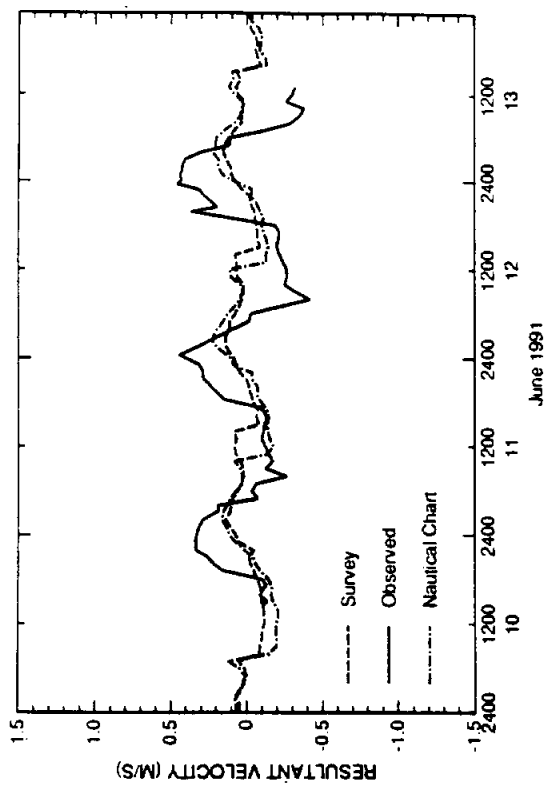


FIG. 10. Brownsville Ship Channel

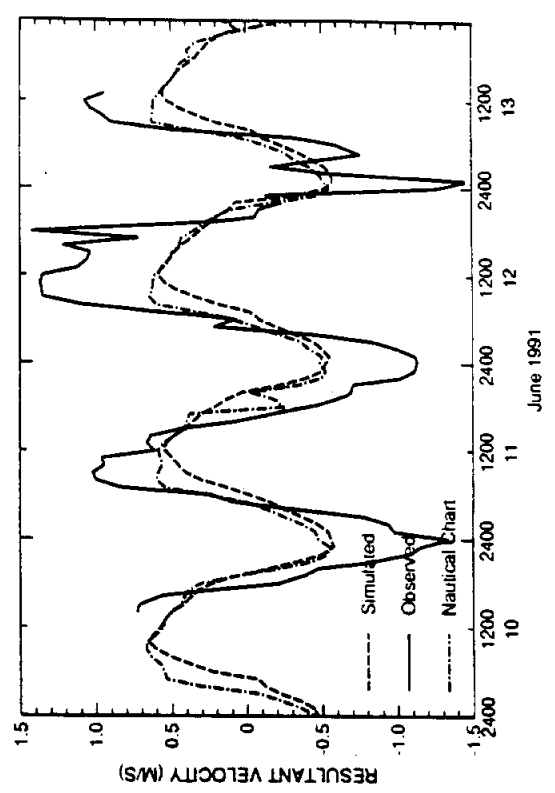


FIG. 12. Brazos Santiago Pass

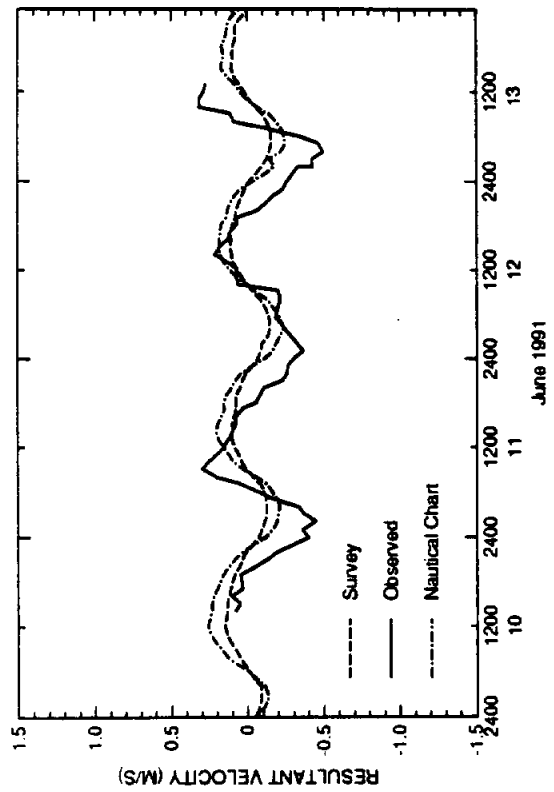


FIG. 9. Port Isabel Channel

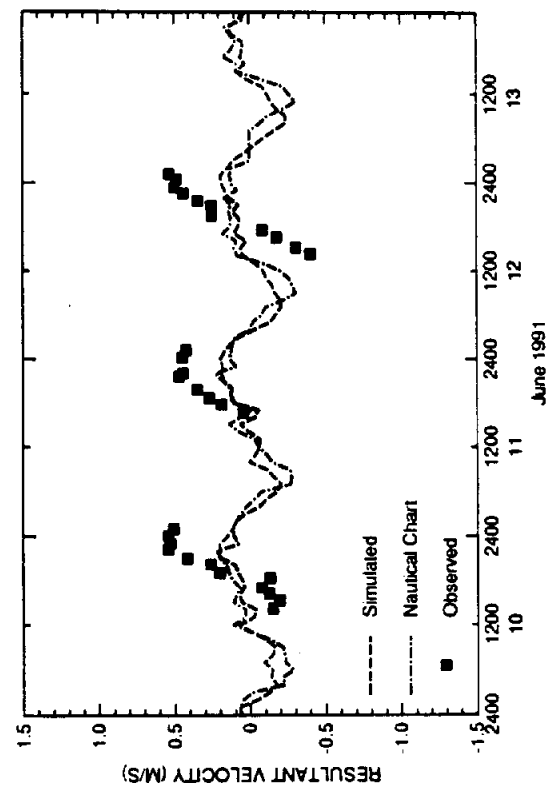


FIG. 11. South Bay Pass

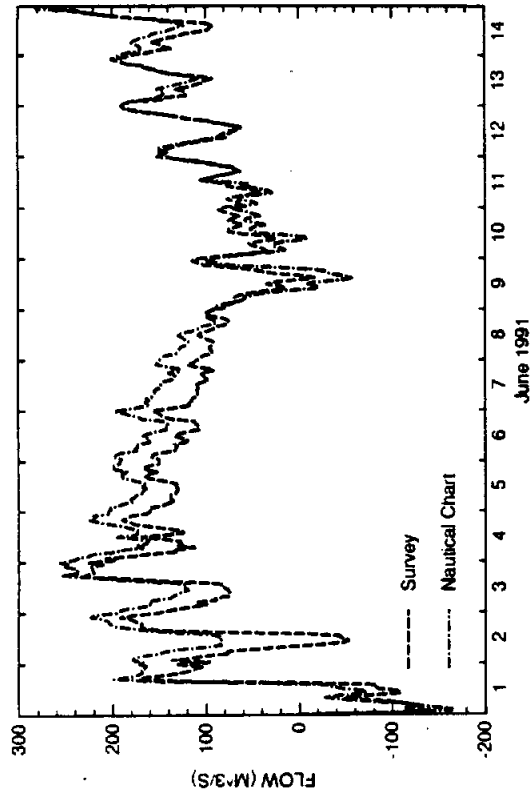


FIG. 1. South Land Cut

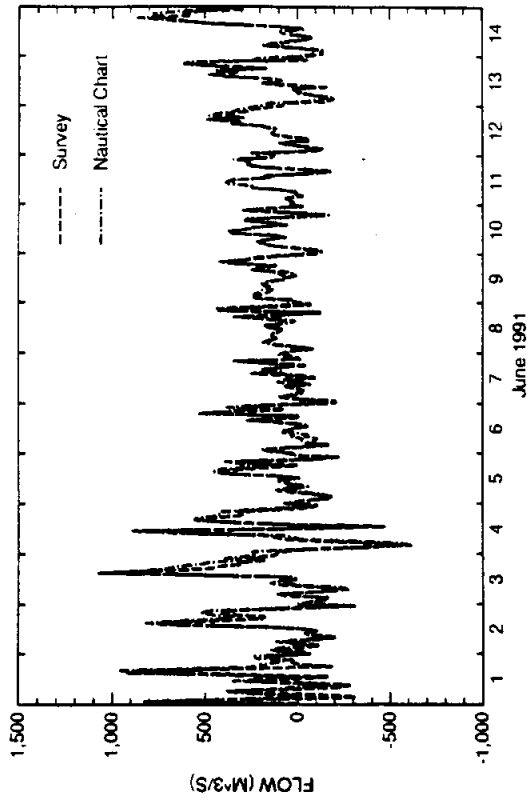


FIG. 2. Laguna Madre North of Port Mansfield

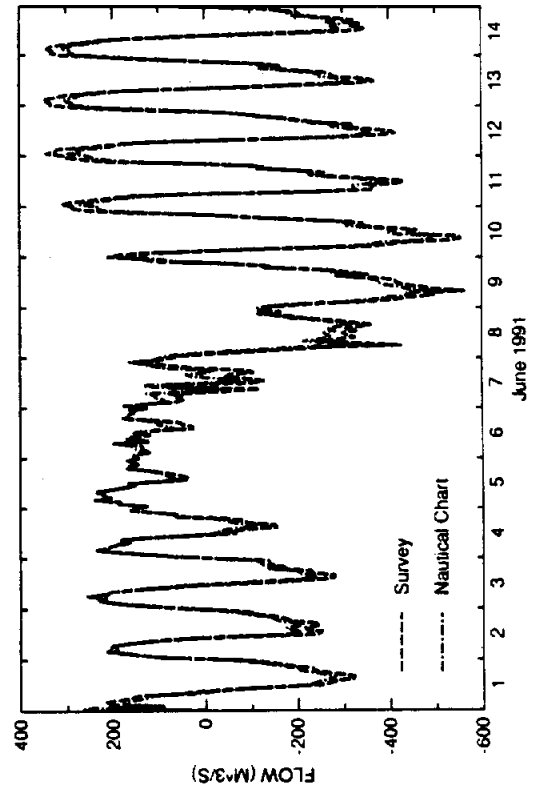


FIG. 3. Port Mansfield Channel

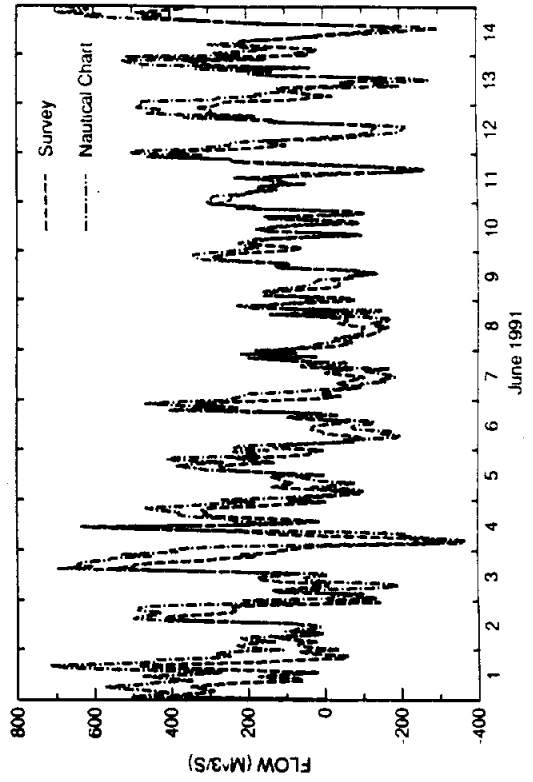


FIG. 4. Laguna Madre South of Port Mansfield

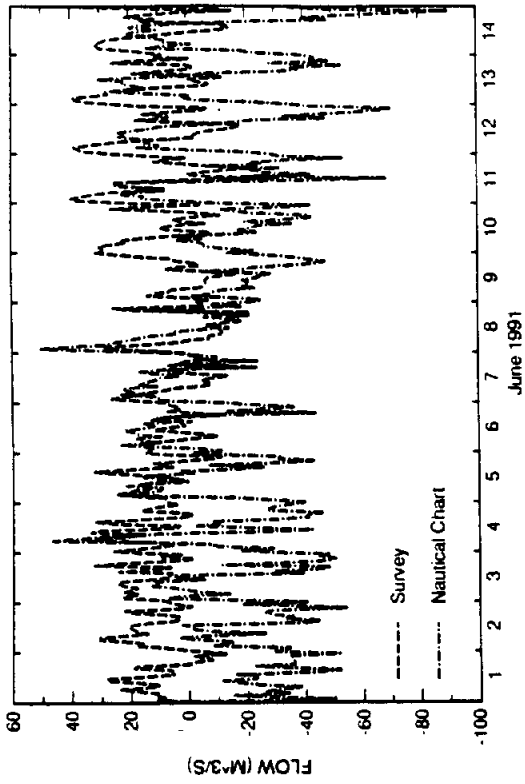


FIG. 6. Arroyo Colorado East of Laguna Atascosa

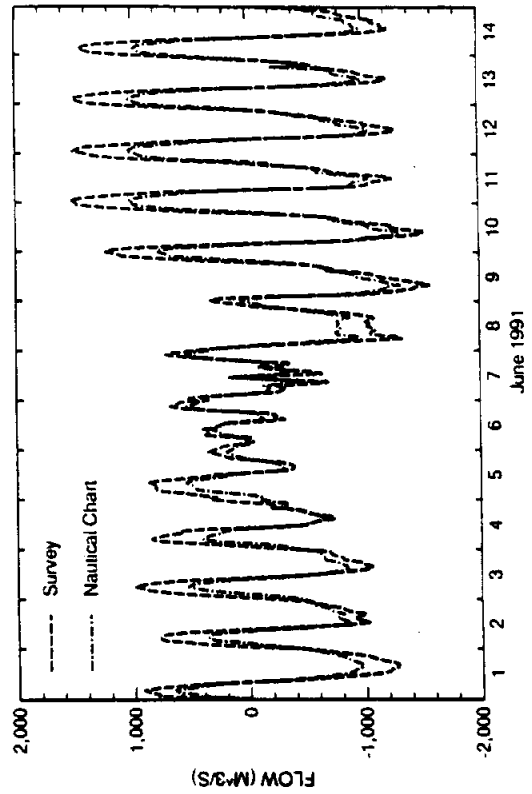


FIG. 8. Brazos-Santiago Pass

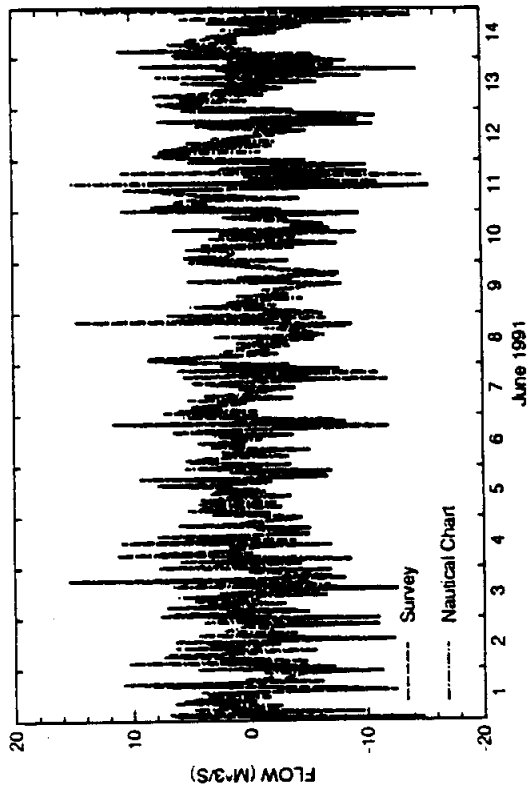


FIG. 5. Arroyo Colorado West of Laguna Atascosa

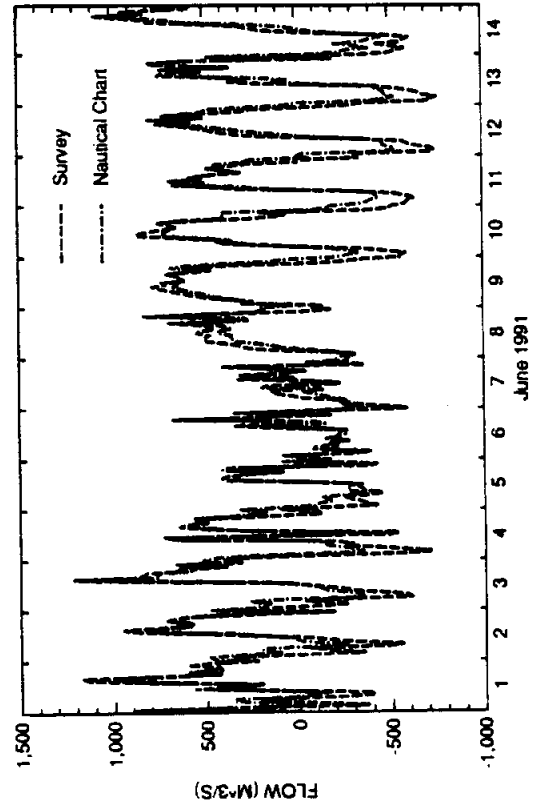


FIG. 7. Laguna Madre North of Port Isabel

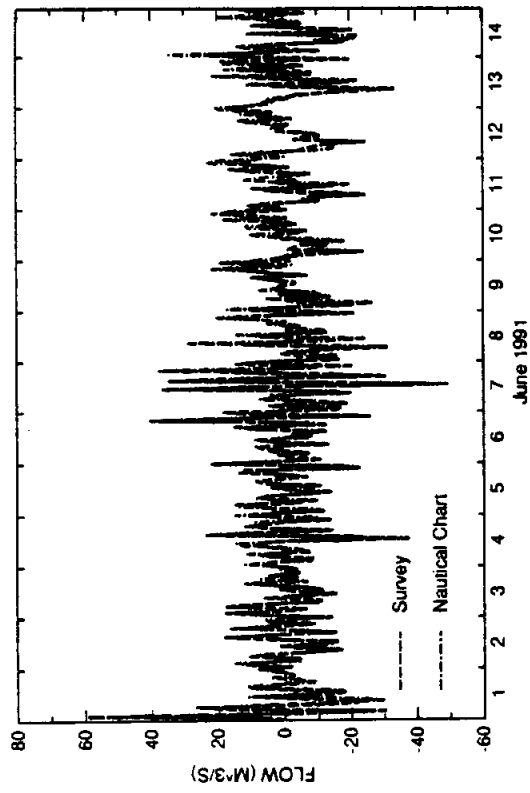


FIG. 9. Brownsville Ship Channel

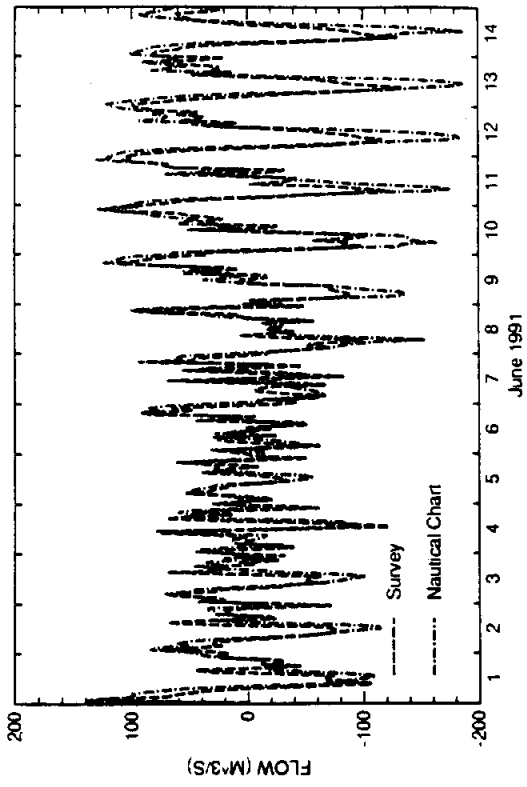


FIG. 10. South Bay Pass

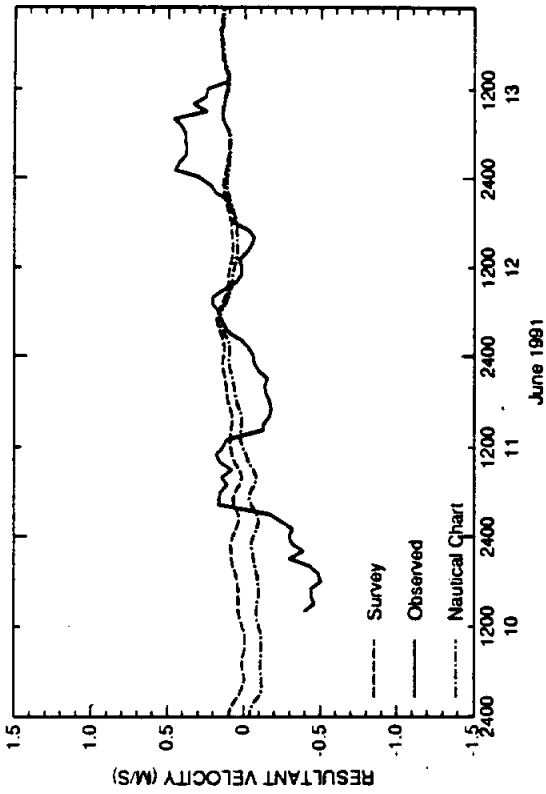


FIG. 1. South Land Cut

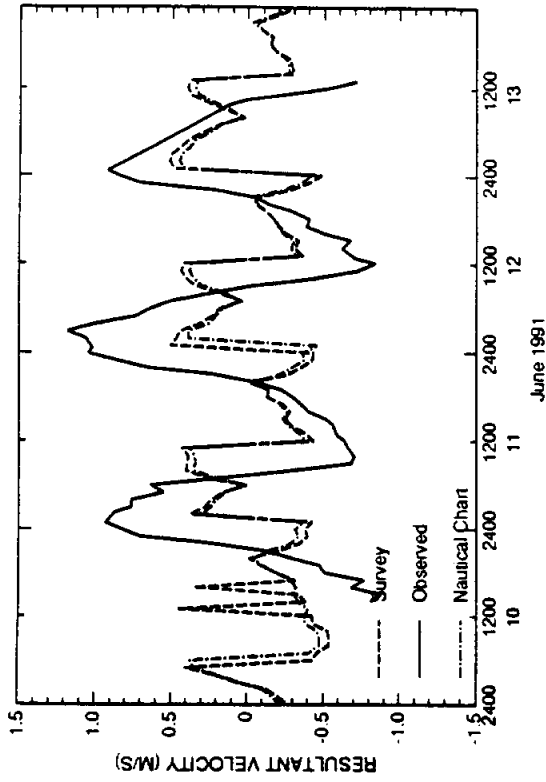


FIG. 2. Port Mansfield Jetties

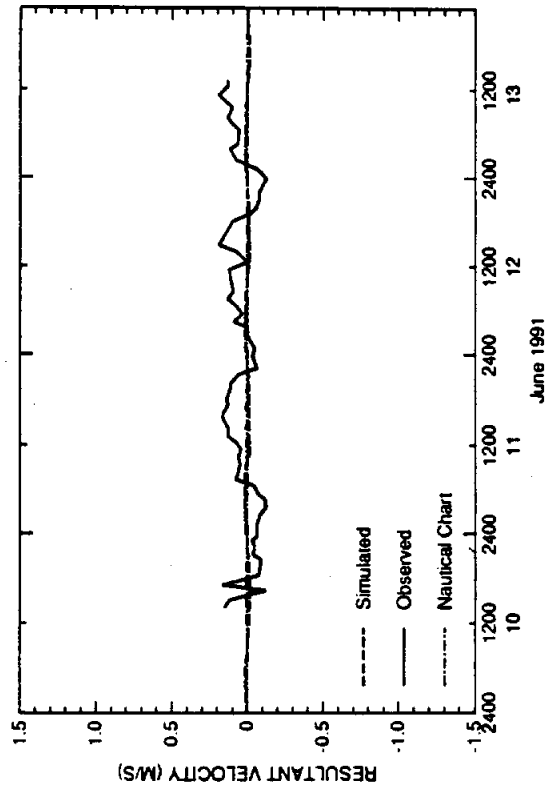


FIG. 3. Mouth of Arroyo Colorado

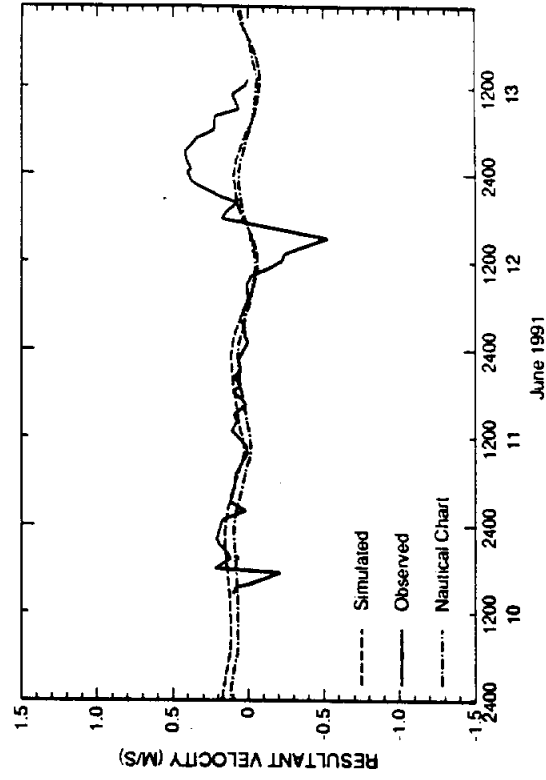


FIG. 4. GIWW North of Arroyo Colorado

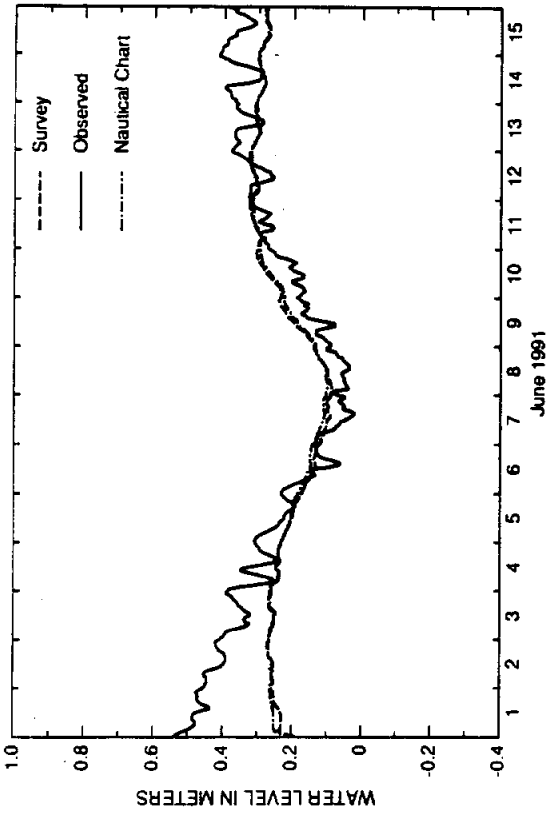


FIG. 1. Rincon Del San Jose Tide Station

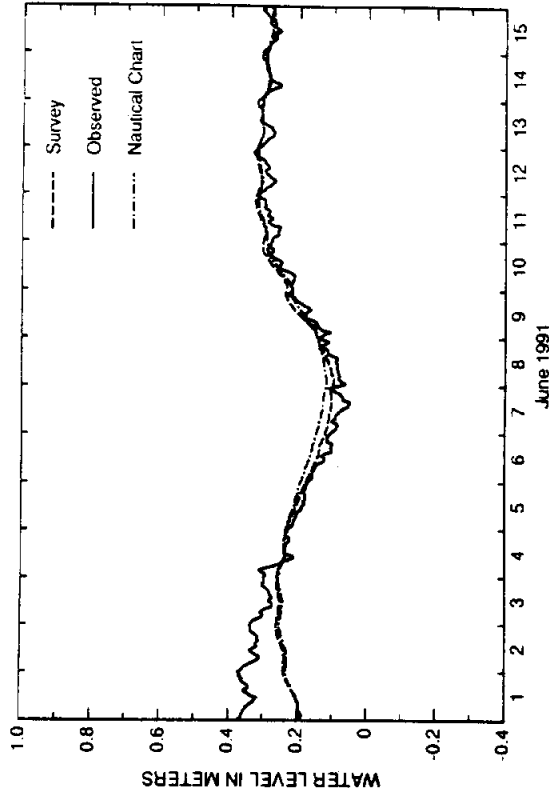


FIG. 2. Port Mansfield Tide Station

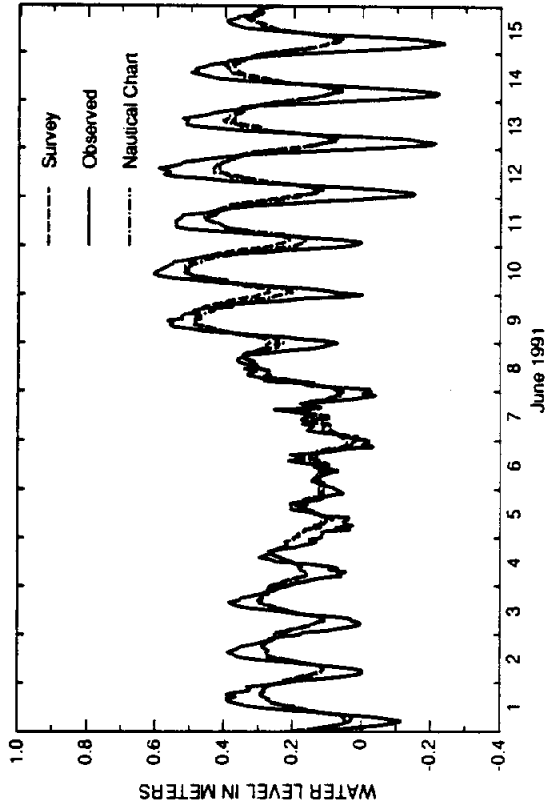


FIG. 3. Port Isabel Tide Station

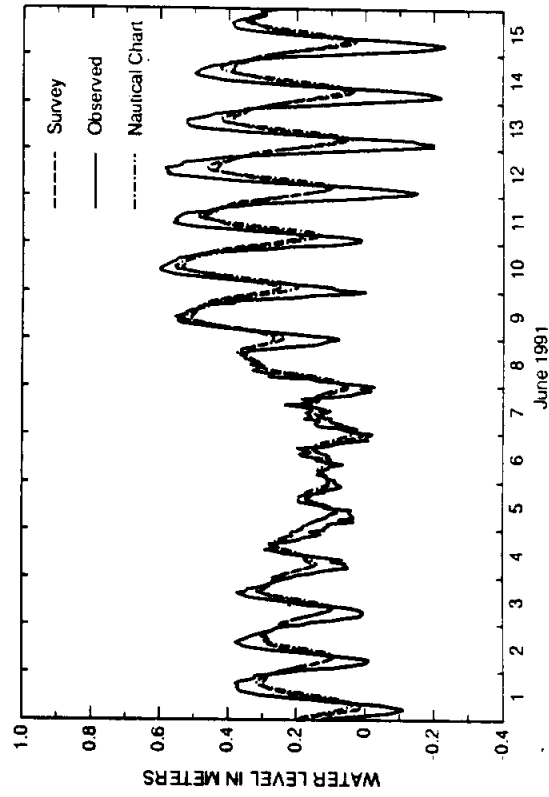


FIG. 4. South Bay Tide Station

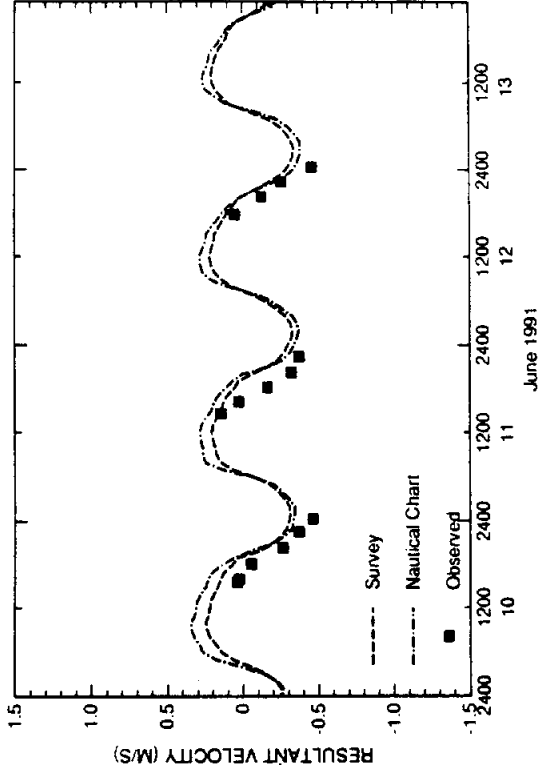


FIG. 6. Old Causeway (Mid East)

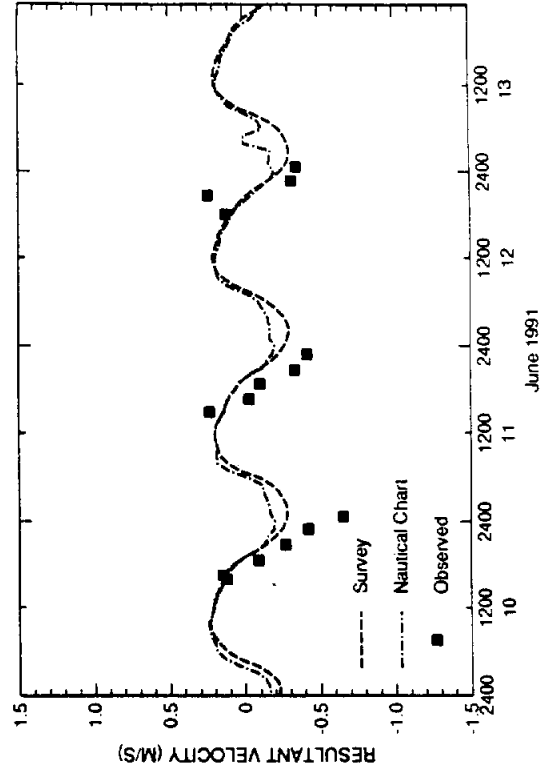


FIG. 8. Old Causeway (Western)

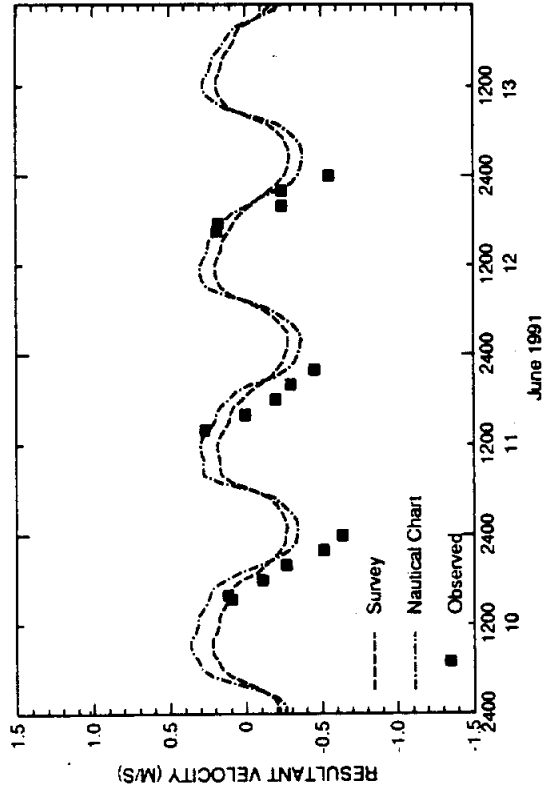


FIG. 5. Old Causeway (Eastern)

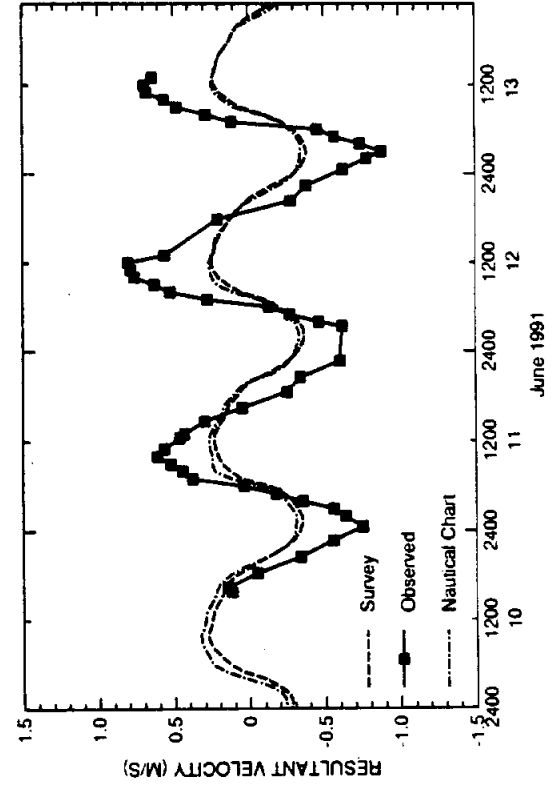


FIG. 7. Old Causeway (Mid West)

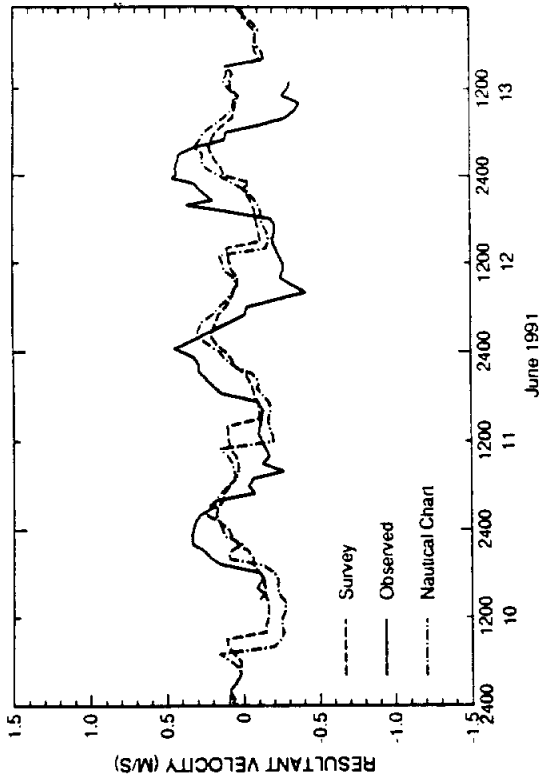


FIG. 10. Brownsville Ship Channel

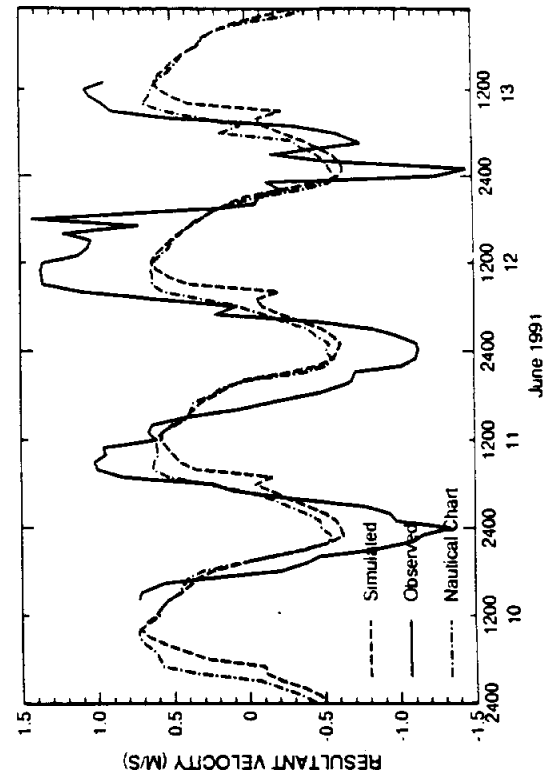


FIG. 12. Brazos Santiago Pass

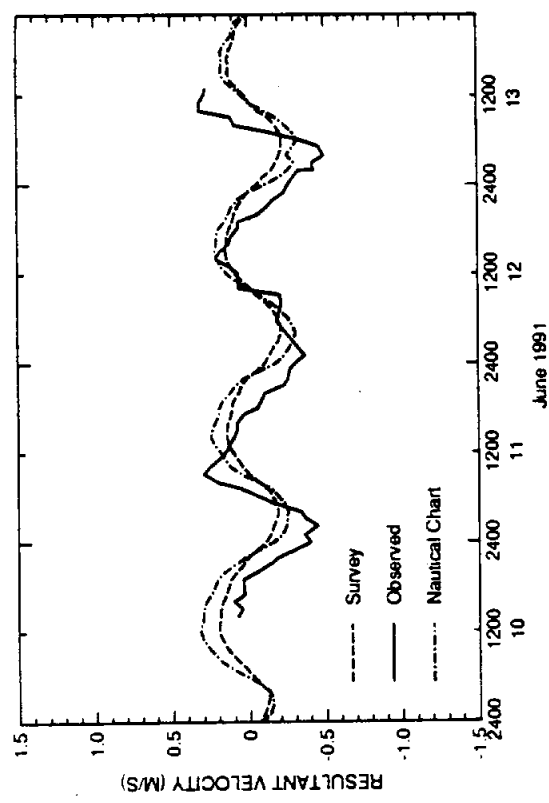


FIG. 9. Port Isabel Channel

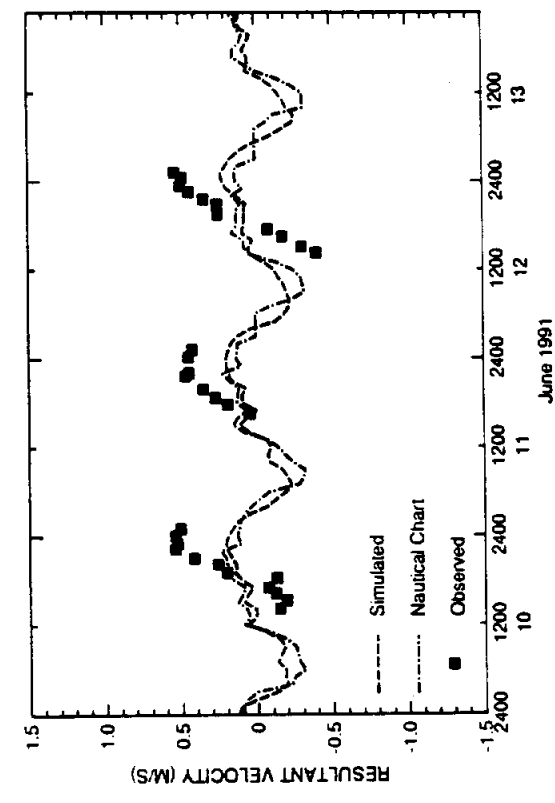


FIG. 11. South Bay Pass

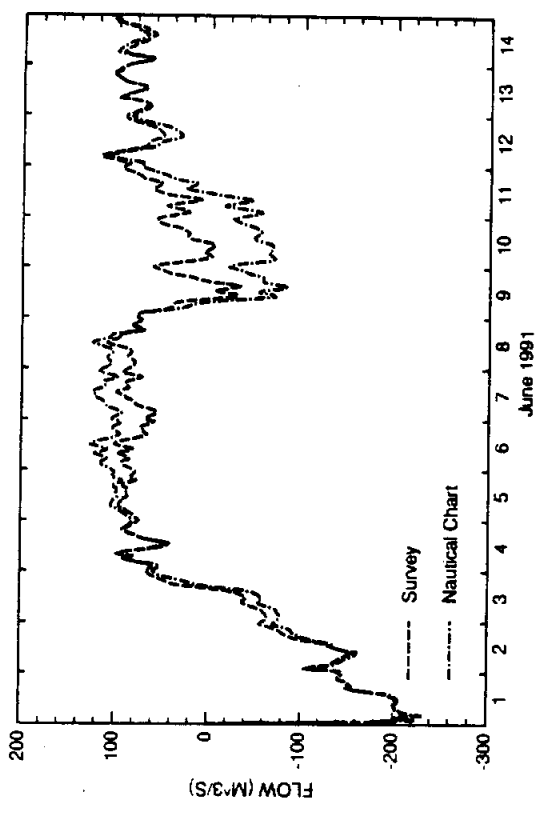


FIG. 1. South Land Cut

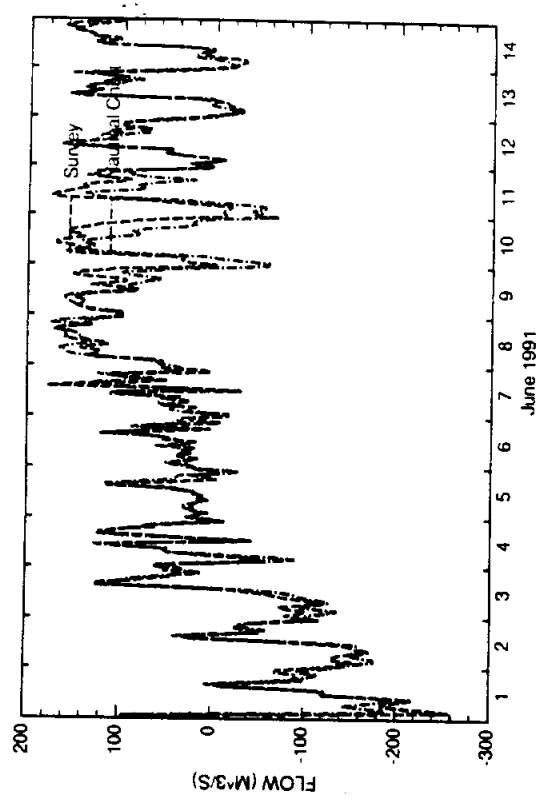


FIG. 2. Laguna Madre North of Port Mansfield

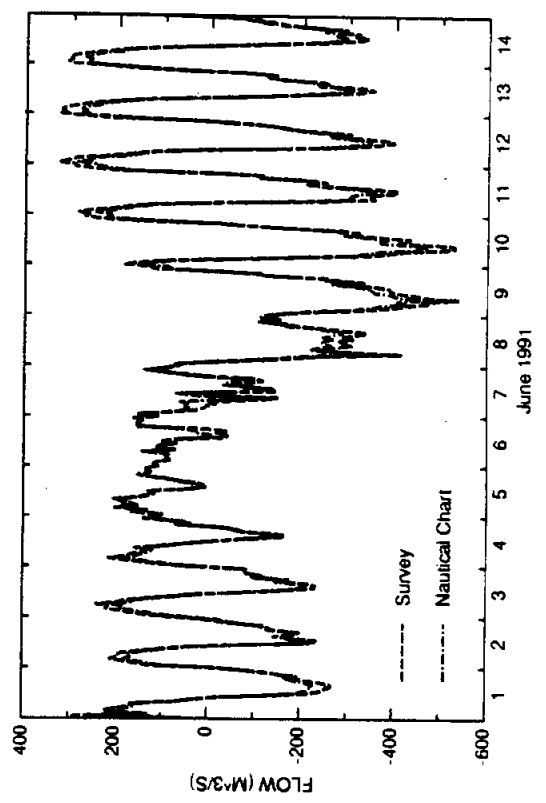


FIG. 3. Port Mansfield Channel

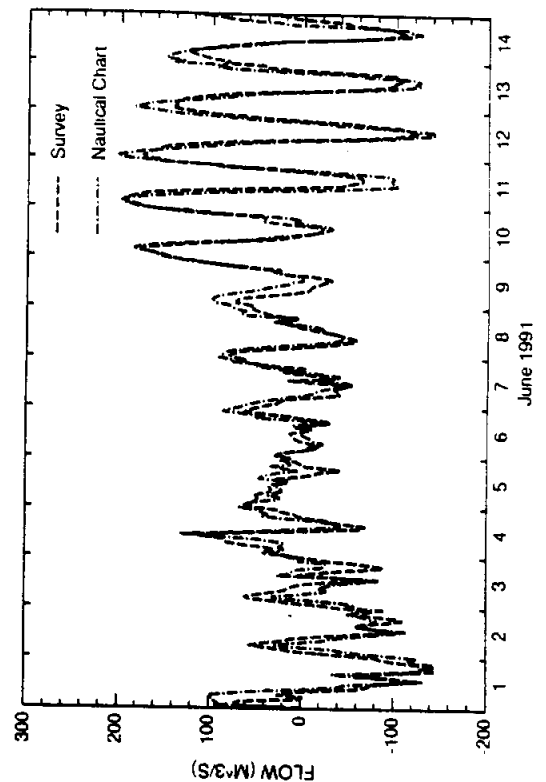


FIG. 4. Laguna Madre South of Port Mansfield

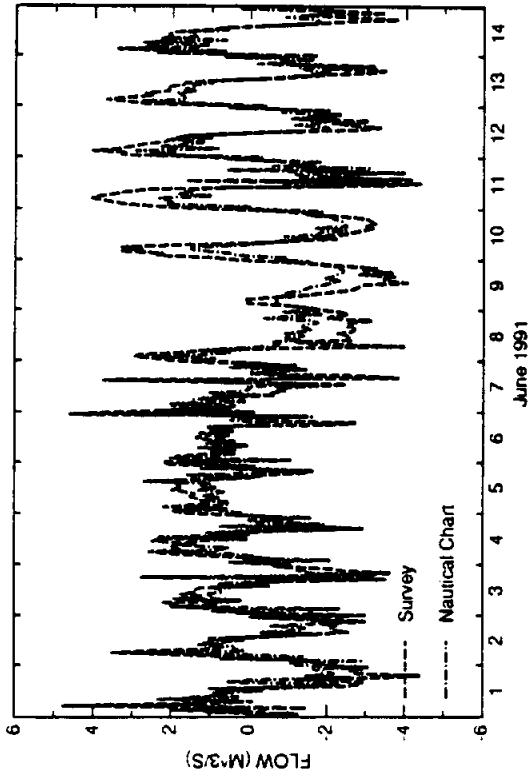


FIG. 5. Arroyo Colorado West of Laguna Atascosa

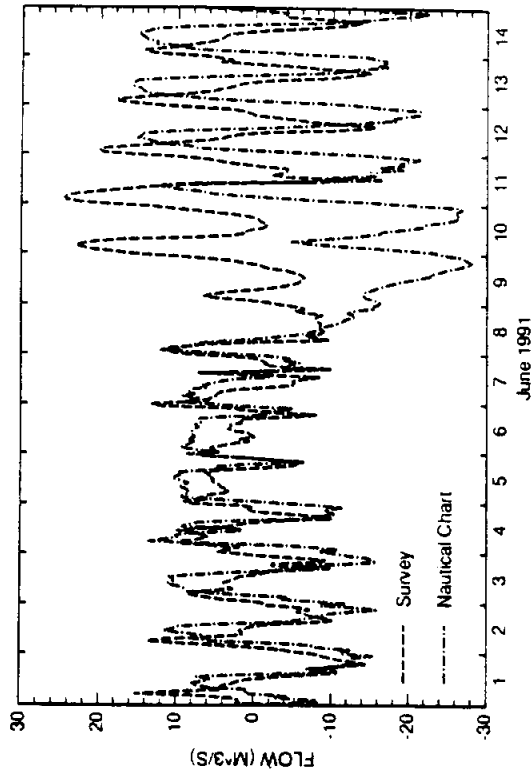


FIG. 6. Arroyo Colorado East of Laguna Atascosa

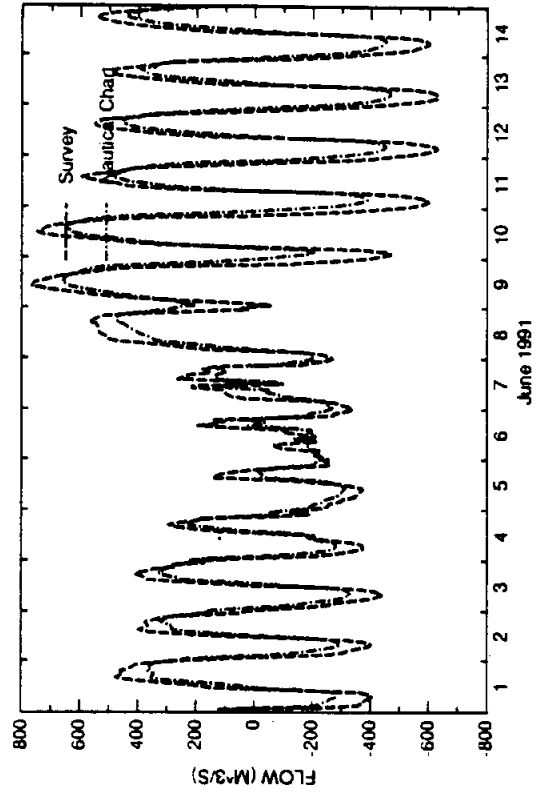


FIG. 7. Laguna Madre North of Port Isabel

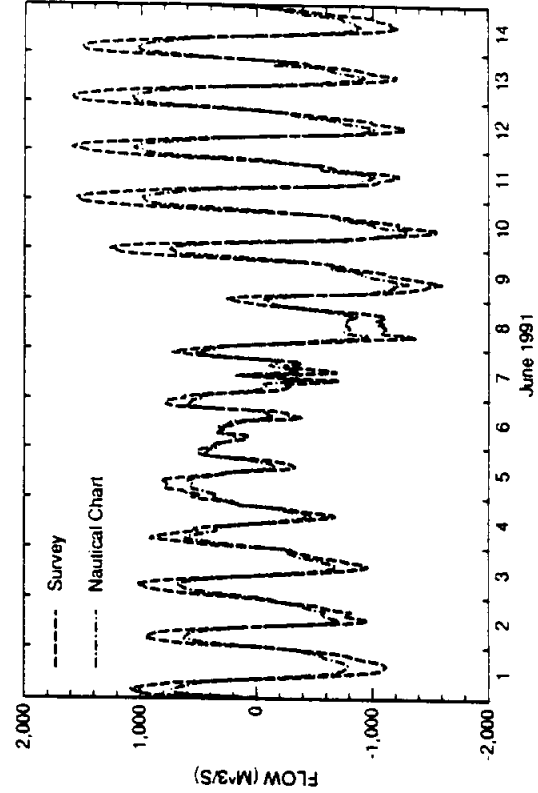


FIG. 8. Brazos-Santiago Pass

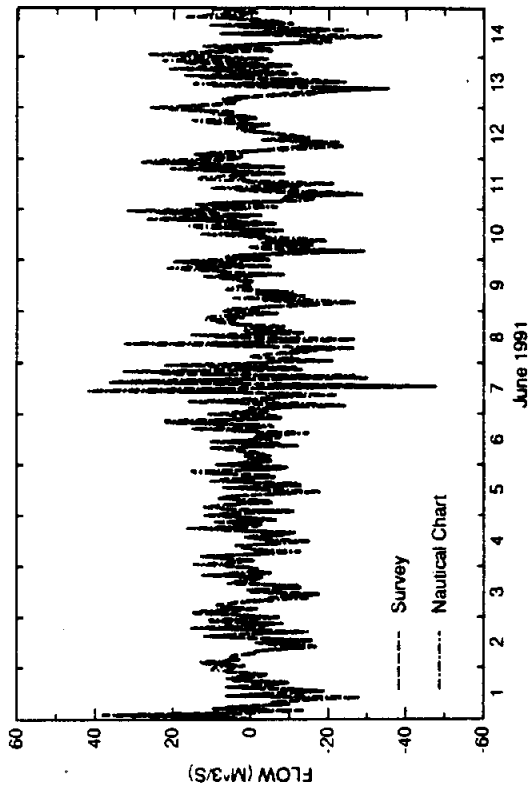


FIG. 9. Brownsville Ship Channel

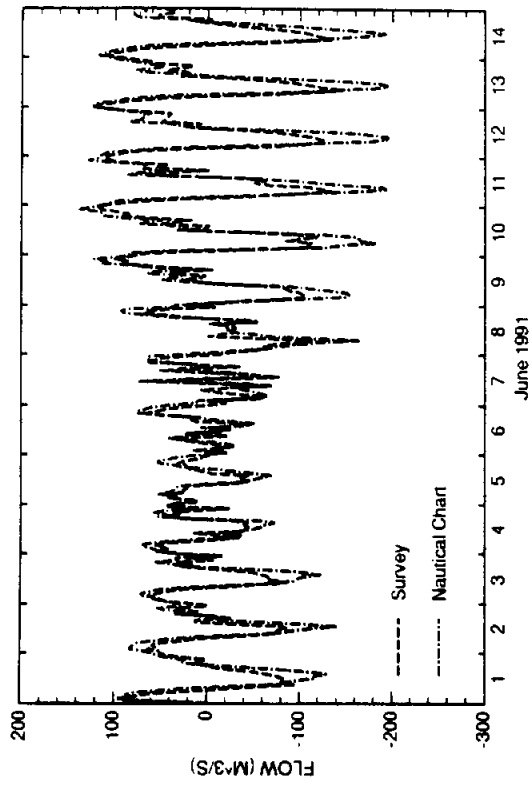


FIG. 10. South Bay Pass

SWIFT2D SIMULATIONS

Wind Stress Variation 2 Simulation

Manning's n = 0.025 in navigation channels
= 0.075 in the vicinity of the old Queen Isabel Causeway
= 0.035 elsewhere

Wind Stress = 0.0026

Time Step = 6 minutes

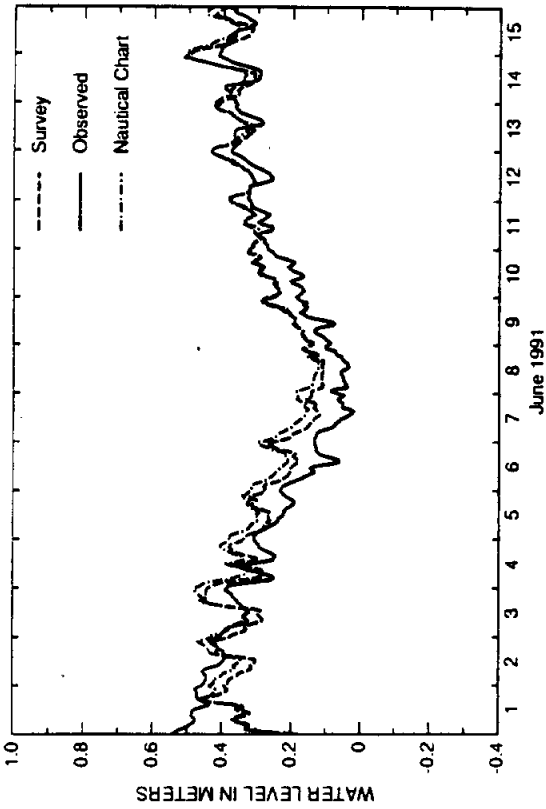


FIG. 1. Rincon Del San Jose Tide Station

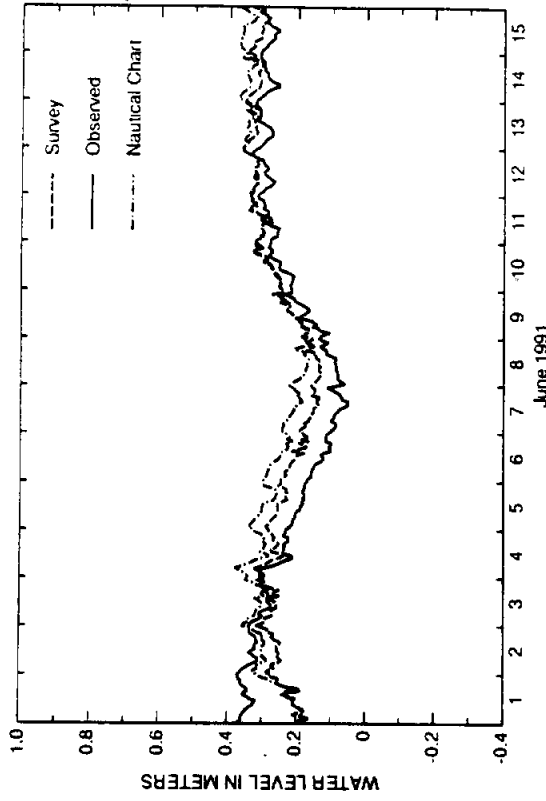


FIG. 2. Port Mansfield Tide Station

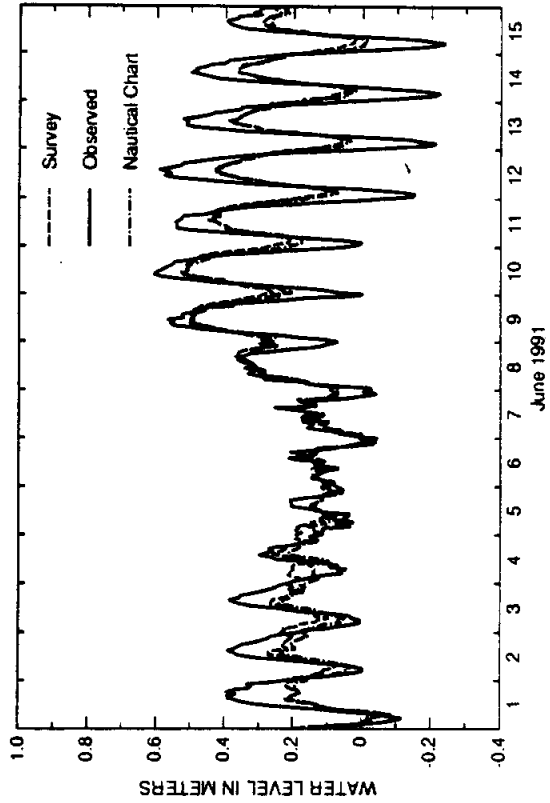


FIG. 3. Port Isabel Tide Station

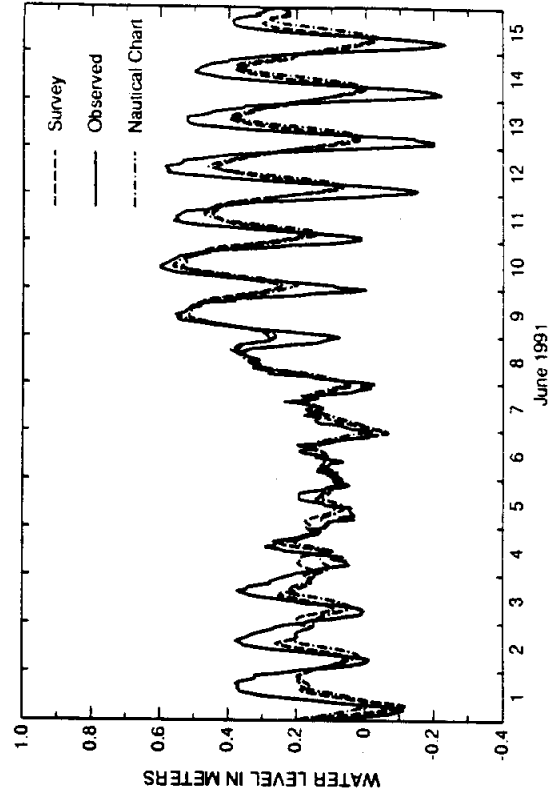


FIG. 4. South Bay Tide Station.

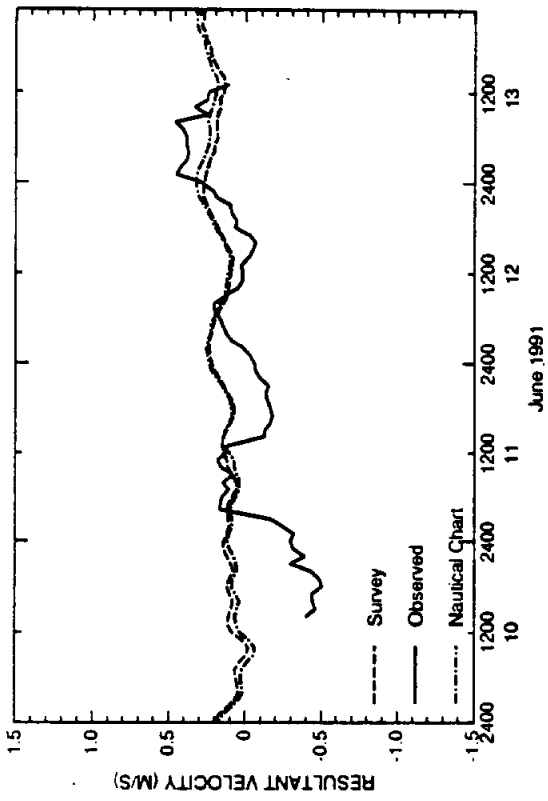


FIG. 1. South Land Cut

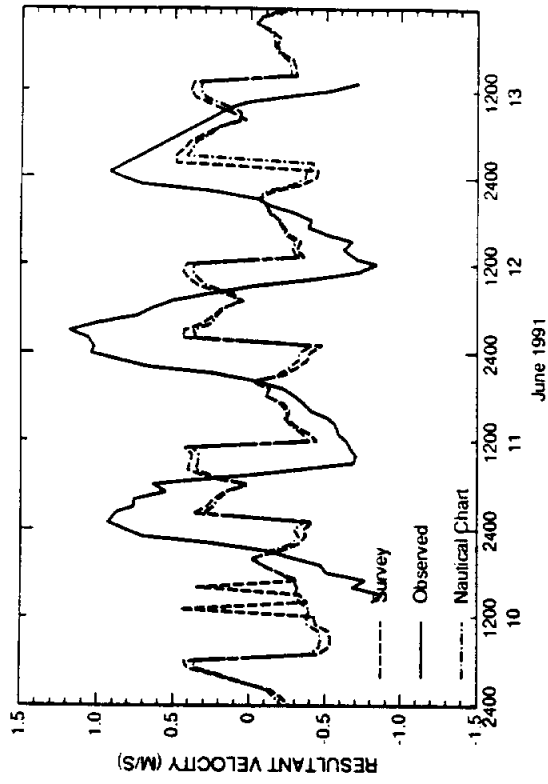


FIG. 2. Port Mansfield Jetties

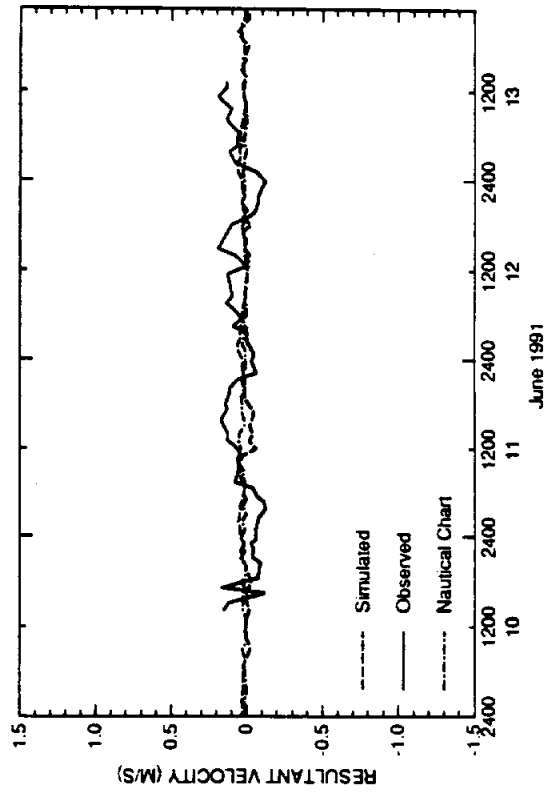


FIG. 3. Mouth of Arroyo Colorado

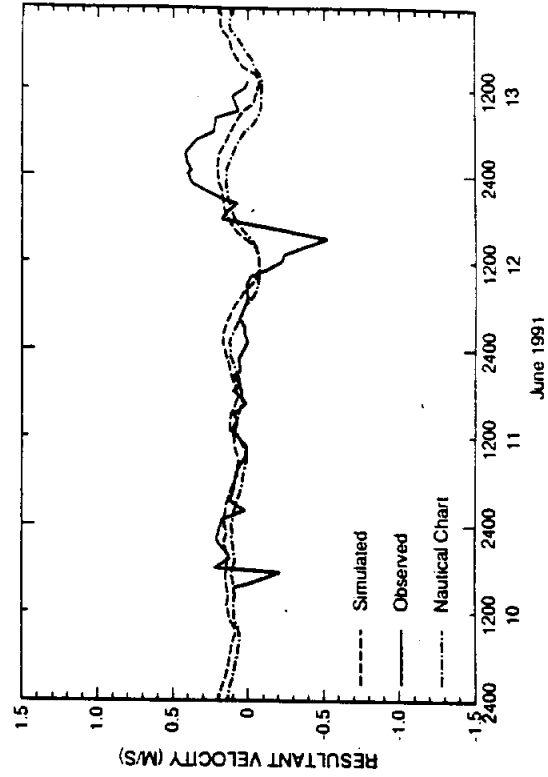


FIG. 4. GIWW North of Arroyo Colorado

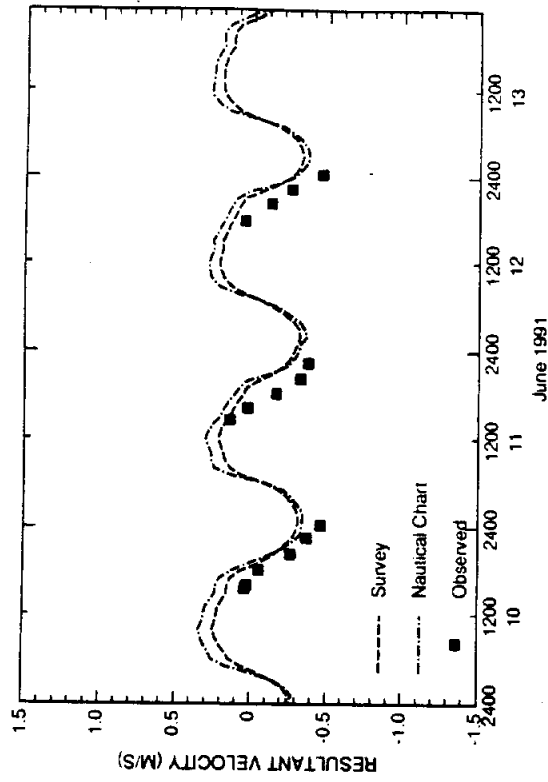


FIG. 6. Old Causeway (Mid East)

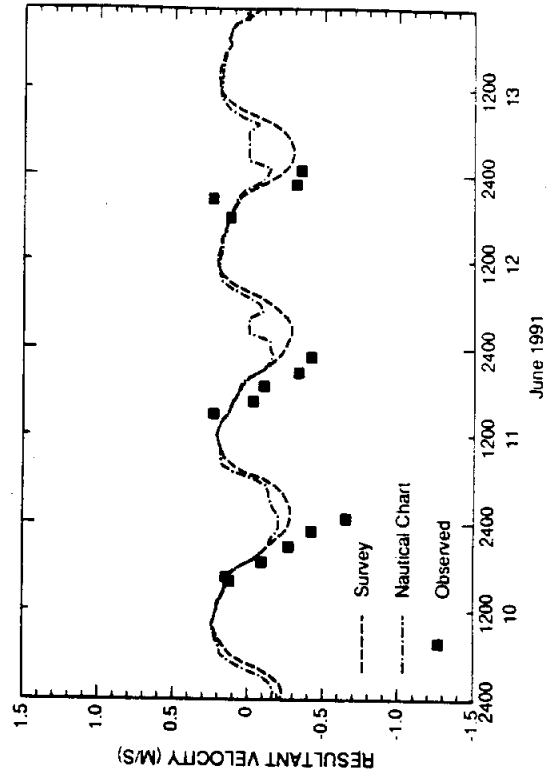


FIG. 8. Old Causeway (Western)

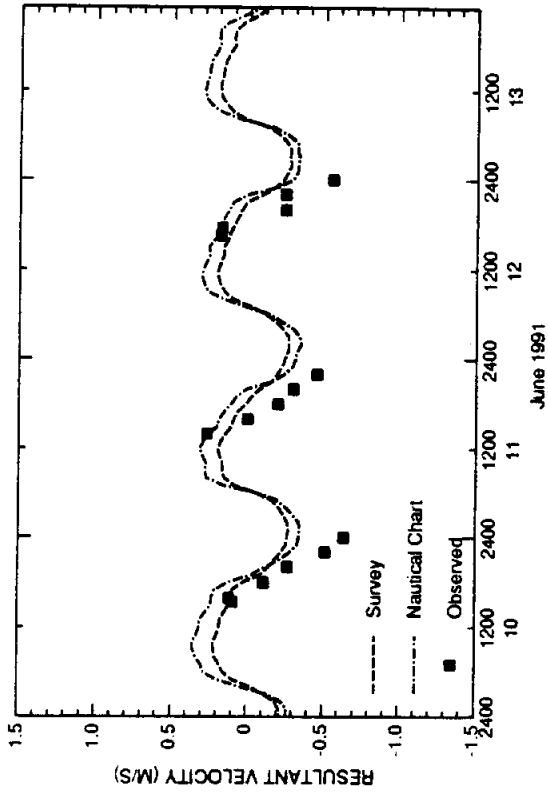


FIG. 5. Old Causeway (Eastern)

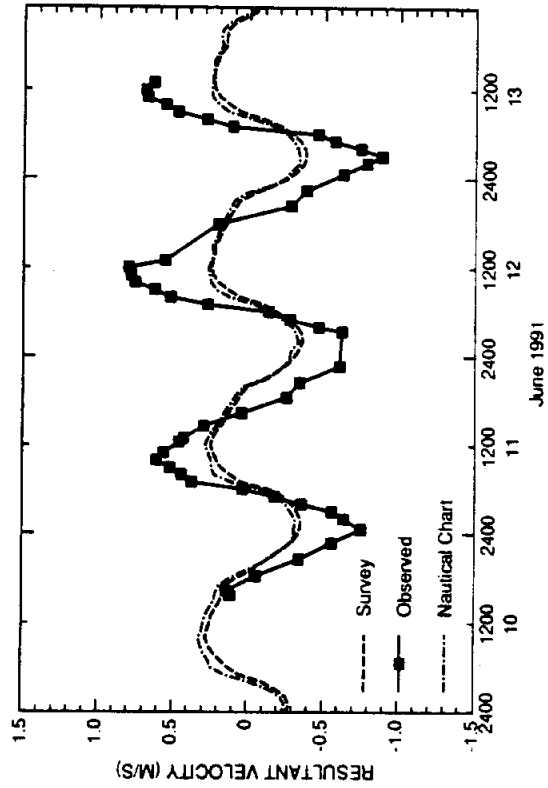


FIG. 7. Old Causeway (Mid West)

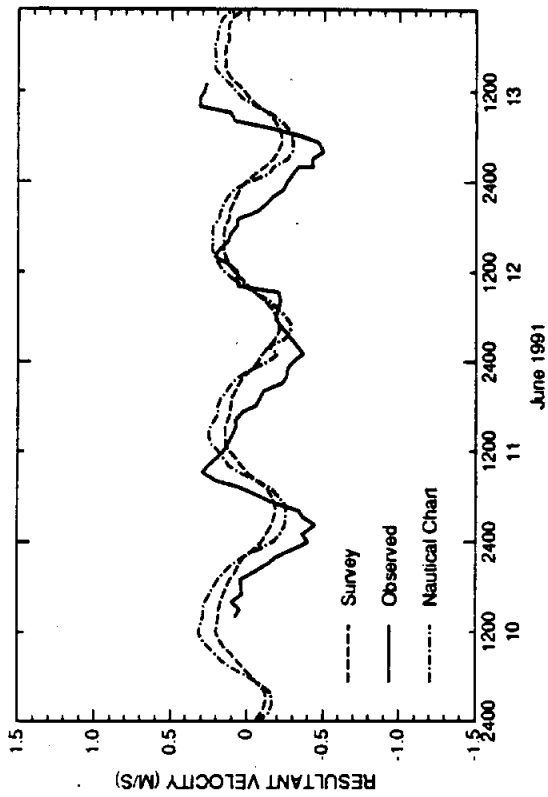


FIG. 9. Port Isabel Channel

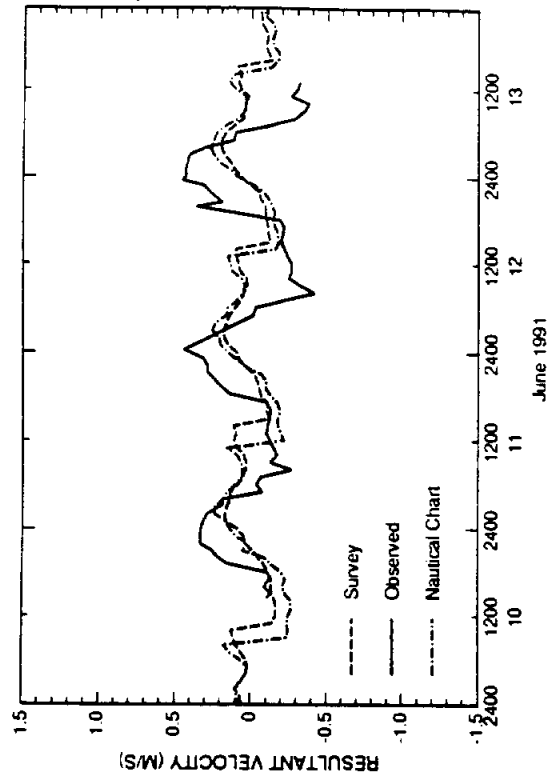


FIG. 10. Brownsville Ship Channel

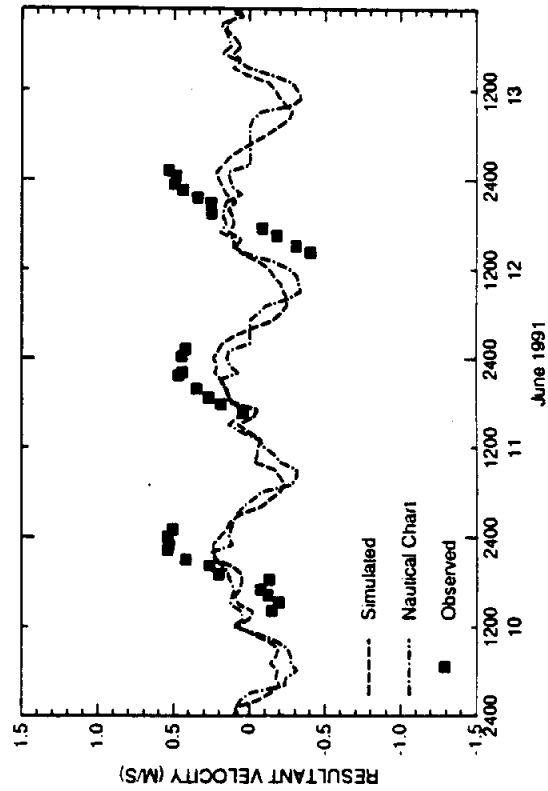


FIG. 11. South Bay Pass

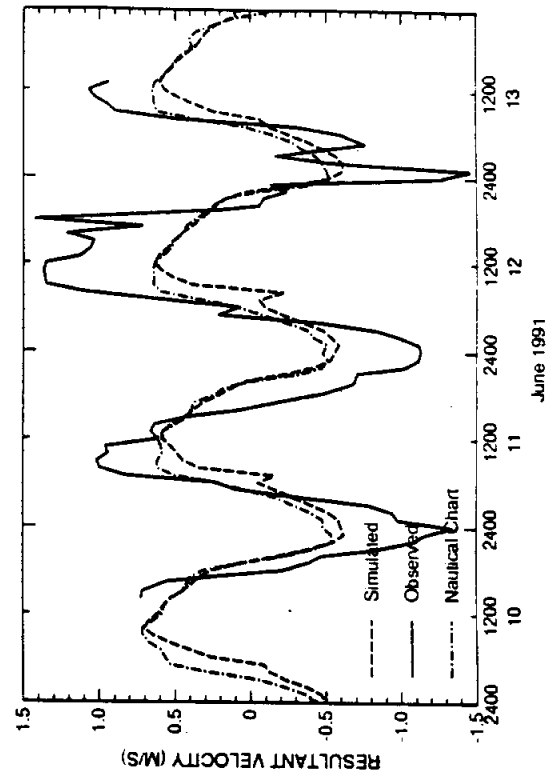


FIG. 12. Brazos Santiago Pass

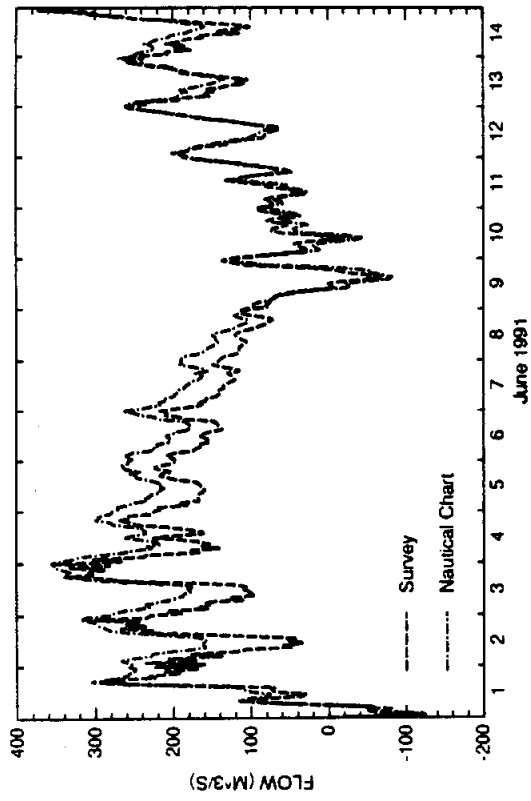


FIG. 1. South Land Cut

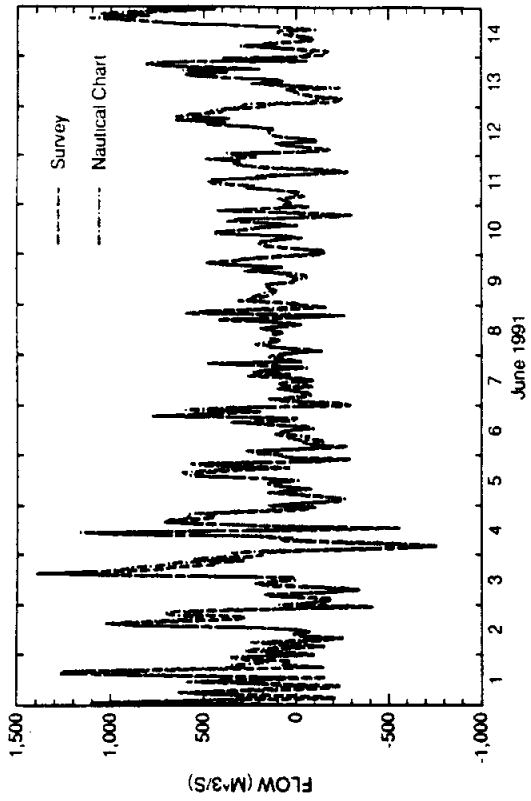


FIG. 2. Laguna Madre North of Port Mansfield

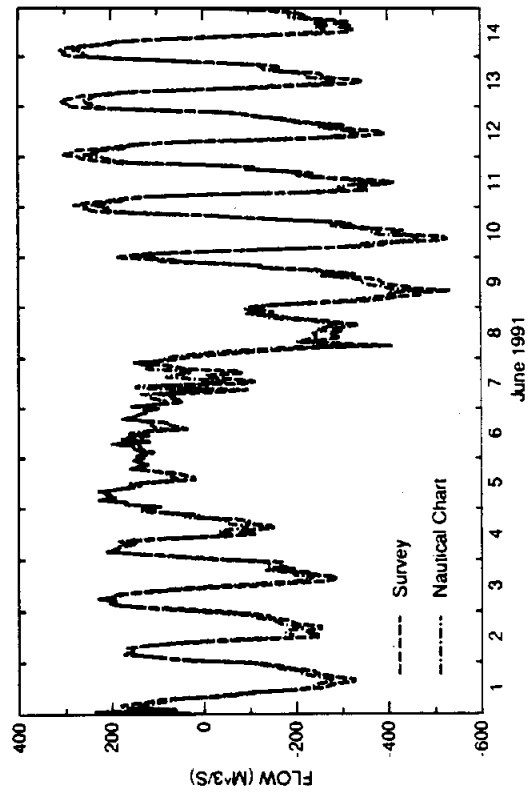


FIG. 3. Port Mansfield Channel

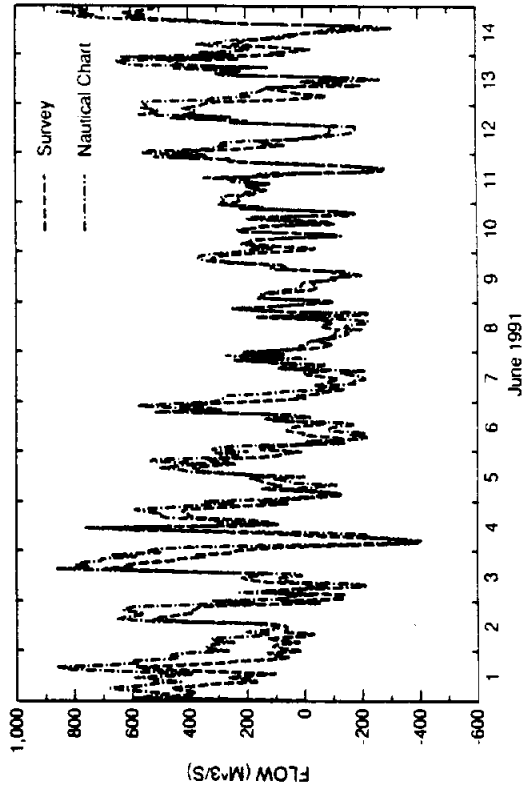


FIG. 4. Laguna Madre South of Port Mansfield

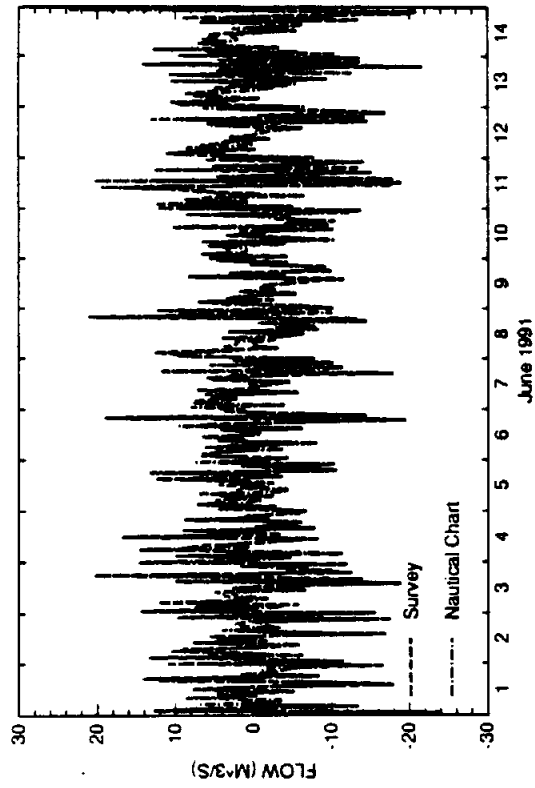


FIG. 5. Arroyo Colorado West of Laguna Atascosa

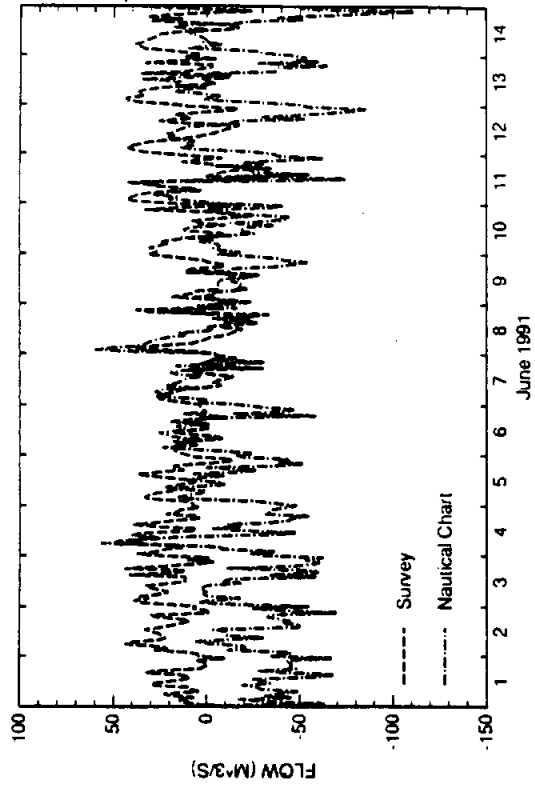


FIG. 6. Arroyo Colorado East of Laguna Atascosa

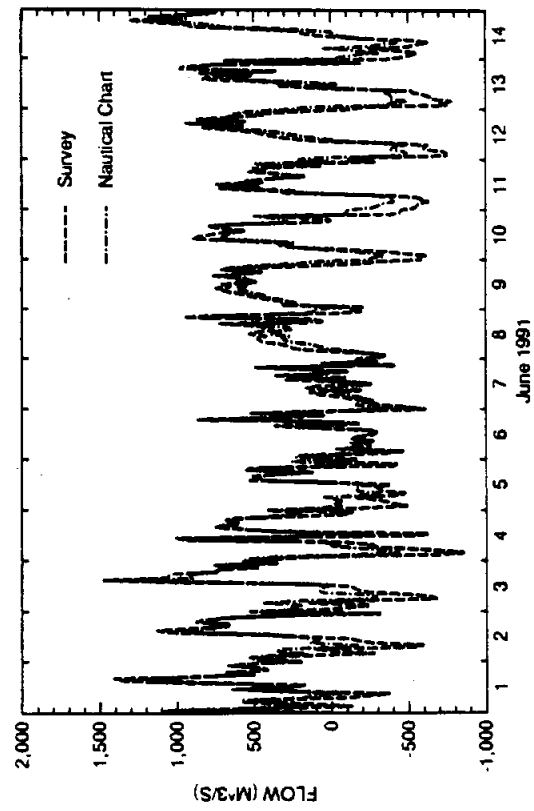


FIG. 7. Laguna Madre North of Port Isabel

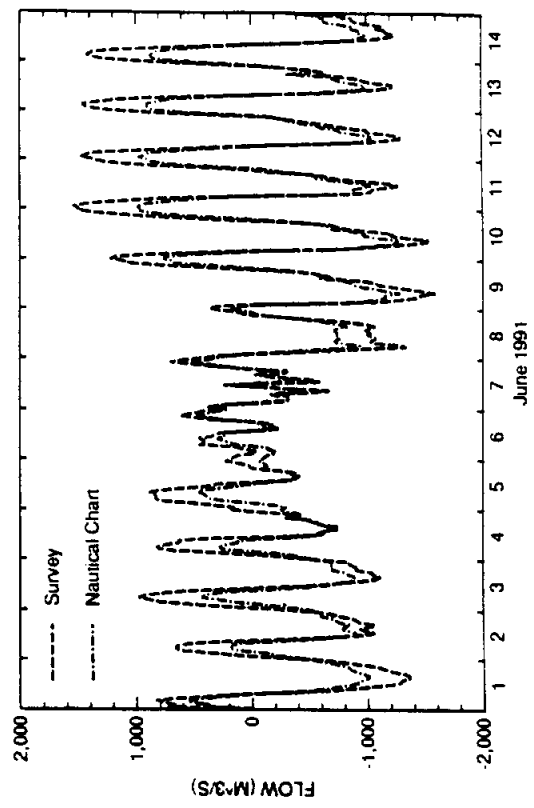


FIG. 8. Brazos-Santiago Pass

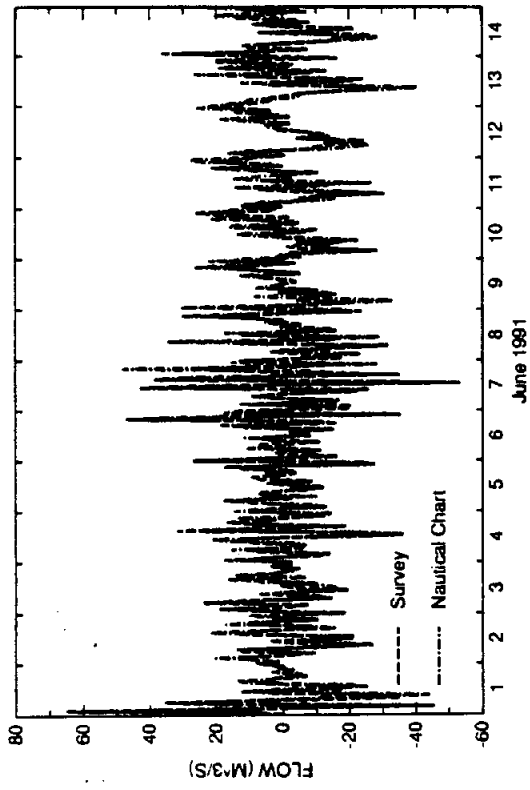


FIG. 9. Brownsville Ship Channel

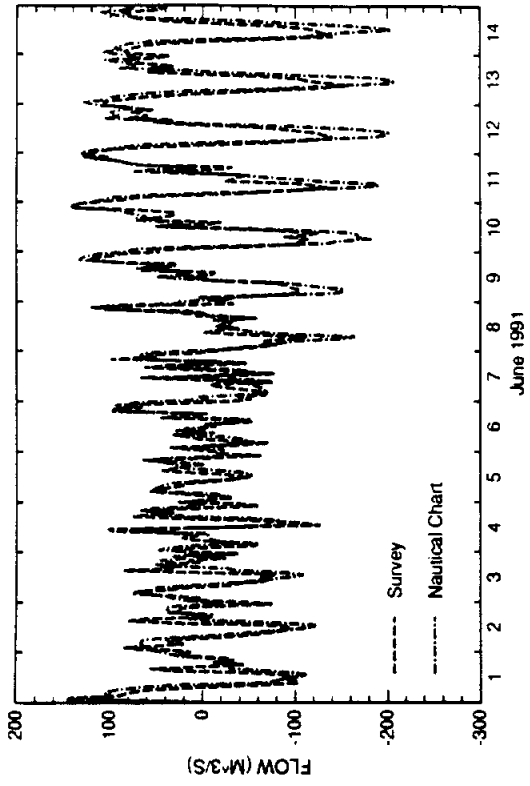


FIG. 10. South Bay Pass

SWIFT2D SIMULATIONS

Time Step Variation Simulation

Manning's n = 0.025 in navigation channels
= 0.075 in the vicinity of the old Queen Isabel Causeway
= 0.035 elsewhere

Wind Stress = 0.0015

Time Step = 12 minutes

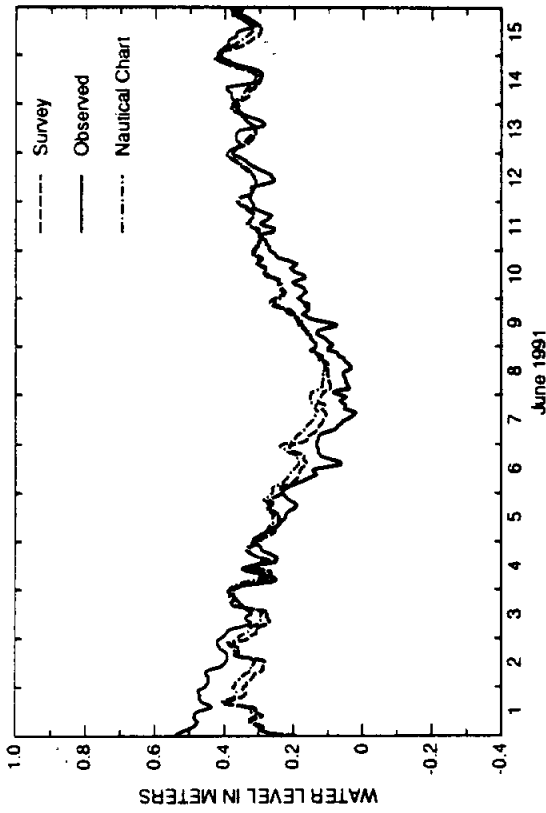


FIG. 1. Rincon Del San Jose Tide Station

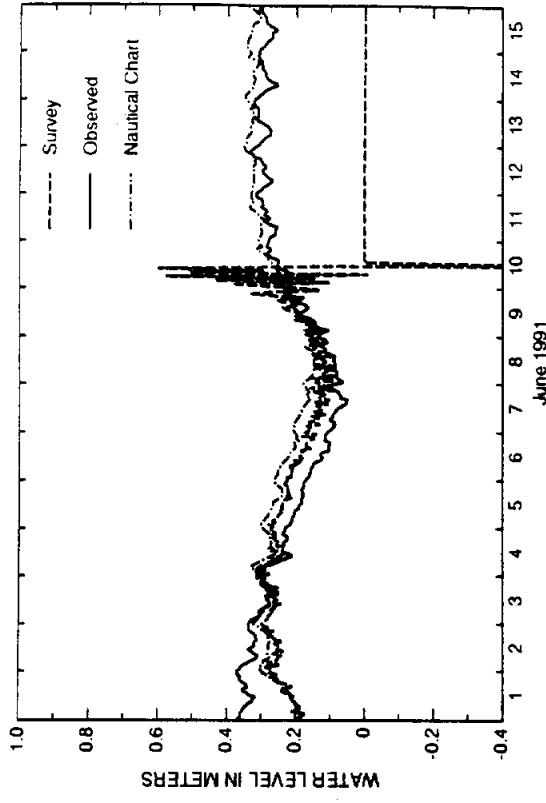


FIG. 2. Port Mansfield Tide Station

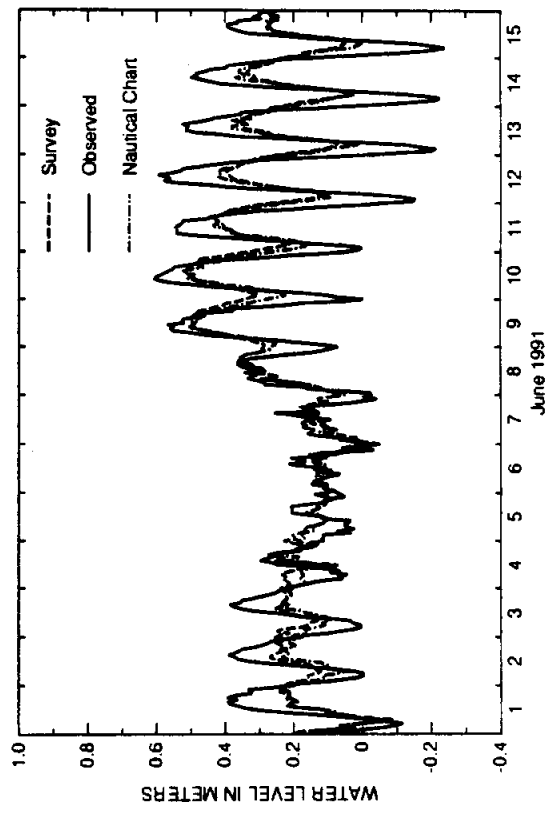


FIG. 3. Port Isabel Tide Station

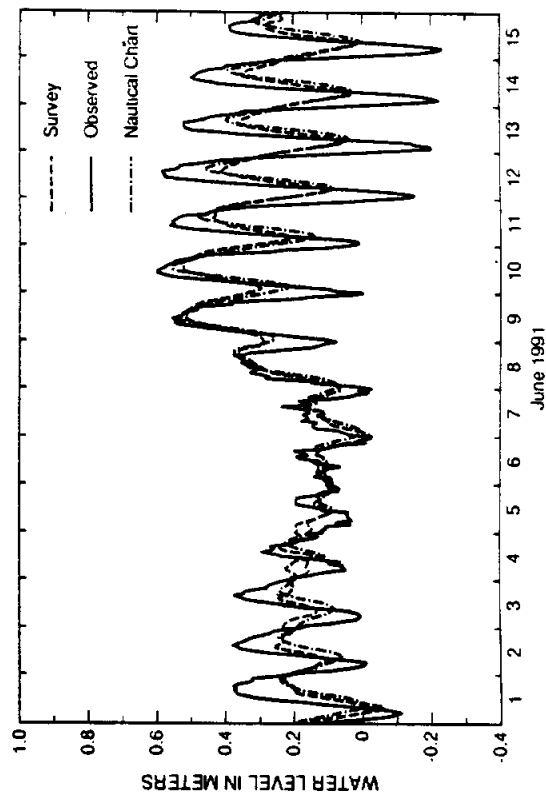


FIG. 4. South Bay Tide Station.

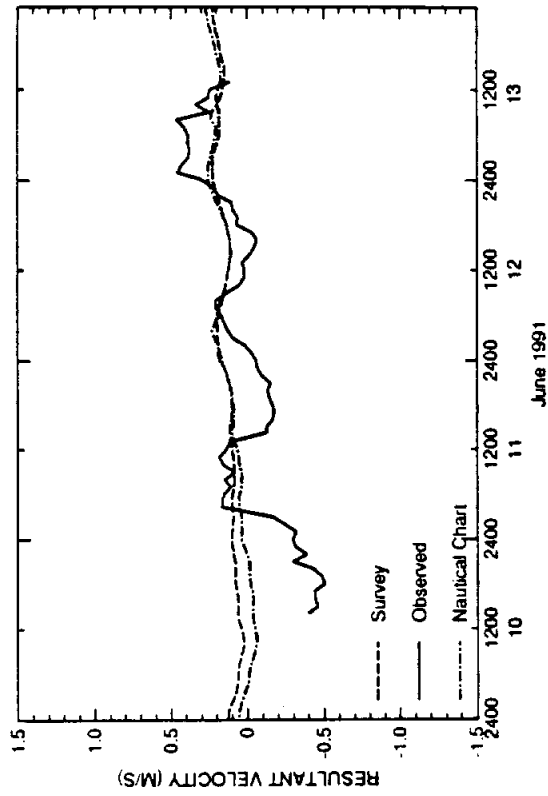


FIG. 1. South Land Cut

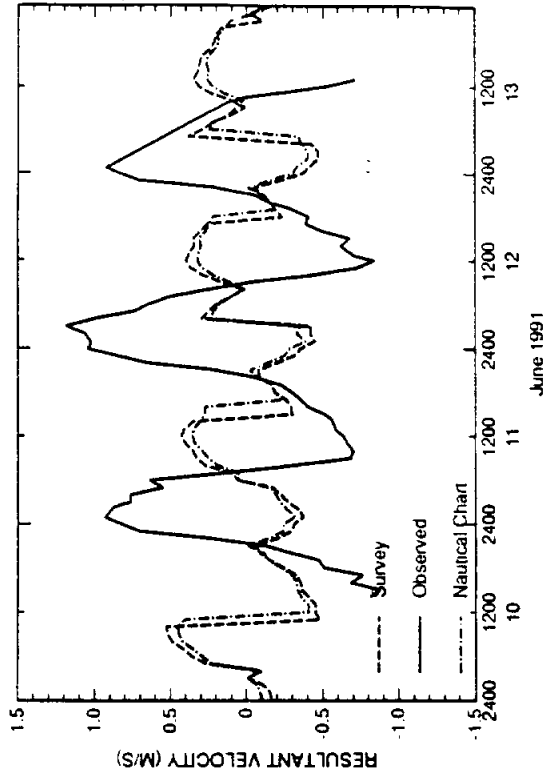


FIG. 2. Port Mansfield Jetties

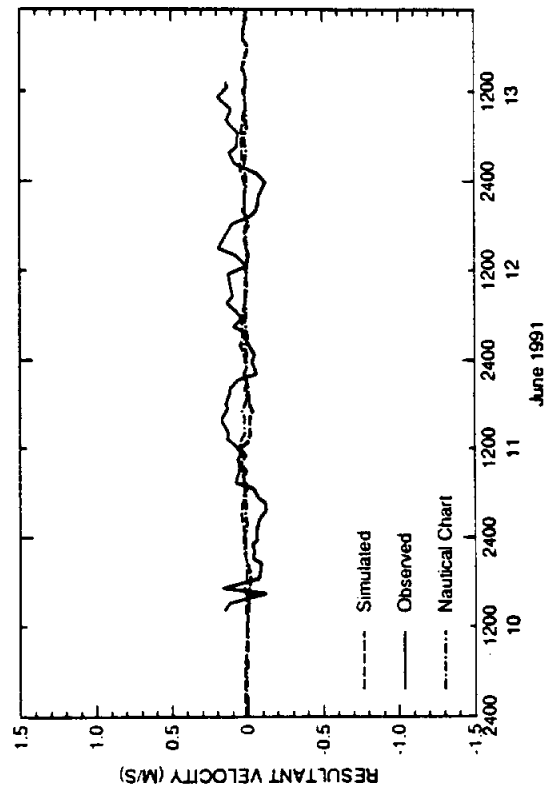


FIG. 3. Mouth of Arroyo Colorado

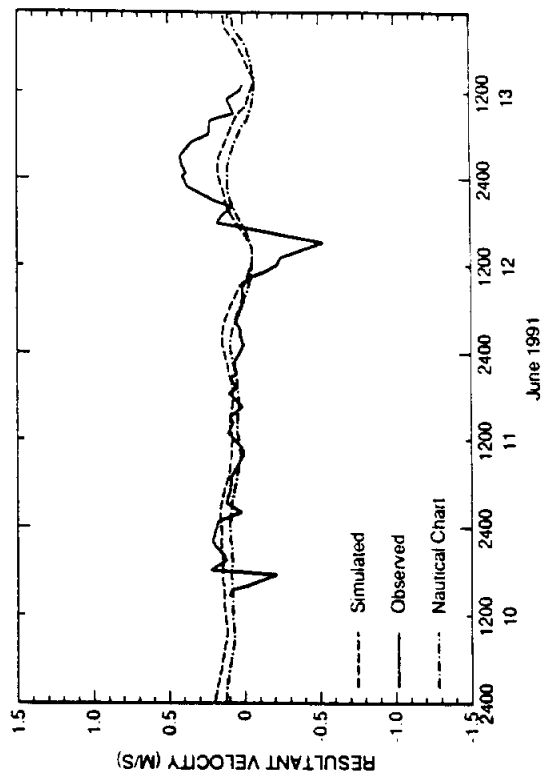


FIG. 4. GIWW North of Arroyo Colorado

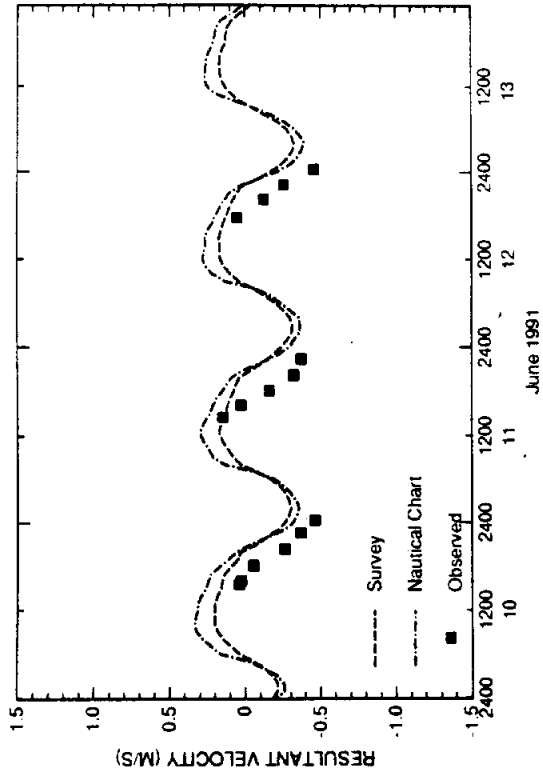


FIG. 6. Old Causeway (Mid East)

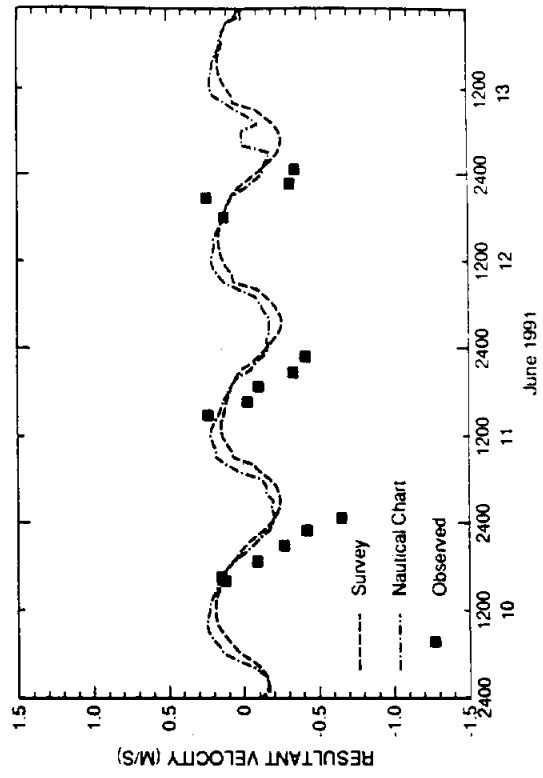


FIG. 8. Old Causeway (Western)

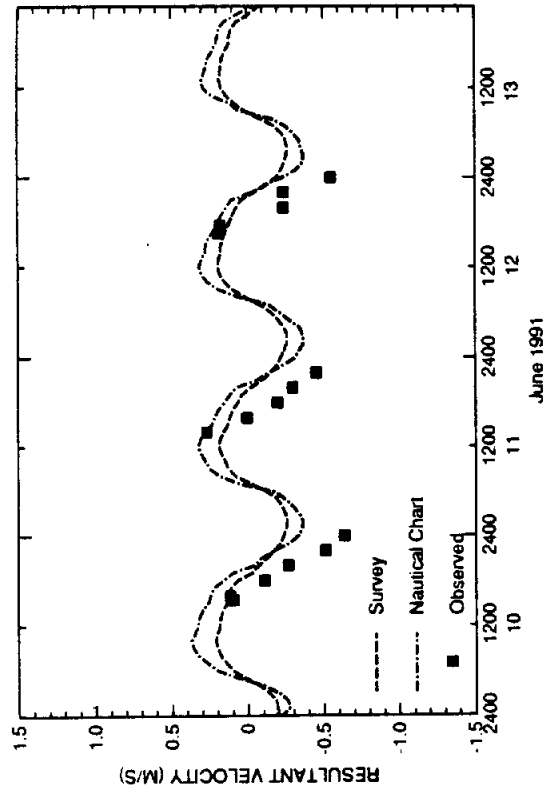


FIG. 5. Old Causeway (Eastern)

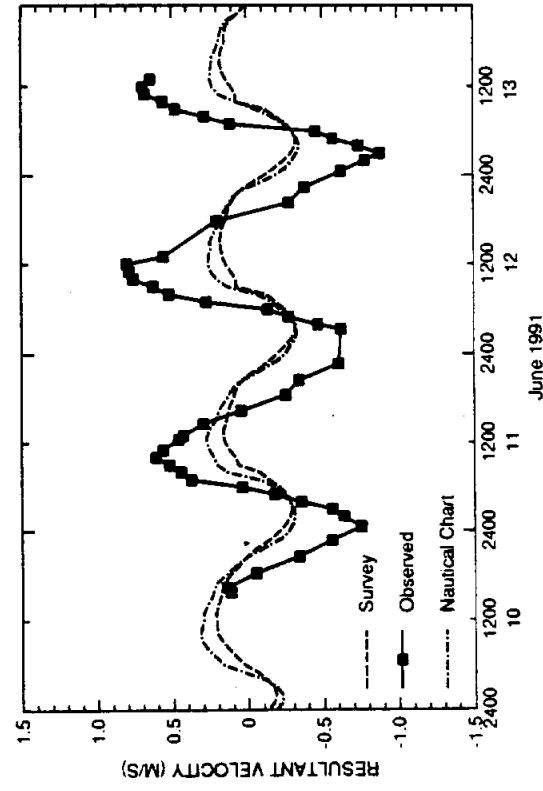


FIG. 7. Old Causeway (Mid West)

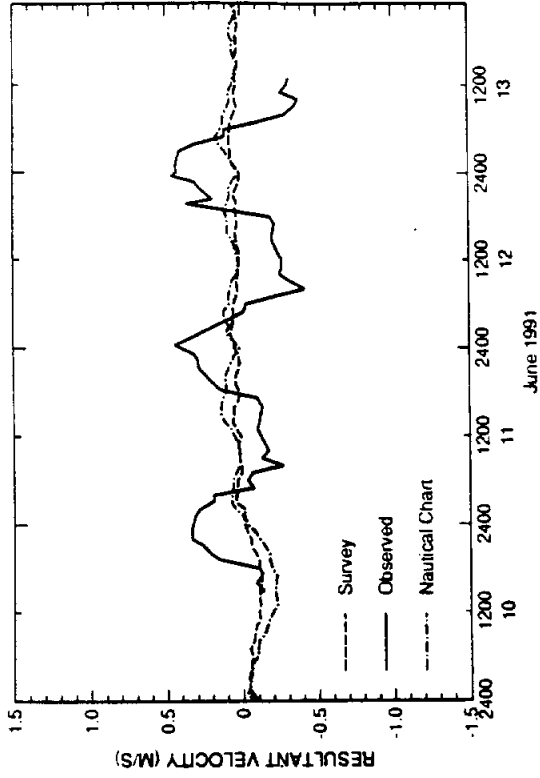


FIG. 10. Brownsville Ship Channel

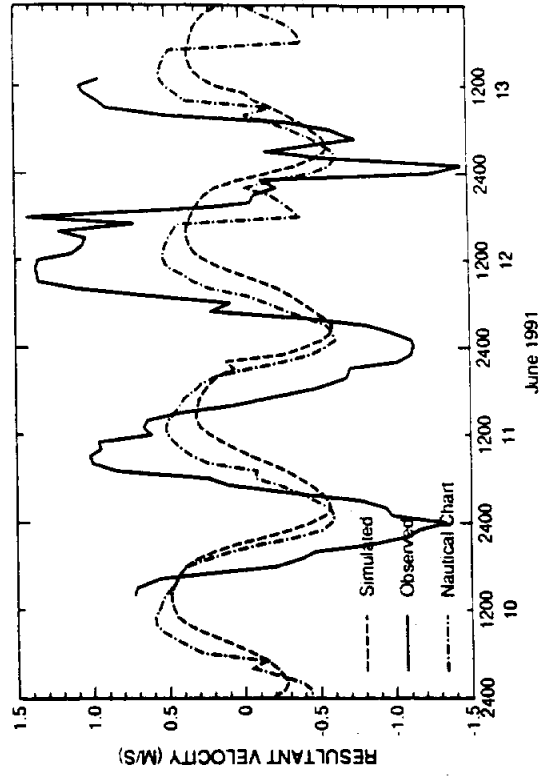


FIG. 12. Brazos Santiago Pass

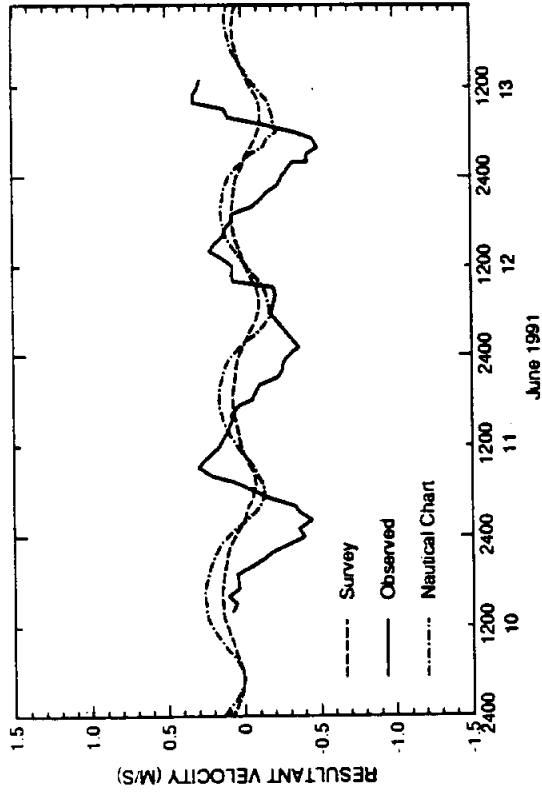


FIG. 9. Port Isabel Channel

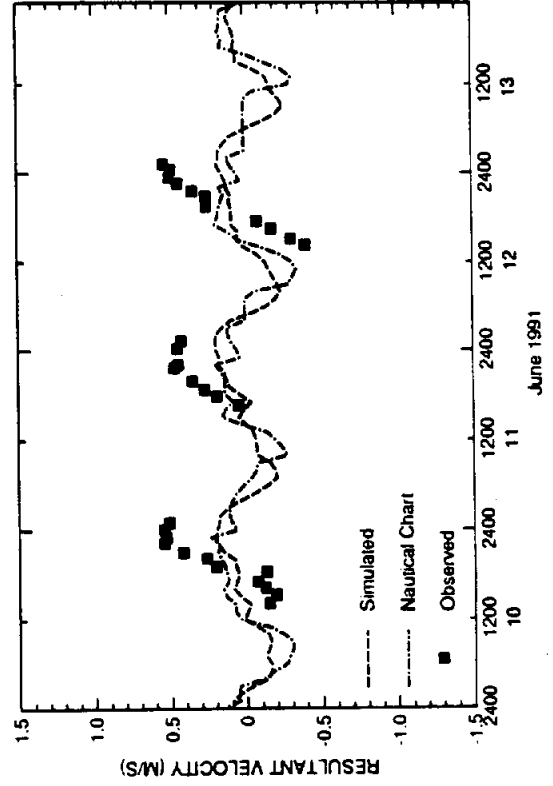


FIG. 11. South Bay Pass

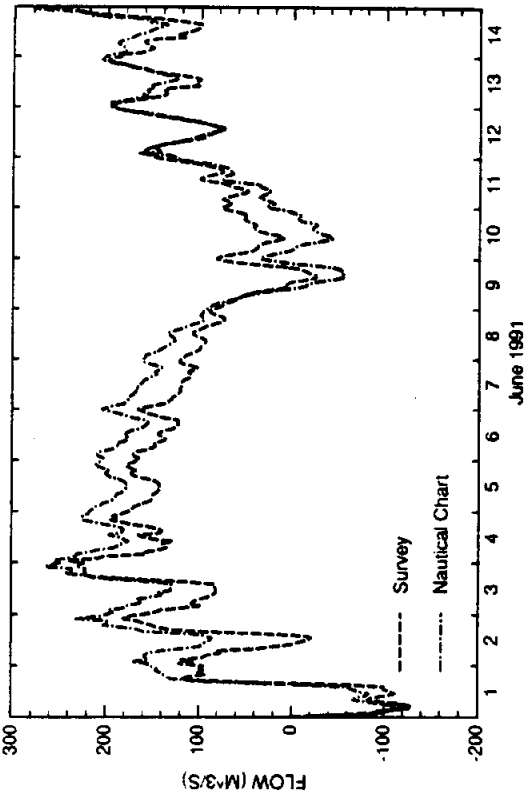


FIG. 1. South Land Cut

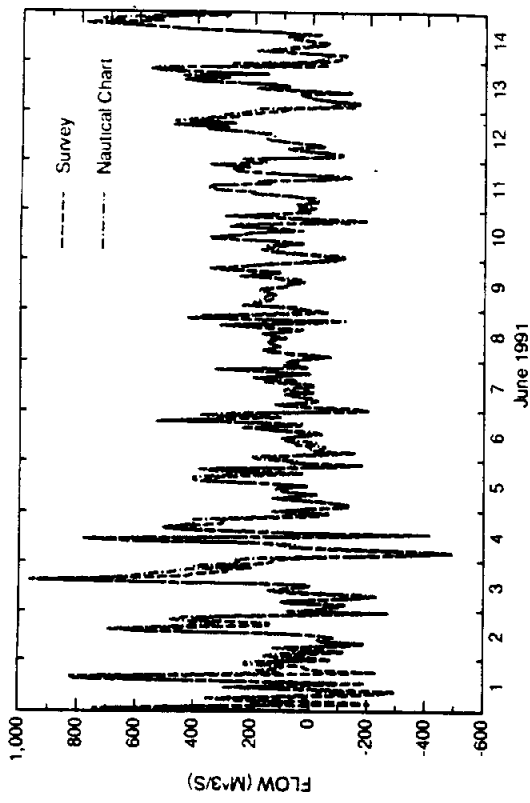


FIG. 2. Laguna Madre North of Port Mansfield

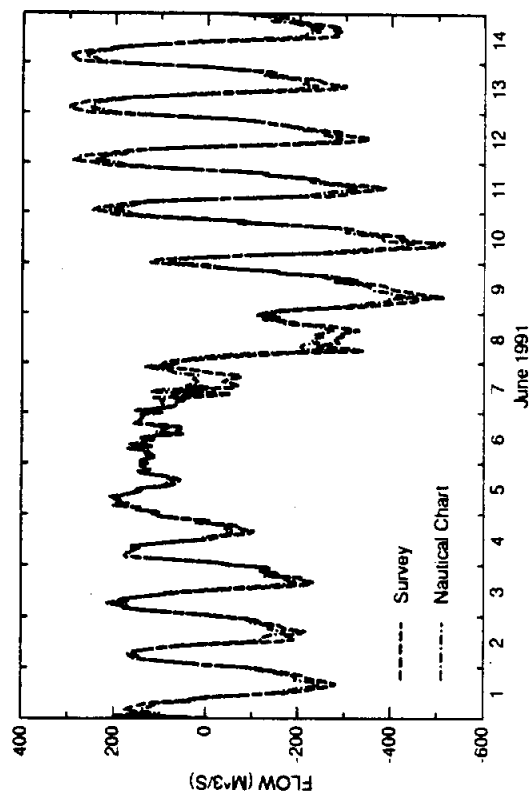


FIG. 3. Port Mansfield Channel

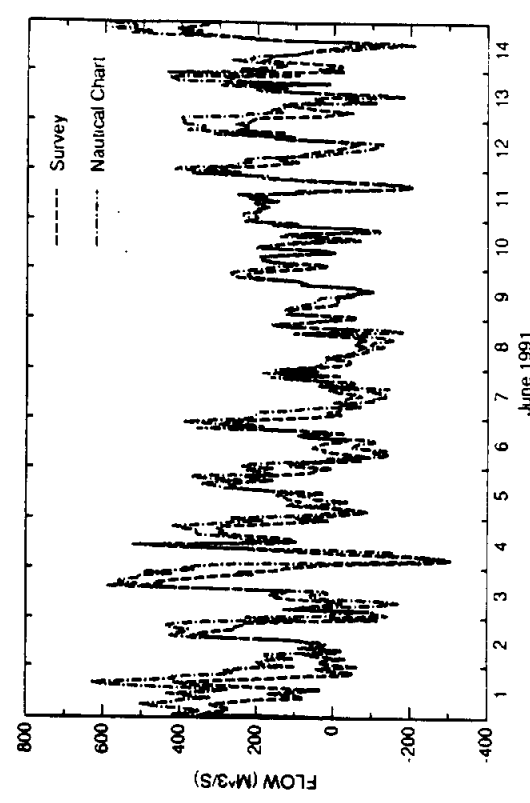


FIG. 4. Laguna Madre South of Port Mansfield

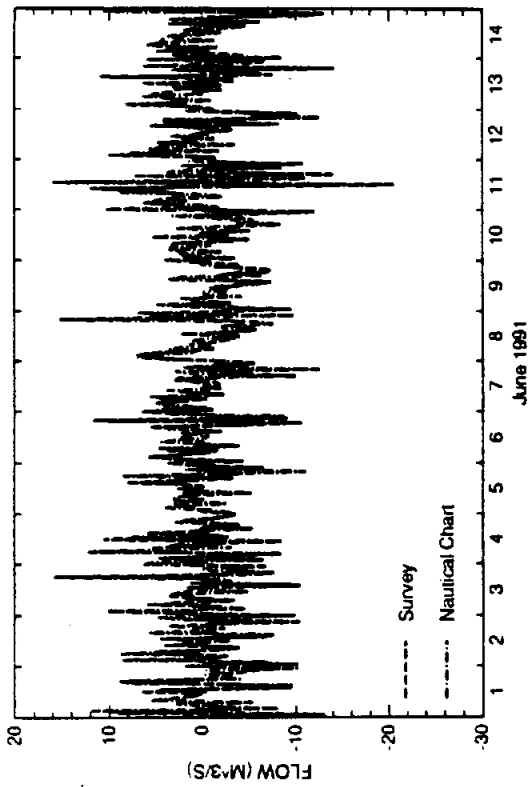


FIG. 5. Arroyo Colorado West of Languna Atascosa

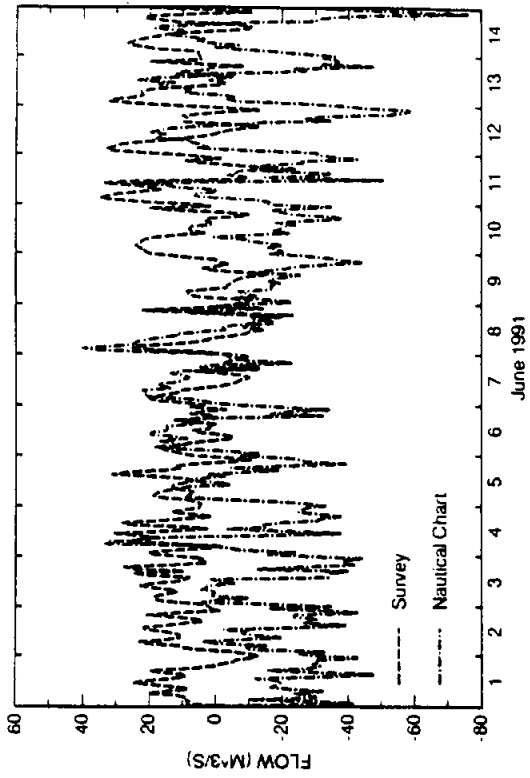


FIG. 6. Arroyo Colorado East of Laguna Atascosa

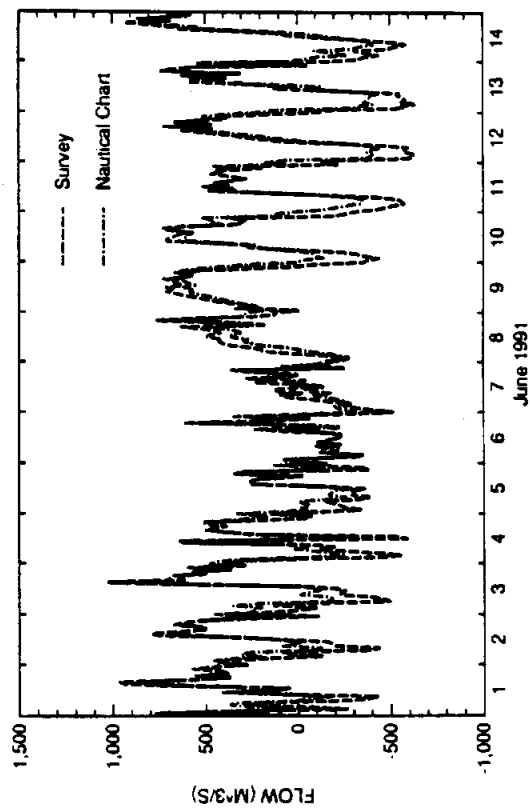


FIG. 7. Laguna Madre North of Port Isabel

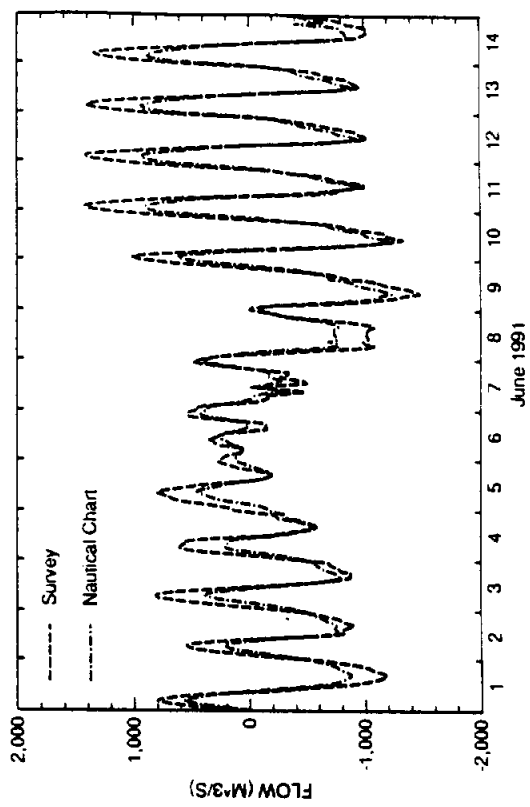


FIG. 8. Brazos-Santiago Pass

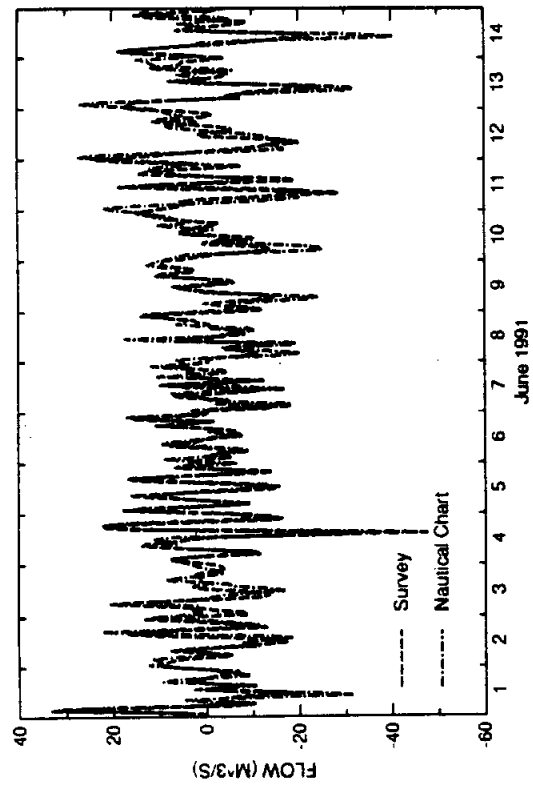


FIG. 9. Brownsville Ship Channel

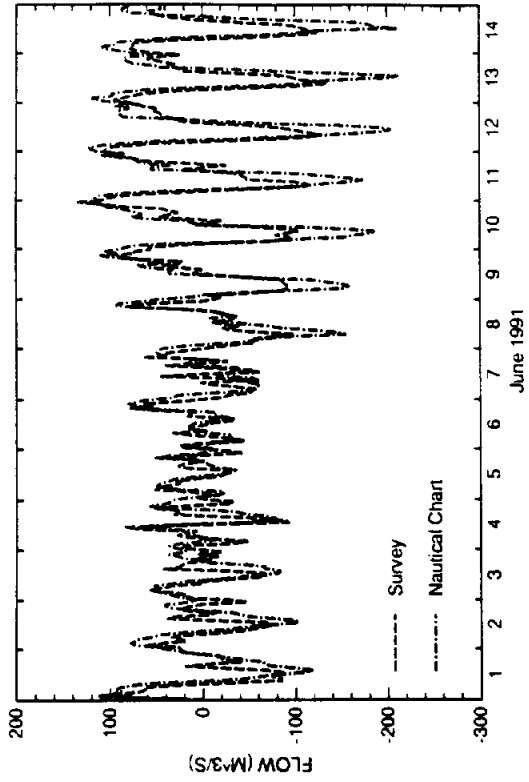


FIG. 10. South Bay Pass

APPENDIX B

LIST OF FILES FOR DELIVERY

INDEX

This file

For all coverages with elevation data the item SPOT represents the elevation (depth) in meters, while the item HOLD represents the elevation (depth) in feet. All coverages are in UTM coordinates with NAD27.

USGS 1:100,000 scale digital line graphs (DLG)
The DLG's were used to develop the boundaries of the mode grids.

baffin_b.hys.e00.Z	Baffin Bay DLG
brownsville.hys.e00.Z	Brownsville DLG
cchristi.hys.e00.Z	Corpus Christi DLG
harlingen.hys.e00.Z	Harlingen DLG
p_mansfld.hys.e00.Z	Port Mansfield DLG
laguna_hys.e00.Z	Combination of DLG's which cover the Laguna Madre

USGS 1:250,000 scale Digital Elevation Model (DEM)
The DEM's could be used to add elevation points on land.

demread	Simple shell script to format DEM data for use in ARC/INFO.
dugdem.txt	Description of demread
brownsville-w.Z	Brownsville DEM
corpus_christi-w.Z	Corpus Christi DEM
port_isabel-w.Z	Port Isabel DEM

Coverages derived from the NOAA/NOS Nautical Charts.

laguna_c.e00.Z	Channels
laguna_con.e00.Z	Contour lines
laguna_d.e00.Z	Depth points
laguna_sd.e00.Z	Supplemental depth points adde by hand

Coverages, grids, amls, etc. used to derive the model grids for the lower Laguna Madre. The grid used in the model was rotated 13 degree in order to reduce the size of the grid needed to represent the estuary. All coverages needed to create the grids are listed below.

r1195grd.aml	AML used to generate the rotated 200 meter grid from the hydrographic survey data (HSD)
r11cgrd.aml	AML used to generate the rotated 200 meter grid from the nautical chart data (NCD)
1195grd.aml	AML used to generate an unrotated grid from the HSD
11cgrd.aml	AML used to generate an unrotated grid from the NCD
1120095_grd.e00.Z	Unrotated 200 meter grid from HSD
11200c_grd.e00.Z	Unrotated 200 meter grid from NCD
1195sup_d.e00.Z	HSD supplemental depth coverage
1laguna_c.e00.Z	NCD channel coverage
1laguna_d.e00.Z	NCD depth coverage
1laguna_i.e00.Z	NCD island coverage
1laguna_sd.e00.Z	NCD supplemental depth coverage
11m95_d.e00.Z	HSD depth coverage
11m95_land.e00.Z	HSD land boundary outline
1ltin_clip.e00.Z	Clip coverage used to create tins
1laguna_land.e00.Z	NCD land boundary outline

Miscellaneous Coverages

lm95xy.e00.Z Coverage of the HSD
stations.e00.Z Coverage with locations of tide, wind,
velocity, water quality, etc. stations
tx95.e00.Z Coverage of the mesh points in the TXBLEND
model

Coverages, grids, amls, etc. used to derive the model grids for
the upper Laguna Madre. All coverages needed to create the grids
are listed below.

ulgrid.aml AML used to create the 200 meter grid (NCD)
for the upper Laguna Madre
ul200_g.e00.Z 200 meter grid (NCD)
ul400_g.e00.Z 400 meter grid (NCD)
ulaguna_c2.e00.Z Channel coverage
ulaguna_d.e00.Z Depth point coverage
ulaguna_i2.e00.Z Island coverage
ulaguna_sd.e00.Z Supplemental depth points
ulland.e00.Z Outline coverage
uloutnc.e00.Z Outline coverage
ultin.e00.Z TIN of the upper Laguna Madre
ultin_clip.e00.Z Clip coverage used to create the TIN

Upper Laguna Madre TIN based on HSD

ulm95tin.aml AML used to create the TIN
ulm95_d.e00.Z HSD depth point coverage
ulm95_tin.e00.Z TIN created from HSD